pharmaceutics

Special Issue Reprint

Population Pharmacokinetics and Its Clinical Applications

Edited by
Katarina Vučićević and Branislava Miljković

mdpi.com/journal/pharmaceutics

MDPI

Population Pharmacokinetics and Its Clinical Applications

Population Pharmacokinetics and Its Clinical Applications

Guest Editors

Katarina Vučićević
Branislava Miljković

MDPI

Basel • Beijing • Wuhan • Barcelona • Belgrade • Novi Sad • Cluj • Manchester

Guest Editors

Katarina Vučićević
Department of Pharmacokinetics and Clinical Pharmacy
University of Belgrade
Belgrade
Serbia

Branislava Miljković
Department of Pharmacokinetics and Clinical Pharmacy
University of Belgrade
Belgrade
Serbia

Editorial Office
MDPI AG
Grosspeteranlage 5
4052 Basel, Switzerland

This is a reprint of the Special Issue, published open access by the journal *Pharmaceutics* (ISSN 1999-4923), freely accessible at: https://www.mdpi.com/journal/pharmaceutics/special_issues/OM1L831CL0.

For citation purposes, cite each article independently as indicated on the article page online and as indicated below:

Lastname, A.A.; Lastname, B.B. Article Title. *Journal Name* **Year**, *Volume Number*, Page Range.

ISBN 978-3-7258-8841-2 (Hbk)
ISBN 978-3-7258-8842-9 (PDF)
https://doi.org/10.3390/books978-3-7258-8842-9

© 2026 by the authors. Articles in this reprint are Open Access and distributed under the Creative Commons Attribution (CC BY) license. The reprint as a whole is distributed by MDPI under the terms and conditions of the Creative Commons Attribution-NonCommercial-NoDerivs (CC BY-NC-ND) license (https://creativecommons.org/licenses/by-nc-nd/4.0/).

Contents

About the Editors . . . . . **ix**

Preface . . . . . **xi**

Katarina M. Vučićević
Population Pharmacokinetic Models at the Forefront of Precision Dosing
Reprinted from: *Pharmaceutics* **2026**, *18*, 535,
https://doi.org/10.3390/pharmaceutics18050535 . . . . . **1**

Anders Larsson, Mats B. Eriksson, Linda Steinholtz and Anna-Karin Hamberg
Patient Median-Based Quality Control in Lamotrigine Therapeutic Drug Monitoring: A 15-Year Retrospective Study
Reprinted from: *Pharmaceutics* **2026**, *18*, 236,
https://doi.org/10.3390/pharmaceutics18020236 . . . . . **6**

Chiara Rossi, Raffaele Simeoli, Giulia Angelino, Sara Cairoli, Fiammetta Bracci, Daniela Knafelz, et al.
Measurement of Anti-TNF Biologics in Serum Samples of Pediatric Patients: Comparison of Enzyme-Linked Immunosorbent Assay (ELISA) with a Rapid and Automated Fluorescence-Based Lateral Flow Immunoassay
Reprinted from: *Pharmaceutics* **2025**, *17*, 421,
https://doi.org/10.3390/pharmaceutics17040421 . . . . . **16**

Nuo Xu, Yufei Shi, Yixue Wang, Wenyao Mak, Wenyu Yang, Kar Weng Ng, et al.
Development and Quality Control of a Population Pharmacokinetic Model Library for Caspofungin
Reprinted from: *Pharmaceutics* **2024**, *16*, 819,
https://doi.org/10.3390/pharmaceutics16060819 . . . . . **32**

Firas Al-Zubaydi, Andrew Wassef, Leonid Kagan and Luigi Brunetti
Development of a Population Pharmacokinetic Gabapentin Model Leveraging Therapeutic Drug Monitoring Concentrations
Reprinted from: *Pharmaceutics* **2024**, *16*, 1514,
https://doi.org/10.3390/pharmaceutics16121514 . . . . . **55**

Maša Roganović, Mirjana Cvetković, Ivana Gojković, Brankica Spasojević, Marija Jovanović, Branislava Miljković and Katarina Vučićević
Population Pharmacokinetics Model of Cyclosporin A in Children and Young Adult Renal Transplant Patients: Focus on Haemoglobin Contribution to Exposure Variability
Reprinted from: *Pharmaceutics* **2026**, *18*, 99,
https://doi.org/10.3390/pharmaceutics18010099 . . . . . **66**

Zorica Pejčić, Valentina Topić Vučenović, Branislava Miljković and Katarina M. Vučićević
Integrating Clopidogrel's First-Pass Effect in a Joint Semi-Physiological Population Pharmacokinetic Model of the Drug and Its Inactive Carboxylic Acid Metabolite
Reprinted from: *Pharmaceutics* **2024**, *16*, 685,
https://doi.org/10.3390/pharmaceutics16050685 . . . . . **79**

Glauco Henrique Balthazar Nardotto, Elin M. Svenson, Valdes Roberto Bollela, Adriana Rocha, Svetoslav Nanev Slavov, João Paulo Bianchi Ximenez, et al.
Effect of Interindividual Variability in Metabolic Clearance and Relative Bioavailability on Rifampicin Exposure in Tuberculosis Patients with and without HIV Co-Infection: Does Formulation Quality Matter?
Reprinted from: *Pharmaceutics* **2024**, *16*, 970, https://doi.org/10.3390/pharmaceutics16080970 . . . . . **92**

Alessandro Di Deo, Sean Oosterholt, Joseph Horrigan, Stuart Evans, Alison McMorn and Oscar Della Pasqua
Population Pharmacokinetics of Tideglusib in Congenital and Childhood Myotonic Dystrophy Type 1: Influence of Demographic and Clinical Factors on Systemic Exposure
Reprinted from: *Pharmaceutics* **2025**, *17*, 1065, https://doi.org/10.3390/pharmaceutics17081065 . . . . . **106**

Charuka Wickramasinghe, Seongho Kim, Yuanyuan Jiang, Xun Bao, Yang Yue, Jun Jiang, et al.
Population Pharmacokinetic Modeling of Total and Unbound Pamiparib in Glioblastoma Patients: Insights into Drug Disposition and Dosing Optimization
Reprinted from: *Pharmaceutics* **2025**, *17*, 524, https://doi.org/10.3390/pharmaceutics17040524 . . . . . **125**

John C. Panetta, Nicholas S. Selvo, David Van Mater and Clinton F. Stewart
Population Pharmacokinetic and Pharmacodynamic Study of Palbociclib in Children and Young Adults with Recurrent, Progressive, or Refractory Brain Tumors
Reprinted from: *Pharmaceutics* **2024**, *16*, 1528, https://doi.org/10.3390/pharmaceutics16121528 . . . . . **141**

Stephanie F. Ling, Kayode Ogungbenro, Adam S. Darwich, Amirah Binti Mohammad Ariff, Nisha Nair, James Bluett, et al.
Population Pharmacokinetic Analysis and Simulation of Alternative Dosing Regimens for Biosimilars to Adalimumab and Etanercept in Patients with Rheumatoid Arthritis
Reprinted from: *Pharmaceutics* **2024**, *16*, 702, https://doi.org/10.3390/pharmaceutics16060702 . . . . . **159**

Srđan Marković, Đorđe Kralj, Petar Svorcan, Tamara Knežević Ivanovski, Olga Odanović, Sanja Obradović, et al.
Vedolizumab Clearance as a Surrogate Marker for Remission in Inflammatory Bowel Disease Patients: Insights from Real-World Pharmacokinetics
Reprinted from: *Pharmaceutics* **2024**, *16*, 1629, https://doi.org/10.3390/pharmaceutics16121629 . . . . . **172**

Karine Rodríguez-Fernández, Javier Zarzoso-Foj, Marina Saez-Bello, Almudena Mateu-Puchades, Antonio Martorell-Calatayud, Matilde Merino-Sanjuan, et al.
Model-Informed Precision Dosing for Personalized Ustekinumab Treatment in Plaque Psoriasis
Reprinted from: *Pharmaceutics* **2024**, *16*, 1295, https://doi.org/10.3390/pharmaceutics16101295 . . . . . **188**

Karine Rodriguez-Fernandez, Javier Zarzoso-Foj, Marina Saez-Bello, Almudena Mateu-Puchades, Antonio Martorell-Calatayud, Matilde Merino-Sanjuan, et al.
Personalized Secukinumab Treatment in Patients with Plaque Psoriasis Using Model-Informed Precision Dosing
Reprinted from: *Pharmaceutics* **2024**, *16*, 1576, https://doi.org/10.3390/pharmaceutics16121576 . . . . . **203**

Judith Kahn, Eva Maria Matzhold, Peter Schlenke and Peter Schemmer
Use of Nuclear Factor of Activated T Cell-Regulated Gene Expression for Monitoring Immunosuppression with Extended-Release Tacrolimus after Liver Transplantation—A Proof of Concept
Reprinted from: *Pharmaceutics* **2024**, *16*, 1317,
https://doi.org/10.3390/pharmaceutics16101317 . . . . . **219**

Hwa Jun Cha, Sungpil Han, Kwan Cheol Pak and Hyungsub Kim
Development of a Web Application for Simulating Plasma Drug Concentrations in Patients with Zolpidem Intoxication
Reprinted from: *Pharmaceutics* **2024**, *16*, 689,
https://doi.org/10.3390/pharmaceutics16050689 . . . . . **235**

About the Editors

Katarina Vučićević

Katarina Vučićević is a Full Professor at the Department of Pharmacokinetics and Clinical Pharmacy, Faculty of Pharmacy, University of Belgrade, Serbia. She is a pharmacist and holds a PhD in Pharmacokinetics, with research interests focused on population pharmacokinetics, pharmacometrics, model-informed precision dosing, therapeutic drug monitoring, pharmacokinetic–pharmacodynamic modeling, and personalized pharmacotherapy. Her research particularly focuses on the application of quantitative approaches to optimize treatment in complex patient populations, including patients with inflammatory bowel diseases, critically ill patients, transplant recipients, and pediatric populations. She is the Principal Investigator of the optYmAb project, funded by the Science Fund of the Republic of Serbia, which aims to improve clinical outcomes in inflammatory bowel disease through population pharmacokinetic–pharmacodynamic modeling and personalized dosing of monoclonal antibodies. In addition, she was Principal Investigator of two bilateral scientific projects with Slovenia and France. Her research activities include the development and evaluation of population pharmacokinetic models, Bayesian forecasting approaches, and implementation of precision dosing strategies in clinical practice. Katarina Vučićević was a Fulbright Visiting Scholar at the University of California, San Francisco, and actively participates in international pharmacometrics and therapeutic drug monitoring initiatives, including the COST Action ENOTTA network. She has authored numerous scientific publications and serves as a reviewer and editor for international journals in pharmacology, pharmacokinetics, and clinical pharmacy. Her current interests include the development of digital platforms for model-informed precision dosing and the translation of pharmacometric methods into routine healthcare practice.

Branislava Miljković

Branislava Miljković is a Full Professor at the Department of Pharmacokinetics and Clinical Pharmacy, Faculty of Pharmacy, University of Belgrade, where she earned her undergraduate degree, completed her master's studies, and obtained her PhD. She also completed postgraduate studies in Clinical Pharmacy at Robert Gordon University, Aberdeen, United Kingdom. As part of her academic training, she undertook research at the Center for Bio-Pharmaceutical Sciences in Leiden, the Netherlands, and was a DAAD scholarship holder at the Institute of Pharmacy, University of Bonn, Germany. Her research focuses on therapeutic drug monitoring, population pharmacokinetics and personalized pharmacotherapy. She is the Head of the Specialist Studies in Clinical Pharmacy and the Academic Specialist Programme in Pharmaceutical Care at the Faculty of Pharmacy, University of Belgrade. Branislava Miljković serves as President of the Pharmaceutical Associations of Serbia, is an expert for the Medicines and Medical Devices Agency of Serbia, and a member of the Editorial Board of the *Pharmacotherapy Guide*. She has also served as a member of the Scientific Committee of the European Association of Hospital Pharmacists (EAHP), a member of the Ethics Committee of the Republic of Serbia, Chair of the Working Group of the Ministry of health of Republic of Serbia for the Development of the National Guidelines on the Use of Medicines During Breastfeeding, and co-author of the EDQM/Council of Europe Medicines Review Guidelines.

Preface

Population pharmacokinetics has become an essential component of modern pharmacotherapy, providing a quantitative framework for understanding variability in drug exposure and supporting individualized treatment strategies. This Reprint was prepared to present recent developments in population pharmacokinetic modeling, model-informed precision dosing, therapeutic drug monitoring, pharmacodynamic assessment, and their translation into clinical practice. The aim of this Reprint is to present current research demonstrating how pharmacometric approaches can address challenges associated with interindividual variability, complex patient populations, and the optimization of therapeutic regimens. The included contributions cover diverse therapeutic areas and populations, illustrating the application of modeling and simulation approaches in improving dose selection, monitoring treatment response, and enhancing medication safety.

This Reprint is intended for researchers, pharmacists, pharmacometricians, clinicians, and healthcare professionals interested in the application of quantitative approaches to precision medicine. It highlights the multidisciplinary nature of population pharmacokinetics and its growing importance in bridging pharmacological research and patient-centered care.

As Guest Editors, we would like to thank all authors for their valuable contributions and for sharing their research findings, which demonstrate the evolving role of pharmacometrics in advancing personalized pharmacotherapy.

Katarina Vučićević and Branislava Miljković
Guest Editors

pharmaceutics

MDPI

Editorial

Population Pharmacokinetic Models at the Forefront of Precision Dosing

Katarina M. Vučićević

Department of Pharmacokinetics and Clinical Pharmacy, Faculty of Pharmacy, University of Belgrade, 11221 Belgrade, Serbia; katarina.vucicevic@pharmacy.bg.ac.rs

1. Population Pharmacokinetics in Focus

Population pharmacokinetics (PopPK) has evolved from a methodological niche into a fundamental pillar of quantitative clinical pharmacology, playing a key role in dose optimization and advancements in individualized therapy and regulatory decision making. By integrating compartmental pharmacokinetic models with nonlinear mixed-effects (NLME) statistical frameworks, PopPK enables the characterization of drug concentration–time profiles and the quantification of variability in drug exposure across individuals within a target population. Interindividual variability is typically explained by identifiable covariates, including demographic, physiological, and disease-related factors such as age, body size, organ function, and underlying clinical conditions [1–3]. Through this framework, PopPK analyses enable us to make better interpretations of clinical observations, guide evidence-based dose adjustments, and support decision making across diverse therapeutic areas. In recent decades, continuous advancements in modeling methodologies, together with increased computational capacity, and the growing availability of high-quality clinical data have substantially strengthened the application of PopPK in both drug development and clinical practice [4,5].

Recent reviews emphasize that model-informed precision dosing (MIPD) represents the next generation of personalized therapy, extending beyond conventional therapeutic drug monitoring (TDM) to incorporate patient-specific characteristics, longitudinal measurements, and predictive modeling, thereby improving the precision of dosing recommendations. Notably, Minichmayr and colleagues demonstrated how MIPD leverages pharmacometric models to facilitate the routine clinical implementation of model-informed approaches, thereby advancing individualized therapy across diverse therapeutic areas, including infectious diseases, oncology, and inflammatory disorders [6].

The Special Issue of *Pharmaceutics* titled "Population Pharmacokinetics and Its Clinical Applications, 2nd edition" built upon the first collection published in 2024, which showcased recent advances in both the development and application of PopPK models across clinical contexts and special populations, highlighting their role in MIPD-TDM, and individualized therapy.

2. Highlights of the Special Issue

The collection of manuscripts published in this Special Issue of *Pharmaceutics*—"Population Pharmacokinetics and Its Clinical Applications"—reflects a coherent and timely advancement in the field of pharmacometrics, with a particular emphasis on PopPK models and their clinical application. Despite the diversity of therapeutic areas, including oncology, neurology, transplantation, inflammatory and rare diseases, the contributions

converge on a shared objective: translating quantitative models into clinically actionable tools that support individualized therapy.

A central theme across the Special Issue is the development and refinement of PopPK models as a foundation for understanding drug disposition and variability. Several studies, including those on gabapentin (Contribution 8), pamiparib (Contribution 13), tideglusib (Contribution 14), and cyclosporin A (Contribution 15), systematically characterize drug absorption, distribution, metabolism, and elimination using an NLME modeling approach. These analyses consistently highlight the role of patient-specific covariates, such as renal function, body weight, age, hemoglobin levels, and prior therapies in explaining interindividual variability in exposure. In rare diseases, the development of a PopPK model for tideglusib demonstrates how modeling approaches can support pediatric extrapolation and inform dosing strategies in conditions with limited clinical data (Contribution 14).

Beyond PopPK model development, several manuscripts extend into PK/PD modeling, linking drug exposure to clinical outcomes. The study of palbociclib in pediatric patients with brain tumor exemplifies this integration by connecting exposure to hematological toxicity endpoints, enabling simulation-based risk assessment (Contribution 9). Similarly, the investigation of vedolizumab in inflammatory bowel disease demonstrates how drug clearance may outperform traditional exposure metric (trough concentration) as predictors of clinical remission (Contribution 11). These findings underscore a paradigm shift toward more mechanistically meaningful biomarkers derived from models rather than empirical thresholds alone.

A distinguishing feature of this Special Issue is its strong focus on MIPD as a bridge between pharmacometric theory and clinical decision making. The paired studies on ustekinumab (Contribution 6) and secukinumab (Contribution 10) in psoriasis provide compelling examples of how PK/PD models can be operationalized to individualize dosing regimens. By explicitly accounting for uncertainty in individual parameter estimates, these works move beyond deterministic predictions and introduce probabilistic frameworks that better reflect clinical reality. Notably, both studies demonstrate that a substantial proportion of patients may benefit from dose optimization or intensification compared to standard regimens, highlighting the clinical impact of MIPD strategies.

Complementing these efforts are contributions that emphasize translational tools and implementation. The development of a web-based application for simulating zolpidem concentrations in intoxication scenarios represents a practical step toward bedside application of PopPK models (Contribution 2). Similarly, the use of simulation platforms in studies such as cyclosporin A (Contribution 15) further illustrates how model outputs can be directly integrated into clinical workflows. These approaches align with the broader vision of digital health and decision-support systems, where complex models are embedded into user-friendly interfaces accessible to clinicians.

Methodologically, the Special Issue also showcases innovation in model design. The semi-physiological model of clopidogrel incorporating first-pass metabolism and metabolite formation highlights the value of mechanistic modeling in capturing complex biotransformation processes (Contribution 1). Meanwhile, the joint modeling of total and unbound drug concentrations, as demonstrated for pamiparib, reflects an increasing recognition of the importance of pharmacologically active fractions in dose optimization (Contribution 13).

The manuscripts included in the Special Issue collectively demonstrate that PopPK has evolved beyond a purely theoretical framework into a clinically applicable discipline that underpins precision medicine in real-world settings. Together, these contributions illustrate the full continuum of PopPK model application: from data generation and rigorous model development using NLME approaches, through model evaluation and simulation, to

https://doi.org/10.3390/pharmaceutics18050535

clinical translation and implementation in decision-support contexts. In this context, the manuscripts complement a growing body of evidence supporting MIPD as an effective framework for optimizing pharmacotherapy.

3. Towards Precision Pharmacology

The field of PopPK is poised for continued transformation as technological advances, computational methods, and clinical integration converge. One of the most promising directions is selection of the adequate PopPK model, and the broader implementation of MIPD in routine clinical practice. This will require not only robust PopPK models but also user-friendly software platforms, integration with electronic health records, and real-time analytics to support clinicians in making data-driven dosing decisions [6]. Nevertheless, integrating biomarkers and pharmacodynamic endpoints with PopPK models will strengthen individualized therapy by linking drug exposure to clinical outcomes. Prospective clinical trials validating these approaches will be essential to translate the promise of MIPD into measurable improvements in patient care, safety, and efficacy.

Artificial intelligence and machine learning are expected to complement traditional population models by identifying hidden covariates, predicting drug response patterns, and integrating complex datasets from genomics, metabolomics, and patient monitoring devices. Such approaches could refine model predictions and extend MIPD to complex multi-drug regimens, especially in oncology, infectious diseases, and transplant medicine [7–9].

In summary, the future of PopPK lies in its full integration into precision medicine, supported by technology, enriched datasets, and validated clinical outcomes. Continued collaboration among modelers, clinicians, regulatory authorities, and software developers will be key to realizing the transformative potential of MIPD in improving patient-centered therapy.

Funding: This research was funded by the Ministry of Science, Technological Development, and Innovation of the Republic of Serbia through two grant agreements with the University of Belgrade–Faculty of Pharmacy (Nos. 451-03-33/2026-03/200161 and 451-03-34/2026-03/200161).

Institutional Review Board Statement: Not applicable.

Informed Consent Statement: Not applicable.

Conflicts of Interest: The author declares no conflicts of interest.

List of Contributions:

1. Pejčić, Z.; Topić Vučenović, V.; Miljković, B.; Vučićević, K. Integrating Clopidogrel's First-Pass Effect in a Joint Semi-Physiological Population Pharmacokinetic Model of the Drug and Its Inactive Carboxylic Acid Metabolite. *Pharmaceutics* **2024**, *16*, 685. https://doi.org/10.3390/pharmaceutics16050685.
2. Cha, H.J.; Han, S.; Pak, K.C.; Kim, H. Development of a Web Application for Simulating Plasma Drug Concentrations in Patients with Zolpidem Intoxication. *Pharmaceutics* **2024**, *16*, 689. https://doi.org/10.3390/pharmaceutics16050689.
3. Ling, S.F.; Ogungbenro, K.; Darwich, A.S.; Mohammad Ariff, A.B.; Nair, N.; Bluett, J.; Morgan, A.W.; Isaacs, J.D.; Wilson, A.G.; Hyrich, K.L.; et al. Population Pharmacokinetic Analysis and Simulation of Alternative Dosing Regimens for Biosimilars to Adalimumab and Etanercept in Patients with Rheumatoid Arthritis. *Pharmaceutics* **2024**, *16*, 702. https://doi.org/10.3390/pharmaceutics16060702.
4. Xu, N.; Shi, Y.; Wang, Y.; Mak, W.; Yang, W.; Ng, K.W.; Wu, Y.; Tang, Z.; He, Q.; Yan, G.; et al. Development and Quality Control of a Population Pharmacokinetic Model Library for Caspofungin. *Pharmaceutics* **2024**, *16*, 819. https://doi.org/10.3390/pharmaceutics16060819.

5. Nardotto, G.H.B.; Svenson, E.M.; Bollela, V.R.; Rocha, A.; Slavov, S.N.; Ximenez, J.P.B.; Della Pasqua, O.; Lanchote, V.L. Effect of Interindividual Variability in Metabolic Clearance and Relative Bioavailability on Rifampicin Exposure in Tuberculosis Patients with and without HIV Co-Infection: Does Formulation Quality Matter? *Pharmaceutics* **2024**, *16*, 970. https://doi.org/10.3390/pharmaceutics16080970.
6. Rodríguez-Fernández, K.; Zarzoso-Foj, J.; Saez-Bello, M.; Mateu-Puchades, A.; Martorell-Calatayud, A.; Merino-Sanjuan, M.; Gras-Colomer, E.; Climente-Martí, M.; Mangas-Sanjuan, V. Model-Informed Precision Dosing for Personalized Ustekinumab Treatment in Plaque Psoriasis. *Pharmaceutics* **2024**, *16*, 1295. https://doi.org/10.3390/pharmaceutics16101295.
7. Kahn, J.; Matzhold, E.M.; Schlenke, P.; Schemmer, P. Use of Nuclear Factor of Activated T Cell-Regulated Gene Expression for Monitoring Immunosuppression with Extended-Release Tacrolimus after Liver Transplantation—A Proof of Concept. *Pharmaceutics* **2024**, *16*, 1317. https://doi.org/10.3390/pharmaceutics16101317.
8. Al-Zubaydi, F.; Wassef, A.; Kagan, L.; Brunetti, L. Development of a Population Pharmacokinetic Gabapentin Model Leveraging Therapeutic Drug Monitoring Concentrations. *Pharmaceutics* **2024**, *16*, 1514. https://doi.org/10.3390/pharmaceutics16121514.
9. Panetta, J.C.; Selvo, N.S.; Van Mater, D.; Stewart, C.F. Population Pharmacokinetic and Pharmacodynamic Study of Palbociclib in Children and Young Adults with Recurrent, Progressive, or Refractory Brain Tumors. *Pharmaceutics* **2024**, *16*, 1528. https://doi.org/10.3390/pharmaceutics16121528.
10. Rodriguez-Fernandez, K.; Zarzoso-Foj, J.; Saez-Bello, M.; Mateu-Puchades, A.; Martorell-Calatayud, A.; Merino-Sanjuan, M.; Gras-Colomer, E.; Climente-Martí, M.; Mangas-Sanjuan, V. Personalized Secukinumab Treatment in Patients with Plaque Psoriasis Using Model-Informed Precision Dosing. *Pharmaceutics* **2024**, *16*, 1576. https://doi.org/10.3390/pharmaceutics16121576.
11. Marković, S.; Kralj, Đ.; Svorcan, P.; Knežević Ivanovski, T.; Odanović, O.; Obradović, S.; Homšek, A.; Jovanović, M.; Savić, R.; Vučićević, K.M. Vedolizumab Clearance as a Surrogate Marker for Remission in Inflammatory Bowel Disease Patients: Insights from Real-World Pharmacokinetics. *Pharmaceutics* **2024**, *16*, 1629. https://doi.org/10.3390/pharmaceutics16121629.
12. Rossi, C.; Simeoli, R.; Angelino, G.; Cairoli, S.; Bracci, F.; Knafelz, D.; Romeo, E.F.; Faraci, S.; Tarantino, G.; Mancini, A.; et al. Measurement of Anti-TNF Biologics in Serum Samples of Pediatric Patients: Comparison of Enzyme-Linked Immunosorbent Assay (ELISA) with a Rapid and Automated Fluorescence-Based Lateral Flow Immunoassay. *Pharmaceutics* **2025**, *17*, 421. https://doi.org/10.3390/pharmaceutics17040421.
13. Wickramasinghe, C.; Kim, S.; Jiang, Y.; Bao, X.; Yue, Y.; Jiang, J.; Hong, A.; Sanai, N.; Li, J. Population Pharmacokinetic Modeling of Total and Unbound Pamiparib in Glioblastoma Patients: Insights into Drug Disposition and Dosing Optimization. *Pharmaceutics* **2025**, *17*, 524. https://doi.org/10.3390/pharmaceutics17040524.
14. Di Deo, A.; Oosterholt, S.; Horrigan, J.; Evans, S.; McMorn, A.; Della Pasqua, O. Population Pharmacokinetics of Tideglusib in Congenital and Childhood Myotonic Dystrophy Type 1: Influence of Demographic and Clinical Factors on Systemic Exposure. *Pharmaceutics* **2025**, *17*, 1065. https://doi.org/10.3390/pharmaceutics17081065.
15. Roganović, M.; Cvetković, M.; Gojković, I.; Spasojević, B.; Jovanović, M.; Miljković, B.; Vučićević, K. Population Pharmacokinetics Model of Cyclosporin A in Children and Young Adult Renal Transplant Patients: Focus on Haemoglobin Contribution to Exposure Variability. *Pharmaceutics* **2026**, *18*, 99. https://doi.org/10.3390/pharmaceutics18010099.
16. Larsson, A.; Eriksson, M.B.; Steinholtz, L.; Hamberg, A.-K. Patient Median-Based Quality Control in Lamotrigine Therapeutic Drug Monitoring: A 15-Year Retrospective Study. *Pharmaceutics* **2026**, *18*, 236. https://doi.org/10.3390/pharmaceutics18020236.

References

1. Ette, E.I.; Williams, P.J. Population pharmacokinetics I: Background, concepts, and models. *Ann. Pharmacother.* **2004**, *38*, 1702–1706. [CrossRef] [PubMed]
2. U.S. Food and Drug Administration. *Population Pharmacokinetics: Guidance for Industry*; FDA: Silver Spring, MD, USA, 2020. Available online: https://www.fda.gov/media/128793/download (accessed on 10 April 2026).

3. European Medicines Agency Committee for Medicinal Products for Human Use (CHMP). *Guideline on Reporting the Results of Population Pharmacokinetic Analyses*; EMA: London, UK, 2007. Available online: https://www.ema.europa.eu/en/documents/scientific-guideline/guideline-reporting-results-population-pharmacokinetic-analyses_en.pdf (accessed on 10 April 2026).
4. Piotrovsky, V.K. Population pharmacodynamic and pharmacokinetic modeling via mixed effects. *Curr. Opin. Drug Discov. Dev.* **2000**, *3*, 314–330. [PubMed]
5. Berezowska, M.; Hayden, I.S.; Brandon, A.M.; Zats, A.; Patel, M.; Barnett, S.; Ogungbenro, K.; Veal, G.J.; Taylor, A.; Suthar, J. Recommended approaches for integration of population pharmacokinetic modelling with precision dosing in clinical practice. *Br. J. Clin. Pharmacol.* **2025**, *91*, 1064–1079. [CrossRef] [PubMed]
6. Minichmayr, I.K.; Dreesen, E.; Centanni, M.; Wang, Z.; Hoffert, Y.; Friberg, L.E.; Wicha, S.G. Model-informed precision dosing: State of the art and future perspectives. *Adv. Drug Deliv. Rev.* **2024**, *215*, 115421. [CrossRef] [PubMed]
7. Le, J.; Le, H.N.; Nguyen, G.; Kim, R.; Avedissian, S.N.; Vo, C.; Le, B.H.; Nguyen, T.H.; Nguyen, D.T.; Do, D.H.; et al. Model-Informed Precision Dosing: Conceptual Framework for Therapeutic Drug Monitoring Integrating Machine Learning and Artificial Intelligence Within Population Health Informatics. *J. Pers. Med.* **2026**, *16*, 76. [CrossRef] [PubMed]
8. Poweleit, E.A.; Vinks, A.A.; Mizuno, T. Artificial Intelligence and Machine Learning Approaches to Facilitate Therapeutic Drug Management and Model-Informed Precision Dosing. *Ther. Drug Monit.* **2023**, *45*, 143–150. [CrossRef] [PubMed]
9. Sibieude, E.; Khandelwal, A.; Girard, P.; Hesthaven, J.S.; Terranova, N. Population pharmacokinetic model selection assisted by machine learning. *J. Pharmacokinet. Pharmacodyn.* **2022**, *49*, 257–270. [CrossRef] [PubMed]

Disclaimer/Publisher's Note: The statements, opinions and data contained in all publications are solely those of the individual author(s) and contributor(s) and not of MDPI and/or the editor(s). MDPI and/or the editor(s) disclaim responsibility for any injury to people or property resulting from any ideas, methods, instructions or products referred to in the content.

pharmaceutics

MDPI

Article

Patient Median-Based Quality Control in Lamotrigine Therapeutic Drug Monitoring: A 15-Year Retrospective Study

Anders Larsson [1,*], Mats B. Eriksson [2,3], Linda Steinholtz [1] and Anna-Karin Hamberg [1]

[1] Department of Medical Sciences, Clinical Chemistry and Pharmacology, Uppsala University, SE-751 85 Uppsala, Sweden; linda.steinholtz@akademiska.se (L.S.); anna-karin.hamberg@akademiska.se (A.-K.H.)
[2] Department of Surgical Sciences, Uppsala University, Uppsala University Hospital, SE-751 85 Uppsala, Sweden; mats.b.eriksson@uu.se
[3] NOVA Medical School, New University of Lisbon, 1099-085 Lisbon, Portugal
* Correspondence: anders.larsson@akademiska.se; Tel.: +46-18-6114271

Abstract

Background/Objectives: Lamotrigine is an anticonvulsant and mood stabilizer with wide interindividual pharmacokinetic variability, necessitating therapeutic drug monitoring (TDM). Patient-based quality control (PBQC) strategies, such as tracking median drug concentrations, may complement traditional quality assurance in routine laboratory practice. **Methods:** We retrospectively analyzed 15,963 lamotrigine results collected between February 2011 and December 2025 at Uppsala University Hospital, Uppsala. Data included age, sex, sampling date, and lamotrigine concentrations. Assays were performed using the Architect platform from February 2011 to January 2021, after which the Cobas Pro c 503 platform was implemented. Yearly patient medians were calculated, and trends, seasonal variation, and method agreement were assessed. **Results:** Of all the results, 5967 were from males and 9996 from females. Median concentrations were slightly higher in males (15.20 µmol/L) than in females (13.71 µmol/L), representing a weak but statistically significant difference (Spearman R = −0.048; $p < 0.0001$). The total number of reported results increased steadily over time, from 402 in 2011 to more than 1500 annually by 2024–2025. Median lamotrigine concentrations increased from 11.85 µmol/L in 2011 to 17.40 µmol/L in 2025 (Spearman R = 0.047; $p < 0.0001$). Seasonal variation in sample volume was observed, with peaks in November and troughs in July and December, but median concentrations remained stable (CV = 3.49%). Method comparison showed strong agreement between Architect and Cobas assays ($R^2 = 0.97$). **Conclusions:** Patient median lamotrigine concentrations serve as a robust PBQC tool, capable of detecting subtle analytical shifts while remaining resilient to seasonal fluctuations and platform transitions. This approach enhances confidence in assay reliability and supports safer therapeutic decision-making in real-world TDM practice.

Keywords: lamotrigine; patient median; therapeutic drug monitoring; immunosuppressive; transplantation; patient-based quality control (PBQC); pharmacokinetics; clinical laboratory quality assurance

1. Introduction

Lamotrigine is a widely used anticonvulsant and mood stabilizer, primarily prescribed for epilepsy and the long-term management of bipolar disorder [1,2]. Its strength lies in preventing depressive relapse, and its generally favorable tolerability profile makes it an

attractive therapeutic option. Nonetheless, careful dose titration is essential to minimize the risk of severe rash, a rare but serious adverse effect [3,4].

Therapeutic drug monitoring (TDM) plays a central role in optimizing lamotrigine therapy [5–7]. Target plasma concentrations typically range between 5 and 60 μmol/L, balancing efficacy in seizure control with the avoidance of toxicity. The substantial interindividual variability in lamotrigine pharmacokinetics—driven by factors such as hepatic function, age, pregnancy, and concomitant enzyme-inducing or -inhibiting medications—necessitates TDM and individualized dose adjustments [8–10]). Recent pharmacokinetic modeling and simulation studies highlight how patient-specific characteristics can markedly influence exposure, underscoring the need for robust and adaptable measurement strategies in clinical laboratories. Retrospective real-world TDM data further illustrate the complexity of dose–concentration relationships, particularly in heterogeneous epilepsy populations undergoing polytherapy, reinforcing the importance of reliable longitudinal assay performance [11].

Traditional quality assurance in TDM relies on internal quality control and external proficiency testing. While indispensable, these approaches may not fully capture subtle, practice-level shifts that accumulate over time. Patient-based quality control (PBQC) strategies—especially those leveraging aggregated patient statistics—offer a complementary framework for continuous surveillance [12,13]. For lamotrigine, PBQC is particularly advantageous because specimens are often collected in stable clinical rhythms and across well-defined care pathways. This consistency can be harnessed to detect analytical drift in near real time, without additional costs or workflow disruption.

Tracking patient median concentrations over defined intervals represents a pragmatic PBQC approach [14,15]. Medians are inherently robust to outliers and skewed distributions, making them well suited to identify small biases or shifts that might elude conventional controls. In lamotrigine TDM, monitoring patient medians across time windows and stratified cohorts (e.g., monotherapy vs. polytherapy, plasma vs. saliva) can provide early warning signals of drift, bias, or imprecision. Such surveillance strengthens confidence in clinical interpretation and supports safer, more effective dose adjustments.

The theoretical concepts introduced—lamotrigine pharmacokinetics, the role of TDM, and the principles of patient-based quality control—are directly tied to the rationale for the study and to the interpretation of the results. Traditional quality assurance strategies, while essential, may not adequately detect gradual or practice-level drifts that can accumulate in high-throughput TDM settings.

Patient-based quality control (PBQC) provides a theoretical framework for addressing this gap. Because lamotrigine samples are often collected within relatively consistent clinical pathways, aggregated patient data—particularly median concentrations—can serve as a stable, real-world indicator of analytical performance. Medians are robust to skewed distributions and outliers, making them suitable for the early detection of systematic bias, instrument drift, or calibration errors. Thus, the theoretical premise directly informs the methodological approach of the present study: by analyzing patient median lamotrigine concentrations over time, we assess whether this PBQC strategy can enhance routine assay surveillance and complement existing quality control procedures.

In this study, we evaluate the use of patient median values as a tool for monitoring the analytical performance of lamotrigine assays in routine TDM practice.

2. Materials and Methods

2.1. Samples

Blood samples submitted for routine lamotrigine monitoring at the Departments of Clinical Chemistry and Pharmacology, Uppsala University Hospital, were collected in

https://doi.org/10.3390/pharmaceutics18020236

serum tubes (BD Vacutainer Systems, Plymouth, UK). The study period spanned from February 2011 through 1 December 2025, comprising 15,963 samples. Data extraction was performed in accordance with ethical approval, ensuring patient anonymity. Only sampling date, age (in years), sex, and lamotrigine concentrations were retained. Ethical clearance was granted by the Uppsala University Ethics Committee (Dnr 01-367).

2.2. Instruments

In February 2011 the Lamotrigine method was transferred to the Architect platform (Abbott Laboratories, Abbott Park, IL, USA), Uppsala, using QMS® Lamotrigine reagent no. 0373795 (Microgenics, Fremont, CA, USA) together with calibrator no. 0373787 and control no. 0374090 (Microgenics). The overall coefficient of variation (CV) was 3.6% at 7.4 µmol/L and 6.0% at 54.4 µmol/L.

In January 2021, the assay was transferred to the Cobas Pro c 503 platform (Roche Diagnostics, Rotkreuz, Switzerland), employing ARK Lamotrigine reagent no. 5023-0001-00 (ARK Diagnostics, Fremont, CA, USA) along with ARK calibrators and controls. External quality controls were provided monthly by LGC Standards (Wesel, Germany). The CV was 5.3% at 7.3 µmol/L and 4.7% at 45 µmol/L. The therapeutic reference range was 5–60 µmol/L.

2.3. Statistical Calculations

Yearly median lamotrigine values were calculated. Statistical evaluations were conducted using Excel 365 (Microsoft Corp., Seattle, WA, USA) and Statistica 10 (Tibco Software, Palo Alto, CA, USA). A non-parametric comparison of lamotrigine concentrations between males and females was performed using the Mann–Whitney U test. The null hypothesis (H_0) stated that the distributions did not differ by sex.

3. Results

3.1. Number of Lamotrigine Results and Sex Distribution

Between 2011 and 2025 a total of 15,963 lamotrigine results were reported. Of these, 6164 were from males and 10331 from females ($\chi^2 = 534.8559$; $p < 0.0001$) (Figure 1).

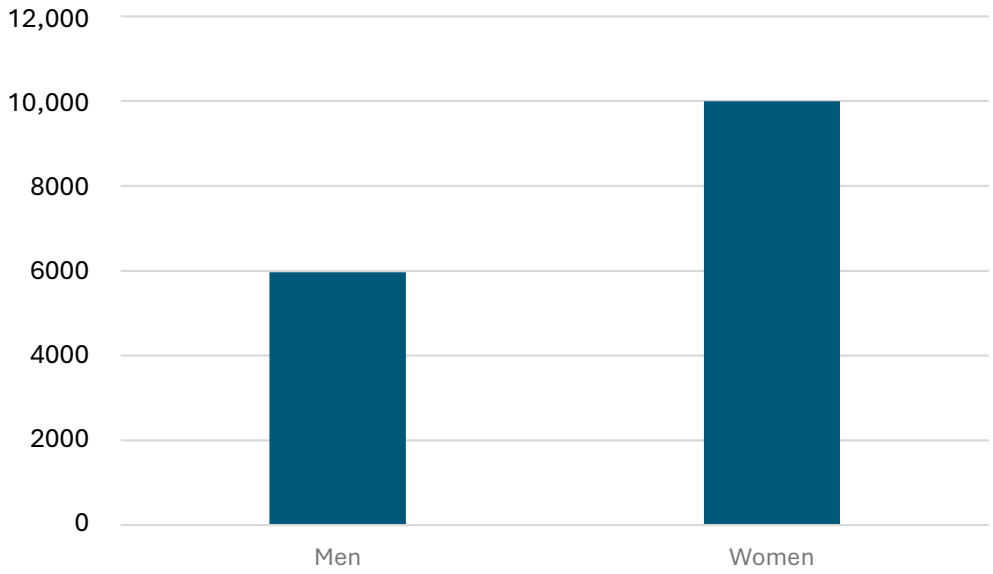


Figure 1. Number of lamotrigine analyses stratified by sex.

The median lamotrigine concentration was 13.71 µmol/L in females and 15.20 µmol/L in males (Table 1). This difference was highly significant according to the Mann–Whitney

U test (Z = 6.162; *p*-value 7.2×10^{-11}). The number of lamotrigine results below 10 µg/L was 5818 and 8450 results were below 15 µg/L, thus below the therapeutic interval. On the other hand 5385 results were above 20 µg/L and 3863 results were above 25 µg/L.

Table 1. Descriptive statistics (mean, median, selected percentiles) of the study variable for the total sample, males, and females.

	Valid N	Mean	Median	0.25	0.75	0.10	0.90
All	15,963	18.23	14.06	7.86	24.50	4.49	37.50
Males	5967	19.04	15.20	8.11	25.90	4.51	39.31
Females	9996	17.75	13.71	7.70	23.70	4.48	36.11

The simulated medians closely matched the reported values, supporting the use of the fitted distributions for this purpose. Under the assumptions of the log normal approximation, these results suggest that the underlying distributions differ between sexes, with males having higher values than females.

3.2. Changes in the Number of Reported Lamotrigine Results over Time

The number of reported results increased from 402 in 2011 to 1543 in 2024 (Figure 2). During the first eleven months of 2025 the number of reported results were 1510, indicating that the total for 2025 will exceed the value for 2024.

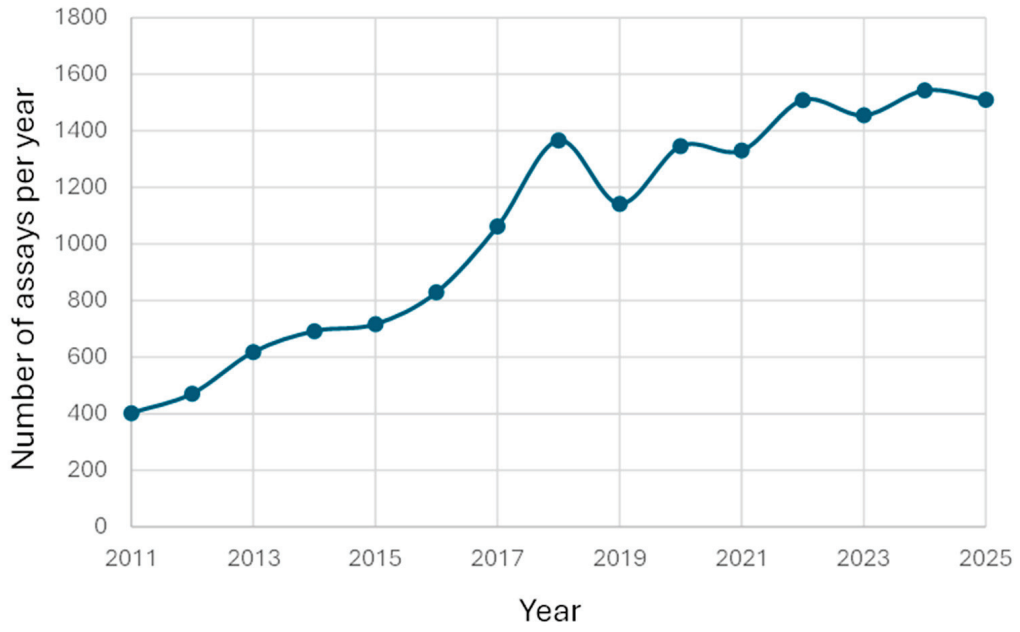


Figure 2. Number of lamotrigine results/year. The data is presented for the time period 1 February 2011–1 December 2025.

3.3. Changes in Median Lamotrigine Concentrations over Time

The median lamotrigine concentrations increased over time from 11.85 µmol/L in 2011 to 17.40 µmol/L in 2025 (Figure 3). This trend represented a weak but highly significant change according to Spearman's rank test (R = 0.047; $p < 1 \times 10^{-9}$).

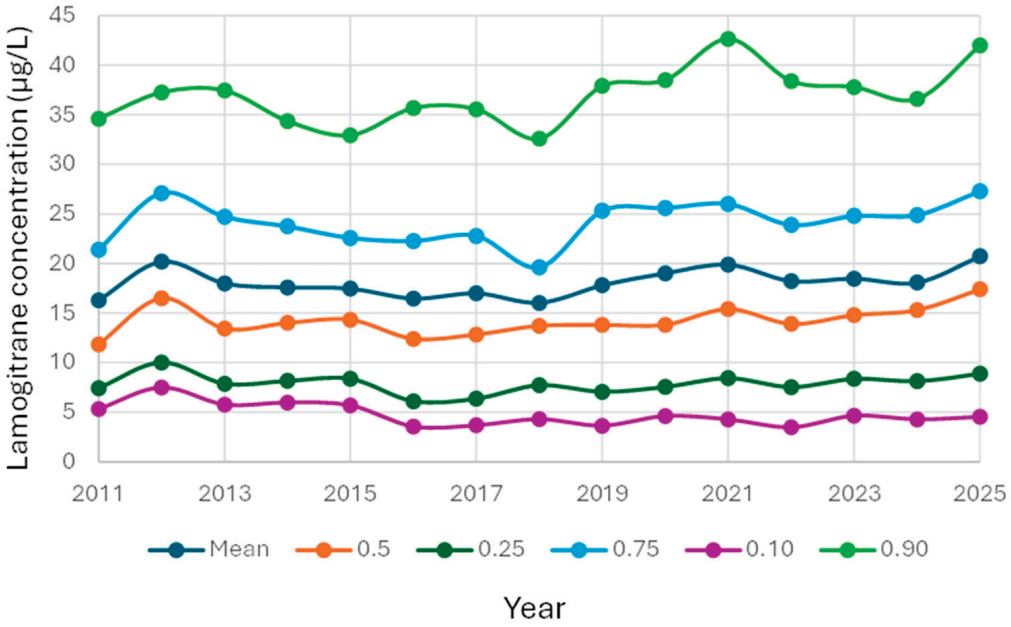


Figure 3. Lamotrigine results over time. The data is presented as 10th percentile, lower quartile, mean, median, upper quartile and 90th percentile per year for the time period 1 February 2011–1 December 2025.

3.4. Seasonal Variation in Lamotrigine Results

The number of reported lamotrigine results was highest in November and lowest in July and December (Figure 4). July is the main vacation month in Sweden and December is also a holiday month. Despite these variations in the number of reported test results across months, the median lamotrigine concentrations remained stable, with a coefficient of variation for the monthly medians of 3.49% (Figure 5).

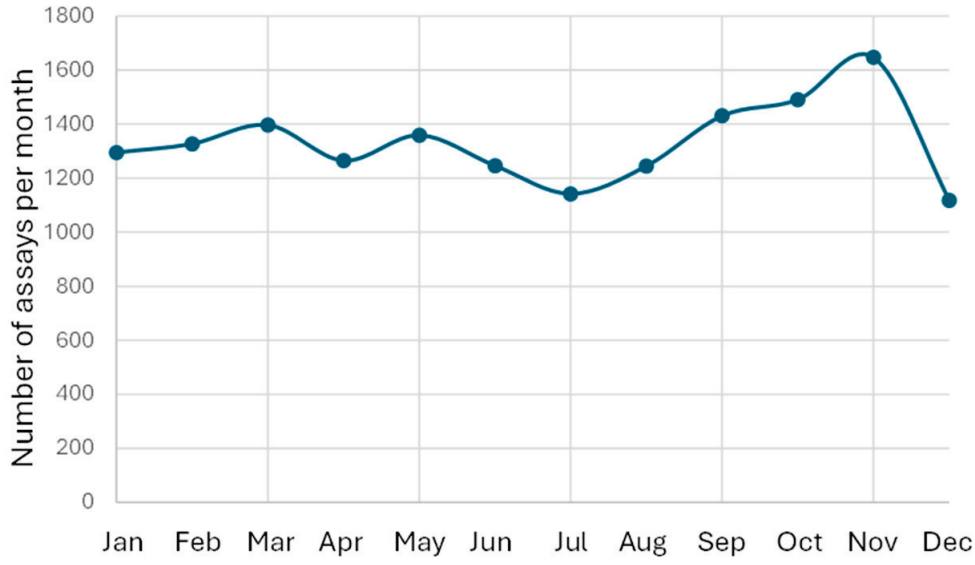


Figure 4. Number of lamotrigine results/month. The data is presented for the time period 2011–1 December 2025.

3.5. Method Comparison Between the Architect and Cobas Lamotrigine Methods

The comparison between the Architect and Cobas lamotrigine methods during the validation process of the Cobas method showed good agreement for patient samples ($y = 0.97x + 0.413$; $R^2 = 0.97$) (Figure 6).

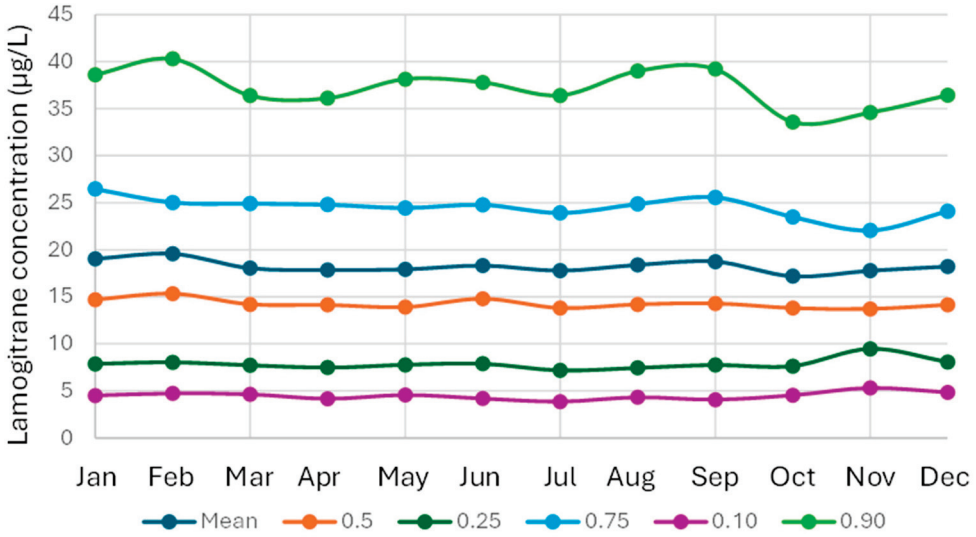


Figure 5. Lamotrigine results per month. The data is presented as 10th percentile, lower quartile, mean, median, upper quartile, and 90th percentile per year for the time period 1 February 2011–1 December 2025.

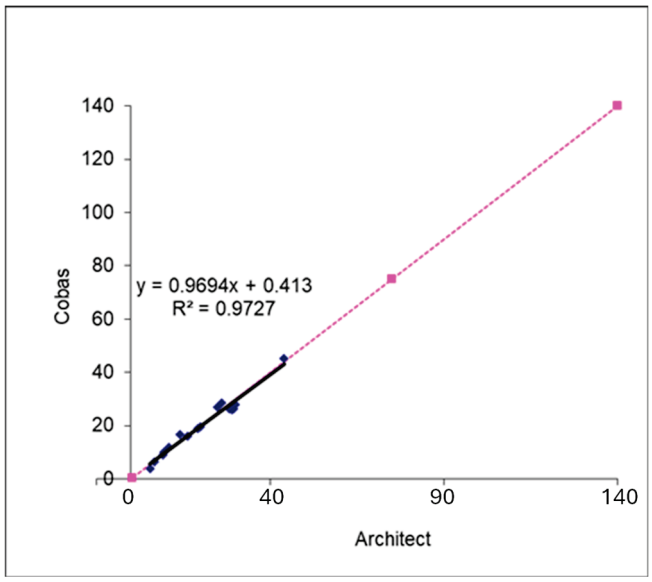


Figure 6. Comparison between the Architect and Cobas lamotrigine methods using patient samples. The blue dots represent individual patient sample results measured on the two analytical platforms. The purple dashed line with squares represents the line of identity (45-degree line), illustrating where results would fall if the two methods produced identical values. The black regression line shows the observed relationship, with the displayed equation and R^2 value indicating the strength of the correlation.

4. Discussion

This large-scale retrospective study demonstrates the value of using patient median values as a pragmatic PBQC strategy for lamotrigine monitoring. Over a 14-year period, we observed consistent trends in assay performance, with increasing median concentrations and rising test volumes reflecting both clinical uptake and evolving therapeutic practice. The weak but statistically significant sex-related differences in median concentrations are consistent with known pharmacokinetic variability, although the magnitude of these differences is unlikely to justify sex-specific reference ranges.

Importantly, seasonal fluctuations in sample volume did not lead to instability in median values, underscoring the robustness of patient medians as a quality control metric. This stability highlights their suitability for continuous monitoring, even in healthcare systems that experience predictable variations in patient flow due to holidays or staffing cycles.

The transition from the Architect to the Cobas platform in 2021 provided a natural opportunity to assess PBQC applicability. The strong agreement between methods ($R^2 = 0.97$) confirms analytical continuity, and patient medians served as an independent safeguard against unnoticed drift during implementation. This real-world validation illustrates how PBQC can complement conventional internal and external quality controls, which may miss subtle practice-level shifts.

The gradual increase in median lamotrigine concentrations over time may reflect evolving prescribing patterns, wider adoption of TDM, or shifts in patient demographics. Although the statistical correlation was weak, its significance suggests that longitudinal monitoring of medians can reveal subtle population-level trends that merit further clinical investigation.

Together, these findings support the integration of patient median tracking into routine lamotrigine TDM workflows. By leveraging data already generated during clinical care, laboratories can enhance quality surveillance without additional cost or workload. This approach not only strengthens analytical reliability but also increases confidence in therapeutic decision-making, ultimately promoting patient safety.

Median plasma lamotrigine concentrations were slightly more than 10% higher in males than in females. This difference should be interpreted cautiously, because the analysis is based on approximate distributions derived from summary statistics rather than individual-level data. Nonetheless, the very small *p*-value from the simulated Mann–Whitney U test indicates that the null hypothesis of identical distributions between males and females can be rejected.

Lamotrigine is metabolized primarily in the liver through UDP-glucuronosyltransferase-mediated glucuronidation, predominantly via UGT1A4, while cytochrome P450 enzymes play only a minimal and clinically negligible role in its metabolism [16,17].

Lamotrigine pharmacokinetics exhibit clinically relevant interindividual variability driven by sex, age, pregnancy, and concomitant antiepileptic and hormonal therapy, underscoring the need for therapeutic drug monitoring (TDM). This aligns with the high number of lamotrigine analyses in our study. Sex-related differences, age, and exposure to exogenous estrogens (combined oral contraceptives and hormone-replacement therapy) substantially influence lamotrigine clearance and plasma concentrations, with important implications for monitoring.

Combined oral contraceptives and other estrogen-containing preparations increase lamotrigine glucuronidation and reduce steady-state concentrations, depending on the hormonal regimen [18]. Pregnancy and rising estradiol levels markedly increase lamotrigine clearance, often necessitating dose escalation and close TDM to avoid seizure breakthrough [19]. Hormone-replacement therapy may produce similar reductions in lamotrigine concentrations in postmenopausal women [20]. While routine, universally applied TDM for lamotrigine is debated [21], targeted monitoring is supported when factors known to alter clearance are present, or when clinical response changes [20]. Evidence supports a pragmatic, individualized TDM approach for lamotrigine—prioritizing patients on polytherapy, women initiating or changing estrogenic therapies, pregnant patients, and those with age-related pharmacokinetic changes—to optimize efficacy and safety [6].

In routine PBQC implementation, defining a pragmatic threshold for when a change in the patient median should trigger investigation is essential. Several laboratories using PBQC frameworks have found that shifts of approximately 5–10% in the patient

median—persisting over several days or multiple analytical batches—generally indicate meaningful analytical or preanalytical issues rather than random variation. For lamotrigine specifically, the monthly coefficient of variation around the median in this study was approximately 3%, demonstrating that the natural biological and workflow-related noise is low. Against this background, a sustained deviation exceeding $\pm 10\%$ from the expected median would therefore be unlikely to arise from random fluctuations and should prompt a review of calibrations, reagent lots, instrument performance, and sample handling workflows.

Smaller deviations (e.g., 5–7%) may still merit attention if they show a consistent directional trend, especially around the time of instrument maintenance, reagent lot changes, or clinical workflow disruptions. Conversely, isolated one day fluctuations are typically attributable to random patient mix effects and should be interpreted with caution.

The performance of PBQC for lamotrigine in this study compares favorably with its application to other routinely monitored therapeutic drugs, particularly immunosuppressants. Lamotrigine displays several features that enhance PBQC performance. First, its intraindividual variability is generally lower under stable dosing conditions, particularly in patients without interacting medications. Second, lamotrigine is typically prescribed for chronic conditions—epilepsy and bipolar disorder—where dose adjustments are less frequent compared with immunosuppressants, leading to more stable population distributions. Third, test volumes for lamotrigine were high and consistent across many years in this study, producing robust medians with low natural variation (monthly CV $\approx 3\%$). The combination of stable pharmacokinetics, large sample numbers, and relatively predictable patient mix results in exceptionally smooth long-term median curves. This stability facilitates early detection of analytical drift because even small systematic deviations become apparent against the otherwise steady background signal.

There are limitations when interpreting the findings of this study. First, the retrospective design inherently restricts control over patient level variables such as diagnosis, dosing regimens, comorbidities, adherence, and concomitant medications, all of which may influence lamotrigine concentrations. The dataset therefore reflects routine clinical practice rather than a controlled population, which limits its ability to attribute observed trends to specific clinical factors. Second, demographic information was limited to age and sex; other pharmacokinetically relevant factors—including pregnancy status, use of estrogen-containing therapies, renal or hepatic impairment, and enzyme-inducing or -inhibiting co-medications—were not available. This constrains interpretation of observed sex differences and broader temporal changes. Third, a platform transition occurred during the 14 year study period. Although method comparisons and external quality assessment demonstrated good agreement, subtle differences in calibration or matrix effects between assays may have contributed to long-term trends in patient medians. Fourth, the analysis relied on aggregated summary statistics rather than repeated measurements from the same individuals. This prevented assessment of intraindividual variability or longitudinal changes within specific patient trajectories.

This study demonstrates that patient median lamotrigine concentrations provide a robust and informative patient-based quality control metric in routine therapeutic drug monitoring. Across 14 years of data, patient medians remained stable despite substantial seasonal fluctuations in sample volume and two major analytical platform transitions. Sex-specific differences and long-term increases in median concentrations were small but detectable, illustrating the sensitivity of PBQC to subtle population level trends while retaining resilience to short term variability.

Strong analytical agreement between the Architect and Cobas platforms confirmed measurement continuity, and the close alignment of patient medians across methods further supports their use as an independent, real-world safeguard against unnoticed drift. Because

medians are simple to compute, resistant to outliers, and derived from routinely generated clinical data, their implementation requires minimal additional resources.

Together, these findings support incorporating patient median monitoring into standard lamotrigine TDM workflows as a complementary tool to traditional quality control systems. By strengthening confidence in assay stability and long-term performance, PBQC has the potential to improve the reliability of therapeutic decision-making and contribute meaningfully to patient safety in everyday clinical practice.

Author Contributions: A.L.: Writing—review and editing, Writing—original draft, Visualization, Validation, Resources, Project administration, Methodology, Investigation, Formal analysis, Data curation, Conceptualization. M.B.E.: Writing—review and editing. L.S.: Review and editing. A.-K.H.: Writing—review and editing, Supervision, Methodology. All authors have read and agreed to the published version of the manuscript.

Funding: The Uppsala University Hospital Research Fund supported this study.

Institutional Review Board Statement: The local ethical committee at Uppsala University approved the collection of samples (01-367). The ethical permit limited the patient information to age in years and sex.

Informed Consent Statement: Patient consent was waived because the data were extracted without patient identifiers, making it impossible to obtain informed consent from the study subjects. All testing was conducted as part of routine patient care, and no additional sampling was performed specifically for this study.

Data Availability Statement: The dataset used and analyzed during the current study is available from the corresponding author on request.

Conflicts of Interest: The authors declare no conflicts of interest.

References

1. Besag, F.M.C.; Vasey, M.J.; Sharma, A.N.; Lam, I.C.H. Efficacy and safety of lamotrigine in the treatment of bipolar disorder across the lifespan: A systematic review. *Ther. Adv. Psychopharmacol.* **2021**, *11*, 20451253211045870. [CrossRef] [PubMed]
2. Prabhavalkar, K.S.; Poovanpallil, N.B.; Bhatt, L.K. Management of bipolar depression with lamotrigine: An antiepileptic mood stabilizer. *Front. Pharmacol.* **2015**, *6*, 242. [CrossRef]
3. Zhang, L.; Yang, P.; Zhu, Y.; Liu, K.; Sun, Z. Toxic epidermal necrolysis following lamotrigine replacement therapy in a woman planning pregnancy: A case report and literature review. *BMC Women's Health* **2025**, *25*, 371. [CrossRef]
4. De Bellis, M.; d'Orsi, G.; Rubino, E.M.; Arigliano, C.; Carella, M.; Sciruicchio, V.; Liantonio, A.; De Luca, A.; Imbrici, P. Adverse effects of antiseizure medications: A review of the impact of pharmacogenetics and drugs interactions in clinical practice. *Front. Pharmacol.* **2025**, *16*, 1584566. [CrossRef]
5. Rambeck, B.; Wolf, P. Lamotrigine clinical pharmacokinetics. *Clin. Pharmacokinet.* **1993**, *25*, 433–443. [CrossRef]
6. Goo, Y.; der Nederlanden, A.M.; Bleasel, A.; Alffenaar, J.W.; Kim, H.Y. Dose Monitoring of Lamotrigine Monotherapy in Pregnancy: Are Pregnant Women with Epilepsy Currently Optimally Managed? A Systematic Review. *Ther. Drug Monit.* **2024**, *46*, 181–194. [CrossRef] [PubMed]
7. Li, J.C.; Miao, C.F.; Lei, Y.; Liu, A.L. Physiologically Based Pharmacokinetic Modeling to Predict Lamotrigine Exposure in Special Populations to Facilitate Therapeutic Drug Monitoring and Guide Dosing Regimens. *Pharmaceuticals* **2025**, *18*, 637. [CrossRef] [PubMed]
8. Reimers, A.; Skogvoll, E.; Sund, J.K.; Spigset, O. Lamotrigine in children and adolescents: The impact of age on its serum concentrations and on the extent of drug interactions. *Eur. J. Clin. Pharmacol.* **2007**, *63*, 687–692. [CrossRef]
9. Böttiger, Y.; Svensson, J.O.; Ståhle, L. Lamotrigine drug interactions in a TDM material. *Ther. Drug Monit.* **1999**, *21*, 171–174. [CrossRef]
10. Yamamoto, Y.; Usui, N.; Kagawa, Y.; Imai, K. Time-Course Changes in Lamotrigine Concentration after Addition of Valproate and the Safety and Long-Term Tolerability of Lamotrigine-Valproate Combination Therapy. *Biol. Pharm. Bull.* **2024**, *47*, 43–48. [CrossRef]
11. Lee, Z.N.; van Nuland, M.; Bognàr, T.; Leijten, F.S.S.; van der Elst, K.C.M. Association of Lamotrigine Plasma Concentrations with Efficacy and Toxicity in Patients with Epilepsy: A Retrospective Study. *Ther. Drug Monit.* **2024**, *46*, 642–648. [CrossRef]

12. van Rossum, H.H. Technical quality assurance and quality control for medical laboratories: A review and proposal of a new concept to obtain integrated and validated QA/QC plans. *Crit. Rev. Clin. Lab. Sci.* **2022**, *59*, 586–600. [CrossRef]
13. Loh, T.P.; Cervinski, M.A.; Katayev, A.; Bietenbeck, A.; van Rossum, H.; Badrick, T. Recommendations for laboratory informatics specifications needed for the application of patient-based real time quality control. *Clin. Chim. Acta* **2019**, *495*, 625–629. [CrossRef]
14. Larsson, A.; Hamberg, A.K.; Cedernaes, J.; Hallberg, P.; Karlqvist, J.H.; Karlsson, M. New Monitoring Recommendations for Digoxin During the Last Decade Are Associated with Decreased Serum Digoxin Concentrations in Patient Samples. *Basic Clin. Pharmacol. Toxicol.* **2025**, *137*, e70083. [CrossRef]
15. Larsson, A.; Saldeen, J.; Duell, F. Recent decline in patient serum folate test levels using Roche Diagnostics Folate III assay. *Clin. Chem. Lab. Med.* **2025**, *63*, e275–e277. [CrossRef]
16. Elwes, R.D.; Binnie, C.D. Clinical pharmacokinetics of newer antiepileptic drugs. Lamotrigine, vigabatrin, gabapentin and oxcarbazepine. *Clin. Pharmacokinet.* **1996**, *30*, 403–415. [CrossRef]
17. Gardner, I.; Heikkinen, A.T.; Tang, L.W.T.; Lapham, K.; Goosen, T.C. Development of a PBPK Model for Lamotrigine which Incorporates Metabolism by UGT2B10: Impact of UGT2B10 Poor Metabolizer Phenotype and Pregnancy. *AAPS J.* **2025**, *27*, 40. [CrossRef]
18. Sabers, A.; Ohman, I.; Christensen, J.; Tomson, T. Oral contraceptives reduce lamotrigine plasma levels. *Neurology* **2003**, *61*, 570–571. [CrossRef]
19. Christensen, J.; Petrenaite, V.; Atterman, J.; Sidenius, P.; Ohman, I.; Tomson, T.; Sabers, A. Oral contraceptives induce lamotrigine metabolism: Evidence from a double-blind, placebo-controlled trial. *Epilepsia* **2007**, *48*, 484–489. [CrossRef]
20. Reimers, A. Hormone replacement therapy with estrogens may reduce lamotrigine serum concentrations: A matched case-control study. *Epilepsia* **2017**, *58*, e6–e9. [CrossRef]
21. Chong, E.; Dupuis, L.L. Therapeutic drug monitoring of lamotrigine. *Ann. Pharmacother.* **2002**, *36*, 917–920. [CrossRef] [PubMed]

Disclaimer/Publisher's Note: The statements, opinions and data contained in all publications are solely those of the individual author(s) and contributor(s) and not of MDPI and/or the editor(s). MDPI and/or the editor(s) disclaim responsibility for any injury to people or property resulting from any ideas, methods, instructions or products referred to in the content.

pharmaceutics

MDPI

Article

Measurement of Anti-TNF Biologics in Serum Samples of Pediatric Patients: Comparison of Enzyme-Linked Immunosorbent Assay (ELISA) with a Rapid and Automated Fluorescence-Based Lateral Flow Immunoassay

Chiara Rossi [1], Raffaele Simeoli [1,*], Giulia Angelino [2], Sara Cairoli [1], Fiammetta Bracci [3], Daniela Knafelz [3], Erminia Francesca Romeo [2], Simona Faraci [3], Giusyda Tarantino [4], Alessandro Mancini [1], Alessia Vitale [1], Carlo Dionisi Vici [1], Silvia Magni Manzoni [4], Paola De Angelis [2] and Bianca Maria Goffredo [1,*]

[1] Division of Metabolic Diseases and Hepatology, Bambino Gesù Children's Hospital, IRCCS, 00165 Rome, Italy; chiara.rossi@opbg.net (C.R.); sara.cairoli@opbg.net (S.C.); alessandro.mancini@opbg.net (A.M.); alessia.vitale@opbg.net (A.V.); carlo.dionisivici@opbg.net (C.D.V.)
[2] Digestive Endoscopy and Surgery Unit, Bambino Gesù Children's Hospital, IRCCS, 00165 Rome, Italy; giulia.angelino@opbg.net (G.A.); efrancesca.romeo@opbg.net (E.F.R.); paola.deangelis@opbg.net (P.D.A.)
[3] Hepatology and Gastroenterology Unit, Bambino Gesù Children's Hospital, IRCCS, 00165 Rome, Italy; fiammetta.bracci@opbg.net (F.B.); daniela.knafelz@opbg.net (D.K.); simona.faraci@opbg.net (S.F.)
[4] Rheumatology Department, Bambino Gesù Children's Hospital, IRCCS, 00165 Rome, Italy; giusyda.tarantino@opbg.net (G.T.); silvia.magnimanzoni@opbg.net (S.M.M.)
* Correspondence: raffaele.simeoli@opbg.net (R.S.); biancamaria.goffredo@opbg.net (B.M.G.); Tel.: +39-0668592174 (B.M.G.); Fax: + 39-0668593009 (B.M.G.)

Abstract: Background: Therapeutic drug monitoring (TDM) of infliximab (IFX) and adalimumab (ADL) mainly relies on the use of enzyme-linked immunosorbent assays (ELISA). More recently, rapid assays have been developed and validated to reduce turnaround time (TAT). Here, we compared IFX and ADL concentrations measured with both ELISA and a new fluorescence-based lateral flow immunoassay (AFIAS). **Methods**: In serum samples from pediatric patients, IFX and ADL drug levels, and total anti-IFX antibodies were measured using clinically validated ELISA kits (Immundiagnostik AG). Samples were further analyzed using a new rapid assay (AFIAS, Boditech Med Inc.) to measure drug levels and total anti-IFX antibodies. **Results**: Spearman's correlation coefficients (rho) were 0.98 [95% confidence interval (CI) 0.97 to 0.99] for IFX ($p < 0.001$) and 0.83 (95% CI 0.72 to 0.90) for ADL ($p < 0.001$). Calculated % bias was −14.09 (95% Limits of agreement, LoA, −52.83 to 24.66) for IFX and 15.79 (LoA −37.14 to 68.73) for ADL. For the evaluation of total anti-IFX antibodies, we did not collect sufficient data to establish a statistically significant correlation between AFIAS and ELISA. The inter-rater agreement showed a "substantial" and a "moderate" agreement for IFX and ADL, respectively. **Conclusions**: Our results show that the AFIAS assay has an accuracy and analytical performance comparable to that of the ELISA method used for TDM of IFX and ADL. Therefore, the introduction of this device into routine clinical practice could provide results more quickly and with similar accuracy as ELISA, allowing clinicians to rapidly formulate clinical decisions.

Keywords: pediatric patients; therapeutic drug monitoring (TDM); anti-TNF biological agents; enzyme-linked immunosorbent assay (ELISA); fluorescence-based lateral flow immunoassay (AFIAS); turnaround time (TAT)

1. Introduction

Inflammatory bowel diseases (IBDs), including Crohn's disease (CD) and ulcerative colitis (UC), are extremely debilitating conditions that can significantly affect patients' quality of life. Inflammatory bowel diseases affect approximately 25% of pediatric patients, and often presents with a more serious disease course compared with adult IBDs [1].

However, owing to significant progress made in biotechnological sciences, medical treatment of IBD has been greatly improved by the introduction of biological agents capable of targeting pro-inflammatory cytokines, such as tumor necrosis factor (TNF)-α, interleukin (IL)-12/23, and $\alpha_4\beta_7$ integrin, which are involved in immune responses [2].

Monoclonal antibodies (mAb) directed against TNF-α (i.e., infliximab, IFX, and adalimumab, ADL) were the first biologics introduced more than a decade ago as therapeutic options for IBD and are still widely used for the treatment of moderate to severe forms of disease [3,4]. In particular, according to the ECCO-ESPGHAN Guideline Update for the Medical Management of Pediatric Crohn's Disease, in new-onset patients at high risk for a complicated disease course, anti-TNF therapy is recommended for inducing remission [5]. Similarly, anti-TNF agents are recommended for induction and maintenance of remission in patients with active CD who do not achieve or maintain remission [5].

Moreover, the introduction of these agents has significantly improved the quality of life of patients, thereby reducing the need for surgical approaches [6].

However, despite their beneficial therapeutic effects, following a primary response to anti-TNF therapy, patients treated with these agents may experience loss of response (LoR) and relapse of the disease [7]. The reasons for these therapeutic failures are not yet fully understood; however, inter-individual variability in drug pharmacokinetics (PK), pharmacodynamics (PD), and immunogenicity are considered possible risk factors [8]. The risk of developing anti-drug antibodies (ADAs) is a serious complication of biological therapies and is often associated with poor response to these treatments [9]. There are multiple mechanisms underlying the development of immunogenicity; however, the presence of specific pharmacogenetic variants and/or prolonged sub-therapeutic drug levels seems to be positively correlated [10–12]. It is also worthwhile to say that a successful therapy with anti-TNF biological agents relays not only on the immunogenicity development but also on the choice of an adequate dosing regimen during both the induction and maintenance of remission [13]. In fact, patients classified as non-responders often display sub-therapeutic drug levels, although typical infusion regimens are given [14]. In addition, considering that biological therapies can also present several side effects and are characterized by high costs, the optimization of tailored therapies should be a desirable endpoint during routine clinical practice.

In this regard, therapeutic drug monitoring (TDM) can be used not only to assess whether low drug levels (with or without the presence of ADAs) could be responsible for therapeutic failures (reactive TDM), but also to allow dose adjustments and ensure that drug levels are within a therapeutic window, thus avoiding risks of future disease relapses (proactive TDM) [15]. In fact, TDM of anti-TNF drug levels and anti-drug antibodies allows for the identification of patients who have lost response to the biological agent but also to potentially define a tailored therapeutic strategy [16]. Specifically, TDM assesses the adequacy of drug plasma concentrations in relation to a target concentration or concentration window at a specific time within a dosing interval [17]. Previously, it has been reported that both primary non-response and secondary LOR in anti-TNF-treated patients commonly result from low trough concentration, high ADA levels, or both [18–20]. Based on this evidence, the ECCO-ESPGHAN Guideline 2020 states that early proactive therapeutic drug monitoring followed by dose optimization is recommended [5].

Proactive TDM is defined as the evaluation of trough concentrations and ADA levels, with the aim of optimizing biological therapy to achieve an effective threshold drug concentration [15]. Moreover, recent data have reported that proactive TDM is associated with better therapeutic outcomes than empirical dose optimization and/or reactive TDM of anti-TNF agents in IBD [21,22]. To date, several TDM-based algorithms have been proposed in real-life clinical practice to guide the tailored optimization of anti-TNF therapies [15,23]. Similarly, clinical outcome predictions in pediatric IBD patients have been suggested by measuring infliximab trough levels at different sampling points during the induction and maintenance phase [15,18].

In fact, proactive TDM allows the maintenance of relatively constant drug levels, creating a personalized and effective therapy and identifying patients suffering from inadequate exposure. Monitoring the serum concentration of the administered drug and the concentration of anti-drug antibodies (ADA) is a fundamental aspect that must be monitored during all phases of therapy, starting from the induction and maintenance phases to complete remission. Only in this way will it be possible to guarantee adequate exposure and reduce the risk of loss of response.

Therefore, based on the evidence that measuring anti-TNF agents and ADA levels improves patient outcomes and could potentially be more cost-effective, several bioanalytical assays have been developed to test both drug and ADA concentrations in serum and plasma samples [16]. These include drug-sensitive solid-phase immunoassays, radioimmunoassay (RIA), homogeneous mobility shift assays (HMSA), and cell reporter gene assays (RGA) [18]. Recently, faster assays, such as fiber-optic surface plasmon resonance (FO-SPR) and lateral flow (LF) tests, have been introduced in the market [22]. Enzyme-linked immunosorbent assay (ELISA) is the most commonly used immunoassay to detect both drug and ADA levels in different biological matrices [24]. Despite its wide adoption across bioanalytical laboratories to measure different analytes, ELISA presents several disadvantages, including time-consuming incubation and washing steps and the need to obtain a certain number of samples before proceeding with evaluation (test in batches). Because ELISA assays require the construction of a calibration curve each time, filling a whole plate by accumulating the desired number of samples could be a valid strategy to reduce costs. Taken together, these aspects can significantly increase the turnaround time (TAT) required to obtain the TDM results. Therefore, in the last decade, there has been growing attention on point-of-care (POC) assays that allow the measurement of drug and anti-drug levels at patient's bedside or in an outpatient clinic in a shorter time (15–20 min) compared to ELISA (3–5 h) [25]. In a study conducted by Curci D and colleagues (2019), two different POC devices based on lateral flow assays were validated to measure serum infliximab levels by comparing their results with those obtained using a reference ELISA kit [26]. More recently, a similar approach was adopted to evaluate the analytical and clinical performance of a new fluorescence-based lateral flow immunoassay (AFIAS) by measuring and comparing infliximab and adalimumab drug levels with those obtained through commercially available ELISA kits [14,27,28]. This rapid assay (20 min) allows the quantitative measurement of IFX, ADL, and anti-drug antibodies on a cartridge ready for direct use on a fully automated instrument (AFIAS). Moreover, the samples did not require repeated dilution, mixing, or separation steps [14,27,28].

So far, previous studies have already compared infliximab drug levels measured with both AFIAS and the gold-standard ELISA in samples from pediatric and adult patients [14,27,28]. However, to the best of our knowledge, this is the first study in which, alongside with AFIAS IFX, the analytical performance of AFIAS ADL has also been evaluated in serum samples collected from pediatric patients during the routine clinical practice. To this aim, here we have used the AFIAS system to quantify IFX and ADL levels in serum

samples from pediatric patients treated with these biological agents. Anti-IFX antibody levels were also measured in the same samples. AFIAS results were then compared with those obtained by using a commercially available ELISA kit considered as a reference assay in our routine clinical practice.

2. Materials and Methods

2.1. Patients' Samples

Samples were obtained from 98 hospitalized pediatric and/or outpatient patients who received biological therapy with infliximab (IFX) or adalimumab (ADL). In particular, n = 44 serum samples were collected for therapeutic drug monitoring (TDM) of IFX and anti-IFX levels, and n = 54 samples were obtained to monitor ADL serum levels. The mean ± SD age of the pediatric patients was 15 ± 9.55 for the IFX group and 15 ± 4.45 ADL. Blood samples were collected immediately before the next dose was administered; therefore, the trough levels (C_{trough}) were monitored for both infliximab and adalimumab. Following centrifugation at 3.500× *g* for 10 min, serum samples were collected, and one aliquot (approximately 300 µL) was used for AFIAS tests, while another aliquot was stored at −80 °C until ELISA assays were conducted. Both tests were performed at the Laboratory of Metabolic Diseases and Hepatology of Bambino Gesù Children's Hospital, IRCCS, in Rome (Italy).

TDM of Infliximab and Adalimumab is well established in the routine clinical practice at Bambino Gesù Children's Hospital. This study was conducted in full observation of the Helsinki Declaration and the protocol was approved by the Ethics Committee of Bambino Gesù Children's Hospital (2333_OPBG_2020) on 4 January 2021.

2.2. Enzyme-Linked Immunoassorbent Assays (ELISA)

Infliximab or Adalimumab levels were determined using commercially available and validated ELISA kits (IDKmonitor®, Immunodiagnostik AG, Bensheim, Germany) according to the manufacturer's instructions. These ELISA assays are designed to quantitatively measure free infliximab or adalimumab levels in serum and EDTA plasma samples, and involve several steps. Briefly, during the first incubation, the free drug contained in the unknown samples was bound to specific anti-drug antibodies coated on a 96-well plate. A washing step was performed to remove all the unbound substances. Finally, after another incubation step, in which a peroxidase-labeled secondary antibody was added to each well, the use of a peroxidase substrate (tetramethylbenzidine-TMB) determined the progress of the reaction, resulting in the formation of a blue-colored product. An acid-containing stop solution was added to terminate the reaction and allow color variation from blue to yellow. The intensity of the yellow color is directly proportional to the concentration of the free drug present in the sample. Using a spectrophotometer, the plate was read at 450 and 620 nm (reference wavelength), and optical densities (ODs) were used to construct a 4PL sigmoidal curve using the calibration standards provided by the kit. The drugs' concentrations in each sample were determined directly by fitting the optical density (OD) values to this curve. Finally, IFX or ADL levels were calculated, multiplying the obtained results by a dilution factor of 200. Results were expressed as µg/mL.

For each ELISA kit (Cat n. K9655 IDKmonitor® infliximab drug level and n. K9657 IDKmonitor® adalimumab drug level), Quality Controls at low (L-QC) and high (H-QC) drug concentrations with relative target ranges were provided by the manufacturer. For infliximab drug levels, target ranges were 7.5–19.5 ng/mL and 39.0–89.0 ng/mL for L-QC and H-QC, respectively. For adalimumab drug levels, target ranges were as follows: 0.9–10.9 ng/mL and 20.0–70.0 ng/mL for L-QC and H-QC, respectively. The validity of

the tests was evaluated by analyzing the QCs together with the unknown samples in each analytical batch.

Similarly, the determination of infliximab total ADA was performed on the same IFX serum samples using an ELISA kit (Cat n. K9654 IDKmonitor® Infliximab Total ADA) provided by Immunodiagnostik AG (Bensheim, Germany). This validated ELISA allows for the semi-quantitative detection of free and bound (total) anti-drug antibodies, even in the presence of infliximab. According to the manufacturer's instructions, serum samples were subjected to preliminary incubation that allowed the separation anti-drug antibodies (ADA) from the therapeutic antibody to detect free ADA. After this incubation step, by adding a conjugate (peroxidase-labeled therapeutic antibody) and tracer (biotinylated therapeutic antibody) to each sample, the unmarked therapeutic antibodies were replaced, and the marked antibodies formed a complex with ADA. This complex binds via biotin to streptavidin-coated microtiter plates via biotin. Thereafter, the complex was detected using a peroxidase conjugate that converted the TMB substrate into a blue product. Finally, the enzymatic reaction was stopped by adding an acid solution, which changed the color of the samples from blue to yellow. The color change was measured using a spectrophotometer at 450 and 620 nm (reference wavelengths). The results were interpreted using the cut-off control sample according to the manufacturer's instructions provided by Immunodiagnostik AG. (Bensheim, Germany). The validity of the tests was assessed by analyzing a Positive and a Negative Control sample provided by the kit, together with unknown samples in each analytical batch. The analytical specifications of the ELISA kits used in this study are listed in Supplementary Table S1.

2.3. Fluorescence-Based Lateral Flow Immunoassay

Infliximab and adalimumab levels were measured in the same serum samples alongside with ELISA by using commercially available kits on the AFIAS-6 instrument (Bodytech Med Inc., 43, Geodudanji 1-gil, Dongnae-myeon, Chuncheon-si, Gangwon-do, Republic of Korea). This fluorescence-based lateral flow immunoassay was developed and validated for the quantitative analysis of IFX (Cat. n. SMFP-75 AFIAS Infliximab) and ADL (SMFP-89 AFIAS Adalimumab) drug levels in whole blood, plasma, and serum samples (Bodytech Med Inc., Republic of Korea). Moreover, AFIAS allows the semi-quantitative analysis of total antibodies against infliximab in both plasma and serum (Cat. n. SMFP-76 AFIAS Total Anti-Infliximab, Bodytech Med Inc., Republic of Korea). AFIAS IFX and ADL were prepared as all-in-one cartridges for direct use and applied to a fully automated instrument, AFIAS (Bodytech Med Inc., Republic of Korea).

For cartridge preparation, three components were used with the kit: a Sample Dilution Buffer, conjugated antibodies, and a nitrocellulose strip.

IFX and ADL levels were measured according to the manufacturer's instructions. Briefly, the assay procedure involved loading the sample (100 μL) into the sample into a specific well on the cartridge. Thereafter, the cartridge was inserted into the cartridge holder in the AFIAS instrument, where the samples were automatically diluted and mixed with the AFIAS reagent. The fluorescence and biotin-labeled anti-infliximab in the buffer bound to infliximab or adalimumab was present in each sample, forming drug–antibody complexes, and migrating onto the nitrocellulose matrix to be captured by the other immobilized streptavidin on a test strip. More drugs are present in the samples, and more drug–antibody complexes will form, leading to a stronger fluorescence signal. Finally, the test results were automatically calculated from a previously loaded calibration ID chip (lot specific) and displayed on the screen within 10 min.

Quality Controls for low (L-QC) and high (H-QC) drug concentrations with relative target ranges were provided by the manufacturer. For infliximab drug levels, target

ranges were 1.5–2.5 μg/mL and 15.0–25.0 μg/mL for L-QC and H-QC, respectively. For adalimumab drug levels, ranges were 2.7–6.3 μg/mL and 11.4–26.6 μg/mL, respectively.

The validity of the tests was evaluated by analyzing the QCs together with the unknown samples before each analytical session.

Similarly, total antibodies (free and bound forms) directed against infliximab were semi-quantitatively measured on the same IFX serum samples using a validated AFIAS Total Anti-Infliximab kit (Bodytech Med Inc., Republic of Korea). This test uses a bridging immunoassay to detect antibodies against infliximab. The assay is based on a system similar to that adopted for the detection of drug levels. Briefly, after loading on the cartridge, the sample was subjected to dissociation, and anti-drug antibodies from the samples were bridged with fluorescence and biotin-labeled infliximab, which resulted in the formation of an immune complex. This immune complex migrates into the nitrocellulose matrix and is captured by immobilized streptavidin on a test strip. More antibodies to infliximab are present in the sample, and more immune complexes will form, leading to stronger intensity of the fluorescence signal, which is processed by the instrument to show total anti-infliximab concentration in a working range of 8–250 AU/mL.

The analytical specifications of the AFIAS kits used in this study are listed in Supplementary Tables S1 and S2.

2.4. Stability

Since ELISA test was performed on frozen and thawed samples, we have evaluated long-term stability by re-assessing infliximab and adalimumab concentrations on randomly selected authentic samples (n = 4) that were stored at −80 °C over a period of one month. The ratio of the concentration after a second freezing/thawing cycle to the initial measurement was used to calculate a percentage difference. Based on EMA guidelines, an acceptable stability should have a percentage difference below 15%.

2.5. Statistical Methods

Nonparametric Passing–Bablok regression and Spearman correlation coefficients were used to evaluate the agreement between drug concentrations measured with both ELISA and AFIAS assays. For the slope and intercept, 95% confidence intervals (CIs) were calculated. Thereafter, the Bland–Altman test was applied to assess the relative differences between the two assays by plotting the % differences against the average anti-TNF agent concentrations measured in serum using ELISA and AFIAS. The mean difference (bias) and standard deviation (SDs) of the mean were calculated. According to The ICH guideline M10 on bioanalytical method validation and study sample analysis. 25 July 2022, EMA/CHMP/ICH/172948/2019 Committee for Medicinal Products for Human Use. Available at https://www.ema.europa.eu/en/ich-m10-bioanalytical-method-validation-scientific-guideline, accessed on 28 August 2023), the difference between the two values obtained should be within 20% of the mean for at least 67% of the repeats. For a qualitative comparison between IFX and ADL drug levels measured by both ELISA and AFIAS, weighted kappa statistics were determined after the stratification of results according to the therapeutic range (IFX < 3 μg/mL, ≥3 to <7 μg/mL, and ≥7 μg/mL) (ADL < 5 μg/mL, ≥5 to <10 μg/mL, and ≥10 μg/mL). Therapeutic intervals were determined according to previously published reports [26,29,30]. Drugs levels measured with both ELISA and AFIAS were expressed as median and interquartile range (IQR). Mann–Whitney test was used to compare two groups of non-parametric data. All statistical analyses were performed using GraphPad Prism, version 10 (GraphPad Software, San Diego, CA 92108, USA).

3. Results

3.1. Comparison of IFX and ADL Serum Levels Measured with Both AFIAS and ELISA Assays

The median concentration of IFX serum levels measured with AFIAS was 4.38 µg/mL (IQR: 5.57), while the median concentration of ELISA measurements was 4.92 µg/mL (IQR: 5.90). A significant difference was not observed in IFX trough levels determined with both assays (p = 0.445). Similarly, the median of ADL trough concentrations measured with AFIAS was 8.73 µg/mL (IQR: 6.07), whereas the median of ADL values found in the same serum samples by using ELISA was 7.09 (IQR: 3.94). Among AFIAS and ELISA ADL trough levels, we have not observed a significant difference (p = 0.135). Paired raw data of IFX and ADL concentrations measured with both methods are reported in Supplementary Table S3. Figure 1 shows the Passing–Bablok correlation plot for IFX and ADL serum concentrations measured by AFIAS and ELISA. For IFX levels, the fit was y = 1.25X − 0.28 (95% CI slope, 0.83 to 1.67; 95% CI intercept, −2.11 to 1.55) (Figure 1A), meanwhile for ADL it was y = 0.72X + 1.07 (95% CI slope, 0.58 to 0.86; 95% CI intercept, −0.04 to 2.19) (Figure 1B). For IFX and ADL, there was an absence of no constant bias, as both the 95% CI intercepts included 0. Exclusively for ADL, the 95% CI slopes did not include 1, indicating the presence of a slight proportional bias.

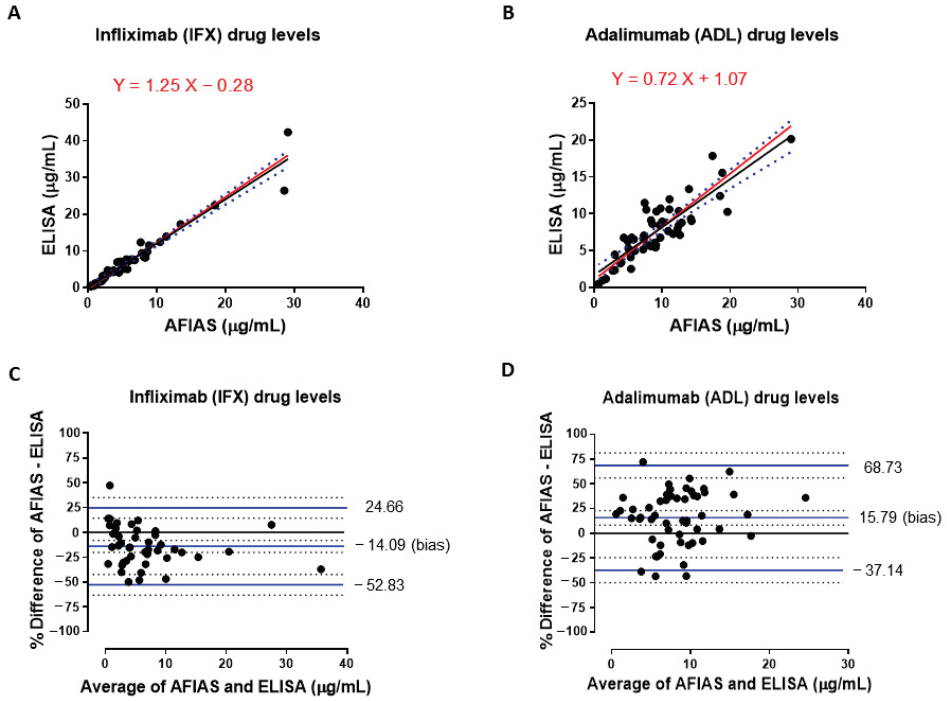


Figure 1. Passing–Bablok correlations and Bland–Altman plots for infliximab (IFX) and adalimumab (ADL) drug levels. Passing–Bablok correlation plots for IFX (**A**) and ADL (**B**) drug levels. Continuous black and red lines indicate the linear and the Deming regression lines, respectively. The dotted blue lines indicate 95% confidence intervals (CIs). Bland–Altman plots of IFX (**C**) and ADL (**D**) drug levels. Continuous horizontal blue lines were drawn from top to down at the upper 95% limits of agreement, the mean difference (bias), and the lower 95% limits of agreement. Dotted horizontal black lines indicate the 95% confidence interval (CI) for the mean and the agreement limits (defined as the mean difference ± 1.96 times the standard deviation of the differences).

The Spearman's correlation coefficients (rho) were 0.98 (95% CI 0.97 to 0.99) for IFX (Figure 1A) and 0.83 (95% CI 0.72 to 0.90) for ADL (Figure 1B), indicating a positive correlation between drug concentrations measured with both assays. Moreover, a significant p value was observed for both IFX (n = 44) and ADL (n = 54) ($p < 0.001$).

The results were further evaluated using the Bland–Altman test (Figure 1). In these graphs, the data are displayed as scatter diagrams of the % difference plotted against the average of two measurements. Continuous horizontal blue lines were drawn at the mean difference (bias) and 95% limits of agreement, which are defined as the mean difference ± 1.96 times the standard deviation of the differences. Dotted horizontal black lines indicate the 95% confidence intervals (CI) for the mean and the agreement limits. The % mean difference values were −14.09 (95% CI −8.08 to −20.1) and 15.79 (95% CI 8.42 to 23.13) for IFX and ADL, respectively (Figure 1C,D).

3.2. Comparison of Total Anti-Infliximab Concentrations in Serum Samples Obtained by Using AFIAS and ELISA Assays

AFIAS Total Anti-infliximab was used for the semi-quantitative detection of antibodies directed against infliximab. For this assay, a working range of 8–250 AU/mL was used, and values below or above this range were displayed as <8 and >250 AU/mL, respectively. Therefore, we did not collect sufficient data to establish a statistically significant correlation between AFIAS and ELISA. However, 39 serum samples were analyzed using AFIAS, which showed a concentration of <8 AU/mL. These samples were also tested using an ELISA kit, which resulted in a median (range) value of 4.78 (2.22–12.31) AU/mL. Similarly, among the AFIAS results, n = 4 serum samples presented a total antibody concentration > 250 AU/mL. The median value obtained with the ELISA assay was 576.5 AU/mL (range 363.1–771.8 AU/mL).

3.3. Qualitative Evaluation of Agreement Between Drug Levels Measured with Both AFIAS and ELISA Assays

To qualitatively compare the serum drug levels obtained with the AFIAS system and the ELISA assay, we evaluated the inter-rater agreement with kappa by stratifying the results into three subgroups according to the therapeutic interval. For IFX, we divided the measurements as follows (<3 μg/mL, ≥3 to ≤7 μg/mL, and ≥7 μg/mL), based on a previously described therapeutic range of 5–7 μg/mL [26,29] (Table 1). Infliximab levels showed "substantial agreement" between the two assays according to the scale suggested by Landis and Koch, G.G. [31]. Overall, the weighted kappa was 0.73 (95% CI 0.58, 0.87), and the number of observed agreements between the reference ELISA and the AFIAS assay was 33/44 (75% of the observations). In particular, for the n = 13 samples with IFX levels < 3 μg/mL (as measured with reference ELISA assay), an agreement was achieved for 13/13 (100%) samples tested with AFIAS; for samples with infliximab drug levels between 3 and 7 μg/mL (n = 13) obtained with the reference ELISA, agreement was reached for 8/13 (61.5%) of AFIAS samples; and finally, when IFX levels for the reference ELISA were >7 μg/mL (n = 18 samples), 12/18 (66.6%) of AFIAS measurements were in agreement with it. Similarly, ADL drug levels were stratified into three subgroups (<5 μg/mL, ≥5 to ≤10 μg/mL, and ≥10 μg/mL) according to the therapeutic range of 5–10 μg/mL proposed for inflammatory bowel diseases [30] (Table 2). The weighted kappa for adalimumab was 0.52 (95% CI 0.34 to 0.71) denoting a "moderate agreement" [31]. For ADL, the overall number of observed agreements between reference ELISA and AFIAS assay was 35/54 (64.8% of the observations). In detail, for the n = 12 ADL samples with drug levels < 5 μg/mL (measured by ELISA as reference method), agreement was reached for 8/12 (66.6%) samples tested with AFIAS as well; for samples with adalimumab drug levels between 5 and 10 μg/mL (n = 29) measured by ELISA, agreement was obtained for 18/29 (62%) of AFIAS measurements; and finally, at drug levels > 10 μg/mL for the reference ELISA (n = 13), 9/13 (69.2%) samples were in agreement with the results of AFIAS.

Table 1. Comparison between infliximab serum levels measured by enzyme-linked immunosorbent assay (ELISA) and AFIAS stratified by the therapeutic range 3–7 μg/mL [29].

Reference ELISA (IDKmonitor® Infliximab Drug Levels)			
	<3 μg/mL	≥3 to <7 μg/mL	≥7 μg/mL
AFIAS Infliximab			
<3 μg/mL	13	5	0
≥3 to <7 μg/mL	0	8	6
≥7 μg/mL	0	0	12

Table 2. Comparison between adalimumab serum levels measured by enzyme-linked immunosorbent assay (ELISA) and AFIAS stratified by the therapeutic range 5–10 μg/mL [30].

Reference ELISA (IDKmonitor® Adalimumab Drug Levels)			
	<5 μg/mL	≥5 to <10 μg/mL	≥10 μg/mL
AFIAS Adalimumab			
<5 μg/mL	8	2	0
≥5 to <10 μg/mL	4	18	4
≥10 μg/mL	0	9	9

Conversely, when we have stratified IFX drug levels measured with AFIAS, at infliximab levels < 3 μg/mL (n = 18), agreement with ELISA was achieved in 13/18 samples (72.2%); for AFIAS results comprised between 3 and 7 μg/mL (n = 14), agreement with ELISA was reached in 8/14 (57.1%) measurements; and finally, when AFIAS drug levels were >7 μg/mL (n = 12), all the measurements (12/12, 100%) were in agreement with the ELISA results. Similarly, by stratifying AFIAS results for ADL drug levels based on the therapeutic range 5–10 μg/mL, at adalimumab concentrations < 5 μg/mL (n = 10), the agreement with ELISA was 8/10 (80%). For AFIAS results between 5 and 10 μg/mL (n = 26), agreement with ELISA was found in 18/26 (69.2%) measurements; and finally, at AFIAS drug levels > 10 μg/mL (n = 18), 9/18 (50%) samples agreed with the ELISA assay.

3.4. Evaluation of Stability

In order to exclude a possible bias due to the freezing–thawing procedure applied to the ELISA samples, we have randomly selected and re-analyzed n = 4 authentic samples after being stored at −80 °C over a period of one month. Therefore, a second freezing–thawing cycle was executed 30 days after the first one, and revealed a stability of 119.0 ± 15.26% (mean ± SD) for IFX and 97.52 ± 14.98% for ADL compared to the initial drugs' measurements.

4. Discussion

According to the ECCO-ESPGHAN Guideline 2020, early proactive therapeutic drug monitoring followed by dose optimization is recommended for patients treated with anti-TNF agents [5]. Proactive TDM is defined as the evaluation of trough concentrations and ADA levels, with the aim of optimizing biological therapy to achieve an effective threshold drug concentration [15]. In contrast to reactive TDM, which is defined as the evaluation of drug concentration and ADA levels in case of primary non-response or secondary loss of response (LoR) to a biological agent, preliminary data suggest that proactive TDM of anti-TNF therapy is associated with better therapeutic outcomes than cost-expansive

empirical dose optimization and/or reactive TDM [15]. Although the introduction of TNF biological blockers into clinical practice has significantly improved the treatment of inflammatory conditions such as IBDs and juvenile idiopathic arthritis, patients treated with these agents may experience LoR and relapse of the disease [7]. The reasons for these therapeutic failures are not yet fully understood; however, inter-individual variability in drug pharmacokinetics (PK), pharmacodynamics (PD), and immunogenicity are considered possible risk factors [8,15,21]. Although different bioanalytical methods have been proposed to measure anti-TNF agents in both serum and plasma samples, ELISA remains the most commonly used assay [18]. However, over the last few decades, point-of-care (POC) devices based on lateral flow (LF) immunoassays have been developed and validated for measuring both drug and ADA levels with a rapid turnaround time [14,26–28]. Despite ELISA being a reliable technology characterized by the possibility of automating tests, lower costs, and high-throughput analyses, it also presents disadvantages. Among them, ELISA requires several hours of work (4–8 h) executed by appropriately trained personnel, and it is cost-effective only if patient samples are accumulated and tested in batches [18]. Consequently, TAT is significantly prolonged and TDM results are not immediately available to clinicians. Conversely, POC devices allow for single-patient analyses and provide both quantitative and semiquantitative results within 15–20 min [14,27,28,32–34].

Nevertheless, before being adopted by a biochemistry laboratory working on the TDM of anti-TNF blockers, these POC devices should be adequately cross-validated using different bioanalytical assays. In this regard, several reports have been published to date comparing ELISA with different POC tests for the measurement of both drug and ADA levels in serum or plasma samples [14,26–28,32–37]. In our study, we have used the AFIAS system (Bodytech Med Inc., Republic of Korea) to measure IFX and ADL drug levels in serum samples collected from pediatric patients during the routine clinical practice. Additionally, anti-IFX Total ADAs were also tested in the same IFX serum samples.

Both AFIAS IFX and AFIAS ADL are fluorescence-based lateral flow immunoassays that have been successfully developed and validated for quantitative determination of infliximab and adalimumab in different biological matrices, including whole blood, plasma, and serum (Bodytech Med Inc., Republic of Korea). To date, the analytical and clinical performance of these assays have been already evaluated by comparing drugs' concentrations measured with both AFIAS and different ELISA kits used for TDM analysis in adult and pediatric patients [14,27,28]. Results were comparable among the different analytical methods, showing a good correlation between AFIAS and the reference ELISA assays [14,28]. However, in a recent manuscript by Lopez Perez J. and colleagues (2025), the authors have defined the AFIAS system a valid method for monitoring anti-TNF-α inhibitors; however, the interchangeability with ELISA should be further confirmed [27]. Here, to the best of our knowledge, we evaluate for the first time the analytical performance of both AFIAS ADL and AFIAS IFX in serum samples collected from pediatric patients during the routine clinical practice.

Passing–Bablok regression and Bland–Altman plots were used to assess the agreement and relative differences between analytical methods, as previously described [14,26,28]. In our hands, Passing–Bablok regressions for both IFX and ADL drugs' concentrations revealed absence of a constant bias, whereas only for ADL, the 95% CI slopes did not include 1, indicating the presence of a slight proportional bias. Moreover, the Spearman's coefficient was close to 1 for both IFX and ADL and revealed a significant correlation between the ELISA and AFIAS assays ($p < 0.001$) (Figure 1A,B).

The Bland–Altman test showed that the % mean difference between drug concentrations measured by ELISA and AFIAS was −14.09 for IFX (Figure 1C) and 15.79 for ADL (Figure 1D). According to previously reported acceptance criteria, for IFX, at least 66% of

paired samples showed a % difference within ±20%, whereas for ADL, only 46% of the analyzed samples were within this acceptable range [38]. The higher deviation observed for ADL compared to IFX was also evident in the analysis of linear regression residuals (Supplementary Figure S1).

However, our results are in line with previously published reports for AFIAS IFX and ADL [14,28].

It is also worthwhile to say that despite a comparable measurement range for IFX and ADL drug levels (0.20–50 μg/mL for AFIAS vs. 0.40–45.0 μg/mL for ELISA), the higher % differences observed for adalimumab drug levels could be partially explained by an overestimation of AFIAS results compared to ELISA measurements. This observation confirms previous published data and could explain the higher % differences observed for adalimumab rather than for infliximab [28]. However, when comparing only ELISA and AFIAS paired concentrations falling within the suggested therapeutic range (5–10 μg/mL), at least 60% of paired samples showed a % difference within the acceptable range of ±20% [38].

Similarly, we qualitatively evaluated the inter-rater agreement with kappa by stratifying both ELISA and AFIAS drug results into three subgroups according to the IFX and ADL therapeutic interval. In particular, for IFX, we divided measurements as follows (<3 μg/mL, ≥3 to ≤7 μg/mL, and ≥7 μg/mL), based on a previously described therapeutic range of 5–7 μg/mL [26,29]. Infliximab levels showed "substantial agreement" between the two assays according to the scale suggested by Landis and Koch, G.G. [31]. In particular, the weighted kappa was 0.73 (95% CI 0.58 to 0.87), and the number of observed agreements between the reference ELISA and the AFIAS assay was 33/44 (75% of the observations). Similarly, ADL drug levels were stratified into three subgroups (<5 μg/mL, ≥5 to ≤10 μg/mL, and ≥10 μg/mL) according to the therapeutic range of 5–10 μg/mL proposed for inflammatory bowel diseases [30]. For ADL, the weighted kappa was 0.52 (95% CI 0.34 to 0.71), denoting a "moderate agreement" compared to IFX [31]. In particular, the overall number of observed agreements between reference ELISA and AFIAS assay was 35/54 (64.8% of the observations) for ADL. Similar to the observations made for the Bland–Altman results, the reasons behind this "moderate agreement" for adalimumab drug levels could be probably due to the overestimation observed for the AFIAS results compared to ELISA concentrations. In fact, the proportional bias observed between ELISA and AFIAS ADL measurements has been previously described and could additionally explain the discrepancy shown for AFIAS ADL compared to IFX [27].

However, it is worth mentioning that for therapies with biologic agents, slight variations in drug measurement are unlikely to significantly affect the clinical decision process, since dosing is usually guided by therapeutic ranges that are tolerant to small variations in the drug levels. Therefore, we believe that, in our study, this discrepancy does not represent a strong limitation in clinical decision making.

Finally, alongside infliximab serum levels, we measured the amount of total anti-IFX antibodies. The most common cause of failure in biological therapy is the development of anti-drug antibodies [39]. The presence of ADAs vs. IFX is generally associated with a reduced serum IFX concentration, decreased clinical response to IFX, and increased adverse events [40]. Moreover, the presence of anti-ADL antibodies was associated with low or undetectable serum trough ADL levels and reduced clinical efficacy [41]. This aspect was further confirmed by empirical evidence showing that the concomitant use of immunosuppressive drugs reduces immunogenicity and overall ADAs production [39]. Therefore, monitoring ADAs alongside drug levels allows for the identification of patients who have lost response to the biological agent but also to potentially define a tailored therapeutic strategy [16]. Moreover, monitoring antibodies against IFX in CD patients is

more cost-effective than dose-escalating strategies [42,43]. Based on this evidence, several bioanalytical methods have been proposed for the detection of antidrug antibodies, including ELISA, RIA, ECLIA, etc. [39,44,45]. POC devices have also been validated by comparing their clinical performances vs. ELISA assays [28,34,36,37]. Despite the availability of different bioanalytical methods, some questions remain to be answered. Although several TDM-based algorithms have been proposed in real-life clinical practice to guide the tailored optimization of anti-TNF therapies [15,23,46], reference ranges for anti-drug antibodies are still lacking. Moreover, according to different analytical performances, the detection of anti-drug antibodies is often based on cut-off values that provide qualitative or semi-quantitative results. Consequently, the interpretation of data is not straightforward for clinicians. Similarly, from a clinical point of view, the need for routine measurement of anti-drug antibodies alongside drug levels, or just following low-drug C_{trough} detection, is still debated. Finally, the clinical evaluation of free rather than total anti-drug antibodies remains an open question. Together, these aspects represent a significant limitation that hampers both the measurement and subsequent interpretation of ADA levels in routine clinical practice.

Here, we compared the semi-quantitative performance of both ELISA and AFIAS assays. However, because the AFIAS Total Anti-IFX provides a working range of 8–250 AU/mL, values below or above this range are exclusively displayed as <8 and >250 AU/mL, respectively. In contrast, the analysis of total anti-IFX serum levels by ELISA can provide numeric results for antibody concentrations <8 or >250 AU/mL. Therefore, we were not able to pair sufficient data to establish a statistically significant correlation between AFIAS and ELISA results. However, n = 39 serum samples were analyzed using AFIAS, and the results were <8 AU/mL. These samples were also tested using ELISA, resulting in a median (range) value of 4.78 (2.22–12.31) AU/mL. Similarly, n = 4 serum samples analyzed with AFIAS had a total anti-IFX value of >250 AU/mL. The median value obtained for these samples following ELISA assessment was 576.5 AU/mL (range 363.1–771.8 AU/mL). Consequently, we can only assume a positive correlation between anti-IFX levels measured using both ELISA and AFIAS assays. This aspect represents a limitation of our study. Perhaps a larger number of samples could be useful to overcome the variability observed for ADL drug concentrations. Similarly, by including a higher number of samples, it could be possible to provide a more robust correlation between ADA levels measured with both methods. However, it is also worth noting that from a clinical point of view, and in the absence of reference ranges for anti-drug levels, the utility of providing a numeric value whenever the ADAs concentration is <8 or >250 AU/mL remains debated. Another limitation of our study could be the fact that the ELISA and AFIAS assays were not performed at the same time. In fact, whereas the AFIAS tests have been executed on fresh serum samples, ELISA was carried out after one freezing–thawing cycle. To eliminate this potential bias among methods, four authentic samples of IFX and ADL were randomly selected and re-analyzed after being stored at −80 °C for one month. Compared to the initial drugs' concentrations, a second cycle of freezing–thawing showed a 30-day stability of 119% and 97.52% for IFX and ADL, respectively. Therefore, these data demonstrate that ELISA results are not affected by the freezing–thawing procedures.

5. Conclusions

In conclusion, our results show that, although there are slight differences between infliximab and adalimumab, the AFIAS assay has an accuracy and analytical performance comparable to that of the ELISA method used for TDM of IFX and ADL drug levels. Regarding the evaluation of anti-IFX antibodies, we only provided a preliminary comparison between ELISA and AFIAS tests, highlighting the necessity for more exhaustive studies

aimed at addressing this point. However, our data seem to show a positive correlation between total anti-IFX levels measured using both bioanalytical methods. AFIAS IFX and ADL have been already validated as lateral flow immunoassays for the quantitative measurement of infliximab and adalimumab in different biological matrices. As a point-of-care device, the AFIAS is based on a rapid and fully automated process that does not require specialized or well-trained personnel and allows single-sample analyses with results displayed within 15–20 min. The latest represents the main advantage of this method, which could overcome the time- and cost-consuming limitations of current ELISA-based TDM approaches. Therefore, based on our results, the introduction of these devices into routine clinical practice could provide results more quickly and with similar accuracy to ELISA, allowing clinicians to rapidly formulate effective therapeutic plans. In fact, an ad hoc protocol has been established in our center to promote the use of this device, encouraging a proactive TDM strategy and, therefore, facilitating a more cost-effective strategy than the empirical dose-escalating approach.

Supplementary Materials: The following supporting information can be downloaded at https://www.mdpi.com/article/10.3390/pharmaceutics17040421/s1: Table S1: Analytical specifications of AFIAS and ELISA kits used for the quantification of Infliximab (IFX) and Adalimumab (ADL) in serum samples. Table S2: Analytical specifications of AFIAS and ELISA kits used for the detection of total antibodies against infliximab in serum samples. Table S3: Paired concentrations of IFX and ADL drug levels measured with both AFIAS and ELISA assays. Figure S1: Analysis of residuals for the linear regression of (A) IFX and (B) ADL drug levels measured with both AFIAS and ELISA methods.

Author Contributions: Conceptualization, C.R., R.S., P.D.A. and B.M.G.; data curation, C.R., R.S., G.A., F.B., D.K., E.F.R., S.F. and G.T.; formal analysis, C.R., R.S., S.C., A.M. and A.V.; funding acquisition, C.D.V., P.D.A. and B.M.G.; investigation, G.A., F.B., D.K., E.F.R., S.F. and G.T.; methodology, C.R., R.S., S.C., A.M. and A.V; project administration, C.D.V., S.M.M., P.D.A. and B.M.G.; resources, C.D.V., P.D.A. and B.M.G.; software, C.R., R.S., S.C., A.M. and A.V.; supervision, S.M.M., P.D.A. and B.M.G.; validation, C.R., R.S., S.C., A.M., A.V. and B.M.G.; visualization, C.R. and R.S.; writing—original draft, C.R., R.S., G.A., F.B., D.K., E.F.R., S.F. and P.D.A.; and writing—review and editing, C.R., R.S., G.T., S.M.M., P.D.A. and B.M.G. All authors have read and agreed to the published version of the manuscript.

Funding: This work was supported by the Italian Ministry of Health with "Current Research funds".

Institutional Review Board Statement: TDM of infliximab and adalimumab is well established during the routine clinical practice at Bambino Gesù Children's Hospital. This study was conducted in accordance with the Declaration of Helsinki, and the protocol was approved by the Ethics Committee of Bambino Gesù Children's Hospital (2333_OPBG_2020) on 4 January 2021.

Informed Consent Statement: Written informed consent has been obtained from the patients 'parents or their legal guardians to publish this paper.

Data Availability Statement: The original contributions presented in this study are included in the article/Supplementary Materials. Further inquiries can be directed to the corresponding authors.

Conflicts of Interest: The authors declare that they have no known competing financial interests or personal relationships that could influence the work reported in this study.

References

1. D'Arcangelo, G.; Distante, M.; Raso, T.; Rossetti, D.; Catassi, G.; Aloi, M. Safety of Biological Therapy in Children with Inflammatory Bowel Disease. *J. Pediatr. Gastroenterol. Nutr.* **2021**, *72*, 736–741. [CrossRef] [PubMed]
2. Duijvestein, M.; Battat, R.; Vande Casteele, N.; D'Haens, G.R.; Sandborn, W.J.; Khanna, R.; Jairath, V.; Feagan, B.G. Novel Therapies and Treatment Strategies for Patients with Inflammatory Bowel Disease. *Curr. Treat. Options Gastroenterol.* **2018**, *16*, 129–146. [CrossRef] [PubMed]

3. Hyams, J.; Crandall, W.; Kugathasan, S.; Griffiths, A.; Olson, A.; Johanns, J.; Liu, G.; Travers, S.; Heuschkel, R.; Markowitz, J.; et al. Induction and maintenance infliximab therapy for the treatment of moderate-to-severe Crohn's disease in children. *Gastroenterology* **2007**, *132*, 863–873. [CrossRef] [PubMed]
4. Hyams, J.S.; Griffiths, A.; Markowitz, J.; Baldassano, R.N.; Faubion, W.A., Jr.; Colletti, R.B.; Dubinsky, M.; Kierkus, J.; Rosh, J.; Wang, Y.; et al. Safety and efficacy of adalimumab for moderate to severe Crohn's disease in children. *Gastroenterology* **2012**, *143*, 365–374.e362. [CrossRef]
5. van Rheenen, P.F.; Aloi, M.; Assa, A.; Bronsky, J.; Escher, J.C.; Fagerberg, U.L.; Gasparetto, M.; Gerasimidis, K.; Griffiths, A.; Henderson, P.; et al. The Medical Management of Paediatric Crohn's Disease: An ECCO-ESPGHAN Guideline Update. *J. Crohns Colitis* **2020**, *15*, 171–194. [CrossRef]
6. Fernandes, S.R.; Bernardo, S.; Simoes, C.; Goncalves, A.R.; Valente, A.; Baldaia, C.; Moura Santos, P.; Correia, L.A.; Tato Marinho, R. Proactive Infliximab Drug Monitoring Is Superior to Conventional Management in Inflammatory Bowel Disease. *Inflamm. Bowel Dis.* **2020**, *26*, 263–270. [CrossRef]
7. Bots, S.J.; Kuin, S.; Ponsioen, C.Y.; Gecse, K.B.; Duijvestein, M.; D'Haens, G.R.; Lowenberg, M. Relapse rates and predictors for relapse in a real-life cohort of IBD patients after discontinuation of anti-TNF therapy. *Scand. J. Gastroenterol.* **2019**, *54*, 281–288. [CrossRef]
8. Di Paolo, A.; Luci, G. Personalized Medicine of Monoclonal Antibodies in Inflammatory Bowel Disease: Pharmacogenetics, Therapeutic Drug Monitoring, and Beyond. *Front. Pharmacol.* **2020**, *11*, 610806. [CrossRef]
9. Naviglio, S.; Lacorte, D.; Lucafo, M.; Cifu, A.; Favretto, D.; Cuzzoni, E.; Silvestri, T.; Pozzi Mucelli, M.; Radillo, O.; Decorti, G.; et al. Causes of Treatment Failure in Children with Inflammatory Bowel Disease Treated with Infliximab: A Pharmacokinetic Study. *J. Pediatr. Gastroenterol. Nutr.* **2019**, *68*, 37–44. [CrossRef]
10. Sazonovs, A.; Kennedy, N.A.; Moutsianas, L.; Heap, G.A.; Rice, D.L.; Reppell, M.; Bewshea, C.M.; Chanchlani, N.; Walker, G.J.; Perry, M.H.; et al. HLA-DQA1*05 Carriage Associated with Development of Anti-Drug Antibodies to Infliximab and Adalimumab in Patients with Crohn's Disease. *Gastroenterology* **2020**, *158*, 189–199. [CrossRef]
11. Curci, D.; Lucafo, M.; Cifu, A.; Fabris, M.; Bramuzzo, M.; Martelossi, S.; Franca, R.; Decorti, G.; Stocco, G. Pharmacogenetic variants of infliximab response in young patients with inflammatory bowel disease. *Clin. Transl. Sci.* **2021**, *14*, 2184–2192. [CrossRef] [PubMed]
12. Atiqi, S.; Hooijberg, F.; Loeff, F.C.; Rispens, T.; Wolbink, G.J. Immunogenicity of TNF-Inhibitors. *Front. Immunol.* **2020**, *11*, 312. [CrossRef]
13. Roda, G.; Jharap, B.; Neeraj, N.; Colombel, J.F. Loss of Response to Anti-TNFs: Definition, Epidemiology, and Management. *Clin. Transl. Gastroenterol.* **2016**, *7*, e135. [CrossRef] [PubMed]
14. Kim, E.S.; Chon, H.; Kwon, Y.; Lee, M.; Kim, M.J.; Choe, Y.H. Fluorescence-Based Lateral Flow Immunoassay for Quantification of Infliximab: Analytical and Clinical Performance Evaluation. *Ther. Drug Monit.* **2024**, *46*, 460–467. [CrossRef]
15. Papamichael, K.; Cheifetz, A.S. Therapeutic drug monitoring in patients on biologics: Lessons from gastroenterology. *Curr. Opin. Rheumatol.* **2020**, *32*, 371–379. [CrossRef]
16. Scott, F.I.; Lichtenstein, G.R. Therapeutic Drug Monitoring of Anti-TNF Therapy in Inflammatory Bowel Disease. *Curr. Treat. Options Gastroenterol.* **2014**, *12*, 59–75. [CrossRef]
17. Simeoli, R.; Dorlo, T.P.C.; Hanff, L.M.; Huitema, A.D.R.; Dreesen, E. Editorial: Therapeutic Drug Monitoring (TDM): A Useful Tool for Pediatric Pharmacology Applied to Routine Clinical Practice. *Front. Pharmacol.* **2022**, *13*, 931843. [CrossRef]
18. Franca, R.; Curci, D.; Lucafo, M.; Decorti, G.; Stocco, G. Therapeutic drug monitoring to improve outcome of anti-TNF drugs in pediatric inflammatory bowel disease. *Expert Opin. Drug Metab. Toxicol.* **2019**, *15*, 527–539. [CrossRef]
19. Nakase, H.; Motoya, S.; Matsumoto, T.; Watanabe, K.; Hisamatsu, T.; Yoshimura, N.; Ishida, T.; Kato, S.; Nakagawa, T.; Esaki, M.; et al. Significance of measurement of serum trough level and anti-drug antibody of adalimumab as personalised pharmacokinetics in patients with Crohn's disease: A subanalysis of the DIAMOND trial. *Aliment. Pharmacol. Ther.* **2017**, *46*, 873–882. [CrossRef]
20. Bodini, G.; Giannini, E.G.; Savarino, V.; Del Nero, L.; Lo Pumo, S.; Brunacci, M.; De Bortoli, N.; Jain, A.; Tolone, S.; Savarino, E. Infliximab trough levels and persistent vs transient antibodies measured early after induction predict long-term clinical remission in patients with inflammatory bowel disease. *Dig. Liver Dis.* **2018**, *50*, 452–456. [CrossRef]
21. Papamichael, K.; Juncadella, A.; Wong, D.; Rakowsky, S.; Sattler, L.A.; Campbell, J.P.; Vaughn, B.P.; Cheifetz, A.S. Proactive Therapeutic Drug Monitoring of Adalimumab Is Associated with Better Long-term Outcomes Compared with Standard of Care in Patients With Inflammatory Bowel Disease. *J. Crohns Colitis* **2019**, *13*, 976–981. [CrossRef] [PubMed]
22. Vande Casteele, N. Assays for measurement of TNF antagonists in practice. *Frontline Gastroenterol.* **2017**, *8*, 236–242. [CrossRef] [PubMed]
23. Regazzi, M.; Golay, J.; Molinaro, M. Monoclonal Antibody Monitoring: Clinically Relevant Aspects, A Systematic Critical Review. *Ther. Drug Monit.* **2020**, *42*, 45–56. [CrossRef]

24. Vermeire, S.; Dreesen, E.; Papamichael, K.; Dubinsky, M.C. How, When, and for Whom Should We Perform Therapeutic Drug Monitoring? *Clin. Gastroenterol. Hepatol.* **2020**, *18*, 1291–1299. [CrossRef] [PubMed]
25. Ates, H.C.; Roberts, J.A.; Lipman, J.; Cass, A.E.G.; Urban, G.A.; Dincer, C. On-Site Therapeutic Drug Monitoring. *Trends Biotechnol.* **2020**, *38*, 1262–1277. [CrossRef]
26. Curci, D.; Lucafo, M.; Cifu, A.; Bramuzzo, M.; Martelossi, S.; Favretto, D.; De Pellegrin, F.; Fabris, M.; Vascotto, F.; Naviglio, S.; et al. Determination of Serum Infliximab Concentration by Point-of-care Devices in Children with Inflammatory Bowel Disease. *J. Pediatr. Gastroenterol. Nutr.* **2019**, *69*, 474–479. [CrossRef]
27. Lopez Perez, J.; Inda-Landaluce, M.; Nocito-Colon, M.; Martinez-Lostao, L. Comparative Analysis of 2 Commercially Available Assays for Therapeutic Drug Monitoring of Infliximab and Adalimumab. *Ther. Drug Monit.* **2025**, *00*, 1–5. [CrossRef]
28. Iniesta-Navalón, C.; Ríos-Saorín, M.; Añez-Castaño, R.; Rentero-Redondo, L.; Ortíz-Fernandez, P.; Martínez, E.; Urbieta-Sanz, E. Evaluating the Accuracy and Clinical Utility of AFIAS-10 Point of Care Versus Enzyme-Linked Immunosorbent Assay in Therapeutic Drug Monitoring of Infliximab and Adalimumab. *Ther. Drug Monit.* **2024**, *00*, 1–7. [CrossRef]
29. Moore, C.; Corbett, G.; Moss, A.C. Systematic Review and Meta-Analysis: Serum Infliximab Levels During Maintenance Therapy and Outcomes in Inflammatory Bowel Disease. *J. Crohns Colitis* **2016**, *10*, 619–625. [CrossRef]
30. Paul, S.; Moreau, A.C.; Del Tedesco, E.; Rinaudo, M.; Phelip, J.M.; Genin, C.; Peyrin-Biroulet, L.; Roblin, X. Pharmacokinetics of adalimumab in inflammatory bowel diseases: A systematic review and meta-analysis. *Inflamm. Bowel Dis.* **2014**, *20*, 1288–1295. [CrossRef]
31. Landis, J.R.; Koch, G.G. The measurement of observer agreement for categorical data. *Biometrics* **1977**, *33*, 159–174. [PubMed]
32. Afonso, J.; Lopes, S.; Goncalves, R.; Caldeira, P.; Lago, P.; Tavares de Sousa, H.; Ramos, J.; Goncalves, A.R.; Ministro, P.; Rosa, I.; et al. Proactive therapeutic drug monitoring of infliximab: A comparative study of a new point-of-care quantitative test with two established ELISA assays. *Aliment. Pharmacol. Ther.* **2016**, *44*, 684–692. [CrossRef] [PubMed]
33. Cherry, M.; Dutzer, D.; Nasser, Y.; Berger, A.E.; Roblin, X.; Paul, S. Point-of-Care Assays Could Be Useful for Therapeutic Drug Monitoring of IBD Patients in a Proactive Strategy with Adalimumab. *J. Clin. Med.* **2020**, *9*, 2739. [CrossRef]
34. Facchin, S.; Buda, A.; Cardin, R.; Agbariah, N.; Zingone, F.; De Bona, M.; Zaetta, D.; Bertani, L.; Ghisa, M.; Barberio, B.; et al. Rapid point-of-care anti-infliximab antibodies detection in clinical practice: Comparison with ELISA and potential for improving therapeutic drug monitoring in IBD patients. *Therap. Adv. Gastroenterol.* **2021**, *14*, 1756284821999902. [CrossRef]
35. Novakovic, V.; Abdija, S.; Larsen, P.B.; Fenger, M.; Gredal, L.; Jacobsen, K.K. Comparison of the Quantum Blue(R) reader Point-of-Care system versus ELISA technique for therapeutic drug monitoring of Infliximab levels. *Clin. Biochem.* **2019**, *74*, 73–75. [CrossRef] [PubMed]
36. Nasser, Y.; Labetoulle, R.; Harzallah, I.; Berger, A.E.; Roblin, X.; Paul, S. Comparison of Point-of-Care and Classical Immunoassays for the Monitoring Infliximab and Antibodies Against Infliximab in IBD. *Dig. Dis. Sci.* **2018**, *63*, 2714–2721. [CrossRef]
37. Valdes-Delgado, T.; Aguado-Paredes, A.; Merino-Bohorquez, V.; Martin-Manzanares, J.; Alonso, M.M.; Maldonado, B.; Castro, L.; Belvis, M.; Benitez, B.; Caunedo, A.; et al. Performance of a New Rapid Point-of-Care Test for Infliximab Levels in Patients with Inflammatory Bowel Disease: A Comparison to ELISA. *Dig. Dis. Sci.* **2024**, *69*, 228–234. [CrossRef]
38. Jannetto, P.J. Chapter 8-Therapeutic drug monitoring using mass spectrometry. In *Mass Spectrometry for the Clinical Laboratory*; Academic Press: Cambridge, MA, USA, 2017; pp. 165–179.
39. Velikova, T.; Sekulovski, M.; Peshevska-Sekulovska, M. Immunogenicity and Loss of Effectiveness of Biologic Therapy for Inflammatory Bowel Disease Patients Due to Anti-Drug Antibody Development. *Antibodies* **2024**, *13*, 16. [CrossRef]
40. Pascual-Salcedo, D.; Plasencia, C.; Ramiro, S.; Nuno, L.; Bonilla, G.; Nagore, D.; Ruiz Del Agua, A.; Martinez, A.; Aarden, L.; Martin-Mola, E.; et al. Influence of immunogenicity on the efficacy of long-term treatment with infliximab in rheumatoid arthritis. *Rheumatology* **2011**, *50*, 1445–1452. [CrossRef]
41. Bartelds, G.M.; Krieckaert, C.L.; Nurmohamed, M.T.; van Schouwenburg, P.A.; Lems, W.F.; Twisk, J.W.; Dijkmans, B.A.; Aarden, L.; Wolbink, G.J. Development of antidrug antibodies against adalimumab and association with disease activity and treatment failure during long-term follow-up. *JAMA* **2011**, *305*, 1460–1468. [CrossRef]
42. Vermeire, S.; Gils, A.; Accossato, P.; Lula, S.; Marren, A. Immunogenicity of biologics in inflammatory bowel disease. *Therap Adv. Gastroenterol.* **2018**, *11*, 1756283X17750355. [CrossRef] [PubMed]
43. Steenholdt, C.; Brynskov, J.; Thomsen, O.O.; Munck, L.K.; Fallingborg, J.; Christensen, L.A.; Pedersen, G.; Kjeldsen, J.; Jacobsen, B.A.; Oxholm, A.S.; et al. Individualised therapy is more cost-effective than dose intensification in patients with Crohn's disease who lose response to anti-TNF treatment: A randomised, controlled trial. *Gut* **2014**, *63*, 919–927. [CrossRef] [PubMed]
44. Steenholdt, C.; Ainsworth, M.A.; Tovey, M.; Klausen, T.W.; Thomsen, O.O.; Brynskov, J.; Bendtzen, K. Comparison of techniques for monitoring infliximab and antibodies against infliximab in Crohn's disease. *Ther. Drug Monit.* **2013**, *35*, 530–538. [CrossRef] [PubMed]

45. Bloem, K.; van Leeuwen, A.; Verbeek, G.; Nurmohamed, M.T.; Wolbink, G.J.; van der Kleij, D.; Rispens, T. Systematic comparison of drug-tolerant assays for anti-drug antibodies in a cohort of adalimumab-treated rheumatoid arthritis patients. *J. Immunol. Methods* **2015**, *418*, 29–38. [CrossRef]
46. Vincent, F.B.; Morand, E.F.; Murphy, K.; Mackay, F.; Mariette, X.; Marcelli, C. Antidrug antibodies (ADAb) to tumour necrosis factor (TNF)-specific neutralising agents in chronic inflammatory diseases: A real issue, a clinical perspective. *Ann. Rheum. Dis.* **2013**, *72*, 165–178. [CrossRef]

Disclaimer/Publisher's Note: The statements, opinions and data contained in all publications are solely those of the individual author(s) and contributor(s) and not of MDPI and/or the editor(s). MDPI and/or the editor(s) disclaim responsibility for any injury to people or property resulting from any ideas, methods, instructions or products referred to in the content.

pharmaceutics

MDPI

Article

Development and Quality Control of a Population Pharmacokinetic Model Library for Caspofungin

Nuo Xu [1,2,†], Yufei Shi [1,2,†], Yixue Wang [3], Wenyao Mak [1], Wenyu Yang [1], Kar Weng Ng [4], Yue Wu [5], Zhijia Tang [1], Qingfeng He [1,2], Gangfeng Yan [3], Xiaoqiang Xiang [1,*] and Xiao Zhu [1,2,*]

[1] Department of Clinical Pharmacy and Pharmacy Administration, School of Pharmacy, Fudan University, Shanghai 201203, China; 22211030092@m.fudan.edu.cn (N.X.); yufei_shi@fudan.edu.cn (Y.S.); makwenyao@gmail.com (W.M.); 21211030109@m.fudan.edu.cn (W.Y.); zjtang@fudan.edu.cn (Z.T.); qf_he@fudan.edu.cn (Q.H.)
[2] Hunan Key Laboratory for Bioanalysis of Complex Matrix Samples, Changsha 410000, China
[3] Department of Critical Care Medicine, Children's Hospital of Fudan University, National Children's Medical Center, Shanghai 200000, China; yixuewang08@aliyun.com (Y.W.); gangfeng_yan@fudan.edu.cn (G.Y.)
[4] Department of Pharmacotherapy Services, Hospital Kuala Lumpur, Ministry of Health, Kuala Lumpur 50586, Malaysia; nkweng@moh.gov.my
[5] Department of Clinical Pharmacy, Shenzhen Children's Hospital, Medical College, Shantou University, Shenzhen 518000, China; wuyue161@163.com
* Correspondence: xiangxq@fudan.edu.cn (X.X.); xiaozhu@fudan.edu.cn (X.Z.); Tel.: +86-21-51980024 (X.X.); +86-21-51980024 (X.Z.)
† These authors contributed equally to this work.

Abstract: Background: Caspofungin is an echinocandin antifungal agent commonly used as the first-line therapy for invasive candidiasis, salvage therapy for invasive aspergillosis, and empirical therapy for presumed fungal infections. Pharmacokinetic (PK) variabilities and suboptimal exposure have been reported for caspofungin, increasing the risk of insufficient efficacy. Objective: This work aimed to develop a caspofungin population pharmacokinetic (popPK) library and demonstrate its utility by assessing the probability of target attainment across diverse settings. Methods: We established a caspofungin popPK model library following a rigorous literature review, re-implementing selected models in R with rxode2. Quality control procedures included a comparison of different studies and assessing covariate impacts. Model libraries were primarily used to perform Monte Carlo simulations to estimate target attainment and guide personalized dosing in Candida infections. Results: A total of 13 models, one- or two-compartment models, were included. The most significant covariates were body size (weight and body surface area), liver function, and albumin level. The results show that children and adults showed considerable differences in pharmacokinetics. For *C. albicans* and *C. parapsilosis*, none of the populations achieved a PTA of $\geq$90% at their respective susceptible MIC values. In contrast, for *C. glabrata*, 70% of the adult studies reached a PTA of $\geq$90%, while all pediatric studies achieved the same PTA level. Conclusion: At the recommended dosage, adult patients showed notably lower exposure to caspofungin compared to pediatric patients. Considering body size, liver function, and serum albumin is crucial when determining caspofungin dosage regimens. Furthermore, further research is required to comprehensively understand the pharmacokinetics of caspofungin in pediatric patients.

Keywords: caspofungin; individualized dosing; population pharmacokinetics; model library

1. Introduction

Echinocandins, including caspofungin, micafungin, and anidulafungin, represent a breakthrough in antifungal treatment. Caspofungin blocks the synthesis of an essential fungal cell wall component, β-(1,3)-D-glucan, leading to the osmotic instability and lysis of the fungal cell. Due to its selective action on fungal cells, caspofungin is usually well tolerated without common significant side effects. Caspofungin exerts potent activity

against *Candida* and *Aspergillus* spp., serving as the first-line therapy for invasive fungal infections (IFIs), salvage therapy for invasive aspergillosis, and empirical treatment for presumed fungal infections in children over three months and in adults [1,2].

With poor oral bioavailability (<0.2%), caspofungin can only be administered by slow intravenous infusion over approximately one hour. About 97% of caspofungin binds to plasma proteins after entering the bloodstream. Following infusion, the plasma concentration of caspofungin declines in a polyphasic manner. The metabolism process is slow and occurs mainly via hydrolysis and N-acetylation [3].

Caspofungin's favorable safety profile and relatively low potential for drug–drug interactions led to its widespread use in the prophylaxis and treatment of IFIs. However, reported pharmacokinetic (PK) variabilities and suboptimal exposure with standard dosing, especially in critically ill patients, increase the risk of insufficient efficacy [4,5]. Hence, personalized dosage recommendations and tailored adjustments, usually informed by measured observations and model-predicted exposure, are crucial to optimize treatment outcomes.

Caspofungin demonstrates a concentration-dependent inhibition of fungal growth [6]. The clinical efficacy of caspofungin in treating invasive aspergillosis relies on defined pharmacokinetic/pharmacodynamic (PK/PD) indices, like peak concentration/minimum effective concentration (C_{max}/MEC), the area under concentration–time curve/minimum inhibitory concentration (AUC/MIC), and AUC/MEC [7,8]. Common targets include the ratio of the 24 h total drug AUC to MIC ($AUC_{0–24\,h}$/MIC) and the ratio of the 24 h free drug AUC to MIC ($fAUC_{0–24\,h}$/MIC) [9,10]. $AUC_{0–24\,h}$/MIC, the most influential PK/PD index for caspofungin, exhibits substantial variability among intensive care unit (ICU) patients [11,12]. Despite preclinical support, these targets have yet to be confirmed and validated in clinical studies, posing challenges in their application to clinical practice.

Population pharmacokinetic (popPK) models describe the PK profiles of the studied population and can evaluate the effect of various covariates on PK variabilities. When integrated with Bayesian forecasting, which combines prior knowledge with new observational data, this approach has become increasingly utilized for designing and adjusting dosing regimens in clinical practice [13]. The Bayesian method requires a well-defined structural model that includes parameters informed by prior distributions and is continually updated with new clinical observations, ensuring that dosing regimens are tailored to the specific needs and responses of patients. Despite numerous PK/PD studies on caspofungin, existing model information has not been quantitatively integrated to guide further research. Therefore, a model library would be invaluable for facilitating model-informed precision dosing (MIPD) strategies by compiling relevant data.

This study aimed to develop a caspofungin population pharmacokinetic (popPK) library and demonstrate its utility by assessing the probability of target attainment across diverse settings. This consisted of three specific objectives: (1) to identify and re-implement existing popPK models using an open-source R package; (2) to perform a quality control of the developed model library by comparing PK metrics and evaluating the impact of covariates; and (3) to demonstrate the utility of the model library by assessing the probability of target attainment (PTA) across diverse study settings.

2. Materials and Methods

2.1. Development of Model Library

2.1.1. Search Strategy

Four databases, including PubMed, Embase, Web of Science, and Scopus, were searched for popPK model studies of caspofungin published before 25 November 2022, following the Preferred Reporting Items for Systematic Reviews and Meta-Analyses (PRISMA) guidelines [14]. The search strategy encompassed keywords pertinent to the focal medication ('Caspofungin' or 'Cancidas' or 'MK 0991' or 'L 743,872'), along with terms specifically denoting popPK modeling approaches, such as population pharmacokinetic, NONMEM, MONOLIX, or nlmixr. Additionally, all reference lists from selected articles were searched to ensure the comprehensiveness of our study. Two independent authors conducted the literature

research, and another two senior investigators performed the data validation [14]. The comprehensive search strategies employed for each database, as well as the detailed inclusion and exclusion criteria utilized in the study, can be found in the Supplementary Materials.

All studies identified from the databases and other sources were screened to evaluate their eligibility based on the following consolidated criteria: (1) the subject of the studies was human, including healthy volunteers and patients; (2) caspofungin was the study drug; (3) popPK or PK/PD analysis was conducted in the study; and (4) the study was published in English. A publication was excluded if (1) it was not an article or only focused on the methodology, algorithms, or software comparisons or (2) critical PK parameters were insufficient.

2.1.2. Literature Evaluation

Literature evaluations were implemented to diligently identify and resolve any anomalies or inconsistencies pertinent to the construction of the model library [15]. The quality of the popPK study was evaluated based on a checklist with 33 items adapted from the guidelines (see Supplementary Materials) [16,17]. The literature evaluation was divided into five parts: title and abstract, introduction, methods, results, and discussion and conclusion. A risk of bias assessment was conducted. Each item received one point if the study information met the criteria; otherwise, zero points were assigned. Compliance, reflecting popPK study quality, was calculated as compliance% = (items reported/total items) $\times$ 100%. The risk of bias plot was conducted using the "ggplot2" package (version 3.3.5; https://ggplot2.tidyverse.org, accessed on 5 November 2022) in R software (version 4.1.1; http://www.r-project.org, accessed on 5 November 2022).

2.1.3. Data Extraction

A standardized data extraction method was systematically employed to facilitate data collection from all eligible studies. This process encompassed the following key aspects: (1) demographic characteristics (e.g., race, age, sex, and weight range); (2) the study design (e.g., type of study, number of subjects and observations, dosage regimens, administration, sampling schedule, and detection method) [16]; (3) popPK modeling characteristics (e.g., software/algorithm, final PK parameters, model validation); (4) investigated and identified covariates information in popPK models; (5) PK/PD targets used for simulation if applicable; and (6) model application and recommended dosage regimens.

2.1.4. Model Re-Implementation

After extracting all relevant information from the models, we re-implemented them using the open-source R package "rxode2" package (version 2.0.12; https://nlmixr2.github.io/rxode2/index.html, accessed on 8 December 2022), with all parameters set to the final parameter estimates reported in the literature. All of the model codes are provided in the Supplementary Materials.

2.2. Quality Control of Model Library

2.2.1. Comparison of Studies

Quality control (QC) measures were implemented to screen and resolve any discrepancies or issues arising during the establishment of the model library, ensuring rigorous standards were maintained. We constructed three age-stratified virtual patient cohorts (comprising infants, children, and adults), thoughtfully designed to accurately mirror the specific target population of their corresponding models.

Virtual populations were created and divided into three age groups: infants (10 kg, 75 cm, 1 year old), children (20 kg, 100 cm, 6 years old), and adults (70 kg, 40 years old). Infants and children adopted the standard dosage regimen, 70 mg/m^2 on the first day, followed by 50 mg/m^2 once daily, whereas adults followed a different dosage regimen: 70 mg on the first day, followed by 50 mg once daily. Caspofungin was administered intravenously over one hour to all groups once daily. The Mosteller formula [18] was used

to calculate body surface area (BSA) values for infants and children, which were set at 0.441 m^2 and 0.79 m^2, respectively. All patients reached a steady state with the labeled dosing regimen. Concentration–time profiles were simulated with the "rxode2" package (version 2.0.12; https://nlmixr2.github.io/rxode2/index.html) in R.

We conducted a similarity comparison assessment to ensure the accuracy of constructing the developed model library. The idea behind this assessment is straightforward. If the models have been accurately implemented, the concentration–time curves for the models with similar target populations should be comparable as they describe the PK behavior of the same drug in the same population. The model performance is considered comparable if its typical maximum concentration (C_{max}) falls within the range of 50–200% of the median C_{max} across all studies (see Supplementary Materials).

2.2.2. Assessment of Covariates Impact

Clearance (CL) is a crucial parameter for AUC, while the apparent volume of distribution (V_d) is an important PK parameter for C_{max}. AUC and C_{max} play central roles in the individualized dosing of caspofungin. Thus, comparing the effects of different covariates on CL and V_d was necessary. The effect of covariates was presented through a forest plot using the "ggplot2" package (version 2.0.0; Tidyverse packages) in R. For continuous covariates, the maximum and minimum values from the included studies were extracted and used for calculating the range of the effect of different covariates on CL or V_d. For covariates included in multiple studies, a uniform range was set up for the comparison based on the demographic information in the included studies. For binary covariates, such as disease situation. The uncommon condition (critically ill disease) was treated as the reference ($COV_i = 0$), while the uncommon condition (not critically ill disease) was treated as the test ($COV_i = 1$). $CL_i = CL_{common} + CL_{diff} \times COV_i$. The range of CL_i was [CL_{common}, $CL_{common} + CL_{diff}$] (if $CL_{diff} > 0$) or [$CL_{common} + CL_{diff}$, CL_{common}] (if $CL_{diff} < 0$). Then, the values of CL and Vd were further normalized by the reference to the median covariate value (equation). We regarded covariate effects beyond the 80–125% range as clinically significant, in accordance with the standard employed in bioequivalence studies [19].

$$The\ effect\ value\ of\ covariates = \frac{Upper\ or\ lower\ limit}{Reference\ value} * 100\%$$

2.3. Application of PopPK Model Library

Louie et al. reported comparable Candida albicans reductions in kidney tissue and proposed $AUC_{0–24\,h}$/MIC as the optimal PK/PD index for caspofungin [20]. Based on the in vivo PK/PD studies, the PK/PD targets for *C. albicans*, *C. glabrata*, and *C. parapsilosis* were 865, 450, and 1185, respectively [10,21]. According to the clinical and laboratory standards institute (CLSI) MIC breakpoint for the in vitro broth dilution susceptibility testing of *Candida* spp., MICs for each Candida species were selected (*C. albicans*, susceptible $\leq$ 0.25 mg/L; *C. glabrata*, susceptible $\leq$ 0.12 mg/L; *C. parapsilosis*, susceptible $\leq$ 2 mg/L) [22]. After the popPK model library of caspofungin was established, a Monto Carlo simulation was conducted to predict the probability of caspofungin reaching the PK/PD target under labeled dosing regimens and specific MIC. The steps were as follows: (1) simulate PK profiles of caspofungin; (2) calculate the steady-state $AUC_{0–24\,h}$ using the trapezoidal method; and (3) calculate the PTA under specific MIC settings.

3. Results

3.1. Overview of Included PopPK Studies for Caspofungin

3.1.1. Identification of Included Studies

Figure 1 presents the PRISMA flowchart for study identification. From PubMed, Scopus, Web of Science, and Embase, 26, 150, 185, and 61 studies were retrieved, respectively, with no additional records from other sources. A total of 13 studies were included in our model library for subsequent analysis.

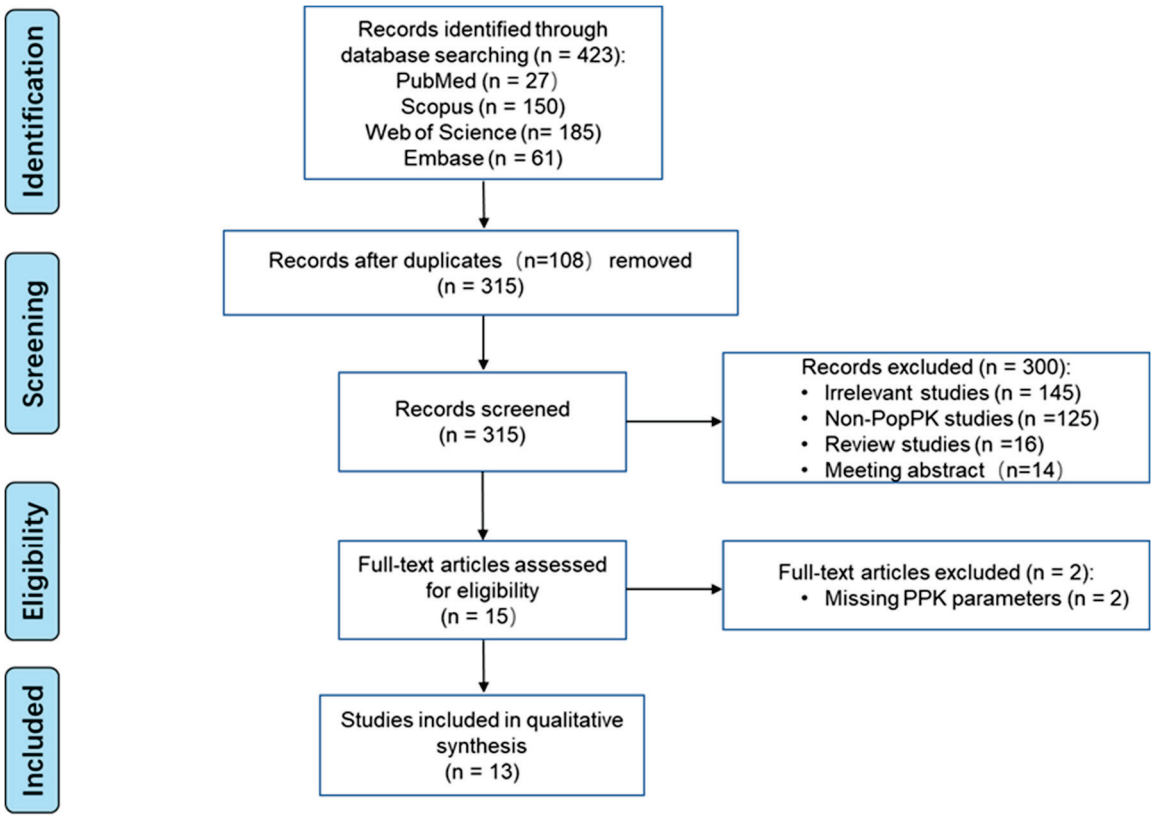


Figure 1. PRISMA flow diagram for the identification of caspofungin population pharmacokinetics (PPK) studies.

3.1.2. Evaluation of Literature

The risk map concerning the bias of the literature is summarized in Figure 2. Two studies lacked a description of PK data in their background sections, and two did not include the sampling schedule. One study did not mention the drug formulation, bioanalytical methods, and the distribution of individual model parameters. None of the included studies detailed the methods of handling missing data, and fewer than 20% of studies reported a specific way of handling the data below the quantification limit. Nevertheless, all studies achieved a compliance rate of 85%, indicating that all studies are of good quality.

3.1.3. Study and PopPK Model Characteristics

The characteristics of each study are summarized in Table 1. All included studies were published from 2011 to 2022, with nine [23–31] being clinical trials and four [11,12,32,33] being observational studies. The total number of participants ranged from 12 to 299 (IQR (19, 48)). Wang et al. [30] and Wu et al. [29] enrolled both patients and healthy subjects, while the others only enrolled invasive candidiasis patients. Three studies enrolled a pediatric population between three months and 18 years, while the rest included adults only. Five studies focused on transplant patients, including allogeneic hematopoietic stem cell transplant [25,32], heart transplant [29], lung transplant [30], and liver transplant [26]. While most studies collected only plasma concentrations, Pressiat et al. [26] collected plasma and peritoneal fluid samples. Sparse sampling strategies were adopted in all three pediatric and two adult studies [23,34], with various bioassay methods used to determine caspofungin concentrations. Despite methodological differences, steady-state plasma concentrations under standard dosing regimens remained above the lowest limits of quantitation (LLOQ, range [0.084–0.6 mg/L]), suggesting their minimal influence on the results.

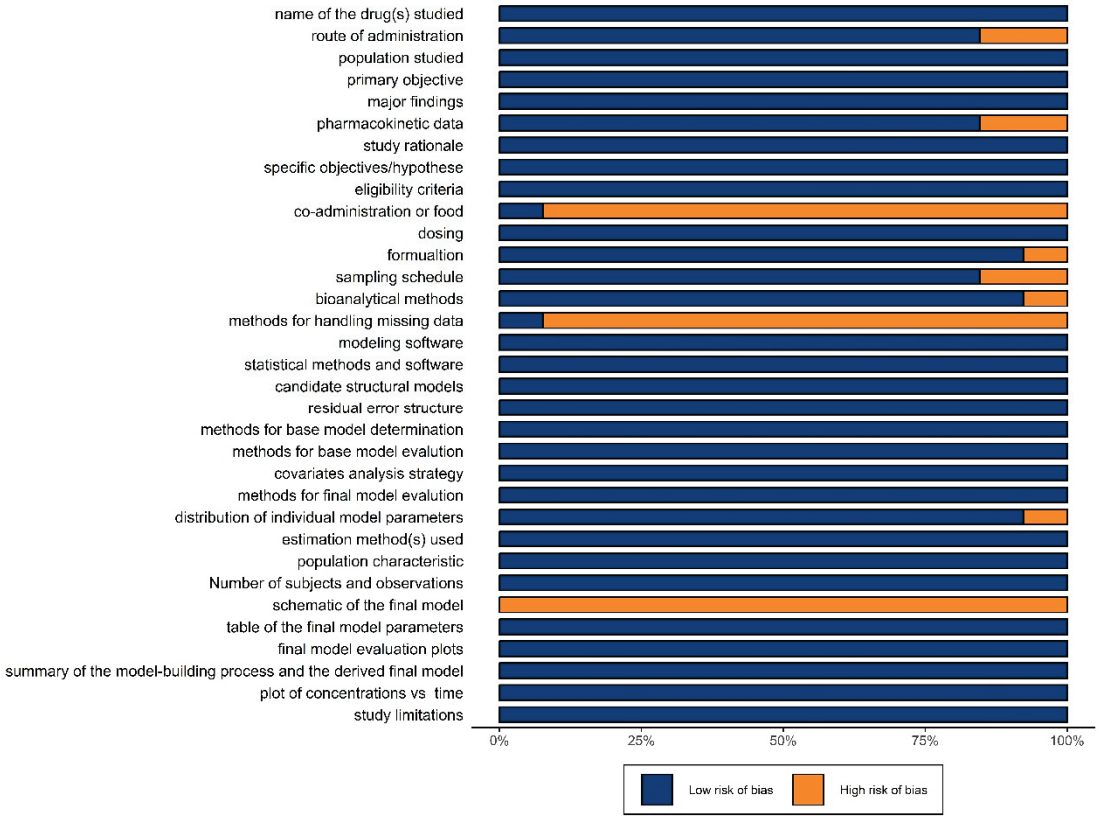


Figure 2. Evaluation of the included population pharmacokinetics studies (the risk bias plot).

The modeling strategies and final PK parameters of the included studies are summarized in Table 2. Ten studies [11,12,23,27–30,32–34] used NONMEM software, with first-order conditional estimation with interaction (FOCE-i) being the most used algorithm [11,12,23,27,28,32–34]. Most studies employed a two-compartment model to describe caspofungin PKs, although two studies [25,34] utilized a one-compartment model due to sparse sampling schedules that may not accurately represent the characteristics of a two-compartment PK model.

All studies incorporated between-subject variability (BSV), with a median of 27.5% (range: 11.8–42.3%) in CL across the 13 studies. Residual unexplained variability was described by proportional [11,23,25–28,31–34], additive [12,30], or combined models [29]. Proportional errors with coefficients of variation ranged from 12.2% to 36% in eleven studies, while three studies [12,29,30] included addictive errors ranging from 0.0941 to 0.73 mg/L. An integration of inter-occasion variability on CL was estimated to be 17.2% and 16.0% in studies by Gastine et al. [33] and Würthwein et al. [28], respectively.

All included popPK models conducted internal validation, including goodness-of-fit tests, a visual predictive check, a predicted–corrected visual predictive check, and normalized prediction distribution error plots. Additionally, ten [11,12,25,27–30,32–34] out of thirteen studies presented results of bootstrap analyses. Würthwein et al. [28] used external validation to further verify their model.

Ten studies [11,12,23,25–27,29,31,33,34] performed Monte Carlo simulations to evaluate existing dosing regimens or optimize caspofungin therapy, comparing different dosage regimens or evaluating caspofungin PKs and drug interaction in specific patient populations. In nine [11,12,23,25,26,29,31,33,34] of these studies, the simulation targeted $AUC_{0–24\,h}$/MIC as the PK/PD. Pressiat et al. [26] concluded that the standard caspofungin dose was sufficient, while five studies [11,12,23,29,34] explicitly advocated for adjusting dosing regimens based on covariates, suggesting higher doses (70–150 mg) considering factors like disease condition, albumin (ALB) levels [29], fungal colony type, and liver function.

Table 1. Characteristics of included population pharmacokinetics studies.

Study (Publication Year)	Country (Type of Study)	Number of Subjects (Male/Female)	Basic Entry Standard	Number of Observation	Sampling Schedule	Age (Years) Mean ± SD Median [Range]	Weight (kg) Mean ± SD Median [Range]	Daily Dose Mean ± SD Median [Range]	Bioassay [LOQ]
Würthwein et al. (2011) [32]	Germany (clinical trial)	19 (11/8)	Adults allo-HSCT recipients, immunocom-promized	239	Day 1 and Day 4: immediately before administration; 0.5 to 1.5 h, 1.5 to 3 h, 3 to 5 h, 5 to 11 h, and 22 to 23 h after administration; Thereafter: random time points twice weekly until the end of treatment	43.4 [20.1–57.6]	71.2 [56–99.2]	70 mg QD on day 1, followed by 50 mg QD, IV infusion over 60 min	HPLC [0.15 mg/L]
Würthwein et al. (2013) [28]	Germany (clinical trial)	46 (21/25)	Adults with invasive Aspergillosis, immunocompro-mized	468	day 1 (immediately prior to dosing and 2 h [peak level], 3 h, 5 to 7 h, and 24 h [trough level] after the start of infusion); peak and trough time points on days 4, 7, 14, 28 h	61 [18–74]	76 [43–104]	70 mg, QD; 100 mg, QD; 150 mg, QD; 200 mg, QD, IV infusion over 120 min	LC-MS/MS [0.084 mg/L]
Pérez-Pitarch et al. (2018) [12]	Spain (clinical trial)	12 (6/6)	Critically ill adults on CVVHD	105	Day 3 and later: predose, 0.5, 1, 1.5, 2, 2.5, 3, 5, 7, 9, 24 h after the start of infusion	73 [56–78]	75 [60–88]	NR	HPLC [NR]
Yang et al. (2019) [27]	France (clinical trial)	48 (28/20)	Children in ICU	159	NR	6.07 ± 2.74 5.09 [2.05–11.77]	22.78 ± 8.71 21 [11.8–47.5]	70 mg/m^2 (loading dose on day 1), 50 mg/m^2 QD.	HPLC/MS [0.25 mg/L]
Wang et al. (2020) [30]	China (clinical trial)	ECMO group 12 (9/3)	Adults on ECMO after LT	271	predose, 0.5, 1, 2, 4, 8, 12, 24 h after the start of the infusion	65 [60–67]	64 [59–69.3]	50 mg QD	UPLC-MS/MS [0.39 mg/L]
		Control group 7 (5/2)	Adult patients never on ECMO after LT			59 [56–62]	65 [53–65]		

Table 1. *Cont.*

Study (Publication Year)	Country (Type of Study)	Number of Subjects (Male/Female)	Basic Entry Standard	Number of Observation	Sampling Schedule	Age (Years) Mean ± SD Median [Range]	Weight (kg) Mean ± SD Median [Range]	Daily Dose Mean ± SD Median [Range]	Bioassay [LOQ]
Bailly et al. (2020) [31]	France (observational study)	13 (10/3)	Adult Patients in ICU with proven or suspected invasive candidiasis	NR	0, 2, 3, 5, 7, 24 h postinfusion	53 [34–55]	76.5 [60–85]	50 mg QD with a 140 mg loading dose, IV infusion over 60 min	LC-MS/MS [0.5 mg/L]
Niu et al. (2020) [25]	China (clinical trial)	48 (31/17)	Children with allo-HSCT	139	an opportunistic sampling strategy	6.58 ± 3.7 [0.61–14]	21.7 ± 10.3 [7.5–54]	loading dose of 70 mg/m^2 followed by 50 mg/m^2	HPLC [0.6 mg/L]
Borsuk-De Moor et al. (2021) [11]	Poland (observational study)	30 (16/14)	ICU patients	180	0.5, 2, 4, 8, 12, 24 h	53 [28–76]	74 [40–150]	70 mg intravenously on the first day and at 50 mg i.v on the consecutive days	HPLC [0.18 µg/mL]
Li et al. (2021) [23]	China (observational study)	42 (31/11)	ICU patients with IFIs	140	1,3,6, 24 h on Day 4	56.82 ± 16.39 [20–88]	59.18 ± 11.40 [41–84.5]	a 70 mg loading dose and a 50 mg maintenance dose	LC-MS/MS [0.2 µg/mL]
Gastine et al. (2022) [33]	Germany (clinical trial)	48 (26/22)	Children aged 3–17	NR	Day 1, Day 4 and Day 9	6 [0–16]	21.5 [9.4–79.5]	CAS I: 1 mg/kg CAS II: 50 mg/m^2 CAS III: 70 mg/m^2 CAS IV: 50 mg/m^2	NR

Table 1. *Cont.*

Study (Publication Year)	Country (Type of Study)	Number of Subjects (Male/Female)	Basic Entry Standard	Number of Observation	Sampling Schedule	Age (Years) Mean ± SD Median [Range]	Weight (kg) Mean ± SD Median [Range]	Daily Dose Mean ± SD Median [Range]	Bioassay [LOQ]
Wu et al. (2022) [29]	China (clinical trial)	HTx group 27 (22/5) non-HTx group 31 (21/10)	27 HTx 31 non-HTx	414	predose, 1, 2, 6, 10, 16, 24 h	HTx group 50 [20–73] Control group 58 [22–78]	HTx group 59.5 [43.5–76] Control group 62 [48–100]	1 h IV infusion at a dose of 50 mg QD after a loading dose of 70 mg	LC-MS/MS [0.4 mg/L]
Pressiat et al. (2022) [26]	France (clinical trial)	20 (9/11)	Adult LT recipients admitted to the liver ICU	395 plasma and 50 PF samples	predose, 1, 2, 4, 8, 12, 24 h D1, D3, D8	45 [40.7–50]	72 [62–81]	A loading dose of 70 mg and then 50 mg per day (or 70 mg per day if the recipient > 80 kg), IV infusion over 1 h	HPLC [0.5 mg/L]
Yang et al. (2022) [34]	China (observational study)	299 (207/92)	Patients who have been diagnosed with confirmed or probable candidiasis	921 plasma samples	C_{min} samples at interval windows of 22–24 h post-dose, other samples at interval windows of 0–12 h and 12–24 h post-dose	44 [18–99]	62.3 [30–100]	1. standard dosage regimen of 70/50 mg; 2. Patients with hepatic insufficiency received 70/35 mg; 3. patients > 75 kg received 70/70 mg	LC-MS [NR]

allo-HSCT: allogeneic hematopoietic stem cell transplantation; ECMO: Extracorporeal membrane oxygenation; HTx: Heart transplantation; IFIs: invasive fungal infections; LT: Liver transplantation; PF: peritoneal fluid; NR: not reported.

Table 2. Modeling strategies and final pharmacokinetics parameters of included studies.

Study (Publication Year)	Software/ Algorithm	Fixed Effect Parameters (RSE)		Between-Subject Variability (%)	Residual Unexplained Variability	Internal Validation	External Validation	Simulation Target	Modeling Application
Würthwein et al. (2011) [32]	NONMEM/ FOCE-I	CL (L/h)	=0.462	25	prop.err = 21%	VPC GOF Bootstrap	NR	NR	Evaluate covariate effects
		V_1 (L)	=8.33	29					
		Q (L/h)	=1.25	/					
		V_2 (L)	=3.59	/					
Würthwein et al. (2013) [28]	NONMEM/ FOCE-I	CL (L/h)	=0.411 × [1 + 0.0102 × (BW-76)]	28.5	prop.err = 14.3%	pcVPC VPC GOF Bootstrap	36/456	NR	Evaluate covariate effects
		V_1 (L)	=5.85 × [1 + 0.0102 × (BW-76)]	28.8					
		Q (L/h)	=0.843	/					
		V_2 (L)	=6.53	66.8					
		IOV(CL)	=0.16	/					
		Cor-CL-V_1	=0.802	/					
Pérez-Pitarch et al. (2018) [12]	NONMEM/ FOCE-I	K_e (h^{-1})	=0.0899	11.8	add.error = 0.0941 mg/L	GOF Bootstrap VPC	NR	AUC/MIC: *C. albicans* 865; *C. glabrata* 450; *C. parapsilosis* 1185; C_{max}/MEC: *Aspergillus* spp. 10–20	Evaluate the efficacy of different dosages
		V_1 (L)	=6.46 × (BW/75) × [1–0.233 × (TP-5.6)]	21.4					
		K_{12} (h^{-1})	=0.494	/					
		K_{21} (h^{-1})	=0.392	/					
Yang et al. (2019) [27]	NONMEM/ FOCE-I	CL (L/h)	=0.165 × (BSA/0.79)$^{1.3}$	24.2	prop.err = 19.6%	GOF VPC NPDEs Bootstrap	NR	C_{min}	Evaluate the efficacy of the dosing regimen; describe PK in a specific population
		V_1 (L)	=1.730 × (BSA/0.79)$^{1.5}$	/					
		Q (L/h)	=0.351	161.6					
		V_2 (L)	=0.943	76.6					

Table 2. *Cont.*

Study (Publication Year)	Software/ Algorithm	Fixed Effect Parameters (RSE)		Between-Subject Variability (%)	Residual Unexplained Variability	Internal Validation	External Validation	Simulation Target	Modeling Application
Wang et al. (2020) [30]	NONMEM/ NR	CL (L/h)	$=0.21 \times (OPT/5)^{1.3}$	20	Add.error = 0.73 mg/L	GOF VPC Bootstrap	NR	NR	Evaluate covariate effects; describe PK in a specific population
		V_1 (L)	$=(2.21 + SEX \times 0.62) \times (OPT/5)^{0.93}$	10					
		V_2 (L)	=2.87	48.0					
		Q (L/h)	$=0.84 \times (SOFA/7)^{1.98}$	/					
Bailly et al. (2020) [31]	Monolix/ SEAM	CL (L/h)	=0.98	42.3	prop.err = 12.2%	GOF VPC	NR	AUC/MIC: 50, 450, 865; C_{max}/MIC 5, 10, 15, 20	Evaluate different dosages
		V_1 (L)	=9.01	42.6					
		Q (L/h)	=5.12	79.9					
		V_2 (L)	=11.9	77.2					
Niu et al. (2020) [25]	Phoenix NLIME	CL (L/h)	$=0.1 \times (BSA/0.79)^{0.89} \times (lnAST/3.38)^{-0.23}$	33.3	prop.err = 26.6%	GOF VPC NPDEs Bootstrap	NR	AUC_{24}/MIC	Dosing optimization against Candida spp.
		V_1 (L)	$=1.36 \times (BSA/0.79)$	32.9					
Borsuk-De Moor et al. (2021) [11]	NONMEM/ FOCE-I	CL (L/h)D1	$=0.563 \times (BW/70)^{0.75}$	24.7	prop.err = 19.9%	pcVPC GOF Bootstrap	NR	AUC_{24}/MIC *C.albicans* 865; *C. glabrata* 450; *C.parapsilosis* 1185	Evaluate covariate effects; describe PK in a specific population
		CL (L/h)D2	$=0.737 * (BW/70)^{0.75}$	24.7					
		CL (L/h)D3	$=1.01 \times (BW/70)^{0.75}$	24.7					
		V_1 (L) D1	$=6.04 \times (BW/70)$	28.6					
		V_1 (L) D2	$=7.32 \times (BW/70)$	28.6					
		V_1 (L) D3	$=7.70 \times (BW/70)$	28.6					
		Q (L/h)	=1.31	/					
		V_2 (L)	=5.13	49.4					
		Cor-CL-V1	=0.868	/					

Table 2. *Cont.*

Study (Publication Year)	Software/ Algorithm	Fixed Effect Parameters (RSE)		Between-Subject Variability (%)	Residual Unexplained Variability	Internal Validation	External Validation	Simulation Target	Modeling Application
Li et al. (2021) [23]	NONMEM/ FOCE-I	CL (L/h)	$= 0.323 \times 0.89 \times (35/ALB)^{1.27}$ (TBIL $\leq$ 22 μmol/L) $= 0.323 \times (35/ALB)^{1.27} \times (TBIL/22)^{0.265}$ (TBIL >22 μmol/L)	22.4	prop.err = 24%	pcVPC GOF NPDEs	NR	AUC_{24}/MIC *C. albicans* 865; *C. glabrata* 450; *C. parapsilosis* 1185	Evaluate covariate effects
		V_1 (L)	$=6.77 \times (WT/70)^{1.08}$	/					
		Q (L/h)	=0.923	/					
		V_2 (L)	=4.58	/					
Gastine et al. (2022) [33]	NONMEM/ FOCE-I	CL (L/h/70 kg)	=0.790	27.5	prop.err = 19.4%	GOF VPC Bootstrap	NR	AUC_{24}/MIC: *C. albicans* 865; *C. glabrata* 450; *C. parapsilosis* 1185; $fAUC_{24}$/MIC: (10–20)	Assess extended twice-weekly dosage using caspofungin
		V_1 (L/70 kg)	=7.75	31.5					
		Q (L/h/70 kg)	=1.20	/					
		V_2 (L/70 kg)	=5.29	15.1					
		IOV(CL)	=17.2%	/					
Wu et al. (2022) [29]	NONMEM/ NR	CL (L/h)	$=0.385 \times (ALB/37.42)^{-1.01}$	33.5	prop.err = 13.4% add.error = 0.213 mg/L	GOF Bootstrap VPC NPDE	NR	AUC_{24}/MIC: *C. albicans* 865; *C. glabrata* 450; *C. parapsilosis* 1185	Evaluate covariate effects
		V_1 (L)	=4.27	67.5					
		Q (L/h)	=2.85	0.0					
		V_2 (L)	=6.01	47.7					

Table 2. *Cont.*

Study (Publication Year)	Software/ Algorithm	Fixed Effect Parameters (RSE)		Between-Subject Variability (%)	Residual Unexplained Variability	Internal Validation	External Validation	Simulation Target	Modeling Application
Pressiat et al. (2022) [26]	Monolix/ FOCE-I	CL (L/h)	=0.38	33.0	prop.err = 36%	GOF pcVPC	NR	$fAUC_{24}$/MIC: *C. albicans* 25.9; *C. glabrata* 13.5; *C. parapsilosis* 35.5	Analyze the PK/PD of caspofungin in a specific population
		V_1 (L)	=6.24	59.0					
		Q (L/h)	=2.58	/					
		V_2 (L)	=6.44	107.0					
		$K_{eff,13}$	=0.08	54					
		$K_{eff,31}$	=0.26	/					
Yang et al. (2022) [34]	NONMEM/ FOCE-I	CL (L/h)	=0.32 × (1 + 0.46 × ALB*) × (1 + 0.98 × WT*) (ALB* = 1, ALB < 35 g/L; ALB* = 0, ALB ≥ 35 g/L; WT* = 1, WT ≥ 70 kg, WT* = 0, WT< 70 kg)	29.2	prop.err = 19.3%	Bootstrap GOF pcVPC	NR	$fAUC_{24}$/MIC *C. albicans* 20; *C. glabrata* 7; *C. parapsilosis* 7	Evaluate covariate effects; describe PK in a specific population
		V_1 (L)	=13.31 × (1 + 0.49 × ALB*) × (1 + 0.24 × WT*) (ALB* = 1, ALB < 35 g/L; ALB* = 0, ALB ≥ 35 g/L; WT* = 1, WT ≥ 70 kg, WT* = 0, WT< 70 kg)	59.2					

CL: clearance; Q: intercompartmental clearance; V_1: central volume of distribution; V_2: peripheral volume of distribution.

Niu et al. [25] concluded that the current recommended dose of caspofungin was sufficient for pediatric patients and did not require higher doses. Gastine et al. [33] reported that a twice-weekly extended dosing regimen of 200 mg/m^2, with a maximal total dose of 200 mg, should yield comparable average weekly exposures to the approved daily-dosing regimen. Additionally, Yang et al. [27] included BSA as a significant covariate on both CL and V_d, supporting the adoption of a BSA-based dosing regimen.

3.2. Overview of PopPK Model Library

3.2.1. Comparison of Caspofungin PK Profiles

Simulated caspofungin concentration–time profiles are displayed in Figure S1. A comprehensive comparison of all simulated PK parameters for caspofungin is shown in Figure 3. The median C_{max} values of children (23.56 mg/L) and infants (25.65 mg/L) were higher than that of adults (8.75 mg/L), likely due to the lower V_d in children and infants (adults vs. pediatric population: [2.21–9.01 L] vs. [1.36–2.21 L]). Moreover, the pediatric population demonstrated a higher CL per kilogram than adults, with weight-normalized median CL values of 0.0083 L/h/kg (range: 0.005–0.011 L/h/kg) and 0.0086 L/h/kg (range: 0.006–0.011 L/h/kg) for children and infants, respectively, compared to 0.0061 L/h/kg (range: 0.003–0.014 L/h/kg) in adults.

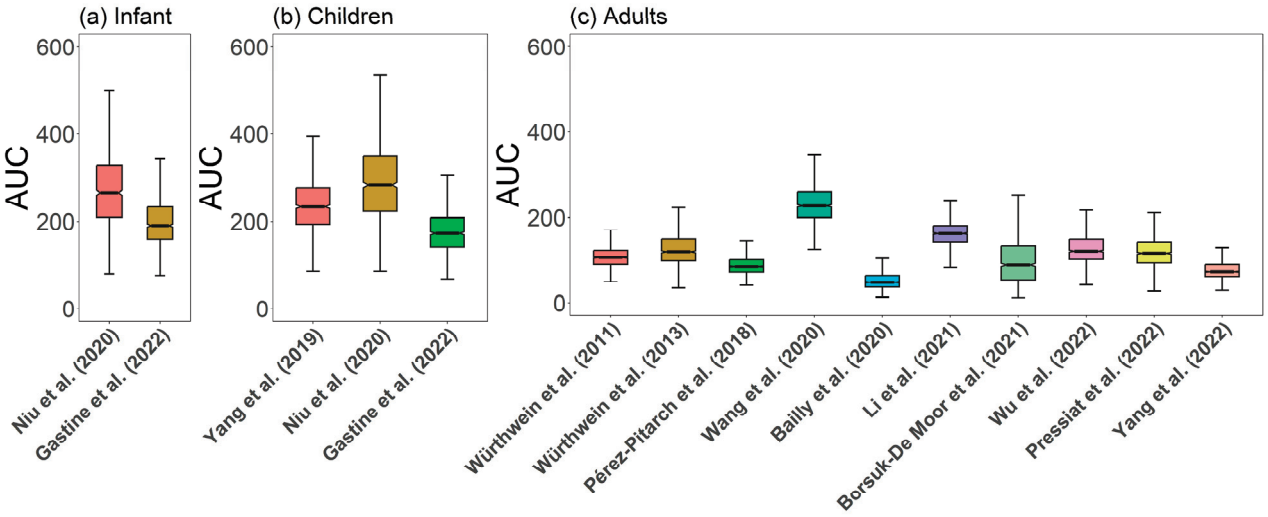


Figure 3. Caspofungin main pharmacokinetic parameter (AUC) at steady state of (**a**) infants, (**b**) children, and (**c**) adults. Virtually all patients were assumed to be male and received caspofungin at a dose of 70 mg on the first day, followed by 50 mg once a day as an infusion for 1 h for adults and 70 mg/m^2 on the first day, followed by 50 mg/m^2 once a day as an infusion for 1 h for infants and children [11,12,25–34].

In the pediatric population, three studies [25,27,33] displayed similar PK characteristics in both infants and children. Among adult patients, Wang et al. [30] reported higher AUC and C_{max} than other studies under the same dosage regimen, while Bailly et al. [31] showed much lower exposure. However, the remaining eight studies showed similar PK profiles despite variations in patients' disease conditions (Figure S1). The subjects in Wang et al.'s study [30] were lung transplantation recipients receiving ICU follow-up treatment, exhibiting lower CL and V_d.

3.2.2. Covariate Screening and Influence Analysis

All tested covariates that affected CL, V_d, intercompartment clearance (Q), and the distribution volume of the peripheral compartment (V_p) are summarized in Table 3. The stepwise covariate screening included forward inclusion and backward elimination. A comparison of identified and investigated covariates is presented in Figure 4.

Table 3. Investigated and identified covariates in population pharmacokinetic models of included studies.

Study (Publication Year)	Tested Covariates			Covariate Selection Criteria		Significant Covariates			
	Demographic	Laboratory Tests	Co-Administration	Forward Inclusion	Backward Elimination	CL	V1	Q	V2
Würthweinet al. (2011) [32]	Sex, Age, Weight, BSA	TBIL, CLCR	Liposomal amphotericin B	$p < 0.001$	$p < 0.001$	NR	NR	NR	NR
Würthwein et al. (2013) [28]	Dose, Sex, Age, Weight	TBIL, CLCR	NR	$p < 0.05$	$p < 0.01$	Weight	Weight	NR	NR
Pérez-Pitarch et al. (2018) [12]	Age, Sex, Weight	TP, SCR, TBIL, CLCR	NR	$p < 0.05$	$p < 0.01$	NR	Weight, TP	NR	NR
Yang et al. (2019) [27]	Age, Weight, BSA	SCR, ALB	NR	NR	$p < 0.05$	BSA	BSA	NR	NR
Wang et al. (2020) [30]	Age, Sex, Weight, BMI, ECMO, OPT, 24 h fluid balance	SOFA, ALT, AST, ALB, TBIL, CLCR, PCT	NR	$p < 0.05$	$p < 0.01$	OPT	Sex	SOFA	NR
Bailly et al. (2020) [31]	Age, Weight, ECMO	ALB, PAL, TBIL, AST, ALT, SCR, SOFA	NR	NR	NR	NR	NR	NR	NR
Niu et al. (2020) [25]	BSA, Weight,	CR, eGFR, ALB, TBIL, DBIL, ALT, AST, γ-GT	NR	$p < 0.05$	$p < 0.01$	BSA, AST	BSA	NR	NR
Borsuk-De Moor et al. (2021) [11]	Age, Weight, Height, Sex, ECMO, CRRT, Survival, dose	SOFA, PCT, UF, ELWI, Cardiac Output, ALB, TP, Liver Failure	NR	NR	$p < 0.01$	NR	NR	NR	NR
Li et al. (2021) [23]	Sex, Age, Weight	ALT, AST, TBIL, ALB, CLCR	NR	$p < 0.05$	$p < 0.01$	ALB, TBIL	Weight	NR	NR
Gastine et al. (2022) [33]	Weight, Age, BSA, Sex, Race	ALB, CLCR	Acyclovir, Vancomycin, Dexamethasone	$p < 0.05$	$p < 0.01$	Weight	Weight	Weight	Weight
Wu. et al. (2022) [29]	Age, Sex, Weight, Height, BMI, ECMO, CRRT	ALB, CLCR, AST, ALT, DBIL, TBIL, PCT, PLT, SCR, TP	NR	$p < 0.05$	$p < 0.001$	ALB	NR	NR	NR
Pressiat et al. (2022) [26]	Age, Sex, Weight, BMI	ALB, TP, TBIL, SCR, CLCR, SOFA, WBC, CRP, MELD, PT	NR	$p < 0.05$	NR	NR	NR	NR	NR
Yang et al. (2022) [34]	Weight, CMT, SOP, SOT, ICU	ALB, MM, CYC, MET	NR	$p < 0.05$	$p < 0.001$	Weight, ALB	Weight, ALB	NR	NR

BMI: body mass index; BSA: body surface area (calculated according to the formula of Mosteller); ALB: albumin; eGFR: the estimated glomerular filtration rate; CLCR: creatinine clearance (determined according to the formula of Cockcroft and Gault); SCR: serum creatinine; PCT: procalcitonin; TP: total protein; TBIL: total bilirubin; DBIL: direct bilirubin; Hb: hemoglobin; AST: aspartate aminotransferase; ALT: alanine aminotransferase; PAL: phenylalanine ammonia-lyase; ECMO: extracorporeal membrane oxygenation; CRRT: continuous renal replacement therapy; SOFA: sequential organ failure assessment; OPT: operative time; ELWI, extravascular lung water index; UF: ultrafiltration rate; PLT: platelet; WBC: leukocyte count; CRP: C-reactive protein; MELD: model for end-stage liver disease; PT: prothrombin time; HT: heart transplantation; NR: not reported.

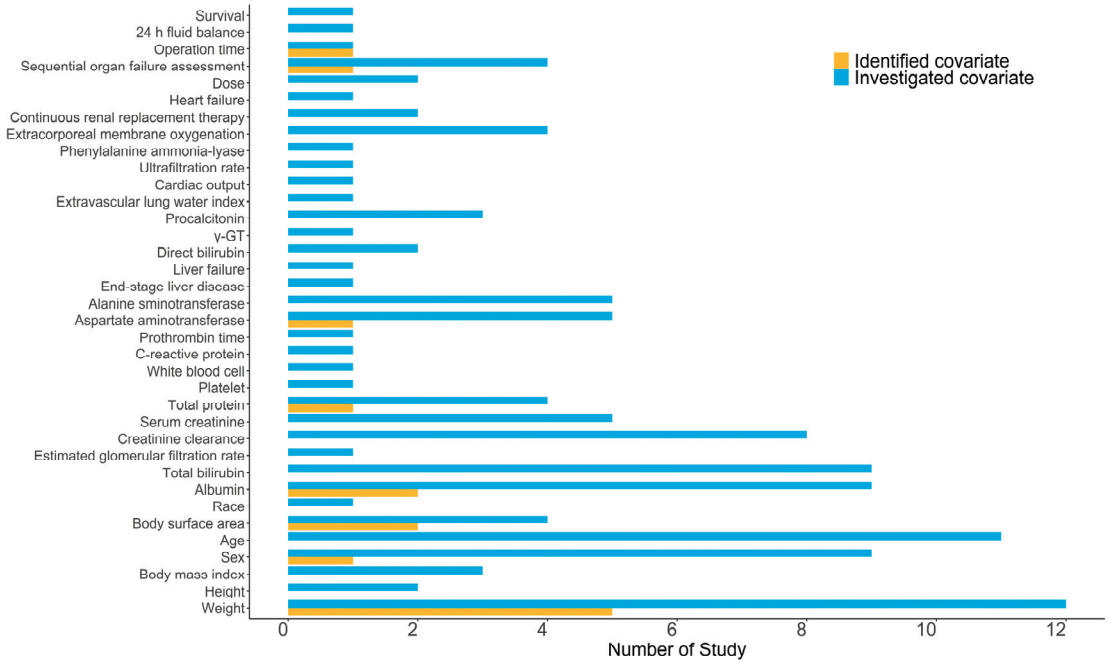


Figure 4. A histogram of the amount of investigated and identified covariates in included studies.

Four studies [11,26,31,32] did not include any covariates, likely contributing to the high consistency of the included patients. The most influential covariate was body size, such as body weight and BSA. Three [15,19,34] studies (23.1%) found body weight closely related to CL, and five studies [12,23,28,33,34] (38.5%) indicated its impact on V_d. Yang et al. [27] and Niu et al. [25] identified BSA as a crucial covariate that affects both CL and V_d. Moreover, three studies [23,29,34] confirmed ALB level as a significant covariate affecting CL. In their final model, Niu et al. [26] and Li et al. [24] included the liver function biomarker as a covariate. Interestingly, among the studies including pediatric populations, two [25,27] identified BSA as a significant covariate on CL and V_d, supporting dosing based on BSA. Würthwein et al. [28] found that the PK of caspofungin was not altered by the coadministration of liposomal amphotericin B. Three studies [11,29,30] investigating the difference in PK characteristics in patient groups who had received continuous renal replacement therapy (CRRT) or extracorporeal membrane oxygenation (ECMO) concluded that these factors had no significant effect.

Identified covariates on CL and V_d were visualized using the forest map in Figure 5. Figure 5A highlights BSA as a pivotal determinant of CL in children, with weight significantly influencing CL in adult and pediatric populations. The impact of body size measures exceeds the conventional range (80–125%), suggesting considerable CL variability. Despite variations in covariates across studies due to different populations, the profound influence of body size on caspofungin CL remains consistent. Compared to the reference value, six [12,23,25,27,29,33] out of the seven studies demonstrated a significant impact of body size on V_d with changes greater than 20% under the normal range of body size. Additionally, two studies [12,27] showed the influence of ALB to exceed a 20% change in V_d within the normal range. Wang et al. found that male gender was associated with increased caspofungin V_d (Figure 5B). Li et al. [23] and Niu et al. [25] showed liver function to have changes over 20% under a wide range of liver functions. Three studies [23,29,34] included ALB as a significant covariate affecting CL, with changes exceeding 20% within the normal range of the ALB level.

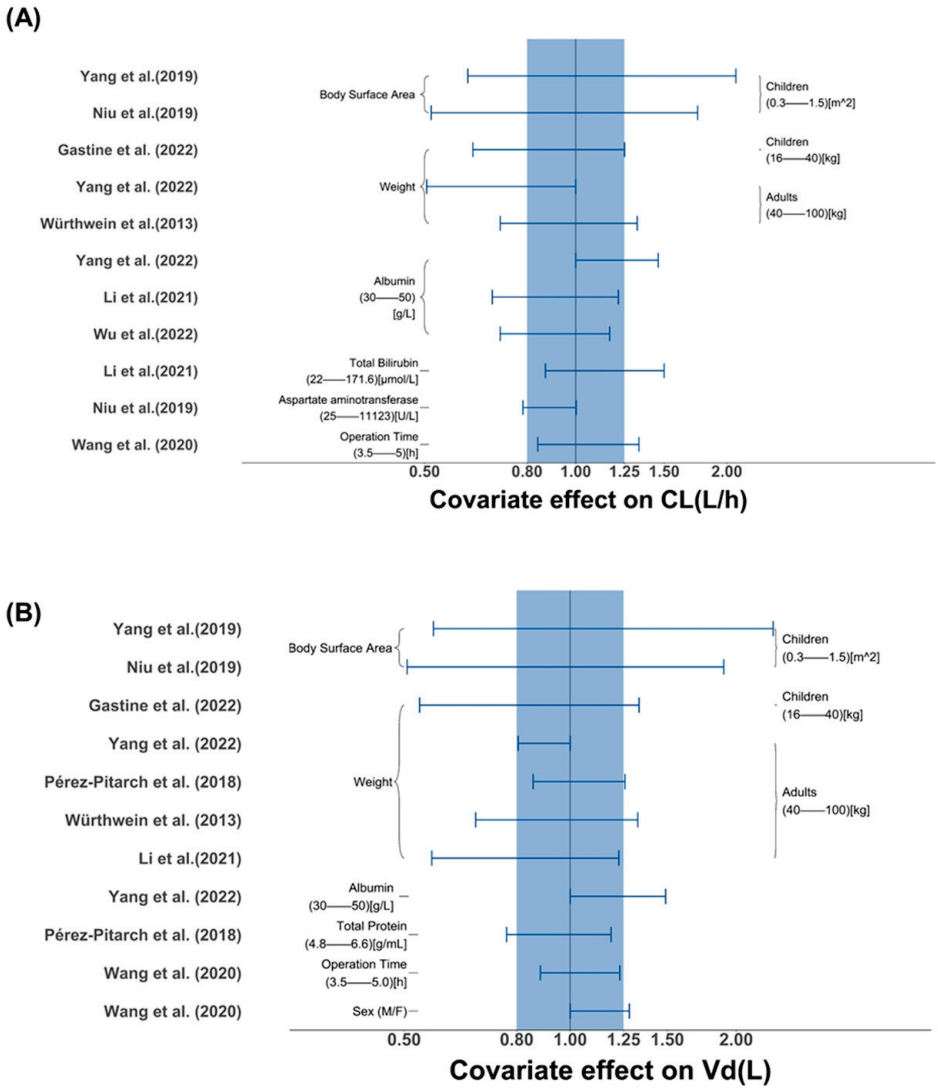


Figure 5. (**A**) The effect of covariates on CL (L/h) of caspofungin in included studies. (**B**) The effect of covariates on V_d (L) of caspofungin in included studies. The horizontal bars represent the covariate effect on clearance in each study. The typical value of clearance in each study was considered to be 1. The effect of each covariate for clearance is displayed by the ratio of clearance in the range of each covariate to the typical clearance value. The shaded area ranges from 0.8 to 1.25 [23,25–30,33,34].

3.3. Model Library Applications

In our model library, 77% of studies incorporated AUC/MIC as the PK/PD target for simulation. The simulated PTA for each published popPK model was assessed with three Candida strains, the results of which are presented in Figure 6. For *C. albicans* (MIC = 0.25 mg/L) and *C. parapsilosis* (MIC = 2 mg/L), none of the populations achieved a PTA of ≥90%. However, for *C. glabrata* (MIC = 0.12 mg/L), 70% of studies focused on adults reached a PTA of ≥90%, while all pediatric patients achieved a PTA of ≥90%. The PTA results suggested that caspofungin may be underexposed in adult patients, indicating the necessity of basing drug dosage on the Candida strains' results and the corresponding MIC value.

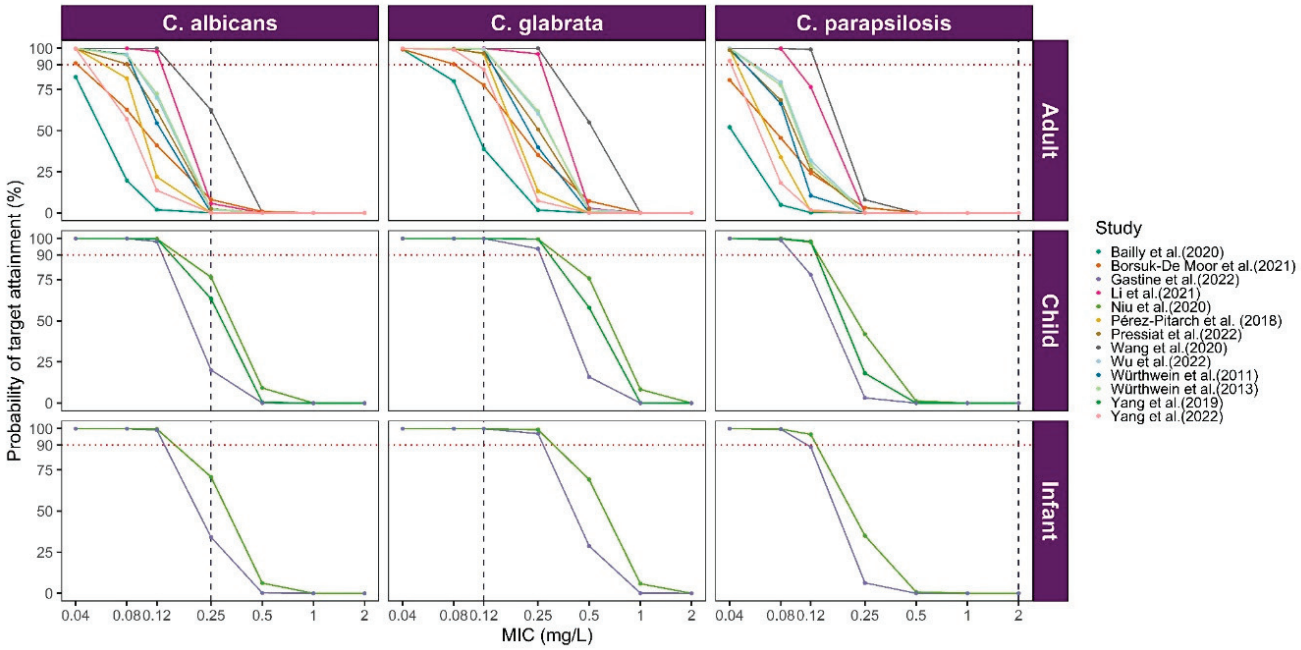


Figure 6. The probability target achievement of caspofungin in included studies. The red dashed line represents a 90% target attainment rate, while the three vertically oriented dashed lines of different colors correspond to the respective clinical breakpoints for MICs of each fungus [11,12,25–34].

4. Discussion

Numerous PK studies on caspofungin have been conducted recently, with several popPK studies aiming to explain PK variability. To our knowledge, this study was the first to build and share a parametric popPK model library of caspofungin. The library is characterized by simulations of concentration–time profiles and covariate effect assessments, where we demonstrated the potential of the constituent models in estimating the AUC, C_{max}, and PTA of caspofungin. This work provides evidence for advocating individualized dosing not only based on body size but also potential covariates such as liver function and hypoalbuminemia.

4.1. Pediatric Patients

The PKs of caspofungin vary substantially among pediatric patients. All three pediatric studies within the model library consistently applied allometric scaling, aligning with the standard pediatric dosing approach that utilizes body surface area as the basis for medication administration. Children showed higher CL (L/h/kg) than adults per kilogram, possibly due to differences in distribution rates into hepatic tissue. In vitro data suggested the involvement of uptake transporters, such as OATP1B1, in caspofungin tissue distribution, particularly in hepatic uptake [35]. Studies [24,36,37] suggested that factors like accelerated liver uptake, larger liver-to-body ratios, and increased hepatic blood flow contribute to heightened caspofungin CL in infants and toddlers. However, conflicting findings exist regarding age-dependent differences in hepatic OATP1B1 expression and its impact on caspofungin uptake. Thomson et al. reported no age-dependent differences in hepatic OATP1B1 expression across pediatric groups. Sáez-Llorens et al. [38] suggested that caspofungin CL increases from infancy to childhood and then decreases through adolescence into adulthood. Pediatric patients generally exhibit higher CL (L/h) and V_d (L) compared to adults under standard dosing regimens, attributed to factors such as reduced blood flow, higher body fat-to-lean mass ratios, and decreased total body water. These physiological and pathological distinctions, particularly pronounced in infants, can significantly influence caspofungin's absorption, distribution, metabolism, and excretion.

Findings from included studies indicated that adjusting the caspofungin daily dose based on BSA, rather than weight, might be more reasonable in pediatric patients. Three studies [25,27,33] focused on children with a median age of around six years used body size for allometric scaling; one included weight, and two studies included BSA. Gastine et al. (48 subjects) estimated weight-normalized CL and V_d, implicitly assuming the power of 1 for the impact of weight on CL and V_d. Niu et al. (48 subjects, 139 observations) showed that the power of BSA on CL was estimated to be 0.89 (RSE 11.36%), and the power of BSA on V_d was fixed to 1, respectively. In Yang et al. (48 subjects, 159 observations), the power of BSA on CL and V_d was estimated to be 1.3 (RSE 13.8%) and 1.5 (RSE 13.5%). Overall, the body size metrics have positive correlations with CL and V_d. Due to the under-power design of the study [39], the slight deviations in the estimated exponents from the theoretical allometric relationship should be interpreted with caution.

Sáez-Llorens et al. [38] found that a BSA-based dosage of 25 mg/m^2 QD in neonates under three months achieved plasma concentration profiles similar to adults receiving a standard 50 mg daily dose [38]. However, PK variability was higher in pediatric patients with a lower body weight, necessitating individualized dose adjustments. Beyond BSA-based dosing, considering blood biochemical parameters and physiological conditions, such as serum ALB level, hepatic function, and blood flow, is crucial. Caspofungin is occasionally used in very low-birth-weight infants, but PK data for this group are scarce [40]. This scarcity emphasizes the necessity for large-scale, prospective trials to establish caspofungin's efficacy, safety, optimal dosage, and role in neonatal candidiasis, particularly in infants under three months with a very low birth weight.

4.2. Adult Patients

Insufficient drug exposure is common with the labeled dosing regimen in adult patients. In this model library, five of the ten adult studies proposed increasing the dosage of caspofungin to achieve target exposure levels. Caspofungin dosing differences exist between adults and children. Lower adult dosages correspond to lower drug concentrations over time compared to children (Figure S1), indicating a need for dosing strategy improvement. In patients with normal liver and kidney function, hypoalbuminemia can result in elevated levels of unbound drugs, potentially leading to an increased CL, especially in highly protein-bound antibiotics like caspofungin. Additionally, as a hydrophilic drug, caspofungin's V_d may increase due to fluid shifts and extensive fluid resuscitation [41,42].

Critically ill patients often present with concomitant conditions such as obesity, hepatic impairment, and specific infusion regimens, contributing to the high BSV of caspofungin PKs [43]. Treatment modalities like ECMO and CRRT are frequently employed in ICU settings. Studies have yielded conflicting results regarding the impact of ECMO on caspofungin CL, with one study [30] suggesting an increase and another [31] finding no discernible effect, likely due to caspofungin's high solubility in water and methanol. Critically ill patients exhibit lower caspofungin exposure compared to healthy subjects [5]. Betts et al. supported a wide safety margin for caspofungin, allowing for higher-dose therapy up to 150 mg daily if clinically indicated [44]. However, arguments against reducing caspofungin doses in critically ill patients with hypoalbuminemia and abnormal liver function suggest that a uniform, flat dosing strategy may not be optimal [45]. Consensus leans towards the importance of therapeutic drug monitoring in critically ill patients with hypoalbuminemia, with or without abnormal liver function, or in cases where strains with elevated minimum inhibitory concentrations need to be addressed.

Borsuk-De Moor et al. [11] noted a time-varying CL of caspofungin in ICU patients: 0.563 L/h on day 1, 0.737 L/h on day 2, and 1.01 L/h on day 3, respectively. This escalating CL may decrease AUC and impair efficacy, but few models considered time-dependent variables. The extended monitoring of caspofungin therapy is recommended for personalized medication optimization.

4.3. Towards Precision Dosing

The model library of caspofungin popPK models developed in this study has the potential to accelerate the implementation of MIPD. Leveraging our model library, researchers could rapidly perform external validations on their data, efficiently selecting the most appropriate model for local use, thereby speeding up individualized dosing [46]. Integration with the "PopED" package further enhances its utility by allowing the selection of published library models as prior information for clinical trial design.

However, translating preclinical PK/PD targets into clinical benchmarks remains challenging. Investigations into the MIC of caspofungin are notably limited, chiefly attributable to the challenges in cultivating fungus, the extended duration of experimental procedures, and an inadequate favorable return on investment. Notably, a recurring theme across studies is the lack of well-established clinical PK/PD targets, leading to reliance on preclinical counterparts. CLSI guidelines specify MIC breakpoints for *Candida* spp. in vitro broth dilution tests, but significant differences in MICs among bacterial species underscore the importance of bacterial culture in clinical practice. In our model library about adults, PK/PD cut-off values vary for *C. albicans*, *C. glabrata*, and *C. parapsilosis*. These findings suggest significant variability in establishing caspofungin cut-off values across populations, posing challenges for clinicians and researchers in determining optimal dosing strategies. For caspofungin, the current target values are derived from preclinical studies and are in urgent need of confirmation through clinical research.

Disparities in PK profiles between pediatric and adult populations highlight the need for further research. The pediatric and adult populations exhibit marked disparities in PK profiles, particularly with much higher caspofungin exposure levels observed in children compared to adults, up to 1.5 times greater with standard dosing regimens. This discrepancy may stem from two potential reasons: differences in the PK/PD relationship between children and adults and the need to optimize the current dosing regimen, suggesting either dose increases for adults or decreases for children. However, due to limited research in pediatric populations, further PK/PD studies in this population are essential to elucidate the underlying causes.

Additionally, assessing the concentration of the free drug is essential, as only the unbound form exerts therapeutic effects, though this aspect is often overlooked in studies of caspofungin. Reduced plasma protein levels in vitro were found to increase the antifungal activity of caspofungin and lower the pharmacodynamic target AUC_{total}/MIC, likely by increasing the free concentration [47]. However, none of the included studies measured free caspofungin concentrations. In cases where $fAUC_{0–24\,h}$/MIC was employed as the PK/PD target, it was calculated based on the total AUC/MIC target and caspofungin's plasma protein binding rate of 97%.

4.4. Limitations

Our research has certain limitations. Firstly, due to the limited number of studies involving pediatric patients, we were unable to comprehensively investigate and compare the PK of children and infants. Furthermore, as this model library focused on summarizing significant covariates influencing caspofungin PKs and comparing popPK modeling across different age groups, we only replicated the published models to align with our study objectives and the characteristics of the medications under investigation. Additionally, PK/PD targets for PTA calculation were derived from in vitro data provided by CLSI, which may lead to discrepancies in PTA accuracy due to the absence of in vivo studies in humans. Finally, our study was restricted to the English-language literature, potentially omitting relevant studies published in other languages.

5. Conclusions

The model library of parametric population pharmacokinetic models for caspofungin is helpful in promoting model-informed precise dosing. The optimization of the caspofungin dosing regimen should consider the patient's liver function and hypoproteinemia.

Additionally, prospective PK/PD studies of caspofungin in pediatrics are warranted to elucidate the exposure–response relationship associated with this medication.

Supplementary Materials: The following supporting information can be downloaded at: https://www.mdpi.com/article/10.3390/pharmaceutics16060819/s1, Figure S1: The steady-state concentration-time profiles of piperacillin for (a) infants, (b) children, and (c) adults when infused intermittently. The solid line represents median of the simulated concentration-time profile. The light shadows represent the 10th–90th percentiles of the simulated concentration-time profiles. All virtual patients were assumed to be male received caspofungin at a dose of 70 mg on the first day, followed by 50 mg once a day as infusion for 1 h for adults and 70 mg/m^2 on the first day, followed by 50 mg/m^2 once a day as infusion for 1h for infants and children. Figure S2: Check List.

Author Contributions: Conceptualization and methodology, N.X., Y.S. and X.Z.; data curation, W.M. and Y.W. (Yixue Wang); software and validation, W.Y., Q.H. and Y.W. (Yixue Wang); formal analysis, N.X. and Y.S.; investigation, W.M. and K.W.N.; visualization, N.X., Y.W. (Yue Wu) and W.Y.; resources, Z.T., Y.W. (Yue Wu), X.X., Q.H. and G.Y.; writing—original draft preparation, N.X. and Y.S.; writing—review and editing, W.M., K.W.N., Y.W. (Yue Wu), Z.T., G.Y. and X.X.; project administration, Z.T. and X.X.; supervision, Q.H., G.Y., X.X. and X.Z.; funding acquisition, X.Z. All authors have read and agreed to the published version of the manuscript.

Funding: Y.W. (Yixue Wang) received research funding from the National Key Research and Development Program of China (2021YFC2701800, 2021YFC2701805). X.Z. received research funding from the Shanghai Municipal Health Commission Clinical Research Youth Project (No. 20224Y0121), the Hunan Key Laboratory for Bioanalysis of Complex Matrix Samples (FZJZ-202305), the National Natural Science Foundation of China (No. 82204544), and the Fudan University Scientific Research Foundation for Talented Scholars (No. JIF301052).

Institutional Review Board Statement: Not applicable.

Informed Consent Statement: Not applicable.

Data Availability Statement: The data generated during and/or analyzed during the current study are available from the published literature.

Acknowledgments: The authors would like to thank Meng Gu from Fudan University for their critical comments and suggestions regarding the data visualization.

Conflicts of Interest: The authors declare no conflicts of interest.

References

1. Pappas, P.G.; Kauffman, C.A.; Andes, D.R.; Clancy, C.J.; Marr, K.A.; Ostrosky-Zeichner, L.; Reboli, A.C.; Schuster, M.G.; Vazquez, J.A.; Walsh, T.J.; et al. Clinical Practice Guideline for the Management of Candidiasis: 2016 Update by the Infectious Diseases Society of America. *Clin. Infect. Dis.* **2016**, *62*, e1–e50. [CrossRef] [PubMed]
2. Hope, W.W.; Castagnola, E.; Groll, A.H.; Roilides, E.; Akova, M.; Arendrup, M.C.; Arikan-Akdagli, S.; Bassetti, M.; Bille, J.; Cornely, O.A.; et al. ESCMID* guideline for the diagnosis and management of Candida diseases 2012: Prevention and management of invasive infections in neonates and children caused by *Candida* spp. *Clin. Microbiol. Infect.* **2012**, *18* (Suppl. S7), 38–52. [CrossRef] [PubMed]
3. HIGHLIGHTS OF PRESCRIBING INFORMATION for CANCIDAS-Merck. Available online: https://www.accessdata.fda.gov/drugsatfda_docs/label/2021/021227Orig1s040lbl.pdf (accessed on 17 September 2023).
4. Sinnollareddy, M.G.; Roberts, J.A.; Lipman, J.; Akova, M.; Bassetti, M.; De Waele, J.J.; Kaukonen, K.M.; Koulenti, D.; Martin, C.; Montravers, P.; et al. Pharmacokinetic variability and exposures of fluconazole, anidulafungin, and caspofungin in intensive care unit patients: Data from multinational Defining Antibiotic Levels in Intensive care unit (DALI) patients Study. *Crit. Care* **2015**, *19*, 33. [CrossRef] [PubMed]
5. van der Elst, K.C.; Veringa, A.; Zijlstra, J.G.; Beishuizen, A.; Klont, R.; Brummelhuis-Visser, P.; Uges, D.R.; Touw, D.J.; Kosterink, J.G.; van der Werf, T.S.; et al. Low Caspofungin Exposure in Patients in Intensive Care Units. *Antimicrob. Agents Chemother.* **2017**, *61*, e01582-16. [CrossRef] [PubMed]
6. van Vianen, W.; de Marie, S.; ten Kate, M.T.; Mathot, R.A.; Bakker-Woudenberg, I.A. Caspofungin: Antifungal activity in vitro, pharmacokinetics, and effects on fungal load and animal survival in neutropenic rats with invasive pulmonary aspergillosis. *J. Antimicrob. Chemother.* **2006**, *57*, 732–740. [CrossRef]
7. Ambrose, P.G.; Bhavnani, S.M.; Rubino, C.M.; Louie, A.; Gumbo, T.; Forrest, A.; Drusano, G.L. Pharmacokinetics-pharmacodynamics of antimicrobial therapy: It's not just for mice anymore. *Clin. Infect. Dis.* **2007**, *44*, 79–86. [CrossRef]

8. Wiederhold, N.P.; Kontoyiannis, D.P.; Chi, J.; Prince, R.A.; Tam, V.H.; Lewis, R.E. Pharmacodynamics of caspofungin in a murine model of invasive pulmonary aspergillosis: Evidence of concentration-dependent activity. *J. Infect. Dis.* **2004**, *190*, 1464–1471. [CrossRef]
9. Louie, A.; Deziel, M.; Liu, W.; Drusano, M.F.; Gumbo, T.; Drusano, G.L. Pharmacodynamics of caspofungin in a murine model of systemic candidiasis: Importance of persistence of caspofungin in tissues to understanding drug activity. *Antimicrob. Agents Chemother.* **2005**, *49*, 5058–5068. [CrossRef] [PubMed]
10. Andes, D.; Diekema, D.J.; Pfaller, M.A.; Bohrmuller, J.; Marchillo, K.; Lepak, A. In vivo comparison of the pharmacodynamic targets for echinocandin drugs against Candida species. *Antimicrob. Agents Chemother.* **2010**, *54*, 2497–2506. [CrossRef]
11. Borsuk-De Moor, A.; Sysiak-Sławecka, J.; Rypulak, E.; Borys, M.; Piwowarczyk, P.; Raszewski, G.; Onichimowski, D.; Czuczwar, M.; Wiczling, P. Nonstationary Pharmacokinetics of Caspofungin in ICU Patients. *Antimicrob. Agents Chemother.* **2020**, *64*, e00345-20. [CrossRef]
12. Pérez-Pitarch, A.; Ferriols-Lisart, R.; Aguilar, G.; Ezquer-Garín, C.; Belda, F.J.; Guglieri-López, B. Dosing of caspofungin based on a pharmacokinetic/pharmacodynamic index for the treatment of invasive fungal infections in critically ill patients on continuous venovenous haemodiafiltration. *Int. J. Antimicrob. Agents* **2018**, *51*, 115–121. [CrossRef] [PubMed]
13. Sheiner, L.B.; Beal, S.; Rosenberg, B.; Marathe, V.V. Forecasting individual pharmacokinetics. *Clin. Pharmacol. Ther.* **1979**, *26*, 294–305. [CrossRef] [PubMed]
14. Page, M.J.; McKenzie, J.E.; Bossuyt, P.M.; Boutron, I.; Hoffmann, T.C.; Mulrow, C.D.; Shamseer, L.; Tetzlaff, J.M.; Akl, E.A.; Brennan, S.E.; et al. The PRISMA 2020 statement: An updated guideline for reporting systematic reviews. *BMJ* **2021**, *372*, n71. [CrossRef] [PubMed]
15. Liu, X.; Ju, G.; Yang, W.; Chen, L.; Xu, N.; He, Q.; Zhu, X.; Ouyang, D. Escitalopram Personalized Dosing: A Population Pharmacokinetics Repository Method. *Drug Des. Devel. Ther.* **2023**, *17*, 2955–2967. [CrossRef] [PubMed]
16. Jamsen, K.M.; McLeay, S.C.; Barras, M.A.; Green, B. Reporting a population pharmacokinetic-pharmacodynamic study: A journal's perspective. *Clin. Pharmacokinet.* **2014**, *53*, 111–122. [CrossRef] [PubMed]
17. Kanji, S.; Hayes, M.; Ling, A.; Shamseer, L.; Chant, C.; Edwards, D.J.; Edwards, S.; Ensom, M.H.; Foster, D.R.; Hardy, B.; et al. Reporting Guidelines for Clinical Pharmacokinetic Studies: The ClinPK Statement. *Clin. Pharmacokinet.* **2015**, *54*, 783–795. [CrossRef] [PubMed]
18. Fancher, K.M.; Sacco, A.J.; Gwin, R.C.; Gormley, L.K.; Mitchell, C.B. Comparison of two different formulas for body surface area in adults at extremes of height and weight. *J. Oncol. Pharm. Pract.* **2016**, *22*, 690–695. [CrossRef] [PubMed]
19. Li, Z.R.; Wang, C.Y.; Zhu, X.; Jiao, Z. Population Pharmacokinetics of Levetiracetam: A Systematic Review. *Clin. Pharmacokinet.* **2021**, *60*, 305–318. [CrossRef]
20. Lewis, R.E. Current concepts in antifungal pharmacology. *Mayo Clin. Proc.* **2011**, *86*, 805–817. [CrossRef]
21. Ernst, E.J.; Klepser, M.E.; Ernst, M.E.; Messer, S.A.; Pfaller, M.A. In vitro pharmacodynamic properties of MK-0991 determined by time-kill methods. *Diagn. Microbiol. Infect. Dis.* **1999**, *33*, 75–80. [CrossRef]
22. CLSI. *Performance Standards for Antifungal Susceptibility Testing of Yeasts*; CLSI: Berwyn, PA, USA, 2022.
23. Li, F.; Zhou, M.; Jiao, Z.; Zou, Z.; Yu, E.; He, Z. Caspofungin pharmacokinetics and probability of target attainment in ICU patients in China. *J. Glob. Antimicrob. Resist.* **2021**, *25*, 238–263. [CrossRef] [PubMed]
24. Mori, M.; Imaizumi, M.; Ishiwada, N.; Kaneko, T.; Goto, H.; Kato, K.; Hara, J.; Kosaka, Y.; Koike, K.; Kawamoto, H.; et al. Pharmacokinetics, efficacy, and safety of caspofungin in Japanese pediatric patients with invasive candidiasis and invasive aspergillosis. *J. Infect. Chemother.* **2015**, *21*, 421–426. [CrossRef] [PubMed]
25. Niu, C.H.; Xu, H.; Gao, L.L.; Nie, Y.M.; Xing, L.P.; Yu, L.P.; Wu, S.L.; Wang, Y. Population Pharmacokinetics of Caspofungin and Dosing Optimization in Children with Allogeneic Hematopoietic Stem Cell Transplantation. *Front. Pharmacol.* **2020**, *11*, 184. [CrossRef] [PubMed]
26. Pressiat, C.; Ait-Ammar, N.; Daniel, M.; Hulin, A.; Botterel, F.; Levesque, E. Pharmacokinetics/Pharmacodynamics of Caspofungin in Plasma and Peritoneal Fluid of Liver Transplant Recipients. *Antimicrob. Agents Chemother.* **2022**, *66*, e0118721. [CrossRef] [PubMed]
27. Yang, X.M.; Leroux, S.; Storme, T.; Zhang, D.L.; de Beaumais, T.A.; Shi, H.Y.; Yang, Y.L.; Wang, X.L.; Zhao, W.; Jacqz-Aigrain, E. Body Surface Area-Based Dosing Regimen of Caspofungin in Children: A Population Pharmacokinetics Confirmatory Study. *Antimicrob. Agents Chemother.* **2019**, *63*, e00248-19. [CrossRef] [PubMed]
28. Würthwein, G.; Cornely, O.A.; Trame, M.N.; Vehreschild, J.J.; Vehreschild, M.J.; Farowski, F.; Müller, C.; Boos, J.; Hempel, G.; Hallek, M.; et al. Population pharmacokinetics of escalating doses of caspofungin in a phase II study of patients with invasive aspergillosis. *Antimicrob. Agents Chemother.* **2013**, *57*, 1664–1671. [CrossRef] [PubMed]
29. Wu, Z.; Lan, J.; Wang, X.; Wu, Y.; Yao, F.; Wang, Y.; Zhao, B.X.; Wang, Y.; Chen, J.; Chen, C. Population Pharmacokinetics of Caspofungin and Dose Simulations in Heart Transplant Recipients. *Antimicrob. Agents Chemother.* **2022**, *66*, e0224921. [CrossRef] [PubMed]
30. Wang, Q.; Zhang, Z.; Liu, D.; Chen, W.; Cui, G.; Li, P.; Zhang, X.; Li, M.; Zhan, Q.; Wang, C. Population Pharmacokinetics of Caspofungin among Extracorporeal Membrane Oxygenation Patients during the Postoperative Period of Lung Transplantation. *Antimicrob. Agents Chemother.* **2020**, *64*, e00687-20. [CrossRef]

31. Bailly, S.; Gautier-Veyret, E.; Lê, M.P.; Bouadma, L.; Andremont, O.; Neuville, M.; Mourvillier, B.; Sonneville, R.; Magalhaes, E.; Lebut, J.; et al. Impact of Loading Dose of Caspofungin in Pharmacokinetic-Pharmacodynamic Target Attainment for Severe Candidiasis Infections in Patients in Intensive Care Units: The CASPOLOAD Study. *Antimicrob. Agents Chemother.* **2020**, *64*, e01545-20. [CrossRef]
32. Würthwein, G.; Young, C.; Lanvers-Kaminsky, C.; Hempel, G.; Trame, M.N.; Schwerdtfeger, R.; Ostermann, H.; Heinz, W.J.; Cornely, O.A.; Kolve, H.; et al. Population pharmacokinetics of liposomal amphotericin B and caspofungin in allogeneic hematopoietic stem cell recipients. *Antimicrob. Agents Chemother.* **2012**, *56*, 536–543. [CrossRef]
33. Gastine, S.; Hempel, G.; Neely, M.N.; Walsh, T.J.; Groll, A.H. Pharmacokinetic modelling of caspofungin to develop an extended dosing regimen in paediatric patients. *J. Antimicrob. Chemother.* **2022**, *77*, 2209–2216. [CrossRef]
34. Yang, Q.; Zhang, T.; Zhang, Y.; Sun, D.; Zheng, X.; Du, Q.; Wang, X.; Cheng, X.; Xing, J.; Dong, Y. The recommended dosage regimen for caspofungin in patients with higher body weight or hypoalbuminaemia will result in low exposure: Five years of data based on a population pharmacokinetic model and Monte-Carlo simulations. *Front. Pharmacol.* **2022**, *13*, 993330. [CrossRef] [PubMed]
35. Sandhu, P.; Lee, W.; Xu, X.; Leake, B.F.; Yamazaki, M.; Stone, J.A.; Lin, J.H.; Pearson, P.G.; Kim, R.B. Hepatic uptake of the novel antifungal agent caspofungin. *Drug Metab. Dispos.* **2005**, *33*, 676–682. [CrossRef] [PubMed]
36. Stader, F.; Wuerthwein, G.; Groll, A.H.; Vehreschild, J.J.; Cornely, O.A.; Hempel, G. Physiology-based pharmacokinetics of caspofungin for adults and paediatrics. *Pharm. Res.* **2015**, *32*, 2029–2037. [CrossRef] [PubMed]
37. Walsh, T.J.; Adamson, P.C.; Seibel, N.L.; Flynn, P.M.; Neely, M.N.; Schwartz, C.; Shad, A.; Kaplan, S.L.; Roden, M.M.; Stone, J.A.; et al. Pharmacokinetics, safety, and tolerability of caspofungin in children and adolescents. *Antimicrob. Agents Chemother.* **2005**, *49*, 4536–4545. [CrossRef] [PubMed]
38. Sáez-Llorens, X.; Macias, M.; Maiya, P.; Pineros, J.; Jafri, H.S.; Chatterjee, A.; Ruiz, G.; Raghavan, J.; Bradshaw, S.K.; Kartsonis, N.A.; et al. Pharmacokinetics and safety of caspofungin in neonates and infants less than 3 months of age. *Antimicrob. Agents Chemother.* **2009**, *53*, 869–875. [CrossRef] [PubMed]
39. Sinha, J.; Al-Sallami, H.S.; Duffull, S.B. Choosing the Allometric Exponent in Covariate Model Building. *Clin. Pharmacokinet.* **2019**, *58*, 89–100. [CrossRef] [PubMed]
40. Fortmann, I.; Hartz, A.; Paul, P.; Pulzer, F.; Müller, A.; Böttger, R.; Proquitté, H.; Dawczynski, K.; Simon, A.; Rupp, J.; et al. Antifungal Treatment and Outcome in Very Low Birth Weight Infants: A Population-based Observational Study of the German Neonatal Network. *Pediatr. Infect. Dis. J.* **2018**, *37*, 1165–1171. [CrossRef]
41. Roch, A.; Woloch, C.; Blayac, D.; Solas, C.; Quaranta, S.; Mardelle, V.; Castanier, M.; Papazian, L.; Sampol-Manos, E. Effect of fluid loading during hypovolaemic shock on caspofungin pharmacokinetic parameters in pig. *Crit. Care* **2011**, *15*, R219. [CrossRef]
42. Roberts, J.A.; Abdul-Aziz, M.H.; Lipman, J.; Mouton, J.W.; Vinks, A.A.; Felton, T.W.; Hope, W.W.; Farkas, A.; Neely, M.N.; Schentag, J.J.; et al. Individualised antibiotic dosing for patients who are critically ill: Challenges and potential solutions. *Lancet Infect. Dis.* **2014**, *14*, 498–509. [CrossRef]
43. Gasperetti, T.; Welte, R.; Oberacher, H.; Marx, J.; Lorenz, I.; Schellongowski, P.; Staudinger, T.; Burgmann, K.; Eller, P.; Santner, T.; et al. Penetration of echinocandins into wound secretion of critically ill patients. *Infection* **2021**, *49*, 747–755. [CrossRef] [PubMed]
44. Betts, R.F.; Nucci, M.; Talwar, D.; Gareca, M.; Queiroz-Telles, F.; Bedimo, R.J.; Herbrecht, R.; Ruiz-Palacios, G.; Young, J.A.; Baddley, J.W.; et al. A Multicenter, double-blind trial of a high-dose caspofungin treatment regimen versus a standard caspofungin treatment regimen for adult patients with invasive candidiasis. *Clin. Infect. Dis.* **2009**, *48*, 1676–1684. [CrossRef] [PubMed]
45. Kurland, S.; Furebring, M.; Löwdin, E.; Eliasson, E.; Nielsen, E.I.; Sjölin, J. Pharmacokinetics of Caspofungin in Critically Ill Patients in Relation to Liver Dysfunction: Differential Impact of Plasma Albumin and Bilirubin Levels. *Antimicrob. Agents Chemother.* **2019**, *63*, e02466-18. [CrossRef] [PubMed]
46. Liu, X.; Ju, G.; Huang, X.; Yang, W.; Chen, L.; Li, C.; He, Q.; Xu, N.; Zhu, X.; Ouyang, D. Escitalopram population pharmacokinetics and remedial strategies based on CYP2C19 phenotype. *J. Affect. Disord.* **2024**, *346*, 64–74. [CrossRef]
47. Kurland, S.; Löwdin, E.; Furebring, M.; Shams, A.; Chryssanthou, E.; Lagerbäck, P.; Tängden, T.; Breuer, O.; Sjölin, J. Human plasma protein levels alter the in vitro antifungal activity of caspofungin: An explanation to the effect in critically ill? *Mycoses* **2022**, *65*, 79–87. [CrossRef]

Disclaimer/Publisher's Note: The statements, opinions and data contained in all publications are solely those of the individual author(s) and contributor(s) and not of MDPI and/or the editor(s). MDPI and/or the editor(s) disclaim responsibility for any injury to people or property resulting from any ideas, methods, instructions or products referred to in the content.

pharmaceutics

MDPI

Article

Development of a Population Pharmacokinetic Gabapentin Model Leveraging Therapeutic Drug Monitoring Concentrations

Firas Al-Zubaydi [1,2], Andrew Wassef [3], Leonid Kagan [3,4] and Luigi Brunetti [1,3,4,5,*]

[1] Department of Pharmacy Practice, Ernest Mario School of Pharmacy, Rutgers, The State University of New Jersey, 160 Frelinghuysen Road, Piscataway, NJ 08854, USA; firas.jawad@copharm.uobaghdad.edu.iq
[2] Department of Pharmaceutics, College of Pharmacy, University of Baghdad, Baghdad 10071, Iraq
[3] Department of Pharmaceutics, Ernest Mario School of Pharmacy, Rutgers, The State University of New Jersey, 160 Frelinghuysen Road, Piscataway, NJ 08854, USA; awassef@scarletmail.rutgers.edu (A.W.); lkagan@pharmacy.rutgers.edu (L.K.)
[4] Center of Excellence in Pharmaceutical Translational Research and Education, Ernest Mario School of Pharmacy, Rutgers, The State University of New Jersey, Piscataway, NJ 08854, USA
[5] Robert Wood Johnson University Hospital Somerset, 110 Rehill Avenue, Somerville, NJ 08876, USA
* Correspondence: brunetti@pharmacy.rutgers.edu; Tel.: +1-848-445-6815

Abstract: Background/Objectives: Gabapentin has variable pharmacokinetics (PK), which contributes to difficulty in dosing and increased risk of adverse events. The objective of this study was to leverage gabapentin concentrations from therapeutic drug monitoring (TDM) to develop a population PK (popPK) model and characterize significant covariates that impact gabapentin PK. **Methods:** Data were retrospectively collected from 82 hospitalized adult patients with TDM gabapentin concentrations. Renal function indicators (i.e., estimated glomerular filtration rate, creatinine clearance, acute kidney injury), body weight parameters (i.e., actual body weight, ideal body weight, adjusted body weight, lean body weight, body mass index, obesity status), fasting plasma glucose levels, and diagnosis of type 2 diabetes were tested as potential covariates. A popPK model was developed in MONOLIX (2020R1, Lixoft, France). **Results**: A one-compartment model best described gabapentin PK with first-order absorption, dose-dependent bioavailability, first-order elimination, and no lag time. Population parameter estimates for the volume of distribution (V_d), and clearance (Cl) were 44.61 L, and 5.73 L/h, respectively. Serum creatinine was a significant covariate on Cl. **Conclusions**: The popPK model highlights the importance of renal function in the interindividual variability of gabapentin PK and suggests that diabetes and body weight parameters have no impact on gabapentin PK. Moreover, our study supports the utility of leveraging data obtained from clinical TDM for popPK model development.

Keywords: gabapentin; gamma-aminobutyric acid; population pharmacokinetics; therapeutic drug monitoring; creatinine

1. Introduction

Gabapentin [1-(aminomethyl)-cyclohexane acetic acid] is an antiepileptic drug with analgesic properties. The drug was first approved by the Food and Drug Administration (FDA) in 1993 [1]. Gabapentin is indicated to treat partial-onset seizures and postherpetic neuralgia and is often used off-label for the treatment of diabetic neuropathy [1–4]. As a structural analog of gamma-aminobutyric acid (GABA), gabapentin was designed to be more lipophilic than GABA and cross the blood–brain barrier more readily [1,5]. The precise mechanism of gabapentin's antileptic and analgesic effects is currently unknown [1]. Gabapentin is actively absorbed in the gut via the L-amino acid transporter system [5–7]. Food has minimal effects on the rate and extent of its absorption [1,5,6]. Gabapentin is largely unbound to plasma proteins [1]. Peak plasma concentration (C_{max}) is achieved within 2–3 h after oral administration. Plasma concentrations are dose-proportional across

typical clinical ranges (300 mg to 400 mg every 8 h), ranging between 1 μg/mL and 10 μg/mL, but are less than dose-proportional at higher dose levels (>600 mg every 8 h) [5–7]. Gabapentin does not undergo metabolism by liver enzymes and is excreted renally as an unchanged drug with a half-life of 5–7 h [1,5–7].

The high interindividual variability of gabapentin pharmacokinetics (PK) contributes to difficulty in reaching effective doses and an increased risk of adverse events [6–10]. The total daily dose of gabapentin is correlated with incidence rates of side effects such as dizziness and somnolence, which negatively impacts patient adherence to therapy [10]. Therefore, identifying covariates that impact gabapentin PK can help guide dose selection and improve the safety and tolerance of gabapentin.

Diabetes mellitus may lead to alterations in drug PK, but there is limited clinical guidance for dosage adjustment in this patient population [11,12]. One of the complications of diabetes is the delayed gastric emptying time; therefore, the absorption rate of orally administered medication may be changed [12]. About 32–47% of untreated patients with type 2 diabetes experience delayed gastric emptying [13].

Theoretically, drugs with carrier-mediated transporter systems are more sensitive to longer gut transit time than drugs absorbed via passive diffusion [11]. Another long-term sequelae of diabetes is altered renal functions, with normal or increased glomerular filtration rate (GFR) during the first five to ten years of the disease and significantly reduced GFR as diabetic nephropathy progresses [11,12,14]. Nephropathy is present in up to 20–40% of patients with diabetes [14]. The volume of distribution can also be altered in patients with diabetes. Chronic hyperglycemia can lead to protein glycation and changing concentration in the circulating free fatty acids, leading to consequent changes in the fraction of unbound drugs [11,12]. The volume of distribution also correlates with the degree of obesity, a common comorbidity in patients with type 2 diabetes [15].

Previous publications have consistently highlighted biomarkers for renal function as a significant covariate on the oral clearance of gabapentin. Creatinine clearance (CrCl) was reported to be linearly correlated with the apparent oral clearance of gabapentin [5,16,17]. Gabapentin elimination is affected directly by age- or disease-related decreases in renal function [6]. However, there is no consensus regarding the effect of diabetes and obesity on gabapentin PK. Ouellet et al. suggested that body weight is a significant covariate on the volume of distribution of gabapentin in the pediatric population. In contrast, other PK studies performed in the adult population did not include body weight in the final model [16,18–20]. A non-compartmental analysis (NCA) by Costa et al. reported that patients with type 2 diabetes exhibited decreased gabapentin C_{max}, increased clearance, and increased volume of distribution compared with the control group [21]. Costa et al. later developed a popPK model, which showed no significant effect of diabetes or hyperglycemia on the PK profile of gabapentin [19]. The paucity in the literature and the conflicting results indicate a need to better characterize covariates for gabapentin PK.

Moreover, previous models were developed using data collected in prospective controlled studies with frequent sampling, which can be resource-intensive. On the other hand, clinical therapeutic drug monitoring (TDM) levels are readily available and may allow for the development of popPK models without additional blood sampling [22,23]. Clinicians have frequently employed TDM to optimize treatment for drugs with a poor correlation between dose and clinical efficacy and in special patient populations with altered PK [24,25]. Patients with diabetes and obese individuals have been proposed to be beneficiaries of TDM [26–28]. This study aimed to develop a popPK model of gabapentin disposition using real-life clinical TDM data and to evaluate the effect of covariates, including diabetes and obesity status, on pharmacokinetic parameters.

2. Methods

2.1. Study Population and Data Collection

The study protocol was approved by the investigational review boards of Rutgers University and Robert Wood Johnson University Hospital Somerset (RWJS), New Jersey,

USA. Data were retrospectively collected from patients with available TDM gabapentin concentrations. Serum gabapentin concentrations were extracted from the electronic health records of all consecutive patients from 1 January 2009 to 7 December 2023. The study included all adult patients (≥18 years) who had received at least one oral dose of gabapentin after admission and had at least one plasma concentration collected after the dose. Pregnant patients and children (<18 years) were excluded. Patients were either taking gabapentin at home or initiated on gabapentin during the hospital stay. The medical indication for gabapentin was not available in the dataset but represents a random general population. The date and time of gabapentin administration before the sample collection and the time of sample collection were recorded. Patients' demographic and clinical characteristics were collected for covariate analysis (Table 1). Lean body weight was calculated using the Janmahasatian equation [29]. Estimated glomerular filtration rate (eGFR) was calculated using the Modification of Diet in Renal Disease (MDRD) equation [30]. Obesity was defined by a body mass index (BMI) of greater than or equal to 30 kg/m^2. The diagnosis of type 2 diabetes was determined based on the admission notes.

Table 1. Demographic and clinical characteristics of individuals included in the analysis (n = 82).

		Mean ± SD	Range
Age (year)		65.7 ± 16.4	22–93
Actual body weight (kg)		84.3 ± 25.9	44.2–195.0
Ideal body weight (kg)		59.9 ± 10.3	43.2–82.2
Adjusted body weight (kg)		69.7 ± 14.3	45.0–123.0
Lean body weight (kg) [a]		54.9 ± 13.4	30.5–91.9
Height (cm)		167.1 ± 9.8	149.9–187.9
BMI (kg/m^2)		30.0 ± 7.9	18–60
Serum creatinine (0.66–1.25 mg/dL)		1.3 ± 1.0	0.4–3.8
eGFR ($mL/min/1.73m^2$) [b]		71.0 ± 42.4	16.0–127
Creatinine clearance (mL/min) [c]		91.67 ± 67.6	13.3–192.7
Fasting plasma glucose (mg/dL)		127.6 ± 78.2	76.0–251.0
Serum concentration (μg/mL)		7.97 ± 7.8	0.6–56.2
ALT (0–49 U/L)		30.8 ± 41.6	8.0–245.0
AST (17–59 U/L)		30.9 ± 44.4	6.0–74.0
Total bilirubin (0.2–1.3 mg/dL)		0.57 ± 0.7	0–2.7
Albumin (3.5–5 g/dL)		3.7 ± 0.7	1.4–4.6
		Median	Range
Single dose amount (mg) [d]		300	100–1200
Total daily dose (mg) [e]		900	100–2700
		n (%)	
Sex	Male	31 (37.8)	
	Female	51 (62.2)	
Race	White	73 (89.0)	
	Asian	1 (1.2)	
	Black	6 (7.3)	
	Other	2 (2.4)	
Type 2 diabetes	Yes	26 (31.7)	
Presence of AKI [f]	Yes	18 (21.9)	
Obesity [g]	Yes	18 (22.0)	

Table 1. *Cont.*

Combined covariate of obesity and diabetes	Obesity + diabetes	8 (9.8)
	Obesity only	22 (26.8)
	"Healthy"	52 (63.4)

ALT: Alanine aminotransferase; AKI: acute kidney injury; AST: aspartate aminotransferase; BMI: body mass index; eGFR: estimated glomerular filtration rate; SD: standard deviation. [a] Lean body weight was calculated using the Janmahasatian formula. [b] eGFR was calculated using the Modification of Diet in Renal Disease (MDRD) equation. [c] Creatinine clearance was calculated with the Cockcroft–Gault formula. The weight factor was adjusted to ideal body weight when the actual body weight was greater or equal to 30% of the ideal body weight. [d] Single-dose amount was defined by the last given dose. [e] Total daily dose was defined by the accumulated total dose over the past 24 h prior to the sample collection. [f] Acute kidney injury was defined by a change in serum creatinine of more than 0.3 mg/dL in the past 48 h. [g] Obesity was defined by BMI $\geq$ 30.

2.2. Bioanalytical Methods

Plasma gabapentin concentrations were quantitated under a service agreement between the medical center and the Mayo Clinical Laboratory using a liquid chromatography–tandem mass spectrometry method [31]. The laboratory determined the assay's performance characteristics to be consistent with Clinical Laboratory Improvement Amendments requirements. The reference range was determined to be 2.0–20.0 μg/mL with a concentration of $\geq$25 μg/mL being considered the toxic concentration.

2.3. Population Pharmacokinetic Analysis

A popPK model was developed in MONOLIX (2020R1, Lixoft, Antony, France) using the stochastic approximation expectation maximization (SAEM) algorithm. The model-building process involves identifying a structural model, optimizing the error model, and assessing covariates.

A one-compartment model with linear elimination was used to describe the disposition of gabapentin, and different absorption models were evaluated, including first-order absorption with or without lag time (T_{lag}) and transit compartment absorption models (Table 2). Both linear and nonlinear bioavailability models were tested for first-order absorption models. The following equation was applied to describe dose-dependent bioavailability, and the parameters were fixed to previously published values [20]:

$$F = \frac{D_{max}}{D_{50} + Dose} \quad (1)$$

where F is gabapentin bioavailability, D_{max} (823 mg/day) is the maximal absorption rate, D_{50} (1120 mg/day) is the dose when the absorption process is 50% saturated, and *Dose* is the last gabapentin dose before the sample collection [20]. Initial values for the population parameters were set to previously reported values. The limited number of concentrations obtained during the absorption phase can undoubtedly cause high variability with the population estimate for the absorption rate constant (k_a) and the delay time (T_{lag}). Therefore, values of 0.778 h^{-1} and 0.31 h were considered as fixed values for k_a and T_{lag}, respectively [16,32]. Models were evaluated based on the likelihood results (i.e., objective function value (OFV), Akaike information criterion (AIC), and Bayesian information criterion (BIC)), relative standard errors (RSEs) of parameters, visual examinations (i.e., visual predictive check (VPC), observation versus prediction plot), and model stability. Structural model stability was assessed in five convergence assessment runs using the SAEM algorithm. Estimated population parameters with high variability were fixed to improve model stability. A constant error model was selected based on the proposal created by MONOLIX.

Table 2. Final model population parameter estimates and bootstrap analysis.

Parameters	Population Estimates (RSEs (%))	Bootstrap Analysis Median (95%CI)
Fixed effects		
k_a (h^{-1})	0.778 (fixed)	0.778 (fixed)
V_d (L)	44.61 (15.94)	45.99 (32.84–65.91)
Cl (L/h)	5.73 (17.62)	7.01 (4.3–12.54)
β_{Cl_SCR}	−0.89 (16.94)	−1.12 ((−1.66)–(−0.58))
Random effects		
ω_{Vd}	0.77 (19.98)	0.75 (0.42–1.07)
ω_{Cl}	0.28 (28.59)	0.26 (0.11–0.48)
Error model parameter		
a	2.03 (17.5)	1.93 (1.1–2.65)

Cl: Clearance; k_a: absorption rate constant; RSE: relative standard error; V_d: volume of distribution; a: constant error model; ω: standard deviation.

Both continuous and categorical covariates were assessed in the covariate model. Continuous covariates include age, body weight parameters (i.e., actual body weight (WT), ideal body weight (IBW), adjusted body weight (ABW), lean body weight (LBW), BMI), renal function indicators (i.e., eGFR, CrCl, SCr), and fasting plasma glucose levels (FPG). The serum creatinine value from the day of gabapentin concentration collection was used to calculate renal function indicators. Categorical covariates include sex, diagnosis of type 2 diabetes, presence of acute kidney injury (AKI), obesity status, and a combined covariate of obesity and diabetes (i.e., patients were categorized into diabetic but not obese, obese but metabolically healthy, both diabetic and obese, and non-diabetic and non-obese). All continuous covariates were log-transformed and centered using mean values. Covariates were selected based on three clinical questions in the following order: the effects of renal function on the clearance (Cl), the effects of body size metric on the apparent volume of distribution (V_d), and the effects of diabetes on absorption rate constant (k_a) and V_d. After all the covariates relevant to the clinical questions were tested, any additional covariates that were significantly correlated ($p \leq 0.01$) with random effects were tested. The covariate was added if the addition of a covariate yielded a reduction of 3.84 or greater in the OFV ($p \leq 0.05$) and if the resulting β coefficient was significantly ($p \leq 0.01$) different from 0 (based on the Wald test and correlation test). Once all covariates were added, a backward deletion was performed. The model retained a covariate if the deletion increased by 6.63 in the OFV ($p \leq 0.01$). VPC, goodness-of-fit plots, RSE, and likelihood results were also used to assess the best model. A bootstrap analysis with 1000 replicates was applied to validate the stability and robustness of the final popPK model.

3. Results

3.1. Participants

A total of 123 gabapentin TDM concentrations from 108 patients were available. Gabapentin TDM concentrations ranged from 0.6 to 56.2 μg/mL (7.97 ± 7.8, mean ± SD). Out of 108 patients, 82 fit the inclusion and exclusion criteria, and their plasma concentrations were used to build the popPK model. The study population was predominantly white, with an average age of 65.7 years and an average BMI of 30 (Table 1). Eighteen (22%) patients had a BMI of greater than 30 and were thus considered obese. Twenty-six (31.7%) patients had a diagnosis of type 2 diabetes. The cohort with diabetes had a higher BMI, higher body weight, higher FPG, lower eGFR, and were older. A total of 18 (21.9%) patients experienced AKI within 48 h of the sample collection. Single gabapentin dosages ranged from 100 mg to 1200 mg (median, 300 mg).

3.2. Population Pharmacokinetic Modeling

A one-compartment model with first-order absorption, no lag time, nonlinear bioavailability, and linear elimination provided a good description of the data and, therefore, was selected as the base structural model. Other potential absorption models were tested but did not provide a significant improvement (Table S1). Moreover, most of the study population received a dose equal to or less than 400 mg, during which dose-proportionality was established [6]. Due to the lower number of concentrations in the dataset, especially in the drug's absorption phase, a simple first-order absorption model with a fixed absorption rate constant (k_a) value (0.778 h^{-1}) was selected over other more complex absorption models. The dose-dependent bioavailability model decreased by 10.98 in OFV when compared with the dose-independent bioavailability model (496.44 versus 507.42), and it was selected as the superior model (Table S1).

Because dose adjustment of gabapentin depends on the patient's renal function, the first step was to assess the effect of renal function on gabapentin clearance. CrCl, SCr, eGFR, and the presence of AKI were tested separately as a covariate on Cl. SCr was selected as a significant covariate on Cl (Table S2). Next, the effect of obesity or body weight on V_d was assessed: WT, IBW, ABW, LBW, BMI, and obesity status were tested separately. None of the covariates resulted in a statistically significant drop in OFV and, therefore, were not included in the model. After that, a diagnosis of diabetes, FPG, and the combined covariate of obesity and diabetes status were tested separately as covariates on k_a and V_d. Similarly, none of the covariates resulted in a statistically significant drop in OFV and, therefore, were not included in the model. After adding SCr to the model, no additional covariates were significantly ($p \leq 0.01$) correlated with random effects.

Population parameter estimates for V_d and Cl were 44.61 L and 5.73 L/h, respectively (Table 2). SCr was included as a significant covariate on Cl. Goodness-of-fit plots showed alignment between observed and predicted gabapentin concentrations (Figure 1A). Individual conditional weighted residuals (IWRESs) were normally distributed and centered around zero (Figure 1B). Plots of IWRESs against time and concentration were evenly centered around zero. Despite the decrease in the model's predictability at low gabapentin concentrations and early time points, the final popPK model demonstrated acceptable adequacy (Figure 1B). As shown in Table 2, the bootstrap analysis resulting from 1000 replicates of the final popPK model validates acceptable robustness and precision. Shrinkage was <5% for all parameters. VPC also demonstrated that simulated data are consistent with observed data (Figure 1C).

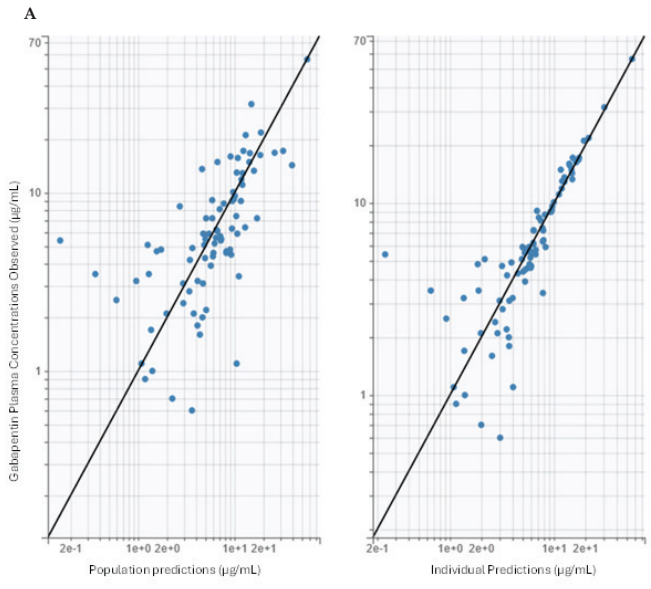


Figure 1. *Cont.*

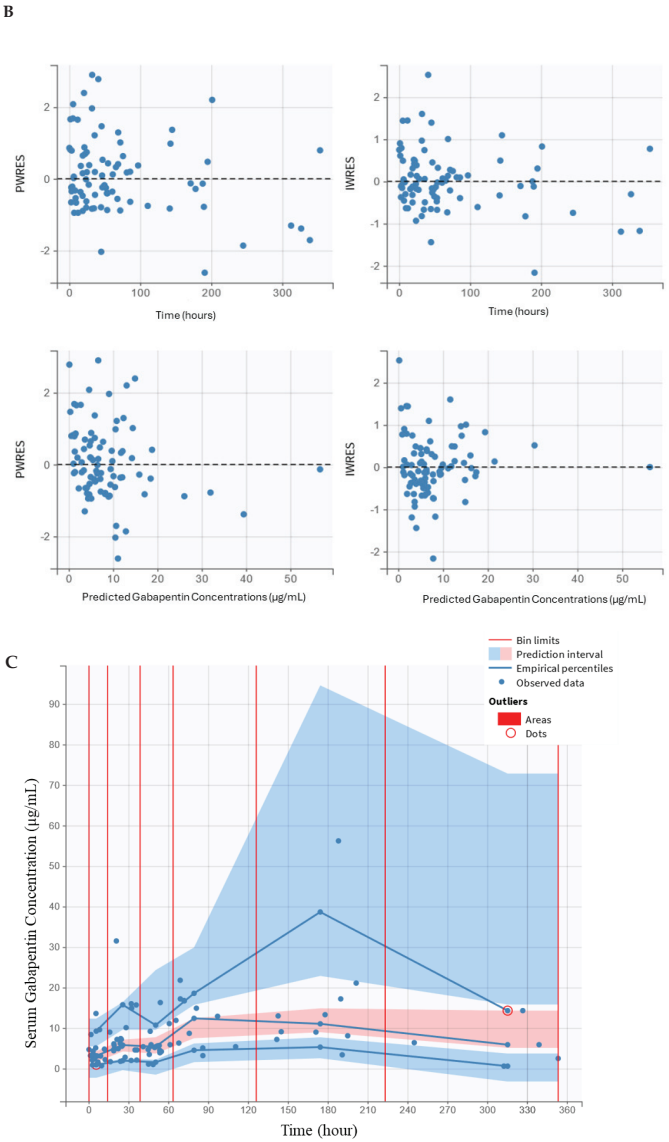


Figure 1. (**A**) Observation versus prediction plots for population and individual predictions. The black linear line is the y = x line. (**B**) Population and individual weighted residuals (PWRESs and IWRESs) plotted against time from the first recorded gabapentin dose (upper panels) and predicted gabapentin concentrations (bottom panels). (**C**) Visual predictive check (VPC) plot for the final model. Observed data are represented by blue dots. The black lines represent the 5th, 50th, and 95th percentiles of the predicted value. The blue areas represent the 95% confidence interval of the predicted percentile. Time 0 was the time of the first recorded gabapentin dose for each individual subject.

4. Discussion

This study aimed to explore the utility of TDM concentrations in developing a non-linear mixed-effect PK model and characterize covariates that affect the PK profile of gabapentin, with a particular interest in diabetes and obesity. Our model suggested that gabapentin PK was best described by a simple one-compartment model with first-order absorption with nonlinear bioavailability and first-order elimination, with SCr as a covariate on Cl.

The population estimate for V_d is approximately similar to the previously reported value (45.4 L) [32]. The population estimate for Cl by this model is smaller than the previously reported values (6.31 L/h) [32]. The inclusion of SCr as a covariate on clearance confirmed the importance of renal function in gabapentin elimination. Previous studies included either CrCl or eGFR as a covariate on clearance in their final popPK models for

gabapentin [16,18–20]. Gabapentin is predominately renally unchanged when excreted (77%) with first-order elimination PK, and a dose reduction of greater than 50% is recommended for adult patients with a CrCl of less than 60 mL/min [1,5]. In addition, oral clearance of gabapentin was reported to be linearly correlated with CrCl [5,16–18]. During the model development, when SCr was compared with CrCl and eGFR as a covariate on clearance, SCr resulted in a significant reduction in OFV. Plasma clearance and renal clearance of gabapentin are directly proportional to the patient's creatinine clearance due to its primarily renal elimination [5,16,17].

In our model, the cohort with diabetes or hyperglycemia had no impact on the PK of gabapentin, and this finding was consistent with previously published popPK models for gabapentin in the adult population with type 2 diabetes [19]. Because patients with type 2 diabetes tend to have a heavier body weight, our model also investigated different body weight parameters as covariates. WT, LBW, ABW, and IBW were evaluated but not included in the final model. This finding was consistent with previously published popPK models for gabapentin in the adult population [16,19,20]. Ouellet et al. concluded that the volume of distribution was related to body weight in their popPK model for gabapentin. However, the study was performed in the pediatric population, with a distinct PK profile from the adult population [18]. Overall, body weight seems to have a minimal effect on gabapentin PK and therefore is not a significant factor for dosing consideration.

Due to gabapentin's considerable interindividual variations in its PK and pharmacodynamics, it has been suggested that TDM may be advantageous. The absence of gabapentin therapeutic effect in certain patients might be due to inadequate drug plasma concentration [8]. In contrast, the high plasma concentrations of gabapentin could result in common adverse effects, such as dizziness and sleepiness, which can significantly impact the well-being and compliance of patients [4,5]. Therefore, TDM could be beneficial in achieving the desired effective drug concentrations and lowering the possibility of adverse effects. The PopPK model developed in this study can describe the interpatient variability of gabapentin by correlating Cl with SCr and the dose-dependent bioavailability. This model can be applied to the prediction of the drug concentration for better individual dose optimization.

Our findings characterized our study population well while confirming several conclusions drawn by previous studies. However, this study has some limitations. Firstly, due to the study's retrospective nature, consistencies and human errors can happen with the sample collection and record documentation. Secondly, our sample size is relatively small as gabapentin TDM concentrations are not routinely collected. We acknowledge residual confounding factors may be present; however, as an observational study, data were limited to what was accessible in the medical record. Further investigation with a larger sample size may allow for a more comprehensive examination of the influence of additional covariates.

The use of TDM concentrations to develop popPK models has been implemented across various disease states and drug classes. This approach has several benefits, including utilizing existing data, conserving resources, and reducing financial burdens. Additionally, employing a real-world population can enhance the external validity of the model. Available concentration data can be used to create a new model or to refine existing published models. In this study, we elected to create a new model due to the differences in the populations used in previously published gabapentin popPK models. Our goal was to focus on developing a model that is applicable to a broad population. While utilizing available gabapentin concentrations from clinical care was a resource-efficient approach, some limitations must be acknowledged in this approach. The development process relies on the available data, which may not cover the entire dosing interval. This can hinder our ability to accurately capture the absorption rate constant (Ka) or the elimination rate constant (Ke). However, we can fix these variables if there are existing data that describes them, as we have performed. Concerns regarding the use of existing data include limited dose ranges, restricted indications, underrepresentation of different races and ethnicities,

and general assumptions, such as the achievement of a steady-state concentration. Taylor and colleagues have provided a concise review of important considerations for developing a popPK model [33]. Despite these limitations, a valuable model can still be created if these issues are addressed during its development and application.

In summary, this study characterized gabapentin PK and demonstrated the potential of repurposing TDM concentrations to develop popPK models, thus addressing the paucity of large-scale prospective PK studies in patients. Previously published gabapentin popPK models in adult populations were based on data collected in prospective PK studies. Our model based on TDM concentrations confirmed the major findings from these prospective studies [16,19,20]. This study demonstrated that TDM concentrations could be utilized to develop popPK models and investigate the unique PK alterations of gabapentin in patients.

5. Conclusions

Gabapentin TDM concentrations were used to develop a popPK model for gabapentin. Gabapentin PK was described by a one-compartment model with first-order absorption with nonlinear bioavailability and first-order elimination. The interindividual variability of gabapentin PK was associated with SCr in our study population. Obesity and diabetes were not significant covariates in the popPK model. The results of this study reinforce the importance of considering renal function when dosing gabapentin.

Supplementary Materials: The following supporting information can be downloaded at: https://www.mdpi.com/article/10.3390/pharmaceutics16121514/s1, Table S1: Summary of structural model selection; Table S2: Summary of the covariate model building process.

Author Contributions: Conceptualization, L.B.; Methodology, L.K. and L.B.; Formal analysis, F.A.-Z., A.W., L.K. and L.B.; Resources, A.W.; Data curation, L.B.; Writing—original draft, F.A.-Z.; Writing—review & editing, F.A.-Z., L.K. and L.B. All authors have read and agreed to the published version of the manuscript.

Funding: This research received no specific grant from any funding agency in the public, commercial, or not-for-profit sectors.

Institutional Review Board Statement: The study was conducted in accordance with the Declaration of Helsinki and approved by the Institutional Review Board of Robert Wood Johnson Somerset Institutional Review Board (protocol code: IRB21-31; approval date 28 September 2021).

Informed Consent Statement: The study was approved on an expedited basis and waiver of consent was granted due to the retrospective nature of the study.

Data Availability Statement: The data that support the findings of this study are available from the corresponding author upon reasonable request.

Conflicts of Interest: The authors declare that there are no conflicts of interest.

References

1. Gabapentin. *Pfizer Inc. NEURONTIN (Package Insert)*; Pfizer Inc.: New York, NY, USA, 2017.
2. Attal, N.; Cruccu, G.; Baron, R.; Haanpää, M.; Hansson, P.; Jensen, T.S.; Nurmikko, T. EFNS guidelines on the pharmacological treatment of neuropathic pain: 2010 revision. *Eur. J. Neurol.* **2010**, *17*, 1113-e88. [CrossRef] [PubMed]
3. Finnerup, N.B.; Attal, N.; Haroutounian, S.; McNicol, E.; Baron, R.; Dworkin, R.H.; Gilron, I.; Haanpää, M.; Hansson, P.; Jensen, T.S.; et al. Pharmacotherapy for neuropathic pain in adults: A systematic review and meta-analysis. *Lancet Neurol.* **2015**, *14*, 162–173. [CrossRef] [PubMed]
4. Moore, R.A.; Wiffen, P.J.; Derry, S.; Rice, A.S. Gabapentin for chronic neuropathic pain and fibromyalgia in adults. *Cochrane Database Syst. Rev.* **2014**, *2014*, Cd007938. [CrossRef] [PubMed]
5. Beydoun, A.; Uthman, B.M.; Sackellares, J.C. Gabapentin: Pharmacokinetics, efficacy, and safety. *Clin. Neuropharmacol.* **1995**, *18*, 469–481. [CrossRef]
6. McLean, M.J. Clinical pharmacokinetics of gabapentin. *Neurology* **1994**, *44*, S17–S22, discussion S31-12.
7. McLean, M.J. Gabapentin. *Epilepsia* **1995**, *36* (Suppl. S2), S73–S86. [CrossRef]

8. Gidal, B.E.; Radulovic, L.; Kruger, S.; Rutecki, P.; Pitterle, M.; Bockbrader, H.N. Inter- and intra-subject variability in gabapentin absorption and absolute bioavailability. *Epilepsy Res.* **2000**, *40*, 123–127. [CrossRef]
9. Bockbrader, H.N.; Wesche, D.; Miller, R.; Chapel, S.; Janiczek, N.; Burger, P. A comparison of the pharmacokinetics and pharmacodynamics of pregabalin and gabapentin. *Clin. Pharmacokinet.* **2010**, *49*, 661–669. [CrossRef]
10. Parsons, B.; Tive, L.; Huang, S. Gabapentin: A pooled analysis of adverse events from three clinical trials in patients with postherpetic neuralgia. *Am. J. Geriatr. Pharmacother.* **2004**, *2*, 157–162. [CrossRef]
11. Gwilt, P.R.; Nahhas, R.R.; Tracewell, W.G. The Effects of Diabetes Mellitus on Pharmacokinetics and Pharmacodynamics in Humans. *Clin. Pharmacokinet.* **1991**, *20*, 477–490. [CrossRef]
12. Dostalek, M.; Akhlaghi, F.; Puzanovova, M. Effect of diabetes mellitus on pharmacokinetic and pharmacodynamic properties of drugs. *Clin. Pharmacokinet.* **2012**, *51*, 481–499. [CrossRef] [PubMed]
13. Goyal, R.K. Gastric Emptying Abnormalities in Diabetes Mellitus. *N. Engl. J. Med.* **2021**, *384*, 1742–1751. [CrossRef] [PubMed]
14. Gheith, O.; Farouk, N.; Nampoory, N.; A Halim, M.; Al-Otaibi, T. Diabetic kidney disease: World wide difference of prevalence and risk factors. *J. Nephropharmacol* **2015**, *5*, 49–56. [CrossRef] [PubMed]
15. Hanley, M.J.; Abernethy, D.R.; Greenblatt, D.J. Effect of obesity on the pharmacokinetics of drugs in humans. *Clin. Pharmacokinet.* **2010**, *49*, 71–87. [CrossRef]
16. Tran, P.; Yoo, H.-D.; Ngo, L.; Cho, H.-Y.; Lee, Y.-B. Population pharmacokinetics of gabapentin in healthy Korean subjects with influence of genetic polymorphisms of ABCB1. *J. Pharmacokinet. Pharmacodyn.* **2017**, *44*, 567–579. [CrossRef]
17. A Blum, R.; Comstock, T.J.; A Sica, D.; Schultz, R.W.; Keller, E.; Reetze, P.; Bockbrader, H.; Tuerck, D.; A Busch, J.; A Reece, P.; et al. Pharmacokinetics of gabapentin in subjects with various degrees of renal function. *Clin. Pharmacol. Ther.* **1994**, *56*, 154–159. [CrossRef]
18. Ouellet, D.; Bockbrader, H.N.; Wesche, D.L.; Shapiro, D.Y.; Garofalo, E. Population pharmacokinetics of gabapentin in infants and children. *Epilepsy Res.* **2001**, *47*, 229–241. [CrossRef]
19. Costa, A.C.C.; de Lima Benzi, J.R.; Yamamoto, P.A.; de Freitas, M.C.F.; de Paula, F.J.A.; Zanelli, C.F.; Lauretti, G.R.; de Moraes, N.V. Population pharmacokinetics of gabapentin in patients with neuropathic pain: Lack of effect of diabetes or glycaemic control. *Br. J. Clin. Pharmacol.* **2021**, *87*, 1981–1989. [CrossRef]
20. Carlsson, K.C.; van de Schootbrugge, M.; Eriksen, H.O.M.; Moberg, E.R.M.; O Karlsson, M.; Hoem, N.O. A population pharmacokinetic model of gabapentin developed in nonparametric adaptive grid and nonlinear mixed effects modeling. *Ther. Drug Monit.* **2009**, *31*, 86–94. [CrossRef]
21. Costa, A.C.C.Y.P.; Benzi, J.R.D.L.; Lauretti, G.R.; de Moraes, N.V. Impact of diabetes on gabapentin pharmacokinetics in patients with neuropathic pain. In Proceedings of the 54th Congress of the European Societies of Toxicology, Brussels, Belgium, 5 September 2018.
22. Bondareva, I. Chapter 19—Individualizing Antiepileptic Therapy for Patients. In *Individualized Drug Therapy for Patients*; Jelliffe, R.W., Neely, M., Eds.; Academic Press: Boston, MA, USA, 2017; pp. 327–371.
23. Rivas, N.; Buelga, D.S.; E Elger, C.; Santos-Borbujo, J.; Otero, M.J.; Domínguez-Gil, A.; García, M.J. Population pharmacokinetics of lamotrigine with data from therapeutic drug monitoring in German and Spanish patients with epilepsy. *Ther. Drug Monit.* **2008**, *30*, 483–489. [CrossRef]
24. Hallworth, M. CHAPTER 39—Therapeutic drug monitoring. In *Clinical Biochemistry: Metabolic and Clinical Aspects*, 3rd ed.; Marshall, W.J., Lapsley, M., Day, A.P., Ayling, R., Eds.; Churchill Livingstone: London, UK, 2014; pp. 767–786.
25. Kang, J.S.; Lee, M.H. Overview of therapeutic drug monitoring. *Korean J. Intern. Med.* **2009**, *24*, 1–10. [CrossRef] [PubMed]
26. Martin, J.H.; Saleem, M.; Looke, D. Therapeutic drug monitoring to adjust dosing in morbid obesity—A new use for an old methodology. *Br. J. Clin. Pharmacol.* **2012**, *73*, 685–690. [CrossRef] [PubMed]
27. Hristova, V.; Clarke, W. Chapter 10—Therapeutic Drug Monitoring in Obese Patients. In *Clinical Challenges in Therapeutic Drug Monitoring*; Clarke, W., Dasgupta, A., Eds.; Elsevier: San Diego, CA, USA, 2016; pp. 231–243.
28. Dekkers, B.G.J.; Akkerman, O.W.; Alffenaar, J.W.C. Role of Therapeutic Drug Monitoring in Treatment Optimization in Tuberculosis and Diabetes Mellitus Comorbidity. *Antimicrob. Agents Chemother.* **2019**, *63*, 20190129. [CrossRef] [PubMed]
29. Janmahasatian, S.; Duffull, S.B.; Ash, S.; Ward, L.C.; Byrne, N.M.; Green, B. Quantification of lean bodyweight. *Clin. Pharmacokinet.* **2005**, *44*, 1051–1065. [CrossRef]
30. Levey, A.S.; Coresh, J.; Greene, T.; Marsh, J.; Stevens, L.A.; Kusek, J.W.; Van Lente, F.; Chronic Kidney Disease Epidemiology Collaboration. Expressing the Modification of Diet in Renal Disease Study equation for estimating glomerular filtration rate with standardized serum creatinine values. *Clin. Chem.* **2007**, *53*, 766–772. [CrossRef] [PubMed]
31. Mayo Clinic Laboratories. Gabapentin, Serum. Available online: https://www.mayocliniclabs.com/test-catalog/overview/80826#Overview (accessed on 19 March 2022).

32. Gidal, B.E.; DeCerce, J.; Bockbrader, H.N.; Gonzalez, J.; Kruger, S.; Pitterle, M.E.; Rutecki, P.; Ramsay, R.E. Gabapentin bioavailability: Effect of dose and frequency of administration in adult patients with epilepsy. *Epilepsy Res.* **1998**, *31*, 91–99. [CrossRef] [PubMed]
33. Taylor, Z.L.; Poweleit, E.A.; Paice, K.; Somers, K.M.; Pavia, K.; Vinks, A.A.; Punt, N.; Mizuno, T.; Girdwood, S.T. Tutorial on model selection and validation of model input into precision dosing software for model-informed precision dosing. *CPT Pharmacometrics Syst. Pharmacol.* **2023**, *12*, 1827–1845. [CrossRef] [PubMed] [PubMed Central]

Disclaimer/Publisher's Note: The statements, opinions and data contained in all publications are solely those of the individual author(s) and contributor(s) and not of MDPI and/or the editor(s). MDPI and/or the editor(s) disclaim responsibility for any injury to people or property resulting from any ideas, methods, instructions or products referred to in the content.

pharmaceutics

MDPI

Article

Population Pharmacokinetics Model of Cyclosporin A in Children and Young Adult Renal Transplant Patients: Focus on Haemoglobin Contribution to Exposure Variability

Maša Roganović [1], Mirjana Cvetković [2,3], Ivana Gojković [2], Brankica Spasojević [2,3], Marija Jovanović [1], Branislava Miljković [1] and Katarina Vučićević [1,*]

[1] Department of Pharmacokinetics and Clinical Pharmacy, Faculty of Pharmacy, University of Belgrade, 11221 Belgrade, Serbia
[2] Department of Nephrology, Dialysis, and Transplantation, University Children's Hospital, 11000 Belgrade, Serbia
[3] Faculty of Medicine, University of Belgrade, 11000 Belgrade, Serbia
* Correspondence: katarina.vucicevic@pharmacy.bg.ac.rs

Abstract

Background/Objectives: Cyclosporine A (CsA) is a key immunosuppressant in post-transplantation therapy protocol characterized by large interindividual and intraindividual pharmacokinetic (PK) variability and a narrow therapeutic range necessitating therapeutic drug monitoring (TDM) to prevent graft rejection and minimize side effects. TDM data can be used for developing PK models with the objective of identification and quantification of variability factors that contribute to the differences in CsA concentrations. **Methods**: Retrospectively collected data from medical records of 58 patients (children and young adults) regarding CsA blood concentrations, concomitant medications, and laboratory findings of significance were used for the population PK model development in NONMEM® (version 7.5) with first-order conditional estimation method with interaction (FOCE-I). Simulation of the concentrations and area under the curve (AUC) was performed in the web application e-campsis®. RStudio (version 4.5.0) was used for the purpose of descriptive statistics analysis and graphs plotting. **Results**: A one-compartment model with first-order absorption and elimination best described the data. Value of clearance (CL/F) was estimated to be 15 L/h, and volume of distribution (V/F) was 71.1 L for a typical patient weighing 40 kg. Interindividual variability (IIV) on CL/F and V/F was 34.91% and 43.05%, respectively. Interoccasional variability (IOV) was 12.25%. Body weight (WT) was introduced allometrically on CL/F and V/F, with the estimated exponent of 0.89 for CL/F and 1 (fixed) for V/F. According to the final model, CL/F decreases with increasing haemoglobin (HGB) value. A difference of almost 22.5% in CL/F was observed among patients' HGB values reported in the study. **Conclusions**: Our findings indicate that HGB levels significantly influence CsA PK, particularly minimum concentration (C_{min}), highlighting the importance of regular HGB levels monitoring together with CsA levels.

Keywords: cyclosporine; population pharmacokinetics; haemoglobin; TDM; NONMEM

1. Introduction

Cyclosporine A (CsA) is an immunosuppressive drug that belongs to the class of calcineurin inhibitors (CNIs) [1]. In combination with other immunosuppressive drugs, CsA forms an essential part of post-transplant therapy protocol aimed at preventing graft

rejection after solid organ transplantation. Although tacrolimus has largely replaced CsA in solid organ transplantation due to lower rejection rates and better long-term outcomes, CsA remains clinically relevant in patients who develop adverse effects such as post-transplant diabetes mellitus and those at higher risk of BK polyomavirus infection [2,3]. It shows marked interindividual and intraindividual pharmacokinetic (PK) variability and has a narrow therapeutic index [4–6]. The absorption and elimination of CsA are highly variable: bioavailability may range from as low as 5% to nearly 90%, and terminal elimination half-life varies from 6.3 to 20.4 h depending on patient-specific factors such as comorbidities and age [7]. Such PK characteristics necessitate regular therapeutic drug monitoring (TDM) to ensure optimal therapeutic exposure and prevent graft rejection [8]. Moreover, its pronounced PK variability and complex absorption mechanisms continue to make CsA an important subject of PK research. Integrating TDM data with population pharmacokinetic (PopPK) modelling can further enhance understanding of the covariates influencing CsA disposition, enabling dose individualization to maximize efficacy and minimize toxicity [9–11]. The side effects of CsA can be serious and include hypertension, nephrotoxicity, an increased risk of malignancy, and neurotoxicity [12,13]. These concerns are particularly pronounced in paediatric patients, whose physiological and biochemical characteristics differ substantially from those of adults. Consequently, variability in PK and pharmacodynamics may lead to a higher incidence of toxicity or therapeutic failure in this vulnerable population, underscoring the need for targeted research [14].

Although numerous PopPK studies have been conducted in both adult and paediatric populations, important knowledge gaps remain, particularly in paediatric population [9,10,15,16]. Research in adults far outweighs that in children, largely due to ethical and logistical challenges inherent to paediatric studies. Moreover, existing studies often involve heterogeneous patient populations, including renal, hepatic, pulmonary, cardiac, and hematopoietic stem cell transplant recipients, making cross-study comparisons difficult due to differences in physiology, comorbidities, and immunosuppressive regimens. The number of studies in paediatric population is still relatively small. TDM practices for CsA also vary substantially among transplant centres. Some institutions measure trough concentrations (C_0, in sample taken immediately before the morning dose), while other centres focus on post-dose concentration (C_2, approximately 2 h after the morning dose), with each applying different target ranges depending on the transplanted organ, biological matrix (most commonly whole blood), and institutional protocols. These inconsistencies reflect the lack of consensus in the literature. Furthermore, although numerous covariates have been associated with CsA PK variability, their relative clinical significance remains uncertain. Specific covariates such as genetic polymorphism and biomarkers related to red blood cells other than haematocrit have not been consistently applied across the models, which highlights a critical need for investigation into these less frequently tested variables.

Therefore, the aim of this study was to develop a PopPK model of CsA in paediatric and young adult renal transplant recipients, with the goal of improving clinical practice through individualized dosing strategies based on identified and quantified covariate effects.

2. Materials and Methods

2.1. Patient Population and Study Design

The study was conducted in the University Children's Hospital, which is currently the only centre in the Republic of Serbia performing renal transplantation in children. The study population included children and young adults who underwent kidney transplantation either at the University Children's Hospital or abroad, but whose post-transplant follow-up was carried out at this institution. All patients who received CsA as part of their

https://doi.org/10.3390/pharmaceutics18010099

immunosuppressive regimen were included in the study, regardless of whether their therapy was subsequently switched to tacrolimus. This was a retrospective study based on data available from patients' medical history. The collected data included CsA dosage regimens, CsA blood concentrations, concomitant medications, and relevant laboratory parameters in kidney transplant recipients. For some patients, pharmacogenetic data were also available, including polymorphisms in *CYP3A4*, *CYP3A5*, *ABCB1*, and *POR* genes. The local ethics committee gave permission for this retrospective study (Ethical Approval No. 16/223, obtained on 7 October 2025). All patients received the same immunosuppressive regimen consisting of CsA, corticosteroid, and mycophenolate acid. CsA was initially administered at a dose of 5 mg/kg/day divided into two or three daily doses. The dose was adjusted to the following target whole-blood levels: C_0 150–200 ng/mL and C_2 1200–1400 ng/mL during the first post-transplant month; C_0 100–150 ng/mL and C_2 800–1200 ng/mL during months two and three; and, thereafter, C_0 100–130 ng/mL and C_2 800–1000 ng/mL depending on the patient's clinical condition.

2.2. Sampling and Cyclosporin A Concentration Measurement

CsA concentrations were measured in whole-blood samples using chemiluminescent microparticle immunoassays developed by Abbott (Abbott Park, IL, USA). The lower limit of quantification of the assay is 30 ng/mL based on functional sensitivity, and the upper limit of quantification is 1500 ng/mL, with imprecision estimated at less or equal to 15% coefficient of variation (CV). Concentrations were measured in samples corresponding to C_0 and C_2, collected after at least three consecutive days of unchanged dosing regimen to ensure that steady-state was reached. The majority of the concentrations in the dataset were obtained approximately one year post-transplantation. For one patient, concentration measurements were collected approximately two years post-transplantation due to unavailable dosing history of CsA during the first-year post-transplant period.

2.3. Population Pharmacokinetic Modelling

PopPK analysis was performed using nonlinear mixed effects modelling with NONMEM® software (version 7.5.0, ICON Development Solutions Inc., Dublin, Ireland) with first-order conditional estimation method with interaction (FOCE-I). NONMEM outputs were handled in R (version 4.5.1, R Foundation for Statistical Computing, Vienna, Austria) within RStudio (version 4.5.0, Posit Software, Boston, MA, USA) for graphical diagnostics and model evaluation. A one-compartment and two-compartment model with first-order elimination were tested. Model selection and comparison were based on a decrease in the objective function value (ΔOFV), as well as on visual inspection goodness of fit (GOF) plots. Additive, exponential, and proportional models were tested to explain interindividual variability (IIV). Residual unexplained variability was explored using additive, proportional, and combined error models.

Initial model development attempted to estimate the absorption rate constant (Ka); however, sparse sampling in the absorption phase did not support reliable estimation of this parameter, leading to model instability and imprecise estimates. Consequently, Ka was fixed during further modelling steps to ensure model identifiability and robustness and allowed reliable estimation of clearance and covariate effects. A similar approach was applied by Xue et al., who fixed Ka at 1.25 h^{-1} [17]. A sensitivity analysis was performed by varying Ka within a plausible range. Interoccasional variability (IOV) was implemented on CL/F. Every pair of concentrations measured on the same day, or a single concentration measured on a given day, was treated as a separate occasion. The correlation between CL/F and V/F was also examined.

https://doi.org/10.3390/pharmaceutics18010099

Covariate model building was performed using the stepwise covariate modelling (SCM) procedure. Continuous covariates that were tested included age (AGE), body weight (WT), height (HT), albumin levels (ALB), cold and warm ischemia time (COLDIH, WARMIH, respectively), haematocrit (HCT), haemoglobin (HGB), serum creatinine levels (CREAT), and creatinine clearance (CLCR) calculated using the Schwartz formula (Equation (1)):

$$\mathrm{CLCR} = \frac{(\mathrm{k}\cdot\mathrm{HT})}{\mathrm{CREAT}} \quad (1)$$

where k is coefficient 0.413 according to the revised Schwartz formula, also known as the bedside Schwartz formula [18]. Influence of categorical covariates was also examined: gender (GEND), type of transplanted graft—live or cadaveric transplantation (TRANS), and genetic polymorphism for *CYP3A4*, *CYP3A5*, *ABCB1*, and *POR*. The forward inclusion process was set for the significance of $p < 0.05$, and the backward elimination process was set to $p < 0.01$. Correlation between the continuous covariates was examined to assess the plausibility of the results of the SCM procedure. Additionally, covariates were considered clinically significant if the change in the parameter value was greater than 20% over the range of the usual values of the covariates [19]. Additionally, the WT effect was carefully considered. Since most of the population was paediatric, the allometric scaling model for both CL/F and V/F was also tested during model development using the equations below (Equations (2) and (3)):

$$\mathrm{CL/F} = \mathrm{CLpop}\cdot\left(\frac{\mathrm{WTi}}{\mathrm{WTmedian}}\right)^{0.75} \quad (2)$$

$$\mathrm{V/F} = \mathrm{Vpop}\cdot\left(\frac{\mathrm{WTi}}{\mathrm{WTmedian}}\right)^{1} \quad (3)$$

Additionally, the effect of WT on CL/F was tested using allometric scaling without fixing the exponent at 0.75 and allowing its estimation to determine whether it improved model fit, given that our population included both children and young adults. Model validation was performed using techniques of internal validation, both graphical and numerical. Graphical evaluation methods included GOF plots and variability- and prediction-corrected visual predictive checks (VPC) based on 1000 simulated samples. Additionally, a bootstrap analysis was performed using 1000 replicates.

2.4. Simulations

Using the web application e-campsis®, simulations of minimal (C_{min}) and maximal (C_{max}) concentrations, as well as areas under the concentration-time curve (AUC) were performed under four different scenarios utilising the developed CsA PopPK model. First, a dataset consisting of 500 girls and 500 boys was simulated in RStudio® using WT distribution data from the Centers for Disease Control and Prevention growth chart for twelve-year-old boys and girls, which corresponds to the median value of age in our population [20]. This dataset was used to calculate means ± standard deviation (SD) of WT for such simulated datasets, so that WT distribution can be used in simulation in e-campsis® for all four different scenarios. Each scenario included 100 patients, with different values of the covariates from the final PopPK model and two occasions per patient considered. Simulations were performed using 5 mg/kg dose, consistent with both our clinical practice and recommended maintenance dose [21].

https://doi.org/10.3390/pharmaceutics18010099

3. Results

3.1. Patients' Characteristics

A total of 58 patients with kidney transplants were included in the study. Most of the population were male patients (34, 58.62%). The patients' age at transplantation ranged from 1 to 25 years, with a median of 12 years (mean 11.78 years). Most of the population were children under the age of 18 (47, 81.03%), and 11 patients (18.97%) were classified as young adults (18–25 years). A total of 30 patients had live donor transplantation, and 28 had an organ transplanted from a cadaver. Genetic polymorphism was available for 33 patients. Other demographic and clinical characteristics of patients are shown in Table 1.

Table 1. Descriptive statistics of patients' characteristics (n = 58).

Characteristics	Mean	SD	Median	Range	IQR
HT (cm)	137.21	25.20	141	78–185	36.5
WT (kg)	39.95	19.53	39.65	9.8–103	26.12
CREAT (μmol/L)	107.50	70.022	87	28–696	58.25
CLCR (mL/min/1.73 m^2)	56.29	19.82	55.21	8.93–131.58	25.39
HGB (g/L)	118.33	14.99	120	73–164	20.25
HCT (%)	35.65	4.37	35.70	21.7–49.8	6.4
PROT (g/L)	61.29	7.026	63	30–77	11
ALB (g/L)	36.91	4.47	37	10–48	3
ALP (IU/L)	146.48	129.55	112	34–964	101.5

SD—standard deviation, IQR—interquartile range, HT—height, WT—body weight, CREAT—serum creatinine, CLCR—creatinine clearance, HGB—haemoglobin, HCT—haematocrit, PROT—total protein, ALB—albumin, ALP—alkaline phosphatase.

3.2. Cyclosporine Concentrations

A total of 974 steady-state concentrations were measured in whole-blood samples taken from the patients: 471 C_0 concentrations, 501 C_2 concentrations, one concentration measured in a sample taken 4 h after the morning dose, and one concentration 6 h post morning dose. Statistics regarding CsA concentrations are shown in Table 2.

Table 2. Descriptive statistics of cyclosporine (CsA) concentrations across post-transplant periods.

	PDAY $\leq$ 30 (n = 132)	**30 < PDAY $\leq$ 90 (n = 229)**	**PDAY > 90 (n = 611)**
C_0 (ng/mL)			
n	65	112	294
Mean (SD)	119.39 (77.54)	142.07 (68.17)	113.50 (47.42)
Range	9.00–462.00	37.20–506.60	33.50–470.00
Median	113	129.7	103.15
C_2 (ng/mL)			
n	67	117	317
Mean (SD)	897.18 (376.60)	915.79 (342.29)	716.69 (243.68)
Range	317.50–1850.40	111.40–2306.00	201.60–1414.00
Median	811.15	896	684

C_0—trough concentration, C_2—concentration 2 h after dose, PDAY—post-transplant day, SD—standard deviation.

Figure 1 shows the percentage of C_0 and C_2 concentrations measured across post-transplant periods 1, 2, and 3 (corresponding to the period of PDAY $\leq$ 30, 30 < PDAY $\leq$ 90, and PDAY > 90, respectively) that are above and below the aforementioned target concentration range. The most pronounced deviation from the target concentration range was for both C_0 and C_2 in the first post-transplant period, with over 75% concentrations being below the desired range.

https://doi.org/10.3390/pharmaceutics18010099



Figure 1. Percentage of cyclosporine A (CsA) trough (C_0) and 2 h post-dose (C_2) concentrations above (green) and below (red) the target concentration range across post-transplant periods. Period 1: post-transplant day (PDAY) $\leq$ 30; Period 2: 30 < PDAY $\leq$ 90; Period 3: PDAY > 90.

3.3. Population Pharmacokinetic Model

The one-compartment model with first-order absorption and elimination best described the data. A base model was developed using the ADVAN2 TRANS2 subroutine and CL/F and V/F were estimated, while Ka was fixed to the value of 1.15 1/h, as it could not be reliably estimated due to limited data in the absorption phase. A sensitivity analysis was performed by varying Ka within a plausible range, demonstrating that changes in Ka had minimal impact on the primary parameter estimates, confirming that the model results are robust to the fixed Ka value. IIV was introduced using an exponential model for both parameters. IOV was kept on CL/F. The maximum number of occasions per patient was 33 over one year period. The correlation between CL/F and V/F was also accounted for in the model. After completion of the SCM procedure, the model included a linear WT effect on CL/F and V/F, and HGB, CREAT, and CLCR as covariates on CL/F. HCT, although tested, was not included in either forward inclusion or backward elimination steps. *CYP3A4* genetic polymorphism was included after forward selection step, but was not retained in the final model, and when tested manually, its effect lacked robustness, as the 95% bootstrap confidence interval included zero, likely due to the limited sample size (genotype data available for only 33 patients). Other polymorphisms were not selected during the SCM procedure in either the forward or backward steps and were therefore not tested manually. To further refine these results and assess their plausibility, a correlation analysis of continuous covariates was performed. Results from the correlation analysis are shown in Figure 2.

As CRCL and CREAT were found to be highly correlated, the final model was refined by testing each covariate separately. First, a model was evaluated with CRCL and HGB on CL/F, and WT on V/F. WT on CL/F was excluded since WT is highly correlated with HT, which is already incorporated in the calculation of CRCL. However, the relative standard error (RSE) for the CRCL effect on CL/F was extremely high (572.7%).

Next, a model including CREAT and WT on CL/F, and WT on V/F, was tested. In this case, the RSE for the CREAT effect on CL/F was much smaller (58.8%) compared to the RSE for the CRCL effect on CL/F, but still high. Nevertheless, although the effect of CREAT on CL/F was statistically significant, the magnitude of its influence was not considered clinically relevant since the change in the parameter value across the range of usual values was less than 20%, and thus the covariate was not retained.

https://doi.org/10.3390/pharmaceutics18010099

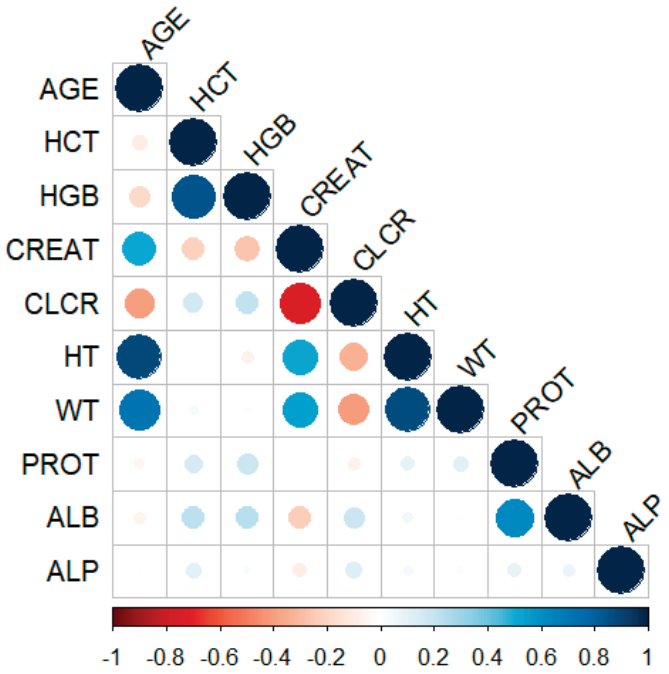


Figure 2. Correlation between continuous covariates. Circle size represents the strength of the correlation (larger circles indicate a stronger correlation) and colour indicates direction (blue for positive, red for negative). Colour intensity reflects the strength of correlation (darker shades indicate a stronger correlation).

The model was subsequently refined to include a linear effect of HGB on CL/F, and WT on both CL/F and V/F. Given that the study population was predominantly paediatric, allometric scaling was evaluated: CL/F was tested with a fixed exponent of 0.75, as well as with estimation of the exponent for CL/F (while the exponent for V/F was kept fixed at 1). WT was centred to the rounded median value of 40 kg. The latter approach yielded the most stable and robust model. This model was therefore selected as the final model. Parameter estimates are summarized in Table 3.

Table 3. Parameter estimates and bootstrap median of the final population pharmacokinetic (PopPK) model of cyclosporine (CsA).

Parameter (Units)	Estimated Value (%RSE)	Bootstrap Median (95% CI)
CL/F (L/h/40 kg)	15 (4.7)	14.92 (13.63–16.35)
V/F (L/40 kg)	71.1 (5.8)	70.76 (63.034–79.71)
Wp (%)	0.258 (4.3)	0.26 (0.23–0.28)
θ_ALL	0.89 (5.7)	0.89 (0.78–0.98)
θ_HGB	−0.00279 (24)	−0.0028 (−0.0041–−0.0016)
ω (CL-V)	0.136 (27.3)	0.13 (0.068–0.20)
IIV_{CL} (%)	34.91 (15.5)	33.83 (22.56–44.65)
IIV_{V} (%)	43.05 (11.8)	41.83 (31.7–52.49)
IOV_{CL} (%)	12.25 (12.5)	12.14 (8.7–15.87)

CL/F—clearance, V/F—volume of distribution, Wp—proportional error, θ_ALL—estimated allometric coefficient for CL/F, θ_HGB—haemoglobin effect on CL/F, ω (CL-V)—covariance between CL and V, IIV_{CL}, IIV_{V}—interindividual variability for CL and V, respectively, IOV_{CL}—interoccasional variability on CL.

Below are shown Equations (4) and (5) from the final model for CL/F and V/F, where WTi and HGBi are the individual WT and individual value of HGB, respectively.

$$CL/F = 15 \cdot \left(\frac{WTi}{40}\right)^{0.89} \cdot (1 - 0.00279 \cdot (HGBi - 120)) \quad (4)$$

$$V/F = 71.1 \cdot \left(\frac{WTi}{40}\right)^{1} \quad (5)$$

Model appropriateness was checked using basic GOF and variability and prediction corrected VPC (Figures 3 and 4, respectively). As it can be seen, the graph of the dependent variable, i.e., observed concentrations vs. population predicted concentrations, shows reasonable distribution of points around the line of identity, while the graph of observed concentrations vs. individual predicted concentrations shows symmetrically distributed points around line of identity with an almost perfect match. The graph of conditional weighted residual (CWRES) vs. population predictions shows that the majority of CWRES lies between ±2 units of the ordinate.

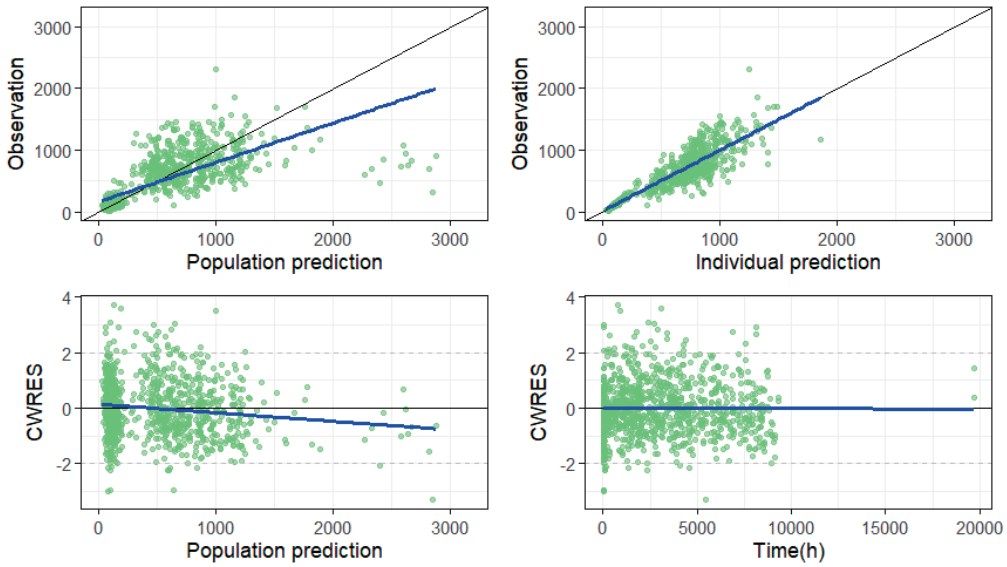


Figure 3. Goodness of fit plots. Observation vs. population prediction and observation vs. individual prediction graphs: dots represent individual data points, black line represents line of identity (y = x), blue line represents regression line; CWRES vs. population prediction and CWRES vs. time: black line represents line of identity (y = 0), blue line represents regression line.

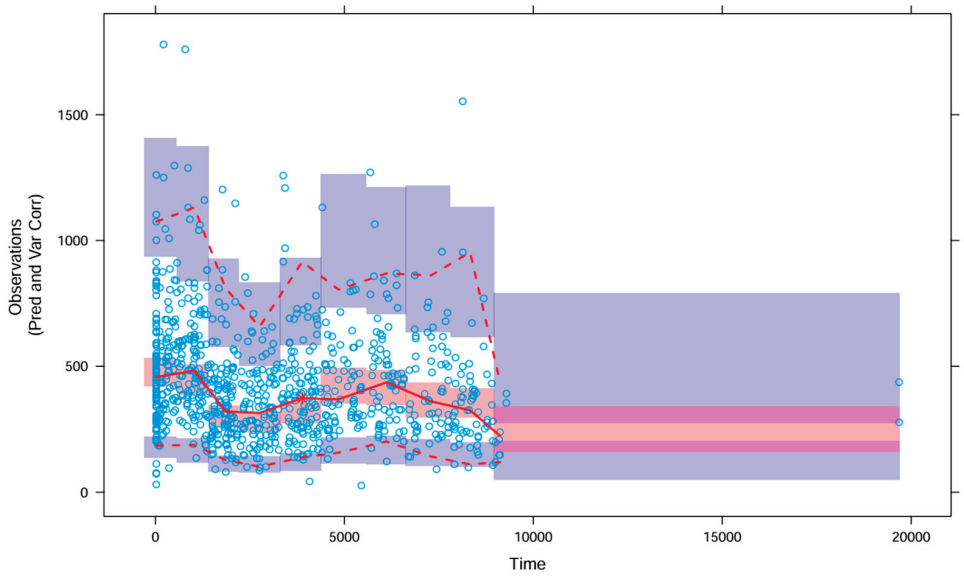


Figure 4. Prediction and variance corrected visual predictive check (VPC). Observed concentrations are shown as circles. Solid and dashed red lines represent median, 5th and 95th percentile of the observed data, with shaded 95% confidence intervals of the simulation-based prediction intervals for median (red) and the 5th and 95th percentiles (purple).

The VPC (Figure 4) demonstrated adequate agreement between observed and predicted concentrations, with only a few observations falling outside the prediction intervals. Data points around 20,000 h (time since first dose) correspond to a single patient, for whom PK data were available approximately two years after therapy initiation.

3.4. Simulation Results

The simulation was performed based on a WT distribution for a typical 12-year-old. The mean value of WT calculated from the simulated dataset that consisted of 1000 12-year-old patients, with 50% being boys, and 50% being girls, was calculated to be 43.03 kg and SD of 9.89 kg. Four different scenarios were simulated: two groups where patients had a low value of HGB (73, taken from the data range that we observed in our real dataset) on occasions 1 and 2, and two groups with a normal value of HGB 120 (also median value of our dataset) simulated on two occasions. Simulated AUC, C_{max}, and C_{min} are shown in Table 4. From the values in the table, the group with normal HGB had higher AUC, C_{max}, and C_{min} on both occasions. Compared with target C_0 and C_2 concentration ranges (regardless of the post-transplant period), simulated concentration values are higher. The higher simulated concentrations are likely due to dosing per kg being applied to a narrower range of WT, whereas the original dataset used to develop the model included a much wider WT range (9.8–103 kg).

Table 4. Simulated exposure metrics.

Metric	Low HGB OCC1 *n* = 100 [1]	Normal HGB OCC1 *n* = 100 [1]	Low HGB OCC2 *n* = 100 [1]	Normal HGB OCC2 *n* = 100 [1]
AUC (ng·h/mL)	6343 (3784–12,189)	7857 (3666–13,174)	6687 (3891–14,707)	7210 (3908–15,118)
C_{min} (ng/mL)	215 (119–528)	331 (173–597)	221 (120–528)	318 (154–631)
C_{max} (ng/mL)	1851 (1093–3545)	2265 (1019–3793)	1918 (1092–4255)	2035 (1121–4340)

[1] Median (5% Centile–95% Centile). AUC—area under the concentration–time curve, C_{min}—minimal CsA concentration, C_{max}—maximum CsA concentration, HGB—haemoglobin, OCC—occasion number, *n*—number of patients per group.

4. Discussion

We developed a CsA one-compartment model with first-order absorption and elimination in this mixed population, with children (<18 years old) being a major part of the studied population. CL/F and V/F were estimated for a typical patient with 40 kg at 15 L/h and 71.1 L, respectively, while Ka was fixed to the value of 1.15 1/h. Among the tested covariates, allometrically scaled WT on CL/F and V/F, and HGB on CL/F are retained. To our knowledge, this is the first population model to describe the influence of HGB on CsA CL/F variability in paediatric patients.

Depending on how sparse or rich the concentration data was, different models were used as a structural model for CsA in previous studies. Similar to our model, many studies used a one-compartment model [17,22–28]. There are also studies that used a two-compartment or even three-compartment model [4,29,30].

A study by Lukas et al. estimated CL/F to the value of 17 L/h with IIV of 27% in adult renal transplant patients, which is very close to the value we estimated. The same study estimated V/F to be 134 L, and that is larger than our estimated value of V/F [31]. Yin et al. reported V/F being 4.5 L/kg, which is again higher than the value we reported [32]. Both studies had Ka fixed to higher values (4 1/h and 2 1/h, respectively) compared to our estimate, which likely resulted in the larger estimated V/F values [31,32]. Previously published parameter values reported by Parke et al. (Ka 1.25 1/h and V/F 77.4 L), are close to our fixed Ka value and V/F estimate, supporting their plausibility [33]. However, it is

important to keep in mind that some differences in disposition parameters may be related to the weight differences between children and adults.

Including maturation functions is a common practice in PopPK models, where the population studied includes children [14]. Due to the limited number of very young children (3 patients in total being under or equal to the age of 2), no maturation function was applied in our study. This is physiologically plausible, as CsA metabolism reaches near-adult levels at the age of 2, and most patients in this dataset were older than 2 years. Allometric scaling of PK parameters is based on physiological principles: CL/F typically scales with WT to the 0.75 power, reflecting the relationship between body size, organ blood flow, and metabolic capacity, while V/F scales approximately linearly with WT, reflecting tissue and body water mass [14,34]. The estimated allometric exponent for CL/F was 0.89, slightly higher than the usual 0.75, whereas CL/F increases somewhat more steeply with larger body size. This finding is physiologically plausible and supports the use of WT-based dosing in this population. A study by Kim et al. also included WT as a power function, with the difference in WT being centred on 70 kg and the estimated exponent being much smaller than ours (0.419) [35]. Fanta et al. also used allometrically scaled WT, but with fixed exponents of 0.75 and 1 for CL/F and V/F, respectively [4].

A key novel finding of this study is the identification of HGB as a significant determinant of CsA CL/F. To our knowledge, this is the first study that incorporates HGB as a covariate in the PopPK model of CsA. HGB was included as a linear covariate on CL/F. According to our model, the difference between the lowest and highest HGB levels (range 73–164 g/L) corresponds to a difference of almost 22.5% change in CL/F, with CL/F decreasing as HGB increases across the range. Simulation results showed that HGB had a consistently large effect on C_{min} on both occasions, with patients with an HGB value of 120 g/L having substantially higher C_{min} compared with those with HGB of 73 g/L (53.95% on occasion 1 and 43.89% on occasion 2). However, the impact of HGB on C_{max} and AUC was less pronounced, where patients with HGB 120 g/L again exhibited higher exposure (22.37% and 23.87% increase, respectively, on occasion 1 and 6.10% and 7.82%, respectively, on occasion 2), which is expected, since these parameters are less dependent on CL/F compared to C_{min}.

This effect may be of particular clinical relevance in renal transplant patients, who frequently present lower HGB levels compared with healthy children or adults [36]. Given that even modest alterations in CsA exposure can markedly affect the risk of under- or over-immunosuppression, HGB-related variability in CL/F and consequently in C_{min}, C_{max}, and AUC warrants careful consideration. A possible explanation for this HGB effect on CsA CL/F is that HGB may influence CsA disposition due to erythrocyte binding; a lower HGB could reduce total CsA binding, effectively increasing CL/F. Many studies showed that HCT, another biomarker related to the erythrocyte, can have an effect on CL/F for the same reason related to the distribution of CsA [4,6,9,17,24,26,32]. Nevertheless, our results suggest that HGB may serve as a more sensitive and clinically relevant biomarker for capturing variability in CsA PK, particularly in paediatric and young adult renal transplant recipients.

This study has several limitations. Firstly, the sample size is relatively small and did not include the full paediatric age spectrum, particularly younger patients in whom hepatic enzyme ontogeny plays a more prominent role. The median age of the study population was 12 years, indicating that most patients were beyond early developmental maturation. Therefore, the observed PK variability is more likely attributable to interindividual differences in physiological and haematological parameters rather than ongoing enzyme maturation. Data were collected retrospectively, which probably affected their accuracy to some extent. Furthermore, data on genetic polymorphism were not available for all

https://doi.org/10.3390/pharmaceutics18010099

patients, which, combined with the small sample size, resulted in the model in which none of the polymorphisms were included in explaining variability in CsA PK parameters. Such downsides and challenges could be overcome with a prospective study that includes more patients and more complete data.

5. Conclusions

The results of this research suggest that CsA PK can be influenced by HGB levels, representing, to our knowledge, the first report of such a finding. As kidney transplant patients are prone to anaemia, CsA therapy in this population should involve careful monitoring of drug concentrations and HGB, which is routinely checked in these patients, along with other biomarkers, making this convenient for everyday practice. As shown, large changes may occur mainly in C_{min}, while C_{max} and AUC changes are moderate compared with C_{min}. These variations can result in significant deviations from target concentration ranges, which are crucial for effective and safe therapy in this vulnerable population.

Author Contributions: M.R. data curation, data analysis, writing—original draft; M.C., I.G. and B.S. data curation, patient recruitment, writing—review and editing; M.J. interpretation of data, writing—review and editing; B.M. conceptualization, writing—review and editing; K.V. conceptualization, interpretation of data, methodology, writing—review and editing, supervision. All authors have read and agreed to the published version of the manuscript.

Funding: This research was funded by the Ministry of Science, Technological Development and Innovation, Republic of Serbia through two Grant Agreements with University of Belgrade—Faculty of Pharmacy No. 451-03-136/2025-03/200161 and No. 451-03-137/2025-03/200161.

Institutional Review Board Statement: The study followed the principles of the Declaration of Helsinki and was approved by the local ethical committee of the University Children's Hospital (approval number 16/223, obtained on 7 October 2025).

Informed Consent Statement: Informed consent was not obtained because this was a retrospective, non-interventional study based exclusively on routinely collected clinical data from medical records.

Data Availability Statement: The data that support the findings of this study are not openly accessible due to ethical restrictions.

Conflicts of Interest: The authors declare no conflicts of interest.

References

1. Filler, G. Calcineurin Inhibitors in Pediatric Renal Transplant Recipients. *Paediatr. Drugs* **2007**, *9*, 165–174. [CrossRef]
2. Kaijansinkko, H.; Tainio, J.; Bjerre, A.; Gjerstad, A.C.; Weinreich, I.D.S.; Jalanko, H.; Wennberg, L.; Westphal Ladfors, S.; Thiesson, H.C.; Bekassy, Z.; et al. Changes in Maintenance Immunosuppression after Pediatric Kidney Transplantation—A Report from the Nordic Pediatric Kidney Transplantation Registry. *Pediatr. Nephrol.* **2025**, *41*, 547–556. [CrossRef]
3. Pape, L. State-of-the-Art Immunosuppression Protocols for Pediatric Renal Transplant Recipients. *Pediatr. Nephrol.* **2019**, *34*, 187–194. [CrossRef]
4. Fanta, S.; Jönsson, S.; Backman, J.T.; Karlsson, M.O.; Hoppu, K. Developmental Pharmacokinetics of Ciclosporin—A Population Pharmacokinetic Study in Paediatric Renal Transplant Candidates. *Br. J. Clin. Pharmacol.* **2007**, *64*, 772–784. [CrossRef]
5. Lindholm, A.; Henricsson, S.; Lind, M.; Dahlqvist, R. Intraindividual Variability in the Relative Systemic Availability of Cyclosporin after Oral Dosing. *Eur. J. Clin. Pharmacol.* **1988**, *34*, 461–464. [CrossRef]
6. Wu, K.H.; Cui, Y.M.; Guo, J.F.; Zhou, Y.; Zhai, S.D.; Cui, F.D.; Lu, W. Population Pharmacokinetics of Cyclosporine in Clinical Renal Transplant Patients. *Drug Metab. Dispos.* **2005**, *33*, 1268–1275. [CrossRef]
7. Ptachcinski, R.J.; Venkataramanan, R.; Burckart, G.J. Clinical Pharmacokinetics of Cyclosporin. *Clin. Pharmacokinet.* **1986**, *11*, 107–132. [CrossRef]
8. Kahan, B.D. Therapeutic Drug Monitoring of Cyclosporine: 20 Years of Progress. *Transplant. Proc.* **2004**, *36*, S378–S391. [CrossRef] [PubMed]
9. Han, K.; Pillai, V.C.; Venkataramanan, R. Population Pharmacokinetics of Cyclosporine in Transplant Recipients. *AAPS J.* **2013**, *15*, 901–912. [CrossRef] [PubMed]

10. Cai, R.; Zhang, L.; Wu, T.; Huang, Y.; Lu, J.; Huang, T.; Wu, Y.; Wu, D.; Qi, J.; Niu, L.; et al. Population Pharmacokinetics of Cyclosporine A in Pediatric Patients with Thalassemia Undergoing Allogeneic Hematopoietic Stem Cell Transplantation. *Eur. J. Clin. Pharmacol.* **2024**, *80*, 685–696. [CrossRef] [PubMed]
11. Xiaoli, D.; Qiang, F. Population Pharmacokinetic Study of Cyclosporine in Patients with Nephrotic Syndrome. *J. Clin. Pharmacol.* **2009**, *49*, 782–788. [CrossRef]
12. Grossman, R.M.; Chevret, S.; Abi-Rached, J.; Blanchet, F.; Dubertret, L. Long-Term Safety of Cyclosporine in the Treatment of Psoriasis. *Arch. Dermatol.* **1996**, *132*, 623–629. [CrossRef] [PubMed]
13. Gijtenbeek, J.M.M.; Van Den Bent, M.J.; Vecht, C.J. Cyclosporine Neurotoxicity: A Review. *J. Neurol.* **1999**, *246*, 339–346. [CrossRef]
14. Jovanović, M.; Vučićević, K. Pediatric Pharmacokinetic Considerations and Implications for Drug Dosing. *Arh. Farm.* **2022**, *72*, 340–352. [CrossRef]
15. Feng, H.; Wang, X.; Zheng, W.; Liu, S.; Jiang, H.; Lin, Y.; Qiu, H.; Chan, T.F.; Huang, M.; Li, Y.; et al. Initial Dosage Optimisation of Cyclosporine in Chinese Paediatric Patients Undergoing Allogeneic Haematopoietic Stem Cell Transplantation Based on Population Pharmacokinetics: A Retrospective Study. *BMJ Paediatr. Open* **2023**, *7*, e002003. [CrossRef]
16. Mao, J.; Qiu, X.; Qin, W.; Xu, L.; Zhang, M.; Zhong, M. Factors Affecting Time-Varying Clearance of Cyclosporine in Adult Renal Transplant Recipients: A Population Pharmacokinetic Perspective. *Pharm. Res.* **2021**, *38*, 1873–1887. [CrossRef]
17. Xue, L.; Zhang, W.W.; Ding, X.L.; Zhang, J.J.; Bao, J.A.; Miao, L.Y. Population Pharmacokinetics and Individualized Dosage Prediction of Cyclosporine in Allogeneic Hematopoietic Stem Cell Transplant Patients. *Am. J. Med. Sci.* **2014**, *348*, 448–454. [CrossRef] [PubMed]
18. Schwartz, G.J.; Muñoz, A.; Schneider, M.F.; Mak, R.H.; Kaskel, F.; Warady, B.A.; Furth, S.L. New Equations to Estimate GFR in Children with CKD. *J. Am. Soc. Nephrol.* **2009**, *20*, 629–637. [CrossRef]
19. Green, B.; Duffull, S.B. Development of a Dosing Strategy for Enoxaparin in Obese Patients. *Br. J. Clin. Pharmacol.* **2003**, *56*, 96–103. [CrossRef]
20. Growth Charts—Percentile Data Files with LMS Values. Available online: https://www.cdc.gov/growthcharts/cdc-data-files.htm (accessed on 9 December 2025).
21. Neoral Oral Solution—Summary of Product Characteristics (SmPC)—(emc) | 5300. Available online: https://www.medicines.org.uk/emc/product/5300/smpc#gref (accessed on 9 December 2025).
22. Chen, B.; Zhang, W.X.; Gu, Z.D.; Li, J.; Zhang, Y.X.; Cai, W.M. Population Pharmacokinetic Study of Cyclosporine in Chinese Renal Transplant Recipients. *Eur. J. Clin. Pharmacol.* **2011**, *67*, 601–612. [CrossRef]
23. Ji, E.; Kim, M.Y.; Yun, H.Y.; Kim, K.I.; Kang, W.; Kwon, K.I.; Kim, I.W.; Lee, H.S.; Shin, W.G.; Oh, J.M. Population Pharmacokinetics of Cyclosporine in Korean Adults Undergoing Living-Donor Kidney Transplantation. *Pharmacotherapy* **2011**, *31*, 574–584. [CrossRef]
24. Zhou, H.; Gao, Y.; Cheng, X.L.; Li, Z.D. Population Pharmacokinetics of Cyclosporine A Based on NONMEM in Chinese Allogeneic Hematopoietic Stem Cell Transplantation Recipients. *Eur. J. Drug Metab. Pharmacokinet.* **2012**, *37*, 271–278. [CrossRef]
25. Li, T.F.; Hu, L.; Ma, X.L.; Huang, L.; Liu, X.M.; Luo, X.X.; Feng, W.Y.; Wu, C.F. Population Pharmacokinetics of Cyclosporine in Chinese Children Receiving Hematopoietic Stem Cell Transplantation. *Acta Pharmacol. Sin.* **2019**, *40*, 1603–1610. [CrossRef]
26. Xue, L.; Zhang, W.J.; Tian, J.X.; Liu, L.N.; Yan, H.H.; Zhang, W.W.; Ding, X.L.; Zhang, J.J.; Miao, L.Y. Multicenter-Based Population Pharmacokinetic Analysis of Ciclosporin in Hematopoietic Stem Cell Transplantation Patients. *Pharm. Res.* **2019**, *37*, 15. [CrossRef]
27. Chen, X.; Yu, X.; Wang, D.; Xu, H.; Li, Z. Initial Dosage Optimization of Ciclosporin in Pediatric Chinese Patients Who Underwent Bone Marrow Transplants Based on Population Pharmacokinetics. *Exp. Ther. Med.* **2020**, *20*, 401–408. [CrossRef] [PubMed]
28. Ling, J.; Yang, X.P.; Dong, L.L.; Jiang, Y.; Zou, S.L.; Hu, N.; Chen, R. Population Pharmacokinetics of Ciclosporin in Allogeneic Hematopoietic Stem Cell Transplant Recipients: C-Reactive Protein as a Novel Covariate for Clearance. *J. Clin. Pharm. Ther.* **2022**, *47*, 483–492. [CrossRef]
29. Irtan, S.; Saint-Marcoux, F.; Rousseau, A.; Zhang, D.; Leroy, V.; Marquet, P.; Jacqz-Aigrain, E. Population Pharmacokinetics and Bayesian Estimator of Cyclosporine in Pediatric Renal Transplant Patients. *Ther. Drug Monit.* **2007**, *29*, 96–102. [CrossRef] [PubMed]
30. Woillard, J.B.; Lebreton, V.; Neely, M.; Turlure, P.; Girault, S.; Debord, J.; Marquet, P.; Saint-Marcoux, F. Pharmacokinetic Tools for the Dose Adjustment of Ciclosporin in Haematopoietic Stem Cell Transplant Patients. *Br. J. Clin. Pharmacol.* **2014**, *78*, 836–846. [CrossRef] [PubMed]
31. Lukas, J.C.; Suárez, A.M.; Valverde, M.P.; Calvo, M.V.; Lanao, J.M.; Calvo, R.; Suarez, E.; Gil, A.D. Time-Dependent Pharmacokinetics of Cyclosporine (Neoral) in de Novo Renal Transplant Patients. *J. Clin. Pharm. Ther.* **2005**, *30*, 549–557. [CrossRef]
32. Yin, O.Q.P.; Lau, S.K.; Chow, M.S.S. Population Pharmacokinetics of Cyclosporine in Chinese Cardiac Transplant Recipients. *Pharmacotherapy* **2006**, *26*, 790–797. [CrossRef]
33. Parke, J.; Charles, B.G. Factors Affecting Oral Cyclosporin Disposition after Heart Transplantation: Bootstrap Validation of a Population Pharmacokinetic Model. *Eur. J. Clin. Pharmacol.* **2000**, *56*, 481–487. [CrossRef] [PubMed]

34. Holford, N.; Heo, Y.A.; Anderson, B. A Pharmacokinetic Standard for Babies and Adults. *J. Pharm. Sci.* **2013**, *102*, 2941–2952. [CrossRef]
35. Kim, M.G.; Kim, I.W.; Choi, B.; Han, N.; Yun, H.Y.; Park, S.; Oh, J.M. Population Pharmacokinetics of Cyclosporine in Hematopoietic Stem Cell Transplant Patients: Consideration of Genetic Polymorphisms. *Ann. Pharmacother.* **2015**, *49*, 622–630. [CrossRef] [PubMed]
36. Schechter, A.; Gafter-Gvili, A.; Shepshelovich, D.; Rahamimov, R.; Gafter, U.; Mor, E.; Chagnac, A.; Rozen-Zvi, B. Post Renal Transplant Anemia: Severity, Causes and Their Association with Graft and Patient Survival. *BMC Nephrol.* **2019**, *20*, 51. [CrossRef] [PubMed]

Disclaimer/Publisher's Note: The statements, opinions and data contained in all publications are solely those of the individual author(s) and contributor(s) and not of MDPI and/or the editor(s). MDPI and/or the editor(s) disclaim responsibility for any injury to people or property resulting from any ideas, methods, instructions or products referred to in the content.

pharmaceutics

MDPI

Article

Integrating Clopidogrel's First-Pass Effect in a Joint Semi-Physiological Population Pharmacokinetic Model of the Drug and Its Inactive Carboxylic Acid Metabolite

Zorica Pejčić [1,2], Valentina Topić Vučenović [3], Branislava Miljković [2] and Katarina M. Vučićević [2,*]

[1] Medicines and Medical Devices Agency of Serbia, Vojvode Stepe 458, 11221 Belgrade, Serbia; pejcic.z@gmail.com
[2] Department of Pharmacokinetics and Clinical Pharmacy, Faculty of Pharmacy, University of Belgrade, Vojvode Stepe 450, 11221 Belgrade, Serbia; branislava.miljkovic@pharmacy.bg.ac.rs
[3] Department of Pharmacokinetics and Clinical Pharmacy, Faculty of Medicine, University of Banja Luka, Save Mrkalja 14, 78000 Banja Luka, Bosnia and Herzegovina; valentina.topic.vucenovic@med.unibl.org
* Correspondence: katarina.vucicevic@pharmacy.bg.ac.rs

Abstract: Clopidogrel (CLO), a pro-drug for preventing thrombotic events, undergoes rapid absorption and extensive metabolism, with approximately 85–90% converted to an inactive carboxylic acid metabolite (CLO-CA) and the remaining to an active thiol (CLO-TH). Few pharmacokinetic models for the drug and its metabolites exist, with most focusing on CLO-TH. Although CLO-CA is inactive, its predominant (compared to its parent drug and metabolites) presence in plasma underscores the importance of characterizing its formation and pharmacokinetic profile. This study aimed to characterize the process of the absorption of CLO and its conversion to CLO-CA via developing a population pharmacokinetic model. Individual participants' data from two bioequivalence studies were utilized. Extensive blood samples were collected at predetermined intervals, including 841 concentrations of CLO and 1149 of CLO-CA. A nonlinear, mixed-effects modelling approach using NONMEM® software (v 7.5) was applied. A one-compartment model was chosen for CLO, while a two-compartment proved optimal for CLO-CA. Absorption from the depot compartment was modeled via two transit compartments, incorporating transit rate constants (K_{tr}). A semi-physiological model explained the first-pass effect of CLO, integrating a liver compartment. The estimated mean transit times (*MTTs*) for the studies were 0.470 and 0.410 h, respectively. The relative bioavailability for each study's generic medicine compared to the reference were 1.08 and 0.960, respectively. Based on the estimated parameters, the fractions metabolized to inactive metabolites (F_{iaM}_st1 and F_{iaM}_st2) were determined to be 87.27% and 86.87% for the two studies, respectively. The appropriateness of the final model was confirmed. Our model offers a robust framework for elucidating the pharmacokinetic profiles of CLO and CLO-CA.

Keywords: clopidogrel; absorption; transit model; FPE; metabolism; PopPK; NONMEM

1. Introduction

Clopidogrel (CLO) is a pro-drug that inhibits platelet aggregation and is indicated for the prevention of atherothrombotic and thromboembolic events in clinical conditions such as myocardial infarction, ischemic stroke, acute coronary syndrome, atrial fibrillation, and peripheral vascular diseases. The absorption of CLO after oral administration is rapid, with the maximum plasma concentration being reached after 45 min and at least 50% of the administered dose being absorbed. Clopidogrel is extensively metabolized in the liver. Most of the absorbed CLO (approximately 85% of an oral dose) is hydrolyzed by esterase to the inactive metabolite clopidogrel carboxylic acid (CLO-CA). Approximately 10–15% of orally absorbed CLO is oxidized in two steps by cytochrome P450 (CYP) isoenzymes to its active metabolite clopidogrel thiol (CLO-TH) [1–4]. In the first oxidation step, which is

catalyzed by CYP1A2, CYP2B6 and CYP2C19, an intermediate metabolite, 2-oxo-CLO, is formed. In the second step, approximately 50% of the 2-oxo-CLO is further oxidized by CYP2B6, CYP2C9, CYP2C19 and CYP3A4/A5 to CLO-TH, which is responsible for the pharmacological effect of the drug. CLO-CA is the major circulating metabolite, with much higher plasma levels than both CLO and CLO-TH [1,2,5].

At the time of the development of the first CLO products, the pharmacokinetic profile of CLO was based on the inactive metabolite CLO-CA, as bioanalytical methods were not sensitive enough to quantify the concentrations of CLO or the active metabolite CLO-TH [6–8]. The introduction of state-of-the-art sensitive analytical methods has made it possible to reliably quantify CLO concentrations. Therefore, the current regulatory guidelines recommend that in the development of generic medicines, the demonstration of bioequivalence between generic and reference CLO medicines is based on the parent pro-drug [6]. Consequently, bioequivalence studies based on CLO [9,10], CLO-CA concentrations [11] or both [12–16] are available in the literature. Bioequivalence studies are designed to include frequent blood sampling, strictly standardized conditions and clearly defined inclusion/exclusion criteria for subjects to allow for good control of all potential sources of variability. A non-compartmental analysis is commonly acknowledged as the gold standard for determining bioequivalence, notwithstanding its' constraints and the availability of compartmental and nonlinear, mixed-effects modeling approaches. The pharmacokinetic data obtained in bioequivalence studies are rich, especially during the absorption phase, and could therefore be used to characterize the absorption process including the first-pass effect (FPE) of the drug in more detail. Moreover, if both parent drug and metabolite concentrations are available, a joint pharmacokinetic model can be developed. For drugs that exhibit high inter-individual and intra-individual pharmacokinetic variabilities, such as CLO, a nonlinear, mixed-effects modeling approach may be more appropriate for delineating and quantifying the various levels of variability [17,18].

To the best of our knowledge, there are only a few published population pharmacokinetic models describing CLO and its metabolites [4,19–24], most of which focus on the CLO-TH metabolite in combination with the parent drug [4,22–24] or alone [21]. Physiologically based pharmacokinetic models have also been developed [3,25–27]. Although the metabolite CLO-CA is inactive, its predominant (compared to its parent drug and metabolites) presence in plasma underscores the importance of characterizing its formation and pharmacokinetic profile. To date, this inactive metabolite's population pharmacokinetics models have been investigated in only a few publications, including a single joint-population pharmacokinetic model with its parent drug [4,19,20]. Hence, the aim of this study was to synthesize data from two bioequivalence studies in order to characterize the process of the absorption of CLO and its conversion to CLO-CA through a joint population semi-physiological pharmacokinetic model.

2. Materials and Methods

2.1. Subjects and Data

Individual participants' data from two bioequivalence studies of CLO formulations, namely Study 1 and Study 2, were utilized. In each study, a single generic 75 mg film-coated tablet of CLO was assessed against Plavix 75 mg film-coated tablets (Sanofi Winthrop Industrie, Ambares, France), serving as the reference medicine. Both studies followed the same 2-way cross-over design (2 treatments, 2 periods, and 2 sequences), with subjects receiving a single CLO dose of 150 mg (2 tablets) under fasting conditions. The studies were conducted at the Military Medical Academy, Belgrade, Republic of Serbia, in compliance with the Declaration of Helsinki [28], the requirements of Good Clinical Practice [29], and the regulatory guidelines for bioequivalence studies conduct [30]. Institutional review board approval from the Military Medical Academy was obtained for the study protocols and informed consent forms. Secondary use of the study data was authorized by the study sponsor.

The eligible subjects were healthy adult volunteers of Caucasian origin of both sexes, with 24 in Study 1 and 26 in Study 2, all of whom had signed an informed consent form and met the predefined inclusion and none of the exclusion criteria. These criteria controlled for various factors that could have potentially influenced the results of the study, leading to more reliable and interpretable results. Study 1 involved healthy subjects aged 21 to 53 years whose body mass indexes (BMIs) ranged from 19 to 26 kg/m^2, while Study 2 participants were aged 19 to 42 years and had BMIs of 19 to 29 kg/m^2. During each study, the subjects each received the generic medicine once and the reference medicine once, according to the randomization scheme. Extensive blood samples were taken at predefined time intervals. In Study 1, sampling was conducted up to 48 h post-medicine administration, with 14 blood samples collected per subject per period, resulting in a total of 672 samples. In Study 2, sampling was performed up to 36 h after medicine administration, with 17 samples per subject per period, yielding a total of 884 samples. Plasma was separated from blood, and concentrations of CLO and CLO-CA were determined in both studies using a validated HPLC-MS analytical method, with a lower limit of quantification (LLOQ) of 0.5 ng/mL for CLO and 0.1 µg/mL for CLO-CA. Our dataset consisted of all demographic and clinical assessment data, including biochemical parameters, randomization scheme, time of dose administration and blood sampling, as well as reported concentrations of CLO and CLO-CA.

2.2. Data Analysis

The dataset for this study encompassed various parameters, including the time of dosing, individual values of the CLO and CLO-CA concentrations, time of blood collection and each study's details (sequence, period and formulation), as well as all demographic (sex, age, body weight, height and BMI) and biochemical parameters (total bilirubin, serum creatinine, aspartate transaminase (AST) and alanine transaminase (ALT)). A descriptive statistical analysis was employed to evaluate the demographic characteristics and biochemical parameters of all 50 subjects from both studies. A population pharmacokinetic analysis was conducted using a nonlinear mixed effects modelling approach with NONMEM® software (v7.5, ICON development solutions Ellicott City, MD, USA) [17,31,32]. Descriptive statistics and graphical presentations of the results were created using the appropriate packages in R® (v4.1.3, R Foundation for Statistical Computing) [33] and RStudio® (v1.4.1717) [34].

A total of 841 non-zero concentrations of CLO and 1149 of CLO-CA were used in the pharmacokinetic modelling. Data below the LLOQ (BLLOQ) were excluded from the analysis. The process of pharmacokinetic model-building involved multiple steps, concentrating on both the structural and statistical parts for both CLO and CLO-CA. The absorption of CLO was evaluated using various models, starting from a simple first-order model without and with a delayed absorption onset. Furthermore, considerations were made for absorption via hard-coded (2, 3 or 4 compartments) and estimated numbers of transit compartments [35]. Both one- and two-compartment models with first-order elimination were explored for both CLO and CLO-CA.

Given that CLO demonstrates an extensive FPE, exceeding 90%, the conversion of CLO to CLO-CA was examined using a model that incorporated a liver compartment. It was presumed that all parent drugs would ultimately undergo metabolism in this compartment. Integrated semi-physiological models of similar structure with FPEs have been previously published [4,24,36,37]. The model employed a physiological liver volume of 1.5 L and a liver plasma flow (Q_h) of 50 L/h [24]. To account for the differences in molecular weights between CLO and CLO-CA (321.82 and 307.80, respectively), a scaling factor of 0.9565 was applied to the formation rate of CLO-CA. The fractions of the dose metabolized to the inactive CLO-CA (F_{iaM}), active metabolite CLO-TH (F_{aM}) and remaining fraction of parent drug (F_P) were assumed to follow a logit-normal distribution. Hence, they were study-specific and coded as follows:

$$F_{iaM} = \frac{FR_1}{1 + FR_1 + FR_2}, \quad (1)$$

$$F_{aM} = \frac{FR_2}{1 + FR_1 + FR_2} \text{ and} \quad (2)$$

$$F_P = \frac{1}{1 + FR_1 + FR_2}, \quad (3)$$

where FR_1 and FR_2 are model parameters supporting the calculation of the corresponding fractions of the dose without any physiological meaning. Certain parameters needed to be fixed to ensure the stability of the model. Hence, F_{aM} was fixed to the estimated value of 12%, which corresponded to the literature data [1–4]. Nevertheless, a sensitivity analysis was performed by varying the values of F_{aM} at 10% and 15%. F_{iaM} and F_P were calculated from the estimated FR_1 in the model for each study. Initially, clearance of the parent drug (CL_P) was estimated at 89.5 L/h, and subsequently, it was fixed at the estimated value in order to stabilize the model. Bioavailability for the reference medicine (F) was fixed at 100%, and the relative bioavailability for the generic medicines from each of the two studies (F_{gen_st1} and F_{gen_st2}) were estimated during modeling.

Inter-individual (IIV) random effects were described by a log-normal distribution of the parameters while a study-specific proportional error model described the intra-individual variability. Moreover, considering the cross-over design of bioequivalence studies, inter-occasional variability (IOV) was incorporated in the absorption parameters.

Classical covariate model-building was not applied, as the inclusion/exclusion criteria ensured a homogenous population of healthy subjects, and there were no differences in the demographic characteristics and biochemical parameters among the studies. However, the incorporation of body-weight via allometric scaling was applied to corresponding clearance(s) using an allometric exponent of 0.75 and volume(s) of distribution with an exponent of 1.

The adequacy of the model was determined based on several criteria, including successful minimization, number of significant digits, gradients in the last iteration, values and changes in objective function (OFV), Akaike information criterion (AIC), Bayesian information criterion (BIC) and precision of parameter estimates. These factors collectively assessed the reliability and accuracy of the model in capturing the observed data and its ability to provide meaningful insights into the underlying pharmacokinetic behavior based on the population semi-physiological model. Furthermore, a graphical evaluation employing goodness-of-fit plots was used to assess the agreement between the observed and predicted values of the CLO and CLO-CA concentrations across the different time points. These diagnostics provided insights into the model's predictive performance [31,38,39].

The nonparametric sample importance resampling (SIR) technique, including 1000 replicates, was employed [40]. The parameters' 95% confidence intervals (CI), obtained through SIR-based simulations, were compared to the estimates derived from the dataset. Additionally, the predicted performance of the final model was assessed using a visual predictive check [41,42], involving 1000 simulations. By plotting the observed data alongside the simulated data from the model, the VPCs allowed for a visual comparison of how well the model predicted the central tendencies and variabilities in the observed data.

3. Results

The demographic characteristics and biochemical parameters of a total 50 subjects from two bioequivalence studies are presented in Table 1. There were no statistically significant differences observed in the subjects' characteristics among the studies.

The final dataset for the pharmacokinetic analysis consisted of 841 non-zero concentrations of CLO and 1149 of CLO-CA. The BLLOQs for CLO and CLO-CA were excluded from the analysis. A majority (87.48%) of the excluded BLLOQs were at/after 6 h for CLO, and 78.50% of those were at/after 12 h for CLO-CA. The maximum plasma concentrations were, on average, 7.2 ng/mL and 4.9 μg/mL for CLO and CLO-CA, respectively. Due to issues with parameter unidentifiability when using the two-compartment model, we opted to utilize a one-compartment model for CLO instead. Conversely, for CLO-CA, the best fit was achieved with the two-compartment model. Absorption from the depot

compartment was best described with a transit model including two transit compartments with a transit rate constant (K_{tr}). The mean transit time (*MTT*) was estimated for each study. As previously described, a hepatic (liver) compartment was utilized to characterize the FPE of CLO. A schematic illustration depicting the structural model for CLO and CLO-CA is presented in Figure 1.

Table 1. Demographic characteristics and biochemical parameters of the subjects.

Characteristics (Units)		Number (%)/Mean ± Standard Deviation (Range)
Gender	Male	29 (58.00)
	Female	21 (42.00)
Age (year)		31.94 ± 8.51 (19–54)
Body-weight (kg)		74.1 ± 13.56 (47–100)
Height (cm)		177.26 ± 9.06 (155–194)
Body mass index (kg/m^2)		23.40 ± 2.66 (19.10–29.30)
Bilirubin (µmol/L)		9.1 ± 4.43 (3–25)
Serum creatinine (µmol/L)		81.5 ± 17.70 (53–114)
Alanine transaminase (ALT) (U/L)		26.2 ± 9.85 (11–52)
Aspartate transaminase (AST) (U/L)		23.7 ± 4.80 (16–35)

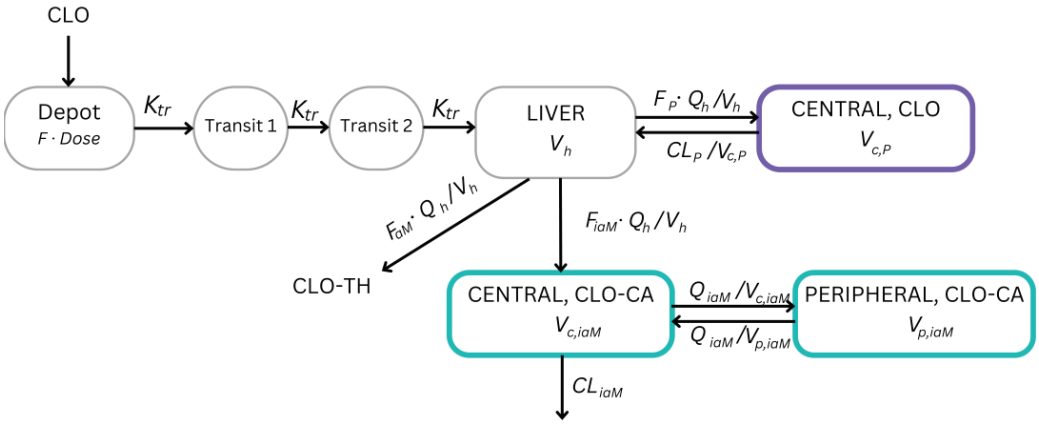


Figure 1. A schematic illustration of the final joint population semi-physiological pharmacokinetic model for clopidogrel (CLO) and its active (CLO-TH) and inactive (clopidogrel carboxylic acid (CLO-CA)) metabolites. CL_{iaM}, clearance of inactive metabolite; CL_P, clearance of parent drug; F, bioavailability; F_{aM}, fraction metabolized to active metabolite; F_{iaM}, fraction metabolized to inactive metabolite; F_P, remaining fraction of the parent drug; K_{tr}, transit rate constant; Q_h, liver plasma flow; Q_{iaM}, intercompartmental clearance of inactive metabolite; $V_{c,iaM}$, volume of central compartment of inactive metabolite; $V_{p,iaM}$, volume of peripheral compartment of inactive metabolite; $V_{c,P}$, volume of distribution of parent drug; V_h, volume of the hepatic (liver) compartment.

Ultimately, the IIV exponential model was incorporated in the volume of distribution of the parent drug ($V_{c,P}$), the volume of the central compartment for the inactive metabolite ($V_{c,iaM}$) and FR_1 and F for each study, separately. When added to the other parameters, IIV resulted in imprecise estimates and over-parameterization of the model. Exponential models ensure positive values for individual parameters, and consequently, they are the most preferred model for IIV. The inclusion of IOV on the absorption parameters F and *MTT* led to a statistically significant reduction in OFV by 284.202 and in AIC by 264.562. AIC as well as BIC values serve as alternatives to OFV for assessing how well a model fits its data while also factoring in its complexity. A lower AIC value suggests a better balance between model fit and its complexity. BIC, on the other hand, leans towards simpler models with fewer parameters while also considering the sample size for assessing model complexity. Hence, statistically significant drops in OFV, AIC and BIC values of 440.102, 420.102 and 364.143, respectively, were observed starting from the base to the final model.

A total of 24 (including 11 structural) model parameters were estimated (Table 2). The estimated *MTT* values for the two studies were 0.470 and 0.410 h, respectively. The relative bioavailability for each generic medicine compared to the reference medicine (F_{gen}_st1 and F_{gen}_st2) were 1.08 and 0.960, respectively, and their 95% CIs included one. Based on the estimated parameters, the fractions metabolized to inactive metabolites (F_{iaM}_st1 and F_{iaM}_st2) were determined to be 87.27% and 86.87% for the two studies, respectively. A summary of the CLO and CLO-CA parameter estimates obtained from the final population semi-physiological pharmacokinetic model is provided in Table 2. The relative standard errors for the structural parameters ranged up to 14.9%.

Table 2. Final parameter estimates for the joint population pharmacokinetic model for clopidogrel (CLO) and its inactive metabolite, clopidogrel carboxylic acid (CLO-CA).

Parameters (Units)	**Dataset**		**Sampling Importance Resampling (SIR)**	
	Estimate	**95% CI**	**Median**	**2.5–97.5 Percentile**
CL_P (L/h/70 kg)	89.5 FIX	-	-	-
$V_{c,P}$ (L/70 kg)	218	188–248	217	189–243
MTT_st1 (h)	0.470	0.425–0.515	0.471	0.429–0.516
F_{gen}_st1	1.08	0.993–1.17	1.08	0.995–1.16
FR_1_st1	119	84.3–154	118	88.2–155
CL_{iaM} (L/h/70 kg)	8.70	7.38–10.0	8.60	7.59–9.73
$V_{c,iaM}$ (L/70 kg)	23.7	19.7–27.7	23.4	20.0–26.9
Q_{iaM} (L/h/70 kg)	10.8	8.02–13.6	10.8	8.94–13.0
$V_{p,iaM}$ (L/70 kg)	61.3	50.3–72.3	60.9	52.4–70.2
Q_h (L/h)	50 FIX	-	-	-
V_h (L/70 kg)	1.5 FIX	-	-	-
MTT_st2 (h)	0.410	0.381–0.439	0.411	0.385–0.438
F_{gen}_st2	0.960	0.818–1.10	0.952	0.840–1.07
FR_1_st2	76.8	64.8–88.8	76.0	66.3–85.9
Inter-Individual (IIV)/Inter-Occasional Variability (IOV)	**Estimate CV (%)**	**RSE (%)**	**Median CV (%)**	**2.5–97.5 Percentile**
IIV *($V_{c,P}$)*	45.82	10.4	45.69	37.38–53.99
IIV *($V_{c,iaM}$)*	25.06	13.2	25.30	18.54–30.38
IIV *(F_st1)*	42.66	13.8	42.40	29.99–51.26
IIV *(F_st2)*	25.88	24.1	26.31	14.16–35.57
IOV *(F_st1)*	8.83	32.9	9.29	3.03–13.33
IOV *(F_st2)*	23.24	13.6	23.76	18.21–28.27
IOV *(MTT_st1)*	25.44	16.8	25.58	16.22–32.97
IOV *(MTT_st2)*	27.48	9.9	27.46	21.86–32.39
IIV *(FR_1_st1)*	72.80	10.5	73.59	57.52–89.97
IIV *(FR_1_st2)*	27.86	13.0	28.36	20.25–34.18
Residual Error	**Estimate (%)**	**RSE (%)**	**Median CV (%)**	**2.5–97.5 Percentile**
Wp (st1)	41.95	3.4	41.98	39.37–44.50
Wp (st2)	29.39	5.7	29.51	27.57–31.62

CL_{iaM}, clearance of inactive metabolite; CL_P, clearance of parent drug; CV, coefficient of variation; FR_1_st1, and FR_1_st2, fraction parameter for inactive metabolite for study 1and study 2, respectively; IIV, inter-individual variability for the corresponding parameter; IOV, inter-occasional variability for the corresponding parameter; *MTT_st1*, mean transit time for study 1; *MTT_st2*, mean transit time for study 2; Q_h, liver plasma flow; Q_{iaM}, intercompartmental clearance of inactive metabolite; F_{gen}_st1 and F_{gen}_st2, relative bioavailability of generic compared to reference medicine for study 1 and study 2, respectively; RSE, relative standard error; $V_{c,iaM}$, volume of central compartment of inactive metabolite; V_h, volume of hepatic compartment; $V_{p,iaM}$, volume of peripheral compartment of inactive metabolite; $V_{c,P}$, volume of distribution of parent drug; *F_st1* and *F_st2*, bioavailability in study 1 and 2, respectively; *Wp*, proportional residual error for the corresponding study.

Diagnostic plots of the final model are presented in Figure 2. Data for the observed and model predicted concentrations of CLO and CLO-CA are presented together; however, the CLO concentration was measured in ng/mL while CLO-CA was measured in µg/mL.

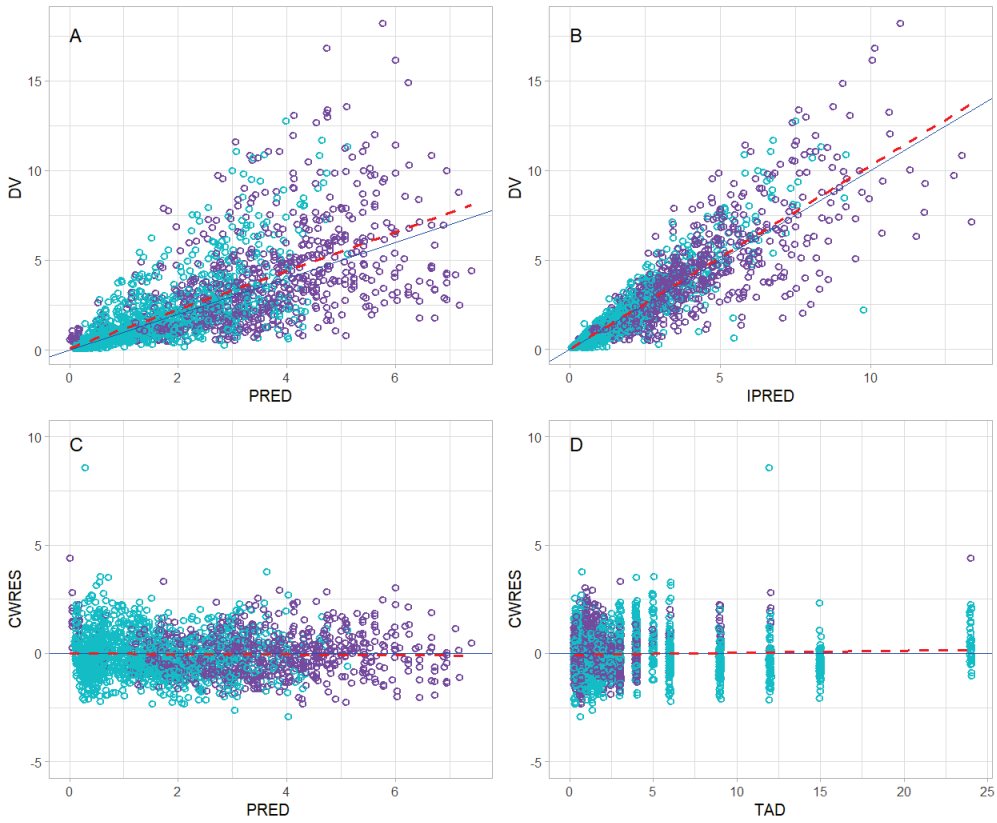


Figure 2. Goodness-of-fit plots of the final model for clopidogrel (CLO), shown in the purple color, and its inactive metabolite, clopidogrel carboxylic acid (CLO-CA), shown in the green color. Data for CLO (ng/mL) and CLO-CA (µg/mL) are presented together. (**A**) The observed (DV) versus population predicted values (PRED); (**B**) DV versus individual model predicted values (IPRED); (**C**) conditional weighted residuals (CWRES) versus PRED; and (**D**) CWRES versus time after dose (hour). The solid lines represent the lines of identity in (**A**,**B**) and the zero lines in (**C**,**D**). The dashed lines represent the regression lines.

The appropriateness of the final population semi-physiological pharmacokinetic model and parameter precision evaluation was confirmed by the SIR technique. The typical parameter estimates, standard errors and 95% CIs using the original dataset were similar to those obtained from 1000 successful replicate runs (Table 2). Moreover, model appropriateness was visually confirmed via VPCs for both CLO and CLO-CA, which showed good agreement between the measured and simulated concentration data (Figure 3).

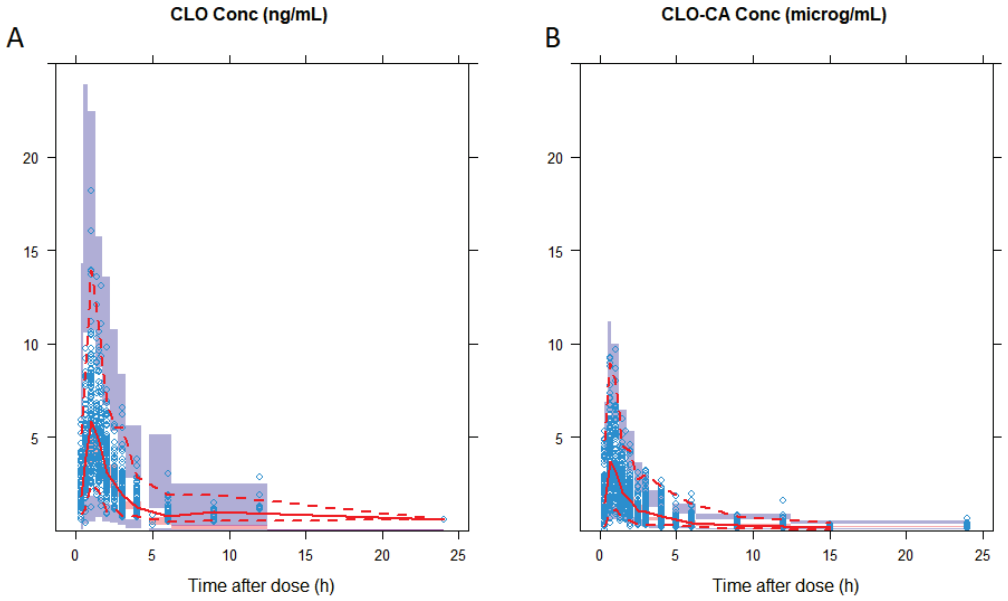


Figure 3. Visual predictive checks of the final joint population pharmacokinetic model for (**A**) clopidogrel (CLO) and (**B**) its inactive metabolite, clopidogrel carboxylic acid (CLO-CA). The observed concentrations are depicted by blue rectangles. The solid and dashed red lines represent the 50th, 5th and 95th percentiles of the predictions, respectively. The semi-transparent red shaded area represents the simulation-based 95% confidence interval (CI) for the median, while the semi-transparent purple fields represent the 95% CI around the 5th and 95th percentiles of the predicted data.

4. Discussion

We developed a joint population semi-physiological pharmacokinetic model for CLO and its inactive metabolite, CLO-CA, using nonlinear, mixed-effects modelling, leveraging data from two bioequivalence studies. The frequent blood-sampling conducted during these studies allowed for the comprehensive pharmaco-statistical characterization of CLO absorption and FPE. Out of 1556 blood samples collected per the protocols, a total of 841 non-zero CLO concentrations (54.04%) and 1149 non-zero CLO-CA concentrations (73.84%) were used in the analysis. Based on our analysis, the terminal half-life of CLO averaged 1.69 (1.46–1.92) hours. Consequently, on average, CLO was expected to completely eliminate after approximately 10 h, indicating that the sampling duration may have been too long. Indeed, a majority of the reported BLLOQs for CLO were at least 12 h after drug administration. This was comparable with the study by Jung et al. [4], where BLLOQ data for CLO were omitted, constituting 27% of the total, with blood-sampling times extending up to 24 h. Considering the sensitivity of the bioanalytical method used in Study 1 and Study 2, it is unsurprising that numerous concentrations of CLO fell into the BLLOQ category. Analogous considerations were applied to the BLLOQ data for CLO-CA, justifying the exclusion of BLLOQ data from the analysis. In each of the studies, the administration of two tablets (150 mg of CLO) was planned per the protocols as it would result in higher concentrations, and the bioanalytical method might have been sensitive enough to accurately quantify them. Therefore, our maximum concentrations and area under the concentration–time curves for both the parent drug and the metabolite exceeded what was expected after 75 mg according to the Summary of Product Characteristics [1].

For a comprehensive understanding of the complete pharmacokinetic profile of CLO, it is crucial to characterize not only its active metabolite CLO-TH, as documented in the literature [21–24], but also the inactive metabolite CLO-CA. CLO is rapidly metabolized, leading to CLO-CA being present in plasma at approximately 2000 times higher concentrations than the parent drug, as previously reported [1,6]. Moreover, studies have demonstrated a linear correlation between CLO and CLO-CA concentrations [43], and CLO-CA concentrations have been previously employed to investigate CLO pharmacokinetics during

bioequivalence studies [6]. Furthermore, studies have reported that assessing CLO-CA plasma concentrations is clinically valuable for identifying poor compliance and variable metabolisms in patients receiving CLO therapy. This suggests that plasma concentrations of CLO-CA serve as reflections of the clinical efficacy of CLO [7]. Although there are limited studies on CLO absorption and FPE to inactive metabolite [4,19,20], it remains crucial to thoroughly describe this process. The models developed by Yousef et al. [19] and Lee et al. [20] were solely based on the concentrations of the inactive metabolite CLO-CA. Therefore, we conducted an in-depth analysis to enhance the understanding of CLO pharmacokinetics, complementing the findings of Jung et al. [4], who developed a comprehensive joint model incorporating both the inactive and active metabolites. However, unlike the authors who kept the fractions fixed at values obtained from the literature, we estimated them.

Despite combining data from two studies and aiming to develop a unified model for CLO, we opted to estimate certain parameters separately for each study (Table 2). This approach was adopted as the data were derived from different study conditions, and as it led to a decrease in OFV and AIC and/or BIC values and stabilized the model.

The final model we developed effectively captured the pharmacokinetic properties of CLO and its metabolite CLO-CA, as evidenced by the numerical and graphical validation. Our model incorporated a liver compartment (Figure 1), aligning with the well-documented and extensive CLO pre-systemic hepatic metabolism of 85–90% of the absorbed CLO [1–4]. Complete metabolism of the parent drug was supported by the return of CLO to the liver from the central compartment (Figure 1). Due to the availability of CLO and CLO-CA concentrations from each study, our aim was to indirectly estimate the fractions, F_{iaM} and F_P, per study, while fixing the fraction of CLO metabolized to CLO-TH at 12%. A sensitivity analysis was performed, and the model was robust (the OFV changed by fewer than two units) to the varying values of F_{aM} of 10% and 15%. The obtained values for the fractions metabolized to CLO-CA were approximately 87% for both studies, aligning closely with the literature values of at least 85–90% [1–4]. This estimation resulted in a one-compartment model for CLO, as in Jiang et al. [24], in contrast to the two-compartment models in [4,23]. This difference was likely attributable to fixing the parameters used for the calculation of the metabolite fractions in Jung et al. [4], whereas we estimated FR_1_st1 and FR_1_st2 directly. CLO exhibits fast absorption, with a time to the maximum concentration of approximately 45 min [1]. Various absorption models have previously been used to characterize the process, including first-order absorption with/without lag time [4,19] and transit compartments [20,23,24]. Erlang-type absorption [44] with two transit compartments improved the absorption phase of CLO compared with the lag model (a statistically significant drop in the AIC of 5.416 units). This model provided a closer description of the absorption that was in line with the physiological conditions. Based on the estimated *MTT*s and two transit compartments, the transit rate constants (K_{tr}) equaled 6.38 h^{-1} and 7.32 h^{-1} for each study, respectively. Overall, the closest in structure to ours was the model established by Jiang et al. [24], but they considered a parent and an active metabolite of CLO, estimating fractions entirely physiologically using well-stirred models for clearances.

The two-compartment model effectively described the CLO-CA concentration-time profile, and the parameters' values were in agreement with previously reported data [19,20]. All final model parameters were estimated with adequate precision (Table 2). The diagnostic plots indicated good agreement between the population/individual predictions and the observed concentrations of CLO and CLO-CA (Figure 2A,B). The conditional weighted residuals (CWRES) were randomly scattered around zero across the population predictions and time after dose (Figure 2C,D). The VPCs, and shown in Figure 3, indicated the good predictive abilities of the model for both the parent drug and the inactive metabolite of CLO.

The model we developed lays a solid groundwork for potential future enhancements to create a more complex model. This could involve incorporating the formation of the active metabolite CLO-TH, genetic variations, and perhaps other factors (such as concurrent drug therapies that interact with CLO) gleaned from patient data.

Despite the strengths of our investigation, there are some limitations to consider. The two bioequivalence studies were independent and involved different subjects, although all were healthy adults with no significant differences in demographic characteristics and biochemical parameters. Therefore, a typical stepwise covariate modeling approach was not justified. This is why body-weight was allometrically included in the model. The impact of varying CYP2C19 and/or carboxylesterase 1 (CES1) phenotypes on CLO pharmacokinetics has been previously recognized [2,22,24,25,45–47]. However, polymorphism data were not available in the studies we used. Nevertheless, even if we had access to CYP2C19 polymorphism data, it is less likely that the covariate would enhance the model, given that CYP2C19 does not play a critical role in CLO-CA formation. On the contrary, as CES1 is responsible for the formation of the inactive metabolite [24,47], the availability of CES1 phenotypes may have resulted in its inclusion in our final model.

5. Conclusions

In conclusion, we have developed a comprehensive joint semi-physiological pharmacokinetic model for CLO and its inactive metabolite, CLO-CA. This model incorporates two transit compartments for absorption and accounts for FPE in a liver compartment. Our model is based on bioequivalence data obtained from two studies, providing a robust framework for understanding the pharmacokinetics of these compounds.

Author Contributions: Conceptualization, B.M. and K.M.V.; methodology, V.T.V. and K.M.V.; formal modeling and simulation analysis, Z.P., V.T.V. and K.M.V.; investigation, Z.P. and V.T.V.; data curation, Z.P.; writing—original draft preparation, Z.P. and V.T.V.; writing—review and editing, B.M. and K.M.V.; supervision, K.M.V. All authors have read and agreed to the published version of the manuscript.

Funding: This research was funded by the Ministry of Science, Technological Development and Innovation, Republic of Serbia through two grant agreements with the University of Belgrade - Faculty of Pharmacy (No. 451-03-65/2024-03/200161 and No. 451-03-66/2024-03/200161).

Institutional Review Board Statement: The primary studies were conducted in accordance with the Declaration of Helsinki, and institutional review board approval from the Military Medical Academy was obtained for the primary study protocols and informed consent forms were provided. The current research based on the secondary use of data was authorized by the studies' sponsors and approved by the Ethics Committee of the University of Belgrade, Faculty of Pharmacy (approval No. 2527/2 dated 17 October 2023).

Informed Consent Statement: Informed consent was obtained from all subjects involved in the primary studies.

Data Availability Statement: The data are unavailable due to privacy restrictions.

Acknowledgments: The authors express their gratitude to the sponsors of the bioequivalence studies for generously providing the primary bioequivalence data for the two generic clopidogrel medicines.

Conflicts of Interest: The authors declare no conflicts of interest.

References

1. European Medicine Agency (EMA). Plavix 75 mg Film-Coated Tablets. EPAR Product Information EMEA/H/C/000174. Available online: https://www.ema.europa.eu/en/documents/product-information/plavix-epar-product-information_en.pdf (accessed on 3 April 2024).
2. Kazui, M.; Nishiya, Y.; Ishizuka, T.; Hagihara, K.; Farid, N.A.; Okazaki, O.; Ikeda, T.; Kurihara, A. Identification of the human cytochrome P450 enzymes involved in the two oxidative steps in the bioactivation of clopidogrel to its pharmacologically active metabolite. *Drug Metab. Dispos.* **2010**, *38*, 92–99. [CrossRef] [PubMed]

3. Loer, H.L.H.; Turk, D.; Gomez-Mantilla, J.D.; Selzer, D.; Lehr, T. Physiologically Based Pharmacokinetic (PBPK) Modeling of Clopidogrel and Its Four Relevant Metabolites for CYP2B6, CYP2C8, CYP2C19, and CYP3A4 Drug-Drug-Gene Interaction Predictions. *Pharmaceutics* **2022**, *14*, 915. [CrossRef] [PubMed]
4. Jung, Y.S.; Jin, B.H.; Park, M.S.; Kim, C.O.; Chae, D. Population pharmacokinetic-pharmacodynamic modeling of clopidogrel for dose regimen optimization based on CYP2C19 phenotypes: A proof of concept study. *CPT Pharmacomet. Syst. Pharmacol.* **2023**, *13*, 29–40. [CrossRef] [PubMed]
5. Karazniewicz-Lada, M.; Danielak, D.; Burchardt, P.; Kruszyna, L.; Komosa, A.; Lesiak, M.; Glowka, F. Clinical pharmacokinetics of clopidogrel and its metabolites in patients with cardiovascular diseases. *Clin. Pharmacokinet.* **2014**, *53*, 155–164. [CrossRef] [PubMed]
6. European Medicine Agency (EMA). Clinical Pharmacology and Pharmacokinetics: Questions and Answers. Bioequivalence Studies for Generic Products Containing Clopidogrel. Available online: https://www.ema.europa.eu/en/human-regulatory-overview/research-and-development/scientific-guidelines/clinical-pharmacology-pharmacokinetics/clinical-pharmacology-pharmacokinetics-questions-answers (accessed on 3 April 2024).
7. Mani, H.; Toennes, S.W.; Linnemann, B.; Urbanek, D.A.; Schwonberg, J.; Kauert, G.F.; Lindhoff-Last, E. Determination of clopidogrel main metabolite in plasma: A useful tool for monitoring therapy? *Ther. Drug Monit.* **2008**, *30*, 84–89. [CrossRef] [PubMed]
8. Pejcic, Z.; Vucicevic, K.; Garcia-Arieta, A.; Miljkovic, B. Adjusted indirect comparisons to assess bioequivalence between generic clopidogrel products in Serbia. *Br. J. Clin. Pharmacol.* **2019**, *85*, 2059–2065. [CrossRef] [PubMed]
9. Heads of Medicines Agencies (HMA). Public Assessment Report Scientific Discussion Agregex 75 mg Film-Coated Tablets, DK/H/1624/001/DC. Available online: http://www.hma.eu/fileadmin/dateien/pipar/dk1624/parmod5_dk1624agregex.pdf (accessed on 30 March 2024).
10. Heads of Medicines Agencies (HMA). Public Assessment Report Scientific Discussion Clopidogrel Sandoz 75 mg Film-Coated Tablets, AT/H/1449/001. Available online: https://mri.cts-mrp.eu/portal/details?productnumber=AT/H/1449/001 (accessed on 29 March 2024).
11. Bahrami, G.; Mohammadi, B.; Sisakhtnezhad, S. High-performance liquid chromatographic determination of inactive carboxylic acid metabolite of clopidogrel in human serum: Application to a bioequivalence study. *J. Chromatogr. B Analyt. Technol. Biomed. Life Sci.* **2008**, *864*, 168–172. [CrossRef] [PubMed]
12. Kim, S.D.; Kang, W.; Lee, H.W.; Park, D.J.; Ahn, J.H.; Kim, M.J.; Kim, E.Y.; Kim, S.W.; Nam, H.S.; Na, H.J.; et al. Bioequivalence and tolerability of two clopidogrel salt preparations, besylate and bisulfate: A randomized, open-label, crossover study in healthy Korean male subjects. *Clin. Ther.* **2009**, *31*, 793–803. [CrossRef] [PubMed]
13. El Ahmady, O.; Ibrahim, M.; Hussein, A.M.; Bustami, R.T. Bioequivalence of two oral formulations of clopidogrel tablets in healthy male volunteers. *Int. J. Clin. Pharmacol. Ther.* **2009**, *47*, 780–784. [CrossRef] [PubMed]
14. Filipe, A.; Almeida, S.; Franco Spinola, A.C.; Neves, R.; Tanguay, M.; Jimenez, C.; Shink, E. Single-dose randomized, open-label, 2-way crossover bioequivalence study of clopidogrel 75 mg tablet in healthy volunteers under fasting conditions. *Int. J. Clin. Pharmacol. Ther.* **2009**, *47*, 187–194. [CrossRef]
15. European Medicine Agency (EMA). CHMP Assessment Report for Clopidogrel Teva Film-Coated Tablets 75 mg, EPAR Scientific Discussion, EMEA/H/C/001053. Available online: https://www.ema.europa.eu/en/documents/assessment-report/clopidogrel-teva-hydrogen-sulphate-epar-public-assessment-report_en.pdf (accessed on 9 April 2024).
16. European Medicine Agency (EMA). CHMP Assessment Report for Zyllt Film-Coated Tablets 75 mg, EPAR—Scientific Discussion, EMEA/H/C/1058. Available online: https://www.ema.europa.eu/en/documents/assessment-report/zyllt-epar-public-assessment-report_en.pdf (accessed on 9 April 2024).
17. Ette, E.I.; Williams, P.J. Population pharmacokinetics I: Background, concepts, and models. *Ann. Pharmacother.* **2004**, *38*, 1702–1706. [CrossRef]
18. Roganović, M.; Homšek, A.; Jovanović, M.; Topić Vučenović, V.; Ćulafić, M.; Miljković, B.; Vučićević, K. Concept and utility of population pharmacokinetic and pharmacokinetic/pharmacodynamic models in drug development and clinical practice. *Arch. Pharm.* **2021**, *71*, 336–353. [CrossRef]
19. Yousef, A.M.; Melhem, M.; Xue, B.; Arafat, T.; Reynolds, D.K.; Van Wart, S.A. Population pharmacokinetic analysis of clopidogrel in healthy Jordanian subjects with emphasis optimal sampling strategy. *Biopharm. Drug Dispos.* **2013**, *34*, 215–226. [CrossRef]
20. Lee, J.; Hwang, Y.; Kang, W.; Seong, S.J.; Lim, M.S.; Lee, H.W.; Yim, D.S.; Sohn, D.R.; Han, S.; Yoon, Y.R. Population pharmacokinetic/pharmacodynamic modeling of clopidogrel in Korean healthy volunteers and stroke patients. *J. Clin. Pharmacol.* **2012**, *52*, 985–995. [CrossRef]
21. Ernest, C.S., 2nd; Small, D.S.; Rohatagi, S.; Salazar, D.E.; Wallentin, L.; Winters, K.J.; Wrishko, R.E. Population pharmacokinetics and pharmacodynamics of prasugrel and clopidogrel in aspirin-treated patients with stable coronary artery disease. *J. Pharmacokinet. Pharmacodyn.* **2008**, *35*, 593–618. [CrossRef]
22. Danielak, D.; Karazniewicz-Lada, M.; Komosa, A.; Burchardt, P.; Lesiak, M.; Kruszyna, L.; Graczyk-Szuster, A.; Glowka, F. Influence of genetic co-factors on the population pharmacokinetic model for clopidogrel and its active thiol metabolite. *Eur. J. Clin. Pharmacol.* **2017**, *73*, 1623–1632. [CrossRef]

23. Zhang, L.; Sun, H.; Liu, Y.; Lai, X.; Gong, Y.; Liu, X.; Li, Y.G.; He, Y.; Zhang, E.Y.; Yan, X. Semi-mechanistic population pharmacokinetics analysis reveals distinct CYP2C19 dependency in the bioactivation of vicagrel and clopidogrel to active metabolite M15-2. *Eur. J. Pharm. Sci.* **2022**, *177*, 106264. [CrossRef]
24. Jiang, X.L.; Samant, S.; Lewis, J.P.; Horenstein, R.B.; Shuldiner, A.R.; Yerges-Armstrong, L.M.; Peletier, L.A.; Lesko, L.J.; Schmidt, S. Development of a physiology-directed population pharmacokinetic and pharmacodynamic model for characterizing the impact of genetic and demographic factors on clopidogrel response in healthy adults. *Eur. J. Pharm. Sci.* **2016**, *82*, 64–78. [CrossRef]
25. Djebli, N.; Fabre, D.; Boulenc, X.; Fabre, G.; Sultan, E.; Hurbin, F. Physiologically based pharmacokinetic modeling for sequential metabolism: Effect of CYP2C19 genetic polymorphism on clopidogrel and clopidogrel active metabolite pharmacokinetics. *Drug Metab. Dispos.* **2015**, *43*, 510–522. [CrossRef]
26. Duong, J.K.; Nand, R.A.; Patel, A.; Della Pasqua, O.; Gross, A.S. A physiologically based pharmacokinetic model of clopidogrel in populations of European and Japanese ancestry: An evaluation of CYP2C19 activity. *Pharmacol. Res. Perspect.* **2022**, *10*, e00946. [CrossRef]
27. Xu, R.J.; Kong, W.M.; An, X.F.; Zou, J.J.; Liu, L.; Liu, X.D. Physiologically-Based Pharmacokinetic-Pharmacodynamics Model Characterizing CYP2C19 Polymorphisms to Predict Clopidogrel Pharmacokinetics and Its Anti-Platelet Aggregation Effect Following Oral Administration to Coronary Artery Disease Patients with or without Diabetes. *Front. Pharmacol.* **2020**, *11*, 593982.
28. World Medical Association. Declaration of Helsinki—Ethical Principles for Medical Research Involving Human Subjects. Available online: https://www.wma.net/policies-post/wma-declaration-of-helsinki-ethical-principles-for-medical-research-involving-human-subjects/ (accessed on 13 April 2024).
29. European Medicines Agency (EMA). Guideline for Good Clinical Practice E6(R2). EMA/CPMP/ICH/135/95. Available online: https://www.ema.europa.eu/en/documents/scientific-guideline/ich-guideline-good-clinical-practice-e6r2-step-5_en.pdf (accessed on 7 April 2024).
30. European Medicine Agency (EMA). Guideline on the Investigation of Bioequivalence. CPMP/EWP/QWP/1401/98 Rev. 1/Corr**. Available online: https://www.ema.europa.eu/documents/scientific-guideline/guideline-investigation-bioequivalence-rev1_en.pdf (accessed on 10 April 2024).
31. Beal, S.; Sheiner, L.; Boeckmann, A.; Bauer, R. *NONMEM 7.4 User's Guides*; Icon Development Solutions: Ellicott City, MD, USA, 1989–2018.
32. Owen, J.; Fiedler-Kelly, J. *Introduction to Population Pharmacokinetic/Pharmacodynamic Analysis with Nonlinear Mixed Effects Models*; John Wiley & Sons: Hoboken, NJ, USA, 2014.
33. R Core Team. *R: A Language and Environment for Statistical Computing*; R Foundation for Statistical Computing: Vienna, Austria, 2022; Available online: http://www.R-project.org (accessed on 1 October 2023).
34. R Studio Team. *RStudio: Integrated Development for R*; RStudio, Inc.: Boston, MA, USA, 2019. Available online: http://www.rstudio.com (accessed on 1 October 2023).
35. Savic, R.M.; Jonker, D.M.; Kerbusch, T.; Karlsson, M.O. Implementation of a transit compartment model for describing drug absorption in pharmacokinetic studies. *J. Pharmacokinet. Pharmacodyn.* **2007**, *34*, 711–726. [CrossRef]
36. Gibiansky, L.; Giraudon, M.; Rayner, C.R.; Brennan, B.J.; Subramoney, V.; Robson, R.; Kamal, M.A. Population pharmacokinetic analysis of oseltamivir and oseltamivir carboxylate following intravenous and oral administration to patients with and without renal impairment. *J. Pharmacokinet. Pharmacodyn.* **2015**, *42*, 225–236. [CrossRef]
37. Yu, H.; Steeghs, N.; Kloth, J.S.; de Wit, D.; van Hasselt, J.G.; van Erp, N.P.; Beijnen, J.H.; Schellens, J.H.; Mathijssen, R.H.; Huitema, A.D. Integrated semi-physiological pharmacokinetic model for both sunitinib and its active metabolite SU12662. *Br. J. Clin. Pharmacol.* **2015**, *79*, 809–819. [CrossRef]
38. Hooker, A.C.; Staatz, C.E.; Karlsson, M.O. Conditional weighted residuals (CWRES): A model diagnostic for the FOCE method. *Pharm. Res.* **2007**, *24*, 2187–2197. [CrossRef]
39. Karlsson, M.O.; Savic, R.M. Diagnosing model diagnostics. *Clin. Pharmacol. Ther.* **2007**, *82*, 17–20. [CrossRef]
40. Gobburu, J.V.; Lawrence, J. Application of resampling techniques to estimate exact significance levels for covariate selection during nonlinear mixed effects model building: Some inferences. *Pharm. Res.* **2002**, *19*, 92–98. [CrossRef]
41. Parke, J.; Holford, N.H.; Charles, B.G. A procedure for generating bootstrap samples for the validation of nonlinear mixed-effects population models. *Comput. Methods Programs Biomed.* **1999**, *59*, 19–29. [CrossRef]
42. Bergstrand, M.; Hooker, A.C.; Wallin, J.E.; Karlsson, M.O. Prediction-corrected visual predictive checks for diagnosing nonlinear mixed-effects models. *AAPS J.* **2011**, *13*, 143–151. [CrossRef]
43. Taubert, D.; Kastrati, A.; Harlfinger, S.; Gorchakova, O.; Lazar, A.; von Beckerath, N.; Schomig, A.; Schomig, E. Pharmacokinetics of clopidogrel after administration of a high loading dose. *Thromb. Haemost.* **2004**, *92*, 311–316.
44. Rousseau, A.; Leger, F.; Le Meur, Y.; Saint-Marcoux, F.; Paintaud, G.; Buchler, M.; Marquet, P. Population pharmacokinetic modeling of oral cyclosporin using NONMEM: Comparison of absorption pharmacokinetic models and design of a Bayesian estimator. *Ther. Drug Monit.* **2004**, *26*, 23–30. [CrossRef]
45. Jiang, X.L.; Samant, S.; Lesko, L.J.; Schmidt, S. Clinical pharmacokinetics and pharmacodynamics of clopidogrel. *Clin. Pharmacokinet.* **2015**, *54*, 147–166. [CrossRef]

46. Song, B.L.; Wan, M.; Tang, D.; Sun, C.; Zhu, Y.B.; Linda, N.; Fan, H.W.; Zou, J.J. Effects of CYP2C19 Genetic Polymorphisms on the Pharmacokinetic and Pharmacodynamic Properties of Clopidogrel and Its Active Metabolite in Healthy Chinese Subjects. *Clin. Ther.* **2018**, *40*, 1170–1178. [CrossRef]
47. Zhu, H.J.; Wang, X.; Gawronski, B.E.; Brinda, B.J.; Angiolillo, D.J.; Markowitz, J.S. Carboxylesterase 1 as a determinant of clopidogrel metabolism and activation. *J. Pharmacol. Exp. Ther.* **2013**, *344*, 665–672. [CrossRef]

Disclaimer/Publisher's Note: The statements, opinions and data contained in all publications are solely those of the individual author(s) and contributor(s) and not of MDPI and/or the editor(s). MDPI and/or the editor(s) disclaim responsibility for any injury to people or property resulting from any ideas, methods, instructions or products referred to in the content.

pharmaceutics

MDPI

Article

Effect of Interindividual Variability in Metabolic Clearance and Relative Bioavailability on Rifampicin Exposure in Tuberculosis Patients with and without HIV Co-Infection: Does Formulation Quality Matter?

Glauco Henrique Balthazar Nardotto [1,2], Elin M. Svenson [3], Valdes Roberto Bollela [4,†], Adriana Rocha [1], Svetoslav Nanev Slavov [5], João Paulo Bianchi Ximenez [1], Oscar Della Pasqua [6] and Vera Lucia Lanchote [1,*]

[1] Faculdade de Ciências Farmacêuticas de Ribeirão Preto, Universidade de São Paulo, Ribeirão Preto 14040-903, Brazil; glauconardotto@gmail.com (G.H.B.N.); drirocha@fcfrp.usp.br (A.R.); joaopaulo.ximenez@usp.br (J.P.B.X.)
[2] Department of Pharmacology and Therapeutics, Roswell Park Comprehensive Cancer Center, Buffalo, NY 14263, USA
[3] Department of Pharmacy, Uppsala University, 75123 Uppsala, Sweden; elin.svensson@farmaci.uu.se
[4] Faculdade de Medicina de Ribeirão Preto, Universidade de São Paulo, Ribeirão Preto 14049-900, Brazil; vbollela@fmrp.usp.br
[5] Center for Viral Surveillance and Serological Evaluation-CeVIVAs, Butantan Institute, Sao Paulo 05503-900, Brazil; svetoslav.slavov@fundacaobutantan.org.br
[6] Clinical Pharmacology & Therapeutics Group, University College London, London WC1J 9JP, UK; o.dellapasqua@ucl.ac.uk
* Correspondence: lanchote@fcfrp.usp.br; Tel.: +55-16-33154195
† Principal Investigator.

Abstract: The present study aims to characterise the pharmacokinetics of rifampicin (RIF) in tuberculosis (TB) patients with and without HIV co-infection, considering the formation of 25-O-desacetylrifampicin (desRIF). It is hypothesised that the metabolite formation, HIV co-infection and drug formulation may further explain the interindividual variation in the exposure to RIF. Pharmacokinetic, clinical, and demographic data from TB patients with (TB-HIV+ group; n = 18) or without HIV (TB-HIV− group; n = 15) who were receiving RIF as part of a four-drug fixed-dose combination (FDC) regimen (RIF, isoniazid, pyrazinamide, and ethambutol) were analysed, along with the published literature data on the relative bioavailability of different formulations. A population pharmacokinetic model, including the formation of desRIF, was developed and compared to a model based solely on the parent drug. HIV co-infection does not alter the plasma exposure to RIF and the desRIF formation does not contribute to the observed variability in the RIF disposition. The relative bioavailability and RIF plasma exposure were significantly lower than previously reported for the standard regimen with FDC tablets. Furthermore, participants weighting less than 50 kg do not reach the same RIF plasma exposure as compared to those weighting >50 kg. In conclusion, as no covariate was identified other than body weight on CL/F and Vd/F, low systemic exposure to RIF is likely to be caused by the low bioavailability of the formulation.

Keywords: pulmonary tuberculosis; human immunodeficiency virus; rifampicin; 25-O-desacetylrifampicin; population pharmacokinetics; bioavailability

1. Introduction

Tuberculosis (TB) remains the world's second leading cause of death from a single infectious agent after COVID-19, and it causes almost twice as many deaths when compared to HIV [1]. However, the immunodeficiency associated with HIV appears to contribute to co-infection, which results in a significant proportion of HIV-positive subjects developing

active TB. In addition, epidemiological data also show that treatment failure and poorer outcomes are higher in HIV-positive subjects [2–4].

Even though such findings must be considered within a much broader context, limited attention has been paid to the variability in drug exposure in subjects who are being treated with antiretrovirals and antitubercular drugs, which are known to have no or minor metabolic interaction. Consequently, an important question to be addressed is the correlation between TB treatment failure and pharmacokinetic variability in subjects with HIV/TB co-infection. Rifampicin (RIF) is an essential component of the first-line anti-tuberculosis drug therapy. Given the significant effect of body weight on RIF disposition, the World Health Organization recommends the use of weight-banded dosing [5,6]. RIF is usually administered daily as part of a four-drug fixed-dose combination (FDC) regimen for TB treatment (RIF, isoniazid, pyrazinamide, and ethambutol). Whilst weight-banded dosing facilitates interventions and an FDC reduces the pill burden, improving adherence to treatment, high intra- and interindividual variability in RIF exposure is observed following therapeutically recommended doses [7–12]. There are many reports on the interindividual variability (IIV) of RIF pharmacokinetics, which attribute it to the formulation type [13], age [14], sex [13,15], HIV co-infection [16], weight (or other body size descriptor) [14,17–20], and comedications [17]. Despite adequate information on the summary of product characteristics regarding the effect of such factors, interindividual variability in the systemic exposure to RIF remains high [16–27], leading to a growing consensus that higher RIF doses are required to ensure efficacy [8,10,12]. However, there is disagreement on whether HIV co-infection, i.e., the potential effect of HIV-related inflammation and changes in the immune response, affects the pharmacokinetics of RIF, and consequently, whether dose adjustment should be considered for TB patients living with HIV [7,16,28].

According to the Biopharmaceutical Classification System, RIF is a class II drug presenting low water solubility and high permeability [29]. Its variable bioavailability is mainly related to the formulation dissolution and disintegration properties [15]. In addition, considering that HIV affects mucosal surfaces with inflammation independently of the viral load [30], it is conceivable that RIF's absorption characteristics related to both the rate and extent of the absorption may be affected in subjects with HIV/TB co-infection.

RIF is eliminated primarily by hepatic mechanisms, but 13–24% of unchanged drug is eliminated renally [31,32]. RIF is metabolised via β-esterase or other esterases in liver microsomes [31,33] to 25-desacetylrifampicin (desRIF, a major contributor) and excreted in bile. At therapeutic doses, RIF's pharmacokinetics is nonlinear (10–40 mg/kg daily), probably due to the saturable active secretion into the bile. However, the transporter involved in this process is unknown [20]. In addition, autoinduction of enzymes and/or transporters leads to a significant decrease in RIF exposure over time. Previous studies have shown that 90% of the maximum induction is reached after two weeks of RIF daily treatment [34]. Thus, RIF pharmacokinetics shows concentration and time-dependent elimination and dose-dependent bioavailability [20]. Moreover, possibly, RIF is a substrate of the efflux transporter P-glycoprotein (P-gp), encoded by the ABCB1 gene [35], and of the organic anion-transporting polypeptide 1B1 (OATP1B1), encoded by the *SLCO1B1* gene [36,37].

Considering that desRIF shows between 50 and 100% of the antimicrobial activity of RIF against *Mycobacterium tuberculosis* [34], it would be of interest to understand whether differences in the metabolite formation contribute to the overall variability in the systemic exposure to RIF, and consequently, whether different metabolic phenotypes may be associated with poorer outcome in patients with HIV/TB co-infection.

Here, we attempt to quantify the effect of interindividual differences in the desRIF formation and HIV-co-infection on the variability in exposure to RIF, taking into consideration the potential contribution of formulation-related differences in the relative bioavailability. A model-based approach is proposed, in which the parent drug and metabolite are evaluated together and separately [34]. Previously, two population pharmacokinetic studies of RIF were developed with the inclusion of desRIF, one in healthy Asian subjects following

rifampicin (600 mg) daily treatment for 14 days [17] and another in patients co-infected with TB and HIV [38]. However, these authors have not considered the potential confounding factor of geographical ancestry and the analysis has been limited to Asian and African, or Latin American, populations [13,39,40].

The present study aims to evaluate the pharmacokinetics of RIF in TB patients from Southeast Brazil with and without HIV co-infection, considering the formation of the metabolite desRIF. It is hypothesised that the metabolite formation, HIV co-infection and drug formulation may further explain the interindividual variation in RIF plasma exposure.

2. Materials and Methods

2.1. Clinical Study

The study protocol was approved by the local Hospital Research Ethics Committee (CEP/FCFRP n°: 405, Process number: 032398/2016), and all the patients signed the informed consent form. This investigation was conducted in accordance with the Declaration of Helsinki and national and institutional standards.

HIV-negative and HIV-positive subjects who were diagnosed with TB (TB-HIV− group, n = 15; TB-HIV+ group, n = 18) were enrolled after they had started the second month of the standard of care therapy. The TB-HIV− and TB-HIV+ groups consisted of 4 female/11 male and 1 female/17 male subjects, respectively. Their age ranged between 18 to 60 years, whereas the body weight of the TB-HIV+ group (range: 38.5 to 65 kg) was lower than the TB-HIV− group (range: 43 to 85.5 kg) ($p < 0.05$; t-test). None of the participants were considered obese. Further details on the participants' demographic data can be found elsewhere [41]. All the subjects were treated with FDC tablets containing rifampicin (150 mg), isoniazid (75 mg), pyrazinamide (400 mg), and ethambutol (250 mg) (Lupin LTD A-28/1, MIDC, Chikalthana, Aurangabad, India and imported by Fundação Osvaldo Cruz-Farmanguinhos, Rio de Janeiro, Brazil). The FDC tablets were administered under fasting conditions based on weight bands: 2 tablets (20–35 kg), 3 tablets (36–50 kg), or 4 tablets (>50 kg) according to the World Health Organization guidelines [5,6]. In addition, the TB-HIV+ subjects were receiving lamivudine, tenofovir (or zidovudine), and raltegravir (or efavirenz). Serial blood samples were collected over the 24 h dose interval at times zero, 0.25, 0.5, 1, 1.5, 2, 2.5, 3, 3.5, 4, 5, 6, 9, 12, 15, 18, 21, and 24 h after antibiotics administration. The plasma aliquots were stored at −80 °C until analysis and then analysed by UPLC-MS/MS as previously described [41].

2.2. Population Pharmacokinetic Models

The population pharmacokinetics of RIF and desRIF was evaluated by nonlinear mixed-effects modelling. To account for the effect of differences in the mass balance, the concentration data of the parent drug and its metabolite were converted into molar units. Evaluation of desRIF as a contributor to the interindividual differences in the pharmacokinetics of RIF was implemented assuming that the parent–metabolite model (RIF-desRIF) is a nested model, including the effect of body weight based on an allometrically function with fixed exponents (0.75 for CL/F and 1 for Vd/F).

Fixed and random effects were included in a stepwise manner. Parameters were estimated using the first-order conditional estimation with interaction method (FOCE-I). One- and two-compartment structural models were considered with first-order or saturable elimination, including autoinduction [18,19]. RIF absorption was modelled considering zero- or first-order absorption, whilst the lag-time was parameterised using a transit compartment [42,43]. Interindividual variability (IIV) was evaluated assuming a log-normal distribution. The residual variability was described by a proportional model with an additive error term [44,45]. As inclusion of covariates and stochastic parameters describing interindividual variability did not fully explain the observed interindividual variation in drug concentrations, random variables were used to characterise the random deviations from the variance of ε, which is assumed to be the same for all subjects. This term allowed different individuals to have residual variability of varying magnitude.

Further details on the model parameterisation are included in the control stream file (Supplementary Materials).

The model-building criteria included the following: (i) successful minimisation and covariance step, (ii) acceptable values of relative standard error (RSE) and shrinkage of each estimate, (iii) number of significant digits, and (iv) acceptable gradients at the last iteration [45,46]. The comparison between hierarchical models was based on graphic and statistical methods that included (1) reduction of the objective function value (OFV) and AIC (Akaike information criteria) [47], (2) goodness of fitting plot (GOF) [45,48] and (3) visual predictive checks (VPCs) [45,48,49], posterior predictive checks (PPC) [50], normalised predictive distribution errors (NPDE) [51] and mirror plots.

The influence of continuous (age and C reactive protein) and categorical (HIV co-infection, antiretroviral treatment and *SLCO1B1* genotype) covariates other than body size on the pharmacokinetic parameters of RIF and desRIF was explored by the stepwise forward inclusion ($p = 0.05$) backward elimination ($p = 0.01$) approach according to the likelihood ratio, with that being that the difference of the -2 log-likelihood value (OFV) between two models is approximately χ^2 distributed with degrees of freedom equal to the difference in the number of parameters between the hierarchical models [52,53]. Attention was also paid to the correlation between the stochastic parameters describing the metabolite formation rate and variability in individual RIF concentrations. Further details on the model evaluation procedures are described in the Supplementary Materials.

The maximum plasma concentration (C_{max}), $AUC_{0–24}$ (trapezoidal rule), and steady state plasma concentration ($Css = {}^{AUC_{0–24}}/_{\text{dosing interval}}$) were derived from the plasma concentrations over time.

Finally, to assess the effect of formulation-related differences on systemic RIF exposure, we compared the $AUC_{0\text{-}24}$ and bioavailability obtained with the final model with those reported previously in the literature [13–15,17]. This was performed by including the parameter estimates of previous RIF models as priors, as implemented in the $PRIOR NWPRI subroutine. The priors were non-informative, with the exception of RIF CL/F and V/F values, which were kept as informative priors.

All the analyses were implemented in NONMEM v. 7.5.0 (ICON Development Solutions, Ellicott City, MD, USA) [46], using PsN v. 5.3.0 [54,55]. Data formatting and the graphical and statistical summaries were performed using R v 4.2.2 [56]. A copy of the control stream files and a summary of the model building process are presented in the Supplementary Materials.

3. Results

Figure 1 presents the observed individual concentration vs. time profiles of RIF and desRIF, as stratified by HIV co-infection. Of note was the finding that the ratio between the area under the concentration vs. time (AUC) curves between desRIF and RIF was comparable across the two groups and did not differ between individuals receiving different doses (i.e., 450 vs. 600 mg RIF).

The RIF and desRIF pharmacokinetics were characterized by a one-compartment model with first-order elimination. The RIF absorption was best described by the transit compartment (Nn = 3) model (Figure 2 and Table 1). The effect of body weight on the clearance and volume of distribution was implemented similarly to that outlined in previous reports, i.e., it was described by an allometric function with fixed exponents for both moieties. None of the other demographic, clinical and genotypical factors included in the covariate analysis were found to be significant.

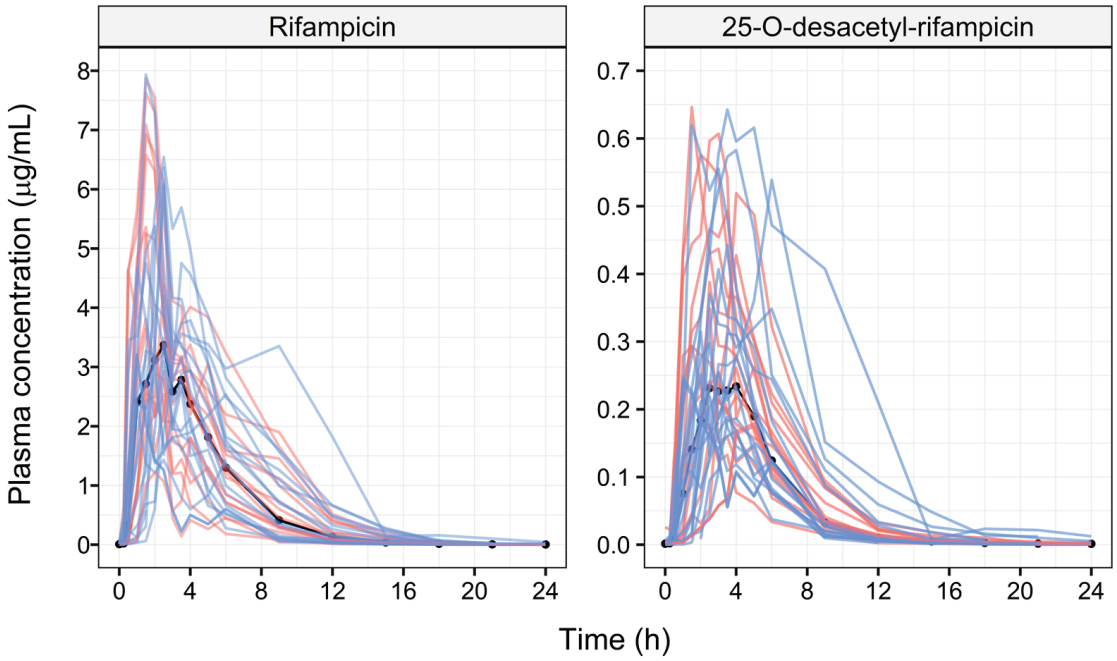


Figure 1. Observed rifampicin (RIF) and 25-O-desacetyl-rifampicin (desRIF) plasma concentration vs. time profiles in subjects with pulmonary tuberculosis with and without HIV co-infection (n = 33). The solid black line describes the median profiles. The red and blue lines depict TB-HIV− and TB-HIV+ subjects, respectively.

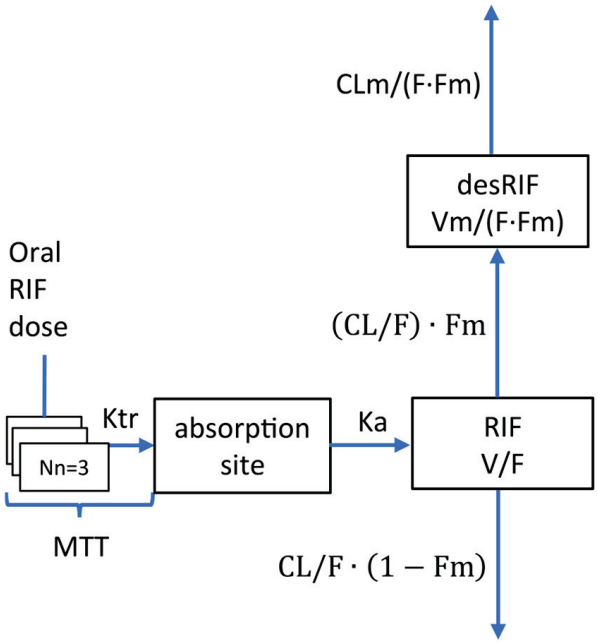


Figure 2. Diagram describing the structural pharmacokinetic model for rifampicin (RIF) and its metabolite 25-O-deacetyl-rifampicin (desRIF). CL/F and CLm/(F·Fm): apparent clearance of RIF and desRIF, respectively; V/F and Vm/(F·Fm): apparent volume of distribution of RIF and desRIF, respectively; Fm: fraction of CL/F converted into desRIF; Nn: number of transit compartments; Ka: RIF absorption rate constant; Ktr: transit absorption rate constant describing the transit time for the absorption of RIF in each compartment, MTT: mean transit time for the absorption of RIF, being: Ka = Ktr = (Nn + 1)/MTT.

Table 1. Final pharmacokinetic parameters of rifampicin (RIF) and desacetyl-rifampicin (desRIF) in subjects with pulmonary tuberculosis, with and without HIV co-infection.

Parameters	Fixed Effects Typical Value (RSE%)	Random Effects CV% (RSE%)
CL/F (L/h)	35.2 (10.1)	26.9 (10.6)
V/F (L)	108.0 (9.4)	
MTT (h)	1.13 (9.0)	53.2 (7.8)
F	----	46.9 (10.7)
Nn	3 (fix)	
Fm	----	38.8 (15.8)
CLm/(F·Fm) (L/h)	368 (9.8)	
Vm/(F·Fm) (L)	226 (15.2)	63.3 (22.0)
Correlation CL/F–Fm		71.5 (2.2)
Residual variability (ε)		
RIF proportional		45.6 (8.5)
RIF additive $(nmol/mL)^2$		1.85×10^{-5} (38.6)
η_1 *		20.4 (37.7)
desRIF proportional		35.5 (10.1)
desRIF additive $(nmol/mL)^2$		3.21×10^{-6} (15.7)
η_2 *		35.1 (28.5)

CV% $= \sqrt{\exp(\omega^2) - 1} \cdot 100$ or $= \sqrt{\exp(\varepsilon^2) - 1} \cdot 100$. * η_1 and η_2 are random deviations of individual i from the variance of ε, which is assumed to be the same for all subjects. RSE: relative standard error.

Model parameterisation:

Ka = Ktr = (Nn + 1)/MTT

$$CL/F = CL/F_{\text{Tipical Value}} \cdot \left(\frac{\text{Weight}}{55.7}\right)^{0.75} \cdot e^{\eta}$$

$$V/F = V/F_{\text{Tipical Value}} \cdot \left(\frac{\text{Weight}}{55.7}\right) \cdot e^{\eta}$$

$$CLm/(F \cdot Fm) = CLm/(F \cdot Fm)_{\text{Tipical Value}} \cdot \left(\frac{\text{Weight}}{55.7}\right)^{0.75} \cdot e^{\eta}$$

$$Vm/(F \cdot Fm) = Vm/(F \cdot Fm)_{\text{Tipical Value}} \cdot \left(\frac{\text{Weight}}{55.7}\right) \cdot e^{\eta}$$

$$F = 1 \cdot e^{\eta}$$

$$Fm = 1 \cdot e^{\eta}$$

CL/F and CLm/F·Fm: apparent clearance of RIF and desRIF, respectively; Fm: fraction of RIF that is converted into desRIF; Ka: RIF absorption rate constant; Ktr: RIF transit rate constant; MTT: mean transit time; Nn: number of transit compartments; V/F and Vm/F·Fm: apparent volume of distribution of RIF and desRIF, respectively; WT: weight; η and ε are random variables with mean 0 and variance ω^2 and σ^2.

The population estimates of the apparent clearance and volume of distribution were, respectively, 35.2 L/h and 108.0 L for RIF and 368 L/h and 226 L for desRIF (Table 1). All the parameters have been estimated with good precision; however, there was no significant reduction in the interindividual or residual variability, as indicated by the stochastic model parameters describing the pharmacokinetics of RIF. Notably, the interindividual variability in bioavailability was essential to accurately describe the individual concentration vs. time profiles of RIF and desRIF.

The VPCs of RIF and desRIF are depicted in Figure 3. As can be seen from the data scattering, the model adequately describes both moieties. Similarly, the model performance was deemed appropriate based on different diagnostic criteria, including the GOF (Figure S1). Posterior predictive checks (PPC) based on the $AUC_{0–24}$ and C_{max} showed the accurate prediction of exposure to RIF and desRIF (Figure S2). The NPDE revealed acceptable, normally distributed errors (Figure S3). In addition, the mirror plots suggest that the variance–covariance structure was well characterised, as the simulated datasets reproduced the dispersion pattern observed in the original data (Figure S4).

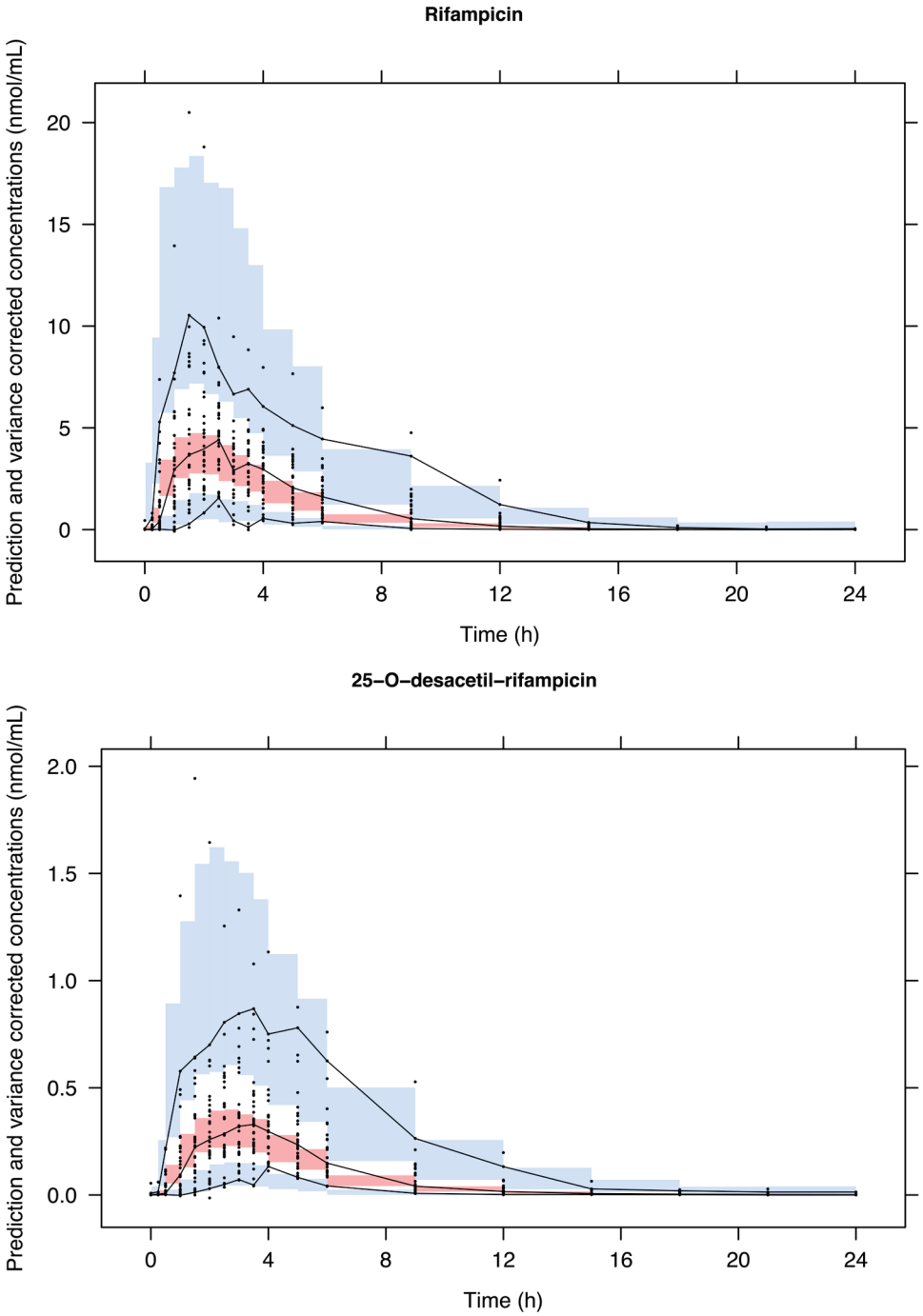


Figure 3. Prediction-corrected visual predictive check (VPC) of rifampicin (**upper** panel) and 25-O-desacetyl-rifampicin (**lower** panel). Dots: observed plasma concentrations. Lines: 2.5th, 50th and 97.5th percentiles of the observed concentrations vs. time profiles. Shaded areas: 2.5th, 50th and 97.5th percentiles of the simulated concentration vs. time profiles (n = 1000).

Given the identification of interindividual variability in the oral bioavailability and the relatively low exposure as compared with previous studies, an assessment of the average relative bioavailability revealed marked differences across studies (Tables 2 and S2–S5), making it evident that the RIF concentrations achieved with the current formulation were significantly lower than those reported elsewhere [13–15,17].

Figure 4 shows how the different metrics of exposure ($AUC_{0–24}$, C_{max}, and Css) vary with body weight, and how our results compare to those of published studies including TB patients with and without HIV co-infection.

Table 2. Comparison of the area under plasma concentration vs. time curve from 0 to 24 h ($AUC_{0–24}$) and the relative bioavailability of the rifampicin (RIF) formulation used in the current study and estimates obtained in previous reports (n = 33).

Priors Included	Frel *	Median $AUC_{0–24}$ (25th–75th Percentiles)	$AUC_{0–24}$ Ratio
Schipani et al., 2016 [14] FDC	0.678	30.83 (10.94–75.77)	0.620
Seng et al., 2015 [17] FDC	0.292	51.26 (16.87–143.27)	1.031
Wilkins et al. 2008 [15] FDC	0.499	28.50 (9.91–72.22)	0.573
Milán-Segovia et al., 2013 [13] Formulation A FDC	0.497	23.28 (9.42–43.11)	0.468
Milán-Segovia et al., 2013 [13] Reference FDC	0.232	49.74 (20.14–92.12)	1
Current study, FDC tablets	---	19.94 (7.15–25.36)	0.330

$AUC_{0–24}$: Area under the plasma concentration vs. time curve from 0 to 24 h obtained from the simulated plasma concentration using the models parameter estimates from the cited references as compared to the current study; $AUC_{0–24}$ ratios: $AUC_{0–24}$ by each model/$AUC_{0–24}$ of the reference FDC by Milán-Segovia et al., 2013 [13]; Frel *: relative bioavailability estimates for the generic formulation used in the current study using priors from parameter estimates obtained previously in [13–15,17], which include a reference FDC tablet and different generic formulations. FDC: fixed-dose combination. Milán-Segovia et al., 2013 [13] reference FDC: Rifater, Sanofi-Aventis, Mexico City, Mexico (rifampicin + isoniazid + ethambutol + pyrazinamide). Milán-Segovia et al., 2013 [13] formulation A FDC: rifampicin + isoniazid + ethambutol + pyrazinamide FDC (unknown brand/manufacturer). Seng et al., 2015 [17]: RIF + Isoniazid FDC (unknown brand/manufacturer). Wilkins et al. 2008 [15]: RIF + isoniazid + ethambutol + pyrazinamide FDC (unknown brand/manufacturer). Current clinical trial and Schipani et al., 2016 [14]: RIF + isoniazid + ethambutol + pyrazinamide FDC (Lupin Pharmaceutical Ltd., Chikalthana, Aurangabad, India).

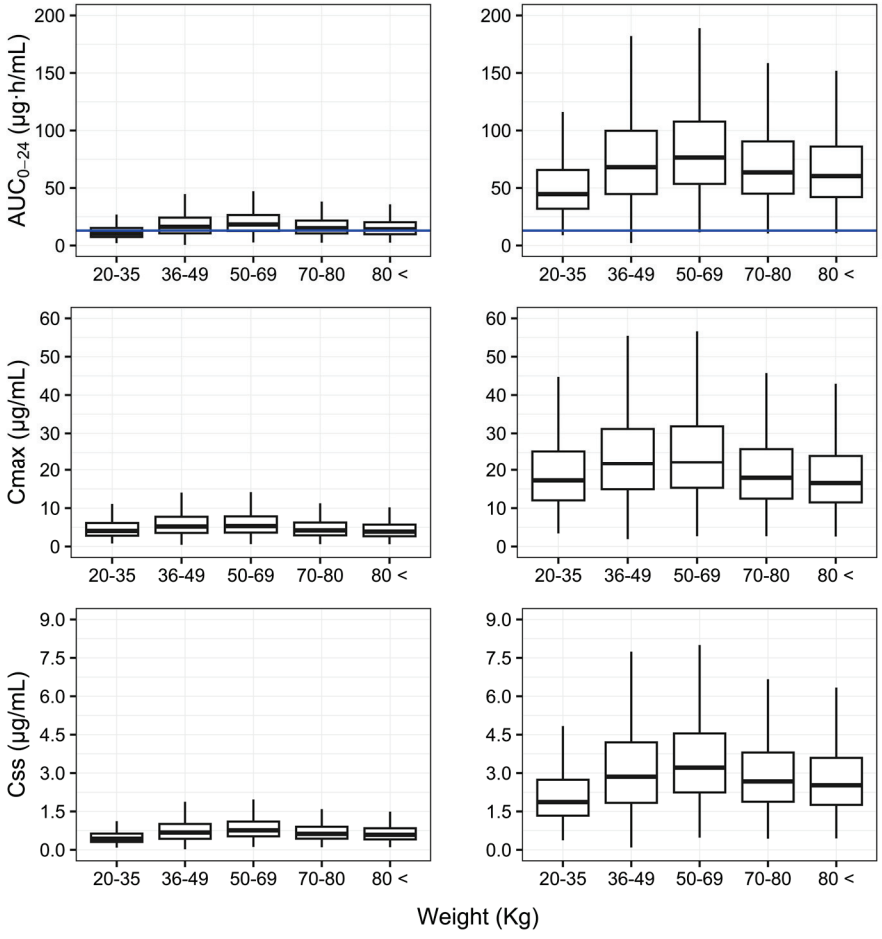


Figure 4. Simulated area under the plasma concentration vs. time curve 0–24 h ($AUC_{0–24}$), maximum plasma concentration achieved (C_{max}) and average steady-state concentration (Css) of rifampicin stratified by body weight (1000 replicates) using the final model (right, generic FDC formulation, Lupin LTD A-28/1,

MIDC, Chikalthana, Aurangabad, India) and the one by Milán-Segovia et al., 2013 [13] (left, reference FDC product, Rifater, Sanofi-Aventis, Mexico City, Mexico). FDC: fixed-dose combination. Blue line: RIF $AUC_{0\text{-}24}$ threshold (13 mg·h/mL) below, which a previous report suggests to be a poor outcome [57]. FDC: fixed-dose combination. Simulations were performed using the final model and reflect the study population (n = 33). The weight bins were arbitrarily selected for description of the covariate effect: 20–35 kg (n = 5; 2 FDC tablets), 36–49 kg (n = 6; 3 FDC tablets), 50–69 kg (n = 9; 4 FDC tablets), 70–80 kg (n = 8; 4 FDC tablets), and >80 kg (n = 5; 4 FDC tablets).

4. Discussion

Despite mounting evidence showing the implications of HIV/TB co-infection for treatment outcomes, there has been limited attention paid to the role of interindividual differences in exposure to anti-tubercular drugs in this group of patients. A previous report by our research group [42] showed that HIV did not influence the pharmacokinetics of RIF in TB patients. Here, we have used a model-based approach to characterise the pharmacokinetics of RIF and its active metabolite, desRIF. First, it is important to highlight that the use of a joint model including the metabolite formation and disposition did not explain the observed interindividual variability in systemic exposure to RIF. In addition, variable exposure cannot be assigned to variable adherence to treatment, as drug administration was ensured through directly observed therapy (DOT). Fasting conditions were also strictly maintained, considering that all the participants were hospitalised (inward period), excluding variability due to potential drug–food interaction. Thanks to the selected group of subjects with HIV/TB co-infection, it was possible to disentangle the potential confounding due to antiretroviral therapy from the intrinsic effect of disease (i.e., the underlying controlled viral infection, with viral load below 50 copies/mL). It is noteworthy that the TB-HIV+ patients had no gastrointestinal disorders such as diarrhoea, vomiting, opportunistic bowel infection, gastric hypoacidity, enteropathy, or comorbidities that may predispose to malabsorption [7,28,41]. None of the antiretroviral drugs showed the potential to impact systemic exposure to RIF.

The median $AUC_{0\text{–}24}$ desRIF/RIF ratio was approximately 0.1, a value that is very close to previously reported data [58,59]. It is also worth mentioning that given the differences in the pharmacological activity of the metabolite, the increased metabolite formation in HIV/TB co-infected subjects could have clinically relevant implications. On the other hand, it became evident that the relatively low concentration vs. plasma profiles of desRIF do not contribute appreciably to explaining the interindividual variability in RIF disposition. Even though these results may not be generalised to other metabolites, such as rifampicin glucuronide and *N*-demethyl rifampicin, it is unlikely that differences in metabolic clearance explicate the residual, random variability in the systemic exposure to RIF.

By contrast, our study reveals that the observed variation in systemic exposure between subjects is unlikely to be caused by first-pass mechanisms. Rather, it may be associated with the dosage form, with significant interindividual differences in the extent of the absorption. These differences do not seem to correlate with the baseline characteristics of the patient population, including geographical ancestry.

Clinical studies in tuberculosis often use distinct RIF formulations from different manufactures [17,18,60,61], either as a single tablet or as an FDC [13–15,19,39,62]. The variation in exposure due to differences across formulations has not been evaluated, as to date no meta-analysis has been performed to assess the impact of the variation between generic formulations on systemic exposure. In addition, as bioequivalence studies are performed in healthy subjects, the interaction with other covariates has been disregarded. Unsurprisingly, disposition parameter estimates show large variation across studies and population pharmacokinetic models, including those observed in the current study. As shown in Table 1, the estimates of apparent clearance (CL/F = 35.2 L/h) and volume of distribution (V/F = 108.0 L) are significantly higher than previously reported. The

CL/F was found to vary between 4.0 and 23.9 L/h, whereas the V/F between 13.8 and 77.4 L [13–15,20,34,41].

It is important to emphasise that a previous pharmacokinetic analysis by Schipani et al., 2016 [14], whose subjects received the same FDC tablet brand as that used in our study (Lupin Pharmaceutical Ltd., India), found relatively lower exposure and clearance estimates (CL/F = 23.9 L/h) that were already beyond the upper range reported to date (i.e., CL/F between 4.0 and 22.8 L/h) [34]. Interestingly, Milán-Segovia et al., 2013 [13] also reported that the bioavailability of RIF in Mexican subjects receiving a generic FDC tablet was only 46.8% as compared to those receiving the reference (Rifater, Sanofi-Aventis, Mexico). Previously, Milán-Segovia et al., 2010 [63] had also shown that the $AUC_{0-\infty}$ test/reference ratio of a generic FDC tablet vs. the reference formulation (Rifater, Sanofi-Aventis, Mexico) was as low as 22.08%. More recently, Medellin-Garibay et al., 2020 [39] reported that a generic FDC formulation showed bioavailability below the range required for bioequivalence (i.e., 0.85–1.25). This pattern seems to persist across different studies, which suggests that FDC formulations have lower bioavailability than RIF single tablets. It also implies that the formulation quality does not seem to be continuously monitored [15].

The issue of variable bioavailability represents a serious concern, as major efforts are being undertaken to optimise dosing regimens and reduce treatment failure in more vulnerable patients, such as those living with HIV. Yet, such an objective cannot be achieved without quality control of the standard of care medicines that are used so widely [64].

The relative bioavailability estimates (Table 2) in the current study were 32.2%, 50.1%, 70.8%, 50.3%, and 76.8% lower than that those, respectively, reported by Schipani et al., 2016 [14] (Malawian subjects taking the same FDC tablets brand as in this study; Table S2), Wilkins et al., 2008 [15] (South African subjects taking FDC tablets; Table S3), Seng et al., 2015 [17] (Asian (mainly Chinese; Table S1) subjects taking RIF + isoniazid FDC tablets), and Milán-Segovia et al., 2013 [13] (Mexican subjects taking a generic and the reference (Rifater, Sanofi-Aventis, Mexico) FDC tablets; Table S4). These differences in bioavailability have direct implications for systemic exposure, including the $AUC_{0–24}$, C_{max} and Css (Figure 4). For instance, median estimates of the $AUC_{0–24}$ (10.39 mg·h/mL) in individuals with body weight <50 kg are likely to result in poor long-term outcomes, according to Pasipanodya et al. [57], who showed that RIF exposure in patients following retreatment weas $\leq$13 mg·h/mL.

From a clinical pharmacology perspective, it becomes clear that any attempt to optimise regimens, so as to ensure achievement of the target exposure across the overall patient population, irrespective of differences in body weight, is pointless if the formulation quality is not warranted. For the sake of completeness, as shown in Figure 4, the effect of body weight on systemic exposure following the currently recommended weight-banded dosing regimen is minor compared to the discrepancies between formulations.

Whilst microbiological and clinical evidence points to the importance of administering higher doses of RIF (e.g., 600 mg) to subjects who have low body weight [27], our study undoubtedly shows that a bigger issue exists, namely the consistency in bioequivalence claims supporting the commercialisation of essential medicines. In the worldwide fight against the threat of TB, and given the vulnerability of subjects living with HIV, there seems to be a gap in policy making, which offsets the advances clinical research has achieved. Accessible, cheaper medicines are crucial in the fight against TB, but medicinal products must comply with regulatory and quality standards. This requirement seems to be overlooked when considering RIF.

5. Conclusions

HIV co-infection does not impact plasma exposure to RIF and the desRIF formation does not contribute to the observed variability in RIF disposition. Surprisingly, our analysis allowed further investigation of the differences in the relative bioavailability, which appeared to be variable across different studies and populations, highlighting a potential quality issue for the most important component of the standard of care therapy for TB.

These findings deserve further attention, as interindividual variability in exposure due to what appears to be a formulation quality issue is clinically unacceptable.

Supplementary Materials: The following supporting information can be downloaded at https://www.mdpi.com/article/10.3390/pharmaceutics16080970/s1, **Figure S1**: Goodness of fit (GOF) plots of rifampicin (RIF) and 25-O-desacetyl-rifampicin (desRIF) by the final model. Observed concentrations (μg/mL) over population and individual predictions (right). Conditional weighted residuals (CWRESs) over population predictions and time (left). Red line: trend line, dashed lines in right plots: identity, and 2- and 0.5-times identity. Dashed lines in left plots: −2, 0 and 2 CWRESs. **Figure S2**: Posterior predictive check (PPC) of rifampicin pharmacokinetics model. Frequency histograms show the predicted distribution of the simulated $AUC_{0–24}$ and C_{max} values (n = 1000 simulations). Red lines: 5th, 50th and 95th percentiles of the observed $AUC_{0–24}$ and C_{max}. Blue lines: 5th, 50th and 95th percentiles of the individual predicted $AUC_{0–24}$ and C_{max}. **Figure S2 (continuation)**: Posterior predictive check (PPC) of 25-O-desacetyl-rifampicin pharmacokinetics model. Frequency histograms show the predicted distribution of the simulated $AUC_{0–24}$ and C_{max} values (n = 1000 simulations). The red lines depict the 5th, 50th and 95th percentiles of the observed $AUC_{0–24}$ and C_{max}; and blue lines depict the 5th, 50th and 95th percentiles of the individual predicted $AUC_{0–24}$ and C_{max}. **Figure S3**: Normalised predictive distribution errors (NPDE) of the model describing the pharmacokinetics of rifampicin and 25-O-desacetly-rifampicin. NPDE vs. predicted concentrations (top left) and time (top right). NPDE histogram (bottom left), NPDE normal quantile-quantile plot (bottom right). **Figure S4**: Mirror plots of rifampicin with the final model. Individual observed concentrations vs. population and individual predicted concentrations. Conditional weighed residuals (CWRESs) vs. population predicted concentrations and time. **Figure S4 (continuation)**: Mirror plots of 25-O-desacetly-rifampicin with the final model. Individual observed concentrations vs. population and individual predicted concentrations. Conditional weighed residuals (CWRESs) vs. population predicted concentrations and time. **Table S1**: Pharmacokinetic parameters of rifampicin (RIF) and 25-O-desacetyl-rifampicin (desRIF) using the model from Seng et al., 2015 [17] as priors. **Table S2**: Pharmacokinetic parameters of rifampicin (RIF) and 25-O-desacetyl-rifampicin (desRIF) using the model from Schipani et al., 2016 [14] as priors. **Table S3**: Pharmacokinetic parameters of rifampicin (RIF) and 25-O-desacetyl-rifampicin (desRIF) using the model from Wilkins et al., 2008 [15] as priors. **Table S4**: Pharmacokinetic parameters of rifampicin (RIF) and 25-O-desacetyl-rifampicin (desRIF) using the model from Milán-Segovia et al., 2013 [13] as priors.

Author Contributions: Conceptualisation, G.H.B.N., V.R.B., O.D.P. and V.L.L.; methodology, G.H.B.N., A.R., S.N.S., J.P.B.X. and V.L.L.; software, G.H.B.N., E.M.S. and O.D.P.; validation, G.H.B.N., E.M.S., A.R. and V.L.L.; formal analysis, G.H.B.N., A.R, S.N.S. and J.P.B.X.; investigation, G.H.B.N. and V.R.B.; resources, E.M.S., S.N.S. and V.L.L.; data curation, G.H.B.N., A.R. and V.L.L.; writing—original draft preparation, G.H.B.N., J.P.B.X., O.D.P. and V.L.L.; writing—review and editing, G.H.B.N., J.P.B.X., O.D.P. and V.L.L.; visualisation, G.H.B.N., J.P.B.X., O.D.P. and V.L.L.; supervision, O.D.P., E.M.S. and V.L.L.; project administration, V.L.L.; funding acquisition, V.L.L. All authors have read and agreed to the published version of the manuscript.

Funding: This research was funded by the São Paulo Research Foundation (FAPESP 2016/05624-0 and 2018/05616-3) and the Brazilian National Council for Scientific and Technological Development (CNPq 303142/2019-7).

Institutional Review Board Statement: The study protocol was approved by the local Hospital Research Ethics Committee (CEP/FCFRP no: 405, process number: 032398/2016). This investigation was conducted in accordance with the Declaration of Helsinki and national and institutional standards.

Informed Consent Statement: Informed consent was obtained from all the subjects involved in the study.

Data Availability Statement: Original data are available from the corresponding author upon request.

Conflicts of Interest: The authors declare no conflicts of interest.

References

1. *Global Tuberculosis Report 2023*; World Health Organization: Geneva, Switzerland, 2023.

2. Gayoso, R.; Dalcolmo, M.; Braga, J.U.; Barreira, D. Predictors of mortality in multidrug-resistant tuberculosis patients from Brazilian reference centers, 2005 to 2012. *Braz. J. Infect. Dis.* **2018**, *22*, 305–310. [CrossRef] [PubMed]
3. Ejeh, F.E.; Undiandeye, A.; Okon, K.; Moshood, K.H. Prevalence of rifampicin resistance tuberculosis among HIV/TB coinfected patients in Benue State, Nigeria. *Pan Afr. Med. J.* **2021**, *38*, 203. [CrossRef] [PubMed]
4. Romaino, S.M.N.; Naing, N.N.; Mat Zuki, M.J. Factors associated with tuberculosis treatment success among tuberculosis and human immunodeficiency virus co-infected patients in Kelantan. *Med. J. Malaysia* **2022**, *77*, 696–703. [PubMed]
5. Ministério da Saúde. *Manual de Recomendações Para o Controle da Tuberculose no Brasil*; Ministério da Saúde, Secretaria de Vigilância em Saúde, Departamento de Vigilância Epidemiológica: Brasília, Brasil, 2019; pp. 1–288.
6. TB CARE I. *International Standards for Tuberculosis Care*; International standards for Tuberculosis Care; University of California: San Francisco, CA, USA, 2014; pp. 1–92.
7. Alsultan, A.; Peloquin, C.A. Therapeutic drug monitoring in the treatment of tuberculosis: An update. *Drugs* **2014**, *74*, 839–854. [CrossRef] [PubMed]
8. Kimerling, M.E.; Phillips, P.; Patterson, P.; Hall, M.; Robinson, C.A.; Dunlap, N.E. Low serum antimycobacterial drug levels in non-HIV-infected tuberculosis patients. *Chest* **1998**, *113*, 1178–1183. [CrossRef] [PubMed]
9. Mehta, J.B.; Shantaveerapa, H.; Byrd Jr, R.P.; Morton, S.E.; Fountain, F.; Roy, T.M. Utility of rifampin blood levels in the treatment and follow-up of active pulmonary tuberculosis in patients who were slow to respond to routine directly observed therapy. *Chest* **2001**, *120*, 1520–1524. [CrossRef] [PubMed]
10. Sahai, J.; Gallicano, K.; Swick, L.; Tailor, S.; Garber, G.; Seguin, I.; Oliveras, L.; Walker, S.; Rachlis, A.; Cameron, W. Reduced plasma concentrations of antituberculosis drugs in patients with HIV infection. *Ann. Intern. Med.* **1997**, *127*, 289. [CrossRef] [PubMed]
11. Strydom, N.; Gupta, S.V.; Fox, W.S.; Via, L.E.; Bang, H.; Lee, M.; Eum, S.; Shim, T.; Iii, C.E.B.; Zimmerman, M.; et al. Tuberculosis drugs' sistribution and emergence of resistance in patient's lung lesions: A mechanistic model and tool for regimen and dose optimization. *PLoS Med.* **2019**, *16*, e1002773. [CrossRef] [PubMed]
12. van Crevel, R.; Alisjahbana, B.; de Lange WC, M.; Borst, F.; Danusantoso, H.; van der Meer JW, M.; Burger, D.; Nelwan RH, H. Low Plasma concentrations of rifampicin in tuberculosis patients in Indonesia. *Int. J. Tuberc. Lung Dis.* **2002**, *6*, 497–502. [CrossRef]
13. Milán-Segovia, R.C.; Ramírez, A.M.D.; Cook, H.J.; Aquino, M.M.; Pérez, M.V.; Brundage, R.C.; Moreno, S.R. Population pharmacokinetics of rifampicin in Mexican patients with tuberculosis. *J. Clin. Pharm. Ther.* **2013**, *38*, 56–61. [CrossRef]
14. Schipani, A.; Pertinez, H.; Mlota, R.; Molyneux, E.; Lopez, N.; Dzinjalamala, F.K.; van Oosterhout, J.J.; Ward, S.A.; Khoo, S.; Davies, G. A simultaneous population pharmacokinetic analysis of rifampicin in Malawian adults and children. *Br. J. Clin. Pharmacol.* **2016**, *81*, 679–687. [CrossRef]
15. Wilkins, J.J.; Savic, R.M.; Karlsson, M.O.; Langdon, G.; McIlleron, H.; Pillai, G.; Smith, P.J.; Simonsson, U.S.H. Population pharmacokinetics of rifampin in pulmonary tuberculosis patients, including a semimechanistic model to describe variable absorption. *Antimicrob. Agents Chemother.* **2008**, *52*, 2138–2148. [CrossRef] [PubMed]
16. Daskapan, A.; Idrus, L.R.; Postma, M.J.; Wilffert, B.; Kosterink, J.G.W.; Stienstra, Y.; Touw, D.J.; Andersen, A.B.; Bekker, A.; Denti, P.; et al. A systematic review on the effect of HIV infection on the pharmacokinetics of first-line tuberculosis drugs. *Clin. Pharmacokinet.* **2019**, *58*, 747–766. [CrossRef]
17. Seng, K.-Y.; Hee, K.-H.; Soon, G.-H.; Chew, N.; Khoo, S.H.; Lee, L.S.-U. Population pharmacokinetics of rifampicin and 25-desacetyl-rifampicin in healthy Asian adults. *J. Antimicrob. Chemother.* **2015**, *70*, 3298–3306. [CrossRef]
18. Nishimura, T.; Kohno, H.; Nagai, H.; Maruoka, D.; Koike, Y.; Kobayashi, M.; Atsuda, K. The population pharmacokinetics of rifampicin in Japanese pulmonary tuberculosis patients. *Drug Res.* **2020**, *70*, 199–205. [CrossRef]
19. Smythe, W.; Khandelwal, A.; Merle, C.; Rustomjee, R.; Gninafon, M.; Lo, M.B.; Sow, O.B.; Olliaro, P.L.; Lienhardt, C.; Horton, J.; et al. A semimechanistic pharmacokinetic-enzyme turnover model for rifampin autoinduction in adult tuberculosis patients. *Antimicrob. Agents Chemother.* **2012**, *56*, 2091–2098. [CrossRef] [PubMed]
20. Svensson, R.J.; Aarnoutse, R.E.; Diacon, A.H.; Dawson, R.; Gillespie, S.H.; Boeree, M.J.; Simonsson, U.S.H. A population pharmacokinetic model incorporating saturable pharmacokinetics and autoinduction for high rifampicin doses. *Clin. Pharmacol. Ther.* **2018**, *103*, 674–683. [CrossRef]
21. Egelund, E.; Alsultan, A.; Peloquin, C. Optimizing the clinical pharmacology of tuberculosis medications. *Clin. Pharmacol. Ther.* **2015**, *98*, 387–393. [CrossRef] [PubMed]
22. Clewe, O.; Karlsson, M.O.; Simonsson, U.S.H. Evaluation of optimized bronchoalveolar lavage sampling designs for characterization of pulmonary drug distribution. *J. Pharmacokinet. Pharmacodyn.* **2015**, *42*, 699–708. [CrossRef]
23. McCune, J.S.; Reynolds, K.S. Developing and using therapeutics for emerging infections. *Clin. Pharmacol. Ther.* **2015**, *98*, 346–351. [CrossRef]
24. Verbeeck, R.K.; Günther, G.; Kibuule, D.; Hunter, C.; Rennie, T.W. Optimizing treatment outcome of first-line anti-tuberculosis drugs: The role of therapeutic drug monitoring. *Eur. J. Clin. Pharmacol.* **2016**, *72*, 905–916. [CrossRef] [PubMed]
25. Vinks, A.A. Therapeutic optimization as part of the precision medicine paradigm. *Clin. Pharmacol. Ther.* **2016**, *99*, 340–342. [CrossRef] [PubMed]
26. Weld, E.D.; Dooley, K.E. State-of-the-art review of HIV-TB coinfection in special populations. *Clin. Pharmacol. Ther.* **2018**, *104*, 1098–1109. [CrossRef] [PubMed]

27. Muliaditan, M.; Della Pasqua, O. How long will treatment guidelines for TB continue to overlook variability in drug exposure? *J. Antimicrob. Chemother.* **2019**, *74*, 3274–3280. [CrossRef] [PubMed]
28. Abulfathi, A.A.; Decloedt, E.H.; Svensson, E.M.; Diacon, A.H.; Donald, P.; Reuter, H. Clinical pharmacokinetics and pharmacodynamics of rifampicin in human tuberculosis. *Clin. Pharmacokinet.* **2019**, *58*, 1103–1129. [CrossRef] [PubMed]
29. Agrawal, S.; Panchagnula, R. Implication of biopharmaceutics and pharmacokinetics of rifampicin in variable bioavailability from solid oral dosage forms. *Biopharm. Drug Dispos.* **2005**, *26*, 321–334. [CrossRef] [PubMed]
30. Bart, G.; Jaber, M.; Giang, L.M.; Brundage, R.C.; Korthuis, P.T. Findings from a pilot study of buprenorphine population pharmacokinetics: A potential effect of HIV on buprenorphine bioavailability. *Drug Alcohol Depend.* **2022**, *241*, 109696. [CrossRef] [PubMed]
31. Jamis-Dow, C.A.; Katki, A.G.; Collins, J.M.; Klecker, R.W. Rifampin and rifabutin and their metabolism by human liver esterases. *Xenobiotica* **1997**, *27*, 1015–1024. [CrossRef] [PubMed]
32. Aristoff, P.A.; Garcia, G.A.; Kirchhoff, P.D.; Hollis Showalter, H.D. Rifamycins—Obstacles and Opportunities. *Tuberculosis* **2010**, *90*, 94–118. [CrossRef]
33. Song, S.H.; Chang, H.E.; Jun, S.H.; Park, K.U.; Lee, J.H.; Lee, E.-M.; Song, Y.-H.; Song, J. Relationship between CES2 genetic variations and rifampicin metabolism. *J. Antimicrob. Chemother.* **2013**, *68*, 1281–1284. [CrossRef]
34. Muda, M.R.; Harun, S.N.; Syed Sulaiman, S.A.; Sheikh Ghadzi, S.M. Population pharmacokinetics analyses of rifampicin in adult and children populations: A systematic review. *Br. J. Clin. Pharmacol.* **2022**, *88*, 3132–3152. [CrossRef] [PubMed]
35. Schuetz, E.G.; Schinkel, A.H.; Relling, M.V.; Schuetz, J.D. P-glycoprotein: A major determinant of rifampicin-inducible expression of cytochrome P4503A in mice and humans. *Proc. Natl. Acad. Sci. USA* **1996**, *93*, 4001–4005. [CrossRef] [PubMed]
36. Chigutsa, E.; Visser, M.E.; Swart, E.C.; Denti, P.; Pushpakom, S.; Egan, D.; Holford, N.H.G.; Smith, P.J.; Maartens, G.; Owen, A.; et al. The SLCO1B1 Rs4149032 polymorphism is highly prevalent in South Africans and is associated with reduced rifampin concentrations: Dosing implications. *Antimicrob. Agents Chemother.* **2011**, *55*, 4122–4127. [CrossRef] [PubMed]
37. Weiner, M.; Peloquin, C.; Burman, W.; Luo, C.-C.; Engle, M.; Prihoda, T.J.; Kenzie, W.R.M.; Bliven-Sizemore, E.; Johnson, J.L.; Vernon, A. Effects of tuberculosis, race, and human gene SLCO1B1 polymorphisms on rifampin concentrations. *Antimicrob. Agents Chemother.* **2010**, *54*, 4192–4200. [CrossRef] [PubMed]
38. Sundell, J.; Bienvenu, E.; Äbelö, A.; Ashton, M. Effect of efavirenz-based ART on the pharmacokinetics of rifampicin and its primary metabolite in patients coinfected with TB and HIV. *J. Antimicrob. Chemother.* **2021**, *76*, 2950–2957. [CrossRef] [PubMed]
39. Medellin-Garibay, S.E.; Huerta-García, A.P.; Rodríguez-Báez, A.S.; Magaña-Aquino, M.; Ortiz-Álvarez, A.; Portales-Pérez, D.P.; del Carmen Milán-Segovia, R.; Romano-Moreno, S. A population approach of rifampicin pharmacogenetics and pharmacokinetics in Mexican patients with tuberculosis. *Tuberculosis* **2020**, *124*, 101982. [CrossRef] [PubMed]
40. Velásquez, G.E.; Brooks, M.B.; Coit, J.M.; Pertinez, H.; Vargas Vásquez, D.; Sánchez Garavito, E.; Calderón, R.I.; Jiménez, J.; Tintaya, K.; Peloquin, C.A.; et al. Efficacy and safety of high-dose rifampin in pulmonary tuberculosis. A randomized controlled trial. *Am. J. Respir. Crit. Care Med.* **2018**, *198*, 657–666. [CrossRef] [PubMed]
41. Nardotto, G.H.B.; Bollela, V.R.; Rocha, A.; Della Pasqua, O.; Lanchote, V.L. No implication of HIV coinfection on the plasma exposure to rifampicin, pyrazinamide, and ethambutol in tuberculosis patients. *Clin. Transl. Sci.* **2022**, *15*, 514–523. [CrossRef] [PubMed]
42. van Beek, S.W.; ter Heine, R.; Alffenaar, J.-W.C.; Magis-Escurra, C.; Aarnoutse, R.E.; Svensson, E.M. A model-informed method for the purpose of precision dosing of isoniazid in pulmonary tuberculosis. *Clin. Pharmacokinet.* **2021**, *60*, 943–953. [CrossRef]
43. Shen, J.; Boeckmann, A.; Vick, A. Implementation of dose superimposition to introduce multiple doses for a mathematical absorption model (Transit compartment model). *J. Pharmacokinet. Pharmacodyn.* **2012**, *39*, 251–262. [CrossRef]
44. Savic, R.M.; Jonker, D.M.; Kerbusch, T.; Karlsson, M.O. Implementation of a transit compartment model for describing drug absorption in pharmacokinetic studies. *J. Pharmacokinet. Pharmacodyn.* **2007**, *34*, 711–726. [CrossRef]
45. Carlsson, K.C.; Savić, R.M.; Hooker, A.C.; Karlsson, M.O. Modeling subpopulations with the $MIXTURE subroutine in NONMEM: Finding the individual probability of belonging to a subpopulation for the use in model analysis and improved decision making. *AAPS J.* **2009**, *11*, 148–154. [CrossRef]
46. Proost, J.H. Combined proportional and additive residual error models in population pharmacokinetic modelling. *Eur. J. Pharm. Sci.* **2017**, *109*, S78–S82.
47. Mould, D.R.; Upton, R.N. Basic concepts in population modeling, simulation, and model-based drug development—Part 2: Introduction to pharmacokinetic modeling methods. *CPT Pharmacomet. Syst. Pharmacol.* **2013**, *2*, e38. [CrossRef]
48. Bauer, R.J. NONMEM Tutorial Part II: Estimation methods and advanced examples. *CPT Pharmacomet. Syst. Pharmacol.* **2019**, *8*, 538–556. [CrossRef] [PubMed]
49. Duffull, S.B.; Wright, D.F.B.; Winter, H.R. Interpreting population pharmacokinetic-pharmacodynamic analyses—A clinical viewpoint. *Br. J. Clin. Pharmacol.* **2011**, *71*, 807–814. [CrossRef]
50. Nguyen, T.H.T.; Mouksassi, M.-S.; Holford, N.; Al-Huniti, N.; Freedman, I.; Hooker, A.C.; John, J.; Karlsson, M.O.; Mould, D.R.; Ruixo, J.J.P.; et al. Model evaluation of continuous data pharmacometric models: Metrics and graphics. *CPT Pharmacomet. Syst. Pharmacol.* **2017**, *6*, 87–109. [CrossRef]
51. Bergstrand, M.; Hooker, A.C.; Wallin, J.E.; Karlsson, M.O. Prediction-corrected visual predictive checks for diagnosing nonlinear mixed-effects models. *AAPS J.* **2011**, *13*, 143–151. [CrossRef] [PubMed]

52. Yano, Y.; Beal, S.L.; Sheiner, L.B. Evaluating pharmacokinetic/pharmacodynamic models using the posterior predictive check. *J. Pharmacokinet. Pharmacodyn.* **2001**, *28*, 171–192. [CrossRef]
53. Comets, E.; Brendel, K.; Mentré, F. Computing normalised prediction distribution errors to evaluate nonlinear mixed-effects models: The Npde add-on package for R. *Comput. Methods Programs Biomed.* **2008**, *90*, 154–166. [CrossRef]
54. Ribbing, J.; Niclas Jonsson, E. Power, selection bias and predictive performance of the population pharmacokinetic covariate model. *J. Pharmacokinet. Pharmacodyn.* **2004**, *31*, 109–134. [CrossRef] [PubMed]
55. Lindbom, L.; Pihlgren, P.; Jonsson, N. PsN-Toolkit—A Collection of computer intensive statistical methods for non-linear mixed effects modeling using NONMEM. *Comput. Methods Programs Biomed.* **2005**, *79*, 241–257. [CrossRef]
56. R Core Team. *R: A Language and Environment for Statistical Computing*; R Foundation for Statistical Computing: Vienna, Italy, 2022.
57. Pasipanodya, J.G.; McIlleron, H.; Burger, A.; Wash, P.A.; Smith, P.; Gumbo, T. Serum drug concentrations predictive of pulmonary tuberculosis outcomes. *J. Infect. Dis.* **2013**, *208*, 1464–1473. [CrossRef]
58. Acocella, G. Clinical pharmacokinetics of rifampicin. *Clin. Pharmacokinet.* **1978**, *3*, 108–127. [CrossRef]
59. Loos, U.; Musch, E.; Jensen, J.C.; Mikus, G.; Schwabe, H.K.; Eichelbaum, M. Pharmacokinetics of oral and intravenous rifampicin during chronic administration. *Klin. Wochenschr.* **1985**, *63*, 1205–1211. [CrossRef]
60. Jing, Y.; Zhu, L.Q.; Yang, J.W.; Huang, S.P.; Wang, Q.; Zhang, J. Population pharmacokinetics of rifampicin in Chinese patients with pulmonary tuberculosis. *J. Clin. Pharmacol.* **2016**, *56*, 622–627. [CrossRef] [PubMed]
61. Marsot, A.; Ménard, A.; Dupouey, J.; Muziotti, C.; Guilhaumou, R.; Blin, O. Population pharmacokinetics of rifampicin in adult patients with osteoarticular infections: Interaction with fusidic acid. *Br. J. Clin. Pharmacol.* **2017**, *83*, 1039–1047. [CrossRef]
62. Chirehwa, M.T.; Rustomjee, R.; Mthiyane, T.; Onyebujoh, P.; Smith, P.; McIlleron, H.; Denti, P. Model-based evaluation of higher doses of rifampin using a semimechanistic model incorporating autoinduction and saturation of hepatic extraction. *Antimicrob. Agents Chemother.* **2015**, *60*, 487–494. [CrossRef] [PubMed]
63. Milán-Segovia, R.C.; Domínguez-Ramírez, A.M.; Jung-Cook, H.; Magaña-Aquino, M.; Romero-Méndez, M.C.; Medellín-Garibay, S.E.; Vigna-Pérez, M.; Romano-Moreno, S. Relative bioavailability of rifampicin in a three-drug fixed-dose combination formulation. *Int. J. Tuberc. Lung Dis. Off. J. Int. Union Tuberc. Lung Dis.* **2010**, *14*, 1454–1460.
64. Johnston, A.; Holt, D.W. Substandard drugs: A potential crisis for public health. *Br. J. Clin. Pharmacol.* **2014**, *78*, 218–243. [CrossRef]

Disclaimer/Publisher's Note: The statements, opinions and data contained in all publications are solely those of the individual author(s) and contributor(s) and not of MDPI and/or the editor(s). MDPI and/or the editor(s) disclaim responsibility for any injury to people or property resulting from any ideas, methods, instructions or products referred to in the content.

pharmaceutics

MDPI

Article

Population Pharmacokinetics of Tideglusib in Congenital and Childhood Myotonic Dystrophy Type 1: Influence of Demographic and Clinical Factors on Systemic Exposure

Alessandro Di Deo [1,†], Sean Oosterholt [1,†], Joseph Horrigan [2], Stuart Evans [2], Alison McMorn [2] and Oscar Della Pasqua [1,*]

[1] Clinical Pharmacology & Therapeutics Group, University College London, London WC1H 9JP, UK
[2] AMO Pharma Ltd., 1 Park Row, Leeds LS1 5AB, UK
* Correspondence: o.dellapasqua@ucl.ac.uk
† These authors contributed equally to this work.

Abstract: Background: GSK3β is an intracellular regulatory kinase that is dysregulated in multiple tissues in Type 1 myotonic dystrophy (DM-1). Tideglusib inhibits GSK3β activity in preclinical models of DM-1 and promotes cellular maturation, normalising aberrant molecular and behavioural phenotypes. It is currently in clinical development for the treatment of paediatric and adult patients affected by congenital and juvenile-onset DM-1. Here, we summarise the development of a population pharmacokinetic model and subsequent characterisation of influential demographic and clinical factors on the systemic exposure to tideglusib. The availability of a population PK model will allow further evaluation of age-and weight-related changes in drug disposition, supporting the dose rationale and implementation of a paediatric extrapolation plan. **Methods:** Given the sparse pharmacokinetic sampling scheme in patients receiving tideglusib, model development was implemented in two steps. First, data from Phase I studies in healthy elderly subjects (i.e., 1832 plasma samples, n = 54) were used to describe the population pharmacokinetics of tideglusib in adults. Then, pharmacokinetic model parameter estimates obtained from healthy subjects were used as priors for the evaluation of the disposition of tideglusib in adolescent and adult DM-1 patients (51 plasma samples, n = 16), taking into account demographic and clinical baseline characteristics, as well as food intake. Secondary pharmacokinetic parameters (AUC, C_{max} and T_{max}) were derived and summarised by descriptive statistics. **Results:** Tideglusib pharmacokinetics was described by a two-compartment model with first-order elimination and dose-dependent bioavailability. There were no significant differences in disposition parameters between healthy subjects and DM-1 patients. Body weight was a significant covariate on clearance and volume of distribution. Median $AUC_{(0–12)}$ and C_{max} were 1218.1 vs. 3145.7 ng/mL·h and 513.5 vs. 1170.9 ng/mL, following once daily doses of 400 and 1000 mg tideglusib, respectively. In addition, the time of food intake post-dose or the type of meal appeared to affect the overall exposure to tideglusib. No accumulation, metabolic inhibition, or induction was observed during the treatment period. **Conclusions:** Even though clearance was constant over the dose range between 400 and 1000 mg, a less than proportional increase in systemic exposure appears to be caused by the dose-dependent bioavailability, which reflects the solubility properties of tideglusib. Despite large interindividual variability in the tideglusib concentration vs. time profiles, body weight was the only explanatory covariate for the observed differences. This finding suggests that the use of weight-banded or weight-normalised doses should be considered to ensure comparable exposure across the paediatric population, regardless of age or body weight.

Keywords: tideglusib; pharmacokinetics; food effect; phase I; myotonic dystrophy; modelling and simulation

1. Introduction

Myotonic dystrophy type 1 (DM-1) is an autosomal dominant, monogenetic disorder caused by expansion repeats of a cytosine-thymine-guanine trinucleotide in the noncoding region of the myotonic dystrophy protein kinase gene on chromosome 19q13.3 [1,2]. Although symptoms most commonly appear in early adulthood, DM-1 can also manifest during childhood (juvenile DM-1) or, in its most severe form, at birth (congenital DM-1), where reduced foetal movements and polyhydramnios can appear already during the prenatal period [3–5]. At birth the main features are severe generalised weakness, hypotonia, and respiratory compromise. Surviving infants experience gradual improvement in motor function during the first decade of life, however they may develop typical features of DM-1, including weakness, myotonia, cataracts, and cardiac complications [6,7].

Tideglusib is a brain penetrant orally administered new chemical entity from the thiadiazolidindione chemical family. It acts as a selective adenosyl triphosphate non-competitive inhibitor of glycogen synthase kinase 3 (GSK-3), an enzyme which has fundamental roles for these protein kinases in memory, behaviour, and neuronal fate determination [8,9]. Dysregulation of signalling pathways involving GSK-3 has been associated with several neurological and psychiatric disorders. These findings offered insights into potential therapeutic interventions for DM-1 patients, in whom intellectual disability affects various cognitive domains, including social cognition, memory, language, and visuospatial functioning is also observed [10].

Tideglusib is currently in clinical development for the treatment of adult and paediatric patients affected by congenital or juvenile DM-1. Recently, a Phase II study aimed at the evaluation of the safety and efficacy of tideglusib in adolescent and adult patients (n = 16) has been completed [11]. Whilst this study provided insight into the potential clinical benefits of tideglusib in the target patient population, relatively large variation has been observed in the systemic exposure to tideglusib, which could be associated with its solubility profile, food effect, metabolic polymorphism or individual patient characteristics, such as body weight. However, to date the determinants of intra- and interindividual variability in pharmacokinetics have not been characterised. The aim of the current investigation was therefore to assess the effect of potential covariate factors on the pharmacokinetics of tideglusib using non-linear mixed effects modelling.

Given the limited pharmacokinetic data available from the Phase II study, which relied on sparse blood sampling, a Bayesian meta-analytical approach was used to characterise the pharmacokinetics of tideglusib. First, data from a Phase I study, in healthy elderly subjects, in which a frequent blood sampling scheme was used, were analysed to ensure the identification of the appropriate pharmacokinetic model structure and relevant parameter distributions. Subsequently, parameter estimates and model structure were used as priors for the assessment of the pharmacokinetics in the DM-1 patients along with an allometric function, describing the effect of developmental growth, including age and body weight on the disposition properties of tideglusib. This approach has been successfully used in previous investigations in children [12–15]. It relies on similar concepts and assumptions applied to historical borrowing, which involves leveraging information from control arms in previous relevant clinical trials, which in turn may further enhance a clinical trial's efficiency [16,17]. The availability of a population pharmacokinetic model will provide the

basis for the dose rationale for younger paediatric patients in future clinical studies. It will also support the implementation of a paediatric extrapolation plan.

2. Materials and Methods

2.1. Study Population and Study Design

Phase I Study in Elderly Healthy Subjects:

NP031112-07A03 was a double blind, randomised, parallel-group, placebo-controlled, multiple ascending dose study to assess the safety, tolerability, and pharmacokinetics of tideglusib in elderly male and female healthy subjects. The study population consisted of six treatment groups each containing twelve participants, with nine of them randomised to receive tideglusib and three subjects to receive placebo (ratio 3:1). An overview of the inclusion and exclusion criteria of the study is included in the Supplementary Materials.

In total, seventy-two subjects (60 years or older) were allocated into one of the following dose groups and administered 300 mg b.i.d., 400 mg b.i.d., 600 mg q.d., 800 mg q.d., 1000 mg q.d. and 1200 mg q.d tideglusib. Repeat dosing of tideglusib or placebo over 14 days was preceded by single-dose administration followed by a wash-out period of 48 h. The investigational product was administered p.o. as a suspension in water of the formulation F06-037F. Blood samples for the evaluation of tideglusib pharmacokinetics were taken on days 1 and 16 at pre-dose (two samples on day 1), at 20 and 40 min, 1, 1.5, 2, 2.5, 3, 4, 6, 8, 12, 16, 24, 30, 36, and 48 h post-dose. Trough samples were collected pre-dose at days 5, 7, 9, 11, 13, and 15. During dose escalation, progression to the next treatment group was determined following a review of all safety, tolerability, and available exposure data from the previous treatment group. This included assessments of increased levels of ALAT, ASAT, GGT, or alkaline phosphatase exceeding 2.5 times the upper limit of normal (ULN), total bilirubin increases greater than 1.5 times the ULN, or any other safety, tolerability, or exposure concerns. All reported adverse events (AEs) were of mild to moderate severity and transient. No severe AEs or deaths occurred during this study and no SAEs were recorded.

Phase II Study in DM-1 Patients:

AMO-02-MD-2-001 was designed as a Phase II, single-blind, placebo-controlled, fixed-dose study of the safety, pharmacokinetics and efficacy of oral treatment with tideglusib (400 mg or 1000 mg q.d.), in which adolescent and adult patients, aged between 13 and 34 years, with congenital or juvenile onset DM-1 were dosed with tideglusib for 12 weeks [11]. An overview of the inclusion and exclusion criteria can be found in the Supplementary Materials.

Subjects were assigned to either 400 mg or 1000 mg q.d. doses of tideglusib according to a 1:1 ratio. In total, 16 subjects were enrolled in the study. All subjects were treated for 2 weeks with single-blind placebo before starting the single-blind active phase, during which they received the assigned dose and dosing schedule for 12 weeks. Subjects in the 400 and 1000 mg cohorts were combined for the main efficacy analysis. Blood samples for the evaluation of tideglusib pharmacokinetics were taken pre-dose, and between 2- and 4 h post-dose at weeks 2 and 12 after the start of the active treatment. Throughout the study, tideglusib was administered following overnight fasting and food intake was restricted for at least one hour after each daily administration. Compliance with food restriction was monitored through a daily diary. Dosing, blood sampling, and food intake times were recorded for each patient. The primary objective of the study was to investigate the safety and tolerability of tideglusib in this patient population. The secondary objectives were to investigate the pharmacokinetics and efficacy of tideglusib, as assessed by the improvement in clinical endpoints between baseline and end-of-treatment.

2.2. Data and Demographic Characteristics

A total of 1832 plasma samples from 54 healthy elderly subjects enrolled in study NP031112-07A03 were included in the pharmacokinetic analysis. The subjects were equally distributed between the six dose groups (nine subjects for each active treatment group). The age of the subjects ranged from 60 to 74 years [mean: 64.3, s.d. = 3.5 years], whereas body weight ranged from 50.7 to 98.1 kg [mean: 74.5, s.d. = 9.9 kg]. Twenty-four subjects were female while 30 were male (Table 1). The observed tideglusib plasma concentration versus time profiles stratified by dose levels are shown in Figure S1 (Supplementary Materials).

From study AMO-02-MD-2-001, a total of 51 evaluable plasma samples from 16 adolescent and adult DM-1 patients were available for the data analysis. Nine samples were found to be below the lower limit of quantification (LLOQ), two of which showed no peak. All these samples were pre-dose (i.e., trough) measurements. As shown in Figure S2 (Supplementary Materials), the observed tideglusib plasma concentration versus time profiles showed large interindividual variability, but with proportionally higher concentrations in patients receiving the 1000 mg q.d. dosing regimen.

The age of patients included in the analysis ranged from 13.8 to 34.9 years [mean: 20.9, s.d. = 5.9 years], whereas body weight ranged from 36.8 to 122.6 kg [mean: 63.6, s.d. = 19.6]. Six of the 16 subjects were female (Table 1).

Table 1. Demographic baseline characteristics of the population included in the pharmacokinetic analysis.

	Dose Group (mg)	Dosing Regimen	Subjects (n/Female)	Body Weight (kg)	Height (cm)	Age (Years)
NP03112-07A03	300	b.i.d.	9/4	78.0 (62.5–93.7)	171 (158–180)	61 (60–68)
	400	b.i.d.	9/5	77.1 (59.5–98.1)	166 (157–188)	68 (62–72)
	600	q.d.	9/4	74.4 (66.4–88.9)	169.0 (163–182)	64 (60–71)
	800	q.d.	9/5	75.6 (64.2–87.6)	168 (159–182)	65 (61–74)
	1000	q.d.	9/2	72.5 (57.6–87.5)	170 (156–180)	63 (60–65)
	1200	q.d.	9/4	72.7 (50.7–92.7)	167 (155–181)	64 (60–70)
AMO-02 MD-2-001	400	q.d.	8/1	60.3 (36.8–81.4)	168.5 (156–179)	19.4 (13.8–32.6)
	1000	q.d.	8/5	58.7 (45.1–122.6)	160.5 (148–178)	20.8 (17.2–34.9)

Values are summarised by median (minimum–maximum). Summary statistics, including means and standard deviations, are presented in Table S1 (Supplementary Materials).

2.3. Bioanalytical Method

The bioanalysis of the human plasma samples was based on a high-performance liquid chromatography with tandem mass spectrometry (HPLC-MS/MS). The method was validated in a previous Phase I study (S01091) and revalidated in Study S29871 in terms of specificity, linearity and intra-assay accuracy and precision, using an UPLC® (Waters) -MS/MS API4000 (AB SCIEX, Marlborough, MA, USA) system. The lower and upper limits of quantification (LLOQ and ULOQ) in human plasma were set at 1 and 2000 ng/mL, respectively. Linearity was evaluated using nine concentrations (spiked plasma samples from calibration standards) ranging between LLOQ and ULOQ. The processing of the chromatograms, the calculation of correlation coefficients (r) and values for the calibration curve slope and intercept were performed using the Analyst® Processing

Manager (Analyst® Version 1.4.2, AB SCIEX, Marlborough, MA, USA). The linear regression used a $1/x^2$ weighting factor. The precision of the bioanalytical procedure was evaluated calculating the intra-assay coefficient of variation, expressed as CV%.

2.4. Population Pharmacokinetic Modelling

2.4.1. Model Development Using Phase I Adult Data

Given the aims of the current investigation, an initial exploratory analysis included data from three Phase I studies (CL031112-05A01, CL031112-06A02 and NP031112-07A03) in which different formulations (Labrasol®/water, F05-052, and F06-037F) were used. These data indicated that formulation differences had an important effect on the pharmacokinetics and overall safety profile of the compound. Labrasol® formulation used in the first two studies was found to be unsuitable for longer studies in animals. In addition, it was also found to produce throat irritation in human volunteers. F05-052 was developed as a powder intended to be orally administered following reconstitution in water. In study NP031112-07A03 formulation F06-037F, an evolution of the F05-052 formulation, demonstrated better dispersibility and organoleptic properties. This finding led to further assessment of its pharmaceutical properties and subsequent development for future clinical trials with tideglusib. Consequently, only data from study NP031112-07A03 were used for the development of a population pharmacokinetic model for tideglusib.

Pharmacokinetic modelling was implemented using a non-linear mixed effects approach. First, a base model was built testing different compartments to describe the observed disposition characteristics. Then, the appropriate stochastic components describing the inter-individual variability were identified and added to the base model. Inter-individual variability in pharmacokinetic parameters was assumed to be log-normally distributed. The residual error was characterised using a proportional error model.

Given the anticipated use of the model as a prior for parameter estimation in subsequent studies including sparse blood sampling in paediatric and/or adult subjects, model development was based on allometric principles, assuming body weight as a significant covariate factor on the pharmacokinetics of tideglusib. This effect was parameterised using a reference body weight of 70 kg and fixed allometric exponents on clearance (0.75) and volumes (1). Even so, a covariate analysis was implemented to explore measurable sources of variability in the pharmacokinetics of tideglusib. In addition to body weight, several factors were considered (e.g., age, BMI, dose, and food intake, i.e., fasting or fed state). In situations in which collinearity exists between covariates, such as age and weight, the choice of covariates to be selected was guided by a careful review of the factors that are most likely to be the primary cause of interindividual differences in pharmacokinetic parameters. A standard forward inclusion backward deletion procedure was used to select the covariates [18]. Statistically significant covariates as well as those considered clinically relevant were added to the base model, with one covariate into one parameter at a time.

Briefly, a comparison between hierarchical models was based on the difference in -2 log likelihood, which is assumed to be approximately χ^2-distributed, with degrees of freedom equal to the difference in the number of parameters between two tested models. A reduction in the OFV $\geq$ 3.84, $\chi^2 < 0.05$ for 1 degree of freedom (df) using the FOCE-I estimation method was considered statistically significant. The significance test as well as the inclusion steps were repeated until all significant covariates were evaluated, and the final model was defined. During the final modelling steps, only the covariates which resulted in an OFV reduction of $\geq$7.88 ($p < 0.005$) were kept in the model. After the full model was identified, the significance of each covariate was tested individually by removal one at a time from the full model (backward deletion). A covariate was retained in the model if, upon removal, the OFV increased by more than 6.64 points ($\chi^2 < 0.01$ 1 df) [18].

2.4.2. Parameter Estimation in DM-1 Patients

The use of a rich sampling scheme in study NP031112-07A03 has allowed the identification of the model structure along with relevant parameter distributions describing the inter-and intraindividual variability in pharmacokinetic parameters (Figure 1). These estimates were subsequently used as prior information for the characterisation of the systemic exposure in DM-1 patients. The analysis was performed according to the $PRIOR NWPRI subroutines in NONMEM. When using NWPRI, fixed-effect parameters are assumed to be normally distributed, whereas the random effects (ω^2 and σ^2) are assumed to be described by an inverse Wishart distribution [19,20].

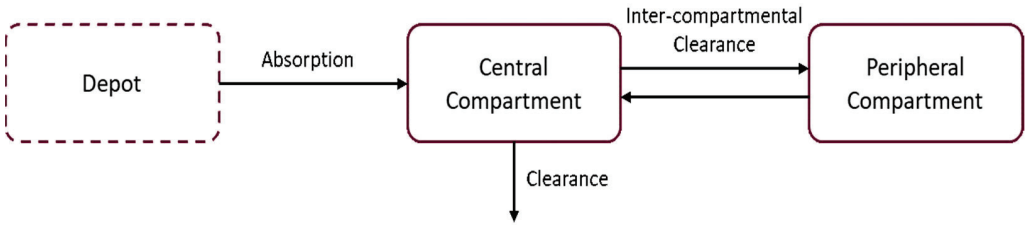


Figure 1. Schematic representation of the pharmacokinetic model structure of tideglusib in elderly healthy subjects. Tideglusib pharmacokinetics was described by a two-compartment model with first-order elimination and dose-dependent bioavailability. The full model included additional terms describing the effect of body weight as a covariate on clearance (CL), intercompartmental clearance (Q), and volumes of distribution (V2 and V3), as well as a dose-dependent effect on the absorption rate constant (KA) and bioavailability (F1).

Both informative and non-informative priors have been tested. Informative prior distributions for fixed-effect parameters were implemented using the full variance-covariance matrix from the pharmacokinetic model in healthy elderly subjects. For informative priors on random effects, the degree of freedom was calculated with the formula:

$$df = 2 \cdot [\omega^2 / (\text{SE of } \omega^2)]^2 + 1 \quad (1)$$

Empirical Bayesian post hoc estimates were then derived for DM-1 patients.

2.4.3. Model Evaluation

Model performance was assessed by numerical, graphical, and statistical procedures, including standard goodness-of-fit plots, visual predictive check (VPC), bootstrapping, normalised prediction discrepancy error (NPDE) and mirror plots. In detail, goodness-of-fit was assessed by graphical methods, including population and individual predicted vs. observed concentrations, conditional weighted residuals vs. observed concentration or time, correlation between parameters. Further evaluation of the variance-covariance structure and overall random effects in the model was based on NPDE diagnostics [21].

VPCs were used to evaluate the adequacy of the final model parameter estimates, including the effects of statistically significant covariates [22]. One thousand replicates of the original data set were simulated, and the 90% prediction interval was computed. The observed concentration versus time data were plotted along with the prediction intervals to visually assess the concordance between predicted and observed data.

Bootstrapping was performed to assess bias, model stability, generate standard errors and confidence intervals for the parameter estimates [23]. For bootstrapping, 1000 new data sets were generated by sampling individuals with replacement from the original data set and then fitting the model to each new data set [24].

Subsequently, to generate mirror plots, the parameter estimates of the final model were used to simulate plasma concentrations in patients with similar demographic characteristics,

dosing regimens, and sampling schemes as those in the original clinical study. Mirror plots of individual predicted versus observed concentration were created to evaluate the variance-covariance structure, which can be assessed by the degree of similarity between the original fit and the pattern obtained from the simulated datasets.

The same model validation procedures have been applied for the analysis of the pharmacokinetic data in healthy adult elderly subjects and DM-1 patients.

2.5. Secondary Pharmacokinetic Parameters

The final parameter estimates were used to simulate individual concentration vs. time profiles based on 6 min sampling intervals. Secondary metrics of exposure were then derived by non-compartmental methods, namely: peak concentration (C_{max}), trough concentration (C_{min}), area under the concentration vs. time curve ($AUC_{(0–24)}$ or $AUC_{(0–12)}$), time at which peak concentration occurs (T_{max}), elimination half-life ($T_{1/2}$) and average steady-state concentration (C_{ss}).

2.6. Exploratory Analysis of the Effect of Food Intake on the Systemic Exposure in DM-1 Patients

Throughout the Phase II clinical study (AMO-02-MD-2-001), tideglusib was administered to DM-1 patients following overnight fasting. Food intake was then restricted for at least one hour after each administration. Food intake times as well as type of meal were recorded, according to the following categories: light, standard or other.

In total, 30 evaluable records, collected from two different visits were used for the purpose of this analysis. Thus, to explore the effect of food on the extent and rate of absorption of tideglusib, $AUC_{(0–12)}$, $AUC_{(0–24)}$, and C_{max} values on visit 4 and visit 9 were compared by stratifying the results by meal type. Results were summarised by median and range.

2.7. Effect of Body Weight on the Pharmacokinetics of Tideglusib and Dose Rationale for the Paediatric Population

Simulation scenarios were implemented to explore the implications of age/weight-related changes in the systemic exposure to tideglusib. As there is limited information *in vivo* on the metabolism of tideglusib, scaling of disposition parameters was based on allometric principles, with total body weight as the primary determinant of changes in pharmacokinetics.

Given the importance of minimising dispensing errors and ensuring a child-friendly dosing regimen, fixed dose weight-banded regimens were prioritised during this evaluation. Scenarios consisted of a virtual population of 71 patients per weight band, and dose level, considering a uniform distribution of weight ranging from 5 to 75 kg. For each dose group, 1000 iterations have been performed. Simulated steady state profiles were generated using a rich sampling scheme (every 0.1 h) with fixed dosing intervals (once daily, every 24 h).

The adequacy of the proposed dosages has been evaluated by comparing the predicted exposure measures, $AUC_{0–24}$ and C_{max}, with the corresponding reference values in adult subjects with a body weight between 70 and 75 kg receiving 1000 mg dose of tideglusib under fasting conditions. Reference values [median (90% prediction interval)] were 2560.8 (1282.5–5286.7) ng/mL·h and 929.6 (446.4–1834.4) ng/mL for $AUC_{0–24}$ and C_{max}, respectively. In addition to summary statistics, the proportion of subjects exceeding the 95th percentile of the exposure range in adults was also calculated. Even though a maturation function cannot be defined in absence of further data, the proposed dosing regimen does take into account the implications of interindividual variability and time-dependent changes in metabolic clearance (i.e., CYP3A4 metabolism, as initially suggested by *in vitro* data). It also considers dose-dependent solubility and its effect on the bioavailability of tideglusib.

2.8. Software

Clinical and demographic baseline data as well as dose and drug concentrations were imported into R (version 4.4.0, R Core Team, 2021) [25] for exploratory analysis and formatted for subsequent modelling and simulation in NONMEM version 7.5.1 (ICON Development Solutions, Baltimore, MD, USA). The analysis was conducted in combination with PsN 5.3.1. All required data manipulation, including graphical and statistical summaries were performed in R.

3. Results

3.1. Tideglusib Pharmacokinetics in Elderly Healthy Subjects and DM-1 Patients

Tideglusib pharmacokinetics in elderly healthy subjects was adequately described by a 2-compartment model. Despite linear pharmacokinetics, the concentration vs. time profiles of tideglusib were found to be dose-dependent, with systemic exposure probably being affected by the limited solubility of the compound. This phenomenon was described by the different estimates for the first-order absorption rate constant (KA) and relative bioavailability (F1). Weight was the only covariate to have a significant effect on CL, V2, V3 and Q. In addition, interindividual variability (IIV) was estimated for CL, V2, V3, Q and KA. Residual variability was parameterised using a proportional error model (Table 2), but a separate parameter was required for doses lower and higher than 400 mg. All parameters were well estimated without significant correlations between them. Fixed-effect parameters were estimated with good precision (%RSE < 27.4%) as were the inter-individual variabilities (%RSE < 41.1%). The VPC (Figure 2) showed that the observed tideglusib concentrations fall within the 90% confidence interval of the simulated values for oral dosing. The non-parametric bootstrap estimates of the model parameters indicated model stability, with acceptable confidence intervals for all parameter estimates.

The diagnostic plots did not reveal any bias or significant deviation between predicted and observed data. This was corroborated by the NPDE plots, which displayed normally distributed prediction errors and did not show any specific bias in model predictions (Supplementary Materials, Figures S3–S5). The final model was therefore deemed to have acceptable predictive performance to be used as priors in conjunction with sparse blood sampling (Table 2).

In fact, tideglusib exposure in adolescent and adult patients with congenital and juvenile-onset DM-1 was adequately described by the model. Similarly to the differences observed in healthy subjects, dose (strength) was found to have a statistically significant effect on residual variability in the patient population, with different parameter estimates for doses higher than 400 mg. Weight was the only covariate to have a significant effect on the disposition of tideglusib. All parameters were well estimated with good precision (%RSE < 23%) as were the IIV (%RSE < 32%). A VPC (Figure 3) shows that the observed tideglusib concentrations fall within the 90% prediction interval. The predictive accuracy and the stability of the final model is corroborated by NDPE and mirror plots. Finally, diagnostic plots indicate that the model adequately describes the data and produces unbiased population and individual predictions (Supplementary Materials, Figures S6–S11). Therefore, the final model was deemed to have acceptable predictive performance for simulation purposes.

Table 2. Final population pharmacokinetic parameter estimates for tideglusib in healthy elderly subjects and DM-1 patients.

	AMO-02-MD-2-001			NP031112-07A03		
Parameter (Unit)	**Population Estimate**	**RSE (%)**	**Bootstrap Median (5th–95th Percentiles)**	**Population Estimate**	**RSE (%)**	**Bootstrap Median [a] (5th–95th Percentiles)**
Clearance, CL (L/h)	341	12.4	336 (268–389)	327	17.0	333 (260–408)
Volume of distribution central compartment, V2 (L)	154	16.4	151 (108–183)	152	27.4	156 (93–239)
Absorption rate constant, kA (1/h)	0.767	6.8	0.760 (0.677–0.828)	0.78	11.3	0.78 (0.67–1.09)
Absorption rate constant, kA (dose > 400 mg) (1/h)	0.609	1.6	0.608 (0.589–0.623)	0.61	6.6	0.61 (0.55–0.69)
Intercompartmental clearance, Q (L/h)	66.1	22.1	64.6 (41.9–82.2)	66.1	26.0	67.0 (46.8–94.1)
Volume of distribution peripheral compartment, V3 (L)	986	18.3	971 (692–1180)	1010	21.1	1021 (759–1375)
Bioavailability (doses $\leq$ 400 mg)	1	FIXED	FIXED	1	FIXED	FIXED
Bioavailability (doses > 400 mg)	0.88	13.2	0.87 (0.68–1.01)	0.85	18.8	0.86 (0.64–1.11)
Interindividual Variability	**Population Estimate (CV%) [b]**	**RSE (%)**	**Bootstrap Median (5th–95th Percentiles)**	**Population Estimate (CV%) [b]**	**RSE (%)**	**Bootstrap Median [a] (5th–95th Percentiles)**
ηCL variance	0.186 (43.1)	22.7	0.18 (0.13–0.27)	0.18 (43.5)	16.9	0.18 (0.12–0.24)
ηQ variance	1.15 (107.2)	31.6	1.09 (0.71–1.83)	0.96 (98.2)	23.5	0.93 (0.61–1.31)
ηV3 variance	1.01 (100.5)	28.6	0.96 (0.67–1.57)	0.90 (95.1)	22.2	0.89 (0.59–1.24)
ηV2 variance	0.321 (56.7)	3.1	0.32 (0.31–0.34)	0.33 (57.8)	36.5	0.32 (0.15–0.58)
ηKA variance	0.069 (26.4)	2.2	0.07 (0.07–0.07)	0.06 (26.2)	41.1	0.06 (0.02–0.11)
Residual Error	**Population Estimate**	**RSE (%)**	**Bootstrap Median (5th–95th Percentiles)**	**Population Estimate**	**RSE (%)**	**Bootstrap Median [a] (5th–95th Percentiles)**
Proportional error (doses $\leq$ 400 mg)	0.54	1.8	0.54 (0.53–0.56)	0.56	7.2	0.55 (0.49–0.62)
Proportional error (doses > 400 mg)	0.46	0.9	0.46 (0.45–0.47)	0.45	4.0	0.45 (0.42–0.48)

Abbreviations: CV = coefficient of variation, RSE = percent relative standard error, θ = PK fixed-effect parameter; η = inter-individual variability; Ω = variance of inter-individual variability in population PK parameter; σ = residual variance. [a]: Non-parametric bootstrap results are presented as median and 5th–95th percentiles. Bootstrapping was based on re-sampling of 1500 data sets from the original data set and subsequent re-estimation using the final model. [b]: Coefficient of variations have been calculated as: $CV = \mathrm{sqrt}\left(\exp\left(\Omega^2\right)\right) \times 100$.

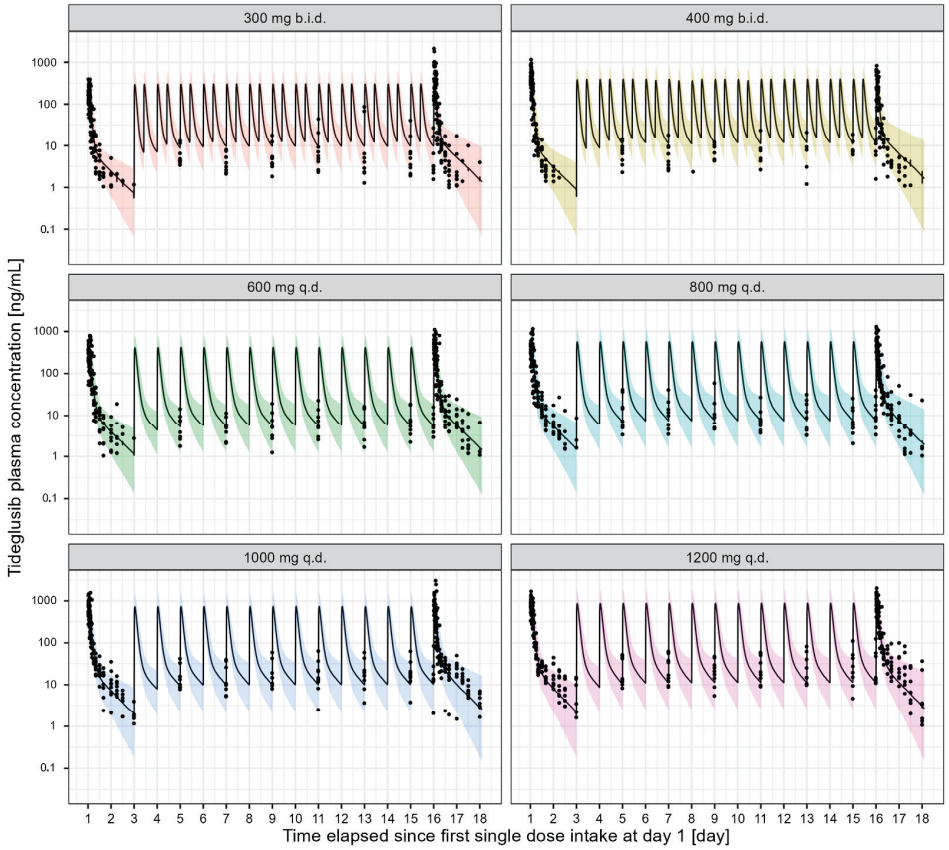


Figure 2. Visual predictive checks describing the performance of the final model of tideglusib in elderly healthy subjects (n = 54), stratified by dose level. The solid circles are the observed concentrations; solid black lines represent the median of the simulated data. The shaded areas depict the 90% prediction intervals for the simulated profiles.

3.2. Secondary PK Parameters

Using the final population model, predicted plasma concentration vs. time profiles were derived using a serial sampling scheme. Median estimates for adolescent and adult DM-1 patients receiving doses of 400 mg and 1000 mg were, respectively, 1218.1 and 3145.7 ng/mL·h for $AUC_{0–12}$ and 513.5 and 1170.9 ng/mL for C_{max}. The median elimination half-life ($T_{1/2}$) ranged between 1.7 h and 2.0 h.

These results show that administration of fixed doses irrespective of interindividual differences in body weight leads to higher exposure in the younger subjects, who have lower body weight. The summary statistics for the secondary pharmacokinetic parameters are shown in Table 3.

Table 3. Statistical summary of the secondary pharmacokinetic parameters of tideglusib in elderly healthy subjects (n = 54) and in adolescent and adult DM-1 patients (n = 16).

Study	Dose (mg)	C_{max} (ng/mL)	C_{min} (ng/mL)	C_{SS} (ng/mL)	T_{max} (h)	$T_{1/2}$ (h)	$AUC_{(0–12)}$ (ng/mL·h)
NP03112-07A03 [a]	400 b.i.d.	504.7 (312.0–624.9)	9.8 (7.2–22.4)	79.2 (57.3–126.4)	0.7 (0.4–1.0)	1.5 (1.0–2.8)	949.7 (687.9–1516.1)
	1000 q.d.	702.0 (550.3–1453.3)	18.5 (7.0–37.8)	78.3 (59.4–219.0	0.7 (0.3–1.3)	4.0 (1.8–6.7)	1749.8 (1376.7–4947.7)
AMO-02 MD-2-001 [b]	400 q.d.	513.5 (342.9–615.4)	4.1 (2.1–11.3)	56.9 (30.7–74.4)	0.75 (0.3–1.0)	2.0 (1.3–5.4)	1218.1 (660.3–1713.8)
	1000 q.d.	1170.9 (573.3–1450.1)	5.6 (3.4–16.2)	141.6 (68.8–220.3)	0.7 (0.6–1.2)	1.7 (1.0–2.5)	3145.7 (1571.4–5109.4)

Data are medians and (5th–95th percentiles). [a] For study NP03112-07A03, secondary pharmacokinetic parameters have been derived at day 16. [b] For study AMO-02-MD-2-001, secondary pharmacokinetic parameters have been derived from Visit 4.

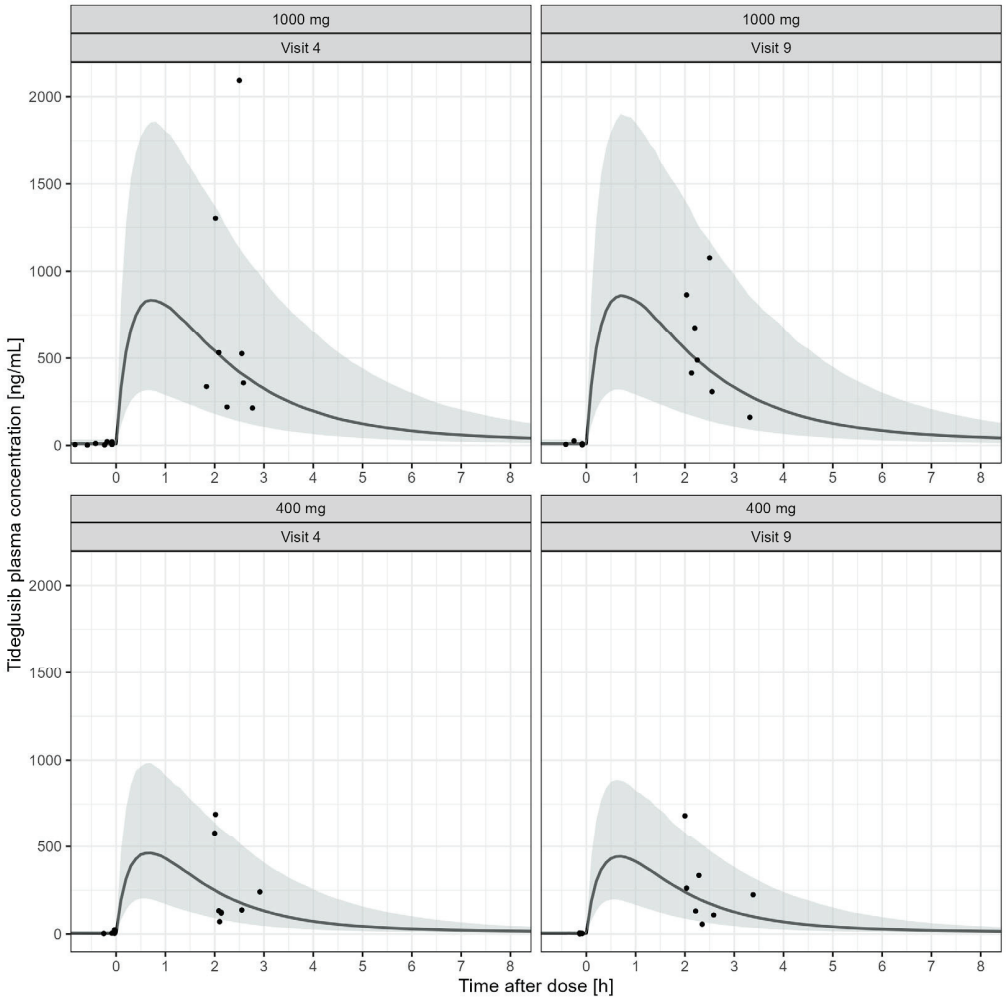


Figure 3. Visual predictive check for the final model of tideglusib in DM-1 patients (n = 16). The black circles are observed concentrations, and the solid black line represents the median of the simulated data. The shaded area indicates the 90% prediction interval of the simulated profiles. Data are stratified by dose group and treatment visit. Time in the *x*-axis is the time after the last dose. Observed concentrations at or before t = 0 are trough samples collected prior to the last dose.

3.3. Influence of Type and Time of Food Intake on the Systemic Exposure to Tideglusib

In the 400 mg dosing group, three patients had a standard meal, seven had a light meal and five had another type of meal. In the 1000 mg dosing group, six patients had a standard meal while three had a light meal and six had other types of meals. Food intake took place at different times after drug administration under fasting conditions. There was no evidence of an effect of food or meal type on the predicted exposure to tideglusib. As shown in Figure 4, there are no clear differences in AUC and C_{max} across dose levels for the different meal types. The intake of food at different times after dosing does not seem to affect systemic exposure; no trends are observed even after stratification of the data by body weight. In Table 4, the secondary PK parameters of interest, $AUC_{(0–24)}$, $AUC_{(0–12)}$ and C_{max} are stratified by meal type.

3.4. Influence of Body Weight on Systemic Exposure to Tideglusib

Body weight was identified as a covariate on the clearance and volume of distribution of tideglusib. This effect is also observed when exploring the correlation between secondary pharmacokinetic parameters and body weight in both healthy elderly subjects and adolescent and adult DM-1 patients. Despite the relatively large interindividual variability,

it seems that higher exposure is expected to occur in subjects with lower body weight (Figure 5).

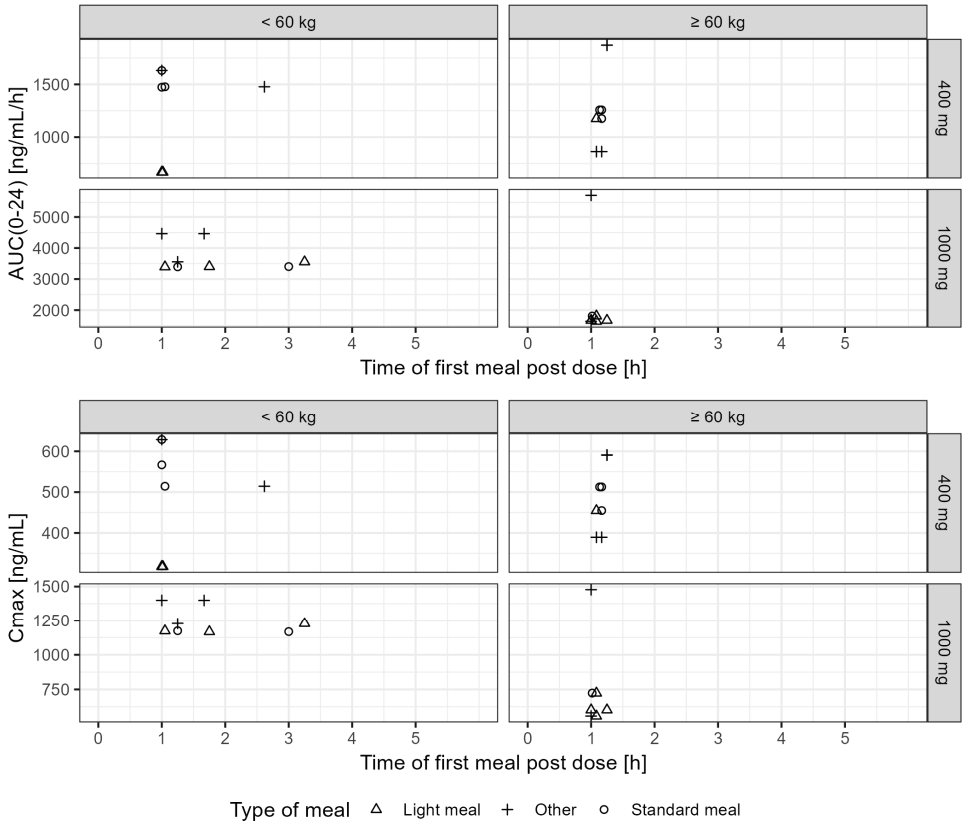


Figure 4. Effect of type of meal on exposure to tideglusib administration in DM-1 patients. Upper and bottom panels show, respectively, $AUC_{(0–24)}$ and C_{max} vs. the time of the first meal post dose. Data are stratified per dose level (rows) and into two body weight groups, i.e., below or above the population median (60 kg). Points depict the individual predicted parameter values. Each meal type is depicted by a different symbol.

Table 4. Statistical summary of the secondary pharmacokinetic parameters per type of meal.

	Dose (mg)	Weight (kg)	n	C_{max} (ng/mL)	$AUC_{(0–12)}$ (ng/mL·h)	$AUC_{(0–24)}$ (ng/mL·h)
Light Meal	400	<60	1	317.9	590.8	669.2
		≥60	1	454.8	1143.5	1175.8
	1000	<60	3	1174.1 (1167.8–1227.8)	3153.4 (3138.1–3462.7)	3402.9 (3394.4–3555.8)
		≥60	3	602.1 (557.8–723.6)	1586.6 (1563.2–1743.7)	1672.7 (1640.7–1810)
Standard Meal	400	<60	3	566.8 (514.3–628.7)	1402.3 (1237.3–1560.0)	1477.2 (1473.0–1631.5)
		≥60	2	483.8 (454.8–512.7)	1171.3 (1143.5–1199.1)	1216.9 (1175.7–1258.1)
	1000	<60	2	1170.9 (1167.8–1174.1)	3145.8 (3138.1–3153.4)	3398.7 (3394.5–3402.9)
		≥60	1	723.6	1743.8	1810.0
Other Meal	400	<60	2	571.5 (514.3–628.7)	1481.1 (1402.3–1560.0)	1554.3 (1477.2–1631.5)
		≥60	2	490.1 (389.4–590.8)	1293.1 (789.4–1796.7)	1367.3 (863.5–1871.2)
	1000	<60	2	1313.5 (1227.8–1399.2)	3817.5 (3462.7–4172.4)	4009.4 (3555.8–4463.0)
		≥60	2	1017.7 (557.8–1477.6)	3588.6 (1563.2–5614)	3685.8 (1640.7–5730.8)

Data are summarised by median (range); n is the number of subjects.

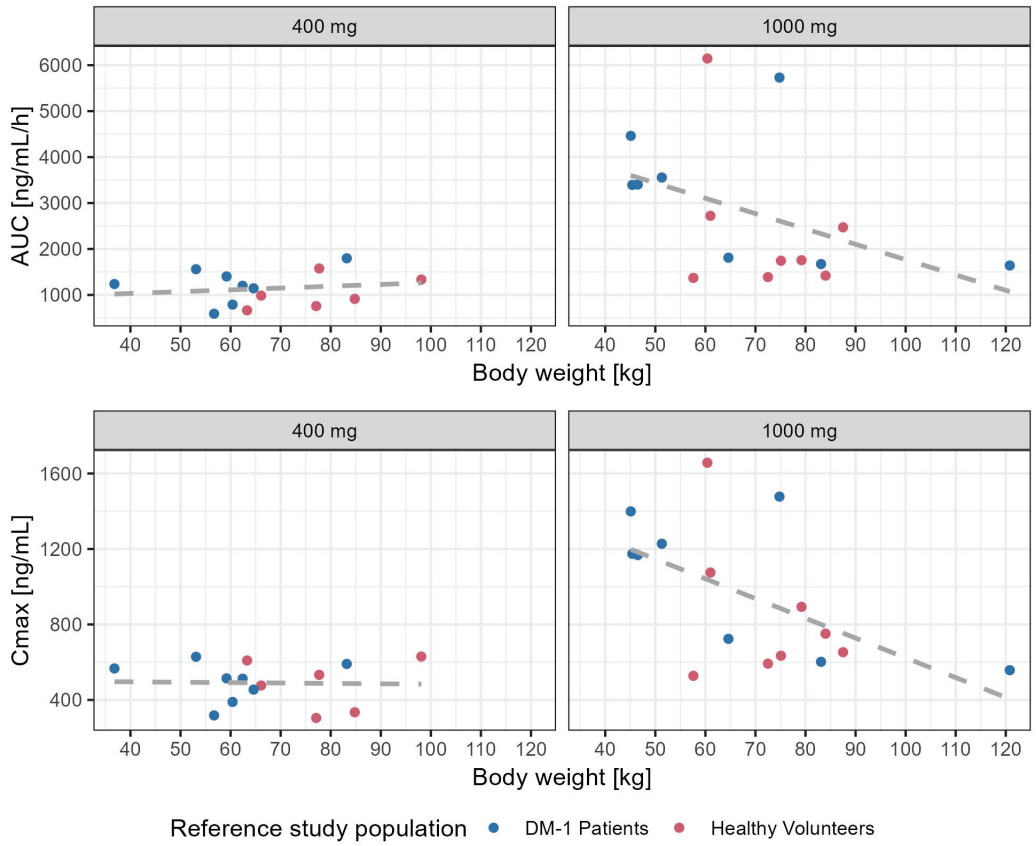


Figure 5. Effect of body weight on systemic exposure (AUC) and peak concentration C_{max}) of tideglusib in elderly healthy subjects and DM-1 patients. Solid circles depict the predicted values while dashed lines are a general linear function describing the trends in the data.

3.5. Dose Rationale for Paediatric Patients

The final pharmacokinetic model in DM-1 patients was used to support prediction and extrapolation of the pharmacokinetic properties of tideglusib across different age groups, assuming that the exposures observed in adults and adolescents following 1000 mg q.d. dose are clinically relevant and can be considered as a target for efficacy. Based on the putative mechanism of action of tideglusib, the approach also assumes a similar pharmacokinetic-pharmacodynamic relationship for tideglusib in adults and children affected by DM-1, despite the heterogeneity in the onset and clinical presentation of the condition in children. Simulation scenarios enabled the identification of suitable dosing regimens that maximise the proportion of subjects who achieve the observed exposure range in adult and adolescent patients receiving 1000 mg dose of tideglusib (Table 5). This scenario provided the highest proportion of patients meeting the target exposure range.

Table 5. Overview of the proposed weight-banded dosing regimen for tideglusib in paediatric and adult patients with DM-1.

	Weight-Banded Dosing Regimen (mg/kg)						
Weight-band (kg)	*≥5–<10*	*≥10–<15*	*≥15–<20*	*≥20–<35*	*≥35–<45*	*≥45–<60*	*60+*
Maintenance Dose (mg)	100	200	300	400	600	800	1000

Figure 6 depicts, the predicted $AUC_{0–24}$ and C_{max} in a paediatric population stratified by dose and body weight. These results are summarised per median (90% prediction

intervals) and mean (±SD) in the Supplementary Tables S2 and S3. For completeness, to address potential tolerability concerns in the youngest subjects, a weight-banded regimen has been explored considering the 400 mg as the reference dose in adults (Table S4). This scenario could be implemented as a run-in phase at the start of treatment prior to the use of a higher (maintenance) dose. The results from this simulation scenario are summarised in the Supplementary Materials Tables S5 and S6 and presented graphically in Figure S12.

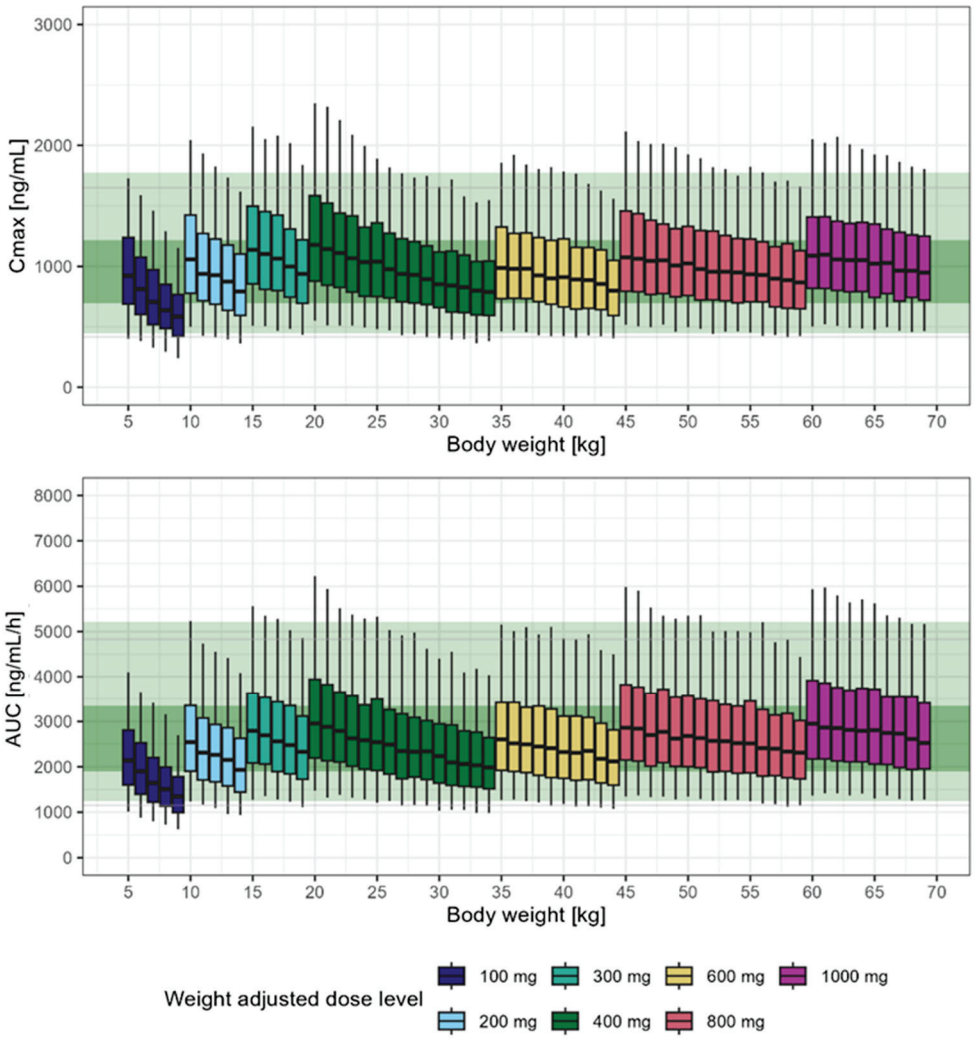


Figure 6. Predicted C_{max} (upper panel) and $AUC_{0–24}$ (lower panel) in children and adults stratified by bodyweight. Shaded green area depicts the reference exposure range (5th–95th and 25th–75th percentiles) predicted in adults with body weight equal to 70–75 kg and receiving 1000 mg. The horizontal line in the whisker-box plots represents the median, bottom and top edge of the box are the 25th and 75th percentiles. The vertical line (whiskers) represents the 5th and 95th percentiles of the data distribution. Each box refers to a specific weight group.

Whilst the current modelling and simulation study relies primarily on allometric principles, the age/weight-related changes in exposure reflect the well-established role of developmental growth (size and organ function) on drug disposition. Implementation of a protocol including interim steps and protocol inclusion based on a staggered approach would allow assessment of potential age-related changes, and further refinement of the recommended weight bands and doses for children affected by congenital and juvenile onset DM1.

4. Discussion

Under the EU Paediatric Regulation and US Best Pharmaceuticals for Children Act (BPCA) and the Pediatric Research Equity Act (PREA) amendments of 2007, pharmaceutical companies are expected to conduct clinical studies in the paediatric population. Evidence from these studies does not only support the regulatory approval of the medicinal product but also provides the basis for prescribing information.

Whilst evidence generation in paediatric diseases with relatively high incidence and prevalence should not represent a challenge for the implementation of a paediatric development plan, this is not the case for orphan drugs developed for rare diseases. As a matter of fact, four main issues thwart the drug development process: 1. poor diagnostics and assessment of disease progression; 2. the large heterogeneity in disease pathophysiology and treatment effects; 3. lack of treatment-sensitive endpoints and biomarkers to predict and quantify treatment outcomes, and 4. paucity of patients and data availability to draw robust conclusions regarding the efficacy and safety profile of a medicinal product based on standard statistical approaches. Our investigation focuses on the latter point, highlighting the application of modelling, simulation and extrapolation approaches as a tool to maximise the use of data, thereby optimising evidence generation during the early stage of development of an orphan drug [26–28]. In a setting in which the lack of data constitutes the main burden to be overcome, the use of quantitative clinical pharmacology concepts allow the implementation of the learning vs. confirming paradigm, providing insight into issues that are critical for the implementation of conclusive study protocols, such as the dose rationale, and understanding of the determinants of variability in drug exposure [29,30].

As shown in the current study, the availability of Phase I data in elderly healthy subjects provided the basis for the characterisation of the population pharmacokinetics of tideglusib. These data allowed for parameter estimates describing the absorption, distribution and elimination processes with adequate accuracy and precision. Parameter estimates were subsequently used as priors for the assessment of systemic exposure in DM-1 patients, taking into account the effect of body weight as an important covariate affecting the disposition characteristics of tideglusib. This effect has been identified for most drugs used in children and reflects the effect of developmental growth on metabolic processes [13,26]. Eventually, this effect can be parameterised together with a maturation function, describing the impact of ontogeny on drug biotransformation (clearance) [12–15].

The main finding from our model is that tideglusib shows dose-dependent bioavailability across the dose range evaluated in healthy elderly subjects as well as in congenital and juvenile onset DM-1 patients. This effect is likely to be caused by the limited solubility of the compound, even though other factors, such as variable first-pass metabolism may also play a role. Our parameterisation suggests that oral bioavailability decreases with increasing doses, even though we have not been able to quantify these changes in a continuous manner. Instead, bioavailability and absorption rate constant were dichotomized into two levels, with exposure data following a 400 mg dose as reference. Accurate description of the individual concentration vs. time profiles at higher dose levels required the use of lower estimates for the oral bioavailability and absorption rate constant.

From a pharmacokinetic perspective, there was no accumulation, metabolic inhibition, or induction observed during treatment. Despite the evidence of dose-dependent bioavailability, the population estimate for the apparent volume of distribution at steady state (i.e., sum of the volumes of distribution for the central and peripheral compartments) was 1140 L, which suggests that tideglusib distributes into tissues well beyond total body water. Mean population estimates for the apparent systemic clearance of 341 L/h likely indicate drug elimination taking place at a rate close to the hepatic blood flow [31]. In addition,

whilst no formal comparison or pooled analysis was performed including healthy elderly subjects and congenital and juvenile onset DM-1 patients, model parameter estimates reveal that the disease does not affect the pharmacokinetics of tideglusib. This is in line with previous reports indicating no significant disease-related changes in hepatic metabolism, haemodynamics or vascular permeability [31].

Time of food intake post dose did not affect the pharmacokinetics of tideglusib, suggesting a favourable safety profile of tideglusib in terms of altered liver enzymes when administered using the selected F06-037F formulation. Thus, in addition to its better dispersibility and organoleptic properties compared to the previous dosage forms, these findings confirm the decision to use this formulation in the subsequent development in DM-1 patients. Indeed, in studies CL031112-05A01 and CL031112-06A02 a marked effect of food was observed in healthy young and elderly volunteers dosed with 200 mg or 400 mg of formulation F05-052 following a high-fat or a normal breakfast within 30 min before drug administration. In detail, plasma levels were substantially increased, and peak concentrations were delayed in fed conditions. Administration with a meal also resulted in a higher frequency of transaminase elevations than administration in fasting conditions. Abnormalities in serum transaminases have been observed, particularly in a twice-daily dosing regimens, when the drug was administered with food and at the highest doses. However, it is worth noting that the increase in liver enzymes observed with previous formulations may be associated with GSK-3 β inhibition for the induction of liver repairing and regeneration process. Evidence from in vitro protocols shows that numerous GSK-3 β inhibitors (LY 2090314, AR-A014418, tideglusib, solasodine, CHIR99021, 9-ING-41, SB-216763) play an important role in stimulating the liver regeneration process through Wnt/β-catenin signalling pathway [31]. Given the chronic nature of this treatment, further evaluation of the administration of lower doses of tideglusib with food should be considered. An exposure range comparable to that observed following administration of tideglusib under fasting conditions may be achieved with the use of lower doses with food. Slower gastric emptying may also allow for lower peak concentrations.

The identification of body weight as a covariate on the parameters describing the disposition of tideglusib is not unexpected, as such an effect is often observed with drugs showing similar distributional properties, especially when considering adolescents or other groups with different demographic characteristics [32–34]. In fact, the use of allometric principles to extrapolate pharmacokinetics from adult subjects to children is widely accepted [32–34]. Based on the available data, no other source of variability has been identified that would further contribute to improving model performance and consequently support the optimisation of the dose level to be used in future trials.

We acknowledge some limitations of our investigation. First, it should be recognised that as there is incomplete data on the primary route of metabolism in vivo, neither a maturation function nor an age-dependent allometric exponent were included in the simulated scenarios [32–34]. In addition, given potential safety concerns, the magnitude of food-drug interaction has not been characterised in the target population. Our approach focused therefore on the time window of food intake after drug administration. Similarly, we have not been able to retrieve detailed information on meal caloric content, which prevented us from exploring these factors as potential covariates. Consequently, they were excluded from the dosing optimisation process, with the assumption that all individuals were in a fasting state. Nevertheless, the use of priors based on the pharmacokinetics in adults has been successfully implemented for several products [32–34]. It has proved to be very effective in a situation that reflects early clinical development of drugs for rare diseases, such as transfusion-dependent haemoglobinopathies, anthrax infection, eosinophilic oesophagitis [32–34].

In conclusion, tideglusib shows dose-dependent bioavailability, with systemic exposure increasing less than proportionally with increasing doses. Despite the relatively high intra- and interindividual variability in plasma concentrations, body weight was found to be a covariate on clearance and volume of distribution, with higher AUCs and C_{max} values observed in subjects with decreasing body weight. Moreover, the availability of a population pharmacokinetic model allowed for extrapolation and prediction of the pharmacokinetics in the paediatric population, supporting the dose rationale for future clinical trials in children affected by myotonic dystrophy.

Supplementary Materials: The following supporting information can be downloaded at: https://www.mdpi.com/article/10.3390/pharmaceutics17081065/s1. Section S1. Inclusion and Exclusion Criteria (Study NP031112-07A03). Section S2. Inclusion and Exclusion Criteria (Study AMO-02-MD-2-001). Section S3. Bioanalytical Method (Study NP031112-07A03). Section S4. Bioanalytical Method (Study AMO-02-MD-2-001). Section S5. Supplementary tables and figures. Table S1. Demographic baseline characteristics of the population included in the pharmacokinetic analysis. Table S2. Predicted area under the concentration vs. time curve ($AUC_{0–24}$) after oral administration of a weight-banded dosing regimen of tideglusib (maintenance phase). Table S3. Predicted peak concentration (C_{max}) after oral administration of a weight-banded dosing regimen of tideglusib (maintenance phase). Table S4. Proposed lower weight-banded dosing regimen for tideglusib in paediatric and adult patients with DM-1. Table S5. Predicted area under the concentration vs. time curve ($AUC_{0–24}$) after oral administration of a weight-banded dosing regimen of tideglusib (titration phase). Table S6. Predicted peak concentration (C_{max}) after oral administration of a weight-banded dosing regimen of tideglusib (titration phase). Figure S1. Scatter plots of observed plasma tideglusib concentrations in elderly healthy subjects stratified by dose group in study NP031112-07A03. Figure S2. Scatter plots of observed plasma tideglusib concentrations in adolescents and adults DM-1 patients enrolled in study AMO-02-MD2-001. Figure S3. Predicted tideglusib concentration vs. time profiles in elderly healthy subjects. Figure S4. Goodness of fit for the final pharmacokinetic model in elderly healthy subjects (study NP031112-07A03). Figure S5. NPDE results for the final model in elderly healthy subjects (study NP031112-07A03). Figure S6. Predicted tideglusib concentration vs. time profiles in adolescent and adult DM-1 patients following oral administration of a 400 or 1000 mg dose. Figure S7. Goodness of fit for the final pharmacokinetic model in adolescent and adult DM-1 patients (study AMO-02-MD2-001). Figure S8. NPDE results for the final model in adolescent and adult DM-1 patients (study AMO-02-MD2-001). Figure S9. Mirror plots. Individual predicted vs. observed tideglusib concentrations from the simulated data using the final model. Figure S10. Final model: distribution of weighted residuals and conditional weighted residuals. Figure S11. Correlations between the inter-individual random effects. Figure S12. Predicted C_{max} (upper panel) and $AUC_{0–24}$ (lower panel) in children and adults stratified by bodyweight and receiving the proposed lower weight-band dosing regimen (titration dosing).

Author Contributions: Conceptualization, J.H., A.M. and O.D.P.; Methodology, A.D.D., S.O. and O.D.P.; Formal Analysis, A.D.D., S.O. and O.D.P.; Writing—original draft preparation, A.D.D.; Writing—review and editing, A.D.D., J.H., A.M., S.E. and O.D.P.; Supervision, J.H., A.M. and O.D.P. All authors have read and agreed to the published version of the manuscript.

Funding: This research was funded by AMO Pharma Ltd.

Institutional Review Board Statement: Study NP03112-07A03 was conducted at a single centre (Parexel International GmbH, Berlin, Germany). The study was conducted in accordance with GCP-guidelines and all applicable regulatory requirements and in full conformance with the principles of the Declaration of Helsinki. The final, approved protocol and the Informed Consent Forms were reviewed by the responsible Ethics Committee (Ethics Committee of the Land Berlin, Germany). The study was registered on the EU Clinical Trials Register (2007-007774-29, on 5 March 2008). Study AMO-02-MD-2-001 (IRAS 199733, approved on 25 May 2016) was conducted at a single investigative site, a specialised centre for DM-1 (Newcastle-upon-Tyne Hospitals NHS Trust, Newcastle Upon

Tyne, United Kingdom). The study has been conducted in full conformance with the principles of the Declaration of Helsinki. All experimental procedures were in accordance with ICH- and GCP-guidelines. The study protocol was approved by the Ethics Committee (Northeast–Newcastle and North Tyneside 2 Research Ethics Committee, UK). The study was registered on Clinicaltrials.gov (NCT02858908, on 5 March 2008) and on the EU Clinical Trials Register (2016-000067-16, on 5 March 2008).

Informed Consent Statement: Study NP03112-07A03: written informed consent was obtained from each subject before screening. Study AMO-02-MD-2-001: consent was obtained for all subjects before screening; in most cases consent was provided by the subject's parent or legally authorised representative, where the subjects were younger than 16 years or did not have the capacity to consent for themselves.

Data Availability Statement: The data can be shared up on request.

Conflicts of Interest: Joseph Horrigan, Alison McMorn, and Stuart Evans are all employees for AMO Pharma, who were the Sponsors of this clinical trial. AMO Pharma funded the positions of Sean Oosterholt and Alessandro Di Deo.

References

1. Bird, T.D. Myotonic Dystrophy Type 1. In *GeneReviews®*; Adam, M.P., Feldman, J., Mirzaa, G.M., Pagon, R.A., Wallace, S.E., Amemiya, A., Eds.; University of Washington: Seattle WA, USA, 1993.
2. Prior, T.W. American College of Medical Genetics Laboratory Quality Assurance, Technical Standards and Guidelines for Myotonic Dystrophy Type 1 Testing. *Genet. Med.* **2009**, *11*, 552–555. [CrossRef] [PubMed]
3. Pavicevic, D.S.; Miladinović, J.; Brkušanin, M.; Šviković, S.; Djurica, S.; Brajušković, G.; Romac, S. Molecular genetics and genetic testing in myotonic dystrophy type 1. *BioMed Res. Int.* **2013**, *2013*, 391821. [CrossRef] [PubMed]
4. Udd, B.; Krahe, R. The myotonic dystrophies: Molecular, clinical, and therapeutic challenges. *Lancet Neurol.* **2012**, *11*, 891–905. [CrossRef]
5. Heatwole, C.; Bode, R.; Johnson, N.; Quinn, C.; Martens, W.; McDermott, M.P.; Rothrock, N.; Thornton, C.; Vickrey, B.; Victorson, D.; et al. Patient-reported impact of symptoms in myotonic dystrophy type 1 (PRISM-1). *Neurology* **2012**, *79*, 348–357. [CrossRef]
6. Kroksmark, A.K.; Stridh, M.L.; Ekstrom, A.B. Long-term follow-up of motor function and muscle strength in the congenital and childhood forms of myotonic dystrophy type 1. *Neuromuscul. Disord.* **2017**, *27*, 826–835. [CrossRef] [PubMed]
7. Petri, H.; Vissing, J.; Witting, N.; Bundgaard, H.; Køber, L. Cardiac manifestations of myotonic dystrophy type 1. *Int. J. Cardiol.* **2012**, *160*, 82–88. [CrossRef]
8. Kaidanovich-Beilin, O.; Woodgett, J.R. GSK-3: Functional Insights from Cell Biology and Animal Models. *Front. Mol. Neurosci.* **2011**, *4*, 40. [CrossRef]
9. King, M.K.; Pardo, M.; Cheng, Y.; Downey, K.; Jope, R.S.; Beurel, E. Glycogen synthase kinase-3 inhibitors: Rescuers of cognitive impairments. *Pharmacol. Ther.* **2014**, *141*, 1–12. [CrossRef]
10. Okkersen, K.; Buskes, M.; Groenewoud, J.; Kessels, R.P.; Knoop, H.; van Engelen, B.; Raaphorst, J. The cognitive profile of myotonic dystrophy type 1: A systematic review and meta-analysis. *Cortex* **2017**, *95*, 143–155. [CrossRef]
11. Horrigan, J.; Gomes, T.B.; Snape, M.; Nikolenko, N.; McMorn, A.; Evans, S.; Yaroshinsky, A.; Della Pasqua, O.; Oosterholt, S.; Lochmüller, H. A Phase 2 Study of AMO-02 (Tideglusib) in Congenital and Childhood-Onset Myotonic Dystrophy Type 1 (DM1). *Pediatr. Neurol.* **2020**, *112*, 84–93. [CrossRef]
12. Bellanti, F.; Del Vecchio, G.C.; Putti, M.C.; Maggio, A.; Filosa, A.; Cosmi, C.; Mangiarini, L.; Spino, M.; Connelly, J.; Ceci, A.; et al. Population pharmacokinetics and dosing recommendations for the use of deferiprone in children younger than 6 years. *Br. J. Clin. Pharmacol.* **2017**, *83*, 593–602. [CrossRef]
13. Borella, E.; Oosterholt, S.; Magni, P.; Della Pasqua, O. Use of prior knowledge and extrapolation in paediatric drug development: A case study with deferasirox. *Eur. J. Pharm. Sci.* **2019**, *136*, 104931. [CrossRef]
14. Glaze, D.G.; Neul, J.L.; Kaufmann, W.E.; Berry-Kravis, E.; Condon, S.; Stoms, G.; Oosterholt, S.; Della Pasqua, O.; Glass, L.; Jones, N.E.; et al. Double-blind, randomized, placebo-controlled study of trofinetide in pediatric Rett syndrome. *Neurology* **2019**, *92*, e1912–e1925. [CrossRef]
15. Oosterholt, S.P.; Della Pasqua, O. Extrapolation and dosing recommendations for raxibacumab in children from birth to age <18 years. *Br. J. Clin. Pharmacol.* **2021**, *87*, 4709–4717. [CrossRef]
16. Hsu, C.H.; Steven Xu, X.; Wang, J.; Zhang, L.; Liu, C.; Wang, Y. Utilization of Adult Data in Designing Pediatric Pharmacokinetic Studies: How Much Are Historical Adult Data Worth? *J. Clin. Pharmacol.* **2019**, *59*, 989–996. [CrossRef] [PubMed]

17. Edwards, D.; Best, N.; Crawford, J.; Zi, L.; Shelton, C.; Fowler, A. Using Bayesian Dynamic Borrowing to Maximize the Use of Existing Data: A Case-Study. *Ther. Innov. Regul. Sci.* **2024**, *58*, 1–10. [CrossRef] [PubMed]
18. Piana, C.; Zhao, W.; Adkison, K.; Burger, D.; Jacqz-Aigrain, E.; Danhof, M.; Della Pasqua, O. Covariate effects and population pharmacokinetics of lamivudine in HIV-infected children. *Br. J. Clin. Pharmacol.* **2014**, *77*, 861–872. [CrossRef] [PubMed]
19. Chan Kwong, A.H.P.; Calvier, E.A.M.; Fabre, D.; Gattacceca, F.; Khier, S. Prior information for population pharmacokinetic and pharmacokinetic/pharmacodynamic analysis: Overview and guidance with a focus on the NONMEM PRIOR subroutine. *J. Pharmacokinet. Pharmacodyn.* **2020**, *47*, 431–446. [CrossRef]
20. Knebel, W.; Gastonguay, M.R.; Malhotra, B.; El-Tahtawy, A.; Jen, F.; Gandelman, K. Population pharmacokinetics of atorvastatin and its active metabolites in children and adolescents with heterozygous familial hypercholesterolemia: Selective use of informative prior distributions from adults. *J. Clin. Pharmacol.* **2013**, *53*, 505–516. [CrossRef]
21. Brendel, K.; Comets, E.; Laffont, C.; Laveille, C.; Mentré, F. Metrics for external model evaluation with an application to the population pharmacokinetics of gliclazide. *Pharm. Res.* **2006**, *23*, 2036–2049. [CrossRef]
22. Yano, Y.; Beal, S.L.; Sheiner, L.B. Evaluating pharmacokinetic/pharmacodynamic models using the posterior predictive check. *J. Pharmacokinet. Pharmacodyn.* **2001**, *28*, 171–192. [CrossRef]
23. Ette, E.I. Stability and performance of a population pharmacokinetic model. *J. Clin. Pharmacol.* **1997**, *37*, 486–495. [CrossRef] [PubMed]
24. Lindbom, L.; Ribbing, J.; Jonsson, E.N. Perl-speaks-NONMEM (PsN)—A Perl module for NONMEM related programming. *Comput. Methods Programs Biomed.* **2004**, *75*, 85–94. [CrossRef]
25. R Core Team. *R: A language and Environment for Statistical Computing*; R Foundation for Statistical Computing: Vienna, Austria, 2021.
26. Bellanti, F.; Della Pasqua, O. Modelling and simulation as research tools in paediatric drug development. *Eur. J. Clin. Pharmacol.* **2011**, *67* (Suppl. S1), 75–86. [CrossRef]
27. Basu, C.; Ahmed, M.A.; Kartha, R.V.; Brundage, R.C.; Raymond, G.V.; Cloyd, J.C.; Carlin, B.P. A hierarchical Bayesian approach for combining pharmacokinetic/pharmacodynamic modeling and Phase IIa trial design in orphan drugs: Treating adrenoleukodystrophy with Lorenzo′s oil. *J. Biopharm. Stat.* **2016**, *26*, 1025–1039. [CrossRef]
28. Simeoli, R.; Lava, S.A.G.; Di Deo, A.; Roversi, M.; Cairoli, S.; Tambucci, R.; Rea, F.; Malamisura, M.; Angelino, G.; Biondi, I.; et al. Pharmacokinetic Evaluation of Oral Viscous Budesonide in Paediatric Patients with Eosinophilic Oesophagitis in Repaired Oesophageal Atresia. *Pharmaceutics* **2024**, *16*, 872. [CrossRef]
29. Danhof, M.; Delange, E.; Dellapasqua, O.; Ploeger, B.; Voskuyl, R. Mechanism-based pharmacokinetic-pharmacodynamic (PK-PD) modeling in translational drug research. *Trends Pharmacol. Sci.* **2008**, *29*, 186–191. [CrossRef]
30. Lyauk, Y.K.; Jonker, D.M.; Lund, T.M. Dose Finding in the Clinical Development of 60 US Food and Drug Administration-Approved Drugs Compared With Learning vs. *Confirming Recommendations. Clin. Transl. Sci.* **2019**, *12*, 481–489. [CrossRef]
31. Pang, K.S.; Rowland, M. Hepatic clearance of drugs. I. Theoretical considerations of a "well-stirred" model and a "parallel tube" model. Influence of hepatic blood flow, plasma and blood cell binding, and the hepatocellular enzymatic activity on hepatic drug clearance. *J. Pharmacokinet. Biopharm.* **1977**, *5*, 625–653. [CrossRef] [PubMed]
32. Jusko, W.J.; Chiang, S.T. Distribution volume related to body weight and protein binding. *J. Pharm. Sci.* **1982**, *71*, 469–470. [CrossRef] [PubMed]
33. Kersting, G.; Willmann, S.; Würthwein, G.; Lippert, J.; Boos, J.; Hempel, G. Physiologically based pharmacokinetic modelling of high- and low-dose etoposide: From adults to children. *Cancer Chemother. Pharmacol.* **2012**, *69*, 397–405. [CrossRef] [PubMed]
34. Piana, C.; Danhof, M.; Della Pasqua, O. Influence of covariate distribution on the predictive performance of pharmacokinetic models in paediatric research. *Br. J. Clin. Pharmacol.* **2014**, *78*, 145–157. [CrossRef] [PubMed]

Disclaimer/Publisher's Note: The statements, opinions and data contained in all publications are solely those of the individual author(s) and contributor(s) and not of MDPI and/or the editor(s). MDPI and/or the editor(s) disclaim responsibility for any injury to people or property resulting from any ideas, methods, instructions or products referred to in the content.

pharmaceutics

MDPI

Article

Population Pharmacokinetic Modeling of Total and Unbound Pamiparib in Glioblastoma Patients: Insights into Drug Disposition and Dosing Optimization

Charuka Wickramasinghe [1], Seongho Kim [1], Yuanyuan Jiang [1], Xun Bao [1], Yang Yue [1], Jun Jiang [1], Amy Hong [2], Nader Sanai [2] and Jing Li [1,*]

[1] Karmanos Cancer Institute, Wayne State University School of Medicine, Detroit, MI 48201, USA
[2] Barrow Neurological Institute, St. Joseph's Hospital & Medical Center, Phoenix, AZ 85013, USA
* Correspondence: lijing@wayne.edu

Abstract: Background: This study aimed to develop a population pharmacokinetic (PK) model that characterized the plasma concentration–time profiles of the total and unbound pamiparib, a PARP inhibitor, in glioblastoma patients and identified patient factors influencing the PK. **Methods:** The total and unbound pamiparib plasma concentration data were obtained from 41 glioblastoma patients receiving 60 mg of pamiparib twice daily. Nonlinear mixed-effects modeling was performed using Monolix (2024R1) to simultaneously fit the total and unbound drug plasma concentration data. The covariate model was developed by covariate screening using generalized additive modeling followed by stepwise covariate modeling. Model simulations were performed following oral doses of 10–60 mg BID. **Results:** The total and unbound pamiparib plasma concentration–time profiles were best described by a one-compartment model with first-order absorption and elimination. Creatinine clearance and age were the significant covariates on the apparent volume of distribution (V/F) and apparent clearance (CL/F), respectively, explaining ~22% and ~5% of IIV of V/F and CL/F. Population estimates of the absorption rate constant (Ka), V/F, CL/F, and unbound fraction for the total drug were 1.58 h^{-1}, 44 L, 2.59 L/h, and 0.041. Model simulations suggested that doses as low as 20 mg BID may be adequate for therapeutic effects in a general patient population, assuming that a target engagement ratio (i.e., unbound $C_{ss,min}$/IC50) of 5 or above is sufficient for full target engagement. **Conclusions:** The total and unbound pamiparib plasma PK are well characterized by a linear one-compartment model, with creatinine clearance as the significant covariate on V/F. Model simulations support further clinical investigation into dose reduction to optimize the benefit-to-risk ratio of pamiparib, particularly in combination therapies.

Keywords: population pharmacokinetic model; pamiparib; PARP inhibitor; unbound plasma concentrations; dosing optimization; glioblastoma

1. Introduction

Pamiparib is a selective, orally bioavailable inhibitor of Poly (ADP-ribose) polymerase-1 (PARP1) and PARP2, enzymes that play a crucial role in DNA damage repair [1,2]. PARP enzymes detect and repair single-strand DNA breaks (SSBs) through the base excision repair (BER) pathway. Pamiparib binds to the catalytic domain of PARP1/2, preventing them from synthesizing Poly (ADP-ribose) (PAR) chains, which are essential for recruiting DNA repair proteins [1,2]. In addition, pamiparib traps PARP1/2 on damaged DNA, leading to the accumulation of double-strand breaks, which are particularly lethal to cancer cells with

defective homologous recombination (HR) repair mechanisms [1]. Tumors with mutations in BRCA1 or BRCA2 (key HR repair genes) are unable to repair double-strand breaks effectively. As such, pamiparib exploits synthetic lethality to selectively target cancer cells with DNA repair deficiencies while sparing normal cells, making it a potential therapeutic option for tumors with BRCA mutations and other DNA damage repair defects [1,3].

Pamiparib has been extensively evaluated in clinical trials for treating a variety of cancers, particularly those associated with DNA damage repair deficiencies such as BRCA-mutated malignancies. A phase I study demonstrated that pamiparib was well tolerated and exhibited preliminary antitumor activity in patients with high-grade epithelial non-mucinous ovarian cancer [4]. A phase II trial demonstrated the significant clinical benefit of pamiparib [3], leading to its approval in China for the treatment of germline BRCA mutation-associated recurrent advanced ovarian, fallopian tube, or primary peritoneal cancer in patients previously treated with two or more lines of chemotherapy. In addition, pamiparib, as a monotherapy or in combination with chemotherapy or checkpoint inhibitors, has been evaluated in other solid tumors, including triple-negative breast cancer, prostate cancer, and advanced gastric cancer [5–8].

Notably, unlike some other PARP inhibitors, pamiparib is not a substrate of P-glycoprotein (P-gp), which enhances its ability to cross the blood–brain barrier (BBB), making it a promising candidate for treating brain tumors, such as glioblastoma [1,9]. In a phase 0/II trial, pamiparib demonstrated good central nervous system (CNS) penetration, achieving potentially therapeutic concentrations in both enhancing and non-enhancing tumors of glioblastoma patients [10]. Leveraging its ability to cross the BBB and potentiate DNA damage in cancer cells, pamiparib is under clinical evaluation in combination with temozolomide and radiation therapy for patients with newly diagnosed or recurrent gliomas.

The recommended dose of pamiparib is 60 mg twice daily, which is administered continuously until disease progression or unacceptable toxicity. However, due to significant interindividual pharmacokinetic (PK) variability, a one-size-fits-all dosing approach may lead to suboptimal treatment outcomes. Tailored dosing regimen for pamiparib is crucial to maximizing its therapeutic efficacy while minimizing toxicity in individual patients. Population pharmacokinetic (PK) modeling can aid in dose optimization by quantifying patient variability in drug disposition and identifying key factors influencing this process. This study aimed to develop a population PK model to characterize the plasma concentration–time profiles of total and unbound pamiparib in glioblastoma patients and to identify patient characteristics (such as demographics, renal and hepatic function, and combination therapy) that contribute to PK variability. The findings provided critical insights into the drug disposition and have clinical implications for guiding the optimization of dosing strategies in patients with glioblastoma and other cancers.

2. Materials and Methods

2.1. Clinical Study and PK Data

The total and unbound pamiparib plasma concentration data used in the population PK analysis were obtained from a phase 0/II study (ClinicalTrials.gov ID: NCT04614909), which enrolled 41 patients with newly diagnosed or recurrent glioblastoma. The protocols were approved by the Institutional Review Board of the Barrow Neurological Institute. Written informed consent was obtained from all participants.

Eligible patients were required to have newly diagnosed or recurrent glioblastoma and meet the following criteria: age >18 years, Eastern Cooperative Oncology Group (ECOG) performance status $\leq$2, and adequate bone marrow and organ functions. Adequate bone marrow function was defined as an absolute neutrophil count $\geq 1.5 \times 10^9$/L, a platelet count

$\geq 100 \times 10^9$/L, and hemoglobin $\geq$ 9 g/dL. Adequate liver function was defined as serum transaminase (AST and ALT) levels $\leq$ 3 times the institutional upper limit of normal (ULN) and total bilirubin $\leq 1.5 \times$ ULN. Adequate kidney function was defined as a glomerular filtration rate (eGFR) $\geq$ 30 mL/min/1.73 m^2 estimated by the Chronic Disease Epidemiology Collaboration (CKD-EPI) equation, and either serum creatinine $\leq 1.5 \times$ ULN or creatinine clearance $\geq$60 mL/min for those with serum creatinine levels above $1.5 \times$ ULN. Patients were required to have discontinued any prior anticancer treatment for at least 21 days before study entry. Patient demographic and characteristic data are summarized in Table 1.

Table 1. Patient demographic and characteristic data.

	Median (Range) or Number of Patients
Baseline characteristics	
Race (white/non-white) †	38/3
Sex (male/female) †	20/21
Age (years) *	60 (31–80)
Weight (kg) *	80 (45–129)
Height (cm) *	173 (155–193)
BSA (m^2) *	1.99 (1.41–2.53)
Liver function *	
Predose total bilirubin (mg/dL)	0.5 (0.3–1.8)
Post-operation total bilirubin (mg/dL)	0.5 (0.2–1.5)
Predose AST (IU/L)	19 (9–44)
Post-operation AST (IU/L)	23 (9–106)
Predose ALT (IU/L)	24 (8–135)
Post-operation ALT (IU/L)	45 (14–193)
Predose plasma albumin (mg/dL)	4.1 (3.5–5)
Post-operation plasma albumin (mg/dL)	3.9 (3–4.5)
Kidney function *	
Predose serum creatine (mg/dL)	0.83 (0.56–1.34)
Post-operation serum creatine (mg/dL)	0.75 (0.41–1.3)
Predose creatine clearance (mL/min)	98 (39–154)
Post-operation creatine clearance (mL/min)	111 (59–169)
Predose GFR (mL/min)	92 (48–116)
Post-operation GFR (mL/min)	101 (48–117)
Concomitant drugs	
Coadministered drugs during the trial (yes/no) †	36/5
Dexamethasone (given/not given) †	34/7
Total dexamethason dose (mg) *	19 (0–66)

* Values are shown as median (range). † Data indicate the number of patients. Abbreviations: AST, aspartate aminotransferase; ALT, alanine aminotransferase; GFR, glomerular filtration rate.

The patients received oral pamiparib (60 mg twice daily) for three days before undergoing surgical tumor resection. Blood samples were collected at predose and at 0.5, 1, 2, 4, 7, and 24 h following the 9th oral dose. Plasma was separated from whole blood by centrifugation at 1000× *g* and 4 °C for 10 min and then stored at −80 °C until analysis. The total and unbound pamiparib concentrations in plasma samples were quantified using a validated liquid chromatography coupled with tandem mass spectrometry (LC-MS/MS) method [11].

2.2. Population PK Modeling Analysis

The population PK model was developed in two steps: (1) basic (structural) model development and (2) covariate model development. All analyses were performed us-

ing the nonlinear mixed-effects modeling program MONOLIX version 2024R1 (Lixoft, Antony, France).

2.2.1. Structure Model Development

The structural model was developed to simultaneously characterize total and unbound pamiparib plasma concentration–time profiles following an oral administration of 9 doses (60 mg, twice daily) in individual glioblastoma patients. A one-compartment model with first-order absorption (without lag time) and first-order elimination was selected to describe the multiple-dose plasma concentration–time data. The primary PK parameters included apparent oral clearance (CL/F), apparent volume of distribution (V/F), absorption rate constant (Ka), and fraction of unbound drug in plasma (Fu). The relationship between total (Cp) and unbound (Cu) drug concentrations was incorporated into the model using the equation Cu = Cp × Fu. All concentration data were log-transformed to stabilize variance and improve model fitting. Population mean PK parameters, interindividual variability, and residual error were assessed in the population PK model. Interindividual variability was modeled using an exponential function, assuming log-normal distribution for all PK parameters.

Various residual error models, including constant, proportional, and combined error models, were evaluated. The combined model, incorporating both proportional and additive error components, was selected as the optimal error model (Equation (1)).

$$y_{i,j} = f(t_{i,j}, \psi_i) + g(t_{i,j}, \psi_i, \xi)\varepsilon_{i,j} \quad (1)$$

Here, ψ_i is the parameter vector of the structural model f for individual i, and the residual error model is defined by the function g that depends on an additional parameter vector ξ. The residual errors $\varepsilon_{i,j}$ are standardized Gaussian random variables with a mean of 0 and a standard deviation of 1. In this analysis, the combined error model was defined as $g = (a + bf^c)$, where the function g consists of a constant term, a, and a term proportional to the structural model f, with b as the proportionality constant. The parameter vector ξ includes a and b, while c is fixed at 1 by default.

Population mean PK parameters were estimated using the Stochastic Approximation Expectation–Maximization (SAEM) algorithm, a robust method for handling complex nonlinear mixed-effects models. Individual patients' PK parameter estimates were obtained through post hoc Bayesian estimation, utilizing the conditional distributions derived from the Markov Chain Monte Carlo (MCMC) procedure.

2.2.2. Covariate Model Development

The covariate model was developed using a stepwise approach to systematically identify and incorporate significant covariate effects. Initial screening for potential covariates was conducted using generalized additive modeling (GAM) with R version 4.4.1. The candidate covariates, listed in Table 1, were evaluated based on their relationship with Bayesian-estimated individual pharmacokinetic (PK) parameters from the structural model, including CL/F, V/F, Ka, and Fu. For patients with missing covariate data, values were imputed using the population median, as the proportion of missing data was low (<2%). Continuous covariates (e.g., body surface area [BSA]) were centered around their median values, while categorical covariates were encoded as binary variables (e.g., male = 1 and female = 0). Potentially significant covariates identified via GAM were further assessed in the stepwise covariate modeling (SCM) procedure, where covariate relationships were

explored using linear, exponential, or power functions. The exponential function (as shown in Equation (2)) was identified to best describe the covariate effects.

$$\theta_i = \theta_{pop} \times e^{\beta_{COV} \times COV_j} \quad (2)$$

Here, θ_i represents the PK parameter for the i^{th} patient, θ_{pop} is the mean population value of the parameter, β_{COV} is the estimated covariate effect coefficient, and COV_j is the identified covariate.

Discrimination between hierarchical models was based on both statistical and graphical criteria. First, model comparisons were conducted using the likelihood ratio test, where a reduction in OFV (-2 log-likelihood, -2LL) was used to assess model improvement. Covariates were retained if the addition of the covariate resulted in a reduction in OFV > 3.875 ($p < 0.05$) during forward selection and if the removal of the covariate led to an increase in OFV > 10.828 ($p < 0.001$) during backward elimination. In addition, model improvement was visually assessed through diagnostic goodness-of-fit plots, including observed vs. predicted concentrations to check for bias and weighted residuals vs. predicted concentrations to ensure random scatter around zero. Additional criteria for covariate inclusion were the increased precision in parameter estimates (i.e., reduced relative standard error [RSE]) and a reduction in interindividual variability of key PK parameters. Collectively, by integrating statistical selection criteria with graphical diagnostics, the final covariate model was refined to optimize predictive performance and biological plausibility.

2.3. Model Evaluation

The precision and stability of parameter estimates were assessed by bootstrap analysis with R (version 4.4.1) [12–14]. This nonparametric resampling method involves generating multiple datasets by randomly sampling, with replacement, from the original dataset. Each resampled dataset was used to re-estimate the model parameters, and this process was repeated 500 times to construct an empirical distribution of parameter estimates. The median and 95% confidence intervals (CIs) of the bootstrap-derived estimates were computed to evaluate the robustness of the parameter estimates. The agreement between the original parameter estimates and the mean of the bootstrap replicates was checked to confirm model stability and ensure that parameter uncertainty was adequately captured [12–14].

The predictive performance of the model was assessed by visual predictive checks (VPCs), which involve simulating 500 datasets using the estimated population parameters and then comparing the simulated concentration–time profiles to the observed data [15,16]. The 50th percentile (median) and the 5th and 95th percentiles (forming the 95% prediction interval) of the predicted concentrations were plotted alongside the observed concentrations. If most observed data points fall within the 95% prediction interval and align well with the simulated percentiles, it indicates that the model can adequately capture the central trend and variability in the data. A systematic deviation between observed and simulated percentiles may suggest model misspecification or the need for further refinement.

In addition, prediction distribution plots were constructed to compare observed concentration data with the theoretical distribution of model-predicted data [17]. Unlike standard VPCs, these plots rely on multiple simulations of the individuals in the dataset without residual error, focusing on the variability arising from structural and random-effects components alone [17]. These simulations use the estimated fixed and random effects from the population model while ignoring parameter uncertainty. By doing so, prediction distribution plots help identify potential systematic deviations between observed data and model predictions, particularly in the presence of model misspecification, overdispersion, or unexplained variability.

2.4. Model Simulations

To guide dose optimization, the developed population PK model was utilized to predict the unbound pamiparib plasma concentration–time profiles following twice-daily oral administration at doses of 10, 20, 30, 40, and 60 mg. Simulations of 200 datasets were performed using the estimated population parameters along with their respective interindividual variability. The median (50th percentile) and 5th and 95th percentiles of the predicted concentration–time profiles were generated. All simulations were executed using R (version 4.4.1).

3. Results

3.1. Population PK Model

The total and unbound pamiparib plasma concentration–time profiles following multiple-dose oral administration were well described by a one-compartment model with first-order absorption (with no lag time) and first-order elimination. Stepwise covariate model development identified creatinine clearance as a significant covariate on the V/F of both the total and unbound drug, explaining ~23% and ~22% of the respective IIV, and age as a significant covariate on the CL/F of the total and unbound drug, explaining ~ 6% and ~4% of the respective IIV. As such, the final covariate model consisted of a one-compartment model with first-order absorption and first-order elimination, incorporating creatine clearance as a covariate on pamiparib V/F and age as a covariate on the CL/F.

The population PK parameters for the total and unbound pamiparib along with their respective interindividual variability (IIV) estimates, from the structural and final covariate models, are summarized in Table 2. The population mean absorption rate constant (Ka) was 1.58 h^{-1}, with substantial IIV (~400%), indicating rapid but variable oral absorption. The population mean CL/F for total pamiparib was 2.59 L/h, with an IIV of 50%. The inclusion of age as a covariate on CL/F accounted for only 6% of the unexplained IIV, suggesting that other factors, which were not assessed in this study, may contribute more significantly to variability in pamiparib clearance. The estimated population mean V/F for total pamiparib was 44 L, suggesting a distribution volume exceeding blood volume. The addition of creatinine clearance as a covariate on V/F explained approximately 23% of the IIV. The population mean elimination half-life ($T_{1/2}$) was estimated to be ~12 h, which is consistent with the estimated $T_{1/2}$ of 13 h in the first in-human study (BGB-290-AU-002; NCT02361723) [4] and supporting a twice-daily dosing regimen. The population mean fraction of unbound pamiparib in plasma was 0.041, indicating high plasma protein binding.

Table 2. Population PK parameters for the total and unbound pamiparib estimated from the base (structure) model and final covariate model.

Parameter *	Total Pamiparib		Unbound Pamiparib	
	Base Model	**Final Model**	**Base Model**	**Final Model**
OFV	9226	9210	9226	9212
TV_KA (h^{-1})	1.64	1.58	1.55	1.7
TV_V/F (L)	44	44 †	1017	1060 †
TV_CL/F (L/h)	2.73	2.59 ‡	65.0	62.5 ‡
TV_Fu	0.042	0.041	0.042	0.042
θ_1 (Ka)	1.64 (42)	1.58 (42)	1.55 (51)	1.7 (44)
θ_2 (V/F)	44 (9.7)	15 (28)	1017 (9.1)	402 (28)
θ_3 (CL/F)	2.73 (8.0)	6.76 (38)	65.0 (8.2)	163 (39)
θ_4 (Fu)	0.042(2.8)	0.041 (2.8)	0.042 (2.7)	0.042 (2.6)
β_1 (PCC on V/F)	-	0.0094 (25)	-	0.0087(26)

Table 2. *Cont.*

Parameter *	Total Pamiparib		Unbound Pamiparib	
	Base Model	**Final Model**	**Base Model**	**Final Model**
β_2 (Age on CL/F)	-	−0.016 (37)	-	−0.016 (38)
IIV of Ka (%)	397 (18)	410 (20)	612 (21)	380 (20)
IIV of V/F (%)	53 (16)	41 (17)	50 (17)	41 (19)
IIV of CL/F (%)	53 (11)	50 (11)	54 (11)	52(11)
IIV of Fu (%)	12 (22)	12 (20)	112 (24)	11 (28)

* PK parameter estimates are expressed as the population mean (% relative standard error of estimation). † $TV\_V = \theta_2 * e^{\beta_1 * PCC}$, with the population median PCC being 111.5. ‡ $TV\_CL = \theta_3 * e^{\beta_2 * Age}$, with the population median age being 60. Abbreviations: θ, population mean PK parameter estimate from the final covariate model; TV, typical population mean PK parameter; Ka, elimination rate constant; CL/F, apparent volume of distribution; V/F, apparent volume of distribution; Fu, fraction of unbound drug in plasma; PCC, post-operation creatine clearance; IIV, interindividual variability.

3.2. Model Evaluation

The prediction performance of the final population PK model was evaluated using goodness-of-fit plots, nonparametric bootstrap analysis, visual predictive check, and prediction distribution plots. The goodness-of-fit plots (Figures 1 and 2) demonstrated a good correlation between the model-predicted total or unbound pamiparib concentrations and the observed data, and the residual plots showed randomly scattered residuals around the horizontal zero line. These data collectively indicated no systematic prediction bias.

The robustness of the parameter estimates was assessed via bootstrap analysis. Table 3 summarizes the population mean PK parameter estimates of the final model alongside the mean and 95% confidence intervals of the bootstrap-derived estimates. The agreement between the population mean PK parameter estimates and the mean of bootstrap replicates, with both falling within the 95% confidence intervals of bootstrap replicates, confirmed the stability of parameter estimation from the final population PK model.

Table 3. Population PK parameters estimated from the final covariate model and bootstrap analysis.

	Total Pamiparib			Unbound Pamiparib		
Parameter	**Population Mean**	**Bootstrap Mean**	**Bootstrap 95% CI**	**Population Mean**	**Bootstrap Mean**	**Bootstrap 95% CI**
θ_1 (Ka) (h^{-1})	1.58	1.71	(0.64, 4.15)	1.7	1.86	(0.67, 4.07)
θ_2 (V/F) (L)	15	17	(8, 30)	402	441	(219, 787)
θ_3 (CL/F) (L/h)	6.76	7.76	(3.6, 15.9)	163	185	(83, 454)
θ_4 (Fu)	0.041	0.041	(0.039, 0.044)	0.042	0.041	(0.039, 0.044)
β_1 (PCC)	0.0094	0.0089	(0.0035, 0.015)	0.0087	0.0083	(0.0027, 0.014)
β_2 (Age)	−0.016	−0.017	(−0.03, −0.0054)	−0.016	−0.016	(−0.032, −0.0053)
Ka_SD	1.7	1.6	(1.0, 2.3)	1.66	1.66	(1.1, 2.34)
V/F_SD	0.39	0.35	(0.16, 0.5)	0.39	0.35	(0.16, 0.5)
CL/F_SD	0.47	0.46	(0.35, 0.56)	0.49	0.46	(0.37, 0.37)
Fu_SD	0.12	0.11	(0.06, 0.16)	0.11	0.11	(0.059, 0.15)

Abbreviations: θ, population mean PK parameter estimate; Ka, elimination rate constant; CL/F, apparent volume of distribution; V/F, apparent volume of distribution; Fu, fraction of unbound drug in plasma; PCC, post-operation creatine clearance; SD, standard deviation.

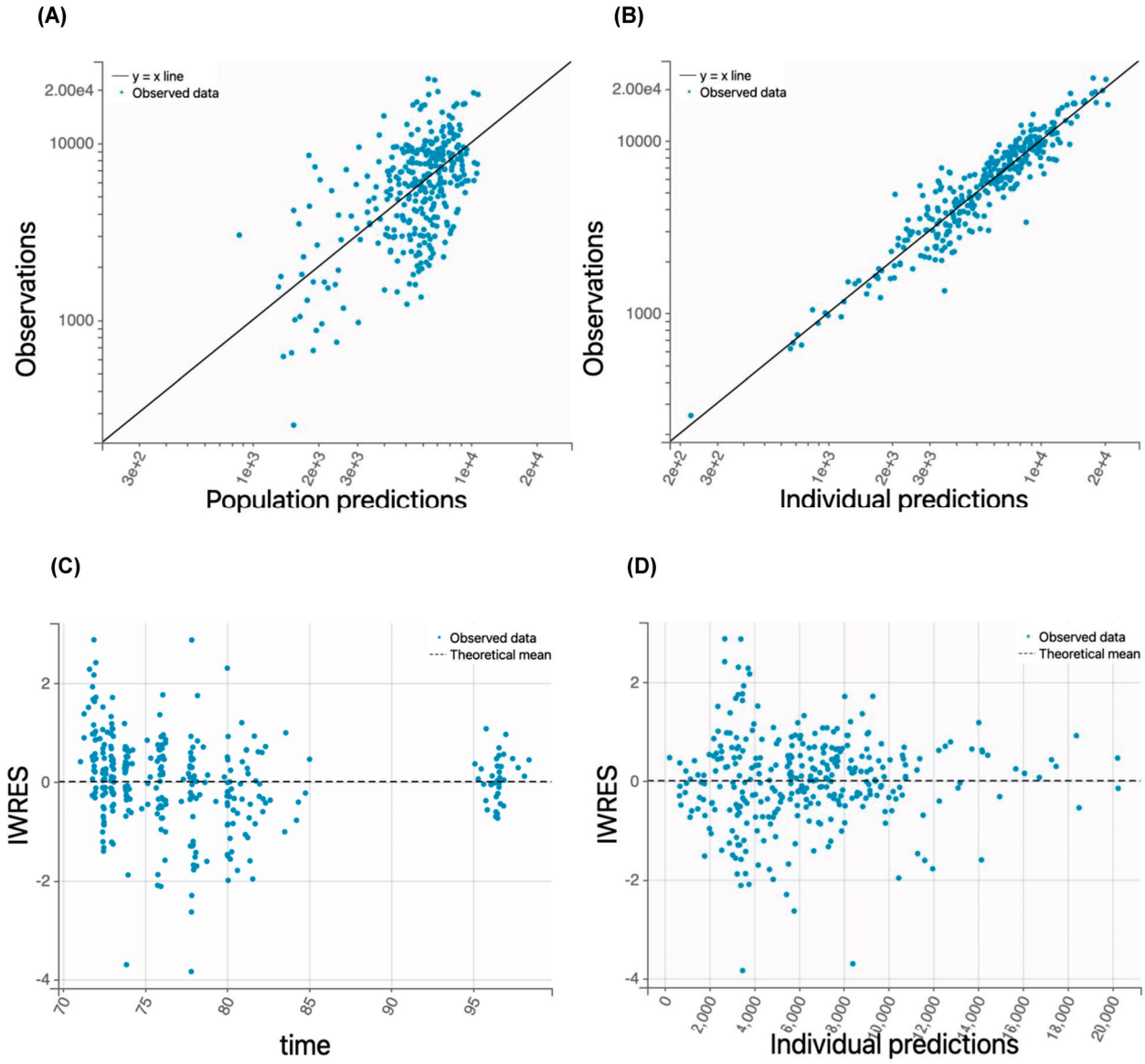


Figure 1. Goodness-of-fit plots for the total plasma pamiparib concentration–time course data fitted by the final covariate model. (**A**) The relationship between the observed and population parameter-predicted total drug concentrations. The solid line is the line of identity. (**B**) The relationship between the observed and individual parameter-predicted total drug concentrations. The solid line is the line of identity. (**C**) Individual weighted residues (IWRESs) versus time. The dashed line is the mean IWRES. (**D**) Individual weighted residues (IWRESs) versus the individual parameter-predicted total drug concentrations. The dashed line is the mean IWRES.

Model predictive performance was evaluated through visual predictive checks (Figure 3A,B). The observed total or unbound pamiparib concentrations fell within the 95% prediction interval and aligned well with the simulated percentiles (50th, 5th, and 95th percentiles), demonstrating that the model adequately captured both the central trend and variability of the observed data. Prediction distribution plots (Figure 3C,D) further assessed predictive accuracy, detecting potential systematic deviations due to model misspecification, overdispersion, or unexplained variability. As shown in Figure 3C,D, >95% of the observed data fell within the 95% prediction intervals and aligned well with the simulated percentiles, indicating no model misspecification.

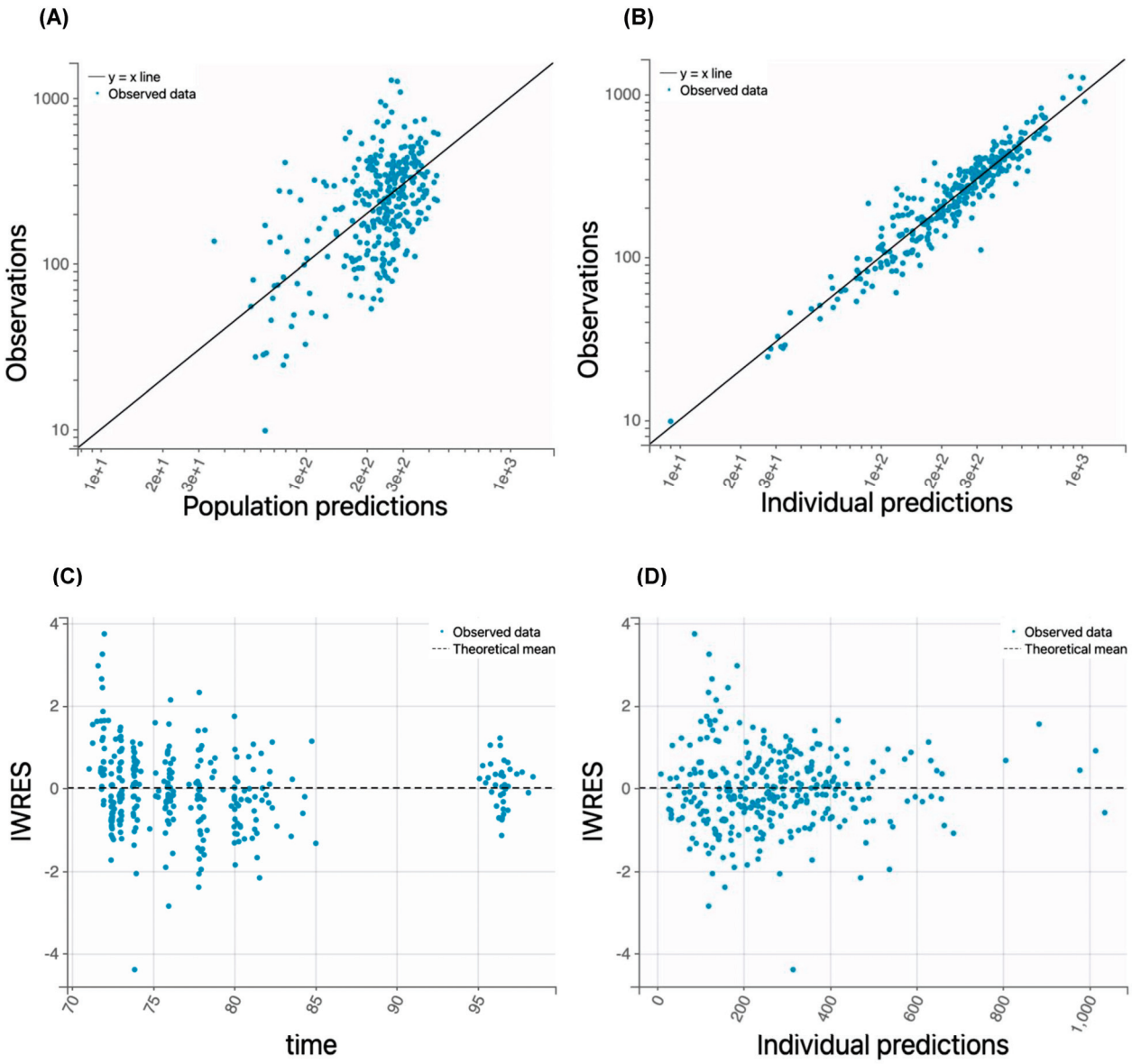


Figure 2. Goodness-of-fit plots for the unbound plasma pamiparib concentration–time course data fitted by the final covariate model. (**A**) The relationship between the observed and population parameter-predicted unbound drug concentrations. The solid line is the line of identity. (**B**) The relationship between the observed and individual parameter-predicted unbound drug concentrations. The solid line is the line of identity. (**C**) Individual weighted residues (IWRESs) versus time. The dashed line is the mean IWRES. (**D**) Individual weighted residues (IWRESs) versus the individual parameter-predicted unbound drug concentrations. The dashed line is the mean IWRES.

Collectively, the goodness-of-fit plots, bootstrap analysis, visual predictive checks, and prediction distribution plots provided a comprehensive assessment of parameter stability and model predictive performance. These results confirmed that the developed one-compartment population PK model with a combined residual error model adequately well characterized the observed total and unbound pamiparib plasma concentration–time profiles in glioblastoma patients.

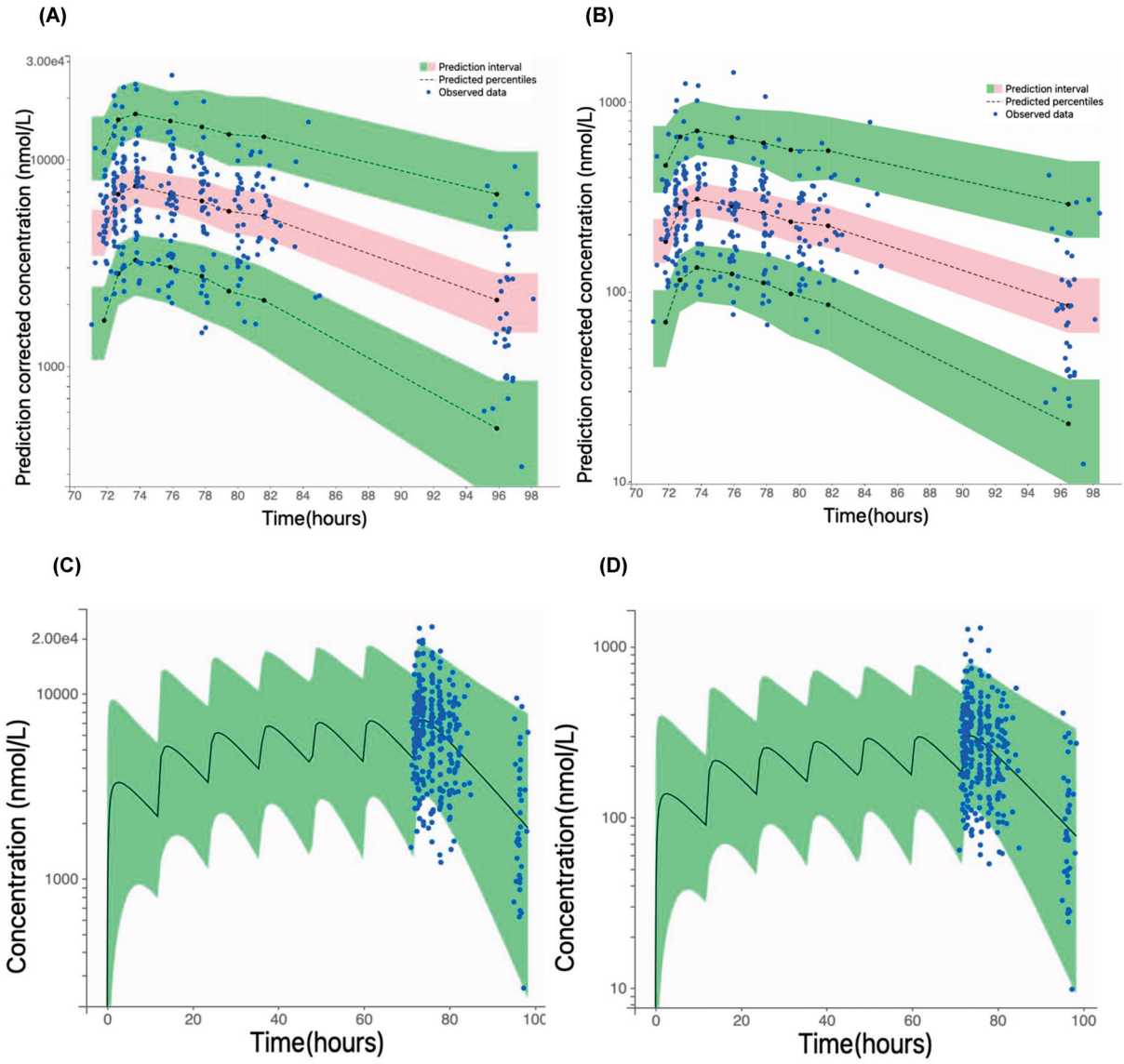


Figure 3. Model evaluation. (**A**,**B**) Visual predictive check of the final covariate model for the total and unbound pamiparib plasma concentrations. The dashed lines represent the 50th, 5th, and 95th percentiles of the model-predicted concentration–time profiles. The shaded areas represent the 95% confidence intervals of the percentiles. Symbols represent the observed drug concentration data. (**C**,**D**) Prediction distribution plots for the total and unbound pamiparib plasma concentration–time profiles following multiple-dose oral administration (60 mg BID). The solid lines represent the model-predicted population mean drug concentration–time profile, and the shaded areas represent the 95% confidence intervals. Dot symbols represent observed concentration data.

3.3. Model Simulation

Figure 4 shows the population PK model-predicted unbound pamiparib plasma concentration–time profiles (including the 50th, 5th, and 95th percentiles) following 5 days of twice-daily oral administration at doses of 10, 20, 30, 40, and 60 mg in a general patient population. Table 4 summarizes the model-predicted steady-state peak, trough, and average plasma concentrations of the unbound pamiparib following twice-daily oral doses of 10–60 mg. When doses increased from 10 to 60 mg BID, the median trough steady-state unbound drug concentrations ($C_{ss,min}$) ranged from 29 to 175 nM, with the 5th percentile ranging from 3 to 16 nM and the 95th percentile ranging from 97 to 581 nM. Given pamiparib's potent PARP inhibition (IC50, ~1 nM) and strong PARP trapping ability, a target engagement ratio (i.e., unbound $C_{ss,min}$/IC50) of 5 or above was considered sufficient for

full target engagement and pharmacological activity. Model predictions suggested that doses as low as 20 mg BID may be adequate for therapeutic effects, even in patients with rapid clearance, where the unbound pamiparib $C_{ss,min}$ was approximately 5 nM (i.e., 5th percentile) (Table 4).

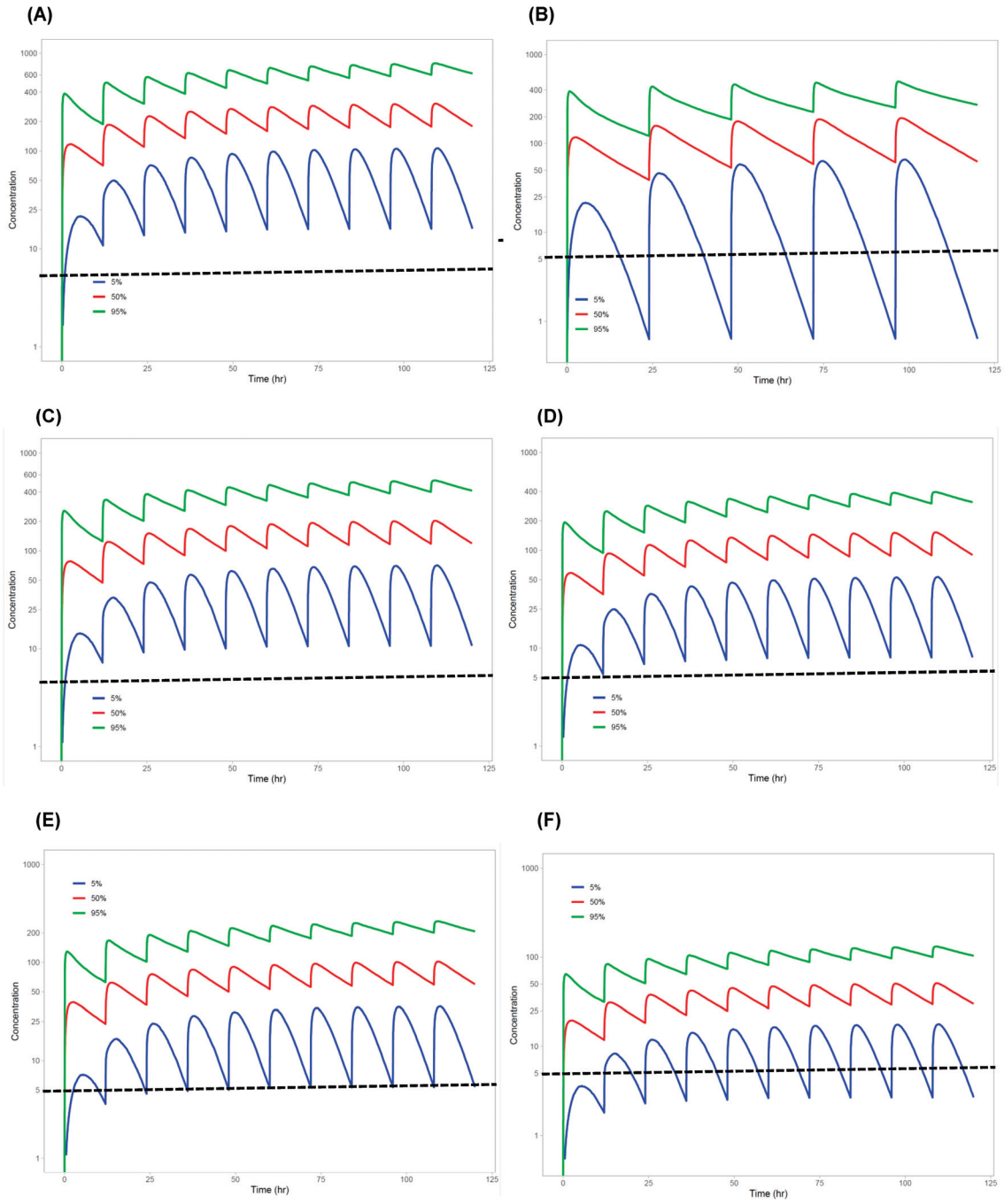


Figure 4. Model-predicted unbound pamiparib concentration–time profiles following oral administration of pamiparib at different dosing regimens: (**A**) 60 mg BID, (**B**) 60 mg QD, (**C**) 40 mg BID, (**D**) 30 mg BID, (**E**) 20 mg BID, and (**F**) 10 mg BID. The red, green, and blue lines represent the 50th, 5th, and 95th percentiles of the predicted concentration profiles. The dashed lines represent the target engagement ratio of 5, which is assumed to be the threshold for therapeutic efficacy.

Table 4. Population PK model-predicted steady-state plasma concentrations of the unbound pamiparib at the 5th, 50th, and 95th percentiles in a general patient population following 5 days of treatment at different dosing regimens.

Dosing Regimen	$C_{ss,max}$			$C_{ss,min}$			$C_{ss,ave}$		
	5th	50th	95th	5th	50th	95th	5th	50th	95th
60 mg BID	105	302	774	16	175	581	47	233	673
60 mg QD	63	193	485	0.6	61	253	14	115	357
40 mg BID	68	201	515	11	117	388	31	155	448
30 mg BID	53	151	387	8	88	291	24	116	336
20 mg BID	35	101	258	5	58	194	16	78	224
10 mg BID	18	50	129	3	29	97	8	39	112

Abbreviations: $C_{ss,max}$, steady-state peak concentration; $C_{ss,min}$, steady-state trough concentration; $C_{ss,ave}$, average steady-state drug concentration; BID, twice-daily dosing; QD, once-daily dosing.

4. Discussion

Due to its strong PARP–DNA trapping ability, favorable PK properties, CNS penetration, and therapeutic potential, pamiparib was evaluated, as a monotherapy or in combination with other therapies, for the treatment of various cancers, particularly BRCA-mutated or homologous recombination-deficient tumors [1,3–6,18]. In this study, we developed a population PK model that well characterized the plasma PK profiles of both total and unbound pamiparib in glioblastoma patients. The model provides a robust framework for optimizing dosing regimens to enhance the clinical development and therapeutic success of this novel PARP inhibitor in oncology.

The pamiparib plasma pharmacokinetic profile following oral administration is characterized by rapid absorption (population mean Ka, 1.58 h^{-1}), low apparent clearance (population mean CL/F, 2.59 L/h), which is significantly lower than human hepatic blood flow (~ 80 L/h), extensive distribution (population mean V/F, 44 L), and high plasma protein binding (population mean Fu, 0.041). These PK parameters align well with pamiparib's physicochemical properties and metabolic characteristics. Pamiparib is a small-molecule drug (molecular weight: 298.3) with moderate lipophilicity (LogP: 2.03), enabling good passive permeability across biological membranes. Notably, it is not a substrate for the efflux transporters ABCB1 and ABCG2, which may contribute to its extensive tissue distribution, including good penetration into the brain [1,9]. Consistent with its low intrinsic clearance determined in human liver microsomes, a mass balance study in patients with solid tumors demonstrated that unchanged pamiparib is the primary circulating component in plasma, comprising 67% of total radioactivity, indicating limited metabolic conversion in humans [18]. Collectively, these observations, in line with our estimated population PK parameters, support that pamiparib exhibits high oral bioavailability (driven by efficient passive permeability and an insignificant first-pass effect), low systemic clearance (due to limited liver metabolism), and extensive tissue distribution.

The population PK analysis suggests that pamiparib exhibits a large interindividual PK variability in patients, with > 50% IIV observed in Ka, V/F, and CL/F (Table 2). While creatinine clearance and age were identified as statistically significant covariates influencing V/F and CL/F for both total and unbound drug, they account for only about 22% and 5% of the respective IIV (Table 2). This suggests that other unassessed patient factors contribute substantially to the interindividual PK variability of pamiparib. One potential factor is the activity of liver enzymes, such as CYP3A4 and CYP2C8, which play key roles in pamiparib metabolism [18]. Potential drug–drug interactions should be considered, particularly with strong CYP3A4 inhibitors or inducers, although the present population PK analysis did not identify any concomitant drugs as significant covariates on pamiparib

PK. A mass balance study in patients revealed that pamiparib metabolites contribute to approximately 33% of the total radioactivity in plasma [18]. The major metabolic pathways involve the oxidation and, to a lesser extent, phase II conjugation of oxidative metabolites. M3 (oxy-dehydro pamiparib) is the most abundant metabolite in human plasma, urine, and feces [18]. Pamiparib and its metabolites undergo both renal and fecal excretion, accounting for approximately 58% and 27% of total radioactivity, respectively [18]. The present study enrolled patients with adequate liver and renal functions. However, given the critical roles of liver metabolism and renal excretion in pamiparib disposition, the impact of severe liver impairment or severe renal dysfunction (creatinine clearance < 30 mL/min) on pamiparib PK remains to be investigated.

Pamiparib is a potent and selective inhibitor of PARP1 and PARP2 enzymes, with a half-maximal inhibitory concentration (IC50) of approximately 1 nM [2]. In addition, it exhibits strong PARP trapping potency, surpassing olaparib and rucaparib but slightly weaker than niraparib and much weaker than talazoparib (the most potent PARP trapper, ~100-fold stronger than olaparib) [19]. PARP trapping is a key mechanism underlying the cytotoxicity of PARP inhibitors, particularly in BRCA-mutated and homologous recombination-deficient cancers [20,21]. Trapped PARP-DNA complexes were more cytotoxic than unrepaired single-strand breaks caused by PARP inactivation, positioning PARP inhibitors as agents that not only inhibit enzyme activity but also act as poisons by trapping PARP on damaged DNA [20,21].

Pamiparib monotherapy has demonstrated clinically meaningful antitumor activity in patients with platinum-sensitive ovarian cancer harboring germline BRCA mutations [3]. However, its efficacy is limited in patients with recurrent ovarian cancer previously treated with PARP inhibitors [22]. In general, PARP inhibitor monotherapy (e.g., olaparib, rucaparib, niraparib, and pamiparib) is most therapeutically effective in maintenance settings for tumors (e.g., breast and ovarian cancer) with BRCA mutations or homologous recombination deficiency [23]. However, broader patient populations or aggressive tumors often require combination therapy for improved clinical efficacy [24]. Combining a PARP inhibitor and a chemotherapeutic agent can lead to synergistic effects, as PARP inhibition prevents DNA repair following DNA damage caused by chemotherapy (e.g., platinum-based drugs and alkylating agents) [24,25]. Additionally, combination strategies may help overcome resistance mechanisms that can develop with monotherapy [24,25]. The efficacy and toxicity of pamiparib-based combination therapies with DNA-damaging agents, radiation, targeted therapies, and immunotherapy are under clinical investigation across multiple cancer types [7]. While pamiparib monotherapy has a manageable safety profile, with primarily hematologic toxicities such as anemia and neutropenia, combination regimens often increase the risk of hematologic and gastrointestinal toxicities. Therefore, optimizing pamiparib dosage or scheduling in combination therapies is critical for balancing efficacy and tolerability to maximize clinical benefit.

The dose– or exposure–response relationships for PARP inhibitors have been explored in preclinical and clinical studies [26,27]. In general, these drugs exhibit a plateau effect, meaning that increasing the drug dose beyond a certain threshold does not significantly enhance efficacy but does increase toxicity [26]. For instance, rucaparib has a threshold dose where higher concentrations do not improve efficacy but increase toxicity; olaparib shows a nonlinear dose–response relationship; and niraparib exhibits dose-dependent hematologic toxicity [26]. Additionally, an imaging study of olaparib in SCLC PDX models demonstrated that olaparib achieved 50% target engagement at the dose of 3.17 mg/kg (ED50) and complete target engagement at 15 mg/kg (~ 5-fold of ED50), with no further benefit beyond 15 mg/kg [27]. These findings align with the observed plateau effect in

clinical settings. While the exact dose– or exposure–response relationship for pamiparib is yet to be fully established, a similar plateau effect is expected.

The current standard pamiparib dose (60 mg BID), established as the maximum tolerated dose in monotherapy [4], may exceed the optimal biological dose required for therapeutic efficacy while minimizing toxicity. Given pamiparib's excellent tissue distribution (including brain penetration), its unbound plasma concentrations could serve as a surrogate for pharmacologically active concentrations at the target site. The target engagement ratio, defined as the unbound drug trough steady-state plasma concentration ($C_{ss,min}$) relative to the IC50 for PARP inhibition (1 nM), can be used as an indicator of potential therapeutic effects. Model simulations following twice-daily oral administration at doses of 10, 20, 30, 40, and 60 mg suggest that pamiparib achieves the target engagement ratio ($C_{ss,min}$/IC50) of 29–175 (50th percentile) in patients with a typical population mean apparent clearance (CL/F), 97–581 (95th percentile) in patients with low CL/F, and 3–16 (5th percentile) in patients with high CL/F (Figure 4 and Table 4). Assuming that a target engagement ratio of 5 or above is sufficient for full target engagement and pharmacological activity, doses as low as 20 mg BID may be adequate for therapeutic effects even in patients with rapid clearance, where the target engagement ratio is 5 (i.e., 5th percentile) (Figure 4 and Table 4). These findings support further clinical investigation into dose reduction to optimize pamiparib's benefit-to-risk ratio, particularly in maintenance settings for BRCA-mutated or homologous recombination-deficient tumors, which may respond to lower PARP inhibitor doses. Furthermore, in combination therapies, where dose–response dynamics may shift due to synergistic effects, lower pamiparib doses would enhance tolerability while maintaining efficacy. Continued clinical investigation into the optimization of the pamiparib dosing regimen is essential for refining its clinical application and maximizing therapeutic benefit.

In conclusion, the total and unbound pamiparib plasma PK are well characterized by a linear one-compartment model, with creatinine clearance as the significant covariate on V/F. Model simulations support further clinical investigation into dose reduction to optimize the benefit-to-risk ratio of pamiparib, particularly in combination therapies.

Author Contributions: Conceptualization, J.L.; methodology, C.W., S.K., Y.J., J.J., Y.Y., X.B., A.H., N.S. and J.L.; software, C.W. and S.K.; formal analysis, C.W. and J.L.; resources, J.L. and N.S.; data curation, Y.J., J.J., Y.Y., X.B. and A.H.; writing—original draft preparation, C.W. and J.L.; writing—review and editing, C.W., S.K., Y.J., J.J., Y.Y., X.B., A.H., N.S. and J.L.; supervision, J.L.; project administration, J.L.; funding acquisition, J.L. All authors have read and agreed to the published version of the manuscript.

Funding: This study is supported by the National Cancer Institute of the National Institute of Health (NIH), R01CA255124 (JL), and the NIH Cancer Center Support Grant P30CA022453 (Karmanos Cancer Institute Pharmacology and Metabolomics Core).

Institutional Review Board Statement: The study was conducted in accordance with the Declaration of Helsinki, and approved by the Institutional Review Board of St. Joseph's Hospital and Medical Center (protocol code 2020-12 and date of approval 12 July 2020).

Informed Consent Statement: Informed consent was obtained from all subjects involved in the study.

Data Availability Statement: The data generated in this study are available within the paper. The raw data used for the population PK analysis and creating graphs are available from the corresponding author upon reasonable request.

Conflicts of Interest: The authors declare no conflicts of interest.

References

1. Xiong, Y.; Guo, Y.; Liu, Y.; Wang, H.; Gong, W.; Liu, Y.; Wang, X.; Gao, Y.; Yu, F.; Su, D.; et al. Pamiparib is a potent and selective PARP inhibitor with unique potential for the treatment of brain tumor. *Neoplasia* **2020**, *22*, 431–440. [CrossRef] [PubMed]
2. Wang, H.; Ren, B.; Liu, Y.; Jiang, B.; Guo, Y.; Wei, M.; Luo, L.; Kuang, X.; Qiu, M.; Lv, L.; et al. Discovery of Pamiparib (BGB-290), a Potent and Selective Poly (ADP-ribose) Polymerase (PARP) Inhibitor in Clinical Development. *J. Med. Chem.* **2020**, *63*, 15541–15563. [CrossRef] [PubMed]
3. Wu, X.; Zhu, J.; Wang, J.; Lin, Z.; Yin, R.; Sun, W.; Zhou, Q.; Zhang, S.; Wang, D.; Shi, H.; et al. Pamiparib Monotherapy for Patients with Germline BRCA1/2-Mutated Ovarian Cancer Previously Treated with at Least Two Lines of Chemotherapy: A Multicenter, Open-Label, Phase II Study. *Clin. Cancer Res.* **2022**, *28*, 653–661. [CrossRef]
4. Lickliter, J.D.; Voskoboynik, M.; Mileshkin, L.; Gan, H.K.; Kichenadasse, G.; Zhang, K.; Zhang, M.; Tang, Z.; Millward, M. Phase 1A/1B dose-escalation and -expansion study to evaluate the safety, pharmacokinetics, food effects and antitumor activity of pamiparib in advanced solid tumours. *Br. J. Cancer* **2022**, *126*, 576–585. [CrossRef] [PubMed]
5. Xu, B.; Sun, T.; Shi, Y.; Cui, J.; Yin, Y.; Ouyang, Q.; Liu, Q.; Zhang, Q.; Chen, Y.; Wang, S.; et al. Pamiparib in patients with locally advanced or metastatic HER2-negative breast cancer with germline BRCA mutations: A phase II study. *Breast Cancer Res. Treat.* **2023**, *197*, 489–501. [CrossRef]
6. Stradella, A.; Johnson, M.; Goel, S.; Park, H.; Lakhani, N.; Arkenau, H.T.; Galsky, M.D.; Calvo, E.; Baz, V.; Moreno, V.; et al. Phase 1b study to assess the safety, tolerability, and clinical activity of pamiparib in combination with temozolomide in patients with locally advanced or metastatic solid tumors. *Cancer Med.* **2024**, *13*, e7385. [CrossRef]
7. Friedlander, M.; Mileshkin, L.; Lombard, J.; Frentzas, S.; Gao, B.; Wilson, M.; Meniawy, T.; Baron-Hay, S.; Briscoe, K.; McCarthy, N.; et al. Pamiparib in combination with tislelizumab in patients with advanced solid tumours: Results from the dose-expansion stage of a multicentre, open-label, phase I trial. *Br. J. Cancer* **2023**, *129*, 797–810. [CrossRef]
8. Ciardiello, F.; Bang, Y.J.; Cervantes, A.; Dvorkin, M.; Lopez, C.D.; Metges, J.P.; Sanchez Ruiz, A.; Calvo, M.; Strickland, A.H.; Kannourakis, G.; et al. Efficacy and safety of maintenance therapy with pamiparib versus placebo for advanced gastric cancer responding to first-line platinum-based chemotherapy: Phase 2 study results. *Cancer Med.* **2023**, *12*, 13145–13154. [CrossRef]
9. Li, J.; Wickramasinghe, C.; Jiang, J.; Wu, A.; Jiang, Y.; Tovmasyan, A.; Kim, S.; Sanai, N. Mechanistic Modeling of Spatial Heterogeneity of Drug Penetration and Exposure in the Human Central Nervous System and Brain Tumors. *Clin. Pharmacol. Ther.* **2025**, *117*, 690–703. [CrossRef]
10. Kennedy, W.R.; Chang, Y.W.; Jiang, J.; Molloy, J.; Pennington-Krygier, C.; Harmon, J.; Hong, A.; Wanebo, J.; Braun, K.; Garcia, M.A.; et al. A Combined Phase 0/2 "Trigger" Trial Evaluating Pamiparib or Olaparib with Concurrent Radiotherapy in Patients with Newly-Diagnosed or Recurrent Glioblastoma. *Int. J. Radiat. Oncol. Biol. Phys.* **2023**, *117*, e115. [CrossRef]
11. Jiang, J.; Bao, X.; Yue, Y.; Schiff, D.; Bindra, R.; Li, J. Development and validation of a liquid chromatography coupled with tandem mass spectrometry method for determining total and unbound pamiparib in human plasma and brain tumors. *Biomed. Chromatogr.* **2022**, *36*, e5478. [CrossRef] [PubMed]
12. Yafune, A.; Ishiguro, M. Bootstrap approach for constructing confidence intervals for population pharmacokinetic parameters. I: A use of bootstrap standard error. *Stat. Med.* **1999**, *18*, 581–599. [CrossRef]
13. Efron, B. The bootstrap and Markov-chain Monte Carlo. *J. Biopharm. Stat.* **2011**, *21*, 1052–1062. [CrossRef] [PubMed]
14. Efron, B. Bayesian inference and the parametric bootstrap. *Ann. Appl. Stat.* **2012**, *6*, 1971–1997. [CrossRef]
15. Bergstrand, M.; Hooker, A.C.; Wallin, J.E.; Karlsson, M.O. Prediction-corrected visual predictive checks for diagnosing nonlinear mixed-effects models. *AAPS J.* **2011**, *13*, 143–151. [CrossRef] [PubMed]
16. Yano, Y.; Beal, S.L.; Sheiner, L.B. Evaluating pharmacokinetic/pharmacodynamic models using the posterior predictive check. *J. Pharmacokinet. Pharmacodyn.* **2001**, *28*, 171–192. [CrossRef]
17. Comets, E.; Brendel, K.; Mentre, F. Computing normalised prediction distribution errors to evaluate nonlinear mixed-effect models: The npde add-on package for R. *Comput. Methods Programs Biomed.* **2008**, *90*, 154–166. [CrossRef]
18. Mu, S.; Palmer, D.; Fitzgerald, R.; Andreu-Vieyra, C.; Zhang, H.; Tang, Z.; Su, D.; Sahasranaman, S. Human Mass Balance and Metabolite Profiling of [(14) C]-Pamiparib, a Poly (ADP-Ribose) Polymerase Inhibitor, in Patients With Advanced Cancer. *Clin. Pharmacol. Drug Dev.* **2021**, *10*, 1108–1120. [CrossRef]
19. Murai, J.; Huang, S.Y.; Das, B.B.; Renaud, A.; Zhang, Y.; Doroshow, J.H.; Ji, J.; Takeda, S.; Pommier, Y. Trapping of PARP1 and PARP2 by Clinical PARP Inhibitors. *Cancer Res.* **2012**, *72*, 5588–5599. [CrossRef]
20. Hopkins, T.A.; Ainsworth, W.B.; Ellis, P.A.; Donawho, C.K.; DiGiammarino, E.L.; Panchal, S.C.; Abraham, V.C.; Algire, M.A.; Shi, Y.; Olson, A.M.; et al. PARP1 Trapping by PARP Inhibitors Drives Cytotoxicity in Both Cancer Cells and Healthy Bone Marrow. *Mol. Cancer Res.* **2019**, *17*, 409–419. [CrossRef]
21. Hopkins, T.A.; Shi, Y.; Rodriguez, L.E.; Solomon, L.R.; Donawho, C.K.; DiGiammarino, E.L.; Panchal, S.C.; Wilsbacher, J.L.; Gao, W.; Olson, A.M.; et al. Mechanistic Dissection of PARP1 Trapping and the Impact on In Vivo Tolerability and Efficacy of PARP Inhibitors. *Mol. Cancer Res.* **2015**, *13*, 1465–1477. [CrossRef] [PubMed]

22. Zhu, J.; Cheng, F.; Sun, L.; Shao, F.; Wang, J.; Yang, L.; Jiang, G. 778P Efficacy and safety of pamiparib monotherapy in recurrent ovarian cancer (rOC) after prior PARPi exposure: A prospective, open label, single-arm, phase II study. *Ann. Oncol.* **2024**, *35*, S585. [CrossRef]
23. O'Malley, D.M.; Krivak, T.C.; Kabil, N.; Munley, J.; Moore, K.N. PARP Inhibitors in Ovarian Cancer: A Review. *Target. Oncol.* **2023**, *18*, 471–503. [CrossRef] [PubMed]
24. Bhamidipati, D.; Haro-Silerio, J.I.; Yap, T.A.; Ngoi, N. PARP inhibitors: Enhancing efficacy through rational combinations. *Br. J. Cancer* **2023**, *129*, 904–916. [CrossRef]
25. Kim, D.; Nam, H.J. PARP Inhibitors: Clinical Limitations and Recent Attempts to Overcome Them. *Int. J. Mol. Sci.* **2022**, *23*, 8412. [CrossRef]
26. Bruin, M.A.C.; Sonke, G.S.; Beijnen, J.H.; Huitema, A.D.R. Pharmacokinetics and Pharmacodynamics of PARP Inhibitors in Oncology. *Clin. Pharmacokinet.* **2022**, *61*, 1649–1675. [CrossRef]
27. Carney, B.; Kossatz, S.; Lok, B.H.; Schneeberger, V.; Gangangari, K.K.; Pillarsetty, N.V.K.; Weber, W.A.; Rudin, C.M.; Poirier, J.T.; Reiner, T. Target engagement imaging of PARP inhibitors in small-cell lung cancer. *Nat. Commun.* **2018**, *9*, 176. [CrossRef]

Disclaimer/Publisher's Note: The statements, opinions and data contained in all publications are solely those of the individual author(s) and contributor(s) and not of MDPI and/or the editor(s). MDPI and/or the editor(s) disclaim responsibility for any injury to people or property resulting from any ideas, methods, instructions or products referred to in the content.

pharmaceutics

MDPI

Article

Population Pharmacokinetic and Pharmacodynamic Study of Palbociclib in Children and Young Adults with Recurrent, Progressive, or Refractory Brain Tumors

John C. Panetta [1], Nicholas S. Selvo [1], David Van Mater [2] and Clinton F. Stewart [1,*]

[1] Department of Pharmacy and Pharmaceutical Sciences, St. Jude Children's Research Hospital, 262 Danny Thomas Place, Memphis, TN 38105, USA; carl.panetta@stjude.org (J.C.P.); nick.selvo@stjude.org (N.S.S.)
[2] Division of Pediatric Hematology-Oncology, Department of Pediatrics, Duke University Medical Center, Durham, NC 27710, USA; david.vanmater@duke.edu
* Correspondence: clinton.stewart@stjude.org; Tel.: +1-901-595-3665; Fax: +1-901+525-6869

Abstract: Background/Objectives: Palbociclib, an oral CDK 4/6 inhibitor, was evaluated in a Pediatric Brain Tumor Consortium (PBTC) phase 1 (NCT02255461; PBTC-042) study to treat children and young adults with recurrent, progressive, or refractory brain tumors. The objectives of this study were to characterize the palbociclib population pharmacokinetics in children enrolled on PBTC-042, to conduct a population pharmacodynamic analysis in this patient population, and to perform a simulation study to assess the role of palbociclib exposure on neutropenia and thrombocytopenia. **Methods:** The palbociclib population pharmacokinetics and pharmacodynamics were characterized in this patient population (n = 34 patients; 4.9–21.6 years old). Population pharmacokinetics were modeled using a one-compartment model with first-order absorption and elimination. Covariate analysis was performed, evaluating demographics, laboratory values, and concomitant medications. A pharmacodynamic model was used to describe the relation between palbociclib plasma exposure and changes in the ANC and platelet counts. **Results:** The population estimates for the apparent oral volume, apparent oral clearance, and absorption rate constant were 664.5 L/m^2, 36.8 L/h/m^2, and 0.48 h^{-1}, respectively. The palbociclib apparent oral clearance was decreased in patients with higher AST values (p = 0.0066). The ANC and platelet pharmacodynamic models estimated that the median (5th–95th percentile) time individuals had grade 3 or greater neutropenia was 4 (0, 21) days. Simulations showed that given 75 mg/m^2 palbociclib, 49% of the individuals were expected to have grade 3 or greater neutropenia. **Conclusions:** Palbociclib pharmacokinetics and pharmacodynamics were adequately characterized in this patient population, no unexpected adverse reactions were noted, and the drug was well tolerated.

Keywords: palbociclib; CDK4/6; pharmacokinetics; pharmacodynamics; pediatrics; brain tumors; special populations; PK/PD models; nonlinear mixed-effects modeling

1. Introduction

Approximately 4000 new cases of pediatric central nervous system (CNS) tumors occur in the United States per year [1]. The current therapy for pediatric CNS tumors such as medulloblastomas, high-grade gliomas, and ependymomas includes maximal surgical resection and radiation alone or in combination with chemotherapy. Although this approach will lead to excellent outcomes in these tumors, some of these patients will recur or relapse, leading to poor overall survival. For these populations, alternative approaches including molecularly targeted agents are needed [2].

Recent studies at the genomic level have revealed numerous specific molecular alterations that drive the progression of these tumors, but these also may serve as the basis for the design of molecularly targeted drugs, which can control tumor proliferation and spread and, in contrast to cytotoxic therapy, cause less damage to normal tissues [3–5].

Specifically, studies have shown that a significant subset of pediatric CNS tumors harbor mutations in the cyclin-D cyclin-dependent kinase 4 and 6 (CDK4/6)-retinoblastoma (Rb) pathway that is a key regulator of the cell cycle. CDK4/6 inhibitors prevent progression from the G1 phase to the S phase of the cell cycle by inhibiting the phosphorylation of the retinoblastoma protein (RB1), thereby preventing replication [6,7].

Palbociclib is an oral, potent, and highly selective reversible inhibitor of cyclin-dependent kinases CDK4 and CDK6, which prevents RB1 phosphorylation and stops abnormal cellular replication. In children with recurrent or refractory solid or primary CNS tumors, the average time of the maximum observed concentration (T_{max}) after oral palbociclib administration was between 5 and 8 h, and the average half-life was 11.3 to 19.5 h. The palbociclib systemic exposure (i.e., the maximum plasma concentration (C_{max}) and area under the plasma concentration–time curve (AUC)) increased in a proportional manner; however, a large inter-individual variability in pharmacokinetic parameters was reported [8,9].

Myelosuppression, primarily neutropenia, has been the most common adverse event associated with palbociclib administration in both adult breast cancer studies and the pediatric literature [8,10]. This neutropenia is likely on-target since preclinical studies have shown that palbociclib inhibits neutrophil maturation through an effect on early myeloid progenitor cells [11]. The extent of neutropenia is associated with palbociclib systemic exposure in clinical trials in adults and in children with relapsed brain tumors; higher palbociclib systemic exposures (AUC and C_{max}) were associated with severe (grade 3 or 4) neutropenia [8].

Although numerous adult population pharmacokinetic and pharmacodynamic studies have been published, no comprehensive analysis has been performed in children with cancer. Thus, the objectives of this study were to characterize the palbociclib population pharmacokinetics in children with recurrent, progressive, or refractory brain tumors enrolled on PBTC-042, to conduct a population pharmacodynamic analysis in this patient population, and to perform a simulation study to assess the role of palbociclib exposure on neutropenia and thrombocytopenia.

2. Patients and Methods

2.1. Clinical Trial Design

The patients included in this palbociclib population pharmacokinetic/pharmacodynamic analysis were treated in the phase I clinical trial PBTC-042 (NCT02255461), which evaluated single-agent oral palbociclib therapy in children and young adults with recurrent, progressive, or refractory brain tumors. Details of this clinical trial have been reported elsewhere [8]. In adults treated with palbociclib, myelosuppression has been the main dose-limiting toxicity (DLT) reported, and the toxicity is greater in more heavily pretreated patients [12,13]. Thus, patients in this pediatric trial were divided into two strata: stratum I included patients who were not heavily pretreated, while stratum II included heavily pretreated patients [8]. The starting dosage for stratum I was 50 mg/m^2, with planned dose escalations to 75 mg/m^2 and 95 mg/m^2. The planned starting dosage for stratum II was one dosage level below the MTD for stratum I. The Institutional Review Board approved this trial and written informed consent was obtained from patients, parents, or legal guardians before the onset of any study procedures. Assent was obtained from patients as appropriate based on local institutional guidelines.

2.2. Pharmacokinetic Sampling and Bioanalysis

Pharmacokinetic studies of oral palbociclib (PD-0332991) were performed on course 1, day 1 and day 21 to evaluate the population pharmacokinetics of palbociclib. On day 2 of course 1, the palbociclib dose was held. On day 1 of course 1, palbociclib single-dose serial blood samples were drawn pre-dose and 0.5, 1, 2, 4, 8 ($\pm$1), 24 ($\pm$4), and 48 ($\pm$4) hours (immediately prior to the day 3 dose) after the oral dose. On day 21 of course 1,

palbociclib steady-state serial blood samples were collected pre-dose and 1, 2, 4, 8 (±1), and 24 (±4) hours (immediately prior to the day 22 dose) after the dose.

At each time point, whole blood (2 mL) was collected in K_2EDTA tubes, spun to plasma within one hour of collection, and stored at −20 °C until analysis. Palbociclib plasma concentrations were measured using a validated liquid chromatography–mass spectrometric assay method with a lower limit of quantitation (LLOQ) of 1 ng/mL [14].

2.3. Population Pharmacokinetic Analysis

Palbociclib serum concentration–time data from course 1, day 1 and day 21 were analyzed using nonlinear mixed-effects modeling implemented in Monolix software version 2023R1 (Lixoft, Antony, France) using the Stochastic Approximation Expectation Maximization (SAEM) algorithm. Inter-individual and inter-occasion variabilities were assumed to be log-normally distributed. A proportional residual error model was used to quantify the unexplained variability of the model. Error terms were assumed to be normally distributed. A one-compartment model with first-order absorption, the absorption lag time, and first-order elimination was used [15,16]. Specifically, the PK parameters estimated included the absorption lag time (T_{lag}), absorption rate constant (k_a), apparent oral volume (V/F), and apparent oral clearance (CL/F), where F was the bioavailability, which was not identifiable given only oral dosing was used. The inter-individual variability was estimated for all parameters. Additionally, the inter-occasion variability was estimated for the CL/F. The palbociclib dosage (i.e., the palbociclib dosage normalized to the patient body surface area (BSA)) was used as the model input. Data below the limit of quantitation (BLQ) were censored according to the Beal method M3 [17], as implemented in Monolix.

2.3.1. Covariate Analysis

The following covariates were evaluated for their effects on the apparent oral palbociclib clearance: age, body weight, body surface area (BSA), gender, serum creatinine, serum albumin, estimated glomerular filtration rate (eGFR), aspartate aminotransferase (AST), total bilirubin, and concomitant medications reported in at least 10% of the total patients. The eGFR was calculated using a simplified two-covariate equation based on the patient height and serum creatinine, which was developed specifically for pediatric oncology patients [18]. Concomitant medications were tested as categorical variables (i.e., yes/no) and included dexamethasone, ranitidine, famotidine, granisetron, ondansetron, levetiracetam, lacosamide, lorazepam, levothyroxine, gabapentin, and trimethoprim/sulfamethoxazole. Continuous covariates were modeled using a power model scaled to the population median covariate value. Categorical covariates were modeled according to an exponential model.

A stepwise forward inclusion method was used to identify significant covariates. Each covariate was added univariately to the parameter of interest and selected based upon a decrease in the OFV by at least 3.84 units (corresponding to $p < 0.05$ based on the χ^2 test), a decrease in the inter-individual variability, and improved model fits. The covariate displaying the highest change in the OFV was retained in the model and the process was repeated until no covariates were statistically significant.

2.3.2. Population Pharmacokinetic Model Evaluation

The population pharmacokinetic model fit was evaluated using various goodness-of-fit plots including observed vs. population predicted, observed vs. individual predicted, weighted residuals vs. time, and visual predictive checks. The predictive performance of the final model was evaluated using approaches previously employed [19,20]. The precision of the parameters estimated from the final population model was evaluated using a non-parametric bootstrap resampling method. A total of 500 replicates of the original dataset were generated using random sampling with replacement. The model was applied to each replicate dataset. Summary statistics for each parameter were calculated based upon the model runs (i.e., the mean and 90% bootstrap confidence interval). Non-parametric

bootstrapping was performed with the MonolixSuite R-based package Rsmlx 2.0.4 package (Lixoft, Antony, France).

2.4. Pharmacodynamic (PD) Methods

A complete blood count (CBC) with differential was performed pre-therapy, weekly during course 1, and then weekly during courses 2 to 26. The CBC provided platelet and absolute neutrophil counts (ANCs). If an individual only had a single platelet count or ANC observation collected before palbociclib administration, the patient was not included in the pharmacodynamic analysis.

2.4.1. Pharmacodynamic Model

The model describing the ANC and platelet dynamics has been previously described [21]. The model for the ANC consisted of a bone marrow compartment with proliferating neutrophils, three transient compartments that represent the maturation process of the neutrophils from blasts to circulating neutrophils, and a circulating neutrophil compartment. The model included the negative feedback effects of endogenous G-CSF, which affected the growth rate of proliferating cells in a manner inversely proportional to the concentration of circulating neutrophils. We assumed that palbociclib only affected the proliferating neutrophils in the bone marrow compartment. We used a similar structural model for platelet dynamics. The model describing the neutrophil dynamics is shown in Equations (1)–(5) and Figure S1.

$$\frac{N_{PBM}}{dt} = \left[\frac{k_{in}K_M}{K_M + N_{circ}} \frac{IC_{50}^n}{IC_{50}^n + C_{palblociclib}^n} - k_{bp}\right] N_{PBM} \quad (1)$$

$$\frac{dN_{T1}}{dt} = k_{bp}(N_{PBM} - N_{T1}) \quad (2)$$

$$\frac{dN_{T2}}{dt} = k_{bp}(N_{T1} - N_{T2}) \quad (3)$$

$$\frac{dN_{T3}}{dt} = k_{bp}(N_{T2} - N_{T3}) \quad (4)$$

$$\frac{dN_{circ}}{dt} = kpbN_{T3} - k_{out}N_{circ} \quad (5)$$

The model parameters were as follows: N_{PBM}: proliferating bone marrow stem cells; N_{T1}, N_{T2}, and N_{T3}: transient compartments describing the maturation phases of the neutrophils; N_{circ}: circulating neutrophils. Note that we were only able to observe this compartment. The model parameters were defined as follows: k_{in} (1/days): the stem cell proliferation rate; k_{bp} (1/days): the transition rate between transient compartments (the mean transition time from the bone marrow to the circulating neutrophils is $4/k_{bp}$); k_{out} (1/days): the elimination rate of circulating neutrophils; K_M ($10^3/\mu$L): the half-saturation effect of the G-CSF negative feedback; IC_{50} (nM) and n; the half-saturation effect and Hill coefficient of the palbociclib effects on the bone marrow; and $C_{palbociclib}$ (nM): the concentration of palbociclib in the plasma. Prior to treatment, the system was assumed to be steady-state, where N_{circ0} was the steady-state circulating neutrophil level. The following relationship between the model parameters was needed for the system to maintain steady state prior to treatment (Equation (6)).

$$K_M = \frac{k_{bp}}{k_{in} - k_{bp}} N_{circ0} \quad (6)$$

For this relationship to be positive, $k_{in} > k_{pb}$. To ensure this requirement, we defined $k_{pb} = fk_{bp} \cdot k_{in}$ where $fk_{bp} \in [0, 1]$ and estimated fk_{bp}. In addition, the initial conditions for

the system at steady state (i.e., the steady-state solution to the system in the absence of the drug) are (Equation (7))

$$\left[\frac{k_{out}}{k_{bp}}N_{circ0},\ \frac{k_{out}}{k_{bp}}N_{circ0},\ \frac{k_{out}}{k_{bp}}N_{circ0},\ \frac{k_{out}}{k_{bp}}N_{circ0},\ N_{circ0}\right] \quad (7)$$

2.4.2. Parameter Estimation

The parameters for the pharmacodynamic model were estimated using nonlinear mixed-effects modeling with the SAEM algorithm as implemented in the Monolix® software version 2023R1 (Lixoft, Antony, France). The palbociclib pharmacokinetics were fixed to each individual's post hoc estimated parameters (as determined above). The inter-individual and inter-occasion variability were assumed to be log-normally distributed for all parameters except fk_{bp}, which was assumed to be a logit distribution, so its value will be between 0 and 1. A proportional residual error model was used to quantify the unexplained variability of the model. Error terms were assumed to be normally distributed.

2.4.3. Pharmacodynamic Model Simulations

To assess the extent of neutropenia and thrombocytopenia expected at clinically relevant dosages and the effect of prior myelosuppressive therapy on neutropenia and thrombocytopenia, simulations were performed with three fixed dosages (50, 75, or 95 mg/m^2/day for 21 days) using the individual estimated PK (conditional mode) and PD parameters (samples from the conditional distribution). The median and 5th–95th percentiles for the measurements of neutropenia and thrombocytopenia were calculated using the individual PD profiles (based on the individual estimated PD parameters sampled from the individual conditional distribution) of the ANC and platelet dynamics. We evaluated bias in residuals (measured vs. estimated ANC or platelets) between courses (1 and 2 vs. 3 and 4) using the Kruskal–Wallis test. Comparisons of neutropenia and thrombocytopenia between strata were evaluated using the Kruskal–Wallis test.

3. Results

3.1. Summary of Population Pharmacokinetic Data

Pharmacokinetic studies were conducted on the 34 participants enrolled in the study who were assigned oral palbociclib at 50, 75, and 95 mg/m^2/day. One patient who deviated from the protocol by taking concomitant medications of phenytoin (a strong CYP3A inducer) and omeprazole (a proton pump inhibitor) was excluded from the analysis. The remaining 33 patients participated in course 1, day 1 pharmacokinetic studies, and of them, 26 patients participated in course 1, day 21 studies. Among the seven patients who did not participate in course 1, day 21 pharmacokinetic studies, one patient withdrew consent, four patients went off study, one patient was taken off treatment due to progressive disease, and samples from one patient were not collected because of that patient's clinical condition. Patients ranged from 4.9 to 21.6 years old, and over half were Caucasian. All the patient characteristics, including the clinical covariates and concomitant medications of interest, are summarized in Table 1.

This study included 397 samples from these 33 individuals. We excluded 10 samples from three patients, so a total of 387 samples were included in the pharmacokinetic analysis. The 10 samples were excluded for the following reasons: the 24 h sample was higher than the 8 h in two individuals, suggesting that these patients may have taken a dose prior to the sample at 24 h. Therefore, the 24 and following 48 h samples in these two individuals were excluded. One patient had four course 1, day 21 samples that were BLQ (pre-dose and 1, 2, and 4 h post-dose), followed by two samples well above BLQ at 7 and 24 h post-dose. These samples BLQ were spurious given the individual received 21 days of dosing. Therefore, these six samples on day 21 were excluded.

Table 1. Characteristics of patients included in the pharmacokinetic study (n = 33).

Female/male n (%)	12 (36)/21 (64)
† Race n (%)	
Caucasian	19 (58)
Black	4 (12)
Other	10 (30)
Stratum I/II n (%)	21 (64)/12 (36)
Palbociclib dosage n (%)	
50 mg/m^2	6 (18)
75 mg/m^2	21 (64)
95 mg/m^2	6 (18)
Age (y)	12.8 (4.9–21.6)
Height (cm)	147.8 (109–185.1)
Weight (kg)	52.5 (23.8–110.4)
Body surface area (m^2)	1.5 (0.8–2.4)
Albumin (g/dL)	4.2 (3.2–4.9)
Aspartate aminotransferase (AST; U/L)	25 (11–93)
Bilirubin (mg/dL)	0.4 (0.1–1.2)
Creatinine (mg/dL)	0.5 (0.2–1.2)
Concomitant medication: Day 1 n (%); Day 21 n (%)	
Ranitidine	3 (9); 2 (8)
Famotidine	1(3); 1(4)
HT-3 inhibitors (ondansetron/granisetron)	5 (15)/2 (6); 3 (12)/2 (8)
Dexamethasone	8 (24); 5 (19)

Data are reported as the frequency or median (range). † Self-declared ethnicity. Other includes Asian (n = 3), Hispanic (4), American Indian/Alaskan (1), and unknown (n = 2).

3.2. Population Pharmacokinetic and Covariate Analysis

The base population pharmacokinetic estimates for the T_{lag}, k_a, V/F, and CL/F were 0.8 h, 0.48/h, 664.5 L/m^2, and 36.8 L/h/m^2, respectively. A summary of all the population parameters and measures of variability is shown in Table 2. Covariate analysis showed that the palbociclib CL/F was significantly decreased with increasing AST (from 48.2 L/h/m^2 at AST = 10 U/L to 24.1 L/h/m^2 at AST = 100 U/L; $p = 0.0066$; Table S1; Figure 1). With the inclusion of AST, the inter-patient variability of the palbociclib CL/F decreased by 10% (from 0.29 to 0.26) (Table 2). None of the concomitant drugs considered as covariates were significant (Table S1).

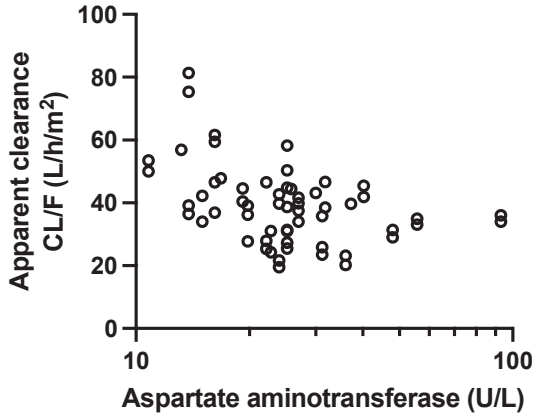


Figure 1. Scatterplot of palbociclib apparent clearance and aspartate aminotransferase levels (Corr: 0.98, $p = 0.0066$).

Table 2. Final pharmacokinetic population parameter estimates.

Parameters *	Base Model Est. (RSE%) *	AST	Mean	Non-Parametric Bootstrap 90% CI
Population estimates				
Absorption lag time T_{lag} (h)	0.8 (12.3)	0.8 (12.1)	0.81	0.65; 0.97
Absorption rate constant k_a (/h)	0.48 (17.9)	0.46 (17.6)	0.51	0.39; 0.70
Volume V/F (L/m^2)	664.5 (4.1)	653 (3.5)	668.5	617.1; 757.1
Clearance CL/F (L/h/m^2)	36.8 (5.8)	36.5 (5.2)	33.5	30.5; 37.9
Covariates				
AST on CL/F		−0.3 (39.3)	−0.24	−0.12; −0.36
Inter-patient variabilities (IIV) *				
Absorption lag time T_{lag}	0.68 (14.4)	0.67 (14.1)	0.69	0.54; 0.88
Absorption rate constant k_a	0.88 (16)	0.87 (14.8)	0.86	0.34; 1.19
Volume V/F	0.076 (58)	0.04 (86)	0.06	0.02; 0.26
Clearance CL/F	0.29 (16.7)	0.26 (16.3)	0.24	0.15; 0.30
Inter-occasion variabilities (IOV)				
Clearance CL/F	0.13 (28)	0.12 (25.4)	0.13	0.09; 0.18
Residual proportional error	0.32 (4.7)	0.32 (4.7)	0.32	0.26; 0.39
2 × Log-likelihood value (OFV)	3198	3191.6		

* RSE%, relative standard error; IIV and IOV are reported as a standard deviation.

The diagnostic plots of the final pharmacokinetic model are shown in Figure 2. The goodness-of-fit plots based on the model observations and predictions did not show any significant bias or model misfits (Figure 2a–d). In addition, the prediction-corrected visual predictive checks based on model simulations showed that the central tendency and the variability of the palbociclib data both after a single dose and at steady state were accurately described by the final population pharmacokinetic model (Figure 2e,f).

The precision of the population parameter estimates for the final model was further assessed using non-parametric bootstraps. The estimated population parameters were close to the mean of the bootstrap estimates, and none of the 90% confidence intervals included a value of zero (Table 2).

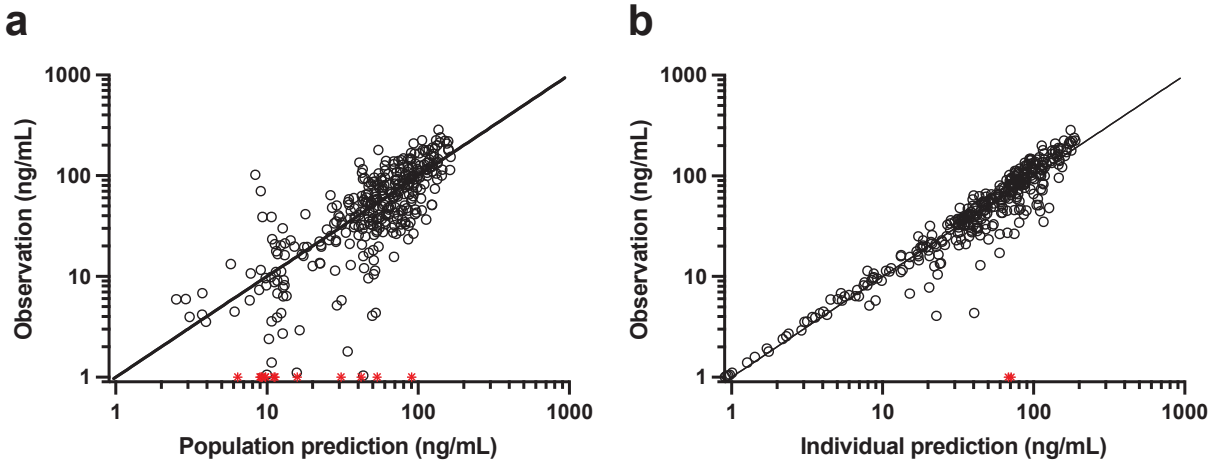


Figure 2. *Cont.*

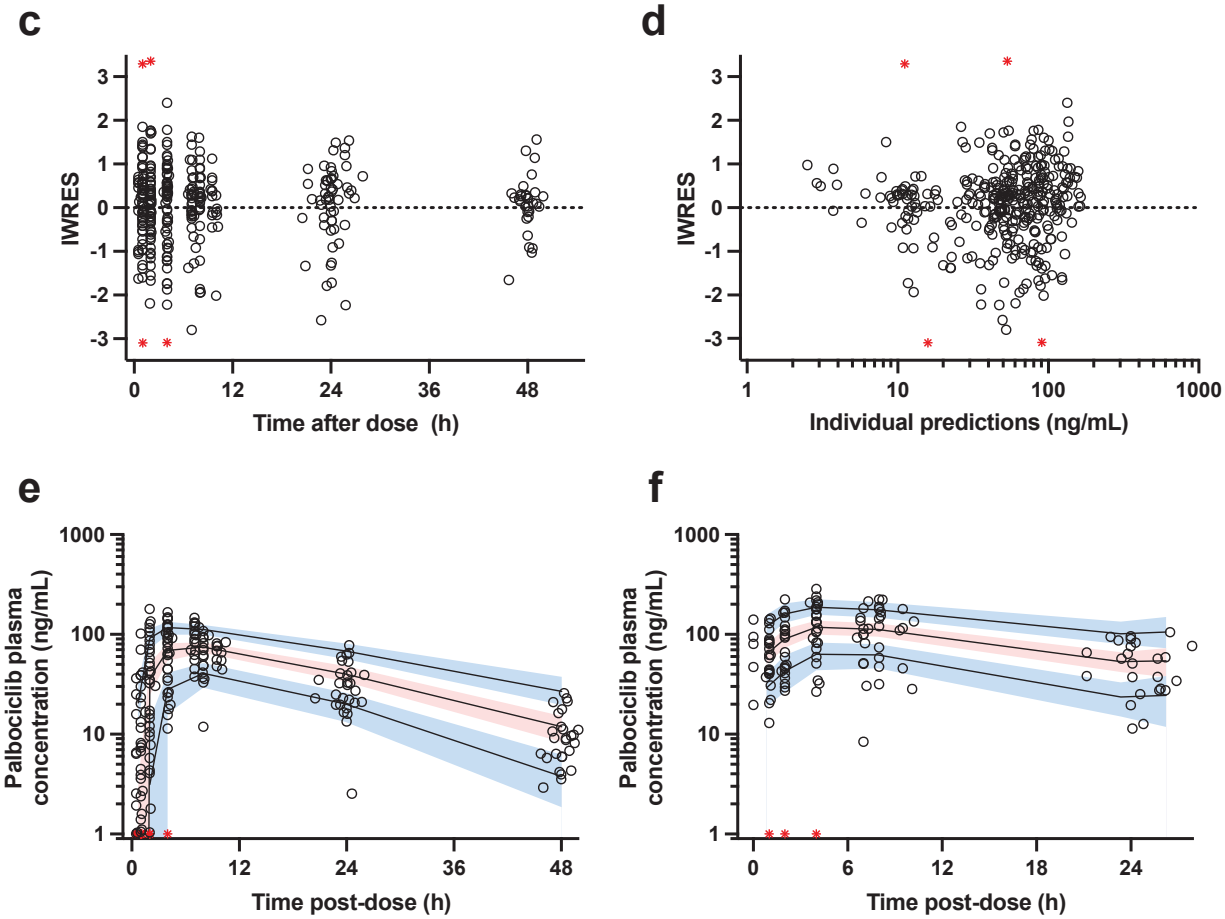


Figure 2. Diagnostic plots for the population pharmacokinetic model. (**a**) Observed concentration–time data vs. population, (**b**) individual model predictions, (**c**) individual weighted residuals (IWRES) vs. time, and (**d**) model predictions. In panels (**a**,**b**), solid lines represent the unity line and red crosses are data below the limit of quantification. The bottom plots show (**e**) the prediction-corrected visual predictive checks for single-dose and (**f**) steady-state data. Circles are observed data, stars in a red color are data below the limit of quantification, the solid lines depict the model-predicted 5th, 50th, and 95th percentiles, respectively, and the shaded areas represent the 90th confidence interval around the model-predicted percentiles.

3.3. Summary of Pharmacodynamic Data

Of the 33 patients used for the population PK model, 2 individuals were not included in the pharmacodynamic analysis as they only had a single ANC and PLT observation collected before the administration of the palbociclib dose. A total of 190 ANCs and 189 PLT observations from 31 individuals were available during course 1 (until the beginning of course 2, day 1). A total of 99 ANCs and PLT observations from 21 individuals were available during course 2 (until the beginning of course 3, day 1). A total of 54 ANCs and 55 PLT observations from six individuals were available during courses 3 and 4. An average of 11 ANC and PLT data points were collected for each patient over all courses.

3.4. Population Pharmacodynamic Parameter Estimation—ANC

We used the ANC data for the first two courses of palbociclib to evaluate the population pharmacodynamic parameters. A summary of the population pharmacodynamic parameters is shown in Table 3A, the goodness-of-fit plots are shown in Figure 3a,b, and individual ANC vs. time plots of the model fits are shown in Figure S2. Based on the individual model estimates, the estimated median (5th–95th percentile) time below an ANC of $1.5 \times 10^3/\mu L$ (i.e., grade 2 neutropenia), $1.0 \times 10^3/\mu L$ (i.e., grade 3 neutropenia), and

$0.5 \times 10^3/\mu L$ (i.e., grade 4 neutropenia) was 15 (0, 35), 4 (0, 21), and 0 (0, 11) days/course for the first two courses, respectively. In addition, the estimated median (5th–95th percentile) nadir based on data from the first two courses was 1.0 (0.4, 3.3) $\times 10^3/\mu L$.

Using the six individuals who also had course 3 and 4 ANC data, we determined the ability to predict these next two courses of treatment given the PKs from course 1 and the PD estimates based on data from courses 1 and 2. Figure S2 shows the individual ANC vs. time plots for all four courses for these six individuals, visually indicating that courses 3 and 4 are described well by the individual model fits to the first two courses. Additionally, we evaluated the residuals (the percent difference between the observed and estimated ANC) during courses 1 and 2 vs. 3 and 4. We observed no bias in the residuals in either group (median [5th–95th percentile]: −1.5% [−41%, 38%], $p = 0.16$, and −6.1% [−69%, 55%], $p = 0.22$, respectively), and the difference in the bias between the two groups was not significant ($p = 0.1$).

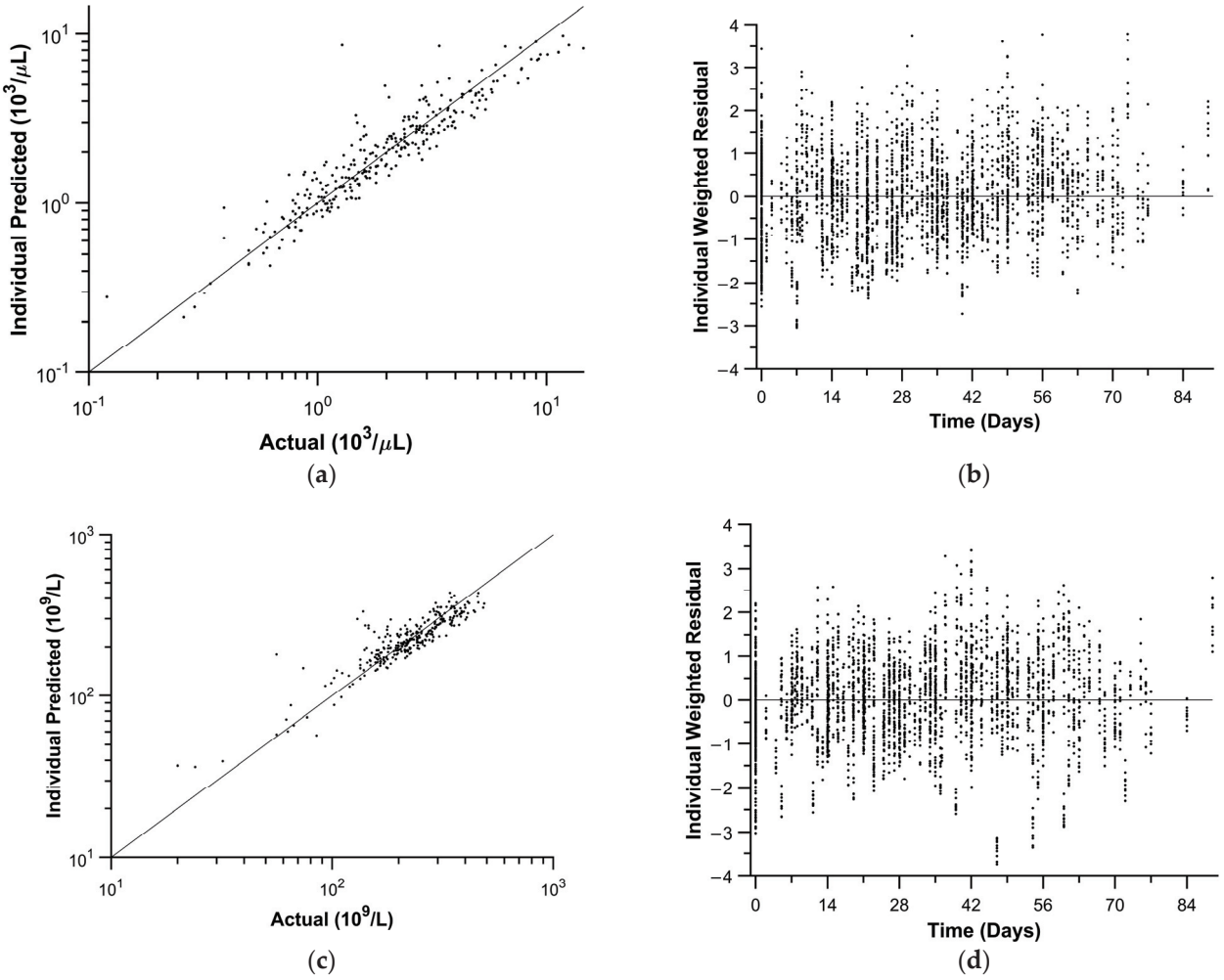


Figure 3. Pharmacodynamic model goodness-of-fit plots for ANC: (**a**) Actual vs. individual predicted ANC. (**b**) Individual weighted residuals for ANC. Pharmacodynamic model goodness-of-fit plots for PLT: (**c**) Actual vs. individual predicted PLT. (**d**) Individual weighted residuals for PLT.

Table 3. (**A**) Population PD parameter estimates for ANC model. (**B**) Population PD parameter estimates for PLT model.

(A)						
Parameter	**Population Estimate**	**RSE (%)**	**IIV (CV%)**	**RSE (%)**	**IOV (CV%)**	**RSE (%)**
N_{circ0} ($10^3/\mu L$)	3.95	8.7	47.0	13.9		
k_{in} (1/days)	0.90	8.6	29.4	50.2	14.3	54.3
k_{bp} (1/days)	0.78	3.5	1.5	203.4	5.8	123.7
k_{out} (1/days)	4.80	Fixed	Fixed			
IC_{50} (nM)	383.5	17.8	25.6	53.0	24.2	149.4
n	1	Fixed	Fixed			
Residual error						
b	0.29	6.0				
(B)						
Parameter	**Population Estimate**	**RSE (%)**	**IIV (CV%)**	**RSE (%)**	**IOV (CV%)**	**RSE (%)**
N_{circ0} ($10^9/L$)	267.40	4.2	21.4	14.4		
k_{in} (1/days)	0.93	3.3	7.6	39.4	4.1	43.8
k_{bp} (1/days)	0.52	5.9	7.6	99.1	5.9	57.2
k_{out} (1/days)	4.80	Fixed	Fixed			
IC_{50} (nM)	559.14	11.2	33.0	33.6	19.6	72.8
n	1	Fixed	Fixed			
Residual error						
b	0.20	6.0				

3.5. Population Pharmacodynamic Parameter Estimation—Platelets

We then used the PLT data for the first two courses of palbociclib to evaluate the population pharmacodynamic parameters. A summary of the population parameters is shown in Table 3B, goodness-of-fit plots are shown in Figure 3c,d, and individual PLT vs. time plots of the model fits are shown in Figure S3. Based on the individual model estimates, only three individuals had grade 1 ($<100 \times 10^9/\mu L$) or greater thrombocytopenia (one grade 1, one grade 2, and one grade 3). In addition, the estimated median (5th–95th percentile) nadir was 169 (59, 240) $\times 10^9/\mu L$.

Using the six patients who also had course 3 and 4 PLT data, we determined the ability to predict these next two courses of treatment given the PKs from course 1 and the PD estimates based on data from courses 1 and 2. Figure S3 shows the individual PLT vs. time plots for all four courses in these six individuals, visually indicating that courses 3 and 4 are described well by the individual model fits to the first two courses. Additionally, we evaluated the residuals (the percent difference between the observed and estimated PLT) during courses 1 and 2 vs. 3 and 4. We observed no bias in the residuals in courses 1 and 2 (median [5th–95th percentile]: −1.9% [−26%, 28%], $p = 0.08$), though there was some bias (over-predicting the PLT depletion) in courses 3 and 4 (−8.0% [−37%, 18%], $p = 4 \times 10^{-4}$). The difference in the bias between the two groups was also significant ($p = 0.006$).

3.6. Pharmacodynamic Simulations

To assess the extent of myelosuppression expected at clinically relevant dosages, we simulated the effects of a fixed palbociclib dosage of either 50, 75, or 95 mg/m^2/day for 21 days on the duration and extent of ANC and PLT depletion. In these simulations, we used PD parameters sampled from each patient's conditional distribution (n = 10 per individual). These results are summarized in Figure 4 and Table 4. These simulations show that given a 50 mg/m^2 dose, 19% of the individuals are expected to have grade 3 or greater neutropenia and none are expected to have grade 3 or greater thrombocytopenia. Furthermore, the median (5th–95th percentile) duration of grade 3 or greater neutropenia was 0 (0, 16) and 12 (0, 30) days for a 50 and 95 mg/m^2 dose, respectively. In addition, given

a 95 mg/m^2 dose, 69% of the individuals are expected to have grade 3 or greater neutropenia and 6% of the individuals are expected to have grade 3 or greater thrombocytopenia, and the median (5th–95th percentile) duration of grade 3 or greater thrombocytopenia was 0 (0, 0) and 0 (0, 11) days for a 50 and 95 mg/m^2 dose, respectively.

To assess the effect of prior myelosuppressive therapy on myelosuppression, we simulated patients subdivided by stratum, and our simulations show that given a dosage of 75 mg/m^2, more grade 3 neutropenia would be expected in a heavily pretreated patient (i.e., stratum 2) than a patient who was not heavily pretreated (i.e., stratum 1) (75% vs. 35%; $p = 2 \times 10^{-18}$; Figure S4) and more grade 3 thrombocytopenia would be expected in stratum 2 vs. 1 (15% vs. 0%; $p = 3 \times 10^{-13}$; Figure S5).

Table 4. Estimated nadir and duration of ANC and PLT depletion when given palbociclib 50, 75, or 95 mg/m^2/day for 21 days.

Nadir of ANC	**50 mg/m^2/day**	**75 mg/m^2/day**	**95 mg/m^2/day**
% <1.5 × 10^3/μL	45	72	79
% <1.0 × 10^3/μL	19	49	69
% <0.5 × 10^3/μL	3.1	13	32
Duration of ANC depletion (days); median (5th–95th percentile)			
Days < 1.5 × 10^3/μL	0 (0, 28)	15 (0, 34)	20 (0, 39)
Days < 1.0 × 10^3/μL	0 (0, 16)	0 (0, 24)	12 (0, 30)
Days < 0.5 × 10^3/μL	0 (0, 0)	0 (0, 11)	0 (0, 19)
Nadir of PLT	**50 mg/m^2/day**	**75 mg/m^2/day**	**95 mg/m^2/day**
% <100 × 10^9/L	6	8	12
% <50 × 10^9/L	0	6	6
% <25 × 10^9/L	0	0	3
Duration of PLT depletion (days); median (5th–95th percentile)			
Days < 100 × 10^9/L	0 (0, 1)	0 (0, 13)	0 (0, 16)
Days < 50 × 10^9/L	0 (0, 0)	0 (0, 6)	0 (0, 11)
Days < 25 × 10^9/L	0 (0, 0)	0 (0, 0)	0 (0, 0)

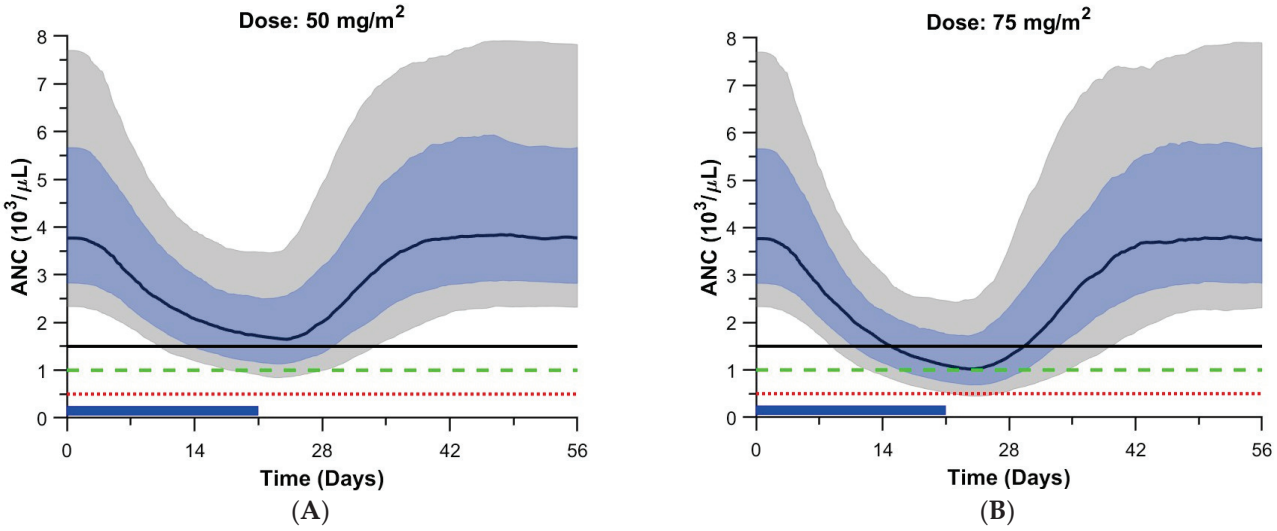


Figure 4. *Cont.*

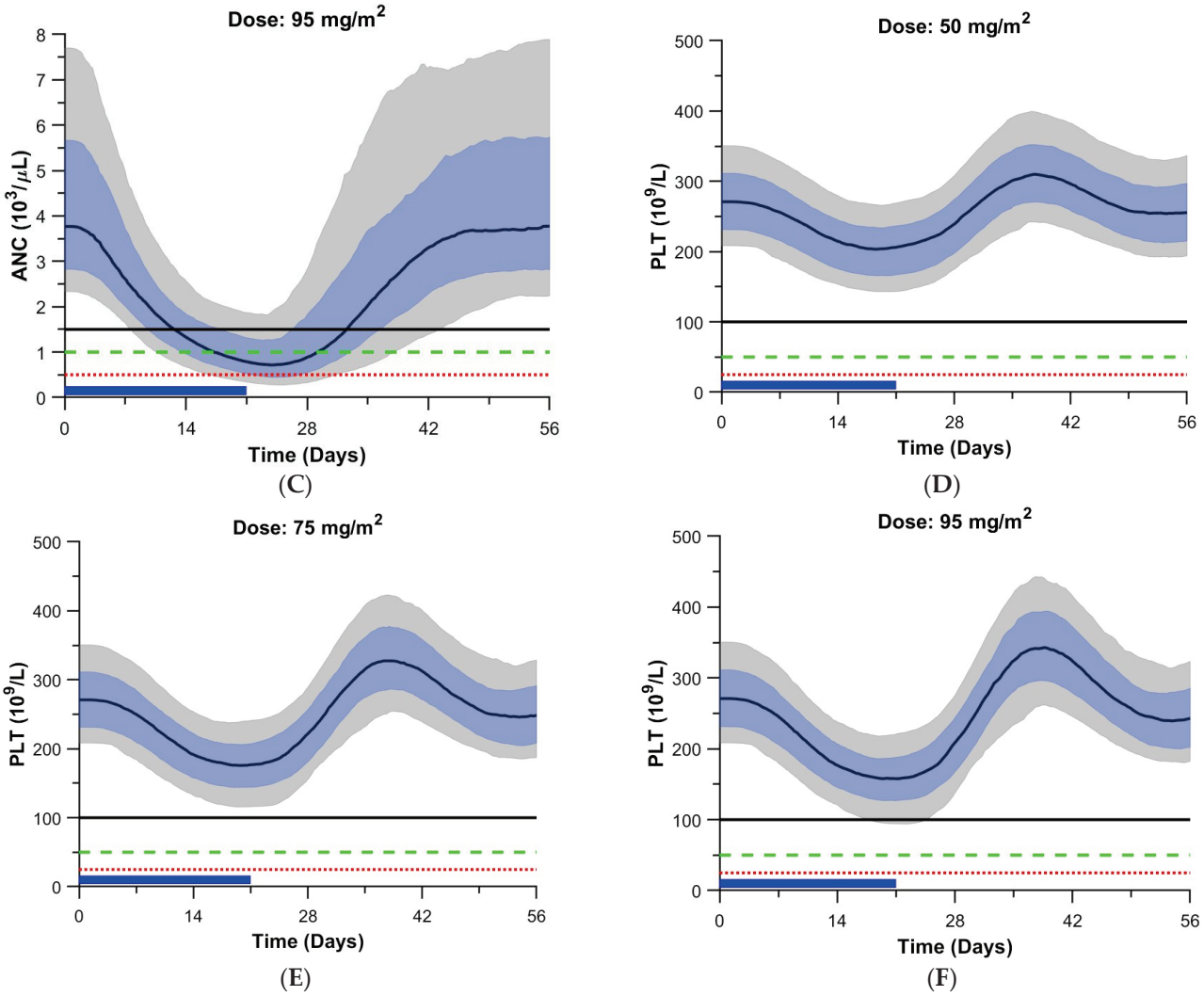


Figure 4. Pharmacodynamic simulations: (**A**): Simulated ANC vs. time for 50 mg/m^2/day palbociclib for 21 days. (**B**): Simulated ANC vs. time for 75 mg/m^2/day palbociclib for 21 days. (**C**): Simulated ANC vs. time for 95 mg/m^2/day palbociclib for 21 days. (**D**): Simulated PLT vs. time for 50 mg/m^2/day palbociclib for 21 days. (**E**): Simulated PLT vs. time for 75 mg/m^2/day palbociclib for 21 days. (**F**): Simulated PLT vs. time for 95 mg/m^2/day palbociclib for 21 days. For all panels of Figure 4—blue bar: dosing interval; black solid line, green dashed line, and red dotted line: mild neutropenia or thrombocytopenia (100 × 10^9/L), moderate neutropenia (1.0 × 10^3/μL) or thrombocytopenia (50 × 10^9/L), and severe neutropenia (0.5 × 10^3/μL) or thrombocytopenia (25 × 10^9/L); black curve: median ANC or PLT; blue shaded region: 25th–75th percentiles; gray shaded region: 5th–95th percentiles.

4. Discussion

The population pharmacokinetics and pharmacodynamics of palbociclib, a CDK4/6 inhibitor, were characterized for the first time in children and young adults with recurrent, progressive, and refractory brain tumors. The results of the covariate analysis showed that the apparent oral clearance of palbociclib was influenced by baseline AST values. Specifically, a 2.5-fold increase in the baseline AST was associated with a 2-fold lower apparent oral palbociclib clearance. Additionally, the ANC and PLT data during the first two courses were well described. Based on the individual model estimates for the ANC and PLT for the first two courses, we predicted the ANC data for six patients for courses 3 and 4 without bias, but the PLT data were biased and slightly over-predicted.

Prior to the current report, only one study had published pharmacokinetic data for palbociclib in pediatric oncology patients. Raetz and colleagues studied the disposition of palbociclib in 12 children with acute lymphoblastic leukemia or lymphoma enrolled in a phase I study [22]. They obtained serial samples on days 1 and 11 for up to 24 h after the oral dose. Both capsule (n = 3) and liquid formulations (n = 9) were used in this study, and a noncompartmental pharmacokinetic analysis approach was used. They reported a mean (range) steady state apparent oral clearance of 40.4 (21.1–102.0) L/h/m^2 and a half-life of 27.9 (4.5–86.8) hours [22].

In adult patients, the results of several population pharmacokinetic studies have been published. Royer and colleagues published the first population pharmacokinetic study of palbociclib utilizing retrospective data collected from therapeutic drug monitoring [15]. Although they studied 124 patients, they only had 151 samples for model building. A one-compartment model with a first-order absorption (Ka), an absorption lag time, and a combined error model was used to describe their data. The noise in the real-world data limited their ability to estimate the parameters of their model (e.g., the absorption); however, their estimate of a palbociclib apparent oral clearance of 58 L/h (34 L/h/m^2) compares well with the one from the present study. They found that the creatinine clearance (CrCl) estimated using the Cockcroft–Gault method, which includes the variables of age, gender, weight, and serum creatinine, was a significant covariate. As the CrCl decreased, the palbociclib apparent oral clearance decreased, and the AUC increased.

That same group conducted a population pharmacokinetic/pharmacodynamic study of palbociclib using therapeutic drug monitoring data for 143 patients, which were retrieved retrospectively from the patient record management software [16]. Similarly to Royer, these authors used a one-compartment model with a first-order absorption (Ka), an absorption lag time, and a combined error model to describe their data. They estimated the palbociclib apparent oral clearance as 57 L/h (34 L/h/m^2), which is remarkably similar to that of Royer and not unexpectedly compares to the one from the present study. As with the study by Royer, these authors also found that CrCl was a significant covariate for the palbociclib apparent oral clearance. However, these authors also found that a hepatic biomarker (alkaline phosphatase; ALP) was a significant covariate for the palbociclib apparent oral clearance with increasing ALP associated with a decreasing palbociclib clearance and increased systemic exposure.

Lastly, Courlet and colleagues conducted a population pharmacokinetic study in adults using data from a clinical trial aimed at optimizing oral targeted anticancer therapies (OpTAT; NCT04484064) [23]. The authors obtained blood samples at routine visits and serial sampling up to 12 h in 45 women with metastatic breast cancer receiving palbociclib. Differently from the Royer analysis, these authors used a two-compartment model with first-order absorption, a lag-time, and a proportional error model to describe their data. The palbociclib apparent oral clearance from their analysis was 67 L/h (39 L/h/m^2), which was similar to both Royer and the current analysis. In this analysis, the palbociclib apparent oral clearance was increased by 56% when taken under fasting conditions along with concomitant proton pump inhibitors; however, the authors never specify exactly which PPIs these patients were administered nor the exact palbociclib formulation used.

The results of our covariate analysis showed that aspartate aminotransferase (AST) was a significant covariate for the palbociclib apparent oral clearance. Our covariate analysis included a measure of renal function (i.e., the estimated GFR) as well as age and BW, but none of these covariates had a significant impact on the palbociclib apparent oral clearance as found by Royer or Marouille in their analyses [15,16]. We did find that a marker of hepatic function, AST, was associated with the palbociclib apparent oral clearance, similarly to that of Royer. Moreover, as reported by those authors, an increase in AST was associated with a decrease in the palbociclib apparent oral clearance and an increase in the palbociclib systemic exposure.

The results of the first phase I studies in adults showed that myelosuppression was the primary dose-limiting toxicity for palbociclib. Thus, investigators performed

exploratory pharmacokinetic and pharmacodynamic analyses of the relation between palbociclib systemic exposure and the ANC and platelet levels during the first two courses of treatment [24,25]. Using a simple Emax model, they established a relationship between the change in the ANC and platelet levels versus the palbociclib plasma exposure with increasing exposures resulting in a saturable decrease from the baseline for both the ANC and platelets. Subsequent studies used a more mechanistic population pharmacokinetic/pharmacodynamic modeling approach based on a previously described semi-mechanistic physiological model developed to describe the effects of cytotoxic chemotherapy agents on neutrophils but not platelets [26]. Although the Friberg approach initially was intended to model the neutropenic effects of cytotoxic chemotherapy, these investigators found that it performed well at modeling the cytostatic effects of palbociclib [16,27,28]. This model has also been used to model the cytostatic effects of other CDK4/6 inhibitors such as ribociclib [29] and trilaciclib [30].

Similarly to the results observed in the adult phase I studies, the recent pediatric phase I study of palbociclib also reported myelosuppression as the most common dose-limiting toxicity [8]. A preliminary regression analysis demonstrated that higher values of the palbociclib Cmax and AUC were associated with more severe (grade 3 or 4) neutropenia and leukopenia [8]. These observations prompted this more thorough analysis of the relation between palbociclib systemic exposure and the ANC and platelet levels. We modeled both the ANC and PLT data in the current study using our previously developed mechanistic mathematical model originally developed to quantify temozolomide myelosuppression [31] and later modified to quantify topotecan neutropenia and thrombocytopenia in neuroblastoma [21]. The results of our current analysis compare closely to several other studies. For example, the baseline ANC ($CIRC_0$) for our model was $3.95 \times 10^3/\mu L$, which compares favorably with $3.63 \times 10^3/\mu L$ from Sun [27], $2.94 \times 10^3/\mu L$ from Marouille [16], and $3.36 \times 10^3/\mu L$ from Jian [28]. In addition, the MTT (the time for committed stem cells to pass through the maturation compartments before entering the circulation) in the three published adult PK/PD studies ranged from 4.33 to 8.25 days, which was similar to the 5.12 days estimated from our current study.

Since six patients had ANC data from the third and fourth courses, we determined the ability of our pharmacodynamic model to use course 1 and 2 individual PD and PK estimates to predict the PD profile for courses 3 and 4. The lack of bias in the residuals indicated that our model was capable of predicting course 3 and 4 ANC values well and that the decreases in ANCs were not cumulative. This observation was consistent with that made in the early phase I study of Schwartz and colleagues [24]. In a larger population PK/PD analysis, Sun and his group also noted neutropenia associated with palbociclib administration was reversible and not cumulative [27].

Using our pharmacodynamic model, we simulated the extent of myelosuppression expected at clinically relevant palbociclib dosages (between 50 and 95 mg/m^2). The simulations provide a quantitative and mechanistic approach to predict the ANC and PLT concentrations expected at any clinically relevant palbociclib dosage. For example, the model predicted that given a palbociclib dosage of 75 mg/m^2, approximately half the patients would have grade 3 or greater neutropenia.

The present study had several limitations. First, as with many pediatric population pharmacokinetic and pharmacodynamic studies, the number of patients studied was relatively small on course 1, day 1, and the number of patients with repeat studies on course 1, day 21 was even smaller. Another limitation of our study is the lack of external model validation. Due to the small patient population, the sample size was not large enough to derive an external validation group to further validate the model. Regardless, our pharmacokinetic and pharmacodynamic findings for this patient population agree with previously published adult results, and our PK/PD model could be very useful for predicting expected ANC- and PLT-related toxicities at relevant doses with the caveat that it will require prospective validation in an independent patient population.

5. Conclusions

This is the first population pharmacokinetic and pharmacodynamic study of palbociclib in children and adolescents with progressive brain tumors. Significant covariates associated with palbociclib disposition identified in our analysis included a decreased apparent oral clearance in patients with increased AST values. The ANC and PLT data during the first two courses were well described. Based on their individual model estimates for the ANC and PLT for the first two courses, we estimated the ANC data for six patients for courses 3 and 4 without bias, but the PLT data were biased and slightly over-predicted.

Supplementary Materials: The following supporting information can be downloaded at: https://www.mdpi.com/article/10.3390/pharmaceutics16121528/s1, Table S1: Comparison of the base pharmacokinetic model's objective function value (OFV) with models including single covariates on apparent clearance (Cl/F); Figure S1: Depicted below is the pharmacodynamic model scheme describing the ANC and platelet dynamics. The model for ANC consists of a bone marrow compartment with proliferating neutrophils, three transient compartments that represent the maturation process of the neutrophils from blasts to circulating neutrophils, and a circulating neutrophil compartment. The model included the negative feedback effects of endogenous G-CSF, which affected the growth rate of proliferating cells in a manner inversely proportional to the concentration of circulating neutrophils. We assumed that palbociclib only affected the proliferating neutrophils in the bone marrow compartment. We used a similar structural model for platelet dynamics; Figure S2_1: ANC vs Time Plots for patient #1. Right Axis: ANC ($10^3/\mu L$), black curve, model estimated curve; black dots measured ANC levels. Left Axis: palbociclib concentration (nM), red dotted curve, model estimated concentration. Horizontal black solid, green dashed, and red dotted lines: ANC thresholds of 1.5, 1.0, and $0.5 \times 10^3/\mu L$, respectively; Figure S2_5: ANC vs Time Plots for patient #5. Right Axis: ANC ($10^3/\mu L$), black curve, model estimated curve; black dots measured ANC levels. Left Axis: palbociclib concentration (nM), red dotted curve, model estimated concentration. Horizontal black solid, green dashed, and red dotted lines: ANC thresholds of 1.5, 1.0, and $0.5 \times 10^3/\mu L$, respectively; Figure S2_14: ANC vs Time Plots for patient #14. Right Axis: ANC ($10^3/\mu L$), black curve, model estimated curve; black dots measured ANC levels. Left Axis: palbociclib concentration (nM), red dotted curve, model estimated concentration. Horizontal black solid, green dashed, and red dotted lines: ANC thresholds of 1.5, 1.0, and $0.5 \times 10^3/\mu L$, respectively; Figure S2_21: ANC vs Time Plots for patient #21. Right Axis: ANC ($10^3/\mu L$), black curve, model estimated curve; black dots measured ANC levels. Left Axis: palbociclib concentration (nM), red dotted curve, model estimated concentration. Horizontal black solid, green dashed, and red dotted lines: ANC thresholds of 1.5, 1.0, and $0.5 \times 10^3/\mu L$, respectively; Figure S2_22: ANC vs Time Plots for patient #22. Right Axis: ANC ($10^3/\mu L$), black curve, model estimated curve; black dots measured ANC levels. Left Axis: palbociclib concentration (nM), red dotted curve, model estimated concentration. Horizontal black solid, green dashed, and red dotted lines: ANC thresholds of 1.5, 1.0, and $0.5 \times 10^3/\mu L$, respectively; Figure S2_25: ANC vs Time Plots for patient #25. Right Axis: ANC ($10^3/\mu L$), black curve, model estimated curve; black dots measured ANC levels. Left Axis: palbociclib concentration (nM), red dotted curve, model estimated concentration. Horizontal black solid, green dashed, and red dotted lines: ANC thresholds of 1.5, 1.0, and $0.5 \times 10^3/\mu L$, respectively; Figure S3_1: PLT vs Time Plots for patient #1. Right Axis: PLT ($10^9/L$), black curve, model estimated curve; black dots measured PLT levels. Left Axis: palbociclib concentration (nM), red dotted curve, model estimated concentration. Horizontal black solid, green dashed, and red dotted lines: PLT thresholds of 100, 50, and $25 \times 10^9/L$, respectively; Figure S3_5: PLT vs Time Plots for patient #5. Right Axis: PLT ($10^9/L$), black curve, model estimated curve; black dots measured PLT levels. Left Axis: palbociclib concentration (nM), red dotted curve, model estimated concentration. Horizontal black solid, green dashed, and red dotted lines: PLT thresholds of 100, 50, and $25 \times 10^9/L$, respectively; Figure S3_14: PLT vs Time Plots for patient #14. Right Axis: PLT ($10^9/L$), black curve, model estimated curve; black dots measured PLT levels. Left Axis: palbociclib concentration (nM), red dotted curve, model estimated concentration. Horizontal black solid, green dashed, and red dotted lines: PLT thresholds of 100, 50, and $25 \times 10^9/L$, respectively; Figure S3_21: PLT vs Time Plots for patient #21. Right Axis: PLT ($10^9/L$), black curve, model estimated curve; black dots measured PLT levels. Left Axis: palbociclib concentration (nM), red dotted curve, model estimated concentration. Horizontal black solid, green dashed, and red dotted lines: PLT thresholds of 100, 50, and $25 \times 10^9/L$, respectively; Figure S3_22:

PLT vs Time Plots for patient #22. Right Axis: PLT (10^9/L), black curve, model estimated curve; black dots measured PLT levels. Left Axis: palbociclib concentration (nM), red dotted curve, model estimated concentration. Horizontal black solid, green dashed, and red dotted lines: PLT thresholds of 100, 50, and 25 $\times$ 10^9/L, respectively; Figure S3_25: PLT vs Time Plots for patient #25. Right Axis: PLT (10^9/L), black curve, model estimated curve; black dots measured PLT levels. Left Axis: palbociclib concentration (nM), red dotted curve, model estimated concentration. Horizontal black solid, green dashed, and red dotted lines: PLT thresholds of 100, 50, and 25 $\times$ 10^9/L, respectively; Figure S4: Simulated ANC vs time given palbociclib dosages of 50, 75, and 95 mg/m^2/day for 21 days for Stratum 1 and 2. Horizontal black solid, green dashed, and red dotted lines: ANC thresholds of 1.5, 1.0, and 0.5 $\times$ 10^3/μL, respectively. Black curve: median ANC; Blue shaded region: 25–75th percentiles; Grey shaded region: 5–95th percentiles; Figure S5: Simulated PLT vs time given palbociclib dosages of 50, 75, and 95 mg/m^2/day for 21 days for Stratum 1 and 2. Horizontal black solid, green dashed, and red dotted lines: PLT thresholds of 100, 50, and 25 $\times$ 10^9/L, respectively. Black curve: median PLT; Blue shaded region: 25–75th percentiles; Grey shaded region: 5–95th percentiles.

Author Contributions: Conceptualization: C.F.S. and D.V.M.; methodology: J.C.P. and C.F.S.; formal analysis: J.C.P.; investigation: N.S.S. and C.F.S.; resources: C.F.S. and D.V.M.; data curation: N.S.S. and J.C.P.; writing—original draft preparation: J.C.P. and C.F.S.; writing—review and editing: J.C.P., N.S.S., D.V.M. and C.F.S.; supervision: C.F.S.; project administration: N.S.S. and C.F.S.; funding acquisition: C.F.S. and D.V.M. All authors have read and agreed to the published version of the manuscript.

Funding: This work was supported by a Cancer Center Support (CORE) Grant CA021765, 2UM1CA081457, and the American Lebanese Syrian Associated Charities (ALSACs). The content is solely the responsibility of the authors and does not necessarily represent the official views of the National Institutes of Health.

Institutional Review Board Statement: This multi-institutional study was conducted in accordance with the Declaration of Helsinki, and approved by the following Institutional Review Boards: Children's Hospital of Los Angeles (CHLA) IRB on 10/08/2014; Baylor College of Medicine IRB on 10/22/2014; Children's National Medical Center IRB on 10/22/2014; The Ann & Robert H. Lurie Children's Hospital of Chicago IRB on 10/28/2014; Cincinnati Children's Hospital Medical Center IRB on 10/28/2014; St. Jude Children's Research Hospital IRB on 10/28/2014; Duke University Health System IRB on 11/14/2014; Stanford University IRB on 11/24/2014; Seattle Children's Hospital IRB on 12/04/2014; Memorial Sloan Kettering Cancer Center IRB on 12/17/2014; University of Pittsburgh IRB on 12/22/2014.

Informed Consent Statement: Informed consent was obtained from all subjects involved in the study.

Data Availability Statement: Any requests for data from this study must be made in writing to the PBTC Operations, Biostatistics, and Data Management Core Executive Director.

Acknowledgments: The authors would like to acknowledge the research nurses and CRA staff at each of the PBTC sites who participated in this clinical trial and provided support to this population PKPD study. We also acknowledge the infrastructure support for the PBTC operation's core personnel. Pfizer provided palbociclib and financial support for the trial conduction, patient research costs, operations costs, and correlative studies. Pfizer reviewed the manuscript but did not have a direct role in the trial design, patient recruitment, data collection, analyses, or manuscript preparation. Lastly, the authors would like to acknowledge Justin T. Hoffman as a technical clinical pharmacology subject matter expert who provided assistance with this study.

Conflicts of Interest: The authors have no conflicts of interest to declare.

References

1. Ostrom, Q.T.; Patil, N.; Cioffi, G.; Waite, K.; Kruchko, C.; Barnholtz-Sloan, J.S. CBTRUS Statistical Report: Primary Brain and Other Central Nervous System Tumors Diagnosed in the United States in 2013–2017. *Neuro-oncology* **2020**, *22*, iv1–iv96. [CrossRef] [PubMed]
2. Plant-Fox, A.S.; O'Halloran, K.; Goldman, S. Pediatric brain tumors: The era of molecular diagnostics, targeted and immune-based therapeutics, and a focus on long term neurologic sequelae. *Curr. Probl. Cancer* **2021**, *45*, 100777. [CrossRef] [PubMed]

3. Weiser, A.; Sanchez Bergman, A.; Machaalani, C.; Bennett, J.; Roth, P.; Reimann, R.R.; Nazarian, J.; Guerreiro Stucklin, A.S. Bridging the age gap: A review of molecularly informed treatments for glioma in adolescents and young adults. *Front. Oncol.* **2023**, *13*, 1254645. [CrossRef] [PubMed]
4. Chen, F.; Chandrashekar, D.S.; Scheurer, M.E.; Varambally, S.; Creighton, C.J. Global molecular alterations involving recurrence or progression of pediatric brain tumors. *Neoplasia* **2022**, *24*, 22–33. [CrossRef]
5. Gajjar, A.; Mahajan, A.; Abdelbaki, M.; Anderson, C.; Antony, R.; Bale, T.; Bindra, R.; Bowers, D.C.; Cohen, K.; Cole, B.; et al. Pediatric Central Nervous System Cancers, Version 2.2023, NCCN Clinical Practice Guidelines in Oncology. *J. Natl. Compr. Cancer Netw.* **2022**, *20*, 1339–1362. [CrossRef]
6. Miklja, Z.; Pasternak, A.; Stallard, S.; Nicolaides, T.; Kline-Nunnally, C.; Cole, B.; Beroukhim, R.; Bandopadhayay, P.; Chi, S.; Ramkissoon, S.H.; et al. Molecular profiling and targeted therapy in pediatric gliomas: Review and consensus recommendations. *Neuro-oncology* **2019**, *21*, 968–980. [CrossRef]
7. Paugh, B.S.; Zhu, X.; Qu, C.; Endersby, R.; Diaz, A.K.; Zhang, J.; Bax, D.A.; Carvalho, D.; Reis, R.M.; Onar-Thomas, A.; et al. Novel oncogenic PDGFRA mutations in pediatric high-grade gliomas. *Cancer Res.* **2013**, *73*, 6219–6229. [CrossRef]
8. Van Mater, D.; Gururangan, S.; Becher, O.; Campagne, O.; Leary, S.; Phillips, J.J.; Huang, J.; Lin, T.; Poussaint, T.Y.; Goldman, S.; et al. A phase I trial of the CDK 4/6 inhibitor palbociclib in pediatric patients with progressive brain tumors: A Pediatric Brain Tumor Consortium study (PBTC-042). *Pediatr. Blood Cancer* **2021**, *68*, e28879. [CrossRef]
9. Glade Bender, J.L.; Lee, A.; Reid, J.M.; Baruchel, S.; Roberts, T.; Voss, S.D.; Wu, B.; Ahern, C.H.; Ingle, A.M.; Harris, P.; et al. Phase I pharmacokinetic and pharmacodynamic study of pazopanib in children with soft tissue sarcoma and other refractory solid tumors: A children's oncology group phase I consortium report. *J. Clin. Oncol.* **2013**, *31*, 3034–3043. [CrossRef]
10. Spring, L.M.; Zangardi, M.L.; Moy, B.; Bardia, A. Clinical Management of Potential Toxicities and Drug Interactions Related to Cyclin-Dependent Kinase 4/6 Inhibitors in Breast Cancer: Practical Considerations and Recommendations. *Oncologist* **2017**, *22*, 1039–1048. [CrossRef]
11. Hu, W.; Sung, T.; Jessen, B.A.; Thibault, S.; Finkelstein, M.B.; Khan, N.K.; Sacaan, A.I. Mechanistic Investigation of Bone Marrow Suppression Associated with Palbociclib and its Differentiation from Cytotoxic Chemotherapies. *Clin. Cancer Res.* **2016**, *22*, 2000–2008. [CrossRef] [PubMed]
12. Finn, R.S.; Martin, M.; Rugo, H.S.; Jones, S.; Im, S.A.; Gelmon, K.; Harbeck, N.; Lipatov, O.N.; Walshe, J.M.; Moulder, S.; et al. Palbociclib and Letrozole in Advanced Breast Cancer. *N. Engl. J. Med.* **2016**, *375*, 1925–1936. [CrossRef] [PubMed]
13. Turner, N.C.; Ro, J.; Andre, F.; Loi, S.; Verma, S.; Iwata, H.; Harbeck, N.; Loibl, S.; Huang Bartlett, C.; Zhang, K.; et al. Palbociclib in Hormone-Receptor-Positive Advanced Breast Cancer. *N. Engl. J. Med.* **2015**, *373*, 209–219. [CrossRef]
14. Sun, W.; Klamerus, K.J.; Yuhas, L.M.; Pawlak, S.; Plotka, A.; O'Gorman, M.; Kirkovsky, L.; Kosa, M.; Wang, D. Impact of Acid-Reducing Agents on the Pharmacokinetics of Palbociclib, a Weak Base with pH-Dependent Solubility, with Different Food Intake Conditions. *Clin. Pharmacol. Drug Dev.* **2017**, *6*, 614–626. [CrossRef]
15. Royer, B.; Kaderbhaï, C.; Fumet, J.D.; Hennequin, A.; Desmoulins, I.; Ladoire, S.; Ayati, S.; Mayeur, D.; Ilie, S.; Schmitt, A. Population Pharmacokinetics of Palbociclib in a Real-World Situation. *Pharmaceuticals* **2021**, *14*, 181. [CrossRef]
16. Marouille, A.L.; Petit, E.; Kaderbhaï, C.; Desmoulins, I.; Hennequin, A.; Mayeur, D.; Fumet, J.D.; Ladoire, S.; Tharin, Z.; Ayati, S.; et al. Pharmacokinetic/Pharmacodynamic Model of Neutropenia in Real-Life Palbociclib-Treated Patients. *Pharmaceutics* **2021**, *13*, 1708. [CrossRef]
17. Beal, S.L. Ways to fit a PK model with some data below the quantification limit. *J. Pharmacokinet. Pharmacodyn.* **2001**, *28*, 481–504. [CrossRef] [PubMed]
18. Millisor, V.E.; Roberts, J.K.; Sun, Y.; Tang, L.; Daryani, V.M.; Gregornik, D.; Cross, S.J.; Ward, D.; Pauley, J.L.; Molinelli, A.; et al. Derivation of new equations to estimate glomerular filtration rate in pediatric oncology patients. *Pediatr. Nephrol.* **2017**, *32*, 1575–1584. [CrossRef]
19. Reddick, S.J.; Campagne, O.; Huang, J.; Onar-Thomas, A.; Broniscer, A.; Gajjar, A.; Stewart, C.F. Pharmacokinetics and safety of erlotinib and its metabolite OSI-420 in infants and children with primary brain tumors. *Cancer Chemother. Pharmacol.* **2019**, *84*, 829–838. [CrossRef]
20. Campagne, O.; Zhong, B.; Nair, S.; Lin, T.; Huang, J.; Onar-Thomas, A.; Robinson, G.; Gajjar, A.; Stewart, C.F. Exposure-Toxicity Association of Cyclophosphamide and Its Metabolites in Infants and Young Children with Primary Brain Tumors: Implications for Dosing. *Clin. Cancer Res.* **2020**, *26*, 1563–1573. [CrossRef]
21. Panetta, J.C.; Schaiquevich, P.; Santana, V.M.; Stewart, C.F. Using pharmacokinetic and pharmacodynamic modeling and simulation to evaluate importance of schedule in topotecan therapy for pediatric neuroblastoma. *Clin. Cancer Res.* **2008**, *14*, 318–325. [CrossRef] [PubMed]
22. Raetz, E.A.; Teachey, D.T.; Minard, C.; Liu, X.; Norris, R.E.; Denic, K.Z.; Reid, J.; Evensen, N.A.; Gore, L.; Fox, E.; et al. Palbociclib in combination with chemotherapy in pediatric and young adult patients with relapsed/refractory acute lymphoblastic leukemia and lymphoma: A Children's Oncology Group study (AINV18P1). *Pediatr. Blood Cancer* **2023**, *70*, e30609. [CrossRef] [PubMed]
23. Bandiera, C.; Cardoso, E.; Locatelli, I.; Digklia, A.; Zaman, K.; Diciolla, A.; Cristina, V.; Stravodimou, A.; Veronica, A.L.; Dolcan, A.; et al. Optimizing Oral Targeted Anticancer Therapies Study for Patients With Solid Cancer: Protocol for a Randomized Controlled Medication Adherence Program Along With Systematic Collection and Modeling of Pharmacokinetic and Pharmacodynamic Data. *JMIR Res. Protoc.* **2021**, *10*, e30090. [CrossRef] [PubMed]

24. Schwartz, G.K.; LoRusso, P.M.; Dickson, M.A.; Randolph, S.S.; Shaik, M.N.; Wilner, K.D.; Courtney, R.; O'Dwyer, P.J. Phase I study of PD 0332991, a cyclin-dependent kinase inhibitor, administered in 3-week cycles (Schedule 2/1). *Br. J. Cancer* **2011**, *104*, 1862–1868. [CrossRef]
25. Flaherty, K.T.; Lorusso, P.M.; Demichele, A.; Abramson, V.G.; Courtney, R.; Randolph, S.S.; Shaik, M.N.; Wilner, K.D.; O'Dwyer, P.J.; Schwartz, G.K. Phase I, dose-escalation trial of the oral cyclin-dependent kinase 4/6 inhibitor PD 0332991, administered using a 21-day schedule in patients with advanced cancer. *Clin. Cancer Res.* **2012**, *18*, 568–576. [CrossRef]
26. Friberg, L.E.; Henningsson, A.; Maas, H.; Nguyen, L.; Karlsson, M.O. Model of chemotherapy-induced myelosuppression with parameter consistency across drugs. *J. Clin. Oncol.* **2002**, *20*, 4713–4721. [CrossRef]
27. Sun, W.; O'Dwyer, P.J.; Finn, R.S.; Ruiz-Garcia, A.; Shapiro, G.I.; Schwartz, G.K.; DeMichele, A.; Wang, D. Characterization of Neutropenia in Advanced Cancer Patients Following Palbociclib Treatment Using a Population Pharmacokinetic-Pharmacodynamic Modeling and Simulation Approach. *J. Clin. Pharmacol.* **2017**, *57*, 1159–1173. [CrossRef]
28. Jian, W.; Xue, J.; Yao, Q.; Chen, R.; Yao, Y.; Wang, M.; Zhou, T. Starting dose selection of palbociclib in Chinese patients with breast cancer based on population kinetic-pharmacodynamic model of neutropenia. *Cancer Chemother. Pharmacol.* **2022**, *90*, 489–497. [CrossRef]
29. Lu, Y.; Yang, S.; Ho, Y.Y.; Ji, Y. Ribociclib Population Pharmacokinetics and Pharmacokinetic/Pharmacodynamic Analysis of Neutrophils in Cancer Patients. *J Clin. Pharmacol.* **2021**, *61*, 1054–1068. [CrossRef]
30. Li, C.; Hart, L.; Owonikoko, T.K.; Aljumaily, R.; Rocha Lima, C.M.; Conkling, P.R.; Webb, R.T.; Jotte, R.M.; Schuster, S.; Edenfield, W.J.; et al. Trilaciclib dose selection: An integrated pharmacokinetic and pharmacodynamic analysis of preclinical data and Phase Ib/IIa studies in patients with extensive-stage small cell lung cancer. *Cancer Chemother. Pharmacol.* **2021**, *87*, 689–700. [CrossRef]
31. Panetta, J.C.; Kirstein, M.N.; Gajjar, A.J.; Nair, G.; Fouladi, M.; Stewart, C.F. A mechanistic mathematical model of temozolomide myelosuppression in children with high-grade gliomas. *Math. Biosci.* **2003**, *186*, 29–41. [CrossRef] [PubMed]

Disclaimer/Publisher's Note: The statements, opinions and data contained in all publications are solely those of the individual author(s) and contributor(s) and not of MDPI and/or the editor(s). MDPI and/or the editor(s) disclaim responsibility for any injury to people or property resulting from any ideas, methods, instructions or products referred to in the content.

pharmaceutics

MDPI

Article

Population Pharmacokinetic Analysis and Simulation of Alternative Dosing Regimens for Biosimilars to Adalimumab and Etanercept in Patients with Rheumatoid Arthritis

Stephanie F. Ling [1,2], Kayode Ogungbenro [3], Adam S. Darwich [4], Amirah Binti Mohammad Ariff [1], Nisha Nair [1,2], James Bluett [1,2], Ann W. Morgan [5,6,7], John D. Isaacs [8,9], Anthony G. Wilson [10], Kimme L. Hyrich [2,11], Anne Barton [1,2] and Darren Plant [1,2,*]

[1] Centre for Genetics and Genomics Versus Arthritis, Centre for Musculoskeletal Research, The University of Manchester, Manchester M13 9PT, UK
[2] NIHR Manchester Biomedical Research Centre, Manchester University NHS Foundation Trust, Manchester Academic Health Science Centre, Manchester M13 9WL, UK
[3] Centre for Applied Pharmacokinetic Research, The University of Manchester, Manchester M13 9PT, UK
[4] Division of Health Informatics and Logistics, KTH Royal Institute of Technology, 11428 Stockholm, Sweden
[5] School of Medicine, University of Leeds, Leeds LS2 9JT, UK
[6] NIHR Leeds Biomedical Research Centre, Leeds Teaching Hospitals NHS Trust, Leeds LS7 4SA, UK
[7] NIHR In Vitro Diagnostic Co-Operative, Leeds Teaching Hospitals NHS Trust, Leeds LS9 7TF, UK
[8] Translational and Clinical Research Institute, Newcastle University, Newcastle-upon-Tyne NE1 7RU, UK
[9] Musculoskeletal Unit, Newcastle-upon-Tyne Hospitals NHS Foundation Trust, Newcastle-upon-Tyne NE7 7DN, UK
[10] School of Medicine and Medical Science, Conway Institute, University College Dublin, Dublin 4 Belfield, Ireland
[11] Centre for Epidemiology Versus Arthritis, Centre for Musculoskeletal Research, The University of Manchester, Manchester M13 9PT, UK
* Correspondence: darren.plant@manchester.ac.uk

Abstract: Efficacy to biologics in rheumatoid arthritis (RA) patients is variable and is likely influenced by each patient's circulating drug levels. Using modelling and simulation, the aim of this study was to investigate whether adalimumab and etanercept biosimilar dosing intervals can be altered to achieve therapeutic drug levels at a faster/similar time compared to the recommended interval. RA patients starting subcutaneous Amgevita or Benepali (adalimumab and etanercept biosimilars, respectively) were recruited and underwent sparse serum sampling for drug concentrations. Drug levels were measured using commercially available kits. Pharmacokinetic data were analysed using a population approach (popPK) and potential covariates were investigated in models. Models were compared using goodness-of-fit criteria. Final models were selected and used to simulate alternative dosing intervals. Ten RA patients starting the adalimumab biosimilar and six patients starting the etanercept biosimilar were recruited. One-compartment PK models were used to describe the popPK models for both drugs; no significant covariates were found. Typical individual parameter estimates were used to simulate altered dosing intervals for both drugs. A simulation of dosing the etanercept biosimilar at a lower rate of every 10 days reached steady-state concentrations earlier than the usual dosing rate of every 7 days. Simulations of altered dosing intervals could form the basis for future personalised dosing studies, potentially saving costs whilst increasing efficacy.

Keywords: rheumatoid arthritis; pharmacokinetics; population pharmacokinetics; simulation; biologics; biosimilars

1. Introduction

Rheumatoid arthritis (RA) is a chronic, autoimmune arthritis with multisystem involvement; permanent joint damage can occur if inflammation is not controlled promptly [1].

Biologic disease-modifying anti-rheumatic drugs (bDMARDs) are commonly used in patients with moderately-to-highly active RA; their prescription in the UK has increased since a reduction in thresholds to commence tumour necrosis factor inhibitors (TNFi, a class of bDMARD) [2]. The TNFi agents adalimumab and etanercept are self-administered by patients in pre-filled auto-injectors at set dosing intervals. Since 2013, a number of biosimilar bDMARDs have also been licensed for prescription for RA [3].

An inefficacy rate of $\leq$40% exists in TNFi [4]; one cause of inefficacy is sub-therapeutic drug levels [5]. Research has consistently demonstrated a significant association between adalimumab/etanercept drug levels and treatment response [5]. There is substantial variability in circulating drug levels between patients [5], referred to as between-subject variability (BSV) in drug exposure [6]. Pharmacokinetic (PK) models aim to describe how drug concentrations vary over time. In basic compartmental analysis, many PK models are structurally defined using "compartments", with each representing a hypothetical part of the body. A single compartment model represents a well-mixed and kinetically homogeneous body compartment, enabling the drug to be described with a single representative concentration at any given time point [7].

Individual PK studies employ detailed drug concentration−time data, which are typically analysed using non-compartmental models. By contrast, population (pop) PK modelling incorporates concentration−time data from multiple individuals and does not require rich or balanced drug concentration sampling [8]. PopPK modelling represents an approach for analysing PK study data; it can be used to analyse sparse data where the standard approach of non-compartmental analysis cannot be used. Typically, popPK models are used to quantify variability (e.g., BSV) in a population study and link this to sources (covariates) that can influence PK (e.g., age, sex). A number of popPK studies have been carried out in patients with RA starting the TNFi adalimumab [9,10] and etanercept [11–14]. However, only one popPK study has been published using an etanercept biosimilar in healthy subjects only [15], and no adalimumab biosimilar studies have been published.

This study aimed to carry out PK studies in RA patients starting biosimilars to adalimumab and etanercept (Amgevita and Benepali, respectively) in a cohort of real-world patients, analysing the data using a popPK modelling approach. Parameters from the models were then used to simulate PK profiles using altered dosing intervals to achieve maximal effect and/or steady-state at accelerated time points.

2. Materials and Methods

2.1. Study Aims and Design

1. To carry out PK studies in real-world patients with RA starting Amgevita and Benepali (adalimumab and etanercept biosimilars, respectively) using a popPK modelling approach.
2. To use parameters from the above popPK models to simulate PK profiles using altered dosing intervals to determine whether maximal effect and/or steady-state plasma drug levels can be attained at accelerated time points.

2.2. Study Setting

Patients with RA were recruited from rheumatology clinics in three centres based in Greater Manchester, UK, into the Biologics in RA Genetics and Genomics Study Syndicate [16] (BRAGGSS, Research Ethics Committee reference: 04/Q1403/37), a prospective multi-centre observational study based in the UK.

2.3. Study Participants

Patients with RA, according to the 1987 American College of Rheumatology classification criteria, were recruited to the Personalised Dosing sub-study of BRAGGSS (BRAGGSS-PD) in compliance with the Declaration of Helsinki. All participants gave written informed consent. As well as a clinical diagnosis of RA, inclusion criteria required participants to be starting Amgevita or Benepali (adalimumab and etanercept biosimilars, respectively), be

bDMARD-naïve, have a pre-treatment Disease Activity Score of 28 Joints (DAS28) $\geq$ 5.1 (indicating high disease activity) at the time of recruitment and be aged $\geq$ 18 years. At the time of the study, this DAS28 threshold was required by the National Institute for Health and Clinical Excellence (NICE) in England and Wales for patients to qualify to start a bDMARD. Patients were excluded if they did not fulfil all inclusion criteria. Participants were recruited between January 2019 and August 2021 and were followed up for a total of 12 weeks. The adalimumab and etanercept biosimilars were self-administered subcutaneously by patients at licensed doses of 40 mg every 14 days and 50 mg every 7 days, respectively. These specific biosimilars were selected for study because they are the two agents that have been approved locally for prescription by National Health Service (NHS) rheumatology departments in Greater Manchester, UK, where this study was carried out.

2.4. Sampling Schedules

Optimal sampling time intervals were proposed using previously defined popPK models from the literature in PopDes software v1, an application software that can be utilised for determining optimal sampling times or windows for popPK studies [17]; further information on this software is detailed in the Supplementary Methods. All samples were collected by the same investigator, and all doses given at study visits were also witnessed by that same investigator.

For the adalimumab biosimilar, a previous PK model derived for adalimumab originator [10] was used to simulate multiple dosing interval models. The optimal sampling design was determined to be at baseline (pre-treatment), 1 hour post-first dose, then 2, 4, 6 and 12 weeks post-first dose. Samples subsequent to the second sample were taken directly before the next dose in order to ensure true trough level sampling. For the etanercept biosimilar, previous PK models derived for etanercept originator [12,13,18] were utilised for simulation. The optimal sampling design was determined to be as for the adalimumab biosimilar, with an additional sampling time point at 6 days post-first dose.

2.5. Sample Processing

All participant samples were processed and stored at the Centre for Musculoskeletal Research (CfMR), the University of Manchester, Manchester, UK, and were processed by CfMR laboratory staff. All sample blood tubes were spun at 1720$\times$ *g* for 10 min, then serum was extracted into aliquots and stored in -150 °C freezers.

2.6. Measurement of Drug Levels

Drug level measurements were carried out by CfMR laboratory staff using commercially available ELISA-based test kits produced by Grifols International, SA (Barcelona, Spain). The Promonitor®-ADL-1DV kit was used to measure the adalimumab biosimilar drug levels and the Promonitor®-ETN-1DV kit was used to measure the etanercept biosimilar drug levels. Both had previously been validated [19,20]. Standard laboratory equipment and a spectrophotometer (SpectraMax® Plus 384 Microplate Reader, Molecular Devices, LLC, San Jose, CA, USA) were used during the experimental procedure. Samples were defrosted for two hours at room temperature prior to thorough mixing before the experimental procedure.

Serum drug levels were measured in triplicate using 96-microwell ELISA plates, which were pre-coated with anti-adalimumab and anti-etanercept human monoclonal antibody according to which drug was being measured. Patient samples were diluted to 1:50 concentration using a dilution buffer and were transferred to separate wells. Pre-diluted calibration samples and positive and negative controls were also included for the purposes of quantification of results and quality control; these were also transferred to separate wells. Any drug present in the patient samples, calibration samples and controls became bound to the immobilised anti-drug antibodies during an incubation period of one hour at room temperature. Following incubation, any unbound material was removed by washing the wells with a 20$\times$ buffer containing phosphate-buffered saline and tween-20. Each well was

then loaded with a second horseradish peroxidase-labelled anti-drug monoclonal antibody to form a sandwich complex. The plate was incubated for a further one hour at room temperature to allow the labelled antibody to bind to the drug attached to the microwells. Unbound enzyme-labelled antibody was again washed away with wash buffer, and a substrate of pre-diluted stabilised tetramethylbenzidine was added to measure enzyme activity. After 15 min, a stop reagent of pre-diluted sulphuric acid solution was added to halt the reaction. Colour intensity as a result of the enzymatic reaction was measured in triplicate using a spectrophotometer at wavelength 450 nm. The generated optical density values were proportional to the drug concentration in each sample.

Softmax Pro 7 software (compatible with the SpectraMax® Plus 384 Microplate Reader, Molecular Devices, LLC, San Jose, CA, USA) was used to interpolate the optical density values and determine drug level concentrations. Interpolated values were multiplied by the dilution factor ($\times 50$) to obtain drug levels in patient samples.

2.7. PopPK Analysis

(i) Software

PK data were analysed using a population approach with Monolix v.2019R2 software (Lixoft, Antony, France). This is a non-linear mixed-effects modelling software package based on the stochastic approximation expectation maximisation (SAEM) algorithm. Monolix works by optimising the maximum likelihood to produce optimal population parameter values; final estimates maximise the likelihood of data, given the model. The default simulated annealing option for SAEM was used in order to maintain a larger parameter space. A maximum of 500 iterations was set to ensure the best possible convergence. For medication doses that were self-administered by patients outside of study visits, nominal dose timings were used for the purpose of modelling.

(ii) PopPK analysis

For each drug studied, one-, two- or three-compartment mammillary models assuming first-order absorption and elimination were tested. Estimated PK parameters were given as apparent values due to extravascular administration via the subcutaneous route. PK parameters were parameterised as clearance (CL) and volume of distribution (V_D). Structural models were compared using the Akaike information criterion (AIC). BSV in PK parameters was described using an exponential model. For parameters where BSV could not be estimated, this was removed from the analysis and, therefore, only typical individual values were estimated. Correlations between parameters were tested. Additive, proportional or combined additive and proportional models were tested for residual unexplained variability (RUV). The following four covariates were investigated: age and body weight (continuous covariates) and sex and concurrent conventional synthetic disease-modifying anti-rheumatic drug (csDMARD) therapy (binary covariates). Covariate models were compared using both -2 log-likelihood (-2LL) and AIC. Models with the lowest significant -2LL value (assessed using a likelihood ratio χ^2 test, LRT) and the lowest AIC, with the simplest combination of covariates and between-variable correlations, were selected.

Goodness-of-fit (GOF) was visually assessed using plots of:

- Population-predicted (PRED) and individual-predicted (IPRED) measurements versus observed measurements (DV).
- IPRED and DV versus time.
- Residuals, represented in plots of:
    - Population weighted residual distributions (PWRES).
    - Individual weighted residual distributions (IWRES).
    - Normalised prediction distribution errors (NPDE). Distribution was tested using the Shapiro–Wilk test at a level of $\alpha = 0.05$.

(iii) Simulation of altered dosing intervals

Using model parameters estimated from final popPK models for each drug, simulations of altered dosing intervals were carried out in the R v.4.0.5 [21] base package. The ggplot2 [22] package was used to visualise simulations. Simulations of altered dosing intervals (with the same dose of pre-filled syringe as licensed) were carried out. For the adalimumab biosimilar, dosing intervals of 40 mg every 7 days, 14 days (usual interval) and 21 days were simulated. For the etanercept biosimilar, intervals of 50 mg every 5 days, 7 days (usual interval) and 10 days were simulated.

All methods above are described in more detail elsewhere [23].

3. Results

3.1. Cohort Characteristics

Ten RA patients commencing Amgevita (adalimumab biosimilar) were recruited (Table 1); nine were female and one was male. All patients were white. The median age was 50.5 years (interquartile range, IQR, 46-61) and the median pre-treatment DAS28 was 5.71 (IQR 5.20–6.09). Six RA patients commencing Benepali (etanercept biosimilar) were recruited (Table 2); four were female and two were male. One patient was West African and the remaining patients were white. The median age was 57.5 years (IQR 56–59) and the median pre-treatment DAS28 was 5.33 (IQR 4.96–5.58). Participant numbers were below those planned, as recruitment was curtailed due to the COVID-19 pandemic.

Table 1. Patient characteristics at baseline, prior to treatment with the adalimumab biosimilar (*n* = 10).

Characteristic	Statistic
Female sex, *n* (%)	9 (90.00)
Age (years), median [IQR]	50.5 [46–61]
Body weight (kg), median [IQR]	85.5 [66–111]
Body mass index (kg/m^2), median [IQR]	36.2 [28.7–43.4] (2 missing observations)
Concurrent csDMARD, *n* (%)	8 (80.00)
DAS28, median [IQR]	5.71 [5.20–6.09]

Abbreviations: Conventional synthetic disease-modifying anti-rheumatic drug (csDMARD), disease activity score of 28 joint counts (DAS28), interquartile range (IQR).

Table 2. Patient characteristics at baseline, prior to treatment with the etanercept biosimilar (*n* = 6).

Characteristic	Statistic
Female sex, *n* (%)	4 (66.67)
Age (years), median [IQR]	57.5 [56–59]
Body weight (kg), median [IQR]	70.5 [69–84]
Body mass index (kg/m^2), median [IQR]	24.6 [22.8–28.2] (1 missing observation)
Concurrent csDMARD, *n* (%)	4 (100.00) (2 missing observations)
DAS28, median [IQR]	5.33 [4.96–5.58]

Abbreviations: Conventional synthetic disease-modifying anti-rheumatic drug (csDMARD), disease activity score of 28 joint counts (DAS28), interquartile range (IQR).

3.2. PopPK Modelling

A total of 58 serum samples of the adalimumab biosimilar and 40 serum samples of the etanercept biosimilar drug concentrations were available for analysis. Drug concentration values at each time point are available in Supplementary Tables S1 and S2. One-compartment PK models were found to be sufficient to describe the data in popPK modelling of participants initiating both the adalimumab and etanercept biosimilars. Combined additive and proportional models were used to describe the residual errors in the data.

In the adalimumab biosimilar model, PK parameters estimated are presented in Table 3. No covariates were included, as covariates tested only demonstrated a modest improvement in -2LL and AIC whilst complicating the sparse-sampling model with redundant variables. Due to a large percentage relative standard error (RSE%) from estimation of ka (minimum 622%), this value was fixed to 0.01167 hour^{-1}, as per Ternant et al. [10], and the random effect (BSV) was not estimated for this parameter. Plots were generated of predicted versus observed measurements for the adalimumab biosimilar serum concentrations, demonstrating that PK parameters described the data adequately (Supplementary Figure S1). Diagnostic plots are presented in Supplementary Figures S2 and S3.

Table 3. Population pharmacokinetic (popPK) model parameter estimates for the adalimumab biosimilar.

Parameter (Units)	Definition	Estimate	Relative Standard Error (RSE, %)
V_D (L)	Apparent volume of distribution	9.19	12.7
CL (L/h)	Apparent clearance	0.00283	23.3
ka (/h)	Rate constant for absorption	0.1167	Fixed
ωV_D (%)	Coefficient of variation (CV) of between-subject variability (BSV) on V_D	15.60	141.0
ωCL (%)	CV of BSV on CL	68.90	24.8
σprop (%)	Standard deviation (SD) of proportional residual error	26.00	15.7
σadd (mg/L)	Standard deviation of additive residual error	10.80	16.0

The relative standard error (RSE, %) was calculated as: RSE = (estimate/standard error) × 100. Abbreviations: Additive error (add), between-subject variability (BSV), clearance (CL), coefficient of variation (CV), proportional error (prop), proportional rate constant for absorption (ka), standard deviation (SD), volume of distribution (V_D).

In the etanercept biosimilar model, the PK parameters estimated are presented in Table 4. No covariates were included due to the same reasons as for the adalimumab biosimilar model. Due to a large RSE% from estimation of ka (minimum 1.070%), this value was fixed to 0.0396 hour-1, as per Korth-Bradley et al. [24], and the BSV was not estimated for this parameter. Additionally, the model had a large RSE% for estimated V_D, so the BSV estimation was removed from this parameter. Finally, the additive error standard deviation (SD) was fixed to 0.0001 to ensure model stability. Plots were generated of predicted versus observed measurements for the etanercept biosimilar serum concentrations, demonstrating that PK parameters described the data adequately (Supplementary Figure S4). Other diagnostic plots are presented in Supplementary Figures S5 and S6.

Table 4. Population pharmacokinetic (popPK) model parameter estimates for the etanercept biosimilar.

Parameter (Units)	Definition	Estimate	Relative Standard Error (RSE, %)
V_D (L)	Apparent volume of distribution	7.76	18.2
CL (L/h)	Apparent clearance	0.0404	10.7
ka (/h)	Rate constant for absorption	0.0396	Fixed
ωCL (%)	Coefficient of variation (CV) of between-subject variability (BSV) on CL	0.173	61.0
σprop (%)	CV of proportional residual error	0.46	13.6

The relative standard error (RSE, %) was calculated as: RSE = (estimate/standard error) × 100. Abbreviations: Between-subject variability (BSV), clearance (CL), coefficient of variation (CV), proportional error (prop), rate constant for absorption (ka), volume of distribution (V_D).

3.3. Simulation of Altered Dosing Intervals

Initially, simulations of 10,000 individuals were carried out using parameter estimates and the final popPK models for the adalimumab and etanercept biosimilars. Typical individual profiles, as well as the median, 5th and 95th percentiles, were simulated using the usual dosing intervals of the adalimumab biosimilar 40 mg every 14 days (Figure 1) or the etanercept biosimilar 50 mg every 7 days (Figure 2), respectively. Simulated profiles were overlaid with observed plasma concentration data; these demonstrated visually that simulated values agreed well with the data.

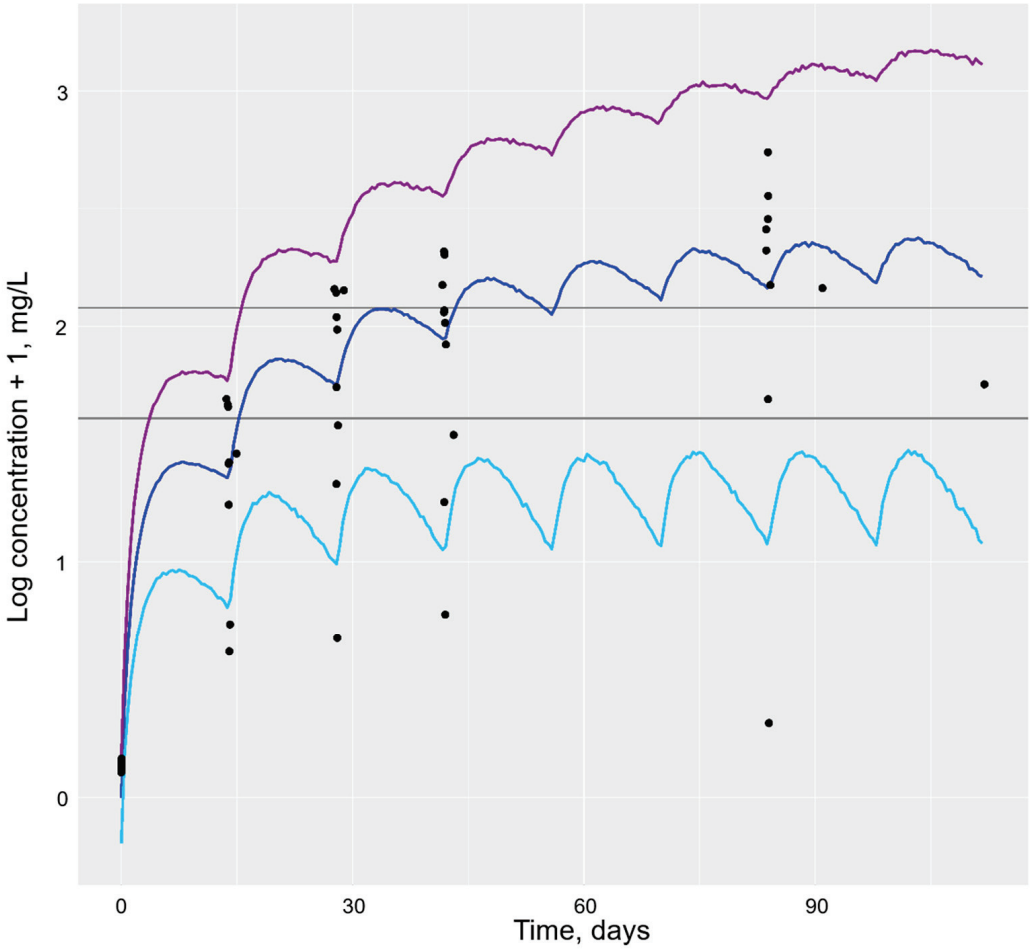


Figure 1. Simulation of the adalimumab biosimilar PK profile for 10,000 individuals using the final popPK model. Legend: Horizontal grey lines represent the adalimumab therapeutic window of 5–8 mg/L proposed by Pouw et al. [25]. The dark blue line represents the population median, the light blue line represents the 5th percentile and the purple line represents the 95th percentile of the population. The black dots represent actual population drug concentration values.

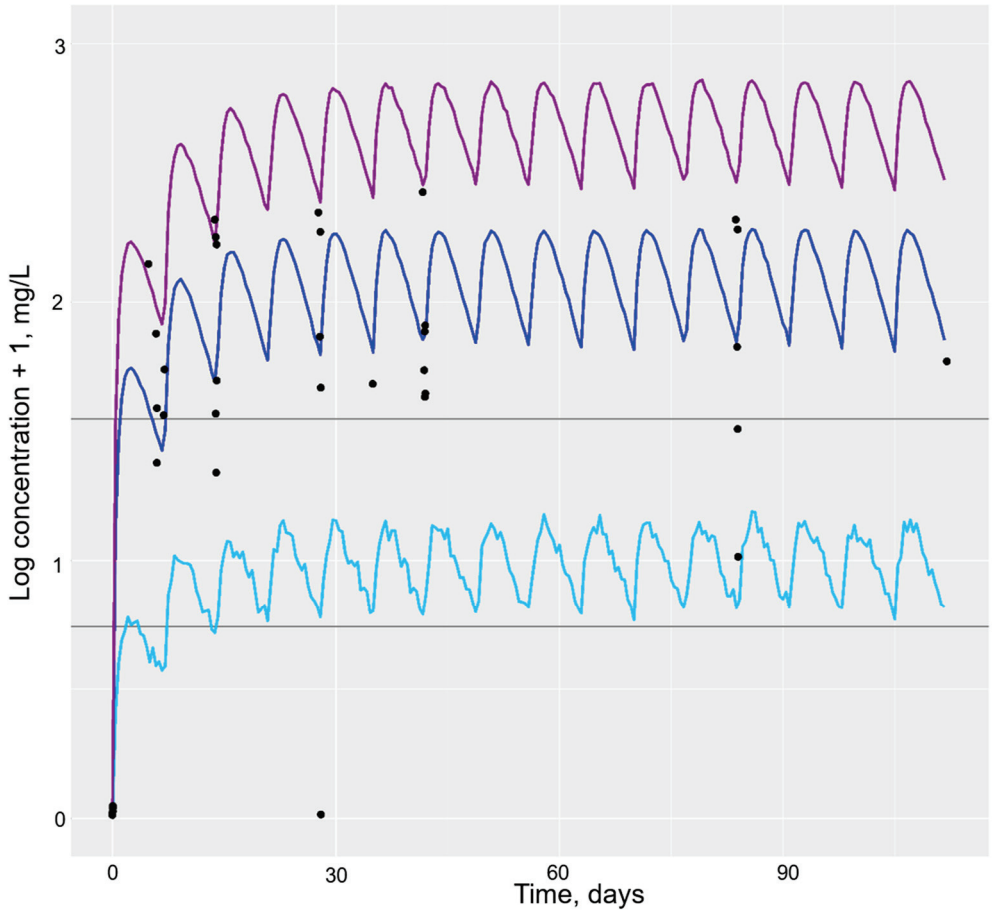


Figure 2. Simulation of the etanercept biosimilar PK profile for 10,000 individuals using the final popPK model. Legend: Horizontal grey lines represent the etanercept therapeutic window of 2.1–4.7 mg/L proposed by Jamnitski et al. [26]. The dark blue line represents the population median, the light blue line represents the 5th percentile and the purple line represents the 95th percentile of the population. The black dots represent actual population drug concentration values.

Once this had been established, alternative dosing regimens were additionally simulated for typical individuals on the adalimumab biosimilar (Figure 3). Both the usual dose rates of 40 mg every 14 days and the increased dose rate of 40 mg every 7 days achieved steady-state drug concentrations within the therapeutic window of adalimumab, defined as between 5–8 mg/L [25]. However, the reduced dose rate of 40 mg every 21 days from initiation did not achieve steady-state concentrations within this proposed window. Time to steady-state drug concentrations had negligible differences between the administration of adalimumab biosimilar 40 mg every 7 or 14 days.

Alternative dosing regimens were also simulated for typical individuals on the etanercept biosimilar (Figure 4). All simulated doses achieved steady-state drug concentrations well above the therapeutic window of etanercept, defined as between 2.1–4.7 mg/L [26]. Time to steady-state drug concentrations had negligible differences between the three simulated dosing regimens of the etanercept biosimilar, although this was marginally quicker with an interval of every 10 days on visual inspection.

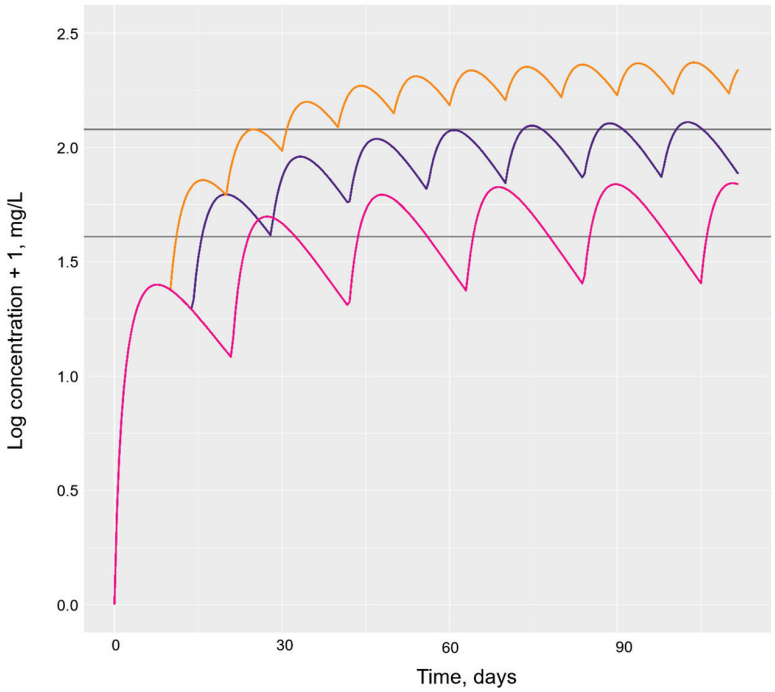


Figure 3. Simulated usual and alternative dosing intervals of the adalimumab biosimilar for a typical patient. Legend: Horizontal grey lines represent the adalimumab therapeutic window of 5–8 mg/L proposed by Pouw et al. [25]. The purple line represents the usual adalimumab biosimilar dosing interval of 40 mg every 14 days, the orange line represents a dosing interval of 40 mg every 7 days and the pink line represents 40 mg every 21 days.

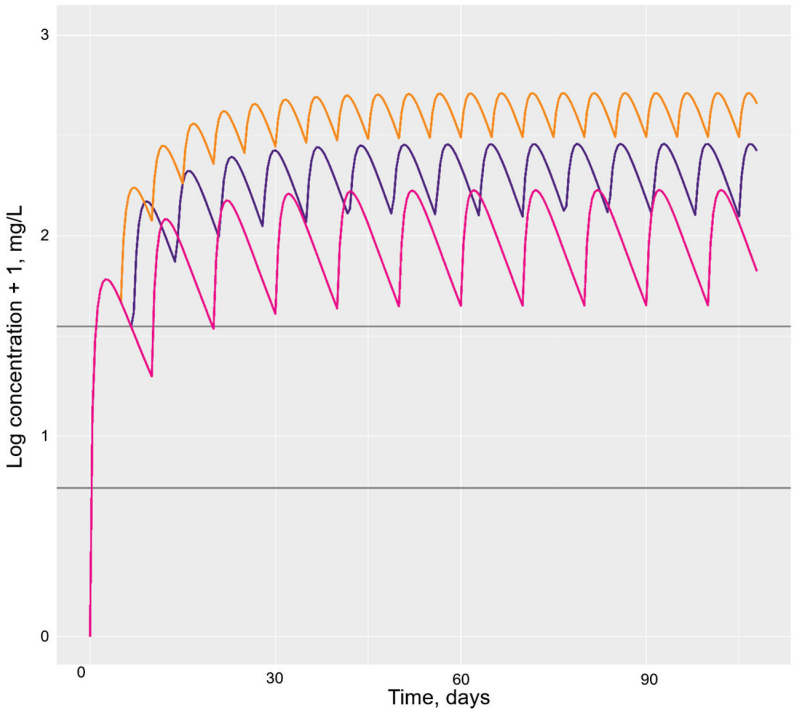


Figure 4. Simulated usual and alternate dosing intervals of the etanercept biosimilar for a typical patient. Legend: Horizontal grey lines represent the etanercept therapeutic window of 2.1–4.7 mg/L proposed by Jamnitski et al. [26]. The purple line represents the usual etanercept biosimilar dosing interval of 50 mg every 7 days, the orange line represents a dosing interval of 50 mg every 5 days and the pink line represents 50 mg every 10 days.

4. Discussion

Using 58 drug concentration samples from ten patients starting the adalimumab biosimilar Amgevita and 40 samples from six patients starting the etanercept biosimilar Benepali, collected over a 12-week period for each patient, popPK models were developed for the study population. Parameter estimates were similar to those from previous studies [10,24], and, alongside acceptable visual checks, this meant that the model fit was determined to be satisfactory. Therefore, values were used to successfully simulate models illustrating altered dosing intervals of both drugs compared to usual dosing in a typical individual. A simulation of dosing Benepali at a lower rate of every 10 days showed drug concentrations reaching steady-state quicker than the usual dosing rate of every 7 days (Figure 4), which has potential cost-saving implications.

There is only one other popPK study of subcutaneously administered adalimumab in RA patients, conducted by Ternant et al. [10], and this study was the basis for the corroboration of estimated PK parameters. In contrast to the present study, Ternant's was a post hoc analysis of a single-centre observational study carried out over 52 weeks, and it used adalimumab originator compound. No popPK analyses have been published for the adalimumab biosimilar Amgevita prior to this study.

The current study is the first published popPK analysis of patients with RA starting the etanercept biosimilar Benepali, and, furthermore, it is the first using the usual dosing regimen of 50 mg subcutaneously every 7 days; other studies have used mixed dosing regimens with a mixture of intravenous and subcutaneous administration [11–13]. The findings of the current study broadly agree with those of Korth-Bradley et al., who carried out popPK analysis in a cohort of healthy controls who received only a single dose of etanercept 25 mg subcutaneously (non-standard dose) [24]. However, whilst subcutaneous delivery of monoclonal antibodies, such as etanercept, is now being used widely, the variations in bioavailability between intravenous and subcutaneous routes and the mechanisms of these variations remain poorly understood [27]. The finding that dosing intervals could potentially be reduced to once every 10 days is interesting; however, given the small sample size, this requires validation in a larger study. Furthermore, because of the size of the study, BSV may not have been described adequately.

Interestingly, patients on the adalimumab biosimilar had an increased median body weight compared with those on the etanercept biosimilar (85.5 kg versus 70.5 kg, respectively). Simulation results for patients receiving the two different biosimilars could, therefore, have been affected by the characteristics of the populations studied, as the adalimumab biosimilar population may have experienced impaired subcutaneous drug absorption secondary to increased adiposity. Furthermore, previous studies have demonstrated that TNFi treatment response is reduced with increased BMI [28].

The majority of patients in the UK are commenced on a biosimilar version of TNFi; therefore, it is important to explore the PK profile of these drugs in patients with RA and how this may influence disease outcome. This study was designed specifically for this purpose and was not carried out as part of a post hoc analysis. The patients were real-world patients managed in UK NHS rheumatology departments, rather than clinical trial participants, so the drug concentrations obtained are likely to be more reflective of day-to-day clinical practice. All samples were collected by the same investigator and delivered to the central processing laboratory within 24 h of blood draw. All blood draws and witnessed dose administrations were documented to the nearest minute by that same investigator, maximising the accuracy of the popPK models. Witnessing of doses at each study visit ensured true trough drug concentrations. Furthermore, because sampling and dose witnessing were all carried out by a single investigator, this ensured no deviations from protocol and consistency of time reporting.

One limitation of this study is that samples were not tested for anti-drug antibodies. Whilst anti-etanercept antibodies occur infrequently, anti-adalimumab antibodies are associated with decreased drug concentrations and reduced rates of treatment response [5]. Due to the low sample numbers, which were ultimately limited due to multiple UK lock-

downs in response to the COVID-19 pandemic, recruitment was below the optimum total of participants. Therefore, including anti-drug antibody seropositivity as a covariate, as with the other covariates tested in this study, would have been unlikely to improve model fit, and hence, was not tested.

Due to low participant numbers, ka had to be fixed in both the adalimumab and etanercept biosimilar models and covariates were not identified, so popPK models may not be completely representative of the study populations. Furthermore, covariate selection can be problematic based on low participant numbers, i.e., although certain covariates can appear as significant/non-significant in a given model, these findings remain uncertain due to sample size [29]. For example, due to the skew between female and male participants, we cannot distinguish between BSV and the effect of sex. Previous work has suggested that a sample size of 20–30 participants per drug would provide a more accurate parameter estimation using a popPK approach [30]. The low study numbers are not necessarily a negative though, as this study itself adds valuable information and data in a space where both are very limited. To this end, it is a rational approach to establish a pilot study before carrying out any larger studies.

5. Conclusions

In conclusion, popPK models for the TNFi biosimilars Amgevita and Benepali were successfully developed in populations of real-world RA patients. Findings from simulations of altered dosing intervals could form the basis for future personalised dosing studies for these two agents.

Supplementary Materials: The following supporting information can be downloaded at: https://www.mdpi.com/article/10.3390/pharmaceutics16060702/s1, Table S1: Drug concentration values for patients receiving the adalimumab biosimilar; Table S2: Drug concentration values for patients receiving the etanercept biosimilar; Figure S1: Observed values of the adalimumab biosimilar concentrations versus population model-predicted values (PRED) and individual prediction values (IPRED); Figure S2: Distribution of population (PWRES) and individual weighted residuals (IWRES) versus individual predictions and normalised prediction distribution error (NPDE) for the adalimumab biosimilar concentrations; Figure S3: Visual predictive check (VPC) of popPK model fit for the adalimumab biosimilar; Figure S4: Observed values of the etanercept biosimilar concentrations versus population model-predicted values (PRED) and individual predicted values (IPRED); Figure S5: Distribution of PWRES and IWRES versus individual predictions and NPDE for the etanercept biosimilar concentrations; Figure S6: VPC of popPK model fit for the etanercept biosimilar.

Author Contributions: Conceptualisation, A.S.D., A.B. and D.P. Methodology, K.O. and A.S.D. Software, S.F.L., K.O. and A.S.D. Validation, S.F.L. and K.O. Formal analysis, S.F.L. and K.O. Investigation, S.F.L., K.O., A.B.M.A. and N.N. Resources, N.N., A.W.M., J.D.I., A.G.W., K.L.H., A.B. and D.P. Data curation, S.F.L., A.B.M.A. and N.N. Writing—original draft preparation, S.F.L. Writing—review and editing, K.O., A.S.D., A.B.M.A., N.N., J.B., A.W.M., J.D.I., A.G.W., K.L.H., A.B. and D.P. Visualisation, S.F.L. and K.O. Supervision, K.O., A.S.D., J.B., A.B. and D.P. Project administration, S.F.L. and N.N. Funding acquisition, A.W.M., J.D.I., A.G.W., K.L.H., A.B. and D.P. All authors have read and agreed to the published version of the manuscript.

Funding: This research was funded by the NIHR Manchester Biomedical Research Centre (BRC, grant reference NIHR203308). The views expressed are those of the authors and not necessarily those of the NHS, the NIHR or the Department of Health. We thank Versus Arthritis for their support (grant reference 21754). A.B. and A.W.M. are NIHR Senior Investigators. Research in JDI's laboratory is supported by the NIHR Newcastle Biomedical Research Centre for Ageing and Multiple Long-Term Conditions and the Research into Inflammatory Arthritis Centre Versus Arthritis (grant reference 22072). Research in A.W.M.'s laboratory is supported by the NIHR Leeds BRC.

Institutional Review Board Statement: A favourable ethics opinion was obtained from the North West–Greater Manchester South Research Ethics Committee (REC), REC reference 04/Q1403/37, IRAS project ID 31668.

Informed Consent Statement: Informed consent was obtained from all subjects involved in the study, in compliance with the Declaration of Helsinki.

Data Availability Statement: The data presented in this study are available on request from the corresponding author due to patient confidentiality.

Acknowledgments: We are grateful for the assistance given by the University of Manchester IT Services and for the use of the Computational Shared Facility.

Conflicts of Interest: A.W.M. received a research grant from Roche and has undertaken consultancy for AstraZeneca and Vifor on behalf of the University of Leeds in the field of vasculitis. J.D.I. has received research grants from Pfizer, GSK and Janssen. He has received consultancy fees (to his employer) from Anaptys Bio, Annexon Biosciences, AstraZeneca, BMS, Cyxone AB, Dragonfly, Eli Lilly, Galapagos NV, Gilead Sciences Ltd, GSK, Istesso Ltd., Jansen, Kenko International, Kira Biotech, Ono Pharma, Pfizer, Revelo Biotherapeutics, Roche and Sanofi. He has received speaker fees from Abbvie and support for meeting attendance from Eli Lilly. K.L.H. has received speaker fees from Abbvie and grant income from Pfizer and BMS. A.B. has received honoraria/grant funding from BMS, Galapagos and Pfizer.

References

1. Smolen, J.S.; Aletaha, D.; Barton, A.; Burmester, G.R.; Emery, P.; Firestein, G.S.; Kavanaugh, A.; McInnes, I.B.; Solomon, D.H.; Strand, V.; et al. Rheumatoid arthritis. *Nat. Rev. Dis. Primers* **2018**, *4*, 18001. [CrossRef] [PubMed]
2. Adalimumab, Etanercept, Infliximab and Abatacept for Treating Moderate Rheumatoid Arthritis after Conventional DMARDs Have Failed. Available online: https://www.nice.org.uk/guidance/ta715 (accessed on 28 September 2021).
3. Biosimilars Approved in Europe. Available online: https://www.gabionline.net/biosimilars/general/biosimilars-approved-in-europe (accessed on 18 July 2023).
4. Finckh, A.; Simard, J.F.; Gabay, C.; Guerne, P.A. Evidence for differential acquired drug resistance to anti-tumour necrosis factor agents in rheumatoid arthritis. *Ann. Rheum. Dis.* **2006**, *65*, 746–752. [CrossRef] [PubMed]
5. Jani, M.; Chinoy, H.; Warren, R.B.; Griffiths, C.E.; Plant, D.; Fu, B.; Morgan, A.W.; Wilson, A.G.; Isaacs, J.D.; Hyrich, K.; et al. Clinical utility of random anti-tumor necrosis factor drug-level testing and measurement of antidrug antibodies on the long-term treatment response in rheumatoid arthritis. *Arthritis Rheumatol.* **2015**, *67*, 2011–2019. [CrossRef] [PubMed]
6. Mould, D.R.; Upton, R.N. Basic concepts in population modeling, simulation, and model-based drug development. *CPT Pharmacometrics Syst. Pharmacol.* **2012**, *1*, e6. [CrossRef] [PubMed]
7. Cobelli, C.; Foster, D.; Toffolo, G. *Tracer Kinetics in Biomedical Research: From Data to Model*; Kluwer Academic/Plenum Publishers: New York, NY, USA, 2000.
8. Sheiner, L.B.; Rosenberg, B.; Melmon, K.L. Modelling of individual pharmacokinetics for computer-aided drug dosage. *Comput. Biomed. Res.* **1972**, *5*, 411–459. [CrossRef]
9. Ducourau, E.; Ternant, D.; Lequerre, T.; Fuzibet, P.; Le Loet, X.; Watier, H.; Goupille, P.; Paintaud, G.; Vittecoq, O.; Mulleman, D. Towards an individualised target concentration of adalimumab in rheumatoid arthritis. *Ann. Rheum. Dis.* **2014**, *73*, 1428–1429. [CrossRef] [PubMed]
10. Ternant, D.; Ducourau, E.; Fuzibet, P.; Vignault, C.; Watier, H.; Lequerre, T.; Le Loet, X.; Vittecoq, O.; Goupille, P.; Mulleman, D.; et al. Pharmacokinetics and concentration-effect relationship of adalimumab in rheumatoid arthritis. *Br. J. Clin. Pharmacol.* **2015**, *79*, 286–297. [CrossRef] [PubMed]
11. Lee, H.; Kimko, H.C.; Rogge, M.; Wang, D.; Nestorov, I.; Peck, C.C. Population pharmacokinetic and pharmacodynamic modeling of etanercept using logistic regression analysis. *Clin. Pharmacol. Ther.* **2003**, *73*, 348–365. [CrossRef]
12. Zhou, H.; Mayer, P.R.; Wajdula, J.; Fatenejad, S. Unaltered etanercept pharmacokinetics with concurrent methotrexate in patients with rheumatoid arthritis. *J. Clin. Pharmacol.* **2004**, *44*, 1235–1243. [CrossRef]
13. Zhou, S.Y.; Shu, C.; Korth-Bradley, J.; Raible, D.; Palmisano, M.; Wadjula, J.; Fatenejad, S.; Bjornsson, T. Integrated population pharmacokinetics of etanercept in healthy subjects and in patients with rheumatoid arthritis and ankylosing spondylitis. *J. Clin. Pharmacol.* **2011**, *51*, 864–875. [CrossRef]
14. Hsu, L.F.; Huang, J.D. Evaluation of etanercept dose reduction in patients with rheumatoid arthritis using pharmacokinetic/pharmacodynamic modeling and simulation. *Int. J. Clin. Pharmacol. Ther.* **2014**, *52*, 776–786. [CrossRef] [PubMed]
15. Shennak, M.; Al-Jaouni, R.; Kshirasagar, S.; Kasibhatta, R.S.; Godse, N.; Al-Ghazawi, A.; Vittala, P.; Bakhle, D. An Open-Label, Randomized, Single-Dose, Crossover, Comparative Pharmacokinetics Study of YLB113 and the Etanercept Reference Product in Healthy Adult Male Subjects. *Eur. J. Drug Metab. Pharmacokinet.* **2020**, *45*, 467–475. [CrossRef]
16. Potter, C.; Cordell, H.J.; Barton, A.; Daly, A.K.; Hyrich, K.L.; Mann, D.A.; Morgan, A.W.; Wilson, A.G.; Biologics in Rheumatoid Arthritis, G.; Genomics Study, S.; et al. Association between anti-tumour necrosis factor treatment response and genetic variants within the TLR and NFκB signalling pathways. *Ann. Rheum. Dis.* **2010**, *69*, 1315–1320. [CrossRef]

17. Gueorguieva, I.; Ogungbenro, K.; Graham, G.; Glatt, S.; Aarons, L. A program for individual and population optimal design for univariate and multivariate response pharmacokinetic-pharmacodynamic models. *Comput. Methods Programs Biomed.* **2007**, *86*, 51–61. [CrossRef]
18. Yim, D.S.; Zhou, H.; Buckwalter, M.; Nestorov, I.; Peck, C.C.; Lee, H. Population pharmacokinetic analysis and simulation of the time-concentration profile of etanercept in pediatric patients with juvenile rheumatoid arthritis. *J. Clin. Pharmacol.* **2005**, *45*, 246–256. [CrossRef]
19. Ruiz-Argüello, M.B.; Magueregui, A.; Martinez, A.; Nagore, D. P329 Adalimumab therapeutic drug monitoring test validated for measuring ABP 501 biosimilar. *J. Crohn's Colitis* **2019**, *13*, S265–S266. [CrossRef]
20. Ghia, C.; Akerkar, S.; Sabnis, S.; Rao, U.R.K.; Rambhad, G. Analytical and clinical evaluation of an immunoassay for estimating immunogenicity of infliximab and etanercept in Indian population. *J. Assoc. Physicians India* **2016**, *64*, 14–17.
21. The R Project for Statistical Computing. Available online: https://www.r-project.org/ (accessed on 24 June 2021).
22. Wickham, H. *ggplot2: Elegant Graphics for Data Analysis*; Springer: New York, NY, USA, 2016.
23. Ling, S. Personalising Dosing of Biologic Therapies in Inflammatory Arthritis to Maximise Cost-Benefit. Ph.D. Thesis, University of Manchester, Manchester, UK, 2022. Available online: https://pure.manchester.ac.uk/ws/portalfiles/portal/267871943/FULL_TEXT.PDF (accessed on 13 May 2024).
24. Korth-Bradley, J.M.; Rubin, A.S.; Hanna, R.K.; Simcoe, D.K.; Lebsack, M.E. The pharmacokinetics of etanercept in healthy volunteers. *Ann. Pharmacother.* **2000**, *34*, 161–164. [CrossRef] [PubMed]
25. Pouw, M.F.; Krieckaert, C.L.; Nurmohamed, M.T.; van der Kleij, D.; Aarden, L.; Rispens, T.; Wolbink, G. Key findings towards optimising adalimumab treatment: The concentration-effect curve. *Ann. Rheum. Dis.* **2015**, *74*, 513–518. [CrossRef]
26. Jamnitski, A.; Krieckaert, C.L.; Nurmohamed, M.T.; Hart, M.H.; Dijkmans, B.A.; Aarden, L.; Voskuyl, A.E.; Wolbink, G.J. Patients non-responding to etanercept obtain lower etanercept concentrations compared with responding patients. *Ann. Rheum. Dis.* **2012**, *71*, 88–91. [CrossRef]
27. Sánchez-Félix, M.; Burke, M.; Chen, H.H.; Patterson, C.; Mittal, S. Predicting bioavailability of monoclonal antibodies after subcutaneous administration: Open innovation challenge. *Adv. Drug Deliv. Rev.* **2020**, *167*, 66–77. [CrossRef] [PubMed]
28. Gialouri, C.G.; Pappa, M.; Evangelatos, G.; Nikiphorou, E.; Fragoulis, G.E. Effect of body mass index on treatment response of biologic/targeted-synthetic DMARDs in patients with rheumatoid arthritis, psoriatic arthritis or axial spondyloarthritis. A systematic review. *Autoimmun. Rev.* **2023**, *22*, 103357. [CrossRef] [PubMed]
29. Vashisht, R.; Bendon, A.A.; Okonkwo, I.; Patel, D.; Fullwood, C.; Ogungbenro, K.; Aarons, L.; Darwich, A.S. A study of the dosage and duration for levobupivacaine infusion by the caudal-epidural route in infants aged 3–6 months. *Paediatr. Anaesth.* **2019**, *29*, 161–168. [CrossRef] [PubMed]
30. Ogungbenro, K.; Aarons, L. How may subjects are necessary for population pharmacokinetic experiments? Confidence interval approach. *Eur. J. Clin. Pharmacol.* **2008**, *64*, 705–713. [CrossRef]

Disclaimer/Publisher's Note: The statements, opinions and data contained in all publications are solely those of the individual author(s) and contributor(s) and not of MDPI and/or the editor(s). MDPI and/or the editor(s) disclaim responsibility for any injury to people or property resulting from any ideas, methods, instructions or products referred to in the content.

pharmaceutics

MDPI

Article

Vedolizumab Clearance as a Surrogate Marker for Remission in Inflammatory Bowel Disease Patients: Insights from Real-World Pharmacokinetics

Srđan Marković [1,2], Đorđe Kralj [1], Petar Svorcan [1,2], Tamara Knežević Ivanovski [1], Olga Odanović [1], Sanja Obradović [3], Ana Homšek [4], Marija Jovanović [4], Rada Savić [5] and Katarina M. Vučićević [4,*]

[1] Department of Gastroenterology and Hepatology, University Hospital Medical Center "Zvezdara", 11120 Belgrade, Serbia
[2] Faculty of Medicine, University of Belgrade, 11000 Belgrade, Serbia
[3] Department of Laboratory Diagnostics, University Hospital Medical Center "Zvezdara", 11120 Belgrade, Serbia
[4] Department of Pharmacokinetics and Clinical Pharmacy, Faculty of Pharmacy, University of Belgrade, 11000 Belgrade, Serbia
[5] Department of Bioengineering and Therapeutic Sciences, University of California, San Francisco, CA 94143, USA
* Correspondence: katarina.vucicevic@pharmacy.bg.ac.rs

Abstract: Background/Objectives: Vedolizumab (VDZ) is approved in the treatment of patients with moderate to severe ulcerative colitis (UC) or Crohn's disease (CD). VDZ exhibits considerable variability in its pharmacokinetic (PK) profile, and its exposure-response relationship is not yet fully understood. The aim was to investigate the variability in VDZ trough levels and PK parameters, to assess the relationship between VDZ PK and biochemical response, as well as clinical and endoscopic outcomes. **Methods**: We included 61 UC and 45 CD patients. Patients' data and trough VDZ concentrations were retrospectively obtained. Population PK analysis was performed using non-linear mixed-effects modelling with NONMEM (version 7.5). Graphs and statistical analyses were performed using R (version 4.1.3). **Results**: In total, 116 trough VDZ concentrations from 106 patients were described by a two-compartment model. For a typical patient, clearance (CL) was estimated at 0.159 L/day, while in patients previously treated with anti-TNFα agents, VDZ CL increased by 26.4% on average. In univariate binary logistic regression, VDZ trough concentration was not statistically significant predictor of remission, whereas CL was. Moreover, combined CL and faecal calprotectin (FCP) were a statistically significant predictors of remission. The hazard ratio (HR) for CL above 0.1886 L/day was 0.35 ($p = 0.05$) and for FCP below 250 μg/g was 2.66 ($p = 0.02$) in a time-to-event analysis. **Conclusions**: Our population PK model incorporates the effect of prior anti-TNFα agents on CL, suggesting its association with more severe forms of IBD. VDZ CL emerged as a more robust and clinically relevant predictor of remission in IBD patients than trough concentration.

Keywords: IBD; monoclonal antibody; NONMEM; pharmacokinetics; therapeutic drug monitoring; clearance

1. Introduction

Inflammatory bowel disease (IBD), which includes ulcerative colitis (UC) and Crohn's disease (CD), considerably impairs patient quality of life due to persistent gastrointestinal inflammation. Vedolizumab (VDZ), a second-line monoclonal antibody targeting the α4β7 integrin, is approved for both the induction treatment and the maintenance of remission in patients with moderate to severe IBD. Its gut-specific mechanism of action reduces systemic immunosuppression and associated adverse effects [1,2].

VDZ exhibits considerable variability in its pharmacokinetic (PK) profile among IBD patients. At trough concentrations above 10 μg/mL, typically achieved after the repeated

dosing of 300 mg every 8 weeks, VDZ demonstrates linear, non-specific elimination [3,4]. Its clearance (CL) varies among patients but generally centres around 0.16 L/day [1,5]. Similar to other monoclonal antibodies, VDZ has a volume of distribution (Vd) between 4.8 and 7.5 L [1,5,6]. This distribution pattern aligns with VDZ's targeted binding within the gut, its large molecular size, which limits its ability to diffuse freely across cell membranes restricting tissue penetration, and its receptor-mediated CL. Consequently, the terminal half-life ($t_{1/2}$) ranges from 15 to 25.5 days, supporting the VDZ dosing schedule every 8 weeks after the initial induction phase [1,5,7]. Despite the established efficacy of VDZ in treating moderate to severe IBD, considerable variability in patient responses remains, with some achieving clinical remission while others experience suboptimal outcomes. This variability is likely influenced by differences in drug pharmacokinetics, including CL and trough concentrations.

Population (Pop) PK modelling approach is the gold standard in identifying sources of variability among patients [8]. However, there is a scarcity of PopPK models of VDZ based on data from real-world studies [5,9–13]. It is important to highlight that these models were primarily developed using data generated during clinical trials, with the majority relying on the model of Rosario et al. [5]. Nevertheless, numerous publications have described and/or studied variations in VDZ trough concentrations using standard statistical approaches [6,7,14–16].

Thus far, several factors are recognised to contribute to the observed variability in VDZ PK. Serum albumin levels are inversely related to VDZ CL, possibly due to increased proteolytic activity or altered drug binding [5,9–13], with a reported cut-off albumin value of 3.2 g/dL [17]. Patients' body weight above 120 kg significantly (and potentially clinically) increases VDZ CL leading to reduced drug exposure and possibly compromising clinical response. Similarly, the presence of neutralising anti-drug antibodies (ADAs) increases CL, but this effect usually was not considered clinically relevant [5,9,12,17]. The concomitant use of immunosuppressive therapies (such as methotrexate, azathioprine, mercaptopurine or aminosalicylates) or prior use of tumour necrosis factor-α (TNF-α) antagonist has shown contradictory results regarding its impact on VDZ CL; however, if statistically significant, it is less likely to be clinically relevant [2,17].

The relationship between VDZ trough concentration and levels of inflammatory biomarkers, clinical response(s) or remission status has been the focus of clinical trials and numerous real-world cohorts [14–16,18–28]. The majority of studies have demonstrated week-specific VDZ exposure-response relationships. These relationships include different variables among studies, reflecting the diverse methodologies and criteria used in the research. In studies where this relationship is evident, higher serum concentrations of VDZ correlate with stable C-reactive protein (CRP), haemoglobin (Hgb), erythrocytes sedimentation rate (ESR), faecal calprotectin (FCP), greater likelihood of achieving better clinical response and reaching sustained clinical remission both in CD and UC patients. These targets of trough VDZ levels greatly vary among studies. Notably, the GEMINI 1 randomised controlled trial indicated that VDZ concentration above 37.1 μg/mL at week 6 (associated with lower CL values) was linked to clinical remission at weeks 14 and 52 [19]. Similarly, a post-hoc analysis of data showed that mucosal healing rates were higher with VDZ concentrations exceeding 35.7 μg/mL at week 6 [29]. In another study by Dreesen et al., VDZ troughs > 30 μg/mL at week 2, >24 μg/mL at week 6, and >14 μg/mL during maintenance were associated with improved outcomes, including both endoscopic and clinical remission [14]. In contrast, the recent ENTERPRET study did not demonstrate a clear benefit of higher VDZ concentrations on clinical outcomes in UC patients [30]. Hence, the inconsistency across reported findings highlights the variability in results between studies, suggesting that the relationship is not yet fully understood. This underscores the need for further research in this area.

Knowledge of the efficacious target VDZ exposure, and understanding the sources of PK variability would enable clinicians to more accurately anticipate which patients will benefit most from VDZ therapy. This insight would allow for dosing regimen adjustments

to improve clinical response and would help in identifying patients who may need to be switched to alternative treatments [14]. Reactive TDM of infliximab has become a critical component in the management of patients with IBD. Moreover, there is increasing evidence supporting the value of proactive TDM, which involves monitoring infliximab levels and adjusting dosing regimens before clinical symptoms arise, to optimise treatment outcomes [31,32]. Consequently, VDZ TDM is increasingly being performed in many clinical settings. The rationale for VDZ TDM includes managing the substantial interpatient variability in drug exposure, and together with clinical parameters, allowing healthcare providers to tailor VDZ dosing regimen more precisely. However, there is no universally accepted TDM protocol for VDZ, as no clear treatment time-dependent and exposure-response specific targets are being established [1,14,33].

Consequently, there is a need for further research to fully elucidate the VDZ PK variability and exposure-response dynamics of VDZ in IBD patients. Addressing these gaps underscores the need for personalised treatment approaches to optimise therapeutic outcomes and improve the clinical decision-making process.

Our research goal was to investigate the variability in VDZ trough levels and PK parameters, utilising a PopPK modelling approach on sparse TDM data. Moreover, we aimed to assess the relationship between VDZ PK and biochemical inflammatory parameters, as well as the clinical and endoscopic remission of patients with IBD in real-world clinical settings.

2. Materials and Methods

2.1. Study Design

A monocentre, retrospective, real-world study was conducted between October 2021 and August 2022, in the University Medical Center "Zvezdara", Belgrade, Republic of Serbia, the centre of excellence for IBD in the country. The research protocol received approval from the institutional Ethics Committee (No. IRB00009457, on 5 October 2022). The study included data obtained from the medical records of all adult patients (aged over 18 years) diagnosed with either CD or UC, who were treated with VDZ therapy and who underwent serum sampling for TDM during the induction or maintenance phase. Exclusion criteria were patients' age below 18 years, incomplete dosing and TDM data information in the medical records.

2.2. Treatment and Therapeutic Drug Monitoring of Vedolizumab

VDZ (Entyvio®, 300 mg vial solution for infusion, Takeda Italia S.P.S) was administered as 30-min intravenous infusion at a standard dose of 300 mg during the induction phase at weeks 0, 2 and 6. Maintenance dosing intervals varied among patients, occurring every 4, 6 or 8 weeks based on clinical judgement and patient response to treatment. Due to limited resources for TDM and the constraints imposed by the COVID-19 pandemic, TDM was performed randomly compared to the therapy initiation. However, it was always conducted before the next VDZ dose as an add-on to routine clinical follow-up of patients.

Blood samples, corresponding to trough VDZ levels, were drawn into 6 mL clot activator tubes. The blood samples were centrifuged at 4000× *g* for 10 min, and the sera were kept frozen at −20 °C until analysis. VDZ concentration was measured using commercially available R-Biopharm® ELISA tests on Dynex DS2 analyser (Dynex Technologies, Chantilly, VA, USA) with measurement ranges from 1 to 50 μg/mL. EasyCal (Eurospital, Trieste, Italy) ready-to-use device was used for the stool sampling and pre-analytical processing of stool specimens, and the prepared extract was used for the measurement of faecal calprotectin (FCP) using the immunoenzymatic test Calprest NG (Eurospital, Trieste, Italy) on Dynex DS2 analyser (Dynex Technologies, Chantilly, VA, USA). Complete blood count and biochemical parameters were routinely analysed using standard methods. All analyses were performed in the biochemical laboratory of University Hospital Medical Center "Zvezdara", Belgrade, Republic of Serbia.

2.3. Data Source

Alongside VDZ therapy and TDM data (date of VDZ therapy initiation, date of administered doses, date of blood sampling for TDM, measured VDZ concentration), prior and current concomitant therapy, detailed demographic (age, sex, body weight), disease characteristics (type of IBD, time of diagnosis, disease severity, phenotype of disease), laboratory, clinical monitoring and colonoscopy data were recorded. Detailed laboratory parameters at baseline of therapy initiation and on TDM sampling day were obtained, and they included the following: albumin (Alb), Hgb, erythrocyte (Er), iron (Fe), ferritin (FER), platelets (Plt), leukocytes (WBC), CRP and FCP. Disease activity was assessed using the Mayo score for UC, and the Simplified Endoscopic Score (SES) was used to assess endoscopic activity in CD. Complete blood count, biochemical parameters and clinical response (for UC: stool frequency, rectal bleeding and physician global assessment; for CD: stool frequency and abdominal pain) were monitored longitudinally at every visit when VDZ administration was scheduled. Clinical remission was defined as a partial Mayo score between 0 and 1 for UC, CD stool frequency ≤ 3 and abdominal pain ≤ 1. For the purpose of this study, we utilised serological and faecal biomarkers of inflammation, and clinical remission at the TDM time point. Gastrointestinal endoscopy was performed approximately every 6–12 months depending on the disease severity. Endoscopic remission was defined as a Mayo score of 0/1 for UC, and SES of 0–2 for CD, and we utilised endoscopic remission data at the subsequent time point following the TDM. Time-to-endoscopic remission was calculated from the TDM time point to the date of documented endoscopic remission or the last follow-up date for censored patients.

2.4. Population Pharmacokinetic Modelling

The analysis of VDZ trough concentrations was done through a non-linear mixed-effects modelling approach using NONMEM® software (version 7.5) [34]. This methodology was selected for the analysis due to its proven ability to model sparse data while accounting for interindividual variability. This is essential for understanding the diverse responses in heterogeneous patient populations. Given the availability of sparse TDM data, the PRIOR approach was utilised [35,36]. This functionality allows the integration of parameter estimates from previous studies to generate more robust estimates in the presence of limited or highly variable data. We used the PopPK model developed by Rosario et al. [5] to inform and stabilise the estimation of structural and statistical model parameters. Due to the limited PK sampling time points, only CL and its variability were estimated, while for other parameters informative priors were used. The non-linear CL described by Rosario et al. was not included since it did not improve the model fit. Decay in concentration over time was described with a bi-exponential model. Between-patient variability was modelled exponentially assuming a log-normal distribution, ensuring positivity of clearance values. Additive, proportional and combined error models were tested to describe residual variability. Furthermore, the relationship between CL and demographic, treatment or clinical characteristics, including age, weight and disease severity, was explored using an automated stepwise covariate model (scm) building procedure. This procedure applied standard criteria based on the $-2\times$ log-likelihood change, which is presented in NONMEM as the objective function value (OFV). When comparing models, a difference in the OFV of 3.84, 7.88 and 10.83 are considered significant at the 0.05, 0.005 and 0.001 levels, respectively. In the covariate analysis, the inclusion criterion was $p < 0.05$, followed by an exclusion criterion of $p > 0.01$ [34]. No outliers were identified in the dataset. PopPK model evaluation is critical and involves assessing goodness-of-fit statistics, diagnostic plots and precision of parameter estimates. Iterative refinement of the model continued until a final model that adequately describes the data is achieved. Bootstrap resampling 1000 datasets was employed to estimate 95% confidence intervals (CI) for the model parameters [8]. Using the final PopPK model, we performed the simulation of the concentration-time profile after various dosing regimens using e-Campsis Pro (Calvagone, Chazay d'Azergues, France).

2.5. Statistical Analysis

Descriptive statistics were employed to summarise the demographic and clinical characteristics of the study population, as well as VDZ therapy and concentration data. Continuous variables are presented as mean ± standard deviation (SD) or median (interquartile range, IQR), depending on their distribution. Categorical variables are summarised as frequencies and percentages.

The Fisher's exact or χ^2 test was applied for the analysis of categorical variables. For paired data, the Student's *t*-test and the Wilcoxon signed-rank test were utilised, while for unpaired data, the unpaired Student's *t*-test or the Mann-Whitney U test was used.

To identify significant predictors of biochemical response, clinical and endoscopic remission, univariate and multivariate stepwise logistic regression and linear regression analyses were employed. Variables with a $p < 0.05$ in the univariate analysis were considered for inclusion in the multivariate model. The strength of association between predictor variables and clinical response or remission was expressed as odds ratios (ORs) with corresponding 95% CI. Cochran-Mantel-Haenszel (CMH) test was used to evaluate the association between two categorical variables while controlling for one or more strata, and appropriate ORs were calculated. To evaluate the diagnostic performance of variables in predicting clinical response and remission in IBD patients, receiver operating characteristic (ROC) curve analysis was conducted. Youden's index was used to determine the optimal cut-off point that maximises the difference between true positive and false positive rates.

Finally, survival analysis was conducted to explore the time to endoscopic remission and to assess the impact of various variables on this outcome. Kaplan-Meier curves were generated to estimate the survival function, and a Cox proportional hazards regression model was employed to evaluate the association between various covariates and the time to endoscopic remission.

Graphs and statistical analyses were conducted with R programming language (version 4.1.3, R Foundation for Statistical Computing, Vienna, Austria) in RStudio (desktop version 1.4.1717).

3. Results

Our cohort included data from 106 IBD patients. The cohort consisted of 62 UC patients (mean age: 49.81 years, 58.1% male) and 45 CD patients (mean age: 49.71 years, 51.9% male). Patients were receiving VDZ as part of their standard clinical care, with concomitant immunomodulatory therapies in 81.1% of patients. Demographic and baseline biochemical characteristics are given in Table 1, while Table S1 describes their disease features.

Table 1. Demographic and baseline biochemical characteristics of patients.

	Ulcerative Colitis (N = 62)	**Crohn's Disease (N = 44)**	**Total (N = 106)**
Age (years)			
Mean (SD)	49.81 (17.56)	49.71 (17.44)	49.76 (17.43)
Range	21–78	21–76	21–78
Sex			
Male	36 (58.1%)	19 (43.2%)	55 (51.9%)
Female	26 (41.9%)	25 (56.8%)	51 (48.1%)
Body weight (kg)			
Mean (SD)	74.29 (11.57)	68.64 (13.74) *	71.94 (12.76)
Range	50–110	44–103	44–110
Haemoglobin (g/L)			
N-Miss	3	2	5
Mean (SD)	126.83 (23.06)	126.74 (18.85)	126.79 (21.31)
Range	75–171	68–161	68–171

Table 1. *Cont.*

	Ulcerative Colitis (N = 62)	Crohn's Disease (N = 44)	Total (N = 106)
Erythrocytes ($\cdot 10^{12}$/L)			
N-Miss	5	1	6
Mean (SD)	4.50 (0.71)	4.41 (0.49)	4.46 (0.63)
Range	2.45–5.84	3.08–5.50	2.45–5.84
Iron (μmol/L)			
N-Miss	10	6 *	16
Mean (SD)	8.47 (5.84)	11.62 (6.74)	9.80 (6.39)
Range	2.0–24.8	2.8–28.2	2.0–28.2
CRP (mg/L)			
N-Miss	3	0	3
Mean (SD)	21.80 (42.97)	8.94 (13.04)	16.31 (34.10)
Range	0.1–205.0	0.1–66.2	0.1–205.0
Albumin (g/L)			
N-Miss	29	13	42
Mean (SD)	39.03 (5.75)	40.55 (6.10)	39.77 (5.92)
Range	28–49	26–52	26–52
Platelets ($\cdot 10^{9}$/L)			
N-Miss	8	1	9
Mean (SD)	332.37 (130.65)	324.86 (118.60)	329.04 (124.87)
Range	123–797	120–701	120–797
Leukocytes ($\cdot 10^{9}$/L)			
N-Miss	6	3	9
Mean (SD)	9.07 (3.54)	9.01 (3.50)	9.05 (3.50)
Range	2.4–18.4	2.8–16.7	2.4–18.4
Ferritin (ng/mL)			
N-Miss	15	6	21
Mean (SD)	58.83 (88.51)	45.58 (47.62)	52.91 (73.03)
Range	3–495	4–164	3–495
Faecal calprotectin (μg/g)			
N-Miss	0	1	1
Mean (SD)	608.63 (573.21)	544.19 (602.01)	582.24 (583.17)
Range	16–1801	12–2055	12–2055
Immunomodulatory drug (azathioprine, 6-mercaptopurine, methotrexate, calcineurin inhibitors)			
No	14 (22.6%)	6 (13.6%)	20 (18.9%)
Yes	48 (77.4%)	39 (86.4%)	86 (81.1%)
Prior anti-TNFα therapy			
No	39 (62.9%)	23 (52.3%)	62 (58.5%)
Yes	23 (37.1%)	21 (47.7%)	44 (41.5%)

SD-standard deviation; N-number; Miss-missing data. * $p < 0.05$ between ulcerative colitis and Crohn's disease groups.

A total of 114 VDZ trough concentration measurements (on average 1.08 samples/patient) were obtained during the follow-up period. These measurements correspond to 56 patients dosed every 4 weeks, 14 patients dosed every 6 weeks, and 36 patients dosed every 8 weeks during the maintenance phase. Due to the practical challenges posed by the COVID-19 pandemic and limited resources, TDM sampling was conducted just before the next dose but at the diverse treatment week-points during the maintenance phase,

and during the induction phase. Previous studies have shown that VDZ trough levels remain stable during the maintenance phase when consistent dosing intervals are used. Accordingly, we summarised all VDZ concentrations obtained during this phase for each dosing interval. Figure 1 illustrates the boxplot of trough VDZ concentrations during the induction and maintenance period based on dosing intervals of 4, 6 or 8 weeks.

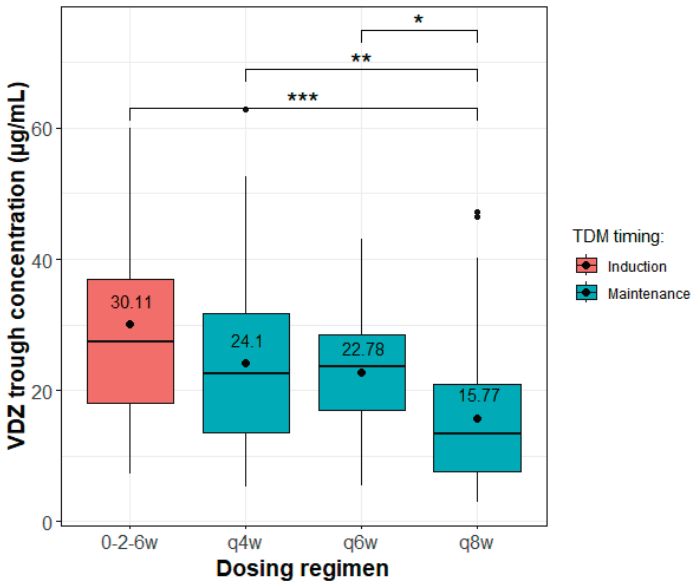


Figure 1. Boxplot of vedolizumab (VDZ) trough concentrations in patients receiving 300 mg as a 30-min infusion during the induction period and every 4, 6 or 8 weeks onwards. The dot represents the mean value, the central line within each box represents the median, and the edges of the box denote the interquartile range (IQR). The whiskers extend to values within 1.5 times the IQR and individual points are outliers beyond this range (* $p < 0.05$, ** $p < 0.01$, *** $p < 0.001$).

By analysing VDZ concentration-time data and accounting for dosing history along with the exact time intervals of dosing and TDM sampling, we characterised the structural PK profile of VDZ as a two-compartment model. A proportional error model better describes residual variability. The covariates were systematically examined, resulting in no significant difference in VDZ CL between UC and CD patients. However, patients with a history of anti-TNFα therapy exhibited an average increase of 26.4% in VDZ CL, as presented in Figure 2. The relationship between typical CL and anti-TNFα therapy is given by Equation (1):

$$TVCL = 0.159 \cdot (1 + 0.264 \cdot ATNF), \quad (1)$$

where ATNF equals 1 if a patient was previously treated with anti-TNFα treatment, or 0 if not. The inclusion of ATNF resulted in an OFV decrease of 13.96 units compared to the base model, corresponding to a *p*-value of 0.000187. 95% CI for the ATNF relationship parameter is 0.117–0.411, further supporting the significance of this covariate in the model.

The typical value of CL based on our final model was estimated at 0.159 L/day with an interindividual variability of 16.4%. The final parameter estimates and their bootstrap values are summarised in Table 2.

The standard goodness-of-fit plot, given in Figure S1, indicates a strong correlation between observed and model-predicted values, validating the accuracy of our model. The PopPK model was used to simulate concentration-time profiles for various VDZ dosing regimens in patients with and without prior anti-TNFα treatment, as shown in Figure S2. Based on these simulations, calculated trough concentrations and cumulative AUCs are given in Table 3.

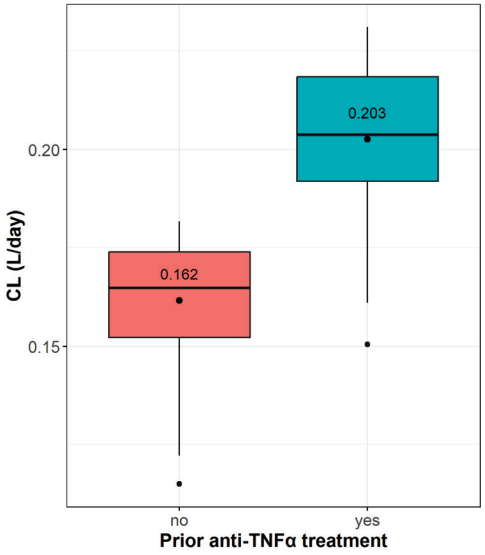


Figure 2. Distribution of individual vedolizumab (VDZ) clearance (CL) estimated from the final population pharmacokinetic (PopPK) model in patients with and without prior anti-TNFα therapy. The dot represents the mean value, the central line within each box represents the median CL, and the edges of the box denote the interquartile range (IQR). The whiskers extend to values within 1.5 times the IQR and individual points are outliers beyond this range.

Table 2. Final vedolizumab (VDZ) population pharmacokinetic (PopPK) parameters estimate using priors and their bootstrap results.

Parameter (Units)	Estimated Value (%RSE)	Bootstrap Median (2.5–97.5th Percentile)
CL (L/day)	0.159 (4.8)	0.160 (0.143–0.177)
Vc (L)	3.19 (1)	3.19 (3.191–3.192)
Q (L/day)	0.120 (3.8)	0.120 (0.119–0.120)
Vp (L)	1.66 (1.8)	1.66 (1.65–1.66)
ATNF	0.264 (28.3)	0.263 (0.105–0.453)
IIV_{CL} (%)	16.4 (25.3)	15.9 (7.91–32.3)
IIV_{Vc} (%)	18.9 (2.8)	18.9 (18.9–18.9)
Proportional residual error	0.458 (11.1)	0.453 (0.226–0.520)

CL—clearance; Vc—volume of distribution of the central compartment; Q—intercompartmental clearance; Vp—volume of distribution of the peripheral compartment; ATNF—increase of CL in the case of prior anti-TNFα therapy; IIV—interindividual variability for corresponding parameter; RSE—relative standard error.

Furthermore, we observed that serological and faecal biomarkers of inflammation stabilised and approached normal ranges at the TDM time point compared to baseline values before VDZ was introduced, at the statistically significant level $p < 0.05$ (Figure S3).

Linear regression analysis was performed to examine the relationship between biochemical parameters at the TDM time point and VDZ trough concentration during the maintenance phase or individual patient CL from the PopPK model. VDZ trough was a significant predictor of only FER levels among all the variables tested ($\beta = 1.0703$, $t_{(73)} = 2.572$, $p = 0.01214$), and the regression model explained 7.1% of the variance in FER. When VDZ CL was examined, the relationship was significant with CRP ($p = 0.0302$), Plt ($p = 2.42 \cdot 10^{-5}$), WBC ($p = 0.000743$), Alb ($p = 0.0354$) and FCP ($p = 0.0137$). Consequently, the relationship was most pronounced between VDZ CL and Plt among all tested variables. The linear regression model shows that CL is in positive association with Plt (Figure S4A), and using binary logistic regression analysis, it was found that having Plt levels greater than

$350 \cdot 10^9$/L is associated with significantly higher VDZ CL (Figure S4B). The area under the receiver operating curve (AUROC) value for VDZ CL in predicting the Plt categorical variable in our study was 76.9 (95% CI 62.8–91.1) with a Youden index of 0.430. However, these relationships were not statistically confirmed when analysing VDZ trough concentrations, although there was a tendency toward lower drug concentrations. The mean VDZ trough in the group of patients with Plt < $350 \cdot 10^9$/L was 23.42 µg/mL versus 18.66 µg/mL in the group where Plt > $350 \cdot 10^9$/L. Figure S5 shows the distribution of VDZ CL based on six categories of FCP defined by different range values.

Table 3. Summary of simulation results based on the population pharmacokinetic (PopPK) model of vedolizumab (VDZ) and dosing regimens. Results are presented as medians (5–95% confidence intervals, CI).

Dosing Regimen	prior Anti-TNFα	C_{trough} (5–95% CI) [ng/mL]	$AUC_{0\text{-}last}$ (5–95% CI) [ng·day/mL]
0–2–6w + 10w + q4w	no	36.6 (20.4–59.8)	16,534 (13,191–22,415)
	yes	25.7 (14.7–39.1)	13,851 (11,069–17,585)
0–2–6w + 14w + q6w	no	20.5 (12.4–35.9)	12,925 (9834–16,107)
	yes	13.4 (5.46–20.4)	10,236 (6877–12,993)
0–2–6w + q8w	no	11.6 (5.92–20.9)	10,860 (7856–14,551)
	yes	6.82 (2.86–13.9)	8531 (6723–12,305)
0–2–6w + 10w + q8w	no	26.4 (14.4–42.4)	11,816 (9279–16,496)
	yes	18.2 (11.4–31.8)	9879 (7380–13,386)

AUC—cumulative area under the concentration-time curve; C_{trough}—trough concentration in steady-state; w—week; q4w, q6w and q8w—dosing interval of 4, 6 and 8 weeks, respectively.

The binary logistic regression results of the statistically significant predictors of remission are given in Table 4. VDZ trough concentration was not a statistically significant predictor of remission. Moreover, clinical remission was associated with endoscopic remission ($p < 0.05$), but with worse performance than Plt, FCP and CL, with an AUROC of 60.1%.

Table 4. Summary of univariate binary logistic regression results for clinical and endoscopic remission including platelets (Plt), faecal calprotectin (FCP) and vedolizumab (VDZ) trough concentration (C_{trough}) and clearance (CL) as predictors.

Predictor Variable	Remission	*p*-Value	AUROC (95% CI)	Youden's Index	Optimal Threshold
Plt (10^9/L)	Clinical	<0.05	57.8 (44.9–70.7)	0.249	392
	Endoscopic	<0.001	70.6 (60.6–80.6)	0.313	257.5
FCP (µg/g)	Clinical	<0.01	74.4 (64.4–84.2)	0.427	164.5
	Endoscopic	<0.001	73.0 (63.6–82.5)	0.347	190.5
VDZ C_{trough} (ng/mL)	Clinical	n.s.	54.0 (42.5–65.5)	0.155	19.84
	Endoscopic	n.s.	49.4 (38.7–60.1)	0.0887	35.71
VDZ CL (L/day)	Clinical	<0.01	67.2 (56.1–78.2)	0.287	0.1886
	Endoscopic	<0.001	72.7 (63.0–82.4)	0.442	0.1886

AUROC—area under receiver operating curve; CI—confidence interval; n.s.—not significant.

In our multivariate binary logistic regression, Plt was not retained in the model. We found negative coefficients for FCP and VDZ CL, indicating lower odds of clinical and endoscopic remission with increasing values of both variables, as shown in Figure 3.

The association between VDZ CL as a categorical covariate using a cut-off of 0.1886 L/day (determined by ROC analysis), and endoscopic remission was evaluated. This analysis was conducted using the Cochran-Mantel-Haenszel (CMH) test, stratified by diagnosis during the maintenance phase. The analysis indicated that the pooled odds ratio (OR) for endoscopic remission associated with CL was 0.157. Higher VDZ CL (>0.1886 L/day) was associated with a lower likelihood of achieving endoscopic remission, accounting for

UC and CD. Analysis of strata-specific ORs revealed some variation, but the pooled OR indicated a consistent trend across both patient groups.

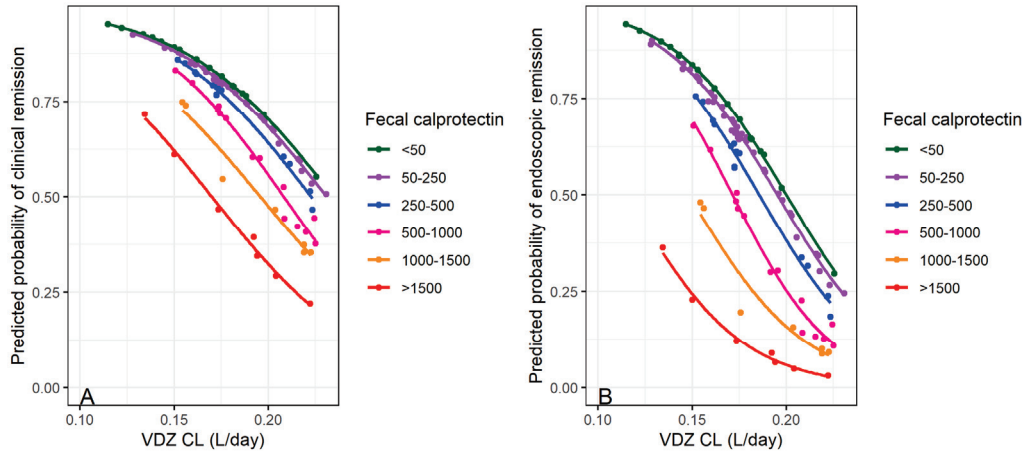


Figure 3. Predicted probability of (**A**) clinical and (**B**) endoscopic remission with vedolizumab (VDZ) clearance (CL) based on faecal calprotectin (FCP) values.

Our final analysis focused on time to endoscopic remission, further supporting the previous findings. This analysis was performed in a limited number of patients (n = 64) with available data on time to remission. FCP, Plt and VDZ CL were statistically significant predictors of endoscopic remission, even though VDZ trough concentration was not. In the multivariable analysis, FCP and VDZ CL emerged as the strongest predictors of the probability of endoscopic remission (Figure 4A). Additionally, the hazard ratio (HR) for CL above the cut-off was 0.35 (95% CI: 0.12–1.0, $p = 0.05$) and for FCP below 250 µg/g, it was 2.66 (95% CI: 1.16–6.1, $p = 0.02$), as given on Figure 4B.

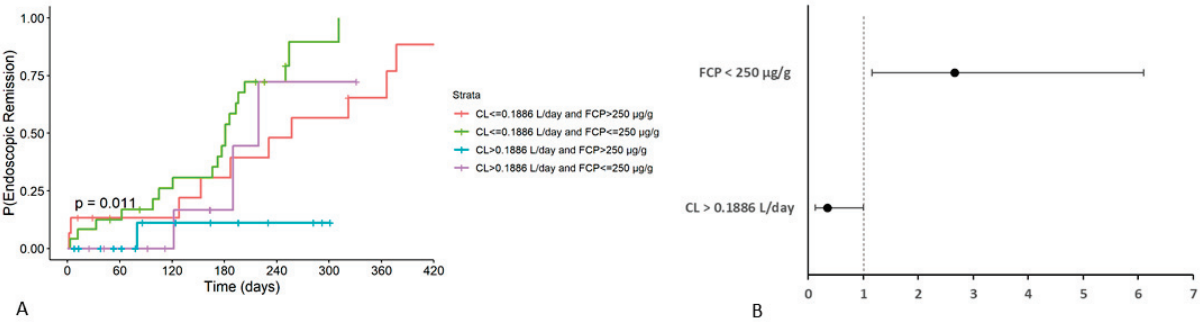


Figure 4. (**A**) Time to endoscopic remission based on vedolizumab (VDZ) clearance (CL) and faecal calprotectin (FCP) categories. (**B**) Forest plot illustrates the estimated effects of VDZ CL and FCP on endoscopic remission where each horizontal line represents a 95% confidence interval (CI).

4. Discussion

The findings from this study shed light on inter-patient variability in the PK profile of VDZ, its characterisation via the PopPK model, and identifying significant factors influencing its CL in IBD patients. Furthermore, our results support that VDZ CL, rather than trough concentration, serves as a more reliable predictor of response. Given the absence of a definitive exposure-response relationship necessary to support VDZ TDM, we hypothesise that VDZ CL may act as a surrogate of response and remission in IBD patients.

The variability in VDZ PK observed in our patient cohort aligns with prior research, showing moderate to high differences in VDZ concentrations among patients. Typically, VDZ trough levels during the standard induction phase are around 27 µg/mL. In the maintenance phase, mean steady-state pre-dose levels are approximately 12 µg/mL and 36 µg/mL for dosing intervals of 8 weeks and 4 weeks, respectively, as reported in the

GEMINI 1, 2 and 3 phase III studies [1,6,7,37]. When an additional dose was administered at week 10, VDZ levels were maintained around 27 μg/mL at both week 10 and week 14. The concentration then drops to expected levels with standard dosing by week 22 and remains stable thereafter [14]. High interpatient variability (above 50%) in VDZ concentrations has been consistently observed across these studies [6,7,14,37]. The trough concentrations obtained in our study (Figure 1) are consistent with these findings [2,14].

Two-compartment model best fitted observed VDZ concentrations; however, our sparse sampling design significantly limited the estimation of structural parameters other than CL. To address this limitation, we used informative priors from the previous model [5] for the remaining PK parameters and their variabilities. The estimated typical value of CL (0.159 L/day) is consistent with previous PK models, which estimated values in the range of 0.155 to 0.215 L/day [5,9,12]. Covariate analysis revealed no statistically significant difference in VDZ CL between UC and CD patients, suggesting that the disease subtype does not affect VDZ PK, as previously reported [2,5,13]. However, prior anti-TNFα therapy significantly affected CL (Figure 2 and Table 2). Specifically, patients with a history of anti-TNFα therapy exhibited an average increase of 26.4% in VDZ CL, which is similar to a previous report by Hanzel et al. (24.5% lower CL in treatment-naïve patients) [12]. Interestingly, other models describe a significant but modest effect of previous anti-TNFα therapy on CL (4–5%), judged as clinically insignificant [5,11]. However, in the exposure-response study, the probability of remission was approximately 10% higher in treatment-naïve patients [18]. We hypothesise that patients previously treated with infliximab or adalimumab may have more severe disease and inflammation, leading to gastrointestinal "leakage" that could contribute to the increased CL. This supports the potential for CL to serve as a pharmacodynamic (PD) marker for VDZ response in IBD patients, a hypothesis that should be further explored in future studies.

One key advantage of PopPK modelling is its ability to provide individual empirical Bayes estimates of PK parameters. As a result, our statistical analysis relied on patient-specific VDZ CL estimates from the final model. Further analysis revealed a positive correlation between VDZ CL and Plt levels (Figure S4A). Specifically, Plt > $350 \cdot 10^9$/L was associated with higher VDZ CL (Figure S4B). A higher CL is expected to lead to lower trough concentration under the same dosing regimen. However, the relationship between trough levels and Plt was not confirmed, although a trend toward lower levels was observed. This finding may suggest that thrombocytosis reflects a higher inflammatory burden, potentially influencing VDZ elimination (Figure S4). Our results align with previous findings that lower VDZ trough levels are associated with biological markers of disease severity [14]. The role of Plts as an inflammatory marker and their association with VDZ CL is a novel observation not yet explored in existing literature [2,17]. Thrombocytosis is commonly observed in active IBD, and our study suggests that the drug's rate of elimination may predict Plt levels. This hypothesis opens new avenues for research, particularly regarding the interplay between inflammation, thrombocytosis and VDZ trough levels or CL in IBD patients.

Previous publications have established correlations between VDZ trough levels and various responses and remissions in IBD patients [7,14,15,18–20,23–25]. The findings from our study (outlined in Table 4) contribute to the existing body of literature by indicating that VDZ CL, rather than trough concentration, is a more reliable predictor of clinical response and remission in IBD patients. Utilizing the CMH test, we demonstrated that after adjusting for diagnosis, a significant association between VDZ CL and the likelihood of achieving endoscopic remission remains both in UC and CD patients (Table 4). The cut-off point for CL as a categorical covariate (0.1886 L/day) is approximately centred within the range of previously reported typical values (0.155–0.215 L/day). In addition to CL, FCP and Plt were identified as independent predictors of endoscopic and clinical remission (Table 4), although the Plt variable was not retained in the multivariate logistic regression model. This is in line with previous findings that patients with lower FCP have a higher probability of remission [2,18]. A recent study showed that FCP < 250 μg/g at

week 8 predicted endoscopic response in both UC and CD patients [38]. Additionally, other research indicated that FCP levels at weeks 16 and 52 were significantly correlated with sustained endoscopic response [39]. Our further analysis, focusing on time to endoscopic remission, supported these findings, indicating that patients with VDZ CL < 0.1886 L/day and FCP < 250 μg/g have the highest probability of achieving endoscopic remission, as presented in Figure 4.

A very important finding of our study is that changes in CL are more closely correlated with clinical and endoscopic remission than VDZ trough levels. Patients with high CL rates require higher doses to reach effective drug exposure to obtain adequate response. These results can be explained by understanding the basic key PK principles and how they apply [40]. CL is a dynamic direct measure of how efficiently the drug is being eliminated from the body, and it integrates multiple processes. In contrast, trough concentration is a static snapshot that may not fully capture the complexity of mAb elimination processes. As a result, CL offers a more comprehensive picture of the drug's behaviour in the body. In addition, there is an intrinsic correlation between the area under the concentration-time curve (AUC), which provides a complete picture of drug exposure, and the CL of the drug. AUC is inversely proportional to CL for a given dose; thus, CL influences the overall (cumulative) drug exposure [40]. Hence, a patient with higher CL will have a lower AUC, and vice versa (Figure S2).

In addition, as previously written, VDZ CL can be influenced by various factors. The development of ADAs can increase CL and potentially reduce drug efficacy [2]. By monitoring CL, clinicians can detect the impact of ADAs and adjust treatment strategies accordingly. Trough concentration alone may not provide this insight, especially if ADAs cause rapid CL fluctuations that are not captured at a single time point. We did not measure ADA in our study, however, the rate of neutralising anti-VDZ antibodies is low at 3% in patients, so, we assume that this small percentage would not influence the study results. Therefore, by focusing on CL, not on a single concentration, we can account for these individual differences, providing a more personalised and accurate assessment of drug exposure [41]. Given that AUC represents complete drug exposure over a dosing interval, it might serve as a more comprehensive predictor of clinical response and remission compared to trough concentration alone. We hypothesise that cumulative AUC-based exposure or time above a certain threshold might better predict outcomes in IBD patients treated with VDZ than single trough concentration. Recently, preliminary results for infliximab support the AUC-response relationship suggesting AUC-guided TDM [42]. Nevertheless, some data indicate that a significant number of IBD patients gain a response over time. These are patients who did not respond to treatment at week 6 but showed a response by week 14 (approximately 10% of patients) or week 30 (around 30% of patients). This may support the importance of extended exposure to drugs over a period of time. The decision to prioritise CL over alternative exposure metrics in the analysis was driven by critical limitations in the dataset. Specifically, TDM was conducted at random intervals. Moreover, the significant variability in therapy duration and outcome timings further complicated the use of individual AUC or time above a specific target, making it challenging to account for these discrepancies. Given these challenges, simulations in a virtual population using typical dosing regimens were performed to gain insights into the underlying dynamics and better understand the situation.

However, it is important to recognise that there is a bidirectional relationship between mAb CL and disease activity. High disease activity, as seen in severe IBD, appears to increase VDZ CL, potentially due to protein loss or a "leaky gut" phenomenon, which in turn reduces drug concentrations. Conversely, elevated CL results in lower drug exposure, which may compromise clinical outcomes by failing to adequately suppress inflammation. To address this, it is crucial to first select patients where non-mechanistic failure exists, and where TDM can assist in optimising dosing to improve outcomes and achieve better disease control. Nevertheless, our ongoing prospective research aims to investigate the correlations

between CL and various exposure metrics with clinical outcomes. We anticipate that this study will contribute to a more comprehensive and reliable approach to TDM of biologics.

Several limitations should be acknowledged. While providing valuable insights, the retrospective nature, the limited sample size, and the few cases in our study may limit the statistical power and restrict the generalisability of the findings. Specifically, the retrospective study design limited obtaining endoscopic results at the same time for each patient. The study was conducted at a single centre, which may introduce biases related to local clinical practices, patient demographics and treatment protocols, further limiting the external validity. Prospective multicentre studies with larger cohorts are necessary to validate these results and refine the pharmacokinetic-pharmacodynamic relationship further. Additionally, exploring the mechanisms behind the altered drug CL observed in patients with previous biological exposure could help in designing more effective treatment regimens. We acknowledge that the current frequency of 1 sample per patient during the maintenance phase may limit precision, and future studies should employ a higher sampling frequency to optimise outcome predictions. Perhaps, after the induction, the sampling before the 4th dose (week 14), every 6 months during the maintenance phase, and at flare-up of symptoms could be considered. Nevertheless, real-world clinical data are crucial for providing a more comprehensive perspective, and that is the greatest strength of this study.

In summary, while trough concentration provides useful information for TDM, VDZ CL offers a more robust and clinically relevant predictor of remission in IBD patients. By understanding CL, we can more accurately tailor dosing regimens to individual patient needs, ultimately enhancing therapeutic outcomes and achieving sustained remission. Furthermore, our ongoing prospective research aims to further investigate the potential of not only CL but also other exposure metrics as surrogates of response and remission in IBD patients. This could provide deeper insights into optimising VDZ therapy.

5. Conclusions

The findings of this study explore various factors of VDZ PK variability and point out a 26.4% increase in VDZ CL with prior anti-TNFα treatment. Moreover, VDZ CL emerged as a more robust and clinically relevant predictor of remission in IBD patients, potentially serving as a PD marker as it can reflect disease activity. Our results reinforce the potential role of CL as a surrogate for remission in IBD patients undergoing VDZ therapy. Future research should focus on exploring the role of VDZ CL together with identifying appropriate exposure metrics to better predict treatment response on evaluating the value of TDM and MIPD-TDM in VDZ optimisation, exploring its PK profile and exposure-response relationship in acute severe UC and fistulizing CD, and assessing its PK in paediatric IBD patients. Additionally, comparative studies of the PK profile of VDZ in comparison to other monoclonal antibodies are needed to identify potential similarities and differences that could inform overall personalised biologics therapy in IBD treatment.

Supplementary Materials: The following supporting information can be downloaded at: https://www.mdpi.com/article/10.3390/pharmaceutics16121629/s1, Table S1: Disease phenotype and clinical characteristics of patients; Figure S1: Goodness-of-fit plots for the vedolizumab (VDZ) final population pharmacokinetic model: observed vs. (A) population (B) individual predicted trough concentration; conditional weighted residual (CWRES) vs. (C) population predicted concentration and (D) time after dose. Values are shown as points with a dashed LOESS trend line through the data, and solid is a line of identity; Figure S2: Simulated concentration-time profiles based on our final population pharmacokinetic model based on previous treatment with anti-TNFα (pink—no, blue—yes) after four dosing regimens (shadow area—95% confidence interval, CI); Figure S3: Individual biochemical parameters at baseline (0) and therapeutic drug monitoring time point (1) and calculated mean difference with p-values using paired Student's *t*-test. (A) Hgb—haemoglobin; (B) Er—erythrocyte; (C) Fe—iron; (D) CRP—C-reactive protein; (E) Alb—albumin; (F) Plt—platelets; (G) WBC—leukocytes; (H) FER—ferritin; (I) FCP—faecal calprotectin; Figure S4: (A) Linear regression and (B) boxplot for logistic regression between vedolizumab (VDZ) clearance (CL) and thrombocytes

(Plt); Figure S5: Distribution of individual vedolizumab (VDZ) clearance (CL) based on faecal calprotectin values categories. The dot represents the mean value, the central line within each box represents the median, and the edges of the box denote the interquartile range (IQR). The whiskers extend to values within 1.5 times the IQR and individual points are outliers beyond this range (* $p < 0.05$).

Author Contributions: S.M., P.S. and K.M.V. conceptualisation and design of the research; Đ.K., T.K.I., O.O., S.O. and A.H. data curation; K.M.V., R.S. and M.J. formal analysis of data; S.M., Đ.K., T.K.I., O.O. and S.O. investigation and patient recruitment; S.M., P.S., Đ.K., T.K.I. and O.O. interpretation of data; R.S. and K.M.V. methodology; K.M.V. project administration; S.M., Đ.K., A.H., M.J. and K.M.V. writing—original draft; P.S., T.K.I., O.O., S.O. and R.S. writing—review and editing. All authors have read and agreed to the published version of the manuscript.

Funding: This research was supported by the Science Fund of the Republic of Serbia, through grant agreement No. *6777*, Improving Clinical Outcomes with Precision Dosing in Patients with Inflammatory Bowel Disease Through Investigating Variability of Monoclonal Antibodies Based on Population Pharmacokinetic-Pharmacodynamic Modelling—optYmAb.

Institutional Review Board Statement: The study followed the principles of the Declaration of Helsinki and was approved by the local ethical committee of the University Clinical Hospital Centre "Zvezdara" (approval code n. IRB00009457).

Informed Consent Statement: Informed consent was obtained from all subjects involved in the study.

Data Availability Statement: The data that support the findings of this study are not openly accessible due to ethical restrictions.

Conflicts of Interest: The authors declare no conflicts of interest.

References

1. SmPC Entyvio. Summary of Product Characteristics for Entyvio 300 mg Powder for Concentrate for Solution for Infusion. Last Updated on the eMC: 02/15/2024. Available online: https://www.medicines.org.uk/emc/product/5442/smpc#gref (accessed on 1 October 2024).
2. Rosario, M.; Dirks, N.L.; Milch, C.; Parikh, A.; Bargfrede, M.; Wyant, T.; Fedyk, E.; Fox, I. A review of the clinical pharmacokinetics, pharmacodynamics, and immunogenicity of vedolizumab. *Clin. Pharmacokinet.* **2017**, *56*, 1287–1301. [CrossRef] [PubMed]
3. Rosario, M.; Wyant, T.; Leach, T.; Sankoh, S.; Scholz, C.; Parikh, A.; Fox, I.; Feagan, B.G. Vedolizumab pharmacokinetics, pharmacodynamics, safety, and tolerability following administration of a single, ascending, intravenous dose to healthy volunteers. *Clin. Drug Investig.* **2016**, *36*, 913–923. [CrossRef] [PubMed]
4. Ward, M.G.; Sparrow, M.P.; Roblin, X. Therapeutic drug monitoring of vedolizumab in inflammatory bowel disease: Current data and future directions. *Therap Adv. Gastroenterol.* **2018**, *11*, 1756284818772786. [CrossRef]
5. Rosario, M.; Dirks, N.L.; Gastonguay, M.R.; Fasanmade, A.A.; Wyant, T.; Parikh, A.; Sandborn, W.J.; Feagan, B.G.; Reinisch, W.; Fox, I. Population pharmacokinetics-pharmacodynamics of vedolizumab in patients with ulcerative colitis and Crohn's disease. *Aliment. Pharmacol. Ther.* **2015**, *42*, 188–202. [CrossRef]
6. Feagan, B.G.; Rutgeerts, P.; Sands, B.E.; Hanauer, S.; Colombel, J.F.; Sandborn, W.J.; Van Assche, G.; Axler, J.; Kim, H.J.; Danese, S.; et al. Vedolizumab as induction and maintenance therapy for ulcerative colitis. *N. Engl. J. Med.* **2013**, *369*, 699–710. [CrossRef] [PubMed]
7. Sandborn, W.J.; Feagan, B.G.; Rutgeerts, P.; Hanauer, S.; Colombel, J.F.; Sands, B.E.; Lukas, M.; Fedorak, R.N.; Lee, S.; Bressler, B.; et al. Vedolizumab as induction and maintenance therapy for Crohn's disease. *N. Engl. J. Med.* **2013**, *369*, 711–721. [CrossRef] [PubMed]
8. Roganovic, M.; Homsek, A.; Jovanovic, M.; Topić Vučenović, V.; Ćulafić, M.; Miljković, B.; Vučićević, K. Concept and utility of population pharmacokinetic and pharmacokinetic/pharmacodynamic models in drug development and clinical practice. *Arh. Farm.* **2021**, *71*, 336–353. [CrossRef]
9. Okamoto, H.; Dirks, N.L.; Rosario, M.; Hori, T.; Hibi, T. Population pharmacokinetics of vedolizumab in Asian and non-Asian patients with ulcerative colitis and Crohn's disease. *Intest. Res.* **2021**, *19*, 95–105. [CrossRef] [PubMed]
10. Pauwels, R.W.M.; Proietti, E.; van der Woude, C.J.; Oudijk, L.; Crombag, M.B.S.; Peppelenbosch, M.P.; Grohmann, U.; Fuhler, G.M.; de Vries, A.C. Vedolizumab tissue concentration correlates to mucosal inflammation and objective treatment response in inflammatory bowel disease. *Inflamm. Bowel Dis.* **2021**, *27*, 1813–1820. [CrossRef] [PubMed]
11. Wyant, T.; Yang, L.; Rosario, M. Comparison of the ELISA and ECL Assay for vedolizumab anti-drug antibodies: Assessing the impact on pharmacokinetics and safety outcomes of the phase 3 GEMINI trials. *AAPS* **2020**, *23*, 3. [CrossRef]
12. Hanzel, J.; Dreesen, E.; Vermeire, S.; Lowenberg, M.; Hoentjen, F.; Bossuyt, P.; Clasquin, E.; Baert, F.J.; D'Haens, G.R.; Mathot, R. Pharmacokinetic-pharmacodynamic model of vedolizumab for targeting endoscopic remission in patients with crohn disease: Posthoc analysis of the LOVE-CD study. *Inflamm. Bowel Dis.* **2022**, *28*, 689–699. [CrossRef]

13. Colman, R.J.; Mizuno, T.; Fukushima, K.; Haslam, D.B.; Hyams, J.S.; Boyle, B.; Noe, J.D.; D'Haens, G.R.; Van Limbergen, J.; Chun, K.; et al. Real world population pharmacokinetic study in children and young adults with inflammatory bowel disease discovers novel blood and stool microbial predictors of vedolizumab clearance. *Aliment. Pharmacol. Ther.* **2023**, *57*, 524–539. [CrossRef] [PubMed]
14. Dreesen, E.; Verstockt, B.; Bian, S.; de Bruyn, M.; Compernolle, G.; Tops, S.; Noman, M.; Van Assche, G.; Ferrante, M.; Gils, A.; et al. Evidence to support monitoring of vedolizumab trough concentrations in patients with inflammatory bowel diseases. *Clin. Gastroenterol. Hepatol.* **2018**, *16*, 1937–1946.e1938. [CrossRef]
15. Cusato, J.; Ribaldone, D.G.; Falzone, M.H.; Manca, A.; Antonucci, M.; Palermiti, A.; Saracco, G.M.; Ceccarelli, L.; Costa, F.; Bottari, A.; et al. Therapeutic drug monitoring as a tool for the clinical outcome prediction in vedolizumab-treated patients: An italian pilot study. *Biomedicines* **2024**, *12*, 824. [CrossRef] [PubMed]
16. Steenholdt, C.; Lorentsen, R.D.; Petersen, P.N.; Widigson, E.S.; Kloft, C.; Klaasen, R.A.; Brynskov, J. Therapeutic drug monitoring of vedolizumab therapy in inflammatory bowel disease. *J. Gastroenterol. Hepatol.* **2024**, *39*, 1088–1098. [CrossRef] [PubMed]
17. Restellini, S.; Afif, W. Update on TDM (Therapeutic Drug Monitoring) with Ustekinumab, Vedolizumab and Tofacitinib in Inflammatory Bowel Disease. *J. Clin. Med.* **2021**, *10*, 1242. [CrossRef]
18. Rosario, M.; French, J.L.; Dirks, N.L.; Sankoh, S.; Parikh, A.; Yang, H.; Danese, S.; Colombel, J.F.; Smyth, M.; Sandborn, W.J.; et al. Exposure-efficacy relationships for vedolizumab induction therapy in patients with ulcerative colitis or crohn's disease. *J. Crohns Colitis* **2017**, *11*, 921–929. [CrossRef] [PubMed]
19. Osterman, M.T.; Rosario, M.; Lasch, K.; Barocas, M.; Wilbur, J.D.; Dirks, N.L.; Gastonguay, M.R. Vedolizumab exposure levels and clinical outcomes in ulcerative colitis: Determining the potential for dose optimisation. *Aliment. Pharmacol. Ther.* **2019**, *49*, 408–418. [CrossRef] [PubMed]
20. Williet, N.; Boschetti, G.; Fovet, M.; Di Bernado, T.; Claudez, P.; Del Tedesco, E.; Jarlot, C.; Rinaldi, L.; Berger, A.; Phelip, J.M.; et al. Association between low trough levels of vedolizumab during induction therapy for inflammatory bowel diseases and need for additional doses within 6 months. *Clin. Gastroenterol. Hepatol.* **2017**, *15*, 1750–1757.e1753. [CrossRef]
21. Al-Bawardy, B.; Ramos, G.P.; Willrich, M.A.V.; Jenkins, S.M.; Park, S.H.; Aniwan, S.; Schoenoff, S.A.; Bruining, D.H.; Papadakis, K.A.; Raffals, L.; et al. Vedolizumab drug level correlation with clinical remission, biomarker normalization, and mucosal healing in inflammatory bowel disease. *Inflamm. Bowel Dis.* **2019**, *25*, 580–586. [CrossRef]
22. Yacoub, W.; Williet, N.; Pouillon, L.; Di-Bernado, T.; De Carvalho Bittencourt, M.; Nancey, S.; Lopez, A.; Paul, S.; Zallot, C.; Roblin, X.; et al. Early vedolizumab trough levels predict mucosal healing in inflammatory bowel disease: A multicentre prospective observational study. *Aliment. Pharmacol. Ther.* **2018**, *47*, 906–912. [CrossRef] [PubMed]
23. Ungaro, R.C.; Yarur, A.; Jossen, J.; Phan, B.L.; Chefitz, E.; Sehgal, P.; Kamal, K.; Bruss, A.; Beniwal-Patel, P.; Fox, C.; et al. Higher trough vedolizumab concentrations during maintenance therapy are associated with corticosteroid-free remission in inflammatory bowel disease. *J. Crohns Colitis* **2019**, *13*, 963–969. [CrossRef] [PubMed]
24. Pouillon, L.; Rousseau, H.; Busby-Venner, H.; De Carvalho Bittencourt, M.; Choukour, M.; Gauchotte, G.; Zallot, C.; Danese, S.; Baumann, C.; Peyrin-Biroulet, L. Vedolizumab trough levels and histological healing during maintenance therapy in ulcerative colitis. *J. Crohns Colitis* **2019**, *13*, 970–975. [CrossRef] [PubMed]
25. Yarur, A.J.; Bruss, A.; Naik, S.; Beniwal-Patel, P.; Fox, C.; Jain, A.; Berens, B.; Patel, A.; Ungaro, R.; Bahur, B.; et al. Vedolizumab concentrations are associated with long-term endoscopic remission in patients with inflammatory bowel diseases. *Dig. Dis. Sci.* **2019**, *64*, 1651–1659. [CrossRef] [PubMed]
26. Singh, S.; Dulai, P.S.; Vande Casteele, N.; Battat, R.; Fumery, M.; Boland, B.S.; Sandborn, W.J. Systematic review with meta-analysis: Association between vedolizumab trough concentration and clinical outcomes in patients with inflammatory bowel diseases. *Aliment. Pharmacol. Ther.* **2019**, *50*, 848–857. [CrossRef] [PubMed]
27. Pouillon, L.; Vermeire, S.; Bossuyt, P. Vedolizumab trough level monitoring in inflammatory bowel disease: A state-of-the-art overview. *BMC Med.* **2019**, *17*, 89. [CrossRef] [PubMed]
28. Vaughn, B.P.; Yarur, A.J.; Graziano, E.; Campbell, J.P.; Bhattacharya, A.; Lee, J.Y.; Gheysens, K.; Papamichael, K.; Osterman, M.T.; Cheifetz, A.S.; et al. Vedolizumab serum trough concentrations and response to dose escalation in inflammatory bowel disease. *J. Clin. Med.* **2020**, *9*, 3142. [CrossRef] [PubMed]
29. Rosario, M.; Abhyankar, B.; Sankoh, S.; Dirks, N.; Lasch, K.; Sandborn, W. Relationship between vedolizumab pharmacokinetics and endoscopic outcomes in patients with ulcerative colitis. *J. Crohns Colitis* **2015**, *9*, S46.
30. Jairath, V.; Yarur, A.; Osterman, M.T.; James, A.; Balma, D.; Mehrotra, S.; Yang, L.; Yajnik, V.; Qasim Khan, R.M. ENTERPRET: A randomized controlled trial of vedolizumab dose optimization in patients with ulcerative colitis who have early nonresponse. *Clin. Gastroenterol. Hepatol.* **2024**, *22*, 1077–1086.e13. [CrossRef]
31. Sethi, S.; Dias, S.; Kumar, A.; Blackwell, J.; Brookes, M.J.; Segal, J.P. Meta-analysis: The efficacy of therapeutic drug monitoring of anti-tnf-therapy in inflammatory bowel disease. *Aliment. Pharmacol. Ther.* **2023**, *57*, 1362–1374. [CrossRef]
32. Cheifetz, A.S.; Abreu, M.T.; Afif, W.; Cross, R.K.; Dubinsky, M.C.; Loftus, E.V., Jr.; Osterman, M.T.; Saroufim, A.; Siegel, C.A.; Yarur, A.J.; et al. A comprehensive literature review and expert consensus statement on therapeutic drug monitoring of biologics in inflammatory bowel disease. *Am. J. Gastroenterol.* **2021**, *116*, 2014–2025. [CrossRef] [PubMed]
33. Di Paolo, A.; Luci, G. Personalized medicine of monoclonal antibodies in inflammatory bowel disease: Pharmacogenetics, therapeutic drug monitoring, and beyond. *Front. Pharmacol.* **2020**, *11*, 610806. [CrossRef] [PubMed]

34. Beal, S.L.; Sheiner, L.B.; Boeckmann, A.J.; Bauer, R.J. *NONMEM 7.5 Users Guides*; Icon Development Solutions: Ellicott City, MD, USA, 1989–2024.
35. Chan Kwong, A.H.P.; Calvier, E.A.M.; Fabre, D.; Gattacceca, F.; Khier, S. Prior information for population pharmacokinetic and pharmacokinetic/pharmacodynamic analysis: Overview and guidance with a focus on the NONMEM PRIOR subroutine. *J. Pharmacokinet. Pharmacodyn.* **2020**, *47*, 431–446. [CrossRef]
36. Gisleskog, P.O.; Karlsson, M.O.; Beal, S.L. Use of prior information to stabilize a population data analysis. *J. Pharmacokinet. Pharmacodyn.* **2002**, *29*, 473–505. [CrossRef] [PubMed]
37. Sands, B.E.; Feagan, B.G.; Rutgeerts, P.; Colombel, J.F.; Sandborn, W.J.; Sy, R.; D'Haens, G.; Ben-Horin, S.; Xu, J.; Rosario, M.; et al. Effects of vedolizumab induction therapy for patients with Crohn's disease in whom tumor necrosis factor antagonist treatment failed. *Gastroenterology* **2014**, *147*, 618–627.e3. [CrossRef]
38. Pauwels, R.W.M.; van der Woude, C.J.; Erler, N.S.; de Vries, A.C. Fecal calprotectin is an early predictor of endoscopic response and histologic remission after the start of vedolizumab in inflammatory bowel disease. *Therap Adv. Gastroenterol.* **2020**, *13*, 1756284820979765. [CrossRef] [PubMed]
39. Pauwels, R.W.M.; de Vries, A.C.; van der Woude, C.J. Fecal calprotectin is a reliable marker of endoscopic response to vedolizumab therapy: A simple algorithm for clinical practice. *J. Gastroenterol. Hepatol.* **2020**, *35*, 1893–1901. [CrossRef] [PubMed]
40. Fan, J.; de Lannoy, I.A. Pharmacokinetics. *Biochem. Pharmacol.* **2014**, *87*, 93–120. [CrossRef]
41. Magro, F.; Fernandes, S.; Patita, M.; Arroja, B.; Lago, P.; Rosa, I.; de Sousa, H.T.; Ministro, P.; Mocanu, I.; Vieira, A.; et al. The influence of subclinical active inflammation on IFX pharmacokinetic modeling and disease progression assessment: Findings from a prospective real-world study in inflammatory bowel disease patients. *J. Crohns Colitis* **2024**, *18*, 1102–1112. [CrossRef] [PubMed]
42. Mohamedi, J.A.; Thomas, D.; Rahier, J.F.; Louis, E.; Baert, F.; Dewint, P.; Lambrecht, G.; Vermeire, S.; Bossuyt, P.; Franchimont, D.; et al. Cumulative Exposure to Infliximab During Induction Therapy Predict Remission in Patients with Crohn's Disease and Ulcerative Colitis. PAGE 32 (2024) Abstr. 11125. 2024. Available online: www.page-meeting.org/?abstract=11125 (accessed on 1 October 2024).

Disclaimer/Publisher's Note: The statements, opinions and data contained in all publications are solely those of the individual author(s) and contributor(s) and not of MDPI and/or the editor(s). MDPI and/or the editor(s) disclaim responsibility for any injury to people or property resulting from any ideas, methods, instructions or products referred to in the content.

pharmaceutics

MDPI

Article

Model-Informed Precision Dosing for Personalized Ustekinumab Treatment in Plaque Psoriasis

Karine Rodríguez-Fernández [1,2,†], Javier Zarzoso-Foj [1,2,†], Marina Saez-Bello [3], Almudena Mateu-Puchades [4], Antonio Martorell-Calatayud [5], Matilde Merino-Sanjuan [1,2], Elena Gras-Colomer [6], Monica Climente-Martí [3] and Victor Mangas-Sanjuan [1,2,*]

[1] Department of Pharmacy and Pharmaceutical Technology and Parasitology, University of Valencia, 46100 Valencia, Spain; karofer@alumni.uv.es (K.R.-F.); javier.zarzoso@uv.es (J.Z.-F.); matilde.merino@uv.es (M.M.-S.)
[2] Interuniversity Research Institute for Molecular Recognition and Technological Development, Polytechnic University of Valencia-University of Valencia, 46100 Valencia, Spain
[3] Pharmacy Service, Doctor Peset University Hospital, Foundation for the Promotion of Health and Biomedical Research in the Valencian Region (FISABIO), 46017 Valencia, Spain; saez_marbel@gva.es (M.S.-B.); climente_mon@gva.es (M.C.-M.)
[4] Dermatology Service, Doctor Peset University Hospital, Foundation for the Promotion of Health and Biomedical Research in the Valencian Region (FISABIO), 46017 Valencia, Spain; mateu_alm@gva.es
[5] Dermatology Service, Hospital Manises of Valencia, 46940 Valencia, Spain; martorell_antcal@gva.es
[6] Pharmacy Service, Hospital Manises of Valencia, 46940 Valencia, Spain; gras_ele@gva.es
* Correspondence: victor.mangas@uv.es; Tel.: +34-963-543-351
† These authors contributed equally to this work.

Abstract: Background/Objectives: Implementing model-informed precision dosing (MIPD) strategies guided by population pharmacokinetic/pharmacodynamic (PK/PD) models could enhance the management of inflammatory diseases such as psoriasis. However, the extent of individual experimental data gathered during MIPD significantly influences the uncertainty in estimating individual PK/PD parameters, affecting clinical dose selection decisions. Methods: This study proposes a methodology to individualize ustekinumab (UTK) dosing strategies for 23 Spanish patients with moderate to severe chronic plaque psoriasis., considering the uncertainty of individual parameters within a population PK/PD model. Results: An indirect response model from previous research was used to describe the PK/PD relationship between UTK serum concentrations and the Psoriasis Area and Severity Index (PASI) score. A maximum inhibition drug effect (I_{max}) model was selected, and a first-order remission constant rate of psoriatic skin lesion (k_{out} = 0.016 d^{-1}) was estimated. Conclusions: The MIPD approach predicted that 35% and 26% of the patients would need an optimized and intensified dosage regimen, respectively, compared to the regimen typically used in clinical practice. This analysis demonstrated its utility as a tool for selecting personalized UTK dosing regimens in clinical practice in order to optimize the probability of achieving targeted clinical outcomes in patients with psoriasis.

Keywords: psoriasis; ustekinumab; pharmacokinetic/pharmacodynamic

1. Introduction

The management of psoriasis, a chronic immune-mediated condition, has been revolutionized with the introduction of therapeutic monoclonal antibody (mAb), with ustekinumab (UTK) constituting one of the available treatment choices [1,2]. UTK targets with high specificity and affinity the shared p40 subunit of interleukin (IL)-12 and IL-23 [3,4]. Both cytokines play an important role in the immune cascade that leads to psoriasis, particularly in modulating the differentiation of naïve T-cells into Th1 and Th17 cells [5–7].

Under the brand name Stelara® (Janssen Biotech, Inc., Horsham, PA, USA) UTK is available in solution for injection and can be administered subcutaneously. The latter formulation offers flexibility in administration, autoinjectors being the most recent [8].

The clinical development programs for UTK have been the most extensive for a biologic agent. Phase III clinical trials [9–12] for UTK in psoriasis have specified a significant decrease in Psoriasis Area and Severity Index (PASI) scores, supporting considerable improvements in the severity of the disease. Additionally, UTK has been directly compared to the tumor necrosis factor inhibitor etanercept [13], representing the first-ever head-to-head comparison of biological agents in psoriasis treatment. UTK is dosed according to body weight, as indicated in the summary of product characteristics (SmPC) [8]. For individuals weighing $\leq$ 100 kg and those weighing > 100 kg, a 45 and 90 mg dose is given, respectively, at weeks 0 and 4 (induction period), followed by subsequent doses every 12 weeks (the maintenance period). UTK typically reaches a steady state within approximately 28 weeks of regular dosing.

A population pharmacokinetic (PK) modeling approach was developed for UTK in clinical trial adult patients with moderate to severe plaque psoriasis [14] and psoriatic arthritis [15] and in real-world data patients [16], using a one-compartment model with first-order absorption and first-order-elimination, demonstrating a comparable PK between adult patients from clinical trials and real-world data. The same model was developed in clinical trial pediatric patients with moderate to severe plaque psoriasis [17]. In addition, an integrated population PK analysis was performed to describe the PK behavior of UTK in healthy subjects and individuals with psoriasis, psoriatic arthritis, Crohn's disease, and ulcerative colitis [18]. The chosen structural PK model for UTK was a two-compartment open model incorporating first-order absorption and elimination kinetics. Notably, parameters such as clearance (CL) and the volume of distribution were found to increase nonlinearly with body weight. This model effectively incorporates the PK characteristics of UTK across all approved inflammatory conditions and in healthy individuals, providing a consistent framework for understanding UTK's PK profile in diverse patient populations. The relationship between serum concentration–time data with longitudinal measures of the PASI in patients with moderate to severe plaque psoriasis was described via an indirect response model in a clinical trial and real-world patient data [16,17,19,20]. The contribution of the UTK effect to the inhibition of the formation rate of psoriatic skin lesions was described by a maximum inhibition drug effect (I_{max}) model [21].

Dermatologists often follow labeled dosing recommendations for initial treatment with UTK, which may not be optimal or safe for every patient [22]. Due to variable psoriasis disease progression in individual patients and the variability in response, they perform changes in the dosing regimen of UTK during the maintenance period of treatment. These changes in routine clinical practice are called optimizations and intensifications of SmPC dosage regimens. Dose regimen optimization involves maintaining the dose but extending the dosing interval or decreasing the dose while maintaining the dosing interval. On the contrary, dose regimen intensification implies maintaining the dose but decreasing the dosing interval or increasing the dose while maintaining the dosing interval. With this approach, the risk of adverse events increases due to drug concentrations that are either supratherapeutic or subtherapeutic because of the lack of a model-informed decision-making process [23]. Additionally, the methods for individualization commonly used in standard clinical practice, such as those based on clinical response and therapeutic drug monitoring (TDM), demand strict adherence to the sampling schedule. Intervention typically occurs only after the drug has reached a steady state, and adjustments are made by comparing the patient's exposure to a target range. If the exposure falls outside this range, the dose is adjusted under the assumption of dose–exposure proportionality at steady state or based on clinical experience [24–27].

Consequently, dermatologists require a flexible approach for psoriasis treatment that considers non-labeled dosing regimens and transitions between different therapeutic modalities of psoriasis to select the optimal treatment for each patient and to solve the cases of suboptimal response, the loss of efficacy over time, or the emergence of adverse effects. These challenges highlight the critical importance of transitioning to model-informed precision dosing (MIPD) strategies guided by population pharmacokinetic/pharmacodynamic

(PK/PD) models. With MIPD, any timed sample can be utilized, allowing interventions at any point, from before the first dose to when a steady state is reached. The intervention method involves calculating a dose that achieves a predefined PK/PD target [27–32]. Implementing PK/PD models in dosing decisions for psoriasis management improves precision dosing and addresses the interindividual variability (IIV) observed in psoriasis treatment responses, enhancing therapeutic outcomes and patient safety [14,17,19,33]. Therefore, the objective of this study was to propose a methodology capable of individualizing dosing strategies of UTK in patients with moderate to severe chronic plaque psoriasis based on the uncertainty of the individual parameters of a population PK/PD model.

2. Materials and Methods

2.1. Study Design

A post-authorization, prospective, and observational clinical practice follow-up study was conducted on Spanish patients with moderate to severe chronic plaque psoriasis from Manises Hospital of Valencia. The authors affirm that all procedures undertaken in this study adhere to the ethical standards established by the pertinent national and institutional committees overseeing human experimentation. Furthermore, they ensure compliance with the Helsinki Declaration of 1975, with revisions made in 2008. The study received approval from the Ethics Committee of La Fe University and Polytechnic Hospital (protocol code VMS-UTK-2020-01 EPA-SP). All participants provided written informed consent. The enrollment period spanned from February 2021 to December 2022, encompassing individuals who had received at least one dose of UTK (Stelara®) and who were under treatment at the time of inclusion. The patients included in the study were receiving dosage regimens individualized (optimized/intensified or not) and authorized by the dermatologist based on their clinical response. Exclusion criteria included individuals below 18 years of age, pregnant individuals, and those with cognitive impairment. Treatment-related variables such as dosage regimen, time, and line of treatment were collected for each patient. Moreover, demographic data were extracted from the hospital's electronic clinical records, including age, sex, weight, and height.

2.2. Blood Sampling and Analytical Quantification of Samples

Patients were administered UTK via subcutaneous injection in the abdomen or upper thigh. The patients received the following dosage regimen as a current treatment: 45 or 90 mg of UTK every 12, 14, and 16 weeks (q12w, q14w, and q16w), 45 mg of UTK every 18 weeks (q18w), and 90 mg of UTK every 8, 10, and 15 weeks (q8w, q10w, q15w). Blood samples for PK analysis were collected using plain red vacutainer tubes immediately before UTK administration and approximately 2, 6, 10, 12, 14, 16, and 18 weeks afterward. After centrifugation, serum samples were transferred to separate tubes and frozen at temperatures between −20 and −80 °C until processing. Serum concentrations of UTK were measured in the laboratory of Manises Hospital using an enzyme-linked immunosorbent assay (ELISA; Promonitor-UTK assay, Progenika Biopharma, Grifols®, Derio, Spain). The Promonitor-UTK quantifies concentrations of UTK in the range of 0.63–20 μg/mL.

2.3. Psoriasis Area and Severity Index Score Measurement

In the dermatology service from Manises Hospital, patients initiating UTK therapy undergo PASI assessments every 3 months during the first year of treatment. Following the initial year, PASI evaluations occur every 6 months. Baseline PASI values, recorded at the onset of UTK therapy, were extracted from patient clinical records. All available PASI scores documented in patient clinal records during the approximately 1.5-year follow-up period were collected.

2.4. Modeling Data Analysis

Figure 1 summarizes the modeling strategy performed. The data analysis was initiated by simulation using the population PK parameters of the 7 reference PK models published

for UTK [14–18,34]. This aided in identifying the model that most accurately represented our data. Subsequently, we applied the chosen model along with the individual UTK serum concentrations gathered during TDM to estimate individual PK parameters.

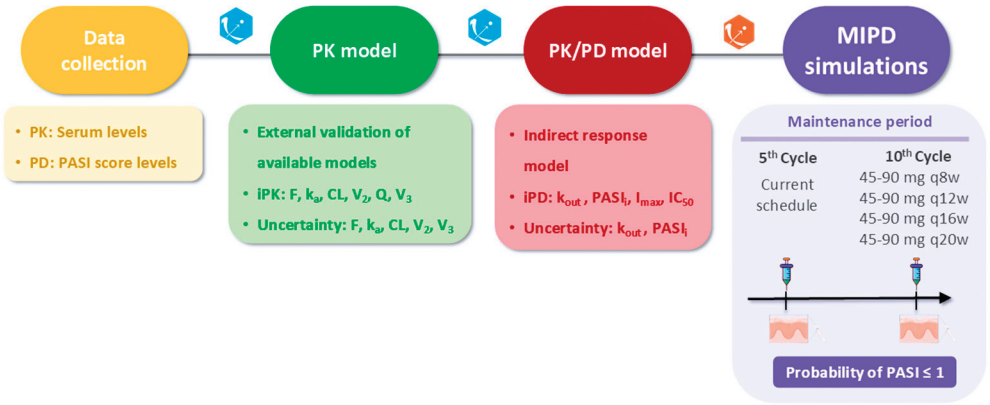


Figure 1. Modeling workflow. PK: pharmacokinetic; PD: pharmacodynamic; PASI: Psoriasis Area and Severity Index; iPK: individual pharmacokinetic parameter; iPD: individual pharmacodynamic parameter; F: bioavailability; k_a: absorption rate constant; CL: clearance; Q: intercompartmental transfer clearance; V_2: central volume of distribution; V_3: peripheral volume of distribution; k_{out}: first-order remission constant rate of psoriatic skin lesion; I_{max}: maximum inhibition drug effect model; $PASI_i$: estimated baseline levels of PASI response; IC_{50}: concentration of the drug needed to inhibit 50% of the response; MIPD: model-informed precision dosing; q8w: once every 8 weeks, q12w: once every 12 weeks; q16w: once every 16 weeks; q20w: once every 20 weeks.

A previously published indirect response model with PASI synthesis inhibition [16] was considered to describe the PK/PD relationship between UTK serum concentrations and the PASI (Figure 2). The ordinary differential equations of the PK/PD model can be found in the Supplementary Materials. This model structure was also previously applied to other mAbs designed for the treatment of psoriasis [19,35–38]. Linear, I_{max}, and sigmoid drug effects functions were evaluated [21].

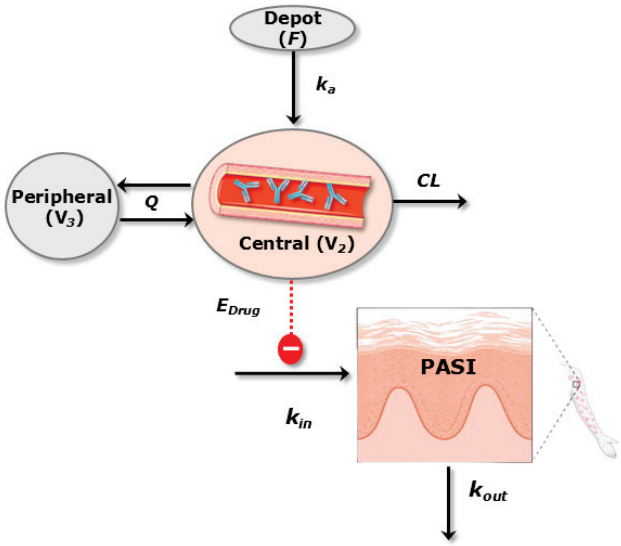


Figure 2. Schematic representation of the final PK/PD model. E_{Drug}: effect of the drug; k_{in}: zero-order progression constant rate of psoriatic skin lesion.

Baseline levels of PASI response ($PASI_i$) were estimated using the B2 method [39], where $PASI_i$ represents the individual predicted baseline level of the PASI, $PASI_{i,o}$ is the

individual observed baseline and $\eta_{i,RV}$ is the estimated individual random component accounting for the difference between $PASI_i$ and $PASI_{i,o}$. This variable has a mean equal to zero and, during parameter estimation, is restricted to having the same variance as the residual unexplained variability (RUV) (Equation (1)). Consequently, we assumed that the variability observed in the rest of the data also applies to the baseline data.

$$PASI_i = PASI_{i,0} \cdot e^{\eta_{i,RV}} \quad (1)$$

The selection of the PK/PD model was based on the comparison of the minimum value of the objective function, a visual exploration of goodness-of-fit plots and the precision of model parameters stated in the standard errors. An evaluation of the selected PK/PD models was performed through simulation-based diagnostics prediction-corrected visual predictive checks (pcVPCs) [40,41]. All data analyses were performed based on the population approach with the software Monolix 2024R1 (Lixoft SAS, a Simulations Plus company, Lancaster, CA, USA) [42]. For graphical and statistical analysis, R software (http://cran.r-project.org, version 4.4.1, accessed on 30 September 2024) was employed [43,44].

2.5. Individual Dosing Regimen Strategy

To explore the performance of the final PK/PD model and its impact on clinical practice, the optimal MIPD regimen in each patient was determined, for which the PK and PD individual parameters and their uncertainties were considered. The individual conditional distributions of PK/PD parameters were estimated in Monolix, which represented the PK and PD individual parameter estimates and their corresponding uncertainty [45]. Uncertainty refers to the degree of accuracy with which PK and PD individual parameters can be determined based on the observed data and covariate value for that individual, considering that the individual belongs to the population for which the typical parameter value (fixed effects) and the variability (standard deviation of the random effects) were previously estimated [45,46].

The determination of individual conditional distributions ($p(\psi_i|y_i)$, with ψ_i being the individual parameters for individual i and y_i the data observations for individual i), was performed with a Markov Chain Monte Carlo (MCMC) procedure called the Metropolis–Hastings algorithm that samples parameter values from these distributions, using the following expression:

$$p(\psi_i|y_i) = \frac{p(y_i|\psi_i) \cdot p(\psi_i)}{p(y_i)} \quad (2)$$

where $p(y_i|\psi_i)$ is the conditional density function of the data when knowing the individual parameter values, $p(\psi_i)$ is the density function for the individual parameters and $p(y_i)$ is a constant that represents the likelihood.

With individual conditional distributions, one hundred clones per patient were generated and were imputed to Simulx 2024R1 (Lixoft SAS, a Simulations Plus company) [47] to predict through stochastic simulations, and the PASI levels expected at the 5th and 10th cycle (maintenance period) of treatment with UTK were as follows:

- 5th cycle: individual simulations of dosing regimens were generated considering 5 cycles of UTK (steady-state conditions) administration with the administered dosage regimen of each patient.
- 10th cycle: following the 5th cycle, we simulated the combination of alternative dose levels (45 and 90 mg) with different posology (q8w, q12w, q16w, and q20w) for each patient during 5 more cycles of treatment with UTK.

For each patient, the probabilities of achieving the response target (a PASI score ≤ 1) with each simulated dose regimen were calculated in cycle 5 and 10 using the following formula:

$$Probability = \frac{n_{PASI}}{T_{PASI}} \times 100 \quad (3)$$

where n_{PASI} represent the amount of simulated PASI score values that reach the response target (a PASI score ≤ 1), and T_{PASI} represent the total amount of simulated PASI score values (100 clones). In the 10th cycle, the regimen with which the patient achieved a probability $\geq 90\%$ (i.e., $\geq$90 virtual patients) was selected as the final dosage regimen. In case the patient achieved the response target with more than one dosage regimen, the optimized dosing regimen was selected as the final regimen, which represented a maintenance of the dose over a wider dosing interval or a decrease in the dose within the same dosing interval. The dosage regimen selected in the 10th cycle was compared with the current dosage regimen from the clinical practice of each patient to determine if the patients continued with their current regimen or required a change (optimization or intensification) in the dosage regimen.

3. Results

3.1. Study Population

The modeling dataset consisted of 23 patients including 75 observations in serum samples (PK), a baseline PASI ($PASI_{i,0}$) for each patient, and 117 individual PASI (PD). Table 1 summarizes the characteristics of the study, including demographic data, comorbidities, TDM data, and treatment characteristics that describe the current dosage regimen from the clinical practice of the subjects enrolled.

Table 1. Summary of patients' characteristics and PK/PD experimental data collected during TDM.

	Mean ± SD	**Range**	**n (%)**
Demographic data			
Age (years)	62 ± 8.19	45–76	
Body weight (kg)	92 ± 18.4	70–135	
Height (m)	1.67 ± 0.06	1.54–1.83	
BMI (kg/m^2)	32.3 ± 6.8	24–50.19	
Gender (male)			14 (64)
Treatment period (years)	5.43 ± 3.3	0.304–11.4	
Biological "naive"			20 (87)
Comorbidities			
AHT			2 (9)
Dyslipidemia			2 (9)
Diabetes			1 (4)
Obesity			4 (16)
Psoriatic arthropathy			2 (9)
Non-alcoholic fatty liver			2 (9)
Anxious–depressive disorder			2 (9)
Others			4 (16)
TDM data			
Total of patients			23
UTK concentration (mg/L)	4.1 ± 3.06	0.27–12.7	
Total of UTK concentrations			75
PASI (no units)	1.096 ± 2.13	0–12	
Total of PASIs			117
$PASI_{i,0}$	14.4 ± 6.23	5–31.9	

Current treatment characteristics							
SmPC		Optimized		Intensified		Summary	
45 mg q12w	1	45 mg q14w	1	90 mg q10w	1	SmPC	9 (40%)
90 mg q12w	8	45 mg q16w	3	90 mg q8w	2	Optimized	11 (48%)
		45 mg q18w	1			Intensified	3 (12%)
		90 mg q14w	1				
		90 mg q15w	2				
		90 mg q16w	3				

SD: standard deviation; BMI: body mass index; AHT: arterial hypertension; TDM: therapeutic drug monitoring; UTK: ustekinumab; PASI: Psoriasis Area and Severity Index; $PASI_{i,o}$: individual observed baseline; SmPC: summary of product characteristics; q8w: once every 8 weeks; q10w: once every 10 weeks; q12w: once every 12 weeks; q14w: once every 14 weeks; q15w: once every 15 weeks; q16w: once every 16 weeks; q18w: once every 18 weeks.

3.2. Population PK Model

A two-compartment model with first-order absorption and linear disposition processes, previously published by Shao et al. [18], was considered as the population PK model (Figure 2). Then, the statistical significance of covariates included in the reference model was tested with the available information and patient population collected. Only the effect of body weight was maintained on CL, intercompartmental transfer clearance (Q), the central volume of distribution (V_2), and the peripheral volume of distribution (V_3). Therefore, body weight was the only covariate that influenced the determination of individual PK parameter values. The results from the model evaluation exercise indicate that the model could capture the individual PK profiles with adequate accuracy since most of the observations were aligned to the identity line (Figure 3). The pcVPC of the PK model is shown in Supplementary Figure S1.

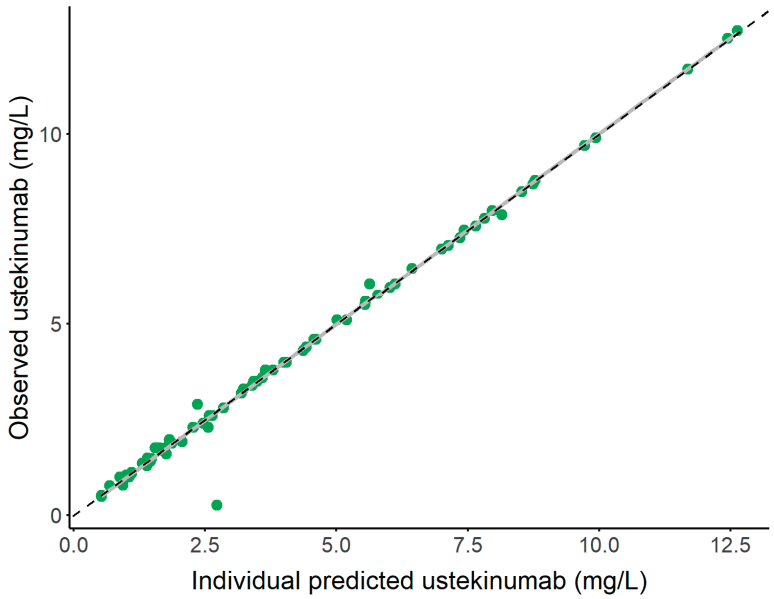


Figure 3. Individual predicted vs. the observed concentrations of UTK in patients with chronic plaque psoriasis.

3.3. Population PK/PD Model

The relationship between UTK concentration and PASI observations was described by an indirect response [48] in which UTK inhibited the zero-order progression constant rate of psoriatic skin lesion (k_{in}) through an I_{max} model. The first-order remission constant rate of psoriatic skin lesion (k_{out}) and the baseline PASI levels using the B2 method were estimated. The concentration of the drug needed to inhibit 50% of the response (IC_{50}) was fixed to a published value [16]. Longitudinal individual PK and PD profiles are shown in Figure 4. Overall, the PK/PD model can characterize the longitudinal behavior of the PASI at the individual level, suggesting that the current framework considers properly the combined drug effect and PASI turnover. The pcVPC of the PK/PD model is shown in Supplementary Figure S2. Parameter estimates of the final population PK/PD model are summarized in Table 2. The mean and standard deviation of individual PK/PD parameters are summarized in Supplementary Tables S1 and S2, respectively.

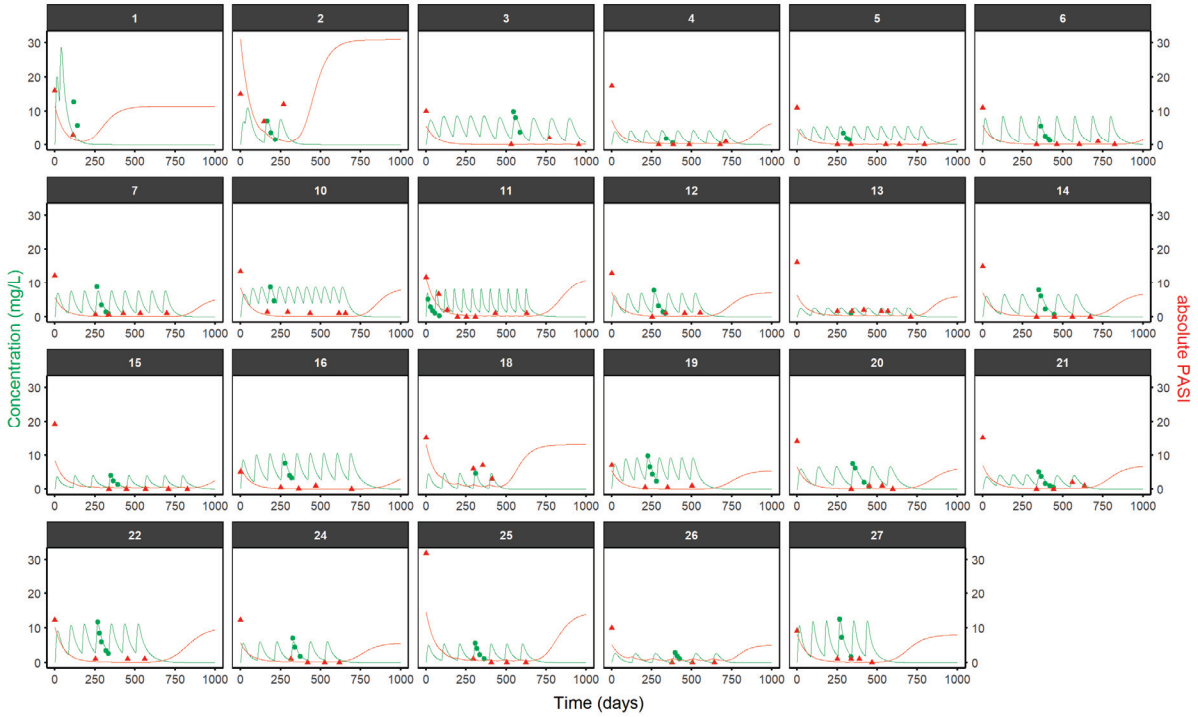


Figure 4. Individual predicted and observed UTK serum concentrations (green) and PASI (red) after UTK administration in patients with chronic plaque psoriasis. The line represents the individual prediction, and the green and red dots represent the UTK and PASI observations, respectively.

Table 2. Population PK/PD estimates after administration of UTK in patients with psoriasis.

Parameter (Units)	Value	RSE (%)
	Fixed effect	
k_{out} (d^{-1})	0.016	22
I_{max}	0.97	0.7
IC_{50} (mg/L)	0.07 FIX	
	Inter-individual variability	
k_{out} (%)	55.87	38.9
	Residual unexplained variability	
Error (%)	0.86	9.95

k_{out}: first-order remission constant rate of psoriatic skin lesion; I_{max}: maximum inhibition drug effect; IC_{50}: concentration of the drug needed to inhibit 50% of the response.

3.4. Individual Dosing Regimen Evaluation

Probabilities across the cycles of treatment evaluated per patient are represented in Supplementary Figure S3. The MIPD strategy predicted that 8/23 (35%) and 6/23 (26%) of patients would require an optimized and intensified dosage regimen, respectively, compared with the current regimen received in clinical practice for the maintenance period. A change to the approved regimen of 45 mg q12w is proposed in 3/23 (13%), representing 38% (3/8) of the total optimized patients. Also, in the optimized patients, non-labeled dosing regimens of 45 mg q16w and 45 mg q8w are suggested in 2/8 (24%) and 3/8 (38%) of patients, respectively. Regarding the patients with intensified dosage regimens, a change to 90 mg q8w (3/6) and 45 mg q8w (3/6), respectively, is recommended. No change in the dosing regimen was predicted in 5/23 (22%) patients. This MIPD strategy additionally allowed us to identify that 4/23 (17%) patients would not achieve the efficacy endpoint selected (a 90% probability of a PASI ≤ 1), contributing to the early identification of patients with therapeutic failure (Figure 5).

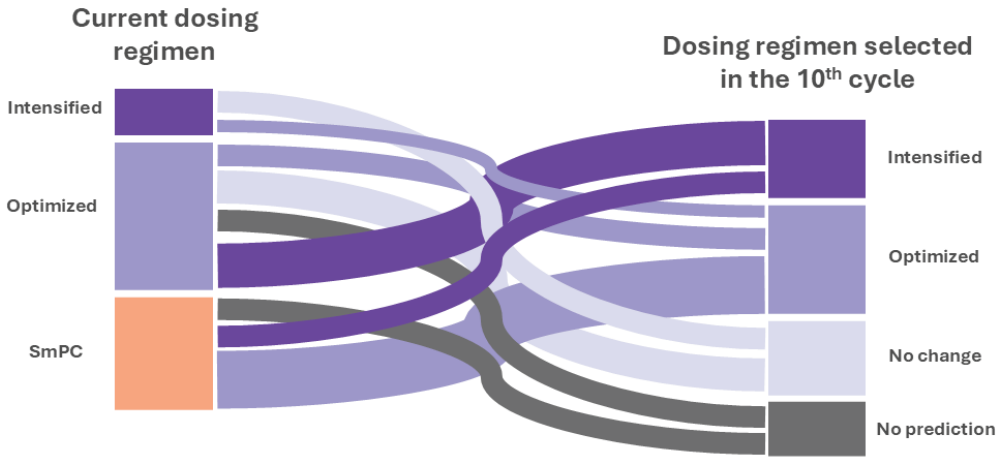


Figure 5. Sankey diagram to indicate the main flows of changes in the individual dose regimen from the current dosage regimen of clinical practice to the predicted dosage regimen in the maintenance period of treatment with UTK (cycle 10). SmPC: summary of product characteristics.

PK and PD simulations with the current dosage regimen from the clinical practice of each subject and the individual optimal dosing regimen established in the 10th cycle are depicted in Supplementary Figure S4. Figure 6 represents the relationship between the absolute PASI and a trough concentration at a steady state ($C_{trough\text{-}ss}$) for each patient, with all dosage regimens tested. Overall, the results suggest a non-linear relationship, indicating that the range of concentration 1.6–1.8 mg/L allows to achieve 90% of patients with a PASI $\leq$ 1.

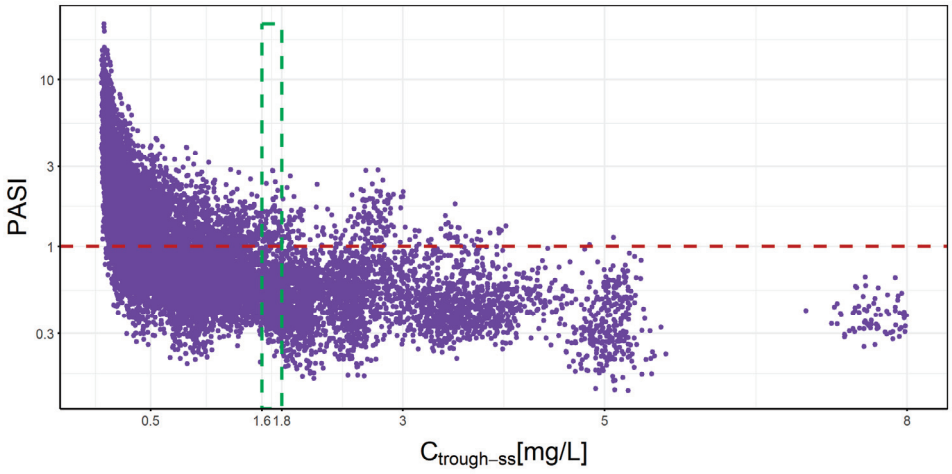


Figure 6. Simulated absolute PASI and trough concentration for each patient after 10 cycles of UTK administration using labeled and non-labeled dosing schemes. $C_{trough\text{-}ss}$: trough concentration at steady state.

4. Discussion

In this study, we developed a procedure capable of individualizing dosing strategies of UTK in clinical practice Spanish patients with moderate to severe chronic plaque psoriasis based on the uncertainty of the individual parameter estimates of a population PK/PD model. Additionally, the inclusion of the uncertainty during the simulation step for a personalized dosing regimen selection facilitates the evaluation of the degree of certainty in model-informed predictions in the clinical setting, providing a probabilistic framework for the MIPD of UTK.

Of the total number of patients who need a dosage regimen modification, 35% would be oriented towards an optimized dosage regimen. In 22% of patients, this optimization is

proposed to be performed using a non-labeled dosage regimen. This represents a reduction of one dose per year, meaning that patients, instead of receiving five doses of UTK in the first year of treatment with SmPC dosing regimens and four from the second year onwards, would receive four doses and three doses, respectively. According to the database of health information on medicines and parapharmacy products [49] the price of Stelara® 45 mg solution for injection in a pre-filled syringe is EUR 2915.4. Assuming the reduction in dosage, this will entail an annual cost per patient of EUR 11,661.6, which will represent a saving of 25%. In addition to fewer expenses related to the purchase of medication, with the lower number of administrations, there is less risk of an occurrence of injection site reactions due to SmPC. The previous fact includes patients who are to receive 45 mg q16w and also those who are to receive 45 mg q8w because the latter take much more intensive dosage regimens during clinical practice, for example, 90 mg q10w.

From our pool of patients, an intensification of the dosage regimen in comparison with the one received in clinical practice is proposed in 26% of the patients. In these patients, individual CL values higher than the typical value are observed; hence, this type of patient will require higher levels of UTK to achieve a successful therapeutic response. It should be taken into consideration that after performing our strategy for MIPD in UTK, dosage regimen optimization is recommended for most of the patients. As a result, an improvement in patient well-being and health system management can be achieved because, in the end, the patients would always be in an optimal therapeutic response range.

The MIPD strategy did not allow us to reach the efficacy endpoint (a 90% probability of a PASI $\leq$ 1) in 17% of patients. This strategy represents an advantage in identifying non-responding patients at the early stages of treatment, improving the effectiveness in the management of psoriasis for those patients, and avoiding the cost of treating these patients during successive cycles. A more in-depth analysis of these patients reveals CL or k_{out} values higher and lower, respectively, than the population average (Supplementary Figure S3), which could serve as a threshold to characterize patients with a low probability of optimal response to UTK.

For the estimation of individual PK/PD parameters, all the PASI and UTK concentration values available at the time of recruitment were used. To implement the proposed MIPD strategy, an adaptive procedure might be implemented. This procedure would involve re-estimating the individual parameters as additional data points become available to ensure the model remains accurate and reflective of the patient's evolving condition. On the other hand, this analysis confirms the need to collect PASI samples from patients during the first weeks of treatment (the induction phase), which enhances the characterization of PK and PD processes and increases the number of observations per patient, leading to a precise and accurate estimation of their individual PD parameters. The non-linear relationship between the PASI score and trough concentration levels of UTK (Figure 6) demonstrates both the impact of the PK and PD parameters to guarantee satisfactory treatment efficacy. Therefore, although it is possible to establish global exposure values for a PASI value, the individualization of treatment through this MIPD strategy allows for the achievement of a greater number of patients with effective therapeutic regimens, reducing therapeutic failure only for non-responding patients. In our study, a $C_{trough\text{-}ss}$ range of 1.6–1.8 mg/L was able to help 90% of patients achieve a PASI $\leq$ 1. Even though the $C_{trough\text{-}ss}$ range obtained in a previous population PK/PD study [17] was 0.0914–0.978 mg/L, it should be noted that this range is representative only for patients weighing 60 to 100 kg with a dosing regimen of 45 mg q12w. Correspondingly, it was generated from the simulated data of patients who were exclusively starting treatment with UTK in pivotal phase III clinical trials, with the efficacy objective of PASI 75 in week 12. However, the range of our study represents a more demanding PD endpoint (PASI $\leq$ 1 or PASI 99), and it is representative of patients with no body weight limit (92 $\pm$ 18.4 [70–135] kg) receiving eight dosage regimens used in clinical practice (45 or 90 mg q8, 12, 16 and 20w) under steady-state UTK therapy conditions. Furthermore, this range provides target $C_{trough\text{-}ss}$ values that are associated with an optimal

response in line with current clinical guideline recommendations (PASI ≤ 1) intended to maximize both clinical outcomes and the quality of life of patients with psoriasis [50,51].

Our work is based on previously published PK /PD models, thus recycling data and using previously developed knowledge, but in addition to our model, we have taken a step forward in the characterization of the relationship between UTK concentrations and response through the PASI observed in real-world clinical data. But also, this study is an example of individual-level precision dosing, which involves a more comprehensive and effective use of precision dosing strategies by recognizing, characterizing, and quantifying the various sources of variability in drug response through PK/PD modeling [23,33]. Such studies are particularly valuable for drugs like UTK that are used to treat heterogeneous conditions like psoriasis, where response variability is significant. While improving our understanding of PK/PD relationships within specific patient subgroups during clinical trials can enhance the identification of precise dosing targets, real-world patients remain significantly more diverse than those in controlled trial settings. Therefore, robust post-marketing surveillance is essential to explore unique precision dosing targets [52]. Advances in data collection and analysis methods from real-world patients offer opportunities to identify new precision dosing algorithms and refine existing ones established in clinical trials. These methods enable the continuous updating and extension of dosing strategies to better meet the individualized needs of patients [33,53]. Thus, our strategy based on MIPD in real-world clinical data could be the first attempt to ensure the most precise individual dosing of patients with plaque psoriasis treated with UTK.

Similar to any real-world study cohort, notable challenges involve the lack of patients (a small patient sample size), a few points available per patient, and therefore the presence of missing data. Due to the study design conditions, many PK/PD observations were taken very spaced out in time, without a continuous characterization (sparse data). For this reason, some unquantified changes in the physiology or the progression of the psoriasis disease could directly impact the obtained results. In the future, similar models could be implemented into a conditional distribution dashboard system [54,55]. This would allow for real-time predictions of treatment response, aiding in informed decisions regarding dosing adjustments and treatment transitions for UTK. In this way, as suggested by Mould and Upton in their recently published review [56], options for alternative dosing strategies based on MIPD and/or TDM could be included in the SmPC of UTK.

5. Conclusions

In conclusion, this study proposes a methodology to individualize UTK dosing strategies considering the uncertainty of individual parameters within a population PK/PD model to optimize the probability of achieving targeted clinical outcomes in patients with moderate to severe chronic plaque psoriasis. This represents an initial step towards performing MIPD for biologics that act on the interleukin pathways of psoriasis, which has been explored very little. Future studies should implement our proposal in a greater cohort of real-world patients.

Supplementary Materials: The following supporting information can be downloaded at: https://www.mdpi.com/article/10.3390/pharmaceutics16101295/s1, Ordinary differential equations for the PK/PD model of UTK and PASI; Figure S1: Prediction-corrected visual predictive check obtained from one thousand simulated studies using the selected population PK model; Figure S2: Prediction-corrected visual predictive check obtained from one thousand simulated studies using the selected population PK/PD model; Table S1: Mean of the individual PK/PD parameters drawn from the conditional distribution task in Monolix; Table S2: Standard deviation of the individual PK/PD parameters drawn from the conditional distribution task in Monolix; Figure S3: Bar plot of 100 simulated absolute PASI for each patient after UTK administration at cycles 5 and 10, using the individual parameters from the final population PK/PD model and their uncertainties; Figure S4: PK and PD simulations with the current dosage regimen from clinical practice and the individual optimal dosing regimen established after simulations in 10th cycle for each patient.

Author Contributions: Conceptualization, M.M.-S., E.G.-C., M.C.-M. and V.M.-S.; methodology, K.R.-F., J.Z.-F., M.M.-S., E.G.-C., M.C.-M. and V.M.-S.; software, K.R.-F., J.Z.-F. and V.M.-S.; validation, K.R.-F., J.Z.-F., M.S.-B., M.M.-S., A.M.-P., A.M.-C., E.G.-C., M.C.-M. and V.M.-S.; formal analysis, K.R.-F., J.Z.-F. and V.M.-S.; investigation, K.R.-F., J.Z.-F. and V.M.-S.; resources, A.M.-P., A.M.-C., E.G.-C. and M.C.-M.; data curation, K.R.-F.; writing—original draft preparation, K.R.-F., J.Z.-F. and V.M.-S.; writing—review and editing, K.R.-F., J.Z.-F., M.S.-B., M.M.-S., A.M.-P., A.M.-C., E.G.-C., M.C.-M. and V.M.-S.; visualization, K.R.-F. and J.Z.-F. ; supervision, E.G.-C., M.C.-M. and V.M.-S.; project administration, E.G.-C., M.C.-M. and V.M.-S.; funding acquisition, A.M.-P., E.G.-C. and M.C.-M. All authors have read and agreed to the published version of the manuscript.

Funding: This research received no external funding.

Institutional Review Board Statement: The study was conducted following the Declaration of Helsinki and approved by the Ethics Committee of La Fe University and Polytechnic Hospital (protocol code: VMS-UTK-2020-01 and date of approval: 27 January 2021).

Informed Consent Statement: Informed consent was obtained from all subjects involved in the study.

Data Availability Statement: The data presented in this study are available on request from the corresponding author due to ethical and legal restrictions.

Conflicts of Interest: The authors declare no conflicts of interest.

Abbreviations

AHT	Arterial hypertension
BMI	Body mass index
$C_{trough\text{-}ss}$	Trough concentration at steady state
CL	Clearance
E_{Drug}	Effect of the drug
F	Bioavailability
IC_{50}	Concentration of the drug needed to inhibit 50% of the response
I_{max}	Maximum inhibition drug effect
IIV	Interindividual variability
IL	Interleukin
k_a	Absorption rate constant
k_{in}	Zero-order progression constant rate of psoriatic skin lesion
k_{out}	First-order remission constant rate of psoriatic skin lesion
mAb	monoclonal antibody
MCMC	Markov Chain Monte Carlo
MIPD	Model-informed precision dosing
n_{PASI}	Amount of simulated PASI score values that reach the response target (PASI score ≤ 1)
$\eta_{i,RV}$	Estimated individual random component accounting for the difference between $PASI_i$ and $PASI_{i,o}$
PASI	Psoriasis Area and Severity Index
$PASI_i$	Estimated baseline levels of PASI response
$PASI_{i,o}$	Individual observed baseline levels of PASI response
pcVPC	Prediction-corrected visual predictive check
PD	Pharmacodynamic
PK	Pharmacokinetic
PK/PD	Pharmacokinetic/pharmacodynamic
Q	Intercompartmental transfer clearance
q8w	Once every 8 weeks
q10w	Once every 10 weeks
q12w	Once every 12 weeks
q14w	Once every 14 weeks
q15w	Once every 15 weeks
q16w	Once every 16 weeks

q18w	Once every 18 weeks
q20w	Once every 20 weeks
RUV	Residual unexplained variability
SD	Standard deviation
SmPC	Summary of product characteristics
TDM	Therapeutic drug monitoring
T_{PASI}	Total amount of simulated PASI score values (100 clones)
UTK	Ustekinumab
V_2	Central volume of distribution
V_3	Peripheral volume of distribution

References

1. Schadler, E.D.; Ortel, B.; Mehlis, S.L. Biologics for the primary care physician: Review and treatment of psoriasis. *Disease-a-Month* **2018**, *65*, 51–90. [CrossRef] [PubMed]
2. Rendon, A.; Schäkel, K. Psoriasis Pathogenesis and Treatment. *Int. J. Mol. Sci.* **2019**, *20*, 1475. [CrossRef] [PubMed]
3. Koutruba, N.; Emer, J.; Lebwohl, M. Review of ustekinumab, an interleukin-12 and interleukin-23 inhibitor used for the treatment of plaque psoriasis. *Ther. Clin. Risk Manag.* **2010**, *6*, 123–141. [CrossRef] [PubMed]
4. Weber, J.; Keam, S.J. Ustekinumab. *BioDrugs Clin. Immunother. Biopharm. Gene Ther.* **2009**, *23*, 53–61. [CrossRef] [PubMed]
5. Mahil, S.K.; Capon, F.; Barker, J.N. Update on psoriasis immunopathogenesis and targeted immunotherapy. *Semin. Immunopathol.* **2016**, *38*, 11–27. [CrossRef]
6. Murphy, K.M.; Reiner, S.L. The lineage decisions of helper T cells. *Nat. Rev. Immunol.* **2002**, *2*, 933–944. [CrossRef]
7. Tesmer, L.A.; Lundy, S.K.; Sarkar, S.; Fox, D.A. Th17 cells in human disease. *Immunol. Rev.* **2008**, *223*, 87–113. [CrossRef]
8. FDA. Approved Drug Products: STELARA (Ustekinumab) Injection, for Subcutaneous or Intravenous Use. March 2024. Available online: https://www.accessdata.fda.gov/drugsatfda_docs/label/2024/761044s013lbl.pdf (accessed on 6 August 2024).
9. Leonardi, C.L.; Kimball, A.B.; Papp, K.A.; Yeilding, N.; Guzzo, C.; Wang, Y.; Li, S.; Dooley, L.T.; Gordon, K.B. Efficacy and safety of ustekinumab, a human interleukin-12/23 monoclonal antibody, in patients with psoriasis: 76-week results from a randomised, double-blind, placebo-controlled trial (PHOENIX 1). *Lancet* **2008**, *371*, 1665–1674. [CrossRef]
10. Papp, K.A.; Langley, R.G.; Lebwohl, M.; Krueger, G.G.; Szapary, P.; Yeilding, N.; Guzzo, C.; Hsu, M.C.; Wang, Y.; Li, S.; et al. Efficacy and safety of ustekinumab, a human interleukin-12/23 monoclonal antibody, in patients with psoriasis: 52-week results from a randomised, double-blind, placebo-controlled trial (PHOENIX 2). *Lancet* **2008**, *371*, 1675–1684. [CrossRef]
11. Thein, D.; Rosenø, N.A.L.; Maul, J.T.; Wu, J.J.; Skov, L.; Bryld, L.E.; Rasmussen, M.K.; Ajgeiy, K.K.; Thomsen, S.F.; Thyssen, J.P.; et al. Drug Survival of Adalimumab, Secukinumab, and Ustekinumab in Psoriasis as Determined by Either Dose Escalation or Drug Discontinuation during the First 3 Years of Treatment–a Nationwide Cohort Study. *J. Investig. Dermatol.* **2023**, *143*, 2211–2218. [CrossRef]
12. Yiu, Z.Z.N.; Mason, K.J.; Hampton, P.J.; Reynolds, N.J.; Smith, C.H.; Lunt, M.; Griffiths, C.E.M.; Warren, R.B. Drug survival of adalimumab, ustekinumab and secukinumab in patients with psoriasis: A prospective cohort study from the British Association of Dermatologists Biologics and Immunomodulators Register (BADBIR). *Br. J. Dermatol.* **2020**, *183*, 294–302. [CrossRef] [PubMed]
13. Young, M.S.; Horn, E.J.; Cather, J.C. The ACCEPT study: Ustekinumab versus etanercept in moderate-to-severe psoriasis patients. *Expert Rev. Clin. Immunol.* **2011**, *7*, 9–13. [CrossRef] [PubMed]
14. Zhu, Y.; Hu, C.; Lu, M.; Liao, S.; Marini, J.C.; Yohrling, J.; Yeilding, N.; Davis, H.M.; Zhou, H. Population pharmacokinetic modeling of ustekinumab, a human monoclonal antibody targeting IL-12/23p40, in patients with moderate to severe plaque psoriasis. *J. Clin. Pharmacol.* **2009**, *49*, 162–175. [CrossRef] [PubMed]
15. Zhu, Y.W.; Mendelsohn, A.; Pendley, C.; Davis, H.M.; Zhou, H. Population pharmacokinetics of ustekinumab in patients with active psoriatic arthritis. *Int. J. Clin. Pharmacol. Ther.* **2010**, *48*, 830–846. [CrossRef]
16. Pan, S.; Tsakok, T.; Dand, N.; Lonsdale, D.O.; Loeff, F.C.; Bloem, K.; de Vries, A.; Baudry, D.; Duckworth, M.; Mahil, S.; et al. Using Real-World Data to Guide Ustekinumab Dosing Strategies for Psoriasis: A Prospective Pharmacokinetic-Pharmacodynamic Study. *Clin. Transl. Sci.* **2020**, *13*, 400–409. [CrossRef]
17. Zhou, W.; Hu, C.; Zhu, Y.; Randazzo, B.; Song, M.; Sharma, A.; Xu, Z.; Zhou, H. Extrapolating Pharmacodynamic Effects from Adults to Pediatrics: A Case Study of Ustekinumab in Pediatric Patients With Moderate to Severe Plaque Psoriasis. *Clin. Pharmacol. Ther.* **2020**, *109*, 131–139. [CrossRef]
18. Shao, J.; Xu, Z.; Xu, Y. Integrated Population Pharmacokinetic Analysis of Ustekinumab Across Multiple Immune-Mediated Inflammatory Disease Populations and Healthy Subjects. *Eur. J. Drug Metab. Pharmacokinet.* **2022**, *47*, 537–548. [CrossRef]
19. Zhou, H.; Hu, C.; Zhu, Y.; Lu, M.; Liao, S.; Yeilding, N.; Davis, H.M. Population-based exposure-efficacy modeling of ustekinumab in patients with moderate to severe plaque psoriasis. *J. Clin. Pharmacol.* **2010**, *50*, 257–267. [CrossRef]
20. Rodríguez-Fernández, K.; Mangas-Sanjuán, V.; Merino-Sanjuán, M.; Martorell-Calatayud, A.; Mateu-Puchades, A.; Climente-Martí, M.; Gras-Colomer, E. Impact of Pharmacokinetic and Pharmacodynamic Properties of Monoclonal Antibodies in the Management of Psoriasis. *Pharmaceutics* **2022**, *14*, 654. [CrossRef]
21. Felmlee, M.A.; Morris, M.E.; Mager, D.E. Mechanism-based pharmacodynamic modeling. *Methods Mol. Biol.* **2012**, *929*, 583–600. [CrossRef]

22. Notario, J.; Bordas, X. Practical management of ustekinumab in moderate-severe psoriasis. *Actas Dermo-Sifiliográficas* **2012**, *103*, 52–58. [CrossRef]
23. Tyson, R.J.; Park, C.C.; Powell, J.R.; Patterson, J.H.; Weiner, D.; Watkins, P.B.; Gonzalez, D. Precision Dosing Priority Criteria: Drug, Disease, and Patient Population Variables. *Front. Pharmacol.* **2020**, *11*, 420. [CrossRef] [PubMed]
24. Syversen, S.W.; Goll, G.L.; Jørgensen, K.K.; Sandanger, Ø.; Sexton, J.; Olsen, I.C.; Gehin, J.E.; Warren, D.J.; Brun, M.K.; Klaasen, R.A.; et al. Effect of Therapeutic Drug Monitoring vs Standard Therapy During Infliximab Induction on Disease Remission in Patients With Chronic Immune-Mediated Inflammatory Diseases: A Randomized Clinical Trial. *JAMA* **2021**, *325*, 1744–1754. [CrossRef] [PubMed]
25. Albader, F.; Golovics, P.A.; Gonczi, L.; Bessissow, T.; Afif, W.; Lakatos, P.L. Therapeutic drug monitoring in inflammatory bowel disease: The dawn of reactive monitoring. *World J. Gastroenterol.* **2021**, *27*, 6231–6247. [CrossRef] [PubMed]
26. D'Haens, G.R.; Sandborn, W.J.; Loftus, E.V., Jr.; Hanauer, S.B.; Schreiber, S.; Peyrin-Biroulet, L.; Panaccione, R.; Panés, J.; Baert, F.; Colombel, J.F.; et al. Higher vs Standard Adalimumab Induction Dosing Regimens and Two Maintenance Strategies: Randomized SERENE CD Trial Results. *Gastroenterology* **2022**, *162*, 1876–1890. [CrossRef]
27. Minichmayr, I.K.; Dreesen, E.; Centanni, M.; Wang, Z.; Hoffert, Y.; Friberg, L.E.; Wicha, S.G. Model-informed precision dosing: State of the art and future perspectives. *Adv. Drug Deliv. Rev.* **2024**, *2024*, 115421. [CrossRef]
28. Olivier, B.G.; Swat, M.J.; Moné, M.J. Modeling and Simulation Tools: From Systems Biology to Systems Medicine. *Methods Mol. Biol.* **2016**, *1386*, 441–463. [CrossRef]
29. Darwich, A.S.; Polasek, T.M.; Aronson, J.K.; Ogungbenro, K.; Wright, D.F.B.; Achour, B.; Reny, J.L.; Daali, Y.; Eiermann, B.; Cook, J.; et al. Model-Informed Precision Dosing: Background, Requirements, Validation, Implementation, and Forward Trajectory of Individualizing Drug Therapy. *Annu. Rev. Pharmacol. Toxicol.* **2021**, *61*, 225–245. [CrossRef]
30. Minichmayr, I.K.; Mizuno, T.; Goswami, S.; Peck, R.W.; Polasek, T.M.; Pharmacology, t.A.S.o.C.; Community, T.P.D. Recent Advances Addressing the Challenges of Precision Dosing. *Clin. Pharmacol. Ther.* **2024**, *116*, 527–530. [CrossRef]
31. Bandín-Vilar, E.; Toja-Camba, F.J.; Vidal-Millares, M.; Durán-Maseda, M.J.; Pou-Álvarez, M.; Castro-Balado, A.; Maroñas, O.; Gil-Rodríguez, A.; Carracedo, Á.; Zarra-Ferro, I.; et al. Towards precision medicine of long-acting aripiprazole through population pharmacokinetic modelling. *Psychiatry Res.* **2024**, *333*, 115721. [CrossRef]
32. Rodríguez-Fernández, K.; Reynaldo-Fernández, G.; Reyes-González, S.; de Las Barreras, C.; Rodríguez-Vera, L.; Vlaar, C.; Monbaliu, J.M.; Stelzer, T.; Duconge, J.; Mangas-Sanjuan, V. New insights into the role of VKORC1 polymorphisms for optimal warfarin dose selection in Caribbean Hispanic patients through an external validation of a population PK/PD model. *Biomed. Pharmacother. Biomed. Pharmacother.* **2024**, *170*, 115977. [CrossRef] [PubMed]
33. Polasek, T.M.; Peck, R.W. Beyond Population-Level Targets for Drug Concentrations: Precision Dosing Needs Individual-Level Targets that Include Superior Biomarkers of Drug Responses. *Clin. Pharmacol. Ther.* **2024**, *116*, 602–612. [CrossRef] [PubMed]
34. Hu, C.; Szapary, P.O.; Mendelsohn, A.M.; Zhou, H. Latent variable indirect response joint modeling of a continuous and a categorical clinical endpoint. *J. Pharmacokinet. Pharmacodyn.* **2014**, *41*, 335–349. [CrossRef] [PubMed]
35. Salinger, D.H.; Endres, C.J.; Martin, D.A.; Gibbs, M.A. A semi-mechanistic model to characterize the pharmacokinetics and pharmacodynamics of brodalumab in healthy volunteers and subjects with psoriasis in a first-in-human single ascending dose study. *Clin. Pharmacol. Drug Dev.* **2014**, *3*, 276–283. [CrossRef]
36. Chigutsa, E.; Velez de Mendizabal, N.; Chua, L.; Heathman, M.; Friedrich, S.; Jackson, K.; Reich, K. Exposure-Response Modeling to Characterize the Relationship Between Ixekizumab Serum Drug Concentrations and Efficacy Responses at Week 12 in Patients with Moderate to Severe Plaque Psoriasis. *J. Clin. Pharmacol.* **2018**, *58*, 1489–1500. [CrossRef]
37. Hu, C.; Yao, Z.; Chen, Y.; Randazzo, B.; Zhang, L.; Xu, Z.; Sharma, A.; Zhou, H. A comprehensive evaluation of exposure-response relationships in clinical trials: Application to support guselkumab dose selection for patients with psoriasis. *J. Pharmacokinet. Pharmacodyn.* **2018**, *45*, 523–535. [CrossRef]
38. van Huizen, A.; Bank, P.; van der Kraaij, G.; Musters, A.; Busard, C.; Menting, S.; Rispens, T.; de Vries, A.; van Doorn, M.; Prens, E.; et al. Quantifying the Effect of Methotrexate on Adalimumab Response in Psoriasis by Pharmacokinetic-Pharmacodynamic Modeling. *J. Investig. Dermatol.* **2024**, *144*, 794–801. [CrossRef]
39. Dansirikul, C.; Silber, H.E.; Karlsson, M.O. Approaches to handling pharmacodynamic baseline responses. *J. Pharmacokinet. Pharmacodyn.* **2008**, *35*, 269–283. [CrossRef]
40. Bergstrand, M.; Hooker, A.C.; Wallin, J.E.; Karlsson, M.O. Prediction-corrected visual predictive checks for diagnosing nonlinear mixed-effects models. *AAPS J.* **2011**, *13*, 143–151. [CrossRef]
41. Upton, R.N.; Mould, D.R. Basic concepts in population modeling, simulation, and model-based drug development: Part 3-introduction to pharmacodynamic modeling methods. *CPT Pharmacomet. Syst. Pharmacol.* **2014**, *3*, e88. [CrossRef]
42. Lixoft. Monolix Suite 2024R1. 2024. Available online: https://lixoft.com/products/monolix/ (accessed on 25 July 2024).
43. Ito, K.; Murphy, D. Application of ggplot2 to Pharmacometric Graphics. *CPT Pharmacomet. Syst. Pharmacol.* **2013**, *2*, e79. [CrossRef] [PubMed]
44. R Core Team. *R: A Language and Environment for Statistical Computing*; R Foundation for Statistical Computing: Vienna, Austria, 2024. Available online: http://www.R-project.org/ (accessed on 30 July 2024).
45. Monolix 2024R1 User Guide. Available online: https://monolix.lixoft.com/single-page/ (accessed on 25 January 2024).
46. Kümmel, A.; Bonate, P.L.; Dingemanse, J.; Krause, A. Confidence and Prediction Intervals for Pharmacometric Models. *CPT Pharmacomet. Syst. Pharmacol.* **2018**, *7*, 360–373. [CrossRef] [PubMed]

47. Lixoft. Simulx 2024R1. 2024. Available online: https://simulx.lixoft.com/ (accessed on 25 July 2024).
48. Dayneka, N.L.; Garg, V.; Jusko, W.J. Comparison of four basic models of indirect pharmacodynamic responses. *J. Pharmacokinet. Biopharm.* **1993**, *21*, 457–478. [CrossRef] [PubMed]
49. BOT PLUS. Available online: https://botplusweb.farmaceuticos.com/ (accessed on 29 August 2024).
50. Torres, T.; Puig, L. Treatment goals for psoriasis: Should PASI 90 become the standard of care? *Actas Dermo-Sifiliográficas* **2015**, *106*, 155–157. [CrossRef] [PubMed]
51. Nast, A.; Smith, C.; Spuls, P.I.; Avila Valle, G.; Bata-Csörgö, Z.; Boonen, H.; De Jong, E.; Garcia-Doval, I.; Gisondi, P.; Kaur-Knudsen, D.; et al. EuroGuiDerm Guideline on the systemic treatment of Psoriasis vulgaris–Part 1: Treatment and monitoring recommendations. *J. Eur. Acad. Dermatol. Venereol.* **2020**, *34*, 2461–2498. [CrossRef]
52. Kamal, M.A.; Ganguly, S.; Kadambi, A.; Smith, P.F. Extended Model-Informed Drug Development: Beyond Clinical Trials and Regulatory Approval. *Clin. Pharmacol. Ther.* **2024**, *116*, 518–521. [CrossRef]
53. Darwich, A.S.; Ogungbenro, K.; Vinks, A.A.; Powell, J.R.; Reny, J.L.; Marsousi, N.; Daali, Y.; Fairman, D.; Cook, J.; Lesko, L.J.; et al. Why has model-informed precision dosing not yet become common clinical reality? lessons from the past and a roadmap for the future. *Clin. Pharmacol. Ther.* **2017**, *101*, 646–656. [CrossRef]
54. Dolan, J.G.; Veazie, P.J.; Russ, A.J. Development and initial evaluation of a treatment decision dashboard. *BMC Med. Inform. Decis. Mak.* **2013**, *13*, 51. [CrossRef]
55. Mould, D.R.; Upton, R.N.; Wojciechowski, J. Dashboard systems: Implementing pharmacometrics from bench to bedside. *AAPS J.* **2014**, *16*, 925–937. [CrossRef]
56. Mould, D.R.; Upton, R.N. "Getting the Dose Right"-Revisiting the Topic with Focus on Biologic Agents. *Clin. Pharmacol. Ther.* **2024**, *116*, 613–618. [CrossRef]

Disclaimer/Publisher's Note: The statements, opinions and data contained in all publications are solely those of the individual author(s) and contributor(s) and not of MDPI and/or the editor(s). MDPI and/or the editor(s) disclaim responsibility for any injury to people or property resulting from any ideas, methods, instructions or products referred to in the content.

pharmaceutics

MDPI

Article

Personalized Secukinumab Treatment in Patients with Plaque Psoriasis Using Model-Informed Precision Dosing

Karine Rodriguez-Fernandez [1,2,†], Javier Zarzoso-Foj [1,2,†], Marina Saez-Bello [3], Almudena Mateu-Puchades [4], Antonio Martorell-Calatayud [5], Matilde Merino-Sanjuan [1,2], Elena Gras-Colomer [6], Monica Climente-Marti [3,*] and Victor Mangas-Sanjuan [1,2,*]

[1] Department of Pharmacy and Pharmaceutical Technology and Parasitology, University of Valencia, 46100 Valencia, Spain; karofer@alumni.uv.es (K.R.-F.); javier.zarzoso@uv.es (J.Z.-F.); matilde.merino@uv.es (M.M.-S.)
[2] Interuniversity Research Institute for Molecular Recognition and Technological Development, Polytechnic University of Valencia–University of Valencia, 46100 Valencia, Spain
[3] Pharmacy Service, Doctor Peset University Hospital, Foundation for the Promotion of Health and Biomedical Research in the Valencian Region (FISABIO), 46017 Valencia, Spain; saez_marbel@gva.es
[4] Dermatology Service, Doctor Peset University Hospital, Foundation for the Promotion of Health and Biomedical Research in the Valencian Region (FISABIO), 46017 Valencia, Spain; mateu_alm@gva.es
[5] Dermatology Service, Hospital Manises of Valencia, 46940 Manises, Spain; martorell_antcal@gva.es
[6] Pharmacy Service, Hospital Manises of Valencia, 46940 Manises, Spain; gras_ele@gva.es
* Correspondence: climente_mon@gva.es (M.C.-M.); victor.mangas@uv.es (V.M.-S.)
† These authors contributed equally to this work.

Abstract: Background/Objectives: Patient care and control of inflammatory disorders, such as psoriasis, can be improved by model-informed precision dosing (MIPD) techniques based on population pharmacokinetic/pharmacodynamic (PK/PD) models. Clinical dose selection decisions based on MIPD strategies need to take account of the uncertainty associated with the individual PK/PD model parameters, which is determined by the quantity of individual observational data collected in clinical practice. **Methods:** The aim of this study was to propose an approach for personalized dosage regimens of secukinumab (SCK) in 22 Spanish patients with plaque psoriasis, whose severity level was considered moderate to severe, taking into account the uncertainty associated with individual parameters in a population-based PK/PD model. **Results:** The link between SCK serum concentrations and Psoriasis Area and Severity Index (PASI) scores was explained using an indirect response model. A maximum inhibition (I_{max}) drug effect model was applied to limit the progression of psoriatic skin lesions within the turnover PD mechanism, which explains the changes in PASI scores during treatment. A first-order remission rate constant for psoriatic lesions (k_{out} = 0.11 day^{-1}) was estimated. **Conclusions:** According to the MIPD strategy, 50% of patients would require an optimized regimen and 14% would require an intensified dosage regimen in comparison to current clinical treatment. This research has shown its usefulness as a tool for choosing individualized SCK dosage regimens in patients with long-lasting plaque psoriasis to improve the probability of achieving satisfactory response levels.

Keywords: psoriasis; secukinumab; pharmacokinetic/pharmacodynamic

1. Introduction

Secukinumab (SCK) is a fully human immunoglobulin G1k (IgG1k) monoclonal antibody (mAb) designated for the treatment of psoriasis [1,2], a chronic autoimmune skin disorder characterized by pro-inflammatory cytokines and keratinocyte hyperproliferation [3–5]. Psoriasis disease is partially explained by an elevation of proinflammatory interleukin (IL)-17A, which binds to the IL-17 receptor present in keratinocytes, triggering the signaling pathway associated with inflammatory processes [6,7]. The pharmacological

mechanism of action of SCK consists in selective binding to IL-17A, which diminishes its interaction with the IL-17 receptor, and therefore, reduces the inflammatory cascade [8].

Currently, SCK (Cosentyx®) is approved as an injection for subcutaneous (SC) use for treating plaque psoriasis, also called psoriasis vulgaris, from moderate to severe modality in adults. As indicated in the summary of product characteristics (SmPC) [9], SCK should be administered in a dose of 300 mg in weeks 0, 1, 2, 3, and 4 (induction period), and then every 4 weeks (maintenance period). For patients with a body weight of 90 kg or more, a maintenance dose of 300 mg every 2 weeks may provide additional benefit [10]. Clinical trials evaluating the efficacy of SCK in psoriasis have reported notable reductions in Psoriasis Area and Severity Index (PASI) scores, reflecting a substantial improvement in disease severity [11–17].

The population pharmacokinetics (PK) properties of SCK have been characterized using pooled results from six clinical trials: one phase I, three phase II, and two phase III studies in patients with psoriasis [11–13,18–20]. A two-compartment PK model with first-order absorption for SC administration and with zero-order infusion for intravenous administration successfully characterized its longitudinal PK behavior in patients with moderate to severe psoriasis [21,22]. SCK shows a terminal half-life of 27 days and slow clearance (CL) (0.19 L/day). Low central (V_2 = 3.61 L) and peripheral (V_3 = 2.87 L) volumes of distribution were estimated. An allometric relationship between body weight and CL and V_2 characterized the influence of body weight on PK disposition parameters of SCK. A disease progression model incorporating a symptomatic drug effect was recently developed for SCK [23]. In this model, the proportion of patients achieving PASI 75 and PASI 90 reported in clinical trials was used as the efficacy index.

The initial treatment with SCK is indicated by dermatologists following the labeled dosing recommendations. This procedure may not be the most favorable or harmless for all patients [24]. When the patient is in the maintenance phase of treatment with SCK because of the variable psoriasis disease progression and the fluctuation in individual response, modifications in SmPC dosage regimens become necessary. These modifications in the routine clinical practice of a dermatology service are called intensifications and optimizations. The goal of dosage regimen optimization is to either decrease the dose while keeping the dosing interval the same or retain the dose whereas the dosing interval is expanded. In contrast, dosage regimen intensification results in keeping the dose but cutting the dosing interval or increasing the dose but keeping the dosing interval. Due to the lack of a model-informed decision-making process, this strategy raises the likelihood of adverse outcomes caused by the emergence of e subtherapeutic or supratherapeutic drug concentrations [25]. Furthermore, rigorous adherence to the sample schedule is required by the individualization techniques that are frequently employed in conventional clinical practice, like those related to therapeutic drug monitoring (TDM) and clinical response. During these techniques, the drug's exposure in patients is compared to an objective range to make modifications, and intervention usually happens only after the medication has achieved a steady state. In cases when the exposure deviates from this range, the dosage is modified based on either clinical experience or the hypothesis of proportionality in dose exposure at a steady state [26–29].

For dosage selection in a patient, the ideal treatment and addressing events of insufficient response, gradual depletion of efficacy, or the advent of side effects, dermatologists must adopt an adaptable approach for treating chronic psoriasis vulgaris that contemplates dosage regimens not included in the SmPC (non-labeled) and transitions between various therapeutic alternatives of the disease. These obstacles underline how crucial it is to switch in the direction of model-informed precision dosing (MIPD) techniques based on population pharmacokinetic/pharmacodynamic (PK/PD) models. Because MIPD allows for the use of any timed sample, interventions can be carried out before the initial dosage or until a steady state is attained. The procedure of intervention determines a dosage that meets a predetermined target for PK/PD [29–34]. Therapeutic results and patient safety are improved when PK/PD models are used in dosage selection for the control of

chronic plaque psoriasis, since they address the interindividual variability (IIV) in therapy responses and increase precision dosing [35–37]. Therefore, this study aims to suggest a strategy for individualizing dosage regimens of SCK in patients with moderate to severe long-lasting psoriasis vulgaris reflecting the uncertainty associated with individual parameters obtained from a population PK/PD model.

2. Materials and Methods

2.1. Research Design

A prospective, observational, post-authorization clinical practice follow-up study was carried out at Dr. Peset University Hospital of Valencia on Spanish patients with chronic psoriasis vulgaris from moderate to severe modality. The study's authors certify that the methods used in the investigation comply with the moral guidelines set out by relevant institutional and national bodies that regulate the use of human subjects in research. Additionally, they guarantee adherence to the 1975 Helsinki Declaration, which underwent amendments in 2008. The Dr. Peset University Hospital Ethics Committee approved the study (protocol code VMS-SCK-2020-01 EPA-SP). Prior to beginning any study procedures, the patients' written informed consent was obtained. The time frame for the study was July 2020–December 2022. Patients who were receiving therapy at the time of registration and had received at least one dose of SCK (Cosentyx®) were eligible to participate. Personalized (optimized/intensified) dose regimens were prescribed to the study participants by the dermatologist, considering their clinical responses. Pregnant women, those under the age of 18, and people with cognitive impairments were all excluded. For every patient, therapy-related information including time, dose, and treatment line were gathered. Demographic information, such as weight, sex, height, and age, were also obtained from the hospital's electronic medical records.

2.2. Blood Collection and Sample Analytical Quantification

The patients received 150 or 300 mg of SCK by SC injection (abdomen or upper thigh) every 4, 5 and 6 weeks (q4w, q5w and q6w). Blood samples for PK analysis were collected using plain red vacutainer tubes immediately before SCK administration and approximately 2, 7, 14, 22, 30, and 40 days afterwards. The collected blood samples were centrifuged for 10 to 15 min at 3500–4000 rpm, and subsequently, the remaining was transferred to another tube and frozen until processing. Concentrations of SCK in serum were measured by A. Menarini Diagnostics (08918 Badalona, Barcelona, Spain) using an ISO 15189 [38] validated enzyme-linked immunosorbent assay (ELISA) in a freedom Evolyzer Tecan. The concentration range of the calibration curve was 0.2 μg/mL to 225 μg/mL.

2.3. Assessment of Psoriasis Area and Severity Index Score

Patients which began SCK therapy at Dr. Peset University Hospital's dermatological service received PASI evaluations between weeks 5 and 6 and weeks 16 and 24 after the induction period. Following this, PASI measurements were performed every 6 months. All the PASI scores that were available and registered in patients' clinical records through the almost 1.5-year follow-up period were used for this investigation. Medical records of the patients were additionally examined to extract the baseline PASI values registered at the beginning of the SCK therapy.

2.4. Modeling Data Analysis

A summary of the modeling approach used is shown in Figure 1. The population PK parameters of the published reference model for SCK [21] were employed for simulation to determine if the available model was able to accurately represent our data. A two-compartment model with an absorption compartment through linear processes (Figure 2) represents the structural PK model. Then, a population PK/PD model was developed to characterize the time course of PASI response [39,40]. Several structural PK/PD models were proposed to characterize the time delay between PK and PD ob-

servations. Linear, maximum inhibition (I_{max}), and functions for sigmoid drug effects were assessed [41]. The first section of the Supplementary Materials provides the ordinary differential equations of the PK/PD model.

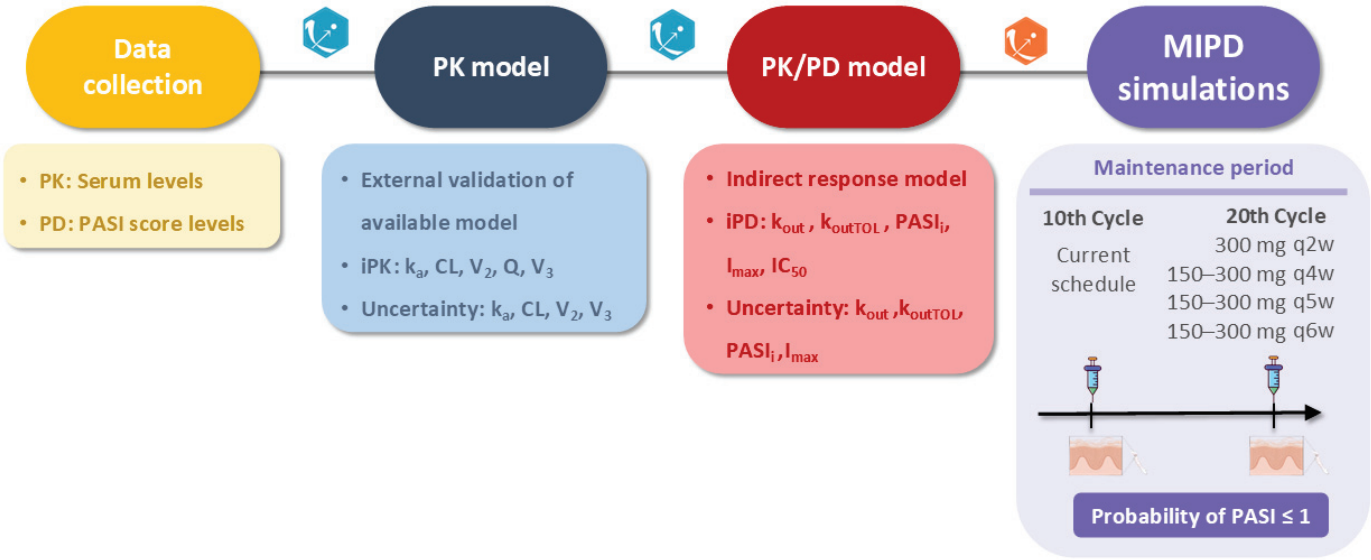


Figure 1. Workflow of the modeling process. PASI: Psoriasis Area and Severity Index; PD: pharmacodynamic; PK: pharmacokinetic; iPK: individual pharmacokinetic parameters; k_a: absorption rate constant; CL: clearance; Q: intercompartmental transfer clearance; V_2: central volume of distribution; V_3: peripheral volume of distribution; iPD: individual pharmacodynamic parameters; k_{out}: first-order reduction constant rate of psoriatic skin lesion; $k_{outTOLt}$: first-order remission constant rate of tolerance; $PASI_i$: estimated baseline levels of PASI response; I_{max}: maximum inhibition drug effect model; IC_{50}: concentration of the drug needed to inhibit 50% of the response; MIPD: model-informed precision dosing; q2w: once every 2 weeks, q4w: once every 4 weeks, q5w: once every 5 weeks, q6w: once every 6 weeks.

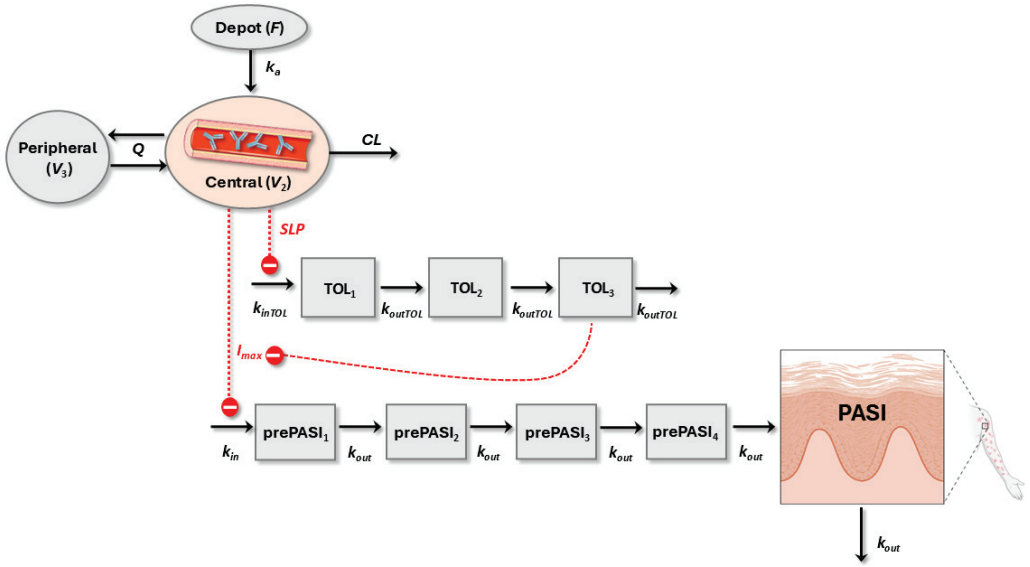


Figure 2. Final PK/PD model representation. *F*: bioavailability; k_{in}: zero-order evolution constant rate of psoriatic skin lesion; k_{inTOL}: zero-order progression constant rate of tolerance; SLP: linear drug effect model.

The B2 method [42] was applied to estimate baseline levels of PASI response, where $PASI_i$ characterizes the individual predicted baseline level of PASI, the individual observed

baseline are represented by $PASI_{i,0}$, and the distinguishing features between $PASI_i$ and $PASI_{i,0}$ are incorporated in the estimated individual random component $\eta_{i,RV}$. The mean of this random component is equal to zero, and its variance is constrained to have the same value as the residual unexplained variability (RUV) (Equation (1)). Hence, we expected that the baseline data would likewise exhibit the variability seen in the remaining data.

$$PASI_i = PASI_{i,0} \cdot e^{\eta_{i,RV}} \quad (1)$$

A comparison of the minimum value of the objective function, a visual examination of goodness-of-fit plots, and the accuracy of model parameters as indicated by the relative standard errors (RSE) were the basis for selecting the PK/PD model. By applying simulation-based diagnostics called prediction-corrected visual predictive checks (pcVPC), the evaluation of the elected PK/PD models was completed [40,43]. The data analyses were conducted via the population approach established in the software Monolix 2024R1 (Lixoft SAS, a Simulations Plus company, Lancaster, CA, USA) [44]. The R software (version 4.4.1; http://cran.r-project.org, accessed on 15 November 2024) [45,46] was used for statistical and graphical analysis.

2.5. Individual Dosage Regimen Approach

The most appropriate MIPD regimen for each patient was found by simulation analysis incorporating the PK and PD individual parameters and their uncertainties, in order to investigate the performance of the final PK/PD model and its influence on clinical practice. The PK and PD individual parameter estimates and their corresponding uncertainty were obtained by computing the individual conditional distributions of PK/PD parameters in Monolix 2024R1 [47]. The degree to which PK and PD individual parameters can be accurately obtained based on the observed data and covariate value for that individual, reflecting that the individual is a member of the population for which the typical parameter value (fixed effects) and the variability (standard deviation of the random effects) were previously estimated, is known as uncertainty [47,48].

A Markov chain Monte Carlo (MCMC) process known as Metropolis–Hastings algorithms was used to determine individual conditional distributions ($p(\psi_i|y_i)$, where ψ_i indicates the individual parameters for individual i , and y_i symbolizes the data observations for individual i. The following expression was used to sample parameter values from these distributions:

$$p(\psi_i|y_i) = \frac{p(y_i|\psi_i) \cdot p(\psi_i)}{p(y_i)} \quad (2)$$

where the constant that denotes the likelihood is $p(y_i)$, the density function for the individual parameters is referred as $p(\psi_i)$, and $p(y_i|\psi_i)$ reflects the conditional density function of the data when the individual parameter values are known.

In order to predict, via stochastic simulations, the PASI levels and trough concentrations at steady state ($C_{trough\text{-}ss}$) expected at the 10th and 20th cycle (maintenance period) of treatment with SCK, one hundred clones per patient were created applying individual conditional distributions and later imputed to Simulx 2024R1 (Lixoft SAS, a Simulations Plus company) [49]. Simulations were performed as follows:

- 10th cycle: using each patient's prescribed dosage regimen, simulations of individual dosage regimens were generated considering 10 cycles of SCK (steady-state conditions) administration
- 20th cycle: once 10 cycles were applied, 10 more cycles of SCK treatment for each patient were implemented additionally, to simulate the combination of alternative dose levels (150 and 300 mg) with different posology (q2w, q4w, q5w, and q6w) (Figure 1).

The probabilities of reaching the response aim (PASI score ≤ 1) in the 10th and 20th cycle for each patient, with each simulated dosage regimen, were calculated applying the following expression:

$$Probability = \frac{n_{PASI}}{T_{PASI}} \times 100 \quad (3)$$

The total quantity of simulated PASI score values (100 clones) corresponds to T_{PASI} , whereas n_{PASI} is the number of simulated PASI score values that accomplish the response target (PASI score ≤ 1). The regimen with a probability $\geq 90\%$ (i.e., $\geq$90 virtual patients) in the 20th cycle was chosen as the final dosage regimen. For methodological reasons, intensified dosing regimens were tested at the 20th cycle; a successful response was achieved even at the 10th cycle. When the response target was reached by the patient with several dosage regimens, it was selected as the final regimen, the one that was the most optimized among all. The most optimized dosage regimen stands for a lower dose while maintaining the dosing interval or equally a larger dosing interval but keeping the dose. After selecting a dosage regimen in the 20th cycle, it was compared with the clinical practice dosing regimen in each patient to determine if it was optimized or intensified, if the patients maintained their current regimen, or if it had not been possible to make a prediction for the patient.

3. Results

3.1. Research Subjects

A total of 22 patients were included in the study. The modeling dataset consisted of 85 concentrations of SCK in samples of serum (PK), 106 individual values of PASI score (PD) and for each patient a baseline PASI ($PASI_{i,0}$). Comorbidities, demographic and TDM data are presented in Table 1. Moreover, the current dosage regimens of the subjects who participated in the study are described as treatment characteristics in Table 1.

Table 1. Overview of the PK/PD experimental data and patient characteristics gathered within TDM.

	Mean ± SD	**Range**	**n (%)**
Demographic data			
Body weight (kg)	74.5 ± 15	46–97	
Height (m)	1.7 ± 0.09	1.54–1.85	
BMI (kg/m^2)	25.5 ± 4.9	16–41	
Age (years)	50.07 ± 13.4	28–76	
Gender (male)			14 (64)
Treatment period (years)	2 ± 1.7	0.005–5.1	
Biological "naive"			19 (86)
Comorbidities			
AHT			5 (23)
Dyslipidemia			7 (32)
Diabetes			3 (14)
Obesity			2 (9.1)
Psoriatic arthropathy			5 (23)
Non-alcoholic fatty liver			1 (4.5)
Anxious–depressive disorder			2 (9.1)
Others			11 (50)
TDM data			
Total of patients			22
SCK concentration (mg/L)	48.2 ± 18.5	7.4–89	85
PASI (no units)	1 ± 1.7	0–12.3	106
$PASI_{i,0}$	11.6 ± 5.8	2–27.5	22

Table 1. *Cont.*

		Mean ± SD		Range	n (%)
Clinical practice treatment characteristics					
SmPC		Optimized		Summary	
300 mg q4w	18	150 mg q4w	2	SmPC	18 (82%)
		300 mg q5w	1	Optimized	4 (18%)
		300 mg q6w	1	Intensified	none

SD: standard deviation; BMI: body mass index; AHT: arterial hypertension; TDM: therapeutic drug monitoring; SCK: secukinumab; PASI: Psoriasis Area and Severity Index; SmPC: summary of product characteristics; q4w: once every 4 weeks; q5w: once every 5 weeks; q6w: once every 6 weeks.

3.2. Population PK Model

The population PK model was a two-compartment model with first-order absorption and linear disposition processes that had been formerly issued by Bruin et al. [21]. The available data and patient population were then used to examine the statistical significance of the covariates enclosed in the original paper. Only body weight on CL (0.8) and V_2 (1) were maintained through an allometric relationship. Given that most of the observations were in line with the identity line, individual characterization of the individual PK profiles was confirmed (Supplementary Figure S1).

3.3. Population PK/PD Model

An indirect response [50] was selected to describe the relationship between SCK concentration and PASI observations in which SCK inhibits the zero-order evolution constant rate of psoriatic skin lesion (k_{in}). The inhibition of k_{in} through an I_{max} model provided a statistically significant reduction in the objective function value (p-value < 0.01). Other mAbs intended to treat moderate to severe chronic psoriasis vulgaris have previously used this model structure [51–56]. To capture the delay between SCK administration and observable effects, an additional chain of four turnover prePASI compartments was added, each representing a step in the disease progression (Figure 2).

The $PASI_i$ was estimated using the B2 method. Also, the value of first-order reduction constant rate of psoriatic skin lesion (k_{out}) was computed. Due to difficulties during the minimization and convergence processes, the concentration of the drug needed to inhibit 50% of the response (IC_{50}) could not be estimated and was fixed to a published value (9.35 mg/L) [23]. A tolerance mechanism was incorporated to account for the increase in PASI score over time during the administration of SCK in four patients (ID: 5, 10, 13, and 16). Tolerance and desensitization phenomena have been previously modeled in preclinical data for proinflammatory cytokines that determine the triggering of plaque psoriasis [57]. A turn-over mechanism including three mediator-like compartments was proposed, where the rate of progression of tolerance (k_{inTOL}) is triggered by drug effects incorporated as a linear function (SLP) of the predicted levels of SCK in serum.

Individual PK and PD profiles across time are reproduced in Figure 3. According to the PK/PD model, the current framework appropriately takes into account the combined action of SCK and PASI turnover, since it can describe the longitudinal behavior of PASI at the individual level. Individual predicted vs. the observed PASI in patients with chronic plaque psoriasis and the pcVPC of the PK/PD model are shown in Supplementary Figures S2 and S3, respectively. Table 2 provides a summary of parameter estimates for the final population PK/PD model. Supplementary Tables S1 and S2 include an overview of the mean and standard deviation of the PK/PD parameters in each patient, respectively.

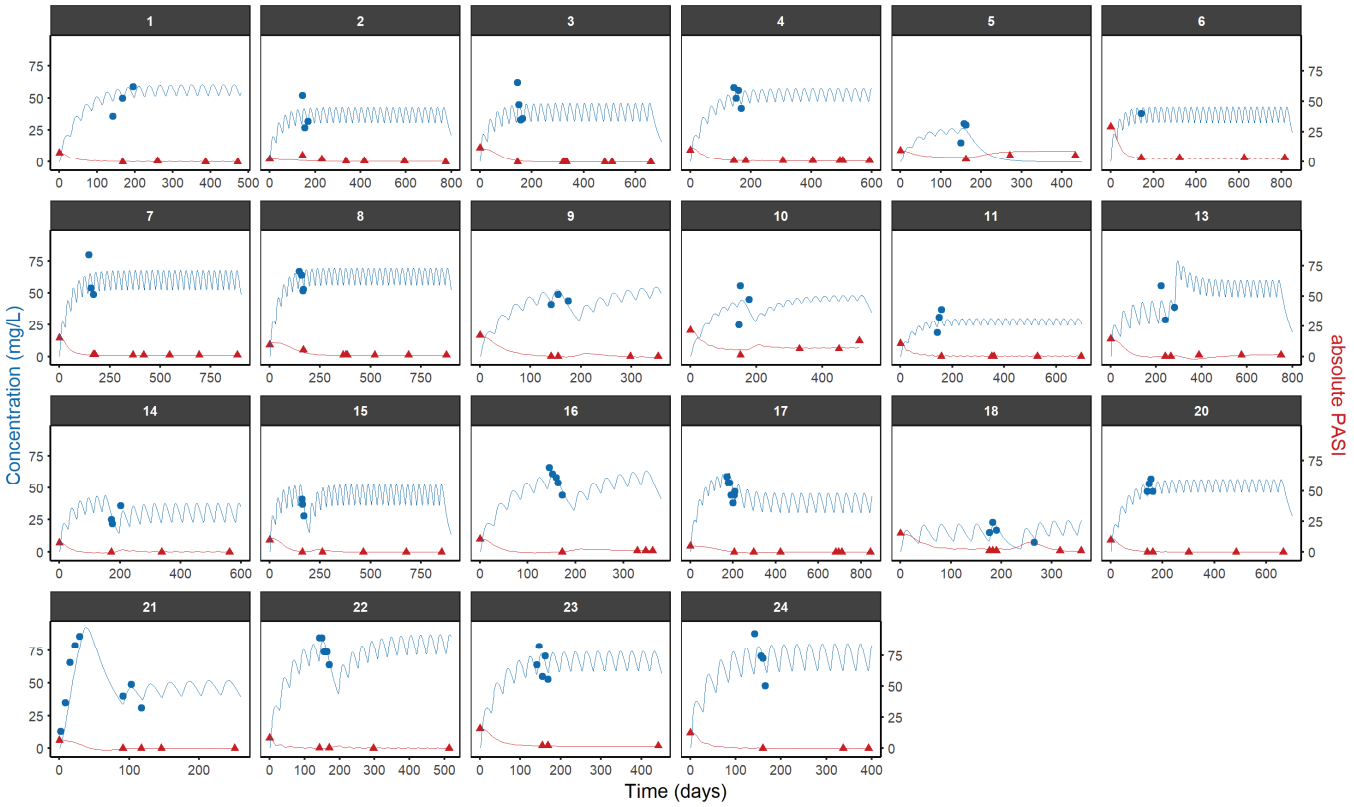


Figure 3. Predicted and observed PASI score (red) and SCK concentrations (blue) after the administration of SCK in patients with long-lasting psoriasis vulgaris. Individual predictions are represented by lines, and the SCK and PASI observations are represented by blue and red dots, respectively.

Table 2. Population PK/PD estimates in patients with chronic plaque psoriasis after administration of SCK.

Parameter (Units)	Value	RSE (%)
Fixed-effect		
k_{out} (day^{-1})	0.11	26.1
k_{outTOL} (day^{-1})	0.003	106
I_{max}	1.19	1.88
IC_{50} (mg/L)	9.35 FIX	
Inter-individual variability		
k_{out} (%)	91.3	20
k_{outTOL} (%)	37.15	431
I_{max} (%)	7.63	18
Residual unexplained variability		
Error (%)	0.76	9.2

RSE: relative standard error; k_{out}: first-order reduction constant rate of psoriatic skin lesion; I_{max}: maximum inhibition drug effect; $k_{outTOLt}$: first-order remission constant rate of tolerance; IC_{50}: concentration of the drug needed to inhibit 50% of the response.

3.4. Individual Dosage Regimen Evaluation

Supplementary Figure S4 illustrates the probabilities across treatment cycles for each patient. The MIPD strategy indicated that 50% (11/22) of patients would require an optimized dose regimen, while 14% (3/22) would need an intensified regimen compared to the clinical practice regimen used during the maintenance period of treatment with SCK. The optimized patients are suggested to follow non-standard dosage regimens: 150 mg q4w

for 9% (1/11), 150 mg q5w for 9% (1/11), 150 mg q6w for 18% (2/11), 300 mg q5w for 45% (5/11), and 300 mg q6w for 18% (2/11) of patients. In patients requiring intensified regimens, switching to 300 mg q2w is advised for all. For 18% (4/22) of patients, no changes to their current regimen were predicted. Furthermore, this MIPD strategy helped identify 18% (4/22) of patients who would not reach the efficacy target (90% probability of PASI ≤ 1), enabling early recognition of those at risk of therapeutic failure. Figure 4 specifies the changes from the dose regimen in clinical practice to the predicted regimen during the maintenance phase of therapy with SCK (cycle 20).

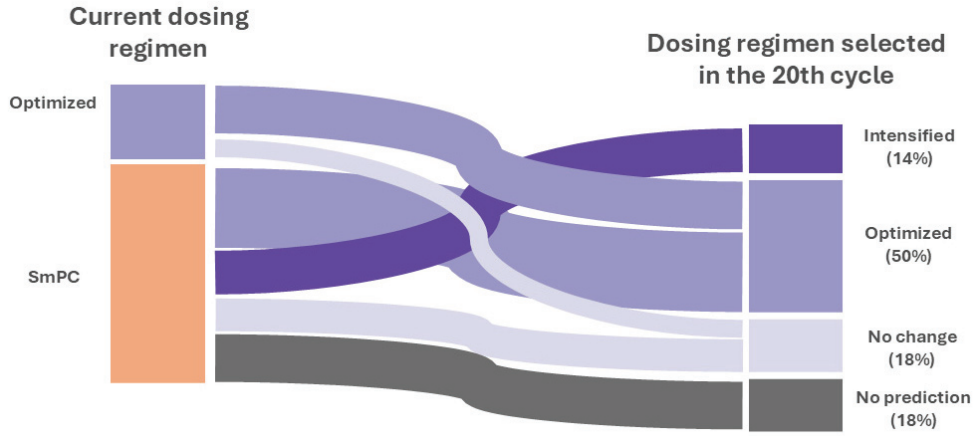


Figure 4. Sankey diagram of the shifts in individual dosage regimens. SmPC: summary of product characteristics.

Supplementary Figure S5 depicts the PK and PD simulations for each patient, comparing the current clinical practice regimen with the optimized dosing regimen determined by the 20th cycle. Figure 5 highlights the connection between absolute PASI scores and steady-state $C_{trough\text{-}ss}$ under all tested regimens. The general findings show a non-linear association, establishing that a $C_{trough\text{-}ss}$ varying from 64.2 to 69.3 mg/L allows a PASI score ≤ 1 in 90% of patients.

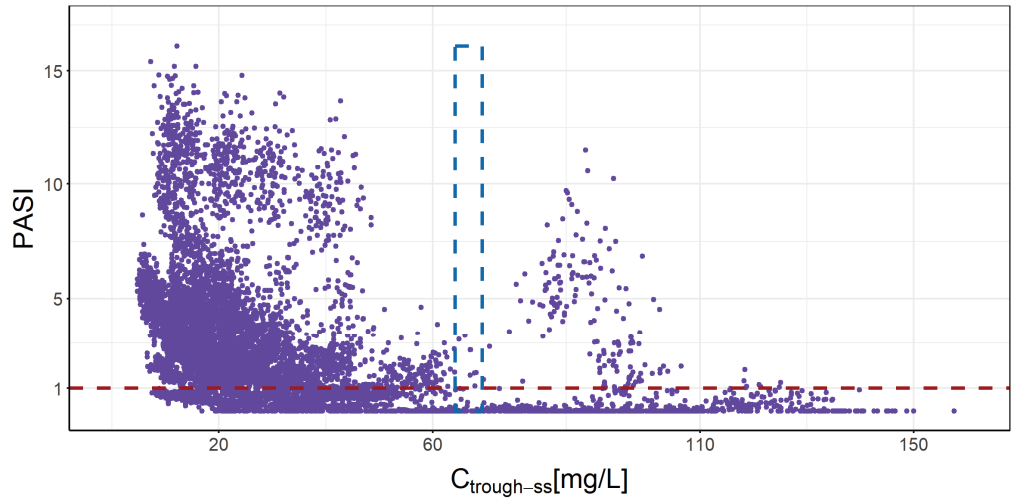


Figure 5. Simulated trough level and absolute PASI score for all subjects after receiving 150 mg q4w, q5w, and q6w; and 300 mg q2w, q4w, q5w and q6w of SCK SC administration in the 20th cycle. The purple dots represent the simulated PASI score and their corresponding $C_{trough\text{-}ss}$. The blue dashed box represents the $C_{trough\text{-}ss}$ (64.2–69.3 mg/L) that allows a PASI score ≤ 1 in 90% of patients. The red dashed line represents the PASI value of 1. $C_{trough\text{-}ss}$: trough concentration at steady state.

4. Discussion

In this study, an exposure–response model was developed for PASI, the most employed endpoint for efficacy in clinical practice patients with persistent psoriasis vulgaris. An indirect-response model was evaluated to characterize the effects of SCK, incorporating an additional series of turnover compartments for prePASI and a tolerance mechanism. This approach was based on the expectation of a time lag between the peak concentrations of SCK and the maximum drug effect on psoriatic lesions, represented by PASI scores. Since SCK inhibits the IL-17A, the exposure–efficacy model represented SCK as having an inhibitory pharmacological effect on the development of psoriatic lesions following drug administration. However, we are aware of the drawbacks in the developed PK/PD model reflected in the low precision in parameter estimation of the tolerance mechanism (RSE of k_{outTOL} and RSE of k_{outTOL} IIV), which is only activated in four patients (5, 10, 13, and 16).

The cornerstone of this study was the development of a procedure for tailoring dosing approaches of SCK in Spanish patients with moderate to severe long-lasting psoriasis vulgaris, based on the uncertainty surrounding individual parameter estimates from a population PK/PD model. Moreover, by integrating uncertainty into the simulation stage designed for personalized dosing regimen choice, it becomes possible to assess the confidence level of model-informed forecasts in clinical practice, offering an approach with probabilistic character for MIPD of SCK. Among the patients needing a modification to their dosage regimen, an optimized dosage regimen is suggested in 50% of them. In almost all optimized patients (91%), the optimization should be to a non-labeled dosage regimen, with 300 mg q5w being recommended in 45% of patients. This adjustment would lead to a decrease of 3 doses for each year, meaning that as an alternative to receiving 14 doses in the following years after the first year of treatment with SKC according to the SmPC dosing guidelines, patients would receive 11 doses. Corresponding to the health information database for medicines and pharmacy products [58], the cost of Cosentyx® 300 mg injection in a pre-filled syringe is EUR 1246.98. With the optimization of SCK therapy, the annual cost per patient would amount to EUR 13717, resulting in savings of 21%. Additionally, fewer medication purchases and a smaller quantity of administrations would decrease the threat of injection site reactions.

In contrast to the clinical practice's dose regimen schedule, intensification was recommended in 14% of the subjects. Because in these patients the I_{max} values were lower (1.06–1.13) than the typical value (1.19), a higher level of SCK dose would be required to achieve a successful therapeutic response. Note that most of the included patients required a dose regimen optimization following the implementation of our MIPD method in SCK. Consequently, since patients are more likely to be within the appropriate treatment response range, it is possible to enhance patient welfare and health system administration. In 18% of subjects, the efficacy endpoint (90% probability of PASI ≤ 1) was not obtained. Therefore, the MIPD strategy proposed in this investigation implies a benefit for identifying patients who are not responding to treatment in the beginning. In this way, the management of plaque psoriasis can be enhanced in these individuals, and unnecessary costs associated with treating them in subsequent cycles could be avoided. Furthermore, their k_{out} values are lower (0.07) than the typically observed (0.11), which might be used as a cutoff point for distinguishing patients who are unlikely to respond optimally to SCK.

The full data of SCK concentrations and PASI scores that were acquirable in each patient included in this study were applied to estimate the individual PK/PD parameters. An adaptable process might be employed to apply the suggested MIPD approach into practice. To make sure the model continues to be accurate and still represent the patient's progressing state, this approach would involve a refining process of the individual parameters as novel data points appear. In this study, the importance of collecting samples of absolute PASI from patients throughout the initial weeks of treatment to accurately determine their individual PD parameters is highlighted. The significance of both PK and PD parameters in ensuring effective treatment outcomes is demonstrated by the non-linear relationship between the simulated absolute PASI and $C_{trough\text{-}ss}$ of SCK

(Figure 5). While it is feasible to set general exposure values corresponding to an absolute PASI, the use of this MIPD approach to personalize treatment can lead to a higher proportion of patients reaching efficient dosage regimens, thereby minimizing treatment failure among non-responders.

A more exigent $C_{trough\text{-}ss}$ range (64.2–69.3 mg/L) was proposed in this study to accomplish in 90% of patients an absolute PASI ≤ 1. A previously reported $C_{trough\text{-}ss}$ range (12.9–62.9 mg/L) was established in a prior population PK modeling investigation [21], which included individuals on a 300 mg q4w dosage regimen, and it was produced using simulated data from clinical trials in patients who were only beginning therapy with SCK, in which the efficacy objective was to achieve in week 12 the PASI 75. Conversely, the $C_{trough\text{-}ss}$ range found in this research stand for a more rigorous PD endpoint (PASI ≤ 1 or PASI 99) from patients in routine clinical practice. Also, the proposed $C_{trough\text{-}ss}$ range aligns with optimal response criteria consistent with current clinical guidelines (PASI ≤ 1), intended to enhance the quality of life and clinical results for those with persistent psoriasis vulgaris [59,60].

This research is based on PK/PD models previously reported. Nevertheless, our work is an example of how to effectively use established knowledge. However, we have gone one step further in the description of the relationship among SCK concentrations and patient responses measured by absolute PASI under real-world circumstances. In addition, this investigation exemplifies individualized precision dosing, representing a more thorough and effective application of precision dosing approaches by identifying, characterizing, and quantifying the different causes of variability in drug response via PK/PD modeling [25,35]. While gaining a deeper comprehension of PK/PD interrelation in particular patient populations during clinical studies can aid in identifying precise dosing objectives, patients from clinical practice are often much more distinct than those in supervised study environments. As a result, efficient post-marketing monitoring is crucial for investigating distinctive precision-dosing aims [61]. Improvements in methods for gathering and analyzing data from real-world patients present chances to discover novel precision-dosing procedures and improve those confirmed in clinical trials. These techniques facilitate the ongoing renewing and enhancement of dosing strategies to more effectively address patient requirements [35,62]. That is why our approach, which is based on MIPD under real-world circumstances, may be a first effort to guarantee the most accurate individual dosage for patients with psoriasis vulgaris receiving SCK.

Some limitations have been played against our investigation. Firstly, as a consequence of the study design conditions, there was a small patient sample size. Secondly, many PK/PD observations were either missing or were captured very distant in time (sparse data), resulting in a small number of points per patient. Because of that, the progression of psoriasis vulgaris or unmeasured physiological transformations may have straightforwardly affected the outcomes obtained. Looking ahead, similar models could be incorporated into a provisional distribution dashboard system for enhanced analysis [63,64]. Regarding the proposed optimization with the unlabeled dosage regimen of 300 mg q5w, and despite its advantages in terms of efficiency and safety, sometimes such optimizations may not be carried out because it would mean extending the frequency of administration by one more week. Changing the dosage could cause some confusion in, for example, elderly patients, patients who are seriously ill at the start of SCK therapy, and patients who have been heavily pretreated with multi-resistant forms. Furthermore, we incorporated tolerance mechanisms because we first developed a PKPD model with all the experimental evidence and then conducted an MIPD approach for evaluating the optimal dosing regimen. Therefore, the tolerance mechanisms could not be anticipated in a traditional TDM approach for prospective prediction without measured PK and PD levels.

The results of this study confirm the recommendations already formulated by other authors, who propose incorporating alternatives for different dosing schemes based on MIPD and/or TDM into the SmPC [65]. This proposal could enhance treatment management in chronic diseases, such as plaque psoriasis, and could facilitate real-time predictions

of treatment responses, helping healthcare providers make informed decisions regarding dosing modifications and therapy transitions for SCK.

5. Conclusions

In conclusion, this study represents a significant initial step for biologists to implement MIPD that targets the IL routes in long-lasting psoriasis vulgaris, an area that has been largely understudied. We propose a methodology to personalize dosing strategies for SCK, which considers the uncertainty of individual parameters within a population PK/PD model to enhance the likelihood of succeeding targeted clinical effects in patients with psoriasis vulgaris from moderate to severe modality. Future research should focus on applying our approach to a larger group of real-world patients and validating the proposed dosing strategies.

Supplementary Materials: The following supporting information can be downloaded at: https://www.mdpi.com/article/10.3390/pharmaceutics16121576/s1, Ordinary differential equations for the PK/PD model of SCK and absolute PASI; Figure S1: Individually predicted vs. the observed concentrations of SCK in patients with chronic psoriasis vulgaris; Figure S2: Individually predicted vs. the observed PASI in patients with chronic psoriasis vulgaris; Figure S3: Prediction-corrected visual predictive check obtained from one thousand simulated studies using the selected population PK/PD model; Table S1: Means of the individual PK/PD parameters drawn from the conditional distribution task in Monolix; Table S2: Standard deviation of the individual PK/PD parameters drawn from the conditional distribution task in Monolix; Figure S4: Bar plot of 100 simulated absolute PASI for each patient after SCK administration at cycles 10 and 20, using the individual parameters from the final population PK/PD model and their uncertainties; Figure S5: PK and PD simulations with the current dosage regimen from clinical practice and the individual optimal dosing regimen established after simulations in 20th cycle for each patient.

Author Contributions: Conceptualization, M.M.-S., E.G.-C., M.C.-M. and V.M.-S.; methodology, K.R.-F., J.Z.-F., M.M.-S., E.G.-C., M.C.-M. and V.M.-S.; software, K.R.-F., J.Z.-F. and V.M.-S.; validation, K.R.-F., J.Z.-F., M.S.-B., M.M.-S., A.M.-P., A.M.-C., E.G.-C., M.C.-M. and V.M.-S.; formal analysis, K.R.-F., J.Z.-F. and V.M.-S.; investigation, K.R.-F., J.Z.-F. and V.M.-S.; resources, A.M.-P., A.M.-C., E.G.-C. and M.C.-M.; data curation, K.R.-F.; writing—original draft preparation, K.R.-F., J.Z.-F. and V.M.-S.; writing—review and editing, K.R.-F., J.Z.-F., M.S.-B., M.M.-S., A.M.-P., A.M.-C., E.G.-C., M.C.-M. and V.M.-S.; visualization, K.R.-F. and J.Z.-F.; supervision, E.G.-C., M.C.-M. and V.M.-S.; project administration, E.G.-C., M.C.-M. and V.M.-S.; funding acquisition, A.M.-P., E.G.-C. and M.C.-M. All authors have read and agreed to the published version of the manuscript.

Funding: This research received no external funding.

Institutional Review Board Statement: This study was conducted following the Declaration of Helsinki and approved by the Ethics Committee of Dr. Peset University Hospital (protocol code: VMS-SCK-2020-01 and date of approval: 30 March 2020).

Informed Consent Statement: Informed consent was obtained from all subjects involved in the study.

Data Availability Statement: The data presented in this study are available on request from the corresponding author due to ethical and legal restrictions.

Conflicts of Interest: The authors declare no conflicts of interest.

Abbreviations

AHT	Arterial hypertension
BMI	Body mass index
$C_{trough\text{-}ss}$	Trough concentration at steady state
CL	Clearance
ELISA	Enzyme-linked immunosorbent assay
F	Bioavailability
IC_{50}	Concentration of the drug needed to inhibit 50% of the response
I_{max}	Maximum inhibition

IIV	Interindividual variability
IL	Interleukin
k_a	Absorption rate constant
k_{in}	Zero-order evolution constant rate of psoriatic skin lesion
k_{inTOL}	Zero-order progression constant rate of tolerance
k_{out}	First-order reduction constant rate of psoriatic skin lesion
k_{outTOL}	First-order remission constant rate of tolerance
mAb	Monoclonal antibody
MCMC	Markov chain Monte Carlo
MIPD	Model-informed precision dosing
PASI	Psoriasis Area and Severity Index
$PASI_i$	Estimated baseline levels of PASI response
$PASI_{i,0}$	Individual observed baseline levels of PASI response
pcVPC	Prediction-corrected visual predictive checks
PD	Pharmacodynamic
PK	Pharmacokinetic
PK/PD	Pharmacokinetic/pharmacodynamic
Q	Intercompartmental transfer clearance
q2w	Once every 2 weeks
q4w	Once every 4 weeks
q5w	Once every 5 weeks
q6w	Once every 6 weeks
RSE	Relative standard error
RUV	Residual unexplained variability
SC	Subcutaneous
SD	Standard deviation
SmPC	Summary of product characteristics
SLP	Linear drug effect model
TDM	Therapeutic drug monitoring
SCK	Secukinumab
V_2	Central volume of distribution
V_3	Peripheral volume of distribution

References

1. Frieder, J.; Kivelevitch, D.; Menter, A. Secukinumab: A review of the anti-IL-17A biologic for the treatment of psoriasis. *Ther. Adv. Chronic Dis.* **2018**, *9*, 5–21. [CrossRef] [PubMed]
2. Garnock-Jones, K.P. Secukinumab: A review in moderate to severe plaque psoriasis. *Am. J. Clin. Dermatol.* **2015**, *16*, 323–330. [CrossRef] [PubMed]
3. Nestle, F.O.; Kaplan, D.H.; Barker, J. Psoriasis. *N. Engl. J. Med.* **2009**, *361*, 496–509. [CrossRef]
4. Schadler, E.D.; Ortel, B.; Mehlis, S.L. Biologics for the primary care physician: Review and treatment of psoriasis. *Disease-a-Month* **2018**, *65*, 51–90. [CrossRef] [PubMed]
5. Rendon, A.; Schäkel, K. Psoriasis Pathogenesis and Treatment. *Int. J. Mol. Sci.* **2019**, *20*, 1475. [CrossRef] [PubMed]
6. Patel, D.D.; Lee, D.M.; Kolbinger, F.; Antoni, C. Effect of IL-17A blockade with secukinumab in autoimmune diseases. *Ann. Rheum. Dis.* **2012**, *72* (Suppl. 2), ii116–ii1123. [CrossRef]
7. Mahil, S.K.; Capon, F.; Barker, J.N. Update on psoriasis immunopathogenesis and targeted immunotherapy. *Semin. Immunopathol.* **2016**, *38*, 11–27. [CrossRef]
8. Lynde, C.W.; Poulin, Y.; Vender, R.; Bourcier, M.; Khalil, S. Interleukin 17A: Toward a new understanding of psoriasis pathogenesis. *J. Am. Acad. Dermatol.* **2014**, *71*, 141–150. [CrossRef]
9. EMA: COSENTYX-EPAR-product information. Available online: https://www.ema.europa.eu/en/documents/product-information/cosentyx-epar-product-information_en.pdf (accessed on 17 September 2024).
10. Phung, M.; Ighani, A.; Georgakopoulos, J.R.; Vender, R.; Giroux, L.; Lansang, P.; Yeung, J. Off-Label High-Dose Secukinumab for the Treatment of Moderate-to-Severe Psoriasis. *J. Cutan. Med. Surg.* **2019**, *23*, 391–393. [CrossRef]
11. Rich, P.; Sigurgeirsson, B.; Thaci, D.; Ortonne, J.P.; Paul, C.; Schopf, R.E.; Morita, A.; Roseau, K.; Harfst, E.; Guettner, A.; et al. Secukinumab induction and maintenance therapy in moderate-to-severe plaque psoriasis: A randomized, double-blind, placebo-controlled, phase II regimen-finding study. *Br. J. Dermatol.* **2013**, *168*, 402–411. [CrossRef]
12. Papp, K.A.; Langley, R.G.; Sigurgeirsson, B.; Abe, M.; Baker, D.R.; Konno, P.; Haemmerle, S.; Thurston, H.J.; Papavassilis, C.; Richards, H.B. Efficacy and safety of secukinumab in the treatment of moderate-to-severe plaque psoriasis: A randomized, double-blind, placebo-controlled phase II dose-ranging study. *Br. J. Dermatol.* **2013**, *168*, 412–421. [CrossRef] [PubMed]

13. Langley, R.G.; Elewski, B.E.; Lebwohl, M.; Reich, K.; Griffiths, C.E.; Papp, K.; Puig, L.; Nakagawa, H.; Spelman, L.; Sigurgeirsson, B.; et al. Secukinumab in plaque psoriasis--results of two phase 3 trials. *N. Engl. J. Med.* **2014**, *371*, 326–338. [CrossRef]
14. Augustin, M.; Jullien, D.; Martin, A.; Peralta, C. Real-world evidence of secukinumab in psoriasis treatment—A meta-analysis of 43 studies. *J. Eur. Acad. Dermatol. Venereol. JEADV* **2020**, *34*, 1174–1185. [CrossRef] [PubMed]
15. Yiu, Z.Z.N.; Mason, K.J.; Hampton, P.J.; Reynolds, N.J.; Smith, C.H.; Lunt, M.; Griffiths, C.E.M.; Warren, R.B. Drug survival of adalimumab, ustekinumab and secukinumab in patients with psoriasis: A prospective cohort study from the British Association of Dermatologists Biologics and Immunomodulators Register (BADBIR). *Br. J. Dermatol.* **2020**, *183*, 294–302. [CrossRef]
16. Leonardi, C.; Zhu, B.; Malatestinic, W.N.; Eastman, W.J.; Guo, J.; Murage, M.J.; Choong, C.K.; Burge, R.; Blauvelt, A. Real-World Biologic Adherence, Persistence, and Monotherapy Comparisons in US Patients with Psoriasis: Results from IBM MarketScan(®) Databases. *Adv. Ther.* **2022**, *39*, 3214–3224. [CrossRef]
17. Thein, D.; Rosenø, N.A.L.; Maul, J.T.; Wu, J.J.; Skov, L.; Bryld, L.E.; Rasmussen, M.K.; Ajgeiy, K.K.; Thomsen, S.F.; Thyssen, J.P.; et al. Drug Survival of Adalimumab, Secukinumab, and Ustekinumab in Psoriasis as Determined by Either Dose Escalation or Drug Discontinuation during the First 3 Years of Treatment—A Nationwide Cohort Study. *J. Investig. Dermatol.* **2023**, *143*, 2211–2218.e2214. [CrossRef] [PubMed]
18. Hueber, W.; Patel, D.D.; Dryja, T.; Wright, A.M.; Koroleva, I.; Bruin, G.; Antoni, C.; Draelos, Z.; Gold, M.H.; Psoriasis Study Group; et al. Effects of AIN457, a Fully Human Antibody to Interleukin-17A, on Psoriasis, Rheumatoid Arthritis, and Uveitis. *Sci. Transl. Med.* **2010**, *2*, 52ra72. [CrossRef]
19. Reich, K.; Papp, K.A.; Matheson, R.T.; Tu, J.H.; Bissonnette, R.; Bourcier, M.; Gratton, D.; Kunynetz, R.A.; Poulin, Y.; Rosoph, L.A.; et al. Evidence that a neutrophil-keratinocyte crosstalk is an early target of IL-17A inhibition in psoriasis. *Exp. Dermatol.* **2015**, *24*, 529–535. [CrossRef]
20. Paul, C.; Lacour, J.P.; Tedremets, L.; Kreutzer, K.; Jazayeri, S.; Adams, S.; Guindon, C.; You, R.; Papavassilis, C. Efficacy, safety and usability of secukinumab administration by autoinjector/pen in psoriasis: A randomized, controlled trial (JUNCTURE). *J. Eur. Acad. Dermatol. Venereol. JEADV* **2015**, *29*, 1082–1090. [CrossRef]
21. Bruin, G.; Loesche, C.; Nyirady, J.; Sander, O. Population pharmacokinetic modeling of secukinumab in patients with moderate to severe psoriasis. *J. Clin. Pharmacol.* **2017**, *57*, 876–885. [CrossRef]
22. Rodríguez-Fernández, K.; Mangas-Sanjuán, V.; Merino-Sanjuán, M.; Martorell-Calatayud, A.; Mateu-Puchades, A.; Climente-Martí, M.; Gras-Colomer, E. Impact of Pharmacokinetic and Pharmacodynamic Properties of Monoclonal Antibodies in the Management of Psoriasis. *Pharmaceutics* **2022**, *14*, 654. [CrossRef] [PubMed]
23. Liu, Y.; Xu, L.; Wang, X.; Wu, L.; Cai, R.; Li, L.; Zheng, Q. Optimization of secukinumab dose regimens in patients with moderate-to-severe plaque psoriasis via exposure-response modeling. *Expert Rev. Clin. Pharmacol.* **2023**, *16*, 999–1008. [CrossRef]
24. Notario, J.; Bordas, X. Practical management of ustekinumab in moderate-severe psoriasis. *Actas Dermo-Sifiliogr.* **2012**, *103*, 52–58. [CrossRef]
25. Tyson, R.J.; Park, C.C.; Powell, J.R.; Patterson, J.H.; Weiner, D.; Watkins, P.B.; Gonzalez, D. Precision Dosing Priority Criteria: Drug, Disease, and Patient Population Variables. *Front. Pharmacol.* **2020**, *11*, 420. [CrossRef] [PubMed]
26. Syversen, S.W.; Goll, G.L.; Jørgensen, K.K.; Sandanger, Ø.; Sexton, J.; Olsen, I.C.; Gehin, J.E.; Warren, D.J.; Brun, M.K.; Klaasen, R.A.; et al. Effect of Therapeutic Drug Monitoring vs Standard Therapy During Infliximab Induction on Disease Remission in Patients with Chronic Immune-Mediated Inflammatory Diseases: A Randomized Clinical Trial. *JAMA* **2021**, *325*, 1744–1754. [CrossRef] [PubMed]
27. Albader, F.; Golovics, P.A.; Gonczi, L.; Bessissow, T.; Afif, W.; Lakatos, P.L. Therapeutic drug monitoring in inflammatory bowel disease: The dawn of reactive monitoring. *World J. Gastroenterol.* **2021**, *27*, 6231–6247. [CrossRef]
28. D'Haens, G.R.; Sandborn, W.J.; Loftus, E.V., Jr.; Hanauer, S.B.; Schreiber, S.; Peyrin-Biroulet, L.; Panaccione, R.; Panés, J.; Baert, F.; Colombel, J.F.; et al. Higher vs Standard Adalimumab Induction Dosing Regimens and Two Maintenance Strategies: Randomized SERENE CD Trial Results. *Gastroenterology* **2022**, *162*, 1876–1890. [CrossRef]
29. Minichmayr, I.K.; Dreesen, E.; Centanni, M.; Wang, Z.; Hoffert, Y.; Friberg, L.E.; Wicha, S.G. Model-informed precision dosing: State of the art and future perspectives. *Adv. Drug Deliv. Rev.* **2024**, *215*, 115421. [CrossRef]
30. Olivier, B.G.; Swat, M.J.; Moné, M.J. Modeling and Simulation Tools: From Systems Biology to Systems Medicine. In *Systems Medicine*; Schmitz, U., Wolkenhauer, O., Eds.; Methods in Molecular Biology; Humana Press: New York, NY, USA, 2016; Volume 1386, pp. 441–463. [CrossRef]
31. Darwich, A.S.; Polasek, T.M.; Aronson, J.K.; Ogungbenro, K.; Wright, D.F.B.; Achour, B.; Reny, J.L.; Daali, Y.; Eiermann, B.; Cook, J.; et al. Model-Informed Precision Dosing: Background, Requirements, Validation, Implementation, and Forward Trajectory of Individualizing Drug Therapy. *Annu. Rev. Pharmacol. Toxicol.* **2021**, *61*, 225–245. [CrossRef]
32. Minichmayr, I.K.; Mizuno, T.; Goswami, S.; Peck, R.W.; Polasek, T.M.; American Society of Clinical Pharmacology; Therapeutics Precision Dosing Community. Recent Advances Addressing the Challenges of Precision Dosing. *Clin. Pharmacol. Ther.* **2024**, *116*, 527–530. [CrossRef]
33. Bandín-Vilar, E.; Toja-Camba, F.J.; Vidal-Millares, M.; Durán-Maseda, M.J.; Pou-Álvarez, M.; Castro-Balado, A.; Maroñas, O.; Gil-Rodríguez, A.; Carracedo, Á.; Zarra-Ferro, I.; et al. Towards precision medicine of long-acting aripiprazole through population pharmacokinetic modelling. *Psychiatry Res.* **2024**, *333*, 115721. [CrossRef] [PubMed]

34. Rodríguez-Fernández, K.; Reynaldo-Fernández, G.; Reyes-González, S.; de Las Barreras, C.; Rodríguez-Vera, L.; Vlaar, C.; Monbaliu, J.M.; Stelzer, T.; Duconge, J.; Mangas-Sanjuan, V. New insights into the role of VKORC1 polymorphisms for optimal warfarin dose selection in Caribbean Hispanic patients through an external validation of a population PK/PD model. *Biomed. Pharmacother.=Biomed. Pharmacother.* **2024**, *170*, 115977. [CrossRef] [PubMed]
35. Polasek, T.M.; Peck, R.W. Beyond Population-Level Targets for Drug Concentrations: Precision Dosing Needs Individual-Level Targets that Include Superior Biomarkers of Drug Responses. *Clin. Pharmacol. Ther.* **2024**, *116*, 602–612. [CrossRef]
36. Zhu, Y.; Hu, C.; Lu, M.; Liao, S.; Marini, J.C.; Yohrling, J.; Yeilding, N.; Davis, H.M.; Zhou, H. Population pharmacokinetic modeling of ustekinumab, a human monoclonal antibody targeting IL-12/23p40, in patients with moderate to severe plaque psoriasis. *J. Clin. Pharmacol.* **2009**, *49*, 162–175. [CrossRef] [PubMed]
37. Zhou, W.; Hu, C.; Zhu, Y.; Randazzo, B.; Song, M.; Sharma, A.; Xu, Z.; Zhou, H. Extrapolating Pharmacodynamic Effects From Adults to Pediatrics: A Case Study of Ustekinumab in Pediatric Patients With Moderate to Severe Plaque Psoriasis. *Clin. Pharmacol. Ther.* **2020**, *109*, 131–139. [CrossRef]
38. *ISO 15189*; Medical Laboratories—Requirements for Quality and Competence. International Organization for Standardization: Geneva, Switzerland, 2022.
39. Mould, D.R.; Upton, R.N. Basic concepts in population modeling, simulation, and model-based drug development. *CPT Pharmacomet. Syst. Pharmacol.* **2012**, *1*, e6. [CrossRef]
40. Upton, R.N.; Mould, D.R. Basic concepts in population modeling, simulation, and model-based drug development: Part 3-introduction to pharmacodynamic modeling methods. *CPT Pharmacomet. Syst. Pharmacol.* **2014**, *3*, e88. [CrossRef]
41. Felmlee, M.A.; Morris, M.E.; Mager, D.E. Mechanism-based pharmacodynamic modeling. In *Computational Toxicology*; Reisfeld, B., Mayeno, A., Eds.; Methods in Molecular Biology; Humana Press: Totowa, NJ, USA, 2012; Volume 929, pp. 583–600. [CrossRef]
42. Dansirikul, C.; Silber, H.E.; Karlsson, M.O. Approaches to handling pharmacodynamic baseline responses. *J. Pharmacokinet. Pharmacodyn.* **2008**, *35*, 269–283. [CrossRef]
43. Bergstrand, M.; Hooker, A.C.; Wallin, J.E.; Karlsson, M.O. Prediction-corrected visual predictive checks for diagnosing nonlinear mixed-effects models. *AAPS J.* **2011**, *13*, 143–151. [CrossRef]
44. Lixoft. Monolix Suite 2024R1 (2024). Available online: https://lixoft.com/products/monolix/ (accessed on 25 July 2024).
45. Ito, K.; Murphy, D. Application of ggplot2 to Pharmacometric Graphics. *CPT Pharmacomet. Syst. Pharmacol.* **2013**, *2*, e79. [CrossRef]
46. R Core Team. *R: A Language and Environment for Statistical Computing*; R Foundation for Statistical Computing: Vienna, Austria, 1999–2024; Available online: http://www.R-project.org/ (accessed on 30 July 2024).
47. Monolix 2024R1 User Guide. Available online: https://monolix.lixoft.com/single-page/ (accessed on 25 January 2024).
48. Kümmel, A.; Bonate, P.L.; Dingemanse, J.; Krause, A. Confidence and Prediction Intervals for Pharmacometric Models. *CPT Pharmacomet. Syst. Pharmacol.* **2018**, *7*, 360–373. [CrossRef] [PubMed]
49. Lixoft. Simulx 2024R1 (2024). Available online: https://simulx.lixoft.com/ (accessed on 25 July 2024).
50. Dayneka, N.L.; Garg, V.; Jusko, W.J. Comparison of four basic models of indirect pharmacodynamic responses. *J. Pharmacokinet. Biopharm.* **1993**, *21*, 457–478. [CrossRef]
51. Zhou, H.; Hu, C.; Zhu, Y.; Lu, M.; Liao, S.; Yeilding, N.; Davis, H.M. Population-based exposure-efficacy modeling of ustekinumab in patients with moderate to severe plaque psoriasis. *J. Clin. Pharmacol.* **2010**, *50*, 257–267. [CrossRef] [PubMed]
52. Salinger, D.H.; Endres, C.J.; Martin, D.A.; Gibbs, M.A. A semi-mechanistic model to characterize the pharmacokinetics and pharmacodynamics of brodalumab in healthy volunteers and subjects with psoriasis in a first-in-human single ascending dose study. *Clin. Pharmacol. Drug Dev.* **2014**, *3*, 276–283. [CrossRef]
53. Tham, L.-S.; Tang, C.-C.; Choi, S.-L.; Satterwhite, J.H.; Cameron, G.S.; Banerjee, S. Population exposure-response model to support dosing evaluation of ixekizumab in patients with chronic plaque psoriasis. *J. Clin. Pharmacol.* **2014**, *54*, 1117–1124. [CrossRef] [PubMed]
54. Pan, S.; Tsakok, T.; Dand, N.; Lonsdale, D.O.; Loeff, F.C.; Bloem, K.; de Vries, A.; Baudry, D.; Duckworth, M.; Mahil, S.; et al. Using Real-World Data to Guide Ustekinumab Dosing Strategies for Psoriasis: A Prospective Pharmacokinetic-Pharmacodynamic Study. *Clin. Transl. Sci.* **2020**, *13*, 400–409. [CrossRef]
55. Kerbusch, T.; Li, H.; Wada, R.; Jauslin, P.M.; Wenning, L. Exposure-response characterisation of tildrakizumab in chronic plaque psoriasis: Pooled analysis of 3 randomised controlled trials. *Br. J. Clin. Pharmacol.* **2020**, *86*, 1795–1806. [CrossRef]
56. Rodríguez-Fernández, K.; Zarzoso-Foj, J.; Saez-Bello, M.; Mateu-Puchades, A.; Martorell-Calatayud, A.; Merino-Sanjuan, M.; Gras-Colomer, E.; Climente-Martí, M.; Mangas-Sanjuan, V. Model-Informed Precision Dosing for Personalized Ustekinumab Treatment in Plaque Psoriasis. *Pharmaceutics* **2024**, *16*, 1295. [CrossRef]
57. DeBonis, J.; Veiseh, O.; Igoshin, O.A. Uncovering the interleukin-12 pharmacokinetic desensitization mechanism and its consequences with mathematical modeling. *CPT Pharmacomet. Syst. Pharmacol.* **2024**. [CrossRef]
58. BOT PLUS. Available online: https://botplusweb.farmaceuticos.com/ (accessed on 29 August 2024).
59. Torres, T.; Puig, L. Treatment goals for psoriasis: Should PASI 90 become the standard of care? *Actas Dermo-Sifiliogr.* **2015**, *106*, 155–157. [CrossRef]
60. Nast, A.; Smith, C.; Spuls, P.I.; Avila Valle, G.; Bata-Csörgö, Z.; Boonen, H.; De Jong, E.; Garcia-Doval, I.; Gisondi, P.; Kaur-Knudsen, D.; et al. EuroGuiDerm Guideline on the systemic treatment of Psoriasis vulgaris—Part 1: Treatment and monitoring recommendations. *J. Eur. Acad. Dermatol. Venereol. JEADV* **2020**, *34*, 2461–2498. [CrossRef] [PubMed]

61. Kamal, M.A.; Ganguly, S.; Kadambi, A.; Smith, P.F. Extended Model-Informed Drug Development: Beyond Clinical Trials and Regulatory Approval. *Clin. Pharmacol. Ther.* **2024**, *116*, 518–521. [CrossRef] [PubMed]
62. Darwich, A.S.; Ogungbenro, K.; Vinks, A.A.; Powell, J.R.; Reny, J.L.; Marsousi, N.; Daali, Y.; Fairman, D.; Cook, J.; Lesko, L.J.; et al. Why has model-informed precision dosing not yet become common clinical reality? lessons from the past and a roadmap for the future. *Clin. Pharmacol. Ther.* **2017**, *101*, 646–656. [CrossRef]
63. Dolan, J.G.; Veazie, P.J.; Russ, A.J. Development and initial evaluation of a treatment decision dashboard. *BMC Med. Inform. Decis. Mak.* **2013**, *13*, 51. [CrossRef] [PubMed]
64. Mould, D.R.; Upton, R.N.; Wojciechowski, J. Dashboard systems: Implementing pharmacometrics from bench to bedside. *AAPS J.* **2014**, *16*, 925–937. [CrossRef]
65. Mould, D.R.; Upton, R.N. "Getting the Dose Right"—Revisiting the Topic with Focus on Biologic Agents. *Clin. Pharmacol. Ther.* **2024**, *116*, 613–618. [CrossRef]

Disclaimer/Publisher's Note: The statements, opinions and data contained in all publications are solely those of the individual author(s) and contributor(s) and not of MDPI and/or the editor(s). MDPI and/or the editor(s) disclaim responsibility for any injury to people or property resulting from any ideas, methods, instructions or products referred to in the content.

pharmaceutics

MDPI

Article

Use of Nuclear Factor of Activated T Cell-Regulated Gene Expression for Monitoring Immunosuppression with Extended-Release Tacrolimus after Liver Transplantation—A Proof of Concept

Judith Kahn [1,*,†], Eva Maria Matzhold [2,†], Peter Schlenke [2] and Peter Schemmer [1,3,*]

[1] Division of General, Visceral, and Transplant Surgery, Department of Surgery, Medical University of Graz, 8036 Graz, Austria
[2] Department of Blood Group Serology and Transfusion Medicine, Medical University of Graz, 8036 Graz, Austria; eva.matzhold@medunigraz.at (E.M.M.); peter.schlenke@medunigraz.at (P.S.)
[3] Bern Visceral Surgery & Pancreas Clinic Switzerland, Hirslanden Hospital Beau-Site, 3013 Bern, Switzerland
* Correspondence: judith.kahn@medunigraz.at (J.K.); peter.schemmer@hirslanden.ch (P.S.); Tel.: +43-316-385-80676 (J.K.)
† These authors contributed equally to this work.

Abstract: Background: There is a narrow therapeutic window for immunosuppression using calcineurin inhibitors. Drug trough levels do not reflect immunosuppression and should be replaced by pharmacodynamic monitoring. This prospective cohort study was designed to evaluate the effect of an extended-release formulation of tacrolimus (LCP Tac) on the nuclear factor of activated T cell-regulated gene expression (NFAT-RGE). Methods: The expression of interleukin-2, interferon-γ, granulocyte-macrophage colony-stimulating factor, and three reference genes was measured. Samples from 23 patients at defined time points in the first year after liver transplantation were analyzed using a droplet digital polymerase chain reaction. Results: All samples were within the targeted trough levels of LCP Tac, and their LCP Tac peak levels and residual NFAT-RGE showed a strong inverse correlation ($r = -0.8$). Most importantly, there was an individual immunosuppressive response to the LCP Tac. The mean individual trough effect of LCP Tac on the three target genes when all time points were pooled was 33% (26–56%) in patients without infection and 81% (53–95%) in those with infection ($p < 0.011$). The mean individual peak effect was 48% (44–64%) in patients without infection and 91% (90–94%) in those with infection ($p < 0.001$). Conclusions: Thus, tailored immunosuppression based on residual NFAT-RGE could prevent infections associated with over-immunosuppression early after liver transplantation.

Keywords: immunomonitoring; nuclear factor of activated T cells (NFAT); residual gene expression (RGE); extended-release Tacrolimus (LCP Tac); liver transplantation

1. Introduction

Calcineurin inhibitors (CNIs) are the backbone of immunosuppression (IS) following liver transplantation (LT); however, treatment with CNIs has many undesirable side effects. Although they are dose-critical drugs with a narrow therapeutic range, adequate monitoring is not currently available. As defined serum CNI trough levels have an individual effect on the immune status of each patient, the current standard for their monitoring does not reflect the overall immunological effect of CNIs. Thus, there is an urgent need to directly monitor the effects of CNIs for tailored IS and to reduce the side effects, such as infections, of these drugs. Careful pre- and post-transplant screening, vaccination pre- and post-LT, and post-LT prophylactic antimicrobials may reduce the risk of infection, which is currently the leading cause of death in these patients. Opportunistic pathogens, such as cytomegalovirus (CMV), which are not harmful to immunocompetent individuals, are

predominantly responsible for this process. In general, IS increases the risk of infection, with the highest prevalence in over-immunosuppressed patients.

Recent evidence suggests that IS can be measured using surrogate markers, such as the Torqueo Teno virus and polyoma (BK) virus load [1,2]. Additionally, CNIs inhibit the phosphatase activity of calcineurin after the formation of CNI/calmodulin complexes in the cytosol of lymphocytes. The main substrate of calcineurin in T cells is the phosphorylated transcription factor, the nuclear factor of activated T cells (NFAT). The dephosphorylation of NFAT by calcineurin is required for the translocation of this transcription factor into the nucleus, allowing for the subsequent transcription of the four key genes needed for T cell activation: interleukin-2 (IL-2), tumor necrosis factor alpha, granulocyte-monocyte colony-stimulating factor (GM-CSF), and interferon-gamma (IFN-γ) [3]. The expression of the three NFAT-regulated genes, IL-2, IFN-γ, and GM-CSF, can be analyzed to directly measure the actual functional effects of CNIs in peripheral blood [4,5]. Using a real-time polymerase chain reaction (PCR), several studies have semi-quantitatively analyzed NFAT-regulated gene expression (RGE) in peripheral blood and have confirmed this approach to be useful for the individualization of CNI dosing. Nearly all studies have shown an association between the level of NFAT-RGE and clinical aspects, which include rejection episodes and complications such as infection and malignancy.

The present study is the first designed to analyze the individual effects of Envarsus® (LCP Tac), a once-daily extended-release Tac formulation with MeltDose™ drug-delivery technology used to control drug release and enhance the drug's overall bioavailability, on the expression of NFAT-RGE. The use of LCP Tac in immunosuppressed patients following kidney transplantation (KT) and LT can potentially increase bioavailability, lower blood peak levels (c_{max}), lower peak-to-trough fluctuations, allow for the faster achievement of therapeutic drug levels, and lower the total daily dose when compared to Prograf® and Advagraf®. Compared to Prograf®, an increase in the concentration/dose ratio has been shown to be associated with improvements in renal function in LT patients, with a significant recovery of their estimated glomerular filtration rate 6 months after conversion [6]. When compared to immediate-release Tac, a lower incidence of tremor, insomnia, and alopecia after conversion with LCP Tac in KT patients within the first year post-transplant was also shown [7]. The aim of this trial is to prove the concept that this diagnostic approach can be used to monitor the degree of IS in LT patients receiving LCP Tac.

2. Materials and Methods

2.1. Patients

This prospective observational cohort study included 23 patients who underwent an LT between February 2019 and June 2020 (phase IV). They were recruited at the Division of General, Visceral, and Transplant Surgery, Department of Surgery, Medical University of Graz, Austria, and were investigated before LT (pre-LT) and at 1 and 2 weeks and 1, 6, and 12 months after LT (post-LT). Measurements were also performed at the time of infection. Infection requiring antimicrobial treatment was defined as exhibiting leukocyte and C-reactive protein values above the normal range, as confirmed by cell culture and viral PCR results, when possible. The diagnosis and treatment of infections were routinely performed. Rejection was primarily diagnosed through clinical assessments and liver function tests, i.e., elevated liver enzymes, after ruling out vascular and biliary complications using imaging techniques. If there was an immediate response to the administration of corticosteroids, a liver biopsy was not performed [8].

Briefly, post-LT patients who provided informed consent and were at an age $\geq$ 18 and <90 years were included in this study. Patients with a known allergy to the study drug, or its constituents, or to medications with a similar chemical structure, as recently published, were excluded from this study (NCT03315858).

Immunosuppressive Treatment

The IS regimen used in this study consisted of LCP Tac, which was introduced directly after LT, with mycophenolate mofetil and corticosteroid tapering for 2 months. Induction therapy with anti-T-lymphocyte globulin (ATG) at 3–5 mg/kg for 4 days was administered to patients <40 years of age with autoimmune hepatitis, with renal insufficiency with a glomerular filtration rate of <60 mL/min, and those receiving grafts from donors after cardiac death. All patients received the extended-release, once-daily formulation of LCP Tac (Envarsus®, Chiesi Farmaceutici S. p. A., 43122 Parma, Italy). The initial oral once-daily dose of LCP Tac was 0.11–0.13 mg/kg, initiated within 24–72 h after surgery. This dose was subsequently adjusted to achieve target trough serum concentrations of 5–10 ng/mL [8]. Their LCP Tac serum levels were also measured 4 h after LCP Tac intake (LCP Tac_{peak}). A total of 1 g of mycophenolate mofetil was administered twice daily. Steroid treatment consisting of 500 mg of methylprednisolone was initiated on day 0, with 160 mg administered on day 1, 80 mg on day 2, and 40 mg from day 3 onward. The dose was progressively decreased to allow patients to be weaned off and discontinue steroids after postoperative day (POD) 60.

Patients with CMV-positive donors received CMV prophylaxis, which included valganciclovir during the first 6 months post-LT. Both CMV-positive and -negative recipients received CMV prophylaxis with valganciclovir during the first 3 months post-LT.

LCP Tac levels were determined by liquid chromatography with tandem mass spectrometry (LC-MS/MS) using ethylendiamintetraacetate (EDTA) anticoagulated blood and a validated CE IVD assay (MassTox® Immunosuppressants in whole blood, Chromsystems).

2.2. Gene Expression Analysis

Heparinized peripheral blood samples (4 mL) were stimulated with 4 mL of complete RPMI-1640 medium (#R8755) containing 5 µg/mL Ionomycin (#I3909) and 100 ng/mL PMA (P1585) (all from Sigma-Aldrich, Burlington, MA, USA). After incubation at 37 °C for 3 h, lysates of the stimulated cells were prepared using Buffer EL (#79217) and RLT (#79216), and their total RNA was isolated using the RNA Blood Mini Kit (#52304) (all from Qiagen). Complementary DNA (cDNA) was reverse-transcribed using the SuperScript III First-Strand Synthesis System for RT-PCR (#18080051) (Invitrogen, Life Technologies), according to the manufacturer's protocols. Reactions consisting of 0.15–1.5 ng of cDNA were used in droplet digital PCR (ddPCR) experiments.

The gene expression levels of IL-2, IFN-γ, GM-CSF, and 3 reference genes, ACTB, GAPDH, and TPT1, were quantified using ddPCR (QX200 Droplet Digital PCR System) with the ddPCR Supermix for Probes (#186-3023) (Both from Bio-Rad, Hercules, CA, USA). Human ddPCR Expression Probe Assays—dHsaCPE5192847 (IL-2), dHsaCPE5034618 (IFNG), and dHsaCPE5039652 (CSF2)—were multiplexed with dHsaCPE5190200 (ACTB), dHsaCPE5031067 (TPT1), and dHsaCPE5031597 (GAPDH), respectively. The absolute number of copies (c) of the target gene transcripts were normalized to the geometric mean of the absolute copies of the 3 reference genes.

At 1 and 2 weeks and 1, 6, and 12 months after LT, the residual expression of NFAT-RGE after an LCP Tac intake was calculated. This percentage (RGE%) was calculated as $c_{peak}/c_0 \times 100$, with c_0 as the number of transcripts at the LCP Tac pre-dose level and c_{peak} as the number of transcripts at the LCP Tac peak level, 4 h after the LCP Tac intake according to whole-blood time–concentration curves observed in stable transplant recipients [9,10].

The peak effect of LCP Tac (Effect LCP Tac_{peak}) on gene expression was determined as c_{peak} for the patients' respective visits, which was adjusted to the pre-LT copy number ($c_{pre\text{-}LT}$). The trough effect of LCP Tac (Effect LCP Tac_0) was determined as c_0 for their respective visits, adjusted to the $c_{pre\text{-}LT}$. [11]. The pooled gene expression was calculated as the average of all copies (IL-2, GM-CSF, and IFN-γ) for each visit, and the mean copies and RGE% were calculated as the mean value over all eligible time points. The median of the pooled values of all patients without infection was compared with the median of the pooled values of all patients with infection.

2.3. Statistical Analysis

Patient characteristics and laboratory data are described as medians and interquartile ranges and counts and proportions, respectively. The study was planned to have a significant correlation of +/− 0.65 with a power of 90% and a 2-sided alpha of 0.05. To assess statistical differences between groups, U-tests based on Mann–Whitney and Wilcoxon's methods were performed. To assess differences between time points, Friedman or Wilcoxon signed-rank tests were used. All reported *p*-values were two-sided, with $p \leq 0.05$ considered statistically significant. Additionally 25 and 75 Percentiles were calculated (q1, q3). Spearman's correlation coefficient (ρ) was used to quantify bivariate relationships. A $\rho > 0.7$ was considered to indicate a strong relationship. The time to infection was described using the Kaplan–Meier method. Statistical analyses were performed using SAS 9.4 software.

3. Results

A total of 23 patients (65.2%, n = 15 male, n = 8 females) with a mean age of 59 underwent LT for either alcoholic liver cirrhosis (43.5%), hepatocellular carcinoma (43.5%), primary or secondary sclerosing cholangitis (8.7%), or primary biliary cirrhosis (4.3%). The median model of end-stage liver disease (MELD) score was 13 (range, 6–38). Two patients underwent another LT within 48 h, one of whom had primary non-function, while the other had hepatic artery thrombosis (Table S1). The follow-up duration was 12 months, and 1 patient died after 3 months due to sepsis after a duodenal perforation. Another 2 patients did not attend follow-ups after 6 months.

3.1. LCP Tac Dosing

Median LCP Tac doses of 6.00 (4.00–9.00, 4.00–10.00, and 4.00–8.00 mg in the 1st week, 2nd week, and 1 month post-LT, respectively), 3.00 (2.00–4.75 mg at 6 months post-LT), and 2.08 mg (1.50–3.50 ng/dL at 12 months post-LT) were given.

LCP Tac trough levels (LCP Tac_0) were within the targeted range. Median LCP Tac_0 serum levels of 8.00 (5.10–9.80), 9.1 (6.30–11.0), 7.50 (6.10–11.20), 6.40 (5.60–7.30), and 6.20 ng/mL (4.70–7.50) were determined in the 1st and 2nd week and at 1, 6, and 12 months post-LT, respectively. These included correspondingly decreasing values in the later course. LCP Tac_0 differed significantly between the time points ($p = 0.014$). Its levels were significantly higher at 1 and 2 weeks post-LT when compared to 12 months post-LT ($p = 0.030$ and $p = 0.042$, respectively). Its levels at 2 weeks post-LT were also higher than at 6 months post-LT ($p = 0.038$) (Figure 1).

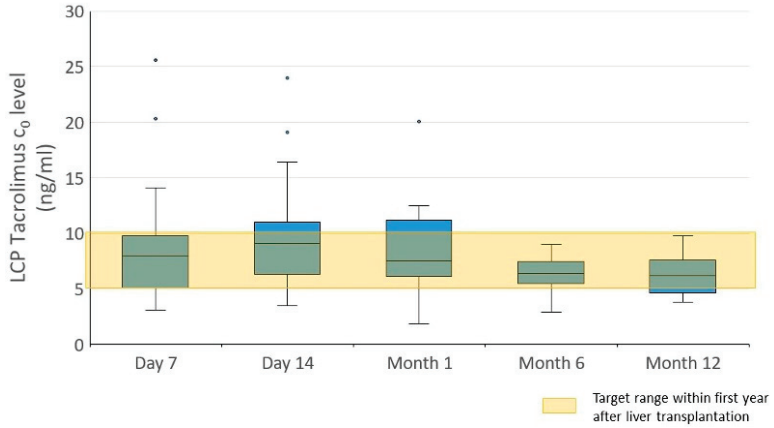


Figure 1. LCP Tacrolimus trough levels (LCP Tac_0) at different time points within the first year after liver transplantation. The trough levels were significantly higher at 1 and 2 weeks than at 12 months ($p = 0.030$ and $p = 0.042$, respectively) and at 2 weeks than at 6 months ($p = 0.038$). The target level aimed for is indicated.

Median LCP Tac_{peak} serum levels of 15.10 (7.70–23.90), 9.1 (7.60–16.20), 16.9 (8.20–21.60), 7.70 (5.90–12.10), and 7.10 ng/mL (5.90–8.80) were determined in the 1st and 2nd week and at 1, 6, and 12 months post-LT, respectively.

No difference in LCP Tac_{peak} serum levels was found between the visits ($p = 0.24$). A proportion of 14.5% of the LCP Tac trough levels were in the subtherapeutic range, 69.1% were in the therapeutic range, and 16.4% were in the supratherapeutic range, with LCP Tac trough levels measured in all patients at all time points (week 1, week 2, month 1, month 6, year 1) (Figure S1, Table S2).

3.2. Cytokine Gene Expression Response

None of the 171 samples used for gene expression measurements were excluded due to methodological or technical problems (i.e., failed RNA extraction or immune activation, respectively).

The NFAT-RGE response, including normalized copy numbers and calculated RGE%, changed significantly with time after LCP Tac intakes. The gene expression levels of IL-2, GM-CSF, and IFN-γ pre- and post-LT, at Tac's pre-dose and peak levels, as RGE%, are expressed over time in Table 1 and Figure 2a,b. Values are expressed as medians (q1,q3).

Table 1. Gene expression of IL2, GM-CSF, and IFN-γ prior to liver transplantation (pre-LT) and prior to LCP Tacrolimus intake (c_0) at different time points. Gene expression of IL2, GM-CSF, and IFN-γ after LCP Tacrolimus intake (c_{peak}) at different time points after liver transplantation. Residual gene expression (RGE%) of IL2, GM-CSF, and IFN-γ after LCP Tacrolimus intake at different time points after liver transplantation.

Normalized Copies	Time Point	Median	q1	q3
IL2 c_0	Pre-LT (cpre-LT)	3.34	2.43	6.16
	Week 1	0.76	0.21	1.53
	Week 2	0.93	0.46	1.84
	Month 1	2.16	1.33	3.86
	Month 6	3.29	2.01	4.17
	Year 1	3.58	2.52	3.73
CSF c_0	Pre-LT (cpre-LT)	3.10	1.67	4.08
	Week 1	0.62	0.16	1.22
	Week 2	0.86	0.35	1.42
	Month 1	1.53	1.00	2.35
	Month 6	2.61	1.63	3.25
	Year 1	2.73	2.05	3.39
IFN-γ c_0	Pre-LT (cpre-LT)	1.76	1.31	3.06
	Week 1	0.36	0.16	0.77
	Week 2	0.63	0.42	0.90
	Month 1	1.04	0.64	2.32
	Month 6	1.64	1.37	2.71
	Year 1	3.01	1.42	4.45
IL2 c_{peak}	Week 1	0.10	0.03	0.30
	Week 2	0.25	0.14	0.31
	Month 1	0.37	0.11	0.89
	Month 6	3.17	1.25	4.38
	Year 1	2.98	2.55	3.83
CSF c_{peak}	Week 1	0.10	0.03	0.27
	Week 2	0.15	0.14	0.40
	Month 1	0.32	0.10	0.63
	Month 6	2.14	1.22	2.67
	Year 1	2.57	2.18	3.15

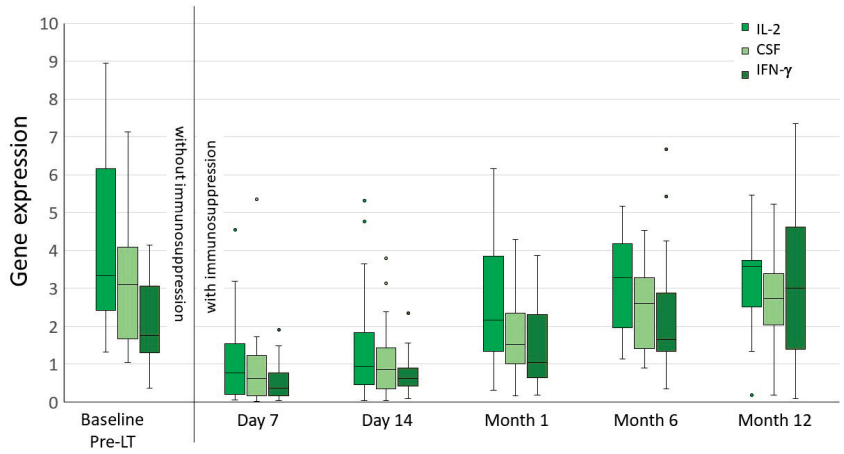
Table 1. *Cont.*

Normalized Copies	Time Point	Median	q1	q3
IFN-γ c_{peak}	Week 1	0.15	0.03	0.40
	Week 2	0.34	0.17	0.50
	Month 1	0.36	0.15	1.01
	Month 6	1.23	0.90	2.40
	Year 1	2.90	1.71	4.03
RGE% IL2	Week 1	22.07	28.50	6.03
	Week 2	25.20	35.37	13.11
	Month 1	16.63	33.36	8.73
	Month 6	81.50	112.93	40.12
	Year 1	100.05	111.65	89.54
RGE% GM-CSF	Week 1	27.38	31.79	7.36
	Week 2	28.23	41.79	15.82
	Month 1	17.75	36.96	9.87
	Month 6	75.62	101.30	39.94
	Year 1	94.35	103.59	85.14
RGE% IFN-γ	Week 1	44.31	61.23	19.65
	Week 2	54.13	62.82	38.68
	Month 1	36.92	68.86	19.18
	Month 6	83.06	99.79	46.83
	Year 1	98.97	117.55	78.67

The expression of IL-2, GM-CSF, and IFN-γ decreased from 1 week to 1 month post-LT and increased to near pre-transplant levels at 6 and 12 months post-LT.

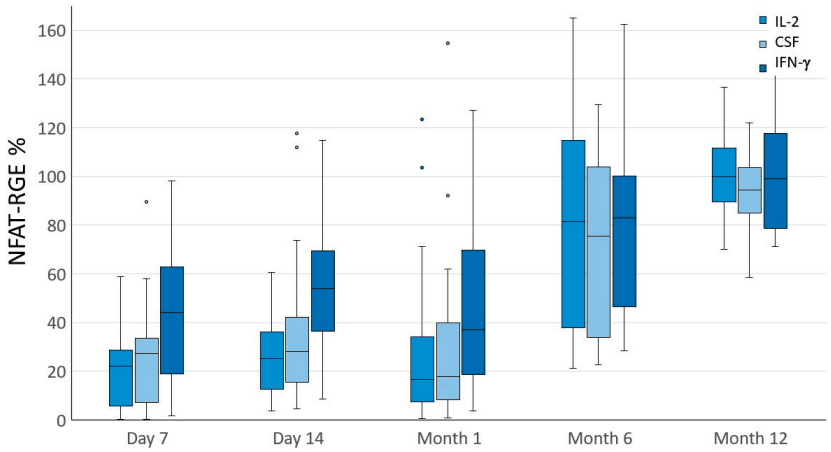
There was no correlation between LCP Tac_0 serum levels and RGE% at any study time point.

LCP Tac_{peak} serum levels and RGE% showed an overall strong inverse correlation at all time points analyzed ($\rho = -0.8$), as described in Table 2. This was also confirmed using dose-normalized LCP-Tac_{peak} concentrations adjusted to the patients' body weight (Tables S3 and S4). Figure 3 representatively displays the relationship between the LCP Tac_{peak} serum levels and RGE% detected at 1 week post-LT.



(**a**)

Figure 2. *Cont.*



(**b**)

Figure 2. (**a**) Gene expression of IL-2, GM-CSF, and IFN-γ, measured before liver transplantation (c_{pre-LT}) and after transplantation at the LCP Tacrolimus pre-dose level (c_0). The expression levels of IL2, GM-CSF, and IFN-γ decreased from week 1 to month 1 and rose again to levels that nearly reached the pre-transplant level at months 6 and 12. Values are presented as medians (q1, q3). (**b**) Gene expression response calculated as the residual expression (RGE%) of IL-2, GM-CSF and IFN-γ after LCP Tacrolimus intake. After liver transplantation, the residual expression of NFAT-regulated genes after LCP Tac intakes was calculated as $c_{peak}/c_0 \times 100$, with c_0 as the number of transcripts at the LCP Tac pre-dose level and c_{peak} as the number of transcripts at the LCP Tac peak level. The strongest suppression of NFAT-regulated genes was observed until the first month after liver transplantation, with high residual NFAT-RGE levels seen after 6 months and 1 year. Values are presented as medians (q1, q3). The circles indicate values of outliers.

Table 2. Residual gene expression (RGE%) of IL2, GM-CSF, and IFN-γ and their correlation with $LCPTac_{peak}$ serum level at different time points after liver transplantation.

Time Point	Gene	RGE% (Median)	Median TAC_{peak} Serum Level (ng/mL)	Correlation Coefficient (ρ)
Week 1	IL2	22.07		−0.753
	GM-CSF	27.38	15.1	−0.827
	IFN-γ	44.31		−0.843
Week 2	IL2	25.20		−0.520
	GM-CSF	28.23	9.1	−0.728
	IFN-γ	54.13		−0.505
Month 1	IL2	16.63		−0.803
	GM-CSF	17.75	16.9	−0.828
	IFN-γ	36.92		−0.730
Month 6	IL2	81.50		−0.808
	GM-CSF	75.62	7.7	−0.647
	IFN-γ	83.06		−0.557
Year 1	IL2	100.05		−0.320
	GM-CSF	94.35	7.1	−0.190
	IFN-γ	98.97		−0.313

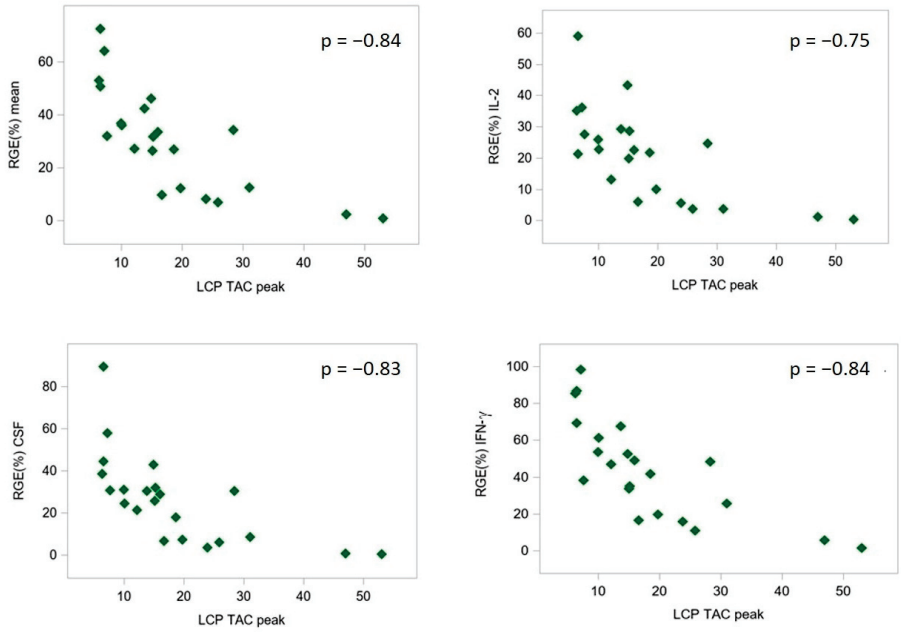


Figure 3. Relationship between LCP Tac_{peak} serum levels and representative residual expressions (RGE%) of IL-2, GM-CSF, and IFN-γ at day 7 after liver transplantation. A strong inverse correlation of the RGE% of each of the three genes with LCP Tac_{peak} serum levels was observed. The green symbols indicate the relationship between RGE% and LCP $Tacp_{eak}$ values.

3.3. Ranges of Residual Gene Expression with Respect to Clinically Significant Events

3.3.1. Infection and Rejection

An infection was observed after a median of 169 days post-LT in 61% (n = 14) of patients (Figure 4). The residual gene expression in individuals at the time of infection and in individuals without infection is shown in Table S5, and infection details are shown in Table S6. The median residual gene expression of NFAT-RGE in stable LT patients without infection 1 year post-LT was 94.25% (86.63–108.32). LT patients had 32.00% (23.30–95.10%) NFAT-RGE% at the time of their first infection post-LT (optional time point).

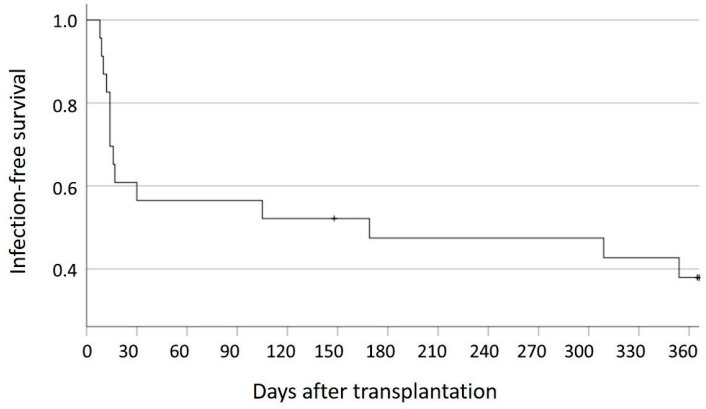


Figure 4. Infections after liver transplantation (LT) and infection-free survival. In 61% (n = 14) of patients, an infection was observed at a median of 169 days after liver transplantation. Eight patients did not experience an infection within the first year after transplantation. + One patient was lost to follow-up after 148 days.

Based on our data and the corresponding existing literature, the optimal NFAT-RGE% range was between 25 and 50% within the first 6 months post-LT (Table 1 and Figure 2b). In the optimal NFAT-RGE% range, we observed infections in four patients, while seven infections were observed in patients who did not meet the optimal NFAT-RGE% range

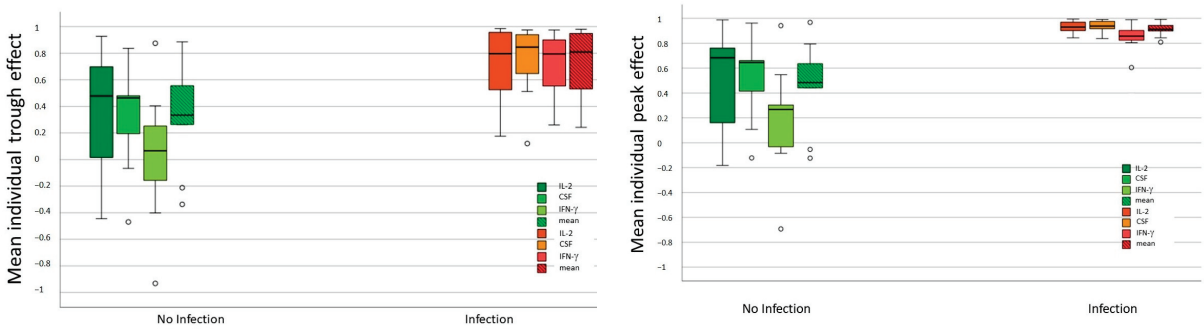
of 25–50%. The NFAT-RGE% values of three patients could not be calculated. The LCP Tacrolimus serum levels seen at the time of infection within the first year after liver transplantation are shown in Figure S2.

Only five rejections were observed, none of which occurred within the optimal NFAT RGE% range.

3.3.2. Individual Immunosuppression Described by Individual LCP Tac Trough and Peak Effects (Effect LCP Tac_0, Effect LCP Tac_{peak})

We assessed the individual effects of LCP Tac on the risk of infection. Medians of the individual trough and peak effects, pooled across the IL-2, GM-CSF, and IFN-γ levels at different time points post-LT, are shown in Table S7. The weakest effects were observed in the later stages (12 months post-LT).

The mean individual trough and peak effects of each of the three NFAT-regulated genes, pooled over all time points, are shown in Table 3 and displayed in Figure 5a,b. The trough and peak effects of the three NFAT-regulated genes were significantly higher in patients with infections than in those without. Additionally, IFN-γ showed the most significant difference of the three genes.



(**a**) (**b**)

Figure 5. Mean individual trough and peak effects of LCP Tacrolimus in patients with infection and without infection: (**a**) The mean individual trough effects of each of the three NFAT-regulated genes, pooled over all measured time points, are shown. The through effect of LCP Tac (Effect LCP Tac_0) was determined using the number of copies before LCP Tac intake (c_0) for the respective visit, adjusted to the copies measured before liver transplantation ($c_{pre\text{-}LT}$). Trough effects were significantly higher in patients with infection compared to patients without infection, with IFN-γ showing the greatest difference of the 3 genes. (**b**) The mean individual peak effects of each of the three NFAT-regulated genes, pooled over all measured time points, are shown. The peak effect of LCP Tac (Effect LCP Tac_{peak}) was determined using the number the copies measured after LCP Tac intake at its peak levels (c_{peak}) for the respective visit, adjusted to the number of copies measured before liver transplantation ($c_{pre\text{-}LT}$). The peak effects of the 3 NFAT-regulated genes were significantly higher in patients with infections than in those without infections. IFN-γ showed the greatest difference of the 3 genes. The circles indicate values of outliers.

Table 3. Individual immunosuppression (Effect LCP Tac_{peak}, Effect LCP Tac_0) of different NFAT-regulated genes pooled across all time points.

Gene	Mean Individual Trough Effect in Patients			Mean Individual Peak Effect in Patients		
	without Infection	with Infection	*p*	without Infection	with Infection	*p*
IL2	0.48 (0.02–0.70)	0.80 (0.53–0.96)	<0.023	0.68 (0.16–0.76)	0.93 (0.90–0.97)	<0.004
GM-CSF	0.46 (0.20–0.48)	0.85 (0.65–0.94)	<0.001	0.65 (0.42–0.66)	0.94 (0.92–0.98)	<0.001
IFN-γ	0.07 (−0.16–0.25)	0.79 (0.55–0.90)	<0.001	0.27 (−0.03–0.30)	0.86 (0.82–0.90)	<0.001
All 3 genes	0.33 (0.26–0.56)	0.81 (0.53–0.95)	<0.011	0.48 (0.44–0.64)	0.91 (0.90–0.94)	<0.001

4. Discussion

The present study investigates the feasibility of measuring NFAT-RGE in LT patients receiving extended-release LCP Tac during their first year post-operation, focusing on over-IS and infection.

We found a strong inverse correlation between the LCP Tac_{peak} serum level and the weight-adjusted LCP-Tac_{peak} concentration and the residual expression of NFAT-regulated genes. The significantly lower infection rate observed in patients with a high NFAT-RGE% range suggests that immunosuppression based on NFAT-RGE measurements could prevent infections associated with over-immunosuppression early after LT.

This is the first study to clearly confirm the feasibility and safety of the present diagnostic methods in patients on IS with LCP Tac. Thus, the proof of concept was realized successfully. Considering the relationship between drug levels and residual NFAT-RGE, we will be able to identify patients with excessive IS. This will allow us to reduce the LCP Tac dose while monitoring the relevant genes' expression. The main objective of further studies should be to develop a tailor-made IS regime for long-term stable LT patients based on the determination of their residual NFAT-RGE.

When reviewing the literature on NFAT-RGE after cyclosporine A, 10 studies comprising 702 patients after kidney transplantation (KT) [9,12–20] and 5 studies containing 153 patients after LT [21–25] were investigated. Of these, two studies included pediatric patients (KT, n = 1; LT, n = 1) and another two studies, comprising 79 heart transplant patients, were reviewed [9,26]. We have found that most of these studies were conducted in patients with long-term stability. There is only one de novo study on the impact of NFAT-RGE in 80 patients after KT. While most trials were prospective, observational, or cross-sectional, only one prospective randomized controlled trial (RCT) was found. In another study, NFAT-RGE and the monitoring of CNI trough levels were compared in 55 stable patients after KT [13]. Most studies have shown an association between high NFAT-RGE levels and rejection episodes after LT, whereas low NFAT-RGE levels have been associated with increased infection rates (Table 4).

Table 4. Clinical studies on the quantitative analysis of NFAT-regulated gene expression in the peripheral blood of solid organ recipients on Cyclosporine A therapy. Clinical studies on the quantitative analysis of NFAT-regulated gene expression in the peripheral blood of solid organ recipients on Tacrolimus therapy.

Reference	Study Design	Patient Cohort	Main Result
Sommerer et al. [12]	Prospective observational	Kidney (n = 176)	Low NFAT-RGE proven as risk factor for BK viremia.
Sommerer et al. [14]	Prospective observational	De novo kidney (n = 80)	Low NFAT-RGE associated with infectious complications and high NFAT-RGE associated with risk of rejection.
Sommerer et al. [15]	Prospective observational	Senior kidney (n = 36)	Low NFAT-RGE associated with opportunistic infections.
Sommerer et al. [16]	Prospective observational	Kidney (n = 133)	Low NFAT-RGE is associated with infections and malignancy.
Giese et al. [9]	Cross-sectional	Kidney (n = 25), liver (n = 14), heart (n = 26)	Pilot study to assess the property of the assay; PK–PD analysis. NFAT-RGE as marker for individual responsiveness.
Sommerer et al. [17]	Prospective observational case–control	Kidney (n = 20), matched controls (n = 20)	Tapering of cyclosporin A, monitored by RGE, improved allograft function and reduced cardiovascular risk factors.

Table 4. *Cont.*

Reference	Study Design	Patient Cohort	Main Result
Sommerer et al. [18]	Prospective observational	Senior kidney (n = 55)	Low NFAT-RGE associated with nonmelanoma skin cancer.
Dannewitz et al. [19]	Prospective observational	Kidney (n = 144)	Low NFAT-RGE associated with cyclosporine A in saliva and gingival hyperplasia.
Sommerer et al. [13]	Prospective interventional randomized-controlled	Kidney (n = 55)	NFAT-RGE leads to an improved cardiovascular risk profile and improves long-term renal allograft function.
Billing et al. [20]	Cross-sectional observational	Pediatric kidney (n = 45)	Low NFAT-RGE is associated with infection episodes.
Billing et al. [21]	Prospective observational	Pediatric liver (n = 33)	Low NFAT-RGE in recurrent infection.
Zahn et al. [22]	Cross-sectional	Liver (n = 45)	Applicability of NFAT-RGE monitoring in liver transplantation confirmed.
Herden et al. [23]	Prospective observational	Liver (n = 20 long-term, n = 20 de novo)	NFAT-RGE correlated with infection parameters.
Steinebrunner et al. [24]	Prospective observational	Liver (n = 13)	High NFAT-RGE in acute rejection.
Steinebrunner et al. [25]	Cross-sectional	Liver (n = 10)	Low NFAT-RGE in CMV infection.
Giese et al. [9]	Cross-sectional	Kidney (n = 25), liver (n = 14), heart (n = 26)	Pilot study to assess the property of the assay; PK–PD analysis. NFAT-RGE as marker for individual responsiveness.
Konstandin et al. [26]	Prospective observational	Heart (n = 53)	Low NFAT-RGE is associated with recurrent infections.
Sommerer et al. [27]	Cross-sectional	Kidney (n = 262)	PK–PD correlation, low NFAT-RGE is associ-ated with recurrent infections and high NFAT-RGE with rejection.
Sommerer et al. [28]	Prospective observational	Kidney (n = 73)	Low NFAT-RGE is associated with CMV viremia.
Sommerer et al. [29]	Prospective observational	Kidney (n = 23)	Low NFAT-RGE as risk factor for BKV viremia.
Keller et al. [11]	Prospective observational	Kidney (n = 10)	Pharmacodynamics of Tac described in dependence of pharmakokinetics.
Bremer et al. [30]	Prospective	Kidney (n = 29)	Potential of NFAT-RGE as a tool for the pharmacodynamic monitoring of Tac therapy in the early phase post-Tx, especially in the context of over-immunosuppression and viraemia confirmed.

Table 4. *Cont.*

Reference	Study Design	Patient Cohort	Main Result
Sommerer et al. [31]	Prospective observational	De novo kidney (n = 60)	NFAT-RGE was confirmed as a potential noninvasive early predictive biomarker in the immediate post-transplant period to detect patients at risk of acute rejection and infectious complications in Tac-treated renal allograft recipients.
Webber et al. [32]	Randomized Controlled Pilot Trial	Kidney (n = 40)	Quantitative analysis of nuclear factor of activated T-regulated gene expression may serve as a reliable assay to lower tac dosing.
Billing et al. [21]	Prospective observational	Pediatric liver (n = 33)	Low NFAT-RGE in recurrent infection.
Zahn et al. [22]	Cross-sectional	Liver (n = 45)	Applicability of NFAT-RGE monitoring in liver transplantation confirmed.
Steinebrunner et al. [24]	Prospective observational	Liver (n = 13)	High NFAT-RGE in acute rejection.
Steinebrunner et al. [25]	Cross-sectional	Liver (n = 10)	Low NFAT-RGE in CMV infection.
Millán et al. [33]	Prospective observational	Liver (n = 56)	Sequential post-transplantation NFAT-RGE monitoring combined with intralymphocytary IL-2 and IFN-γ may be key predictive and diagnostic biomarkers of the risk of TCMAR and SCR and better guide CNi therapy in LT patients.

Few studies have investigated NFAT-RGE after twice-daily Tacrolimus (Tac) treatments. We found four studies, for a total of 428 Tac-treated patients, where long-term stable patients were investigated after KT [11,27–29], two studies including de novo KT patients [30,31], and one RCT. The RCT compared NFAT-RGE measurements with CNI trough level monitoring in 40 stable patients after KT [32]. We found four further studies in which 130 patients given Tac were monitored after LT [21,22,24,25,33] (Table 4).

A study by Bremer et al. [30] was the only one to report NFAT-RGE after once-daily Tac treatment. However, 19 of the 29 patients had been switched from the regular twice-daily formulation of Tac (Prograf®) to a once-daily formulation (Advagraf®) at 1 year post-KT.

According to the literature published in the field, NFAT-RGE measurements might be an optimized way of monitoring and individualizing the level of IS achieved with CNIs. An NFAT-RGE analysis is relatively specific for Tac exposure [9]. As outlined above, most published studies have focused on long-term stable patients, mainly after KT, and two randomized controlled trials on KT patients have been published to date [13,32]. Only 19 cases of once-daily Tac administration in KT patients and NFAT-RGE monitoring 1 year after KT have been reported to date [30].

In our cohort, patients showed the strongest suppression of NFAT-RGE when their residual NFAT-RGE was equivalent to low copy numbers of the three target genes early post-LT, and these numbers increased again after 6 and 12 months. This is in accordance with the published literature. Bremer et al. reported higher residual NFAT-RGEs observed at 1 year on once-daily Tac versus 1 week post-KT with twice-daily Tac, which was suspected to not be explained by the switch in formulations. However, the authors emphasized the

need for further investigation of NFAT-RGE during treatment with once-daily formulations in view of the increasing use of extended-release formulations [30].

A descriptive analysis of our data confirmed that although patients exhibited an LCP Tac trough level within the targeted therapeutic window, a low NFAT-RGE% serum level could result in a higher risk of infection. Based on our data and the corresponding existing literature, the optimal NFAT-RGE% range during the first 6 months after LT is between 25 and 50% [21,22,24,25,33]. Within that range, 43% fewer infections were recorded and no rejections were observed. Outside the optimal range, there were rejections in 19% of the patients. We also assumed a lower tumor recurrence rate, which is of the utmost importance in the face of almost 50% of the patients in our cohort having a malignant disease (hepatocellular carcinoma) before transplantation. An observation period longer than 1 year would be recommended for future studies.

The strengths of the present study are in its prospective design, following patients post-LT, with precisely predefined time points for control visits and a uniform immunosuppressive regimen in all patients. For the first time, we were able to take the immune status of each patient before IS into account, determining the individual peak and trough effects of LCP Tac by referring to each patient's NFAT status pre-LT.

Concerning the individual immunosuppressive status of all patients before transplantation, the individual trough and peak effects of LCP Tac at defined time points post-LT differed significantly between patients with and without infection. In contrast, there was no difference in LCP Tac's trough and peak serum levels. Although only 23 patients were included in our trial, there were significant results within our study, and the primary endpoint was met.

Some limitations of the present study should be kept in mind. As a single-center study, the number of patients included were limited. Therefore, further investigations of different infection types were not possible. Due to the occurrence of heterogeneous infections of unequal severity, the results reported in this proof of concept study have to be interpreted with caution.

Further studies should focus on separate analyses of different types of infections, such as opportunistic infections. Also, a possible relationship between individual LCP-Tac serum levels within different therapeutic ranges and the occurrence of infections needs to be examined in studies with a larger sample size.

In summary, a strong inverse correlation between the LCP Tac_{peak} serum level and the residual expression of NFAT-regulated genes was found, indicating that the quantitative analysis of these genes enables reliable biological IS at the target cell level in de novo LT recipients. There was a difference between NFAT-RGE% in patients with and without infection, which was significant when considering the individual status of IS in each patient pre-LT. In the optimal NFAT-RGE% range, the rates of infection and rejection decreased distinctly, by 43 and 100%, respectively.

This is the first study to clearly confirm both the feasibility and safety of the present diagnostic methods in patients undergoing IS with LCP Tac, and the proof of concept was successfully realized. Considering the relationship between the drug's levels and residual NFAT-RGE, we will be able to identify patients with excessive IS. This will allow us to reduce the LCP Tac dose while monitoring the relevant gene expression. The main objective of further studies should be to develop a tailor-made IS for long-term stable LT patients based on determining their residual NFAT-RGE.

Supplementary Materials: The following supporting information can be downloaded at: https://www.mdpi.com/article/10.3390/pharmaceutics16101317/s1. Table S1: Patient characteristics. Table S2: Results of LCP Tacrolimus trough level measurements, categorized by different therapeutic ranges. Table S3: Residual gene expression (RGE%) of IL2, GM-CSF, and IFN-γ and their correlation with LCP Tac_{peak} concentration, adjusted to patient's body weight at different time points after liver transplantation. Table S4: LCP Tac_0 and LCP Tac_{peak} concentration, adjusted to patient's body weight at different time points after liver transplantation. Table S5: Descriptive statistics of RGE IL-2, RGE GM-CSF, RGE IFN-γ, and RGE mean at the time of infection and without infection. Table S6:

Infection details. Table S7: Individual immunosuppression (Effect LCP Tac_{peak}, Effect LCP Tac_0), pooled across IL-2, GM-CSF, and IFN-γ, after liver transplantation. Figure S1: LCP Tacrolimus trough levels, categorized by different therapeutic ranges. Figure S2: LCP Tacrolimus serum levels at the time of infection within the first year after liver transplantation.

Author Contributions: Conceptualization—J.K. and P.S. (Peter Schemmer); methodology—E.M.M.; investigation—E.M.M.; data curation—J.K. and E.M.M.; writing—original draft; J.K. and E.M.M.; writing—review and editing, P.S. (Peter Schemmer) and P.S. (Peter Schlenke); visualization—J.K.; project administration—J.K.; funding acquisition—P.S. (Peter Schemmer). All authors have read and agreed to the published version of the manuscript.

Funding: This work was funded by Chiesi (Chiesi Farmaceutici S. p. A. Via Palermo 26/A 43122 Parma, Italy) (project-related support).

Institutional Review Board Statement: This observational study was conducted in accordance with the Declaration of Helsinki and Istanbul and was approved by the appropriate ethics and institutional review committees (EK-Nr. 30-444 ex 17/18, NCT03315858, EudraCT number 2018–001290–24 approval date: 11 December 2018). Written informed consent was obtained from all patients.

Informed Consent Statement: Written informed consent has been obtained from the patient(s) to publish this paper.

Data Availability Statement: All of the analyzed data are contained within the article or Supplementary Material. The raw data on gene expression are available on request from the corresponding author.

Acknowledgments: Anja Stoisser, Marie-Therese Melcher, and Lisa Rohrhofer are also acknowledged for their technical assistance. Michael Treiber and Guenther Koellinger are acknowledged for their assistance in data management.

Conflicts of Interest: The authors declare no conflicts of interest. The funders had no role in the design of the study; in the collection, analyses, or interpretation of data; in the writing of the manuscript; or in the decision to publish the results.

References

1. Jaksch, P.; Görzer, I.; Puchhammer-Stöckl, E.; Bond, G. Integrated Immunologic Monitoring in Solid Organ Transplantation: The Road Toward Torque Teno Virus-guided Immunosuppression. *Transplantation* **2022**, *106*, 1940–1951. [CrossRef]
2. Lepore, M.; Crespo, E.; Melilli, E.; Cruzado, J.M.; Torija, A.; Grinyó, J.M.; Bestard, O. Functional immune monitoring of BK Virus and donor-specific T-cell effector immune responses to guide treatment decision-making after kidney transplantation; an illustrative case report and literature review. *Transpl. Infect. Dis.* **2021**, *23*, e13495. [CrossRef]
3. Kel, A.; Kel-Margoulis, O.; Babenko, V.; Wingender, E. Recognition of NFATp/AP-1 composite elements within genes induced upon the activation of immune cells. *J. Mol. Biol.* **1999**, *288*, 353–376. [CrossRef]
4. Giese, T. Development of quantitative RT-PCR tests for the expression of cytokine genes on the LightCycler. In *Rapid Cycle Real-Time PCR: Methods and Applications*; Meuer, S., Wittwer, C., Nakagawara, K., Eds.; Springer: Berlin/Heidelberg, Germany; New York, NY, USA, 2001; pp. 251–261.
5. Sommerer, C.; Giese, T.; Meuer, S.; Zeier, M. Pharmacodynamic monitoring of calcineurin inhibitor therapy: Is there a clinical benefit? *Nephrol. Dial. Transplant.* **2009**, *24*, 21–27. [CrossRef]
6. von Einsiedel, J.; Thölking, G.; Wilms, C.; Vorona, E.; Bokemeyer, A.; Schmidt, H.H.; Kabar, I.; Hüsing-Kabar, A. Conversion from Standard-Release Tacrolimus to MeltDose® Tacrolimus (LCPT) Improves Renal Function after Liver Transplantation. *J. Clin. Med.* **2020**, *9*, 1654. [CrossRef]
7. Bartlett, F.E.; Carthon, C.E.; Hagopian, J.C.; Horwedel, T.A.; January, S.E.; Malone, A. Tacrolimus Concentration-to-Dose Ratios in Kidney Transplant Recipients and Relationship to Clinical Outcomes. *Pharmacotherapy* **2019**, *39*, 827–836, Erratum in *Pharmacotherapy* **2020**, *40*, 719. [CrossRef]
8. European Association for the Study of the Liver. EASL clinical practice guidelines: Liver transplantation. *J. Hepatol.* **2016**, *64*, 433–485. [CrossRef]
9. Giese, T.; Zeier, M.; Schemmer, P.; Uhl, W.; Schoels, M.; Dengler, T.; Buechler, M.; Meuer, S. Monitoring of NFAT-regulated gene expression in the peripheral blood of allograft recipients: A novel perspective toward individually optimized drug doses of cyclosporine A. *Transplantation* **2004**, *77*, 339. [CrossRef]
10. Tremblay, S.; Nigro, V.; Weinberg, J.; Woodle, E.S.; Alloway, R.R. A Steady-State Head-to-Head Pharmacokinetic Comparison of All FK-506 (Tacrolimus) Formulations (ASTCOFF): An Open-Label, Prospective, Randomized, Two-Arm, Three-Period Crossover Study. *Am. J. Transplant.* **2017**, *17*, 432–442. [CrossRef]

11. Keller, F.; Sommerer, C.; Giese, T.; Zeier, M.; Schröppel, B. Correlation between pharmacokinetics of tacrolimus and pharmacodynamics on NFAT-regulated gene expression in stable kidney transplant recipients. *Clin. Nephrol.* **2017**, *87*, 93–99. [CrossRef]
12. Sommerer, C.; Beimler, J.; Meuer, S.; Giese, T.; Zeier, M. Monitoring of NFAT-regulated gene-expression for safe tapering of CNI immunosuppression in BK virus positive renal transplant patients. *J. Am. Soc. Nephrol.* **2007**, *18*, 1000.
13. Sommerer, C.; Brocke, J.; Bruckner, T.; Schaier, M.; Morath, C.; Meuer, S.; Zeier, M.; Giese, T. Improved Pulse Wave Velocity and Renal Function in Individualized Calcineurin Inhibitor Treatment by Immunomonitoring: The Randomized Controlled Calcineurin Inhibitor-Sparing Trial. *Transplantation* **2018**, *102*, 510–520. [CrossRef]
14. Sommerer, C.; Zeier, M.; Meuer, S.; Giese, T. Monitoring of calcineurin inhibitors by NFAT-regulated gene expression in de novo renal allograft recipients. *Clin. Nephrol.* **2015**, *84*, 165–172. [CrossRef]
15. Sommerer, C.; Schnitzler, P.; Meuer, S.; Zeier, M.; Giese, T. Pharmacodynamic monitoring of cyclosporin A reveals risk of opportunistic infections and malignancies in renal transplant recipients 65 years and older. *Ther. Drug Monit.* **2011**, *33*, 694–698. [CrossRef]
16. Sommerer, C.; Konstandin, M.; Dengler, T.; Schmidt, J.; Meuer, S.; Zeier, M.; Giese, T. Pharmacodynamic monitoring of cyclosporine a in renal allograft recipients shows a quantitative relationship between immunosuppression and the occurrence of recurrent infections and malignancies. *Transplantation* **2006**, *82*, 1280. [CrossRef]
17. Sommerer, C.; Giese, T.; Schmidt, J.; Meuer, S.; Zeier, M. Ciclosporin A tapering monitored by NFAT-regulated gene expression: A new concept of individual immunosuppression. *Transplantation* **2008**, *85*, 15. [CrossRef]
18. Sommerer, C.; Hartschuh, W.; Enk, A.; Meuer, S.; Zeier, M.; Giese, T. Pharmacodynamic immune monitoring of NFAT-regulated genes predicts skin cancer in elderly long-term renal transplant recipients. *Clin. Transplant.* **2008**, *22*, 549. [CrossRef]
19. Dannewitz, B.; Kruck, E.M.; Staehle, H.J.; Eickholz, P.; Giese, T.; Meuer, S.; Kaever, V.; Zeier, M.; Sommerer, C. Cyclosporine-induced gingivalover growth correlates with NFAT-regulated gene expression: A pilot study. *J. Clin. Periodontol.* **2011**, *38*, 984–991. [CrossRef]
20. Billing, H.; Giese, T.; Sommerer, C.; Zeier, M.; Feneberg, R.; Meuer, S.; Tönshoff, B. Pharmacodynamic monitoring of cyclosporine A by NFAT-regulated gene expression and the relationship with infectious complications in pediatric renal transplant recipients. *Pediatr. Transplant.* **2010**, *14*, 844–851. [CrossRef]
21. Billing, H.; Breil, T.; Schmidt, J.; Tönshoff, B.; Schmitt, C.; Giese, T.; Engelmann, G. Pharmacodynamic monitoring by residual NFAT-regulated gene expression in stable pediatric liver transplant recipients. *Pediatr. Transplant.* **2012**, *16*, 187–194, Erratum in *Pediatr. Transplant.* **2012**, *16*, 304. [CrossRef]
22. Zahn, A.; Schott, N.; Hinz, U.; Stremmel, W.; Schmidt, J.; Ganten, T.; Gotthardt, D.; Meuer, S.; Zeier, M.; Giese, T.; et al. Immunomonitoring of nuclear factor of activated T cells-regulated gene expression: The first clinical trial in liver allograft recipients. *Liver Transplant.* **2011**, *17*, 466–473. [CrossRef]
23. Herden, U.; Kromminga, A.; Hagel, C.; Hartleb, J.; Nashan, B.M.F.F.; Sterneck, M.; Fischer, L. Monitoring of nuclear factor of activated T-cell regulated gene expression in de novo and long-term liver transplant recipients treated with cyclosporine A. *Ther. Drug Monit.* **2011**, *33*, 185–191. [CrossRef]
24. Zahn, A.; Steinebrunner, N.; Sandig, C.; Sommerer, C.; Hinz, U.; Giese, T.; Stremmel, W. Pharmacodynamic monitoring of nuclear factor of activated T-cell regulated gene expression in liver allograft recipients on immunosuppressive therapy with calcineurin inhibitor in the course of time and correlation with acute rejection episodes—A prospective study. *Ann. Transplant.* **2014**, *19*, 32–40.
25. Steinebrunner, N.; Sandig, C.; Sommerer, C.; Hinz, U.; Giese, T.; Stremmel, W.; Zahn, A. Reduced residual gene expression of nuclear factor of activated T-cells-regulated genes correlates with the risk of cytomegalovirus infection after liver transplantation. *Transpl. Infect. Dis.* **2014**, *16*, 379–386. [CrossRef]
26. Konstandin, M.H.; Sommerer, C.; Doesch, A.; Zeier, M.; Meuer, S.C.; Katus, H.A.; Dengler, T.J.; Giese, T. Pharmacodynamic cyclosporine A-monitoring: Relation of gene expression in lymphocytes to cyclosporine blood levels in cardiac allograft recipients. *Transpl. Int.* **2007**, *20*, 1036. [CrossRef]
27. Sommerer, C.; Zeier, M.; Meuer, S.; Giese, T. Individualized monitoring of nuclear factor of activated T-cells-regulated gene expression in FK506-treated kidney transplant recipients. *Transplantation* **2010**, *89*, 1417–1423. [CrossRef]
28. Sommerer, C.; Zeier, M.; Czock, D.; Schnitzler, P.; Meuer, S.; Giese, T. Pharmacodnamic disparities in tacrolimus treated patients developing CMV viremia. *Ther. Drug Monit.* **2011**, *33*, 373–379. [CrossRef]
29. Sommerer, C.; Baghdadi, J.; Theissing, T.; Zeier, M.; Giese, T. Detection of patients on increased risk of BKV replication by NFAT-regulated gene expression. *Transpl. Int.* **2015**, *28*, 19.
30. Bremer, S.; Vethe, N.T.; Skauby, M.; Kasbo, M.; Johansson, E.D.; Midtvedt, K.; Bergan, S. NFAT-regulated cytokine gene expression during tacrolimus therapy early after renal transplantation. *Br. J. Clin. Pharmacol.* **2017**, *83*, 2494–2502. [CrossRef]
31. Sommerer, C.; Brunet, M.; Budde, K.; Millán, O.; Perich, L.G.; Glander, P.; Meuer, S.; Zeier, M.; Giese, T. Monitoring of gene expression in tacrolimus-treated de novo renal allograft recipients facilitates individualized immunosuppression: Results of the IMAGEN study. *Br. J. Clin. Pharmacol.* **2021**, *87*, 3851–3862. [CrossRef]

32. Webber, A.B.; Tatapudi, V.; Maw, T.T.; Peralta, C.; Leung, J.C.; Vincenti, F. Nuclear Factor of Activated T Cell-regulated Cytokine Gene Expression for Adjustment of Tacrolimus in Kidney Transplant Recipients: A Randomized Controlled Pilot Trial. *Transplant. Direct.* **2018**, *4*, e369. [CrossRef]
33. Millán, O.; Ruiz, P.; Fortuna, V.; Navasa, M.; Brunet, M. Nuclear factor of activated T cells as potential pharmacodynamic biomarker for the risk of acute and subclinical rejection in de novo liver recipients. *Liver Int.* **2020**, *40*, 931–946. [CrossRef]

Disclaimer/Publisher's Note: The statements, opinions and data contained in all publications are solely those of the individual author(s) and contributor(s) and not of MDPI and/or the editor(s). MDPI and/or the editor(s) disclaim responsibility for any injury to people or property resulting from any ideas, methods, instructions or products referred to in the content.

pharmaceutics

MDPI

Article

Development of a Web Application for Simulating Plasma Drug Concentrations in Patients with Zolpidem Intoxication

Hwa Jun Cha [1,2], Sungpil Han [1,2], Kwan Cheol Pak [3] and Hyungsub Kim [4,*]

[1] Department of Pharmacology, College of Medicine, The Catholic University of Korea, Seoul 06591, Republic of Korea; clex9604@catholic.ac.kr (H.J.C.); shan@catholic.ac.kr (S.H.)
[2] PIPET (Pharmacometrics Institute for Practical Education and Training), College of Medicine, The Catholic University of Korea, Seoul 06591, Republic of Korea
[3] Yuhan Corporation, Seoul 06927, Republic of Korea; kcpak4175@yuhan.co.kr
[4] Department of Paramedicine, College of Health Sciences, Eulji University, Seongnam 13135, Republic of Korea
* Correspondence: hkim@eulji.ac.kr; Tel.: +82-31-740-7130; Fax: +82-31-740-7357

Abstract: Zolpidem is a widely prescribed hypnotic Z-drug used to treat short-term insomnia. However, a growing number of individuals intentionally overdose on these drugs. This study aimed to develop a predictive tool for physicians to assess patients with zolpidem overdose. A population pharmacokinetic (PK) model was established using digitized data obtained from twenty-three healthy volunteers after a single oral administration of zolpidem. Based on the final PK model, a web application was developed using open-source R packages such as rxode2, nonmem2rx, and shiny. The final model was a one-compartment model with first-order absorption and elimination with PK parameters, including clearance (CL, 16.9 L/h), absorption rate constant (K_a, 5.41 h^{-1}), volume of distribution (V_d, 61.7 L), and lag time (ALAG, 0.394 h). Using the established population PK model in the current study, we developed a web application that enables users to simulate plasma zolpidem concentrations and visualize their profiles. This user-friendly web application may provide essential clinical information to physicians, ultimately helping in the management of patients with zolpidem intoxication.

Keywords: zolpidem; drug intoxication; pharmacokinetics; simulator; web application

1. Introduction

Insomnia is conceptualized to be hyperarousal at night caused by the inability to switch off arousal-related circuits, which may be a risk factor for various psychiatric disorders such as depression, anxiety, and substance use disorders [1]. The estimated prevalence of insomnia is over 10% of the adult population, and patients with insomnia complain of difficulty with sleep onset, sleep maintenance, or early awakenings. Several factors have been related to insomnia, including abnormal glucose metabolism, increased activation of the autonomic nervous system, decreased GABA (gamma-aminobutyric acid) levels, and reduced melatonin secretion [2,3]. To treat insomnia pharmacologically, several positive allosteric modulators of $GABA_A$ receptors, such as benzodiazepines (triazolam, estazolam, temazepam, quazepam, and flurazepam) and Z-drugs (zaleplon, zolpidem, and zopiclone) were approved and widely used [1,4]. However, because of withdrawal effects, tolerance, and rebound insomnia from benzodiazepines, Z-drugs are prescribed as a first-line hypnotic agent. Among the Z-drugs, approximately 3.8 million adults are prescribed zolpidem annually in the United States, and zolpidem has been ranked first in the global market share for more than 10 years [5–7]. Due to this widespread use, a variety of formulations are available, including an oral spray and sublingual tablets. Different from the benzodiazepines, zolpidem binds selectively to alpha subunits of benzodiazepine-sensitive $GABA_A$ receptors [1]. Pharmacokinetically, zolpidem (*N*, *N*-6-trimethyl-2-[4-methylphenyl] imidazo [1,2-α] pyridine-3-acetamide hemitartrate) has a relatively short

half-life of 1.5–2.5 h after a single oral dosing and it is predominantly metabolized to inactive metabolites by CYP3A4 isoform in the liver [8,9]. The bioavailability is 70% with plasma peak within 2 h. Zolpidem is associated with several adverse effects affecting more than 1% of individuals, such as central and peripheral system depressant effects (drowsiness, dizziness, headache, ataxia, and euphoria), nausea, vomiting, myalgia, or diplopia. In rare instances, more severe complications such as hallucination, abnormal thinking, or respiratory depression can occur. The recommended initial dose is 5 mg or 10 mg of immediate-release formulation for men before bedtime. Women, the elderly, and patients with decreased liver function receive the lower dose of 5 mg [10,11]. In post-marketing reports of overdose with zolpidem alone or in combination with CNS-depressant agents, increased risks of consciousness ranging from drowsiness to coma and fatal results have been reported [10,12]. In terms of clinical toxicology, the therapeutic range of plasma zolpidem concentration is 80–200 ng/mL, and the toxic, comatose, and fatal thresholds are over 500, 1500, and 4000 ng/mL, respectively [13]. In cases of zolpidem overdose, treatment typically involves gastric lavage, and activated charcoal administration may be considered in the early stages of overdose to minimize further absorption of zolpidem, as well as supportive care. In severe cases, flumazenil, a benzodiazepine receptor antagonist, may be used to reverse the sedative effects of zolpidem.

Suicide is a serious social and health problem, and South Korea's suicide rate is the highest among the OECD countries [14]. Among suicide methods in South Korea, acute poisoning is the most common, and the primary causative substances frequently involved in drug intoxication are benzodiazepines, zolpidem, and antipsychotics [15,16]. From 2014 to 2016, the National Forensic Service found that drugs were the most common causative substances among 699 cases of suspected poisoning in Seoul and its metropolitan area, 142 of which involved a combination of two or more drugs, and zolpidem was detected most frequently in the Republic of Korea [17]. Acute drug intoxication, especially sedation- and sleep-inducing drugs, is the most common reason for emergency room (ER) visits due to drug overdose-related suicide attempts. Patients who visit the ER due to drug intoxication often lose consciousness and experience life-threatening complications, such as respiratory depression. Therefore, it is difficult to assess and treat patients, because it is difficult to confirm whether the drug has caused poisoning, even if poisoning is suspected. Moreover, the blood concentration of a specific drug cannot be measured quickly in any medical institution.

Pharmacometrics is a field that contributes to drug development by minimizing errors in initial dose determination and safety prediction through population pharmacokinetic (PK) modeling by non-linear mixed-effect modeling (NONMEM) using early clinical trial data [18]. NONMEM is software that explains observed data through the model by addressing population means and interindividual variations [19]. Through the mean and interindividual variation of the parameters estimated in the model, each individual's observed data are described relative to the population means, accounting for differences between individuals. By expanding these scientific advances in emergency medicine, we aimed to develop a new tool to estimate the blood concentration of zolpidem, a frequently prescribed sleep drug, in patients with acute zolpidem intoxication, ultimately helping to quickly assess and treat patients in the ER. In the present study, we attempted to establish a population PK model using digitized data from South Korean volunteers and developed a web application to predict the plasma concentration of zolpidem in patients with acute intoxication.

2. Materials and Methods

2.1. Study Design and Data

An open-label, one-period, parallel-group, single-dose study was conducted to investigate the pharmacokinetic profile of 10 mg zolpidem (film-coated tablet, immediate-release formulation) in 30 healthy Korean volunteers (15 subjects for each sex) registered with the Clinical Research Information Service (KCT0003934; date of registration:

28 August 2018) [20]. Blood samples for PK analysis were collected using K_2–EDTA tubes at the following time points: pre-dose (0 h) and post-dose at 0.25, 0.5, 0.75, 1.0, 1.5, 2, 3, 4, 6, 8, and 12 h. Using WebPlot Digitizer, we extracted concentration data from a graph of individual plasma profiles for population PK modeling [21,22]. After data extraction, a non-compartment analysis (NCA) was conducted to compare the digitized dataset against the original PK data using the R NonCompart package (version 0.7.0) [23,24]. NCA parameters such as C_{max}, area under the curve (AUC), clearance (CL/F), slope of the elimination phase (lambda z), terminal half-life, volume of distribution (V_d/F), and T_{max} were compared, and AUC was calculated using the linear-up and log-down method.

2.2. Population PK Model

Population PK analysis was performed using non-linear mixed-effects modeling (NONMEM software, version 7.5.0 with a subroutine ADVAN14; ICON Development Solutions, Ellicott City, MD, USA) [25]. One-, two-, and transit-compartment models with first- or zero-order absorption kinetics, including absorption lag time, were tested. Population PK parameters, interindividual variability, and residual variability were estimated using the first-order conditional estimation with interaction (FOCE-I) method. The interindividual variability of each parameter was described using a lognormal distribution.

$$P_i = \theta_{pop} \cdot \exp(\eta_i)$$

P_i is the individual parameter, θ_{pop} is the typical parameter value for the population, and η_i represents the interindividual variability, which follows a normal distribution with a mean of zero and variance of ω^2. The residual variability was modeled as a proportional error.

$$DV_{ij} = DV_{ipred.ij} \cdot (1+ \varepsilon_{prop.ij})$$

DV_{ij} is the jth measured concentration in ith individual, $DV_{ipred.ij}$ is the jth model prediction in ith individual, and $\varepsilon_{prop.ij}$ represents the proportional residual variability which follows a normal distribution with a mean of zero and variance of σ^2. Covariate analysis was performed, particularly in terms of sex, based on a previous report [26].

Graphical assessments and statistical analyses of each model were performed to evaluate the significance of the model improvements. Differences in the objective function value between the two fits of the hierarchical models were approximately chi-squared distributed with degrees of freedom equal to the difference in the number of parameters between the models. A significance level of 0.05 was considered for the likelihood ratio test during model building, meaning that a drop of >3.84 in the objective function value after adding a single model parameter was deemed a statistically significant improvement in the model. Additionally, basic goodness-of-fit plots, including observed data versus population prediction, observed data versus individual prediction, conditional weighted residuals (CWRES) versus population prediction, and CWRES versus time after the dose, were assessed.

2.3. Model Evaluation

The visual predictive check (VPC) and bootstrap methods were used to evaluate the final PK model. One thousand bootstrap datasets were generated by resampling the participants from the original dataset, and the median and 95% confidence intervals of the parameters were calculated to compare the parameter estimates of the final model. Using the 1000 simulated datasets obtained from the Monte Carlo simulation. R software version 4.3.3 (R Foundation for Statistical Computing, Vienna, Austria) was used for data preparation, graphical diagnosis, and statistical analyses [27].

2.4. RxODE Conversion and Simulation

After the final population PK modeling, two open-source R packages were utilized for conducting simulations in the R environment. These included nonmem2rx (ver-

sion 0.1.3) [28], and rxode2 (version 2.1.0) [29,30]. The role of the nonmem2rx package is to convert the NONMEM control stream into RxODE syntax. In this process, the package reads NONMEM files such as the output file and dataset and conducts the comparative analysis to show how well the conversion was conducted by comparing the population prediction (PRED), individual prediction (IPRED), and individual weighted residuals (IWRES) of NONMEM and converted RxODE model. The rxode2 package was used to perform and manage the simulation within R. It facilitates fast and efficient simulations of ordinary differential equation-based models in various user-defined dosing regimens.

2.5. Development of A Web-Application

The web application was developed using an open-source shiny R package that provides the framework of user-interactive web applications [31]. Users can define various dosing regimens for zolpidem, and the application then simulates and predicts the drug's plasma concentration profile and pharmacokinetic parameters. The user interface is designed to be user-friendly, allowing for easy adjustments of input values and facilitating the straightforward visualization of results, making it clear to see the impact of different dosing regimens on zolpidem's PK [32].

3. Results

3.1. Pharmacokinetic Analysis

Data from seven subjects were excluded from the Ministry of Food and Drug Safety (MFDS) report due to errors such as duplicated graphs [33]. Upon closer examination, it was found that the pharmacokinetic profiles of these subjects were identical to other participants' graphs. Consequently, data from 23 subjects (12 males and 11 females) were used for the population pharmacokinetic analysis in this study. Demographic characteristics of 23 subjects could not be summarized due to unavailability of the individual data. However, demographic results are expected to be similar to the original study with a smaller standard deviation. Mean age, height, and weight of male participants (N = 15) were 30.2 $\pm$ 5.9 years, 173.5 $\pm$ 5.5 cm, and 73.1 $\pm$ 7.6 kg, and 29.9 $\pm$ 6.2 years, 159.9 $\pm$ 5.6 cm, and 54.7 $\pm$ 3.9 kg for female participants (N = 15), respectively [33]. NCA was performed to compare the similarity of the data. The results were similar, with no statistically significant differences in any PK parameters between the digitized and original data (Table 1). Digitized concentration data for zolpidem are shown in Figure 1.

Table 1. Non-compartment analysis results of digitized data.

Parameters	Male		Female	
	Original (N = 15)	**Digitized (N = 12)**	**Original (N = 15)**	**Digitized (N = 11)**
C_{max} (ng/mL)	161.21 (46.74)	162.72 (47.04)	187.64 (59.44)	189.22 (59.85)
$AUC_{0–12h}$ (ng h/mL)	537.9 (202.3)	542.5 (197.5)	696.9 (221.7)	688.1 (221.3)
CL/F (L/h)	19.76 (7.25)	18.88 (6.06)	14.72 (4.07)	14.93 (4.22)
Lambda z (1/h)	0.27 (0.09)	0.22 (0.06)	0.23 (0.03)	0.24 (0.04)
Half-life (h)	2.93 (1.14)	3.58 (1.10)	3.05 (0.35)	3.02 (0.52)
V_d/F (L)	74.8 (16.2)	92.2 (35.7)	63.6 (15.6)	63.5 (16.5)
T_{max} (h)	0.94 (0.58–1.80)	0.96 (0.58–1.78)	0.83 (0.58–3.33)	0.84 (0.57–3.36)

Data are presented as the mean (standard error), except for Tmax (min–max). N = number of subjects; Cmax, maximum concentration; $AUC_{0–12h}$, area under the concentration curve from zero to 12 h; CL/F, apparent clearance (dose/AUC_{inf}); lambda z, terminal slope of the time-log-transformed concentration curve; half-life (h) = In(2)/lambda z; V_d/F, apparent volume of distribution (CL/F/Lambda z); Tmax, time to reach the maximum concentration.

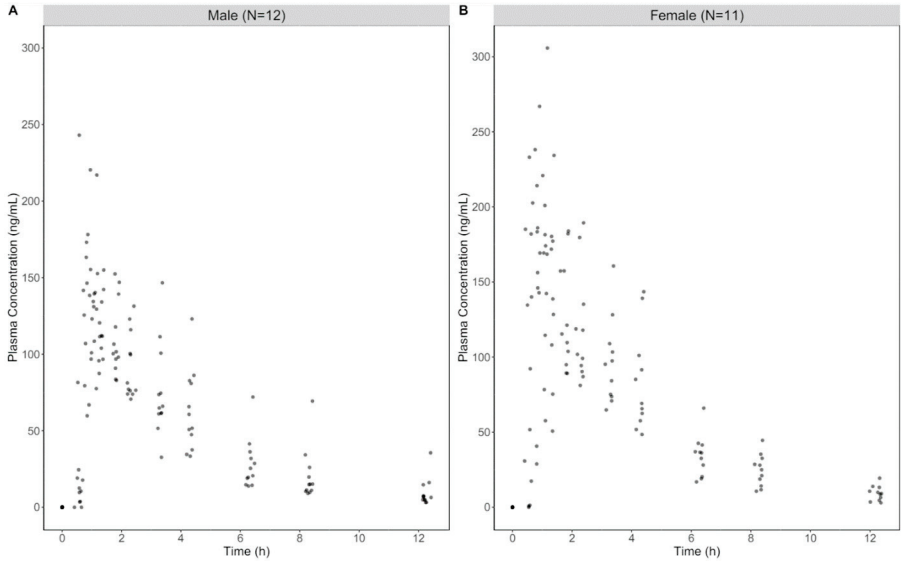


Figure 1. Observed data of plasma zolpidem concentrations. The raw data were digitized using the WebPlot Digitizer from the research report available on the Ministry of Food and Drug Safety website. (**A**) Male participants (N = 12); (**B**) female participants (N = 11).

3.2. Population PK Model

A one-compartment linear model with delayed onset best described the plasma concentrations after the oral administration of zolpidem. The introduction of a parameter reflecting time delay (ALAG) in the PK model significantly improved the model (ΔOFV = 25.3). No other structural models, including various absorption models that explain the early absorption phase, showed any significant improvement. However, the result of the covariate analysis showed that sex was not significant in the current study. The PK parameter estimates for the final model are summarized in Table 2. The population parameter estimates of the final model were close to the median values of the parameter estimates from 1000 bootstrap replicates, and their 95% confidence intervals demonstrated the robustness of the final model (Table 2).

Table 2. Parameter estimates in the final pharmacokinetic model with bootstrap results.

Parameters	Estimates (RSE [a] %)	Bootstrap	
		Median	95% CI
Fixed effects			
K_a (1/h)	5.41 (45.47)	5.66	3.24–11.24
V_d/F (L)	61.70 (5.82)	61.33	54.89–68.64
CL/F (L/h)	16.90 (8.40)	16.87	14.29–19.50
ALAG (h)	0.394 (6.24)	0.394	0.385–0.493
Interindividual variability (IIV)			
ω^2_{Ka} (CV [b] %)	158.91 (43.65)	157.81	69.76–444.98
ω^2_{Vd} (CV%)	22.10 (47.17)	20.98	12.0–29.68
ω^2_{CL} (CV%)	32.60 (45.54)	31.74	20.96–41.65
$\rho_{Vd\text{-}CL}$	0.853	0.853	0.796–0.869
Residual variability			
Proportional error	0.284 (6.16)	0.283	0.242–0.319

[a] RSE (%), relative standard error (standard error/parameter estimate); [b] CV (%), coefficient of variance; K_a, absorption rate constant; V_d/F, apparent central volume of distribution; CL/F, apparent clearance; ALAG, absorption lag time.

The basic goodness-of-fit plot demonstrated adequate predictive performance, and no specific trend was observed, as shown in Figure 2. In addition, the visual predictive

check plot showed adequate predictive properties of the final model, even though slight underprediction was observed (Figure 3).

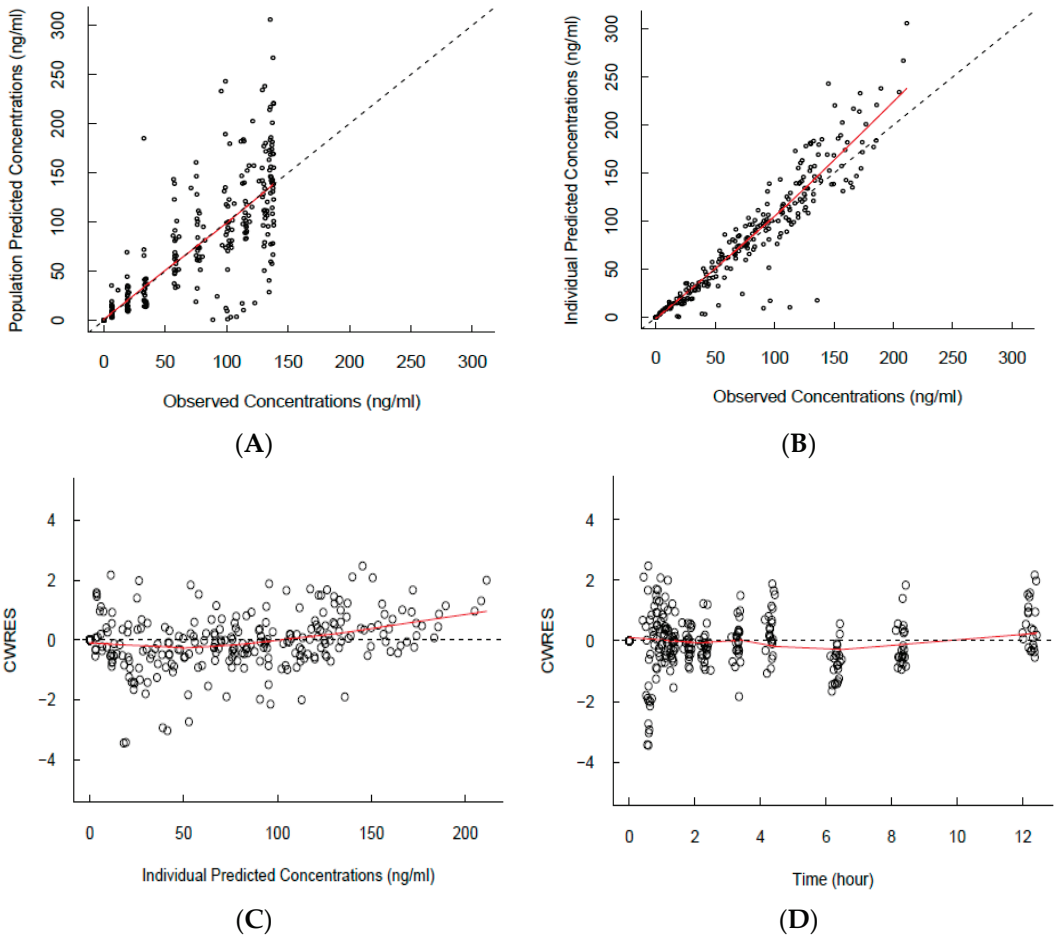


Figure 2. Basic goodness-of-fit plots of the final population pharmacokinetic model. Circles indicate the observed/predicted blood concentrations. The black dashed lines indicate the identity or zero line. The red lines indicate the locally weighted scatterplot smoothing line. (**A**) Scatterplot of PRED (population predictions) versus observed concentrations. (**B**) Scatterplot of IPRED (individual predictions) versus observed concentrations. (**C**) Scatterplot of conditional weighted residuals (CWRES) vs. individual predictions. (**D**) Scatterplot of CWRES vs. time after dosing.

3.3. RxODE Conversion and Simulation

After developing the population PK model, it was converted into RxODE syntax using the nonmem2rx package. This conversion allowed us to easily translate the PK model into R, laying the groundwork for developing the base model. The sampling time for the simulation was specified by the PK characteristics of zolpidem. As shown in Table 1, while the median T_{max} values were between 0.75 and 2.6 h, the T_{max} for females extended up to 3.36 h. To accommodate this observed variability and optimize more accurate simulation, we specified the sampling time to be more frequent up to 4 h to monitor the extended absorption phase. Beyond this, the sampling intervals were widened to reduce the overall simulation time. This simulation model with adjusted sampling times was used as the base model for the shiny web application.

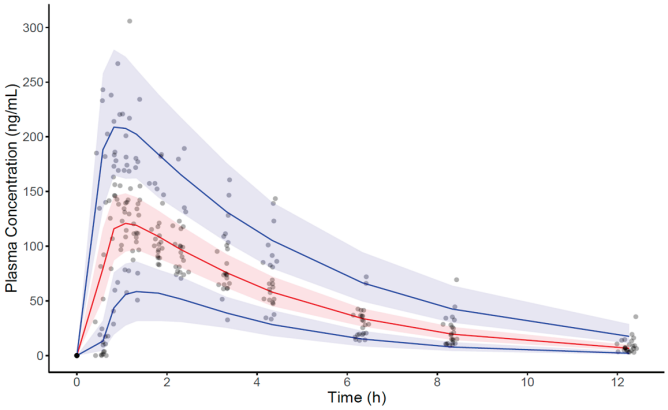


Figure 3. Visual predictive check (VPC) for zolpidem concentrations using the final PK model. Observed concentrations are depicted as gray dots. The figure presents the VPC with the prediction intervals for the 5th, 50th, and 95th percentiles of simulations from bottom to top. The solid lines correspond to 5th, 50th, and 95th percentiles. The blue shaded areas correspond to 95th confidence interval of the 5th and 95th percentile. The red shaded area corresponds to 95th confidence interval of the 50th percentile.

3.4. Zolpidemsim: Web Application

Using the shiny package in R, a web-based user-interactive pharmacokinetic simulation application (Zolpidemsim) was constructed. After developing the population PK model, it was converted into RxODE syntax using the nonmem2rx package. This conversion allowed us to easily translate the PK model into R, laying the groundwork for the development of web applications. The utilization of rxode2 allows for swift and efficient simulations across various dosing scenarios, providing a rapid and reliable computational platform crucial for dynamic pharmacokinetic modeling and analysis. This application consists of three panels, "Dosage regimen", "Simulation results", and "About", and is available online for a responsive simulation (https://pipettox.shinyapps.io/Zolpidem (accessed on 13 April 2024)). In the "Dosage regimen" panel, users can define their preferred dosage regimens via various sidebars, such as dose strength, number of tablets, and number of simulations. Based on the user input, the total dose of zolpidem is automatically calculated and displayed on top of the sidebar. The simulation is initiated by clicking the "Simulate" button. Then, users can view the simulation plot which visually represents the outcomes including 5th, 50th, and 95th percentiles along with the reference range of zolpidem concentration. Also, a summary of the simulation such as predicted parameters, current zolpidem concentration, and duration of toxic concentration is displayed. For a comprehensive analysis, users can navigate to the "Simulation results" panel, which shows detailed simulation outcomes This includes both population PK parameters and NCA results, such as C_{max}, T_{max}, AUC, and half-life. In addition, this application illustrates the duration for which plasma concentrations remain above therapeutic, toxic, and fatal thresholds. A representative example of the simulation in a patient administered 200 mg of zolpidem is displayed in Figure 4.

3.5. Simulation Results at Various Doses

Demonstrative simulations using the application were conducted at four different doses to evaluate the PK profiles of zolpidem. These regimens included a single dose of 10 mg, the recommended daily dose of zolpidem as a reference [10,12]. An additional simulation was performed at a dose of 280 mg, equivalent to the total amount prescribed for four weeks, contained in one package. We then simulated doses of 560 and 1120 mg, which were equivalent to two and four packages, respectively (Figure 5). These doses were selected based on the total dose in a single package and the regulatory context in South Korea, where zolpidem is recommended for up to 28 days.

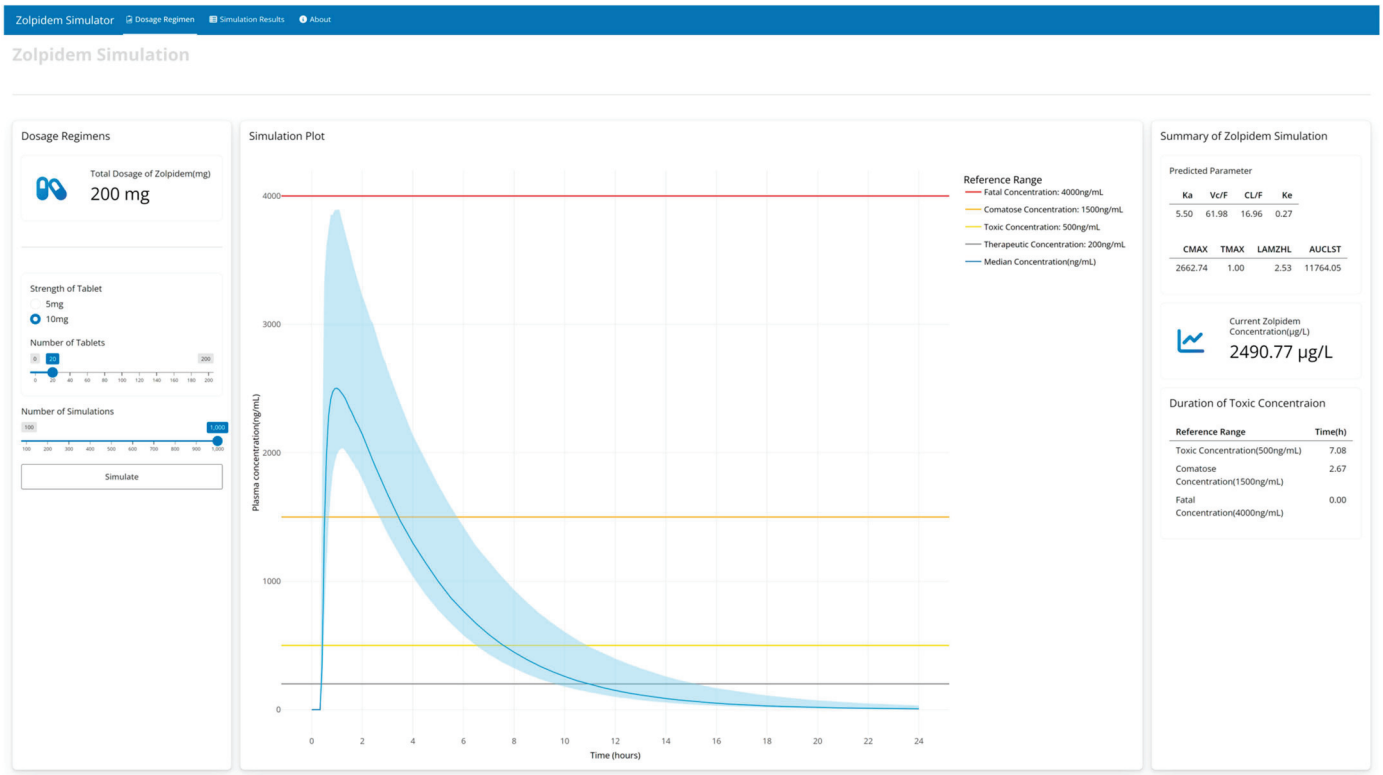


Figure 4. An example of the web application simulated in the case of a 200 mg zolpidem overdose (20 tablets of 10 mg zolpidem).

As shown in Figure 5, the simulated profiles of a single administration of 10 mg of zolpidem remained mostly below the therapeutic threshold and did not reach the toxicity threshold. However, at higher doses, the plasma zolpidem concentration remained above the toxic and comatose levels for a considerable period. In the case of 280 mg dosing, fatal concentrations were simulated in 21.4% of the total simulations within 1 h after dosing. As expected, a remarkable increase was noted at a dose of 1120 mg, where the fatal concentration level was maintained for over 3 h in 98.4% of the total simulations (Table 3).

Table 3. The percentage of the simulation number that reached toxic, comatose, and fatal concentration levels after zolpidem dosing.

	Doses (mg)	NR [a] (%)	<1 h (%)	1–2 h (%)	2–3 h (%)	>3 h (%)
Toxic concentration (500–1500 ng/mL)	10	100	0	0	0	0
	280	0	0	0	0	100
	560	0	0	0	0	100
	1120	0	0	0	0	100
Comatose concentration (1500–4000 ng/mL)	10	100	0	0	0	0
	280	0.2	0.4	0.8	15.0	83.6
	560	0	0	0	0.4	99.6
	1120	0	0	0	0	100
Fatal concentration (>4000 ng/mL)	10	100	0	0	0	0
	280	58.8	21.4	15.6	4.0	0.2
	560	2.6	1.6	11.2	31.4	53.2
	1120	0	0	0	1.6	98.4

[a] NR, not reached. The percentages indicate the proportion of total simulations that were maintained within the toxic, comatose, and fatal concentration ranges after the administration of 10, 280, 560, and 1120 mg of zolpidem.

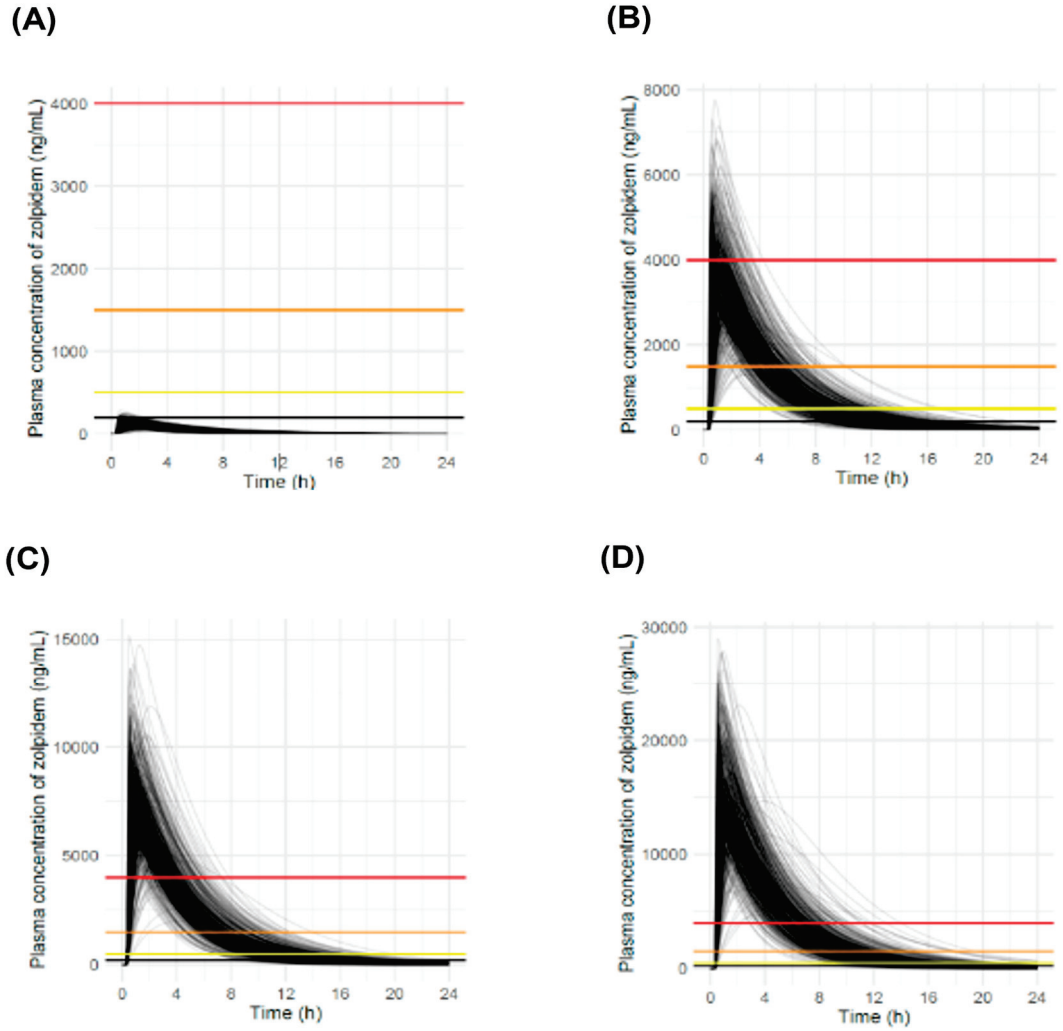


Figure 5. Simulated PK profiles of zolpidem after oral single dosing (N = 500): (**A**) 10 mg zolpidem; (**B**) 280 mg zolpidem; (**C**) 560 mg zolpidem; (**D**) 1120 mg zolpidem. The colored lines indicate concentration thresholds: the red line represents the fatal concentration threshold (4000 ng/mL), the orange line represents the comatose concentration threshold (1500 ng/mL), and the yellow line represents the toxic concentration threshold (500 ng/mL).

4. Discussion

Previous clinical trials using zolpidem demonstrated that its plasma concentration increased rapidly and decreased in the PK profile [22,34]. According to a PK/PD study, this was adequately explained by the sigmoid E_{max} model based on ligand-binding theory [35]. Although zolpidem is known to be a relatively safe compound owing to its short duration of action, it may cause life-threatening complications such as anaphylaxis or respiratory depression upon overdose. In fact, coadministration of zolpidem with alcohol, H1 antihistamines (first generation), benzodiazepines, phenobarbital, and opioids increased the risk of CNS depression and respiratory depression due to the drug–drug interaction (DDI) [10].

To develop a web application for simulating plasma zolpidem concentrations in patients with drug intoxication, we constructed a population PK model using digitized data from 23 healthy volunteers (12 males and 11 females). This website (https://pipettox.shinyapps.io/Zolpidem (accessed on 13 April 2024)) is mainly targeted at physicians who treat patients with drug intoxication in the ER. Therefore, we focused on the maximum concentration (C_{max}) and time to reach the therapeutic level, which is related to severity and recovery time, respectively. Additionally, our simulation results at various doses showed a direct correlation between the zolpidem dose and the duration for which the

plasma concentrations remained above critical levels. This finding suggests that as the dose increases, the duration of critical plasma concentrations increases, indicating an increased potential for adverse effects.

In our study, we chose to run the simulations in the R environment because of its robust suite of tools for analyzing and visualizing data, enhanced by the release of the shiny package, which allows easy development of interactive web-based interfaces. These capabilities make R an ideal platform for pharmacokinetic simulations that benefit from real-time interaction and data representation. Building upon R's capabilities, we incorporated the rxode2 and nonmem2rx packages, enhancing the simulation process for ODE-based PK/PD models. This collaboration between these two packages offers distinct advantages over other available packages such as mrgsolve [36], PKPDsim [37], and deSolve [38]. The nonmem2rx package enables the direct conversion of NONMEM models to RxODE syntax, which markedly simplifies the simulation process by reducing manual scripting. This reduces the risk of human error and significantly saves the time required to set up the simulation. Additionally, the rxode2 package enables specification of dosing scenarios and offers more rapid execution times for these simulations than other packages [31]. Thus, integrating rxode2 and nonmem2rx into our R environments not only enhances our capacity for sophisticated PK/PD simulation but also ensures a more efficient, accurate, and user-friendly experience, ultimately contributing to the robustness and reliability of pharmacokinetic analyses.

Drover et al. reported that a one-compartment model with first-order absorption and elimination phases described PK kinetics and none of the covariates produced a significant improvement [34]. In contrast, Saldanha et al. reported that a two-compartment model with lag time, first-order absorption, and linear elimination best described zolpidem cases [22]. Thus, zolpidem is suitable for various PK models, depending on the concentration data of individuals. In the original study, which included 30 subjects, a two-compartment model combining the Erlang-type and zero-order absorption models was constructed as the basic PK model [33]. However, in this study, the plasma concentration of zolpidem was best described by a one-compartment model without a covariate (N = 23). Although exposure to zolpidem was approximately 30% higher in females than in males, according to a previous report, our results demonstrated that sex was not selected as a covariate. None of the PK parameters from the NCA was significantly different between males and females, except for the volume of distribution ($p < 0.05$). Although this study used digitized data from a limited number of participants, our results are meaningful and reasonable for evaluating patients with intoxication from an emergency medicine perspective.

This study had several limitations. In cases of drug intoxication, patients typically take dozens to hundreds of tablets, which can interfere with absorption. As a result, the maximum concentration (C_{max}) of the drug in the bloodstream would decrease owing to the low dissolution or absorption delay, as mentioned previously. In addition, patients with acute zolpidem overdose occasionally take it with alcohol or other psychotropic drugs, which can lead to a more severe condition than expected from the plasma drug concentrations due to the drug interaction [9]. Because of the short duration of an immediate-release formulation, a controlled-release (CR) formulation has been prescribed to improve sleep maintenance. Therefore, further studies applicable to various clinical situations, including DDI and CR formulation, are needed. Another limitation was the inability to assess the influence of demographic factors on the pharmacokinetics of zolpidem due to the unavailability of individual demographic data other than sex. However, based on the methodology established in the present study, although it uses digitized data, this approach is expected to expand in the future as a platform capable of easily simulating the blood concentrations of acutely intoxicated drugs.

5. Conclusions

We developed a web application that enables physicians to perform various easy-to-use simulations of zolpidem dosing using a web browser. This web application might help

understand how plasma zolpidem concentration changes over time and how long toxic zolpidem concentration levels persist. Thus, this web tool may be helpful in the clinical assessment and management of patients with zolpidem intoxication in the ER.

Author Contributions: Conceptualization, K.C.P. and H.K.; methodology, H.J.C.; software, H.J.C. and S.H.; validation, K.C.P. and H.K.; formal analysis, H.J.C. and K.C.P.; investigation, H.J.C. and K.C.P.; resources, S.H. and H.K.; data curation, H.J.C.; writing—original draft preparation, H.J.C.; writing—review and editing, S.H., K.C.P. and H.K.; visualization, H.J.C.; supervision, S.H. and H.K.; project administration, H.K.; funding acquisition, H.K. All authors have read and agreed to the published version of the manuscript.

Funding: This paper was supported by Eulji University in 2023 (EJRG-23-06).

Institutional Review Board Statement: Not applicable. In this study, we used only virtual data extracted from the graphs of individual plasma profiles in clinical reports published previously.

Informed Consent Statement: Not applicable.

Data Availability Statement: The dataset used in this study is available from the corresponding author upon request.

Acknowledgments: All authors would like to thank all the contributors who belonged to the hospital and MFDS for the clinical trial. We also would like to thank J. Sunwoo (CNUH, Daejeon, Republic of Korea) and Y. Hong (AIMS BioScience, Seoul, Republic of Korea) for their helpful assistance.

Conflicts of Interest: Kwan Cheol Pak was employed by Yuhan Corporation. The remaining authors declare that the research was conducted in the absence of any commercial or financial relationships that could be construed as a potential conflict of interest.

References

1. Stahl, S.M.; Grady, M.M.; Muntner, N. *Stahl's Essential Psychopharmacology, Neuroscientific Basis and Practical Application*, 5th ed.; Cambridge University Press: Cambridge, UK, 2021; pp. 418–424. [CrossRef]
2. Holm, K.J.; Goa, K.L. Zolpidem: An update of its pharmacology, therapeutic efficacy and tolerability in the treatment of insomnia. *Drugs* **2000**, *59*, 865–889. [CrossRef] [PubMed]
3. National Institutes of Health. National Institutes of Health State of the Science Conference statement on Manifestations and Management of Chronic Insomnia in Adults, 13–15 June 2005. *Sleep* **2005**, *28*, 1049–1057. [CrossRef] [PubMed]
4. Moore, T.J.; Mattison, D.R. Assessment of patterns of potentially unsafe use of zolpidem. *JAMA Intern. Med.* **2018**, *178*, 1275–1277. [CrossRef] [PubMed]
5. Morlock, R.J.; Tan, M.; Mitchell, D.Y. Patient characteristics and patterns of drug use for sleep complaints in the United States: Analysis of National Ambulatory Medical Survey data, 1997–2002. *Clin. Ther.* **2006**, *28*, 1044–1053. [PubMed]
6. Thompson, K.S.; Lewis, R.J.; Ritter, R.M. Analysis of zolpidem in postmortem fluids and tissues using ultra-performance liquid chromatography-mass spectrometry. *J. Anal. Toxicol.* **2014**, *38*, 507–512. [CrossRef] [PubMed]
7. Lee, M.H.; Choi, J.W.; Lee, J.; Shin, A.; Oh, S.M.; Jung, S.J.; Lee, Y.J. Trends in prescriptions for sedative-hypnotics among Korean adults: A nationwide prescription database study for 2011–2015. *Soc. Psychiatry Psychiatr. Epidemiol.* **2019**, *54*, 477–484. [CrossRef] [PubMed]
8. Salvà, P.; Costa, J. Clinical Pharmacokinetics and Pharmacodynamics of Zolpidem. *Clin. Pharmacokinet.* **1995**, *29*, 142–153. [CrossRef] [PubMed]
9. Monti, J.M.; Spence, D.W.; Buttoo, K.; Randi-Perumal, S.R. Zolpidem's use for insomnia. *Asian J. Psychiatry* **2017**, *25*, 79–90. [CrossRef] [PubMed]
10. U.S. Food and Drug Administration. FDA Drug Safety Communication: FDA Approves New Label Changes and Dosing for Zolpidem Products and Recommendation to Avoid Driving the Day after Using Ambien CR. US FDA. 2013. Available online: https://www.fda.gov/drugs/drug-safety-and-availability/fda-drug-safety-communication-fda-approves-new-label-changes-and-dosing-zolpidem-products-and (accessed on 21 January 2024).
11. Scharner, V.; Hasieber, L.; Sönnichsen, A.; Mann, E. Efficacy and safety of Z-substances in the management of insomnia in older adults: A systematic review for the development of recommendations to reduce potentially inappropriate prescribing. *BMC Geriatr.* **2022**, *22*, 87. [CrossRef] [PubMed]
12. Sanofi-aventis. U.S. LLC. AMBIEN® (Zolpidem Tartrate) Tablets, for Oral Use. Label. 2022. Available online: https://www.accessdata.fda.gov/drugsatfda_docs/label/2022/019908s40s044s047lbl.pdf (accessed on 9 April 2024).
13. Uges, D.R. TIAFT Reference Blood Level List of Therapeutic and Toxic Substances. Available online: https://www.fnusa.cz/wp-content/uploads/therap_tox_levels.pdf (accessed on 13 January 2024).

14. Organization for Economic Cooperation and Development. *OECD Factbook 2015–2016: Economic, Environmental and Social Statistics*; OECD Publishing: Paris, France. 2016. Available online: https://www.oecd-ilibrary.org/economics/oecd-factbook-2015-2016_factbook-2015-en (accessed on 21 January 2024).
15. Lee, E.S.; Kim, S.J.; Cho, G.C.; Lee, M.J.; So, B.H.; Kim, K.S.; Song, J.; Lee, S.W. The 2022 annual report on toxicology surveillance and severe poisoning cases at emergency departments in Korea. *J. Korean Soc. Clin. Toxicol.* **2023**, *21*, 1–16. [CrossRef]
16. Pai, K.H.; Lee, S.W.; Kim, S.J.; Han, K.S.; Song, J.; Lee, S.; Park, J.H.; Song, J. Patterns of self-harm/suicide attempters who visited emergency department over the past 10 years and changes in poisoning as a major method (2011–2020). *J. Korean Soc. Clin. Toxicol.* **2023**, *21*, 69–80. [CrossRef]
17. Park, M.; Park, J.; Lee, S.; In, S. Analysis of death due to poisoning in the national capital region (2014–2016). *J. Korean Soc. Clin. Toxicol.* **2017**, *15*, 101–106. [CrossRef]
18. Powell, J.R.; Gobburu, J.V.S. Pharmacometrics at FDA: Evolution and impact on decisions. *Clin. Pharmacol. Ther.* **2007**, *82*, 97–102. [CrossRef] [PubMed]
19. Bauer, R.J. NONMEM Tutorial Part I: Description of Commands and Options, With Simple Examples of Population Analysis. *CPT Pharmacomet. Syst. Pharmacol.* **2019**, *8*, 525–537. [CrossRef] [PubMed]
20. Korea Clinical Trials Information Center. Available online: https://cris.nih.go.kr/cris/search/listDetail.do?search_yn=Y&searchWord=KCT0003934 (accessed on 12 January 2024).
21. Rohatgi, A. WebPlotDititizer, Version 4.7 [Computer Software]. 2021. Available online: https://apps.automeris.io/wpd (accessed on 12 January 2024).
22. Saldanha, L.; Costa, B.; Vale, N. In silico personalized study for zolpidem based on sex difference. *Future Pharmacol.* **2022**, *2*, 99–116. [CrossRef]
23. Kim, H.; Han, S.; Cho, Y.S.; Yoon, S.K.; Bae, K.S. Development of R packages: 'NonCompart' and 'ncar' for noncompartmental analysis (NCA). *Transl. Clin. Pharmacol.* **2018**, *26*, 10–15. [CrossRef] [PubMed]
24. NonCompart: Noncompartmental Analysis for Pharmacokinetic Data. R package Version 0.7.0. Available online: https://cran.r-project.org/web/packages/NonCompart/ (accessed on 2 April 2024).
25. NONMEM. ICON plc. Available online: https://iconplc.com/solutions/technologies/nonmem (accessed on 21 January 2024).
26. Yoon, S.; Jeong, S.; Jung, E.; Kim, K.S.; Jeon, I.; Lee, Y.; Cho, J.Y.; Oh, W.Y.; Chung, J.Y. Effect of CYP3A4 metabolism on sex differences in the pharmacokinetics and pharmacodynamics of zolpidem. *Sci. Rep.* **2021**, *11*, 19150. [CrossRef] [PubMed]
27. The R Project for Statistical Computing. R. Available online: http://www.r-project.org (accessed on 22 November 2023).
28. nonmem2rx: 'nonmem2rx' Converts 'NONMEM' Models to 'rxode2'. R Package Version 0.1.3. Available online: https://cran.r-project.org/web/packages/nonmem2rx/ (accessed on 12 December 2023).
29. Rxode2: Facilities for Simulating from ODE-Based Models. R Package Version 2.1.0. Available online: https://cran.r-project.org/package=rxode2/ (accessed on 30 January 2024).
30. Wang, W.; Hallow, K.M. A Tutorial on RxODE: Simulating Differential Equation Pharmacometric Models in R. *CPT Pharmacomet. Syst. Pharmacol.* **2016**, *5*, 3–10. [CrossRef] [PubMed]
31. Shiny: Web Application Framework for, R. R Package Version 1.8.1.1. Available online: https://cran.r-project.org/web/packages/shiny/ (accessed on 2 April 2024).
32. bslib: Custom 'Bootstrap' 'Sass' Themes for 'Shiny' and 'Rmarkdown'. R Package Version 0.7.0. Available online: https://cran.r-project.org/web/packages/bslib/ (accessed on 9 April 2024).
33. Lee, Y.; Oh, W.Y.; Kim, K.S.; Jung, E.; Jeong, S.M.; Lee, J.G.; Yi, J.Y.; Chung, J.; Ryu, S.A.; Park, Z.W. Development of Pharmacometrics-Based Modeling for Optimal Dosage (Korean). Research Report of Ministry of Food and Drug Safety (MFDS), Republic of Korea. 2018. Available online: https://rnd.mfds.go.kr/download/rnd/1125833?mode=download (accessed on 22 January 2024).
34. Drover, D.; Lemmens, H.; Naidu, S.; Cevallos, W.; Darwish, M.; Stanski, D. Pharmacokinetics, pharmacodynamics, and relative pharmacokinetic/pharmacodynamic profiles of zaleplon and zolpidem. *Clin. Ther.* **2000**, *22*, 1443–1461. [CrossRef] [PubMed]
35. de Haas, S.L.; Schoemaker, R.C.; van Gerven, J.M.A.; Hoever, P.; Cohen, A.F.; Dingemanse, J. Pharmacokinetics, pharmacodynamics and the pharmacokinetic/pharmacodynamic relationship of zolpidem in healthy subjects. *J. Psychopharmacol.* **2010**, *24*, 1619–1629. [CrossRef] [PubMed]
36. mrgsolve: Simulate from ODE-Based Models. R Package Version 1.4.1. Available online: https://cran.r-project.org/web/packages/mrgsolve/ (accessed on 9 April 2024).
37. PKPDsim: Tools for Performing Pharmacokinetic-Pharmacodynamic Simulations. R Package Version 1.3.0. Available online: https://cran.r-project.org/web/packages/PKPDsim/ (accessed on 9 April 2024).
38. deSolve: Solvers for Initial Value Problems of Differential Equations ('ODE', 'DAE', 'DDE') R Package Version 1.40. Available online: https://cran.r-project.org/web/packages/deSolve/ (accessed on 9 April 2024).

Disclaimer/Publisher's Note: The statements, opinions and data contained in all publications are solely those of the individual author(s) and contributor(s) and not of MDPI and/or the editor(s). MDPI and/or the editor(s) disclaim responsibility for any injury to people or property resulting from any ideas, methods, instructions or products referred to in the content.

MDPI AG
Grosspeteranlage 5
4052 Basel
Switzerland
Tel.: +41 61 683 77 34

Pharmaceutics Editorial Office
E-mail: pharmaceutics@mdpi.com
www.mdpi.com/journal/pharmaceutics



Disclaimer/Publisher's Note: The title and front matter of this reprint are at the discretion of the Guest Editors. The publisher is not responsible for their content or any associated concerns. The statements, opinions and data contained in all individual articles are solely those of the individual Editors and contributors and not of MDPI. MDPI disclaims responsibility for any injury to people or property resulting from any ideas, methods, instructions or products referred to in the content.





Academic Open
Access Publishing

mdpi.com

ISBN 978-3-7258-8842-9